



Virginia Commonwealth University
VCU Scholars Compass

Theses and Dissertations

Graduate School

2011

Designing Allosteric Inhibitors of Thrombin

Preetpal Sidhu
Virginia Commonwealth University

Follow this and additional works at: <https://scholarscompass.vcu.edu/etd>



Part of the [Pharmacy and Pharmaceutical Sciences Commons](#)

© The Author

Downloaded from

<https://scholarscompass.vcu.edu/etd/295>

This Dissertation is brought to you for free and open access by the Graduate School at VCU Scholars Compass. It has been accepted for inclusion in Theses and Dissertations by an authorized administrator of VCU Scholars Compass. For more information, please contact libcompass@vcu.edu.

© Preetpal Singh Sidhu 2011

All Rights Reserved

DESIGNING ALLOSTERIC INHIBITORS OF THROMBIN

A Dissertation submitted in partial fulfillment of the requirement for the degree of Doctor of
Philosophy at Virginia Commonwealth University

by

PREETPAL SINGH SIDHU

B.Pharmacy, Rajiv Gandhi University of Health Science, 2006

Director: Umesh R. Desai

Professor, Department of Medicinal Chemistry

Virginia Commonwealth University

Richmond, Virginia

November 2011

Acknowledgements

First and foremost, I take an opportunity to express my deep regards and sincerest gratitude to my advisor Dr. Umesh R. Desai for giving me chance to work under his supervision and support over last four years. I attribute my work to his encouragement and availability for answering the queries and for his valuable guidance. He was very supportive and gave independence to work and explore new things.

I offer my regards and thanks to Dr. Qibing Zhou for his support over the period of my Ph.D. degree. He is excellent guide, mentor and teacher. He inspired me by teaching various aspects of organic synthesis and training me. His advice and suggestions are invaluable, that helped me in learning synthesis technique and tricks that helped me to achieve my current goals and will path my way throughout my career.

I would like to express my gratitude towards my dissertation committee Dr. Glen Kellogg, Dr. Martin Safo, Dr. Frank Gupton and Dr. Scott Gronert for supporting my research work and for their valuable comments and suggestion. I really appreciate their time for reading my thesis and hearing me during my oral proposal, committee meeting and final defense.

I would like to thank Dr. Philip Mosier for his valuable suggestions and solving the issue related to computational work. He has been great support to teach and train me in various software and aspects of drug design. Especially grateful for writing various scripts to tackle the issue raised from “Sulfate” group. His feedbacks while reviewing the manuscript were very advantageous.

I thank Dr. Aiye Liang for performing the biochemical experiments and teaching the various aspects related to thrombin assays and plasma clotting assay. Also not forgetting to thank Akul Mehta to spending his valuable time training and helping me out on FlexStation. I also appreciate the help given by Pooja Ponnusamy for recording Mass Spectra for my compounds.

Department of Medicinal Chemistry and School of Pharmacy played valuable role during my research work. I am very thankful for providing me an opportunity to pursue my degree and financial support. Also, would wish to thank Institute for Structural Biology and Drug Discovery and Department of Chemistry for providing the various facilities.

In particular I wish to thank Niti Vanee for all the motivation and spending endless time in reviewing all the write-ups like manuscript, thesis, emails etc. She had been excellent moral support and source of inspiration over my stay in Richmond. I would also like to acknowledge Nipa Patel for supporting and enhancing my self- confidence over last 9 years.

I extend my thanks to our research group members: Jay, Rami, Rajesh, Shrenik, Tim, Rio, Yingizi and Maliaka for the supportive and lively environment at work and my friends in Richmond for making life enjoyable and smooth.

Lastly, I want to thank my family for emotional and financial support and laying the foundation without which nothing could be possible.

Table of content

Acknowledgement	
List of Tables	viii
List of Figures	x
Abbreviation	xiii
Abstract	xv
Chapter 1 Introduction	1
1.1 Background	1
1.2 Blood Coagulation Mechanism.....	2
1.2.1 Primary Hemostasis	3
1.2.2 Secondary Hemostasis	3
1.2.3 Tertiary Hemostasis	5
1.3 Regulation of Coagulation	6
1.4 Anticoagulant Therapy and Targets	7
1.5 Limitation of Current Therapy	15
1.6 Thrombin, role and function	16
1.6.1 Active Site.....	18
1.6.2 Exosite-I.....	20
1.6.3 Exosite-II	21
1.6.4 Role of Chain-A	21
1.6.5 Sodium Binding Site	23
1.6.6 Platelet Activation and Role of Thrombin	27
1.7 Therapeutic Uses of Thrombin	28
1.8 Other Component of Coagulation System	30
1.8.1 Factor VII/VIIa	30
1.8.2 Factor IX/IXa.....	31

1.8.3 Factor XI/Xia	32
1.8.4 Factor XII/XIIa	33
1.8.5 Thrombomodulin and Protein C	34
1.9 Thrombin Engineering	38
Chapter 2 Hypothesis	42
2.1 The era of Small Molecule Inhibitors of Thrombin	42
2.2 Inhibition of Thrombin Through Exosites	43
2.3 Advantage of Allosteric Over Active Site DTIs	44
2.4 Rational for Design of Benzofuran Scaffold.....	45
Chapter 3 Synthesis of Library of Sulfated Benzofuran Monomers and Dimers	50
3.1 Introduction.....	50
3.2 Synthesis	53
3.2.1 Simple Synthesis Procedure of Highly Functionalized Benzofuran Unit.....	53
3.2.2 Synthesis of Benzofuran Monomer and Dimer.....	58
3.2.3 Hydrolysis of Ethyl Ester	58
3.2.4 Reduction of Benzofuran Unit to Diversify the Number and Position of Sulfate Group	60
3.3 Results and Discussion	62
3.3.1 Design of the Sulfated Benzofuran Scaffold.....	62
3.3.2 Overall Description of the Sulfated Benzofuran Library	63
3.3.3 Synthesis of Sulfated Benzofuran Monomers.....	64
3.3.4 Synthesis of Sulfated Benzofuran Dimers	66
3.4 Experimental Section	67
3.4.1 Chemicals, Reagents and Analytical Chemistry	67
3.4.2 Detailed Description of Synthesis Procedure.....	68
3.4.3 Determination of Purity by HPLC Method.....	94

Chapter 4 Identification of a Novel Binding Site for Allosteric Regulation of

Thrombin	97
4.1 Introduction.....	97
4.2 Results.....	98
4.2.1 Thrombin Inhibition.....	98
4.2.2 Mechanism of Thrombin Inhibition.....	103
4.2.3 Plasma Studies	105
4.2.4 Other Biochemical Studies	108
4.2.5 Molecular Modeling Studies.....	109
4.2.6 Screening Against Other Proteases	117
4.3 Discussion.....	121
4.4 Experimental Section	123
4.4.1 Enzyme and Chemicals for Biological Experiments	123
4.4.2 Inhibition of Thrombin	124
4.4.3 Michaelis-Menten Kinetics of Spectrozyme TH Hydrolysis.....	125
4.4.4 Prothrombin Time and Activated Partial Thromboplastin Time	125
4.4.5 Molecular Modeling Studies.....	126
4.4.6 Screening for other proteases.....	127

Chapter 5 Synthesis and Biochemical Evaluation of 2nd Generation of Sulfated

Benzofurans	131
5.1 Introduction.....	131
5.2 Results and Discussion	132
5.2.1 Design and Synthesis of 2nd Generation Sulfated Benzofuran Scaffold.....	132
5.2.2 Chemistry	133
5.2.3 Substrate Hydrolysis Assay	138
5.2.4 Biochemical Studies.....	141

5.2.5 Prolongation of Plasma Clotting Time by 9a.....	142
5.2.6 Screening against Other Enzyme	146
5.2.7 FVIIa Inhibition Potential of Designed Sulfated BenzofuranTrimers	147
5.2.8 FIXa Inhibition Potential of Designed Sulfated BenzofuranTrimers	149
5.2.9 FXa Inhibition Potential of Designed Sulfated BenzofuranTrimers	150
5.3 Significance	152
5.4 Experimental Procedures	153
5.4.1 Chemical, Reagents and Analytical Chemistry.....	153
5.4.2 Synthesis	154
5.4.3 Substrate Hydrolysis Assay	176
5.4.4 Michaelis-Menten Kinetics of Substrate Hydrolysis by Thrombin	177
5.4.5 Plasma Assay (PT and aPTT)	177
5.4.6 Protocol for Screening for Proteases.....	178
5.4.7 Inhibition of FVIIa.....	181
5.4.8 Inhibition of FIXa	182
5.4.9 Inhibition of FXa.....	182
Chapter 6 Identification of Novel Allosteric Inhibitor by Exploring the Larger Chemical Space.....	184
6.1 Introduction.....	184
6.2 Results and discussion	185
6.2.1 Pharmacophore Generation	185
6.2.2 Virtual Screening	186
6.2.3 Docking Studies	187
6.2.4 Chemistry	189
6.2.5 Inhibition of Thrombin by Sulfated Compounds.....	191
6.2.6 Prolongation of Plasma Clotting time by Sulfated Compound.....	193

6.2.7 Screening Against Other Serine Proteases.....	196
6.3 Significance	197
6.4 Experimental Section.....	198
6.4.1 Protein Preparation.....	198
6.4.2 Chemical Database for Virtual Screening.....	198
6.4.3 Docking Protocol	199
6.4.4 Chemical, Reagents and Analytical Chemistry.....	200
6.4.5 Substrate Hydrolysis Assay	201
6.4.6 Plasma Studies	202
Chapter 7 Conclusion.....	203
References.....	206
Appendix (NMR and Mass Spectra).....	238

List of Table

Table 01 – Effect of Different Solvent Composition on Reaction Yield	54
Table 02 – Effect of Various Bases and Reaction Time on Reaction Yield	55
Table 03 – Effect of Substitution of Di-carbonyl Compound on reaction Yield	56
Table 04 – Reaction Condition for Hydrolysis of Ethyl Ester group of 12a.....	59
Table 05 – Method Used for Purity Determination	95
Table 06 – Purity of Compound synthesized.....	96
Table 07 – Inhibition of Human α -Thrombin by Sulfated Benzofuran Monomers	100
Table 08 – Inhibition of Human α -Thrombin by Sulfated Benzofuran Dimers.....	101
Table 09 – Effect of Designed Sulfated Benzofurans on Human Plasma Clotting Time	106
Table 10 – Comparison of GOLD scores obtained from docking studies and IC ₅₀ obtained from experimental data.....	113
Table 11 – Structure of sulfated benzofuran dimers 12a-f and 13-15 found to potently inhibit human thrombin.....	116
Table 12 – Residual activity of various proteases obtained by screening the library of monomers.....	119
Table 13 – Residual activity of various proteases obtained by screening the library of monomers.....	119
Table 14 – Inhibition of Human Thrombin by Sulfated Benzofurantrimers.....	139
Table 15 – PT and aPTT Assay Results for 9a	145
Table 16 – % Residual Activity of Proteases at Single Concentration (365 μ M) of each Inhibitor	146
Table 17 – Inhibition of FVIIa by Sulfated BenzofuranTrimers	149
Table 18 – Inhibition of FIXa by Sulfated Benzofuran Trimers.....	150
Table 19 – Inhibition of FXa by Sulfated Benzofuran Trimers	152

Table 20 – Inhibition of Human α -Thrombin by Sulfated Molecules	192
Table 21 – Effect of Sulfated Molecules on Plasma Clotting Time.....	194
Table 22 – Residual Enzyme Activity of Various Proteases at Single Inhibition Concentration.....	197

List of Figures

Figure 01 – Description of the blood coagulation cascade	6
Figure 02 – Structure of warfarin.....	9
Figure 03 – Structure of heparin	10
Figure 04 – Mechanism of action of DTIslepirudin, bivalirudin and argatroban	11
Figure 05 – Structure of direct FXa inhibitor	14
Figure 06 – Role and regulation of thrombin.....	17
Figure 07 – Chemical mechanism of catalysis for serine proteases.....	19
Figure 08 – Graphical model of human thrombin showing interaction of chain-A and B	22
Figure 09 – Graphical model of human thrombin showing location of active site and exosites.....	23
Figure 10 – Stereo view of the molecular environment of the sodium binding site.....	24
Figure 11 – Stereo view of the structural changes induced by the slow-fast transition of thrombin.....	26
Figure 12 – Structure of thrombomodulin	35
Figure 13 – Graphical model of interaction of thrombin-thrombomodulin complex and activation of protein C.....	37
Figure 14 – Schematic model of regulation of thrombin function by binding of sodium ion.....	40
Figure 15 – Structure and scheme of synthesis of LMWLs.....	46
Figure 16 – Design of benzofuran scaffold from DHPs	48
Figure 17 – Synthesis of a Library of Sulfated Benzofuran as Potential Allosteric Regulators of Thrombin.....	57
Figure 18 - Direct inhibition of thrombin by designed sulfated benzofuran	

monomers and dimmers	99
Figure 19 - Michaelis-Menten kinetics of Spectrozyme TH hydrolysis by human thrombin in the presence of dimer 12a.....	104
Figure 20 - Prolongation of plasma clotting time as a function of concentration of sulfated benzofuran monomers and dimmers	107
Figure 21 - Connolly surface of thrombin (PDB ID = 3EQ0), showing the location of several electropositive basic residues	111
Figure 22 – GOLD binding site definitions for 3EQ0, 1H8D and 2UUF.....	112
Figure 23 - Scatter Plot of GoldScore vs. pIC ₅₀ Values for Docked SBDs	114
Figure 24 - Expanded view of the interaction of 12a with its putative binding site.....	115
Figure 25 - Bar graph showing the % residual activity of given proteases at single concentration of each inhibitor.....	120
Figure 26 - Bar graph showing the % residual activity of given proteases at single concentration of each inhibitor	120
Figure 27- Description of Scheme 1 for Synthesis of Library of Reactive Handle (4a-4h)	134
Figure 28 – Description of Scheme 2 for Synthesis of Reactive Handle 6a-6b.....	135
Figure 29 – Description of Scheme 3 for Synthesis of Library of Trimers (9a-9h and 14).....	136
Figure 30 – Description of Scheme 4 for Synthesis of Tetramer.....	137
Figure 31 – Sigmoidal Plot of Human Thrombin Inhibition by Trimer and Tetramer.....	140
Figure 32 - Prolongation of plasma clotting time as a function of concentration of sulfated benzofuran trimer and tetramer.....	144
Figure 33– Bar Graph of % Residual Activity of Different Proteases By Library of Trimer and Tetramer	147

Figure 34 – Sigmoidal Plot of Full Inhibition by 9b and 9e	148
Figure 35 - Sigmoidal Plot of Full Inhibition by 9c, 9d, 9f, 12 and 15.....	150
Figure 36 - Sigmoidal Plot of Full Inhibition by 9b and 9d.....	151
Figure 37 – Pharmacophore	187
Figure 38 – Dual Screening Filter.....	189
Figure 39 – Structure of Sulfated Compounds.....	191
Figure 40 – Direct Inhibition of Thrombin by Sulfated Compound	193
Figure 41 – Prolongation of Clotting Time.....	195
Figure 42 – Bar Graph for Residual Activity for Screening against Various Protease	197

Abbreviation

ABE: Anion binding exosite

APC: Activated protein C

aPTT: Activated partial thromboplastin time

CA: Caffeic acid

CD: Dehydro polymer of caffeic acid

DHP: Dehydro polymer

DIPEA: Diisopropylethylamine

DTI: Direct thrombin inhibitor

EPCR: Endothelial protein C receptor

GA: Genetic algorithm

GAG: Glycoaminoglycan

H8: Octasaccharide

HK: High-molecular-weight kininogen

HPLC: High pressure liquid chromatography

HS: Hill slope

HTS: High throughput screening

K_{cat} : Catalytic efficiency

K_m : Micheals constant

LAH: Lithium aluminium hydride

LMWH: Low molecular weight heparin

mCBPA: meta-Chloroperbenzoic acid

NAP: nematode anticoagulant protein

PAR: protease activated receptor

PDB: Protein data bank

PEG: Polyethylene glycol

PF4: Platelet factor 4

PK: Prekallikrein

PT: Prothrombin time

RMSD: Root mean square deviation

SAR: Structure activity relationship

SBD: Sulfated benzofuran dimer

SOS: Sucrose octasulfate

SPL: SYBYL programming language

TAFI: Thrombin activable fibrinolysis inhibitor

TBDMSCl: Tributyltrimethylsilyl chloride

TF: Tissue factor

TLC: Thin layer chromatography

TM: Thrombomodulin

tPA: Plasminogen activator

TPFI: Tissue factor pathway inhibitor

UFH: Unfractionated heparin

VS: Virtual screening

vWF: Von Willebrand factor

Abstract

Designing Allosteric Inhibitors of Thrombin

By Preetpal Singh Sidhu

A Dissertation submitted in partial fulfillment of the requirements for the degree of Doctor of Philosophy
at Virginia Commonwealth University

Virginia Commonwealth University, 2011

Director: Dr. Umesh R. Desai

Professor, Department of Medicinal Chemistry

Thrombin is a key enzyme of the coagulation cascade exhibiting important roles in both pro-coagulation and anti-coagulation processes. Most clinically used anticoagulant drugs, including polymeric heparin, warfarin, hirudin, argatroban and the recently approved dabigatran, aim to reduce thrombin activity. There are several binding domains on thrombin including the active site, anion-binding exosites I and II, and the sodium binding site. We hypothesized that thrombin may be better regulated through an allosteric process mediated by small molecules binding to either exosite I or II. An appropriately designed allosteric regulator that reduces the procoagulant signal in a finely tuned manner may maintain a delicate balance between procoagulant and anticoagulant signals in blood resulting reduced bleeding complications.

In this work, we synthesized and studied a library of potent, small, aromatic molecules as allosteric inhibitors of thrombin. Of the 28 potential inhibitors, 11 molecules inhibited thrombin with reasonable potency. Structure activity relationship studies showed that sulfation at the 5-position of the benzofuran scaffold was essential for targeting thrombin. Michaelis-Menten kinetic studies indicated a non-competitive, allosteric mechanism of inhibition. Site-directed mutagenesis, competitive binding and molecular modeling studies led to the identification of the most plausible binding pose for a potent sulfated dimer. To further improve the potency, a small library of sulfated benzofuran trimers was synthesized and studied for thrombin inhibition. Further, to find new scaffold to inhibit thrombin allosterically, docking-based virtual screening approach was used. All these molecules were found to be moderately potent thrombin inhibitors and can serve as lead to develop allosteric inhibitor.

Overall, this work presents the first small, synthetic, sulfated aromatic molecules as potent allosteric modulators of thrombin. Finally, this work also highlights the opportunity of exploring allosteric modulators of other coagulation enzymes, e.g., factors Xa, IXa and XIa, based on the sulfated benzofuran scaffold.

Chapter 1 Introduction

1.1 Background

Cardiovascular diseases have been responsible for the highest number of deaths worldwide counting up to 17.1 million people. It is estimated that the mortality may reach 23.6 million by the end of 2030.¹⁻³ Venous thrombocytopenia (including deep vein thrombosis and pulmonary embolism) is a serious and fatal condition. It causes significant mortality and morbidity in modern society that imposes a major burden on healthcare.^{1,4} Approximately one in every 1000 individuals are diagnosed with this condition annually. These numbers may actually be much higher due to unreported cases because of the asymptomatic nature of the ailment.⁵ Other examples of clotting disorders include acute myocardial infarction, unstable angina, disseminated intravascular coagulation, cerebrovascular thrombosis and atrial fibrillation. Complications resulting from mechanical heart valves and surgery are also related. The risk of developing thrombotic disorder is higher in cancer patients.⁶ Besides the enormous interest and research in advancing treatment of thrombotic disorders, safety still remains a major concern. The primary reason for excessive bleeding associated with thrombotic therapy lies in the complexity of hemostatic system and the high sequence homology in proteases involved in the coagulation target.^{1, 7} The primary targets for thrombotic treatment are thrombin and factor

Xa.⁸ Modern therapy has significantly reduced the side effects of traditional therapy, but is still associated with side effects like compromised immune responses, liver toxicity and requires regular blood monitoring. Consequently, there is significant medicinal potential for the design and synthesis of novel anticoagulant agents that are potent and selective with minimal side effects.^{2, 4}

1.2 Blood Coagulation Cascade

Hemostasis is a spontaneous process that arrests the blood flow to prevent the blood loss in the event of damage to the vascular wall.⁹ Blood coagulation can be defined as the body's defense mechanism against blood loss and microbial infiltration upon injury.¹⁰ It is a complex interplay involving various plasma proteins, the cell membrane, tissue factors, platelets and inorganic ions such as calcium and sodium.¹¹ The hemostatic system is comprised of three mechanisms: the platelet-dependent mechanism, coagulation and fibrinolysis, which are also termed as primary, secondary and tertiary hemostasis, respectively. The mechanism of coagulation is highly conserved throughout the animal kingdom.^{12, 13}

Coagulation begins instantly after an injury to the vascular wall that exposes the transmembrane tissue factor. This is a vascular trigger required to initiate coagulation of blood flow. Exposure of the blood to this tissue factor and endothelial cells initiates the changes in the platelet and other proteases required for the generation of a clot. Platelets are thus immediately activated upon exposure to tissue factor and begin to form a plug at the site of the vascular injury.¹⁴ Simultaneously, the secondary hemostasis mechanism is activated leading to a cascade of events for the formation of fibrin, the primary component of a blood clot.¹⁵

1.2.1 Primary Hemostasis Mechanism

The primary hemostasis mechanism (platelet activation) leads to the exposure of collagens on the surface of endothelial cells.¹⁶ Platelets adhere to the exposed collagen through the von Willebrand Factor (vWF), which acts as a bridge between a glycoprotein complex on the surface of platelets and collagen fibrils.¹⁷ The vWF also binds to factor VIII and is required for its survival while circulating in the blood. Upon binding to collagen, platelets release the contents of their granules, which in turn attract more platelets for aggregation.¹⁸ The activation of platelets is also mediated by thrombin binding to specific receptors on the surface of the platelets. Thrombin is important for initiating the signal transduction cascade. Activation of platelets finally leads to formation of a platelet plug.¹⁹

1.2.2 Secondary Hemostasis Mechanism

The secondary hemostasis mechanism is divided into two pathways: intrinsic and extrinsic (Figure 1).²⁰ The intrinsic pathway (also known as the contact activation pathway) is thought to be less significant for blood coagulation than the extrinsic pathway under normal physiological conditions.¹⁵ However, in disease states, such as hyperlipidemic conditions or bacterial infection, the intrinsic clotting cascade initiates the clot formation. In the state of vascular injury, the extrinsic pathway is mainly responsible for the clot formation. Both pathways merge at the point of conversion of inactive factor X to its active form factor Xa into a common pathway leading to generation of thrombin.¹⁰

The intrinsic pathway is comprised of the clotting factors (VIII, IX, X, XI, and XII), proteins including prekallikrein (PK) and high-molecular-weight kininogen (HK), along with

calcium ions and phospholipids.²¹ The intrinsic pathway begins when PK, HK, factor XI and factor XII are exposed to a negatively charged surface such as that of phospholipids, lipoproteins or a bacterial outer membrane. This is known as the “**contact phase**”.²² The accumulation of contact phase components results in conversion of PK to kallikrein, which in turn leads to activation of factor XII to factor XIIa. Upon activation, factor XIIa activates another inactive zymogen factor XI to form factor XIa. Factor XIIa further converts PK to kallikrein through a positive feedback mechanism. In the presence of Ca^{2+} , factor XIa activates factor IX to form factor IXa. Active factor IXa cleaves factor X at an internal Arg-Ile bond, leading to its activation and forming factor Xa. The assembly of factors VIIIa, IXa and X (inactive form of factor Xa) and Ca^{2+} create the intrinsic tenase complex on the surface of activated platelets. This tenase complex is required for activation of factor Xa.^{13, 15, 23} Factor VIIIa acts as receptor for factors IXa and X.²¹ Thrombin regulates the formation of the tenase complex by playing a dual role via regulating the activation (at low concentration) and inhibition (at high concentration) of factor VIIIa.²⁴ The extrinsic pathway (also known as the tissue factor pathway) is initiated at the site of injury in response to exposure of tissue factor to the blood. Tissue factor is a cofactor in the factor VIIa-catalyzed activation of factor X. The exposed tissue factor binds to activated factors VIIa and X to form the extrinsic tenase.¹⁴ The activation of factor VII is regulated by action of thrombin and factor Xa. The activation of factor VII by factor Xa generates the connection between the intrinsic and extrinsic pathways (Figure 1).^{25, 12, 17}

The common point in both pathways is the activation of factor X to factor Xa. In the common pathway, factor Xa activates prothrombin (factor II) to thrombin (factor IIa). This occurs on the surface of activated platelets and requires formation of a **prothrombinase complex**. It is comprised of platelets, phospholipids, Ca^{2+} , factors Va and Xa, and prothrombin.²⁶

Factor V plays the role of cofactor in the formation of the prothrombinase complex, similar to the role of factor VIII in intrinsic tenase complex. Similar to the intrinsic pathway, activation of factor Va is regulated by thrombin in a concentration-dependent manner.²⁷ Thus, thrombin regulates its own production by regulating the activation of factor VIIIa and Va. Once thrombin is activated, it converts the inactive fibrinogen into an active form by release of two polypeptides. This thrombin-mediated release of the fibrinopeptides then generates fibrin monomers, which spontaneously aggregate in a regular array to form a weak fibrin clot. The weak clot is strengthened by the formation of cross-linked covalent bonds between the fibrin monomers by factor XIIIa,²⁸ which is activated by the action of thrombin.²⁹

1.2.3 Tertiary Hemostasis Mechanism

The tertiary hemostasis mechanism, also known as fibrinolysis, is the degradation of a blood clot.²⁸ Plasmin is a serine protease that circulates in the blood in its inactive form, plasminogen. Plasmin degrades the cross-linked fibrin resulting in dissolution of the clot. The inactive plasminogen binds to both fibrinogen and fibrin, thereby being incorporated into a clot.³⁰ Tissue plasminogen activator (tPA) and urokinase are serine proteases that convert plasminogen to plasmin. Plasmin digests the fibrin to a soluble degradation product to which neither plasmin nor plasminogen can bind. Once the plasminogen and plasmin are released from clot, the free circulating plasmin in the blood is rapidly inactivated by α_2 -antiplasmin.³¹

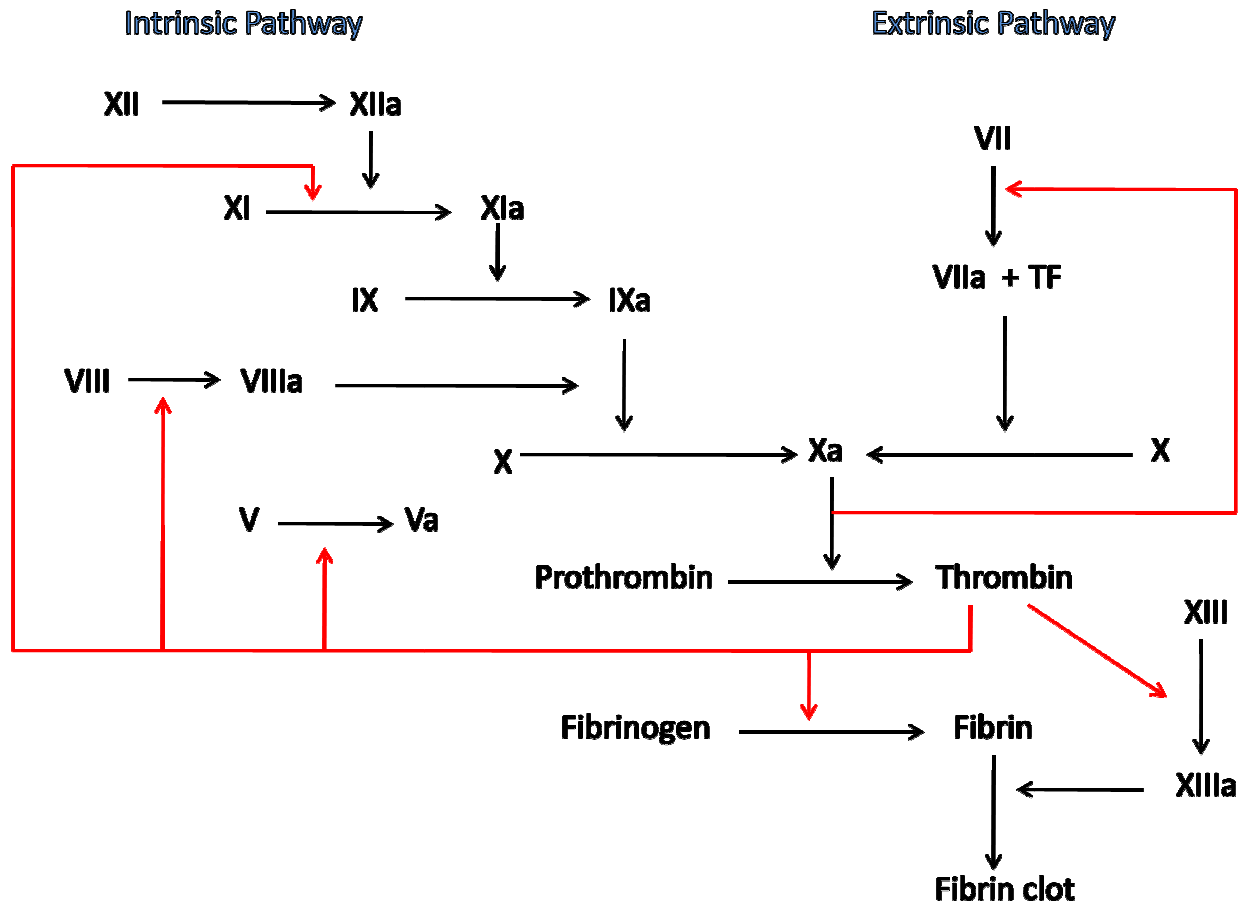


Figure 1. Blood coagulation cascade. The intrinsic and extrinsic pathway merges into a common pathway leading to the formation of a fibrin clot. The red arrows represent the regulation of coagulation by thrombin at various levels.

1.3 Regulation of Coagulation

Several endogenous proteins regulate the coagulation mechanism to prevent the condition of hyper-coagulation by inhibiting various proteases involved in the coagulation process. They also limit the size of the clot formed at the site of injury.

Tissue factor pathway inhibitor (TPFI): TPFI modulates the formation of the extrinsic tenase complex. It mediates the feedback inhibition of the tissue factor-factor VIIa complex, resulting in decreased activation of both factors IX and X.¹² A small amount of factor Xa is required for

TFPI to achieve inhibition of factor VIIa-tissue factor complex. Heparin increases activity of TFPI by 2-4 folds by bringing TFPI and the TF-FVIIa complex closer and hence increasing their interaction. Heparin is also known to increase the release of endothelial stores of TFPI.^{10, 13, 32}

Protein C: Protein C is a vitamin-K dependent inhibitor of the procoagulant system involved in inactivating factors Va and VIIIa. The binding to the thrombin-thrombomodulin complex activates protein C. By inactivating factors Va and VIIa, protein C significantly decreases the thrombin generation, thereby dampening the cascade.^{33, 34}

Antithrombin III: Antithrombin III (AT) directly binds and inactivates thrombin and several serine proteases such as factors IXa, Xa, and XIa.³⁵ The reaction between the serine proteases and AT is relatively slow, but is catalyzed in the presence of heparin. In the presence of heparin or similar sulfated glycosaminoglycans, the reaction between AT and serine proteases is virtually instantaneous, resulting in the immediate arrest of fibrin formation.³⁶

1.4 Anticoagulants Therapy and Targets

Over last five decades, anticoagulant therapy relied mainly on the use of traditional anticoagulants such as heparin and warfarin. The available drugs can be broadly categorized into anticoagulant and antithrombotic, depending on their effects to prolong plasma-based assays. Anticoagulant drugs exert their effect solely by inhibiting the coagulation cascade and hence prolonging the clotting time as indicated in prothrombin (PT) and activated partial thromboplastin time (APTT) assays. In contrast, antithrombotic drugs exert anticoagulation by other mechanisms, apart from any direct effect on the coagulation cascade.³⁷ Recent advances in the development of direct inhibitors of thrombin and factor Xa have resulted in more specific

agents with better pharmacokinetic and pharmacodynamic profiles. Currently, there are three major classes of anticoagulants available in the United States. These are the vitamin-K antagonists, indirect and direct thrombin and factor Xa inhibitors.³⁸

Vitamin-K antagonists: Warfarin was the only oral anticoagulant used over the last 50 years until the discovery of direct inhibitors of thrombin and factor Xa (Figure 2). Warfarin exerts its anticoagulant effects by inhibiting the hepatic synthesis of vitamin-K dependent coagulation factors II, VII, IX and X and anticoagulant proteins C and S. Warfarin not only decreases the synthesis of these coagulation factors, but also reduces their biological activity by inhibiting their activation.³⁹ Warfarin has no effect on circulating coagulation factors, therefore attainment of full antithrombotic effects is delayed depending on the half-lives of the coagulation factors. Warfarin displays an initial transient phase of procoagulation due to the shorter half-life and fast clearance of its anticoagulant protein C.⁴⁰ It has a slow onset of action and needs frequent monitoring of its anticoagulant effects, resulting in increased cost and discomfort to patients. Beside these side effects, warfarin has a narrow therapeutic window due to undesired drug-drug and drug-food interactions. This is even more complicated by significant patient-to-patient variations.⁴¹

Heparins: Unfractionated heparin (UFH) and low molecular weight heparin (LMWH) are used in the clinics as primary anticoagulant therapy. Despite their numerous side effects, they are still considered as first line anticoagulants.³⁸ Heparin is a heterogeneous mixture of polysaccharides chains of molecular weight ranging from 5,000-30,000 Daltons (Figure 3). LMWHs are synthesized by chemical or enzymatic cleavage of UFH to reduce the average molecular weight to 5000 Daltons.⁴² Heparin exerts its biological effect by forming a ternary complex with thrombin and antithrombin.

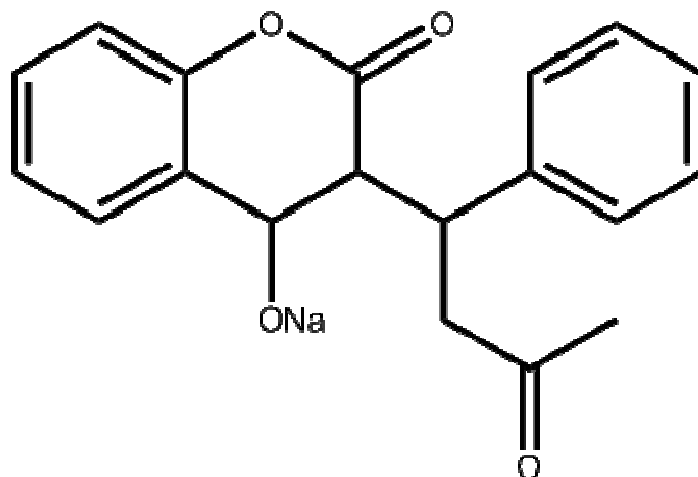


Figure 2. Structure of warfarin, a vitamin-K antagonist.

Heparin binds to antithrombin through a specific pentasaccharide unit causing a major conformational change in antithrombin that accelerates its activity to inhibit factor Xa, thrombin and factor XIa.⁴³ The heparin molecule with the pentasaccharide unit (Figure 3) and an additional 13 saccharide units are able to inhibit thrombin by the bridging mechanism.³⁸ LMWHs having shorter chain lengths are not able to inhibit thrombin as well, but are able to induce a major conformational change in antithrombin that is required to inhibit factor Xa.⁴⁴ The advantages of LMWHs that helped it to replace the clinical usage of UFH is that of longer half-life, allowing the once-daily dosing regimen and its more predictable ADME properties, eliminating the need of regular laboratory monitoring. It also has a lesser risk of thrombocytopenia due to reduced binding to platelet factor 4 (PF4).^{45, 46} The synthetic compound fondaparinux has advantage over LMWHs because it is homogeneous in nature. It is thus safer and carries lower risk of thrombocytopenia than LMWHs and UFH.⁴⁷ Although enormous progress has been made in heparin-based drugs, this class of anticoagulant still has much room for improvement. Heparin and LMWHs are not available orally and require parenteral administration. Heparin also induces thrombocytopenia by binding to PF4. The immune system

produces antibodies for the heparin-PF4 complex, which leads to reduced platelet count.⁴⁸ Fondaparinux is an indirect inhibitor of factor Xa. It is unable to inhibit thrombin due to its shorter chain length. The major drawback of fondaparinux is unavailability of an antidote to neutralize excessive bleeding.⁴⁹⁻⁵¹

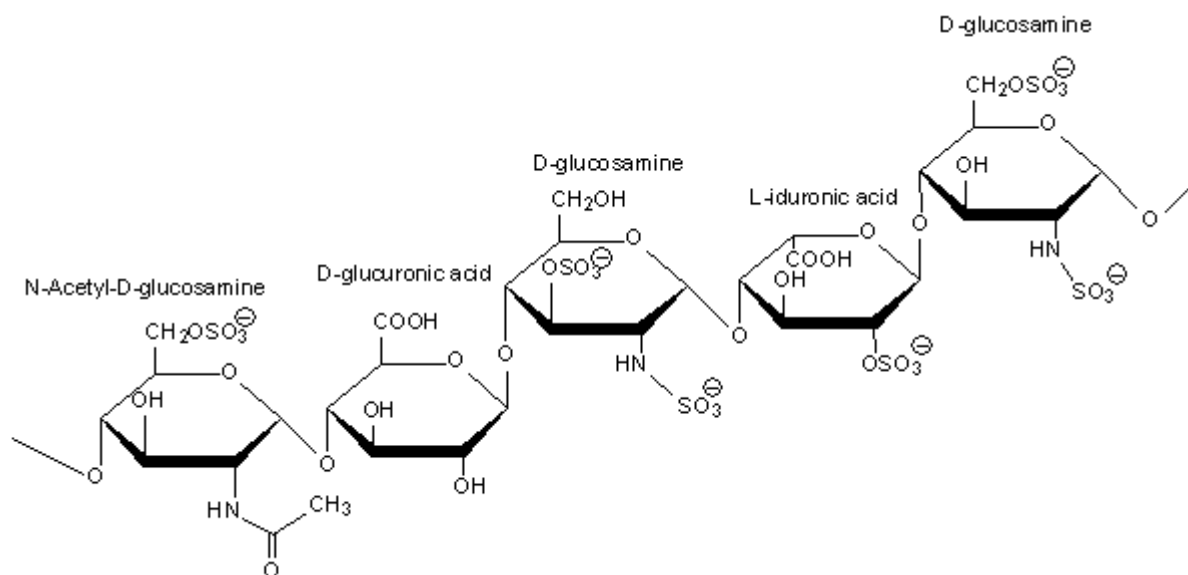


Figure 3. Structure of heparin with various labeled sugar units.

Direct Thrombin Inhibitor (DTI): Hirudin is a peptide-based natural inhibitor of thrombin obtained from the medicinal leech, *hiruda medicinalis*. It is a 65 amino acid long peptide (molecular weight 7000 Daltons), stabilized in three different structural forms by disulfide bridges.⁵² Unlike the heparins, it is a direct inhibitor of thrombin.⁵² It irreversibly inhibits thrombin by binding at two of its sites, thus it is classified as a bivalent DTI.⁵³ Hirudin has other advantages over the heparins by inhibiting both free and clot-bound thrombin.⁵⁴ Hirudin shows no interaction with plasma proteins and has predictable dose response.⁵⁵ Bivalirudin is dodecapeptide from the carboxy-terminal region of hirudin and bridged with an active site-

specific tetrapeptide (D-Phe-Pro-Arg-Pro) by four glycine residues (Figure 4). Like hirudin, it is also a divalent DTI, but only produces transient inhibition of thrombin due to its shorter half-life (Figure 4).⁵⁶ Currently, it is used as alternative to heparin for angioplasty and unstable angina.⁵⁷ On the other hand, hirudin and hirudin-based anticoagulants suffer from serious drawbacks leading to discontinuation of hirudin from clinical use. Hirudin has a strong dependence of the pharmacokinetics of renal function, resulting in difficulties in dosing for elderly patients. Increased risk of bleeding and lack of an antidote worsen the safety profile. In addition, its non-human source and polypeptide nature can lead to serious immune reactions. However, immunogenicity is reduced in bivalirudin and argatroban (a direct active site inhibitor of thrombin).⁵²

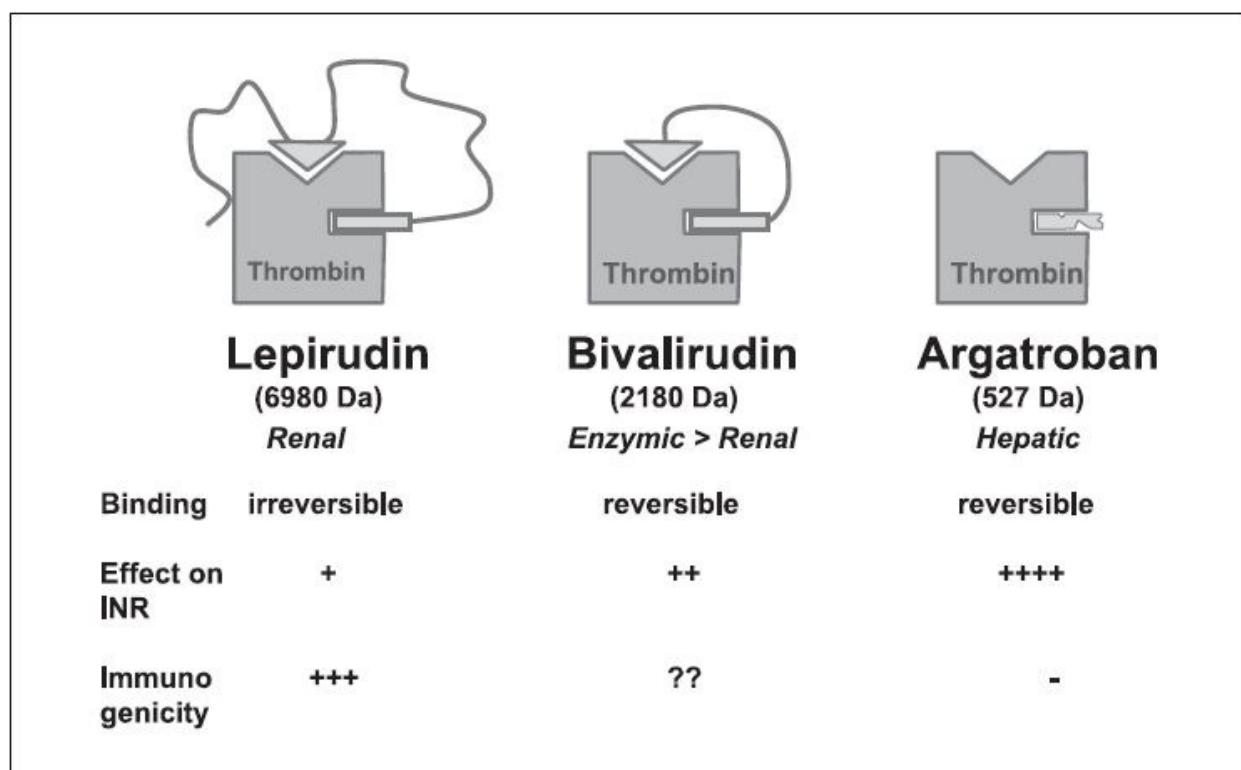


Figure 4. The mechanism of action of DTIs lepirudin, bivalirudin and argatroban. This figure is adapted from Greincher et al.⁵²

Active site inhibitors of thrombin: The design and development of active site inhibitors of thrombin is driven by three major factors: 1) the increasing incidence of immune response against heparin and its analogs, 2) their inhibition of only free thrombin and 3) the non-specific interaction of heparin with other plasma proteins.⁵⁸ Argatroban was the first univalent active site DTI (Figure 4). It is small synthetic molecule derived from L-Arginine and is a competitive and reversible inhibitor.⁵⁷ Melagatran and ximelagatran (prodrug of melagatran) are peptide-based active site DTIs, which significantly eliminated the need of regular laboratory monitoring of anticoagulation level. The clinical success of these inhibitors led the trail for discovery of various other active site DTIs, which are currently under clinical investigation.^{59, 60}

Aptamers: Aptamers are single stranded nucleotides that bind to molecular targets and inhibit their function by physically blocking their interaction with ligands and substrates. The aptamers specific for exosite II (a positively charged patch on the thrombin surface) were successfully designed and tested *in vitro* for competition with exosite II ligands.⁶¹ Toggle-25 is a selective exosite II aptamer that specifically competes with glycosaminoglycan (GAGs) for binding with thrombin. It helps the thrombin to escape inactivation by antithrombin, thus leading to a higher concentration of active thrombin in circulation. It is also known to interfere with binding to the platelets.⁶² HD22 is another aptamer for thrombin that specifically inhibits the activation of platelets by thrombin.⁶³ It is also possible to design aptamers that specifically inhibit the activation of factors VIII and V by thrombin, which could lead to blockage of the positive feedback loop.⁶⁴ Exosite II aptamers could also serve as potential antidotes for exosite II based allosteric inhibitors, such as UFH and LMWHs, to reduce the effect of drug overdose.

Selective indirect factor Xa inhibitors: Fondaparinux is the first known selective anticoagulant designed to inhibit a single protease. It is synthetically derived with a highly specific

pentasaccharide unit of heparin, as required for antithrombin activation. The anticoagulant effect is achieved by high-affinity binding and activation of antithrombin, which further selectively inhibits factor Xa. Fondaparinux accelerates by 300-fold inactivation of factor Xa by antithrombin.⁶⁵ It has a predictable ADME profile and better safety profile than its parent UFH. Owing to its synthetic source and homogeneous nature, there has been reduced incidence of immunogenicity and thrombocytopenia. Idraparinux is a hypermethylated pentasaccharide unit with a very long half-life for once-weekly dosage. It has a 30-fold higher binding affinity for antithrombin and similar clinical properties as fondaparinux.^{66, 67}

Direct factor Xa inhibitors: The successful design of argatroban opened new pathways for design of active site inhibitors of factor Xa. Razaxaban was developed by Bristol-Myers-Squibb as the first direct active site inhibitor of factor Xa to reach higher-stage clinical studies (Figure 5). Razaxaban studies were, however, discontinued due to the development of its congener Apixaban. Apixaban has a more favorable safety profile than Razaxaban and a better ADME profile. Rivaroxaban is another small molecule inhibitor targeting the active site of factor Xa developed by Bayer Health Care (Figure 5). It is currently used for prevention and treatment of thrombosis, marketed under the name of “Xarelto” in the United States. In addition, there are many more active site inhibitors of factor Xa currently under clinical trials.^{20, 68}

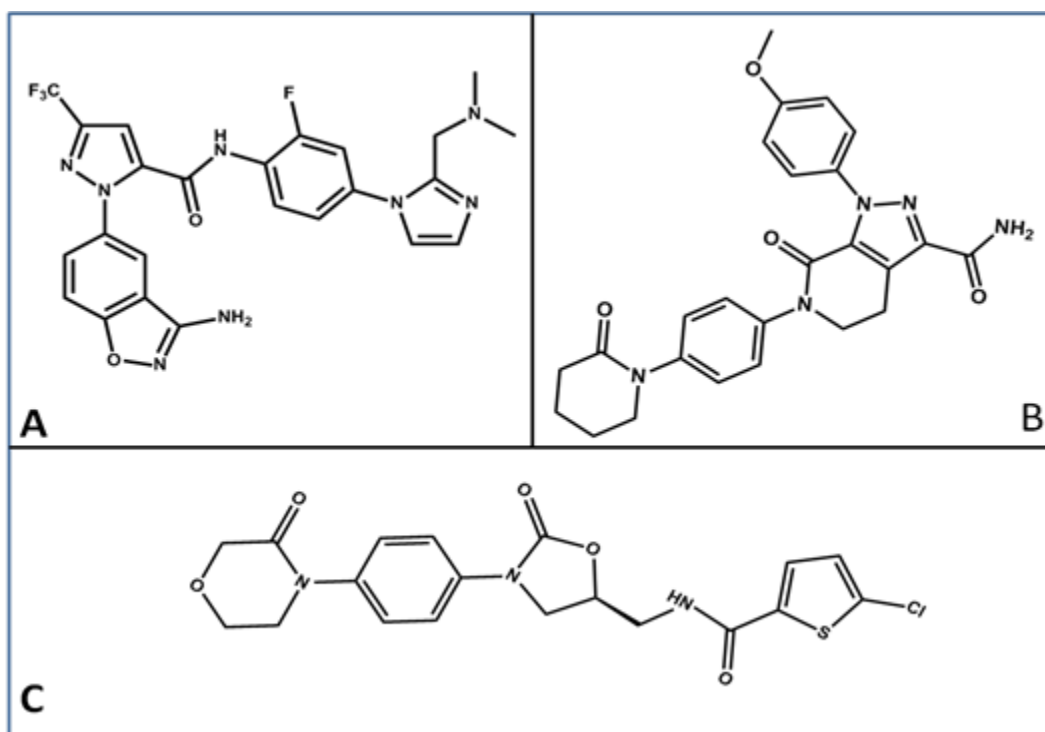


Figure 5. Structures of direct factor Xa inhibitors. A) razaxaban, B) apixaban and C) rivaroxaban.

Factors XIa and IXa active site inhibitors: The development of active site inhibitors targeting factors IXa and XIa is in the early stages. Initial results show promising advantages in terms of the role this class of inhibitors may play.⁶⁹

TF/Factor VIIa inhibitors: The TF/Factor VIIa complex plays an integral part in initiating the extrinsic pathway for blood coagulation. By activating factor XIa, it also initiates the intrinsic pathway.⁷⁰ The function of TF/FVIIa can be blocked by many different approaches: 1) designing antibodies to prevent the complex formation; 2) designing active site inhibitors of factor VIIa; 3) designing exosite inhibitors that prevent binding of TF with factor VIIa; and 4) synthesizing the recombinant protein of naturally occurring inhibitors of the TF/Factor VIIa complex.^{69, 71} The naturally occurring nematode anticoagulant proteins (NAPs) are known to inhibit formation of

the TF/Factor VIIa complex.⁷² The recombinant TFPI also inhibits the activation of factor Xa by the TF/factor VIIa complex.⁷³

1.5 Limitations of Current Therapy

Both heparin and warfarin have been used successfully in the clinics as primary anticoagulant therapy for more than 50 years. Being highly effective, they are associated with numerous side effects and safety issues that make regular blood monitoring obligatory. The interaction of heparin and warfarin with numerous targets leads to side effects, and hence new strategies are required to develop anticoagulants with high degrees of specificity for single targets.⁷⁴ Recently developed anticoagulants like direct thrombin and factor Xa inhibitors are relatively safe as compared to heparin and warfarin. The most important advantage of direct inhibitors is that they can inhibit both free and clot bound thrombin. Thrombin gets entrapped in the growing clot and is responsible for clot maturation. Inhibition of clot-bound proteases is an advantage of direct inhibitors over traditional anticoagulants. Clot-bound thrombin is inaccessible to heparin or other AT-dependent drugs.³⁹ However, the direct inhibitors suffer from side effects such as liver toxicity and lack of available antidotes. Other available anticoagulants such as hirudin, thrombin antibodies and natural products are not orally available and thus have short durations of action. Thus, they require frequent dosing and are associated with higher cost.⁷⁵

1.6 Thrombin: Its Structure and Role

Thrombin is derived from its inactive zymogen prothrombin which is a 70,000 Daltons glycoprotein synthesized in the liver. The inactive prothrombin is converted to its active thrombin form by the prothrombinase complex, consisting of factors Xa and Va, anionic phospholipids and Ca^{2+} .^{24, 76} Factor Xa cleaves prothrombin at Arg320 to generate the meizothrombin and subsequently cleaves meizothrombin to generate active thrombin. The activated thrombin has a very short half-life of few minutes due to its inactivation by antithrombin present in plasma. Thrombin is activated upon cleavage of the Arg15-Ile16 bond, generating a new *N*-terminus end. This new *N*-terminus end, containing Ile16-Val17 residues, inserts into the main body and forms a salt bridge with carboxylate group of residue Asp194. This inward rotation of the side chain causes the outward rotation of the preceding loop causing the opening of the specificity pocket known as “S1”.⁷⁷⁻⁷⁹

Thrombin consists of two polypeptide chains: a 36 amino acid light chain and a 259 residue heavy chain linked by a disulfide bridge. The heavy chain consists of all the functional epitopes of thrombin.^{80, 81} Thrombin molecules have a typical serine protease fold, containing two six-stranded β -barrels packed asymmetrically forming the catalytic triad of His57, Asp102 and Ser195. The 60-loop structures form the upper lid of the active site, restricting the access of solvent to His57 and Ser195. Asp102 anchors His57 in the correct orientation for proton transfer from Ser195. The orientation of the catalytic triad polarizes the side chain of Ser195 for nucleophilic attack on the carbonyl carbon in the scissile bond of the substrate molecules.^{23, 82} In the transition state, the carbon atom attains tetrahedral geometry, which is stabilized by hydrogen bonding between the charged oxygen atom of the scissile bond and the amide hydrogen of Gly193 and Ser195, forming the “oxyanion” hole. The substrate is acylated by the O^γ atom of

Ser195 by transferring the proton to His57 and by losing its *C*-terminal end (Figure 7). The water molecule catalyses the deacetylation process by releasing the carboxylic acid and the *N*-terminal end of the substrate. A particularly striking feature of the thrombin molecule is its uneven distribution of charge over its surface causing patches of both positive and negative charges.⁸³⁻⁸⁶

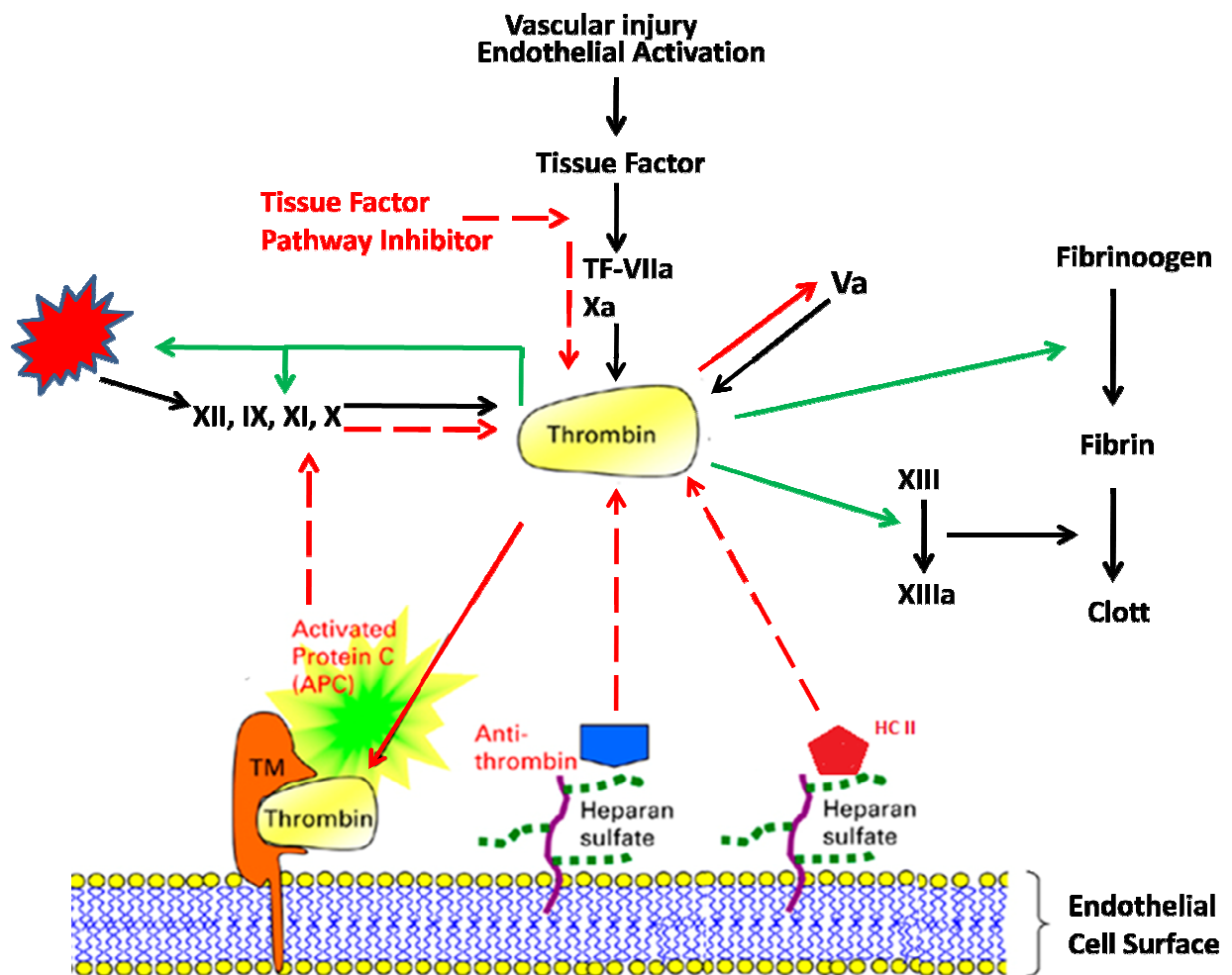


Figure 6. Thrombin plays a central role in blood coagulation regulating its own production by positive and negative feedback loops. Broken red arrows represent the inhibition of thrombin activity, red arrows represent the negative feedback regulation of thrombin to regulate its own production and green arrows represent the positive feedback regulation of thrombin to increase its production.

1.6.1 Active Site

The active site residues are located inside the narrow cleft formed between the two barrels. The active site is divided into various sub-pockets. To the left of the active site resides the S1 specificity site, a narrow deep pocket containing the acidic Asp189 at the bottom.⁸⁷ This pocket is guarded by uncompensated charge of Glu192 residue at the entrance, which plays a significant role in the specificity of thrombin in selecting substrates and inhibitors.⁸⁸ The apolar binding region on the top of the S1 pocket is further divided into two sub-pockets: S2 and S4. These are hydrophobic pockets and also contribute to the specificity of thrombin. The access of substrate and inhibitors to these pockets is limited by the “60-loop”. The S1’ pocket lies on the right side of the catalytic triad. It is limited in size and can only accommodate small polar residues. The natural substrate of thrombin holds the following criteria: medium to bulky hydrophobic P4 residue, proline at the P2 site, positively charged (especially Arg) at the S1 site, serine at P1’, a hydrophobic residue at P2’ and a basic residue at P3’.⁸⁹⁻⁹¹ There are exceptions for this scheme, but suboptimal substrates utilize additional binding sites on thrombin to compensate for the lost binding energy.⁸⁸

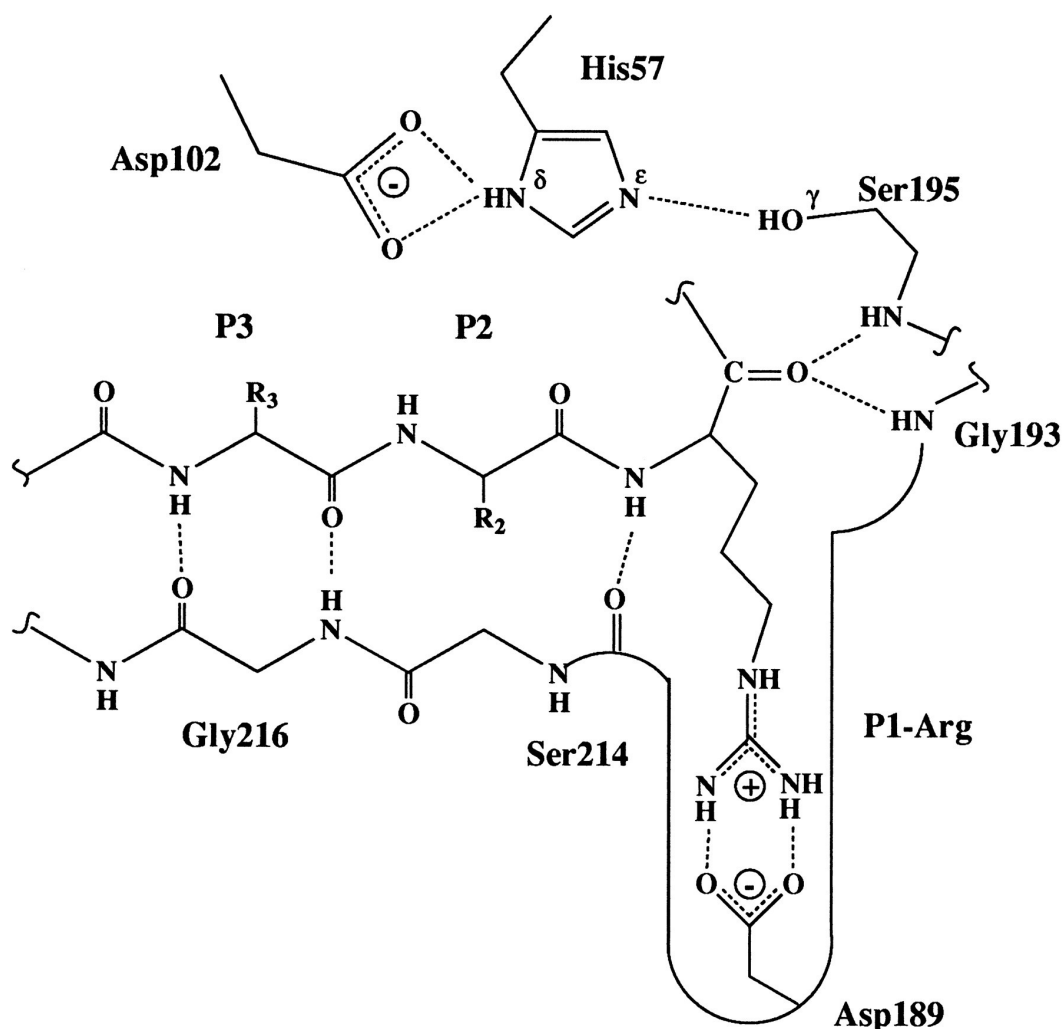


Figure 7. Chemical mechanism of catalysis for serine proteases.

1.6.2 Exosite I

Exosite I is a highly anionic notched surface depression located to the right side of the active site formed by the 70-80 loops. This region is similar to the calcium binding site of trypsin where the required Ca^{2+} is replaced by the insertion of the side chain of Lys70. In the center of the highly positive electrostatic potential formed by Arg63, Arg73, Arg75 and Arg77 lies the hydrophobic region formed by the side chains of Tyr76 and Ile82. Structural and functional data

suggest that exosite I is involved in the binding of thrombin with fibrinogen.^{92, 93} The α - and β -chain fragments of fibrinogen bind at exosite I to provide the additional binding energy required to overcome the suboptimal substrate residues at the cleavage site.^{94, 95} Thrombomodulin binds at exosite I and allosterically induces changes in the active site to reverse the role of thrombin from a procoagulant to potent anticoagulant.⁹⁶ The natural inhibitors, such as hirugen, rhodniin, ornithodorin and triabin, also induce allosteric changes in the catalytic triad.⁹⁷ The nature of interactions for these inhibitors with exosite I varies from ionic to hydrophobic in nature. Thrombin also utilizes exosite I residues to interact with the protease-activated receptor-1 (PAR1).⁹⁸ PAR1 is a thrombin receptor found on the surface of platelets that mediates the action of thrombin in activation of platelets. The specific thrombin inhibitors such as heparin cofactor-II and antithrombin-III utilize the exosite I to interact with thrombin in the blood. It is known that the binding on exosite I communicates changes to the catalytic site and is thus involved in allosteric modulation of thrombin.^{99, 100} The importance of exosite I is demonstrated by the fact that the β - and γ - forms of thrombin, which lack the region of exosite I fail to cleave fibrinogen but retain the catalytic activity at the active site.^{99, 101}

1.6.3 Exosite II

The extreme cluster of positive charge located to the left of the active site is called the anionic exosite II (also known as the heparin-binding site). This is formed primarily by Arg89, Arg98, Arg245, Lys248 and Lys252. Basic arginine residues surround the small hydrophobic Leu234 residue.^{92, 102, 103} Exosite II is known for its interaction with polyanionic ligands like heparin and other GAGs that are required for forming the ternary complex for inhibition of

thrombin by antithrombin. The binding at exosite II allosterically modulates the catalytic site of thrombin by disturbing the position of the Asp102 residue. In addition to its role in GAGs binding, exosite II is also involved in activation of factors V and VIII. The thrombin inhibitor haemadin derived from leech utilizes exosite II for binding with thrombin.^{94, 95}

1.6.4 Role of the Light Chain

The boomerang-like thrombin light-chain is formed in a multiple turn conformation. The light- and heavy-chains are linked mainly by salt bridges (Figure 8). However, the light-chain is devoid of any known epitope for substrate recognition.¹⁰⁴ Due to lack of any catalytic or regulatory function, the light-chain of thrombin has received very little attention and almost can be considered as an “appendage” of thrombin. Various studies have concluded that the bovine thrombin with an omitted light-chain retains most of its catalytic functions. On the contrary, phenotypes with mutations in residues of the light-chain are associated with moderate to severe bleeding. The best explanation for this discrepancy may be the involvement of the light-chain in the activation of prothrombin. The importance of the side light-chain is shown by the single mutation of Lys9, which not only affects the activation of thrombin, but also impairs the catalytic activity of thrombin for the chromogenic substrate, fibrinogen, PAR1 and protein C.¹⁰⁵ It is rich in acidic residues engaged in intra- and intercellular interactions. The major function of the light-chain is in its stabilization of the heavy-chain through various ionic interactions that neutralize the basic residues on the heavy-chain.^{106, 107}

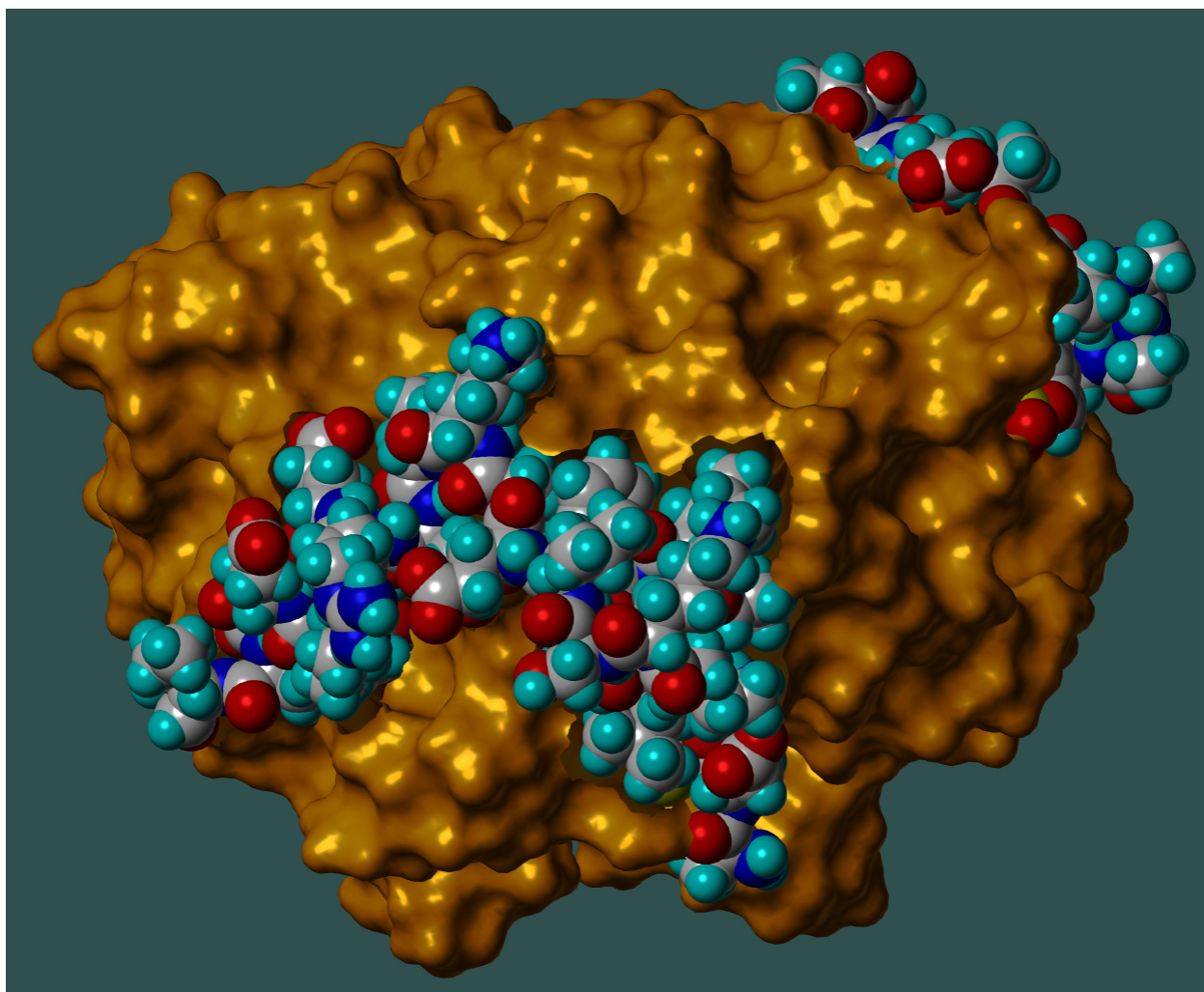


Figure 8. Graphical model of thrombin created by Sybyl8.1 showing the interaction of chain-A (shown in space filled model) with chain-B (shown as molcad surface).

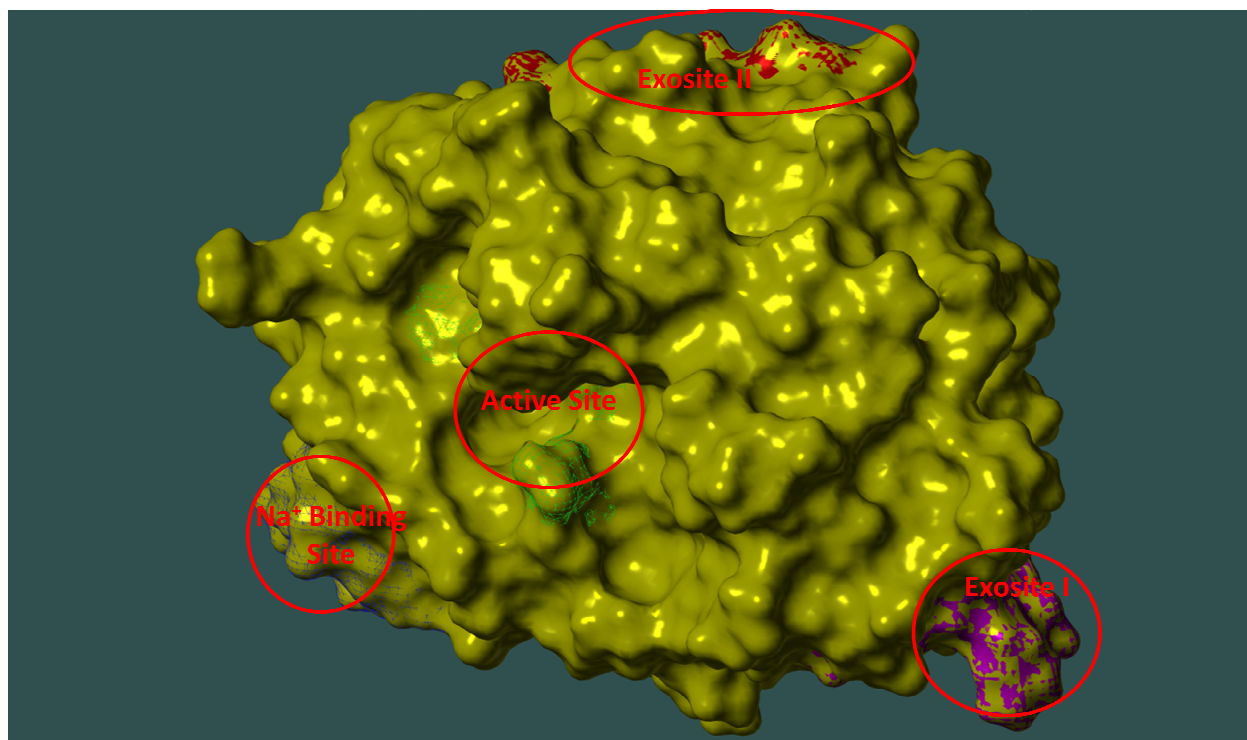


Figure 9. Graphical model of human thrombin generated by Sybyl8.1 shows the location of active site, sodium binding site, exosite I and II. The model is generated from crystal structure co-ordinates obtained PDB (ID: 3EQ0).

1.6.5 Sodium Binding Site

The sodium binding site is located in the center of the 220-loop, 15-20 Å away from the catalytic triad and 5 Å away from Asp189 in the S1 pocket.¹⁰⁸ This site is highly solvent exposed and communicates with the catalytic triad through a network of eleven water molecules. It is located in a cylindrical cavity formed by three antiparallel β -strands. Tyr225 is the most crucial residue controlling sodium binding in thrombin and is conserved in other serine proteases. The three ion pairs formed by Arg221a-Glu146, Lys224-Glu217 and Asp221 and Asp222 bidentate ion pair with Arg187 render stability to this site. The bound sodium ion is octahedrally coordinated by two backbone O atoms from Arg221a and Lys224 and four buried water molecules anchored by the side chains of Asp189 and Asp221 and the backbones of Gly223 and

Tyr184a. Asp189 anchors the orientation of one of the four water molecules ligating sodium ion and thus provides an important link between the sodium site and the P1 residue of the substrate (Figure 10).^{109, 110}

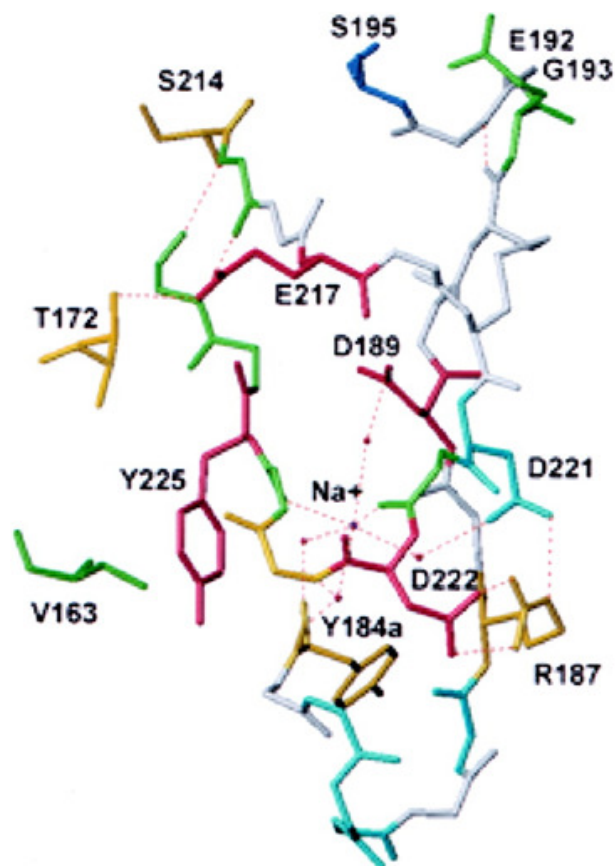


Figure 10. Model of the molecular environment of the Na^+ binding site of thrombin showing the residues of the allosteric core (purple). The bound Na^+ is shown in blue with its coordinating water molecules (purple balls). H-bonds are depicted as broken lines. The residues affecting the Na^+ affinity >3-fold (green) or <3-fold (cyan).¹¹¹

Thrombin displays a striking feature in its ability to get activated by interaction with sodium in a specific and allosteric manner.¹¹² Sodium binding converts thrombin from the low

activity slow state to the high activity fast state.²⁴ This also has a significant effect on thrombin's interaction with procoagulant (fibrinogen), prothrombotic (PAR) and anticoagulant (protein C) substrates.^{85, 113} The K_d of sodium binding is 110 mM at 37 °C and the physiological concentration of sodium is 140 mM.¹⁰⁹ The procoagulant and anticoagulant activities of thrombin correspond to the slow and fast forms, respectively. Hence, any factor that disturbs the sodium binding increases the anticoagulant effect of thrombin leading to prolonged clotting time and reduced platelet activation.⁷⁶

The structures of E (slow form) and E:Na (fast form) are very similar with limited structural changes being required to explain the complexity of the full range of allosteric transitions. The few major structural differences between from slow and fast forms are the favorable orientation of Asp189 in the specificity pocket, which explains the improvement in k_M and the position of Ser195, which explains the improvement in catalytic efficiency (K_{cat}). The most significant structural change is the long-range communication between the sodium binding site and the active site. In the fast form, the network of H-bonds in eleven water molecules allosterically communicate information from the sodium binding site, whereas in the slow form only seven water molecules form this network, thus significantly altering the connectivity.¹¹⁴

The perturbation of the primary specificity pocket is evident in the slow to fast transition of thrombin. In the fast form, orientation of Asp189 is optimal for interaction with the basic P1 residue of the substrate. In the slow form, the carboxylate group of Asp189 rotates 30° from its optimal position and this disturbs the interaction with the basic P1 residue of the substrate. The conformation of Glu192 changes in this transition from fast to slow form. In the slow form, the side chain of Glu192 moves away from active site region and thus minimizes the clash between the acidic residues of P3 and P3' of protein C. The orientation of Glu192 compensates the

deleterious changes in Asp189 and Ser195. This results in a conformation that retains the activity toward protein C, and explains the anticoagulant nature of the slow form of thrombin. The rotation of the hydrophilic side chain of catalytic Ser195 by 35° breaks the critical H-bond with the catalytic His57, which is crucial for catalysis (Figure 11).^{24, 76}

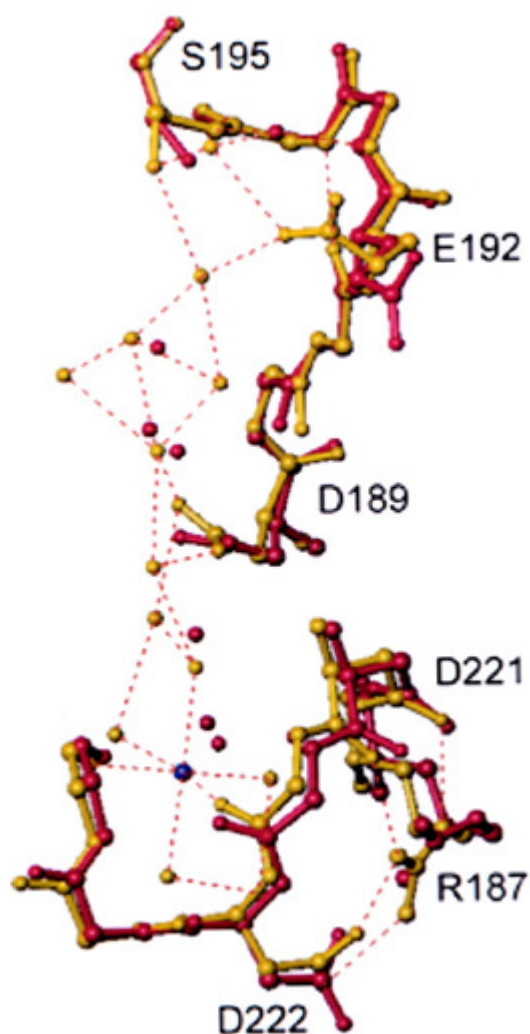


Figure 11. Model of the structural changes induced by the slow \rightarrow fast transition of thrombin depicted by the structures of F (free fast form, gold) and S (free slow form, red).¹¹¹

The physiological importance of sodium binding is demonstrated by bleeding phenotypes such as prothrombin Frankfurt,¹¹⁵ Salakta¹¹⁶ and Greenville.¹¹⁷ Mutations in these phenotypes significantly compromise sodium binding to thrombin. Conditions such as hypernatremia (high sodium conc.) and hyponatremia (low sodium conc.) are associated with thrombosis and bleeding, respectively.

1.6.7 Platelet Activation and Role of Thrombin

Human platelets circulate in the blood in dormant state and their premature activation is prevented by the presence of the endothelial monolayer, prostaglandin and nitric oxide, which limits the local accumulation of platelet agonists.¹¹⁸ Platelets start activating once these barriers are overcome in response to local trauma or rupture of the atherosclerotic plaque.⁸³ Thrombin plays an essential role in activating platelets to form the platelet plug, similar to the formation of the fibrin clot. When thrombin is added to human platelets *in vitro*, it causes the platelets to change shape, stick to each other, and secrete their content of stored granules.^{119, 120}

Thrombin displays many structurally distinct features that help it to interact specifically with different ligands, proteins, receptors and substrates to modulate the various procoagulant and anticoagulant functions responsible for maintaining the fine regulation of hemostasis.¹²¹ The procoagulant role of thrombin is mediated by cleavage of seven transmembrane thrombin receptors that, in turn, activate the platelets. Humans have two prototypes of protease-activated receptors (PAR): PAR1 and PAR4, of which PAR1 is thought to be more important.¹²⁰

PAR1 is characterized as a seven transmembrane domain G-protein-coupled receptor activated by specific cleavage of its *N*-terminal domain by thrombin. Thrombin cleaves at

Arg41-Ser42 exposing a new *N*-terminus that acts as a tethered ligand by binding to the intramolecular body of the receptor and leading to activation of platelets.⁹⁸ PAR1 has “tow” domains that interact with thrombin. Mutant studies showed that the receptors cleavage recognition site and hirudin-like acidic domain are critical for interaction of the receptor with thrombin. The hirudin-like acidic domain interacts with the anionic exosite I and is responsible for overcoming the unfavorable interaction at the cleavage recognition site.¹²² The hirudin-like domain of PAR1 has a similar proportion of acidic and hydrophobic residues to other exosite I ligands of thrombin such as fibrinogen, hirudin and thrombomodulin. Mutant studies showed that these residues are important for receptor activation and, thus, electrostatic and hydrophobic interactions play an important role in PAR1 activation by thrombin.^{123, 124} Synthetic ligands that mimic the newly exposed tethered ligand of PAR1 and PAR4 act as agonists for the receptor and hence can be used as pharmacological tools to study the role of these receptors in various cells.^{125, 126}

1.7 Therapeutic Uses of Thrombin

Since 1930, there has been extensive work on the use of thrombin as a topical agent for the treatment of surface bleeding.¹²⁷ While there is sparsely published literature on the use of thrombin as topical hemostatic agent, it is used extensively in surgery. Thrombin is frequently used as adjuvant therapy to stop the residual bleeding in cardiothoracic and cardiovascular surgery. Thrombin was also used for treatment of burns but now it has been replaced by epinephrine.¹²⁸

The extensive use of thrombin is supported by the minimal risk to system damage due to higher thrombin levels. The reason for such a low risk may be due to the low level of thrombin and its application to confined space. It is also known that thrombin is well contained within fibrin clots and that leaked thrombin is rapidly inactivated by antithrombin and other serpins in systemic circulation. This is further supported by the fact that most of the global parameters such as pro-thrombin time, thrombin time and partial thromboplastin time remain unchanged after topical use of thrombin.³⁴ Bovine thrombin had been extensively used as topical hemostatic agent for a number of years without any reported incidences of adverse effects.¹²⁹ In the last few years, some serious immunological adverse effects were reported, such as the development of antibodies to bovine thrombin or factor V.¹²⁹ Bovine thrombin is available as topical preparation is the most common source of thrombin for therapeutic use. Human thrombin is obtained by use of recombinant DNA technology for therapeutic use. It is available as a lyophilized powder, spray kit and as a syringe spray kit.

Production of native human thrombin is done in a multi-step process involving the separation of crude prothrombin from plasma using the alcohol fractionation process of Cohn.¹²⁹ Prothrombin is absorbed on an insoluble barium salt and subsequently eluted with sodium citrate. In an alternative method, prothrombin is absorbed on the anion-exchanger DEAE-agarose and subsequently eluted. The crude prothrombin is obtained as a mixture of factors VII, IX and X. Prothrombin is activated by adding crude tissue factor, which initiates the activation cascade leading to generation of thrombin. Activated thrombin is purified using a cation-exchange chromatography method.¹²⁹

1.8 Other Components of Coagulation System

1.8.1 Factors VII/VIIa

Factor VIIa along with the tissue factor (TF) initiates the extrinsic pathway upon injury to the vascular wall. The TF/Factor VIIa complex activates factor X to initiate the clotting process.¹³⁰ In addition, this complex also activates factor IX and initiates the intrinsic pathway.¹³¹ The majority of factor VII is present in inactive zymogen, along with traces of the activated form.¹³² Factor VIIa consists of two chains: the heavy chain and the light chain covalently linked by disulfide bridges. The light chain of factor VIIa contains the 10 γ -carboxyglutamic acids residues and two growth factor homology domains, whereas the heavy chain contains the catalytic region.¹³³ The activation of factor VII is also catalyzed by factors XIIa,¹³⁴ IXa, Xa¹³⁵ and thrombin¹³⁶ suggesting the importance of its production in physiology.

Factor VII is activated upon the cleavage of the peptide bond between Arg15 and Ile16, thus generating new *N*-terminal residue Ile16.¹³⁷ After cleavage, Ile16 buries its side chain in a hydrophobic region and forms a salt bridge between its α -amino nitrogen atom and Asp194. The formation of this salt bridge orients the neighboring Ser195 residue of the catalytic triad optimally for proteolytic cleavage. Along with Ser195, three adjacent loops undergo conformational changes to construct the substrate-binding region. Beside cleavage by proteases, activation of factor VII also requires the binding of the TF. The function of TF is partly to protect the chemical modification of the α -amino nitrogen atom of Ile16.¹³⁸ Thus, factor VII exists in equilibrium between its partially and fully active forms. TF binds specifically to the active form of factor VIIa.¹³⁸ TF is expressed in the vascular smooth muscle cells, pericytes and fibroblasts in vessel walls. The binding of factor VII to TF is mediated by calcium ion at the Gla-

containing region. Factor VIIa has three allosteric sites: the TF binding region, the active site binding region and the macromolecular binding exosite.¹³⁹ The binding of TF allosterically enhances both proteolytic and amidolytic activities of factor VIIa.¹⁴⁰

1.8.2 Factors IX/IXa

Factor IX, with a molecular weight of 54,000 Daltons, is a vitamin-K dependent single chain glycoprotein of 415 amino acid residues. Factor IX consists of a Gla-containing region and two epidermal growth factor-like regions. The Gla-region consists of 12 γ -carboxy glutamyl residues and functions as a calcium binding region. It also serves as a site for interaction with phospholipid monolayers.¹⁴¹ Gla is formed by the post-translational modification of a glutamic residue by enzyme γ -glutamyl carboxylase.¹⁴² The two epidermal growth factor-like domains serve as binding sites with various cell receptors.¹⁴³ Factor IX is activated by factor XIa in the presence of calcium ion that, upon activation, binds to the surface of endothelial cells.¹⁴⁴ This is the first calcium dependent reaction in the intrinsic pathway. Activation of factor IX does not require the presence of phospholipids. Factor IX can also be activated by the factor VIIa-TF complex.¹³¹ This reaction bridges the intrinsic and extrinsic pathways. Factor IX is activated upon cleavage at two sites: Arg145-Ala146 and Arg180-Val181. There is no cofactor required for activation of factor IX.¹⁴⁵ The cleavage at these sites generates two polypeptide chains: the light and heavy chains, which are linked covalently by a disulfide bridge. The carboxy-terminal heavy chain contains the catalytic triad formed by Ser365, His221 and Asp269. The structures of both metal-bound and metal-free factor IX have been solved by NMR spectroscopy. The structure of the metal-free form is slightly disordered, whereas the calcium ion bound form is well ordered, containing all the domains.

The vascular surface provides the site for achieving high local concentration of factor IXa to activate the factor X. Factor IXa along with calcium and modified factor VIII activate factor X.¹⁴⁶ Patients deficient in factor IX suffer from the bleeding disorder hemophilia B. Recombinant factor IX is widely used worldwide for treatment of hemophilia A and B.¹⁴⁶

1.8.3 Factors XI/XIa

Factor XI is 160,000 Daltons dimeric protein of two identical 607 amino acid chains containing subunits linked by a disulfide bond.¹⁴⁷ It consists of four apple-like domains and a C-terminal trypsin-like catalytic domain.¹⁴⁸ It circulates in blood complexed of with high molecular weight kininogen.¹⁴⁹ Blood also contains a monomeric homolog of factor XI, prekallikrein. Factor XI zymogen is activated in the blood to form factor XIa and the process is mediated by activators such as thrombin, factor XIIa and XIa (auto activation), by cleaving the Arg369-Ile370 bond.¹⁵⁰ Thrombin activates factor XI in the presence of charged surfaces such as dextran sulfate or heparin.¹⁵¹ The exosite I of thrombin interact with the A1 domain of factor XI, with residues like Glu66, Lys83, and Gln84. These residues are located in close proximity to the activation loop that contains the Arg369-Ile370 cleavage site.¹⁵²

It was postulated earlier that factor XI was involved in fibrin generation,¹⁵² but later it was observed that the patients with factor XII deficiency do not have an excessive bleeding tendency. Thus, there are alternative pathways that can activate factor XI. Recently, factor XIa has been considered as a part of the positive feedback loop to sustain the process of thrombin generation.¹⁵² Activated factor XIa is regulated in blood by plasma serpins such as antithrombin, the C1-inhibitor, protease nexin 1, and protein Z-dependent protease inhibitors.¹⁴⁸ Heparin

enhances the serpin-mediated inactivation by binding on the A3 domain and the catalytic domain through a template mechanism.¹⁵³

The four apple-like domains (A1-A4) of factor XIa are similar to those of other vitamin-K dependent proteases. Each apple domain is comprised of 7 β -strands that fold into curved antiparallel sheets that frame into an α -helix.¹⁵⁴ Two disulfide bonds lock the helix onto the central β 4 and β 5 strands, and the third one connects the *N*- and *C*-terminals. The two loops, β 4- β 5 and β 5- β 6 generate a small pocket on the other side of the α -helix.¹⁵⁵ The dimeric units are attached to each other through the A4 domain, with an interface area of 886 Å.¹⁵⁴ The β -sheets of the two units pack against each other, and Cys321 forms an interchain disulfide bond.¹⁵⁶

1.8.4 Factors XII/XIIa

Factor XII is a glycoprotein with a single polypeptide chain composed of 596 amino acid residues, with a molecular weight ranging from 76,000 to 80,000 Daltons.¹⁵⁷ It is also called the “Hageman” factor. Inactive zymogen factor XII is activated in the presence of negatively charged surfaces by kallikrein, factor XIa and plasmin. Factor XII auto-activates in presence of negatively charged surfaces such as glass, kaolin, ellagic acid, sulfatide micelle, polyethylene, silicon rubber, cartilage, skin, fatty acids, endotoxins, heparins, phospholipids and many more.¹⁵⁸ The fact that factor XII can be auto-activated in the presence of negatively charged surfaces makes it medically important for clinical plasma assays (activated partial thromboplastin time) to well predict the bleeding risk.¹⁵⁹ Activation, either by auto-activation or plasma kallikrein, results in formation of a heavy chain (MW 52,000) and a light chain (MW 28,000) that are covalently linked by a disulfide bridge. The light chain contains the catalytic triad formed by

Ser544, His393 and Asp442, which are responsible for the proteolytic function of the enzyme. After the initial cleavage, a second slower cleavage occurs at the heavy chain thus retaining the activity of the enzyme and resulting in two forms of activated factor XII enzymes in the blood circulation.¹⁶⁰

Once activated, factor XIIa activates factor XI, which is associated with the high molecular weight kininogen and prekallikrein. Beside this, factor XIIa is also involved in the activation of C1 of the complement system, activation of factor VII and down regulation of monocyte receptors of IgG.¹⁶¹ The activity of factor XIIa is inhibited in the blood by a plasma protease inhibitor and the C1 inhibitor. The presence of activating surfaces such as kaolin, dextran sulfate and sulfatides can protect the deactivation of factor XIIa.¹⁶² It has been shown that the presence of factor XII influences the size of thrombus growth and thus makes it an important pharmacological target.¹⁶³ Besides its involvement in blood coagulation, factor XII is also known to play a role as a growth factor. It is important for tissue repair after thrombosis or inflammation.¹⁶⁴

1.8.5 Thrombomodulin and Protein-C

Thrombomodulin (TM) is a glycosylated type-I transmembrane protein of 75 Daltons with no intrinsic enzymatic activity.¹⁶⁵ TM is present in endothelial cells and in capillary rich endothelial cell surfaces.¹⁶⁶ The presence of multiple disulfide bonds ensures TM stability under extreme pH conditions. The mature TM contains six epidermal growth factor (EGF) like-domains.¹⁶⁷ Domains 4, 5 and 6 are involved in thrombin binding and protein C activation (Figure 12).¹⁶⁸ In addition, these domains are also responsible for signaling posttranslational

modifications. Thrombin forms a 1:1 complex with TM with a K_d of 0.5 nM. This complex activates protein C with a K_M of 0.5 μ M on the endothelial cell surface.¹⁶⁵ Almost all of the thrombin is removed from circulation, as it passes through the vascular bed, by a high concentration of TM, leading to inactivation of thrombin by converting its procoagulant role to anticoagulant. Thrombomodulin is regulated by internalization of the molecule with a concomitant loss of capability for activating protein C.^{169, 170}

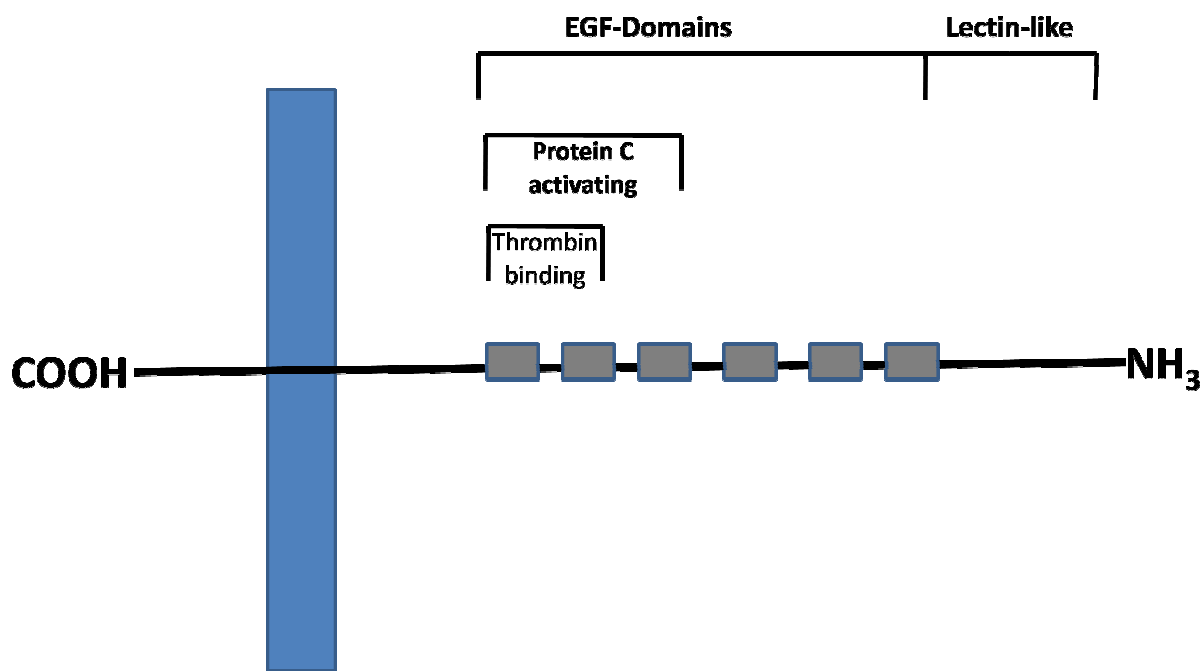


Figure 12. Structure of thrombomodulin showing the domains involved in thrombin binding and protein C activation.

Protein C is a vitamin K-dependent serine protease that upon activation down-regulates the clotting cascade. Protein C is activated by the thrombin-thrombomodulin complex by cleaving a 12 residue peptide in the activation loop.^{171, 172} *In vivo*, activation of protein C by thrombin occurs on endothelial cell surfaces in the presence of the cofactor thrombomodulin and a calcium ion.¹⁷³ Thrombomodulin accelerates the activity of thrombin toward protein C by

1000-fold in the presence of calcium ion.⁷⁸ The presence of endothelial protein C receptor (EPCR) further enhances the reaction by another 10-fold.¹⁷⁴ Protein C can also be activated by factor Xa and plasmin.¹⁷⁵ Activated protein C (APC) circulates in the blood as a light and heavy chain molecule covalently linked by a single disulfide bond.¹⁷⁶ The *N*-terminal light chain of APC contains the non-catalytic Gla domain and two epidermal growth factor domains. The Gla domain mediates calcium dependent interaction with protein S on its negatively charged surface.¹⁷⁷ Protein S is a vitamin K-dependent plasma cofactor of protein C that amplifies the anticoagulant function of protein C. The *C*-terminal heavy chain contains the catalytic site. APC is inactivated in the blood circulation by α_1 -antitrypsin, α_2 -antiplasmin and α_2 -macroglobulin.¹⁷⁸ The APC anticoagulant pathway is also regulated by protein S activity and inhibition of the thrombin-TM complex by antithrombin.^{172,177}

Upon binding to TM, thrombin switches its function from procoagulant to anticoagulant by increasing its specificity to cleave protein C to form APC (Figure 13). The binding of TM induces allosteric changes in the active site of thrombin to alleviate the activating function towards the procoagulant proteases, fibrinogen, PAR-1, and cofactors V and VIII.¹⁷³ Besides activating protein C, TM-thrombin complex also activates the thrombin activatable fibrinolysis inhibitor (TAFI).¹⁷⁹ Hirudin competes with TM for binding with thrombin and thus inhibits the activation of protein C. Thrombin bound to TM is inhibited more rapidly by antithrombin and protein C inhibitor, with a half-life of approximately 2 seconds.¹⁸⁰

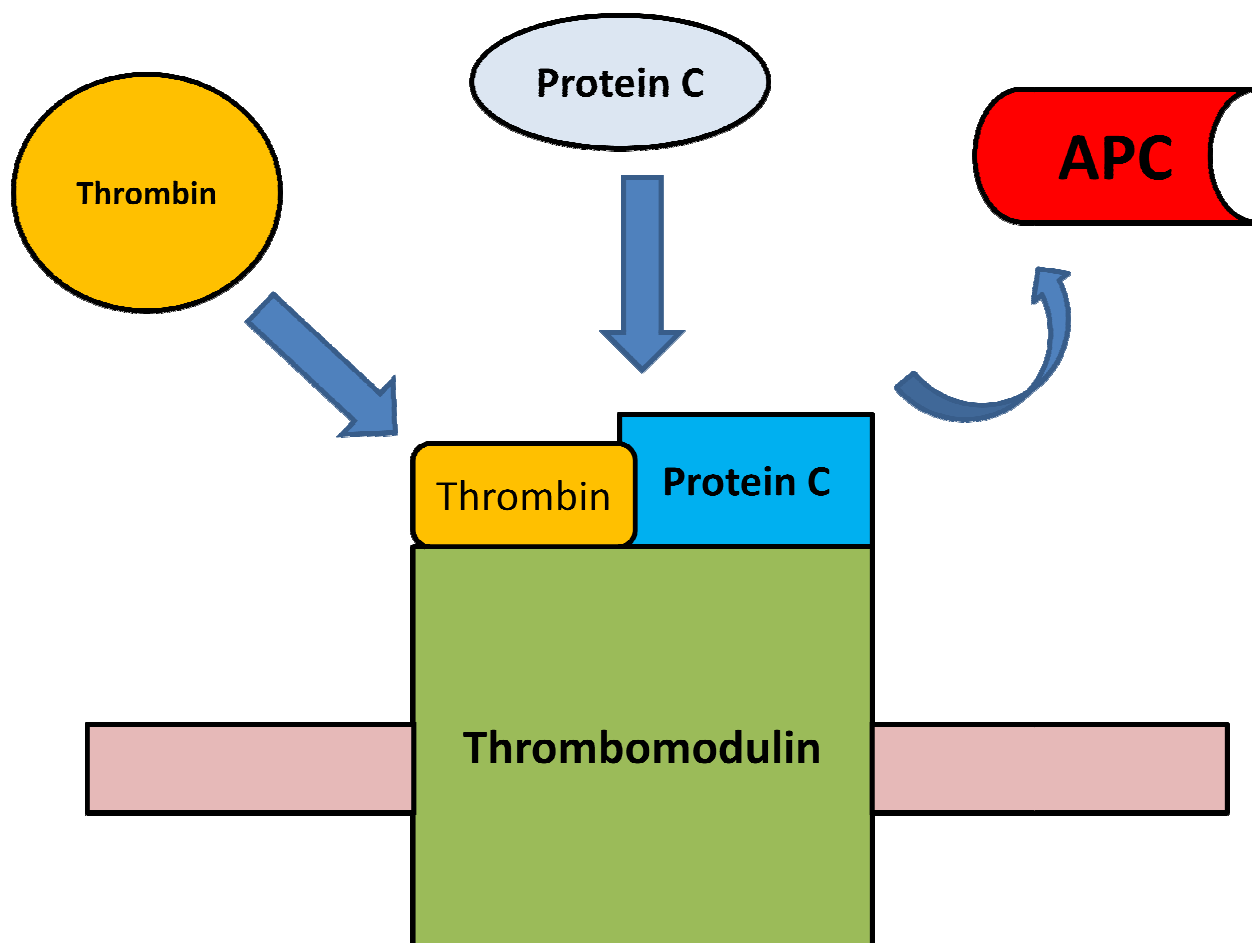


Figure 13. Graphical model of interaction of thrombin-thrombomodulin complex and activation of protein C.

Upon activation, APC dissociates from the thrombin-TM-EPCR complex and binds to protein S.¹⁸¹ Protein S has strong affinity for the surfaces of the negatively charged phospholipids. The APC, in complex with protein S, interacts with phospholipids or with the platelet-bound activated factors Va and VIIIa.¹⁸² APC mediates the anticoagulant function by proteolytically degrading the procoagulant cofactors factors Va and VIIIa, which are essential for activation of thrombin by factor Xa in both the extrinsic and intrinsic pathways.^{172, 183} The inactivation of these cofactors down-regulates the production of thrombin. The inactivation of factor Va by APC requires cleavages at Arg306 and Arg506 in sequential kinetic order, with

initial rapid cleavage at Arg506 followed by slower cleavage at Arg306. The inactivation of factor Va is accelerated by the presence of protein S.¹⁸⁴ In the case of factor VIIIa, APC cleaves the cofactor at Arg336 and Arg562. Cleavage at either of these sites leads to complete inactivation of factors VIIIa, Va and VIIIa, in complex with factors Xa and IXa, are resistant to inactivation by APC, but the presence of protein S inactivates the bound form of factor Va and VIIIa.^{185,186} APC can also inactivate the native forms of factors V and VIII and prevent their participation in the coagulation reaction. APC has a long half-life of 10 minutes in the blood circulation, favoring the enzyme remaining in circulation for localization and degradation of cofactors.¹⁸⁷

The regulation of the TM level is clinically significant, as high levels lead to bleeding, whereas low levels lead to thrombosis. The qualitative and quantitative deficiencies of protein C and protein S and defective APC lead to significant risk of venous thromboembolism and myocardial infarction.¹⁸⁷ APC also exhibits cytoprotective, anti-inflammatory and profibrinolytic properties.^{188, 189}

1.9 Thrombin Engineering

Thrombin has two important but functionally opposite roles in the blood coagulation system. The procoagulant role is initiated by conversion of fibrinogen into an insoluble fibrin clot, followed by activation of platelets to platelet plugs and initiate wound repair.¹⁹⁰ This action is amplified by the activation of factor XIII that stabilizes the fibrin clot, activation of TAFI to inhibit fibrinolysis and activation of factors V, VIII and XI in a positive feedback loop to increase its own production. In its anticoagulant role, thrombin activates protein C upon binding

with TM. This action is amplified in the presence of endothelial cell receptors.⁷⁶ Binding with TM initiates allosteric changes in the active site of thrombin leading to an enhanced specificity for protein C over fibrinogen and PAR1. Activated protein C inactivates the factors Va and VIIIa in a negative feedback loop to decrease the thrombin generation (Figure 14). The role of thrombin is further complicated by the allosteric effect of occupancy of sodium ions at the sodium binding site. Sodium binding converts thrombin from the slow anticoagulant form to its fast procoagulant form. Sodium binding is required for cleavage of fibrinogen, activation of factors V, VIII and XI, and activation of PAR1.¹⁹¹ Sodium binding is the major force driving the procoagulant role of thrombin. A sodium-free state converts thrombin into a slow form to produce an anticoagulant role, by activation of protein C and reduction of the platelet activation. Under physiological conditions, the balance between the procoagulant and anticoagulant roles of thrombin is optimal. Any effect that destabilizes the sodium-binding site converts thrombin into a potent anticoagulant. Several naturally occurring mutants of thrombin and physiological conditions that disturb the sodium binding equilibrium are associated with severe bleeding. There are some examples where multifunctional roles of thrombin were dissociated into procoagulant and anticoagulant activities.¹⁰⁶

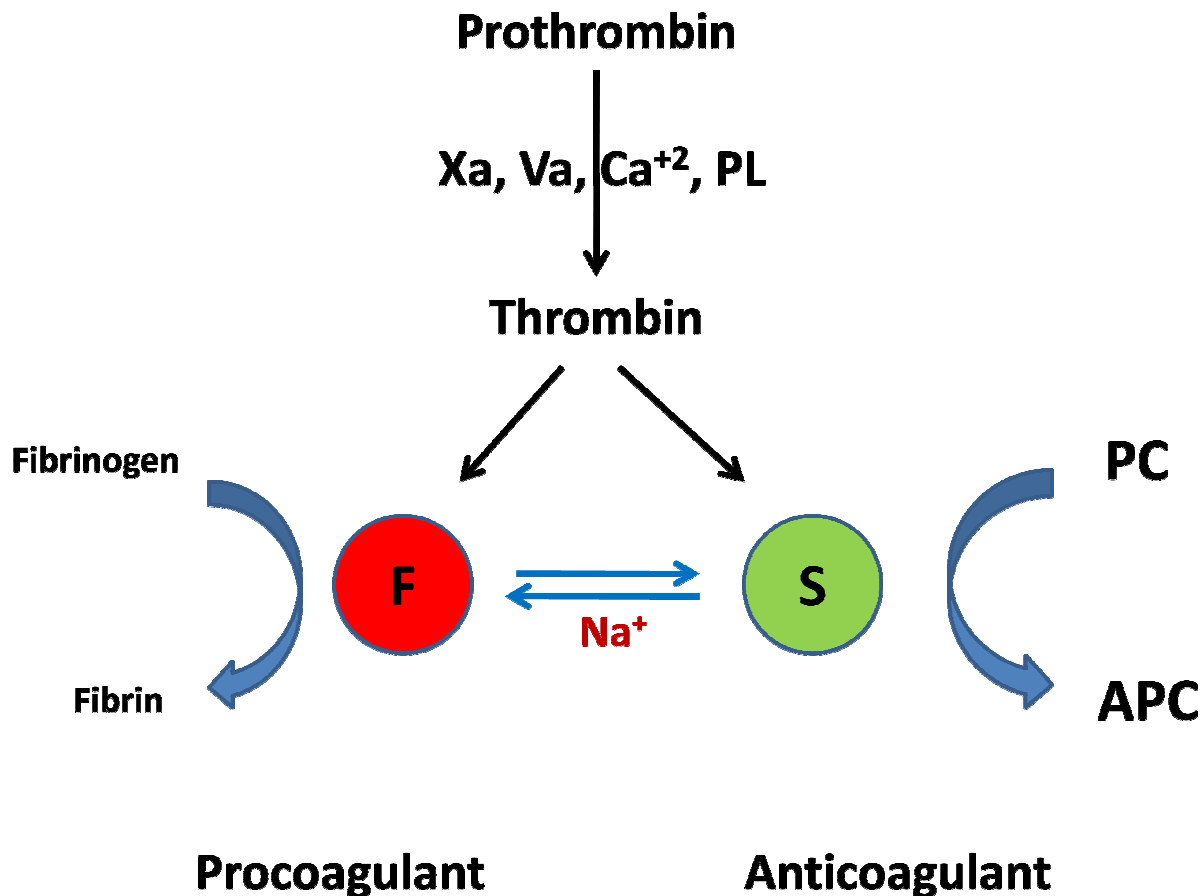


Figure 14. Schematic model of regulation of thrombin function by binding of sodium ion. “F” represents the fast form of sodium with procoagulant function and “S” represents the slow form of thrombin with anticoagulant function.⁸⁵

Mutation of the Arg75 residue to Glu in exosite I of thrombin retains fibrinogen clotting activity but has only 7% protein C activity in the presence of TM. The mutation of Lys60 to Phe leads to a 2-fold increase in activity for protein C but only retains 17% of the original activity for fibrinogen. The most pronounced anticoagulant effect is seen in mutation of Glu217 to Ala or Lys, both of which completely abolishes the procoagulant activity of thrombin. The dissociation of the thrombin functions in these mutations provides an important pharmacological tool to regulate the activity of thrombin and for designing novel methods for treatment of various clotting and bleeding disorders. The residues important for fibrinogen binding to thrombin are

spread over the region of the exosite I, the 60-loop, the sodium binding site, and the active site. In the case of protein C, the surface recognition is limited to the primary specificity pocket and portions of the 60-loop. Thus, it is easy to identify the residues that are significant for fibrinogen binding and to construct mutants with enhanced anticoagulant activity. A thrombin mutant with lower proteolytic cleavage activity for fibrinogen but retaining activity for protein C can act as an anticoagulant by generating APC in blood circulation. In one of the studies by Cera *et al.*,¹⁹² the double mutant W215A/E217A (WE) was found to be a safe and potent anticoagulant in a baboon model. At the dose of 0.011 mg/kg, it reduced the platelet thrombus accumulation by 80%. Subjects treated with WE showed no signs of hemorrhage or organ failure. There was no procoagulant activity observed in plasma until the end of one week. At high doses, it exhausted the cofactors for protein C activation before consuming the substrate reserve and the effect of overdose is thus down regulated rapidly. Protein C activation by WE appeared to be safe when compared with other methods of anticoagulation.¹⁹² In another study by Cera *et al.*, the double mutant R221aA/K224A completely abolished the sodium affinity by retaining the discrimination among monovalent cations. The disturbance of two ions pairs formed by these residues elicited drastic changes in structure such that fibrinogen specificity is completely lost but the specificity for protein C is retained, making the thrombin act as an anticoagulant.¹¹³

Chapter 2 Hypothesis

2.1 The Era of Small Molecule Inhibitors of Thrombin

Thrombin is an attractive target for designing anticoagulants owing to its most central role in the coagulation cascade. “Direct” and “indirect” are the two most important approaches used to target the inhibition of thrombin.⁶⁹ Heparin, an indirect inhibitor of thrombin, mediates its action through activation of antithrombin. Direct inhibitors mediate their action by binding directly to the active site of thrombin.¹⁹³ Hirudin was the first direct inhibitor of thrombin reported in literature. Hirudin is the most potent inhibitor of thrombin, making it an essentially irreversible inhibitor.⁵² Based on the hirudin structure, ximelagatran was the first orally available direct thrombin inhibitor (DTI).⁷⁵ Later, hundreds of small molecules were identified as active site inhibitors of thrombin and factor Xa. Recently, a number of selective inhibitors of thrombin and factor Xa have been identified by exploring the specificity site in the active site region.¹⁹⁴ DTIs have certain advantages over indirect inhibitors. They have the potential to inhibit the fibrin-bound thrombin whereas heparin fails to inhibit it. Secondly, small molecule inhibitors do not elicit thrombocytopenia.¹⁹⁵ Also, the direct inhibitors demonstrate a predictable dose response, which translates into a reduced requirement for regular laboratory monitoring. They

also demonstrate both larger therapeutic windows and rapid onset of action, yet they suffer from certain disadvantages such as higher cost, patient compliance, hepatotoxicity and the need for regular dosage adjustment.⁴⁴

2.2 Inhibition of Thrombin Through Exosites

Thrombin can also be targeted by the action of inhibitors at its two exosites.¹⁹⁶ These exosites can be used for designing allosteric inhibitors of thrombin. Besides acting as functional epitopes for defining high specificity binding, the exosites can also allosterically modulate the proteolytic activity of thrombin. It is known that thrombin has excellent communication between its exosites and active site.⁷⁶ The long range communication of the sodium binding site with the active site through a network of eleven water molecules is the best known example of thrombin's allosteric modulation.¹⁰⁹ The binding of thrombomodulin to exosite I of thrombin distorts the active site in such a way that it changes the specificity from a procoagulant role to an anticoagulant role. This proves that a communication pathway between exosite I and the catalytic site.¹⁶⁸ Sucrose octasulfate (SOS), which is considered to be a surrogate for heparin, binds at exosite II. It is found that SOS weakly inhibits thrombin activity by an allosteric mechanism mediated by binding to exosite II. Low molecular weight lignins (LMWLs) previously synthesized in our group were found to be potent allosteric inhibitors of thrombin. This set of examples encourages a new pathway for designing the inhibitors that mediate the allosteric inhibition of thrombin by binding to one of the exosites.

2.3 Advantages of Allosteric Over Direct Inhibitors

The major disadvantage of DTIs is that they can completely inhibit the catalytic activity of thrombin. Besides inhibiting its procoagulant role, these inhibitors will also block the anticoagulant function of thrombin by inhibiting activation of protein C. This can lead to rebound hyper-coagulability.⁹⁶ The active site DTIs are also known to have an antiplatelet effect through reduced platelets activation. Furthermore, the clinical data on the longer use of DTIs suggests a higher risk of fatal hepatotoxicity and other side effects. However, these effects are asymptomatic and reversible on discontinuation of therapy. Severe hepatotoxicity led to disapproval of ximelagatran by FDA followed by its withdrawal from the European market.¹⁹⁷ Moreover, a suitable monitoring method for anticoagulant therapy using DTIs has not been well established. The activated partial-thromboplastin time (APTT) assay suffers from poor linearity and reproducibility. Recombinant hirudin and its analogs can be monitored with activated partial-thromboplastin.⁴⁴ Finally, the lack of an available antidote for reversing the effect of overdosed active site directed DTIs further increases the risk associated with this therapy. The requirement for an antidote is of extreme necessity in high bleeding risk patients.¹⁹⁸

Beside these limitations, DTIs are also not optimal therapy for most of the thrombotic disorders. None of the DTIs have shown better efficacy and safety profile than LMWHs for long-term treatment of acute coronary syndrome. DTIs are also less effective than LMWHs for treatment of thromboprophylaxis after orthopedic surgery. Altogether, lower efficiency, poor safety profile, hepatotoxicity and the lack of an antidote drives research toward the path of allosterically inhibiting the thrombin for anticoagulant therapy.¹⁹⁹

It is easy to attain selectivity for a single protease in allosteric design of inhibitors. The active sites are mostly conserved in proteases in the coagulation cascade, thus making it difficult

for selective inhibition. Selectivity for a single protease will be translated into lesser side effects and lower risk of excessive bleeding. The partial inhibition of thrombin to maintain the balance between anticoagulation and coagulation can be easily achieved by allosteric inhibitors. One of the major advantages of allosteric inhibitors is the relatively easy design of antidotes for reversal of the effects of accidental over-dosing.

2.4 Rationale for Design of Benzofuran scaffold

To design functional mimics of heparin that are orally available and safe, our laboratory previously designed sulfated LMWLs, which are synthetic versions of naturally occurring lignins.^{200, 201} The synthesis involved enzymatic oxidative coupling of commercially available 4-hydroxycinnamic acids, caffeic acid, sinapic acid and ferulic acid using horseradish peroxidase. The oligomeric intermediates were sulfated to give three sulfated LMWLs, named CDSO₃, SDSO₃ and FDSO₃, having interesting anticoagulant profiles and modes of action.²⁰²

Sulfated LMWLs are oligomeric and polyanionic in nature. Similar to heparin, they are polydisperse and heterogeneous in nature. Beside these similarities with heparin, the mechanism of inhibition of thrombin is significantly different from heparin.²⁰² This is owing to the nature of scaffold being less anionic and more hydrophobic as compared to heparin. The saccharide scaffold chain in heparin is replaced by an aromatic scaffold chain in sulfated LMWLs.

chain lengths and patterns of sulfation. The presence of multiple chiral centers further adds to the heterogeneity of the mixture. A simple calculation gives 262,144 distinct structures in the decamer-length unit.^{200, 203} The average molecular weight of CDSO3 (the most interesting LMWL) was found to be 3320, with a range of chain lengths between 5 and 13 monomeric units. CDSO3 contains an average of 0.4 sulfate groups/unit as compare to 0.7 sulfate groups/unit on heparin.²⁰⁰ The substrate hydrolysis assay of CDSO3 for thrombin in the presence and absence of antithrombin suggested that CDSO3 inhibits thrombin by the direct mechanism.²⁰² Unlike heparin, CDSO3 does not require the presence of antithrombin to inhibit the activity of thrombin.²⁰² Based on these studies, it was found that CDSO3 is a potent direct inhibitor of thrombin. In a Michaelis-Menten kinetics analysis, it was found that the K_M of substrate hydrolysis by thrombin was not affected by the presence of CDSO3. At the same time, V_{Max} was significantly reduced. This result suggested that CDSO3 does not compete with the substrate for binding.²⁰¹ Competitive binding studies with known ligands for exosite I and II indicated strong competition with UFH and H8. Based on these biochemical studies, it was concluded that CDSO3 is a *non-competitive*, direct thrombin inhibitor. Interestingly, human plasma and blood studies indicated that CDSO3 possessed anticoagulant potency similar to clinically approved LMWHs.^{201, 202}

The major concerns with LMWLs are their poly-dispersity and heterogeneity in structure. This can result in batch-to-batch variation in structural population, thus affecting the potency of the mixture. The presence of structures with different binding features can also bind at various non-target sites leading to severe side effects. The lack of structural information of such a heterogeneous mixture presents a hurdle for rational design of newer molecules to improve potency and ADME profiles.

To design homogeneous structures with potent anticoagulant activity based on the sulfated LMWL scaffold, we envisioned sulfated LMWLs as aromatic units formed by various random linkages of 4-hydroxy-cinnamic monomers. Literature suggests an abundance of β -5 linkages in natural lignins.^{204, 205} We initiated the design of new classes of anticoagulants based on the β -5 linkage of sulfated LMWLs (Figure 16). The β -5 linked monomers of CDSO3 form a dihydrobenzofuran moiety having carboxylate and sulfate groups at 3- and 7- positions, respectively. It also has two stereo-centers at the 2- and 3- positions. Simplification of the above structure, gave the benzofuran unit. After incorporating synthetic feasibility, we proposed 5, 6-dihydroxy-benzofuran-3-carboxylate ester as the first designed, small molecule scaffold for allosteric modulation of thrombin's activity.

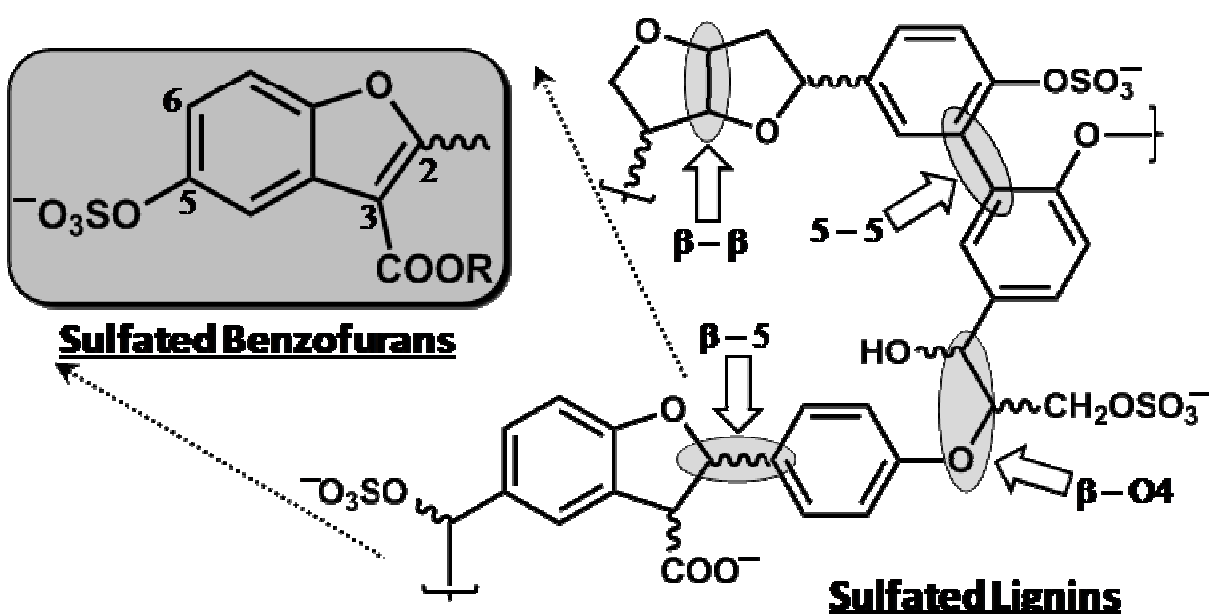


Figure 16. The development of design of benzofuran scaffold from the DHPs, showing various inter-monomeric linkages present in sulfated lignin. The β -5 linkage forms the Dehydrobenzofuran ring, which is modified to benzofuran to remove the complexity of two chiral centers and for ease of synthesis.

Based on this hypothesis, a small library of sulfated benzofuran monomers were synthesized and evaluated for thrombin inhibition. It was found that the selected sulfated monomer inhibited thrombin with low potency but that Michaelis-Menten kinetic analysis revealed that these molecules do not compete with spectrozyme-TH.²⁰⁵ Thus, based on these findings, it can be concluded that, although inhibition potency of sulfated monomers is low, the design of allosteric inhibition of thrombin is proven. This led us to further ask whether:

- 1) Can we design dimeric or higher oligomeric sulfated benzofurans to improve the inhibition potency?
- 2) Can we still retain the allosteric mode of inhibition for higher oligomeric sulfated benzofurans and explore the binding region?
- 3) Can *in vitro* potency of these inhibitors translated in higher systems?
- 4) Is it possible to propose newer scaffolds based as potential leads for allosteric inhibition of thrombin?

Chapter 3 Synthesis of Library of Sulfated Benzofuran Monomers and Dimers

3.1 Introduction

Thrombin is a key enzyme of the coagulation cascade, exhibiting important roles in both pro-coagulation and anti-coagulation processes. Most clinically used anticoagulant drugs, including polymeric heparin, warfarin, hirudin, argatroban and the recently approved dabigatran, aim to reduce thrombin activity.¹⁹⁷ Although these drugs have been successful in treating many thrombotic disorders, anticoagulation therapy continues to suffer from bleeding risk, narrow therapeutic index and other drug-specific adverse effects, which highlight the critical need to develop agents with better therapeutic profiles.

Structurally, thrombin is a complex serine protease of the trypsin family that displays multiple ligand-binding domains that modulate its activity and interactions with other molecules. These domains include the active site, the anion-binding exosites I and II, and the sodium binding site. The design of thrombin inhibitors has focused almost exclusively on blocking the substrate's access to the active site through a competitive process.¹⁹⁷ This paradigm has resulted in the design of thousands of molecules distributed across a large number of scaffolds.^{20, 80, 197, 206} Of these, a select group of scaffolds, including the pyrazoles, naphthylamidines, indoles,

biphenyls, and benzimidazoles, are preferred because of their high thrombin selectivity. Fundamentally, these designed inhibitors attempt to mimic the D-Phe-Pro-Arg recognition sequence through the incorporation of a guanidine or amidine moiety. Recently, however, newer molecules have been designed with a P-1 halophenyl substituent so as to interact with Tyr228 in the S1 pocket, which improves the poor oral bioavailability of most P-1 guanidine-based inhibitors.^{197, 207, 208}

An exciting alternative to competitive inhibition of thrombin is allosteric inhibition through either exosite I or II. It is well established that binding of ligands in these exosites can induce conformational changes in the active site of thrombin.^{79, 86, 209, 210} An example of this is thrombomodulin, which interacts with exosite I so as to change the substrate specificity of thrombin from fibrinogen to protein C.²¹⁰ Likewise, hirugen binding in exosite I increases or decreases the catalytic efficiency of thrombin, depending on the nature of the chromogenic substrate.^{86, 209} Similarly, exosite I – active site allosteric coupling is also the reason why peptides such as bothrojaracin inhibit thrombin.^{101, 102} Nevertheless, no small organic molecule has been designed to date that utilizes exosite I to effect physiological thrombin inhibition.

Exosite II ligands include heparin, chondroitin sulfate, haemadin, and fibrinogen γ' . These can be broadly classified as either highly anionic polysaccharides or traditional peptides. Interaction of heparin with exosite II is known to induce greater reactivity with antithrombin and recent work shows that formation of the antithrombin – thrombin complex disrupts exosite II.²¹¹ Also, exosite II – active site coupling is suggested by the change in fluorescence properties of para-amino benzamidine, a non-covalent active site probe, upon heparin binding to exosite II.²¹² However, no exclusive II ligand has been found to date that reduces the catalytic efficiency of thrombin.

Allosteric regulation is a promising strategy for thrombin inhibition. Nature tends to utilize allostereism to confer specificity of recognition and also to effect regulation. For thrombin, the possibility of regulation, or controlled inhibition, is of considerable importance because nearly all current anticoagulants are associated with risk of bleeding. An appropriately designed allosteric regulator that does not fully nullify the procoagulant signal may maintain a finely tuned balance between procoagulant and anticoagulant signal resulting in reduced bleeding complications. In pursuit of such allosteric regulators, we had earlier designed sulfated low molecular weight lignins (LMWLs) as functional mimetics of heparin targeted to exosite II-like regions of coagulation enzymes, including thrombin.^{213, 214} Sulfated LMWLs, chemo-enzymatic variants of the naturally available lignin (Fig. 1), were found to potently inhibit thrombin with an IC_{50} of 18–34 nM under physiological conditions.²¹³ More importantly, sulfated LMWLs also inhibited blood clotting under *ex vivo* conditions with potency comparable to the LMW heparins.²¹⁵

Despite their excellent *in vitro* and *ex vivo* anticoagulant properties, sulfated LMWLs are challenging because of their polydispersity and microheterogeneity, which parallel that observed with the heparins. Sulfated LMWLs represent a large library of structures arising from multiple inter-monomeric linkages, variable sulfation and chain length, and the presence of many chiral centers.²¹⁶ These variables introduce considerable structural diversity to these molecules, which nevertheless bind to exosite II of thrombin and allosterically induce thrombin inhibition.²¹³ Sulfated LMWLs represent the first examples of an exclusive exosite II-mediated inhibition of the key coagulation protease.

In this and the next chapter, we present a study of 28 monomeric and dimeric sulfated benzofurans, molecules derived from the sulfated LMWL structure, as inhibitors of thrombin.

Enzyme inhibition studies show that the library of molecules displays a range of inhibition potential, while Michaelis-Menten kinetic studies show the inhibition to arise from an allosteric process. Collectively, this work establishes the potential of allosteric inhibition of thrombin through the interesting and unusual features of sulfated benzofurans that direct the interaction with thrombin.

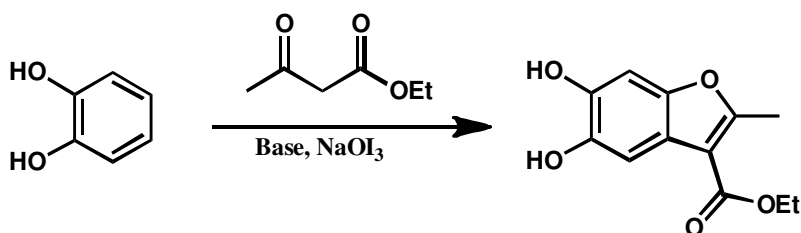
3.2 Synthesis

3.2.1 Simple Synthesis Procedure of Highly Functionalized Benzofuran Unit

Our initial synthesis of ethyl 5,6-dihydroxy-2-methylbenzofuran-3-carboxylate on a 5-gram scale using the method reported by Pei *et al*²¹⁷ produced the desired product only in yields below 20% and required several rounds of chromatographic purification. In order to obtain enough hydroxylated benzofuran as a building block for the thrombin inhibitors, various solvent systems, base and reaction times as well as a simplified purification procedure were investigated. It was found that solvent composition played a crucial role in defining the reactivity of components. Detailed studies indicated that the amount of water played a crucial role in the reaction (Table 1). Whereas 1:1 water – ethanol mixture was completely ineffective, a 3:1 was found to be optimal in yielding the desired highly functionalized benzofuran. Likewise, neither water alone nor ethanol alone yielded any product. The reason for this significant stringency appears to be the insolubility of catechol and ethyl acetoacetate. Yet, other solvents such as acetonitrile or DMF, in which both reactants are fully soluble, also failed to give any product. Attempting to improve solubility by heating to 50 °C also failed as it resulted in tar, possibly due to polymerization. Preventing this tar formation by removing atmospheric oxygen (flushing with nitrogen) gave back the starting materials in nearly quantitative yields. The reaction requires

atmospheric oxygen to promote oxidative addition and cyclization, although no experiments were performed to assess the minimal level of atmospheric oxygen necessary to sustain the reaction.

Table 1. The effect of different solvent composition on reaction yield. The following reaction condition was used: catechol (20 mmol), ethyl acetoacetate (10 mmol), base (40 mmol), NaIO₃ (10 mmol) at room temperature for 14 hours.



Solvent	Yield
Water	0
Water: Ethanol (96:4)	0
Water: Ethanol (90:10)	7%
Water: Ethanol (85:15)	10.5%
Water: Ethanol (80:20)	18%
Water: Ethanol (75:25)	25%
Ethanol	0
Acetonitrile	0
Acetonitrile: Ethanol (80:20)	0
* Water: Ethanol (75:25)	0 (Heating at 50 °C)
* Water: Ethanol (75:25)	0 (under nitrogen)

To further improve the yield of the reaction, various bases with increasing pK_a were screened (Table 2). Bases such as triethylamine and DIPEA improved the yield to 40-50%, most probably arising from better deprotonation of acidic hydrogen from ethyl acetoacetate. Yet, stronger bases such as K-*t*-butoxide ($pK_a = 19$) resulted in no products. Reaction time of 10-12 hours was also found to be critical (Table 2). Extending the reaction time beyond 12 hours led to a significant decrease in yield probably because of oxidative degradation of the product.

Finally, purification of the desired product could be achieved through direct precipitation in ethyl acetate as the yield had increased to a sufficiently high level. Thus, an effective procedure for the synthesis of highly functionalized benzofuran was developed. In this process, catechol (4.4 g), ethyl acetoacetate (5.6 g) and DIPEA (10.14 g) were added and stirred for 5 minutes to make a slurry. Ethanol (50 mL) and then water (150 mL) were added to the slurry, stirred for 10 minutes followed by addition of sodium iodate (4 g). The reaction was allowed to proceed unattended at room temperature for 10 hours, then quenched with ethyl acetate (400 mL) and extracted with acidified brine followed by vacuum concentration. The desired product was obtained with > 95% purity by direct precipitation from ethyl acetate.

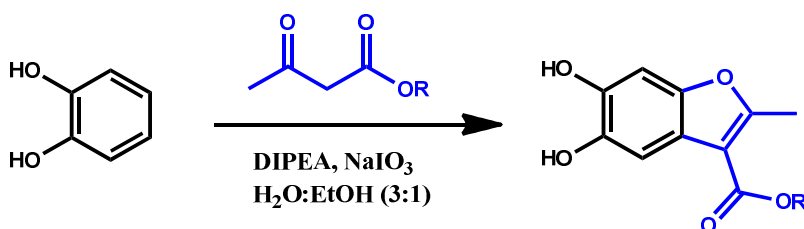
Table 2. The effect of various bases and reaction time on percentage yield of **1a**. The following reaction condition were used: ¹catechol (20 mmol), ethyl acetoacetate (20 mmol), NaIO₃ (10 mmol), water: ethanol (3:1) at room temperature for 14 hours; ²DIPEA (40 mmol) was used as the base.

<i>Impact of different bases¹</i>		<i>Impact of reaction time²</i>	
Base	%Yield	Time (Hours)	% Yield
Pyridine (2 equiv.)	25	8	15
Pyridine (1 equiv)	10	10	60
Triethylamine	40	12	50
DIPEA	50	14	40
K ⁺ O- <i>t</i> Bu	0	24	20

To evaluate the feasibility of this synthetic procedure to other reactants, various commercially available alkyl acetoacetates including methyl, ethyl, *t*-butyl, methoxy ethyl and allyl ester were investigated at a 10 g scale. It was observed that yield improved with polarity of the esters such as methoxyethyl ester and decreased with hydrophobic *t*-butyl ester (Table 3). On

the other hand, the simple purification method of direct precipitation in ethyl acetate is applicable to all of these esters. Thus, overall a significant advance could be achieved in the application of this useful reaction to synthesis of a library of highly functionalized benzofurans.

Table 3. The effect of substitutions on the dicarbonyl compound. The following reaction condition were used: catechol (20 mmol), ethyl acetoacetate (20 mmol), DIPEA (40 mmol), NaIO₃ (10 mmol), water: ethanol (3:1) at room temperature for 10 hour.



Compound	-R	% Yield
1a	-CH ₃	60 %
1b	-CH ₂ CH ₃	60 %
1c	-C(CH ₃) ₃	40 %
1d	-CH ₂ CH ₂ OCH ₃	70 %
1e	-CH ₂ CH=CH ₂	60 %

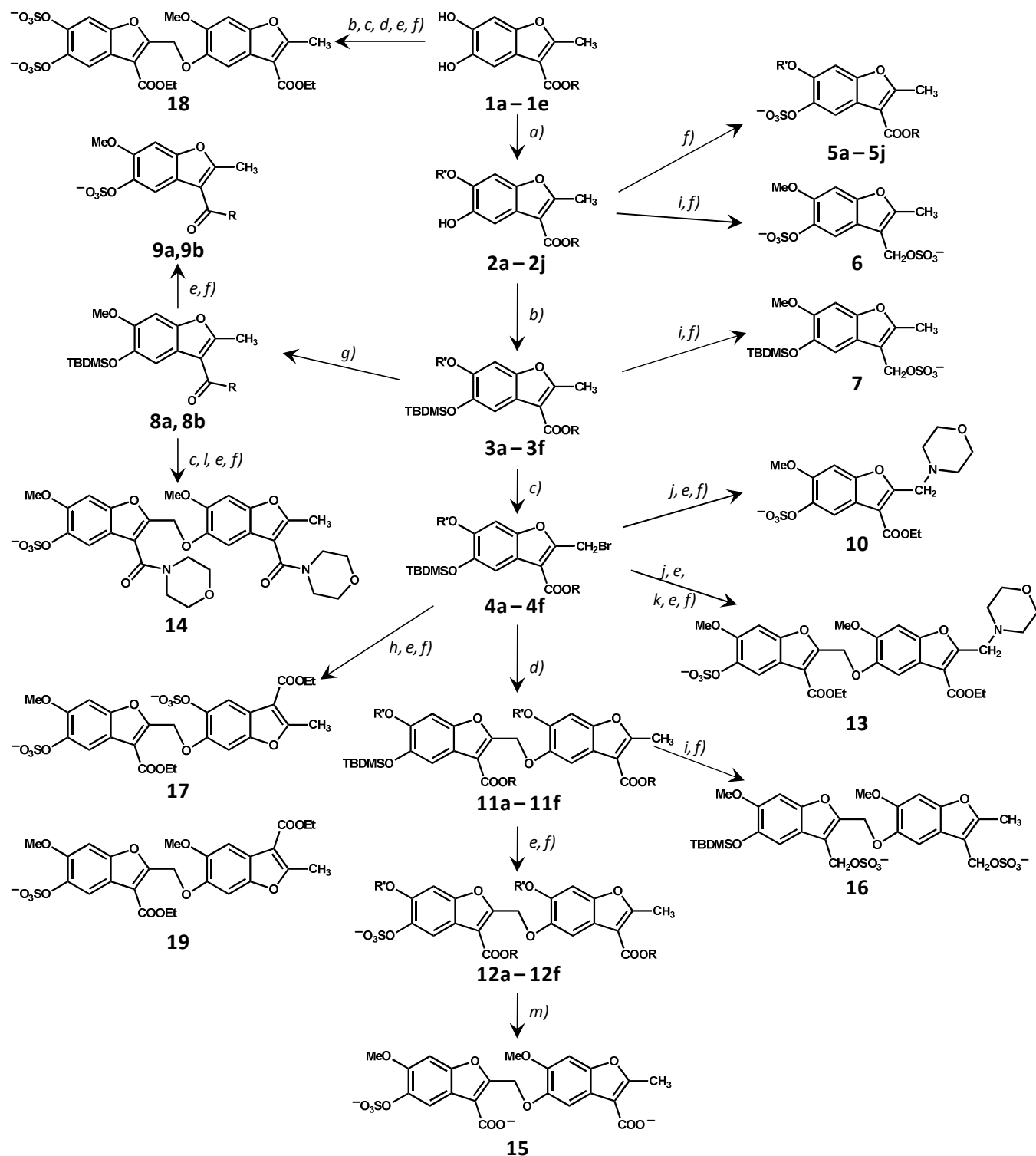


Figure 17. Synthesis of a library of sulfated benzofurans as potential allosteric regulators of thrombin. The library consists of 15 monomers (**5a – 5j**, **6**, **7**, **9a**, **9b**, and **10**) and 13 dimers (**12a – 12f**, **13 – 19**). Reactions: a) Cs₂CO₃, alkyl or acyl halide, an. DMF; b) TBDMSCl, Imidazole,

DMF; c) NBS, CCl₄; d) Cs₂CO₃, **2**; DMF; e) KF, CH₃COOH, DMF; f) Et₃N:SO₃, CH₃CN:DMF (4:1), MW; g) Me₃Al, R-H, toluene; h) Cs₂CO₃, **1a**, DMF; i) LAH, an. THF; j) Cs₂CO₃, morpholine, DMF; k) Cs₂CO₃, **4a**, DMF; l) Cs₂CO₃, DMF, desilylated **8a**; m) alc. LiOH.

3.2.2 Synthesis of Benzofuran Monomer and Dimer Precursors

The detailed protocol for the synthesis of each benzofuran precursor is provided in the Experimental Section (3.4). The overview of the highly branched synthesis scheme is described in Figure 17. This highly branched synthesis scheme was required for the synthesis of a diverse library in term of number and position of sulfate and variable substitutions at the 2-, 3- and 6-positions.

3.2.3 Hydrolysis of Ethyl Ester

Initially, several attempts failed to hydrolyze the ethyl ester present at 3- and 3'- positions of the sulfated benzofuran dimer. In addition to the abundance of literature on mild hydrolysis of ester groups, the reaction required effort to optimize the conditions to hydrolysis ester in the presence of labile sulfate groups (Table 4). The following conditions were tried:

To the solution of **12a** in anhydrous DMSO was added K-t-butoxide (2 equiv) and a catalytic amount of water. The reaction was stirred at room temperature for 12 hours. No product was observed. The use of a different solvent system such as DMF also failed to give the desired product. At low temperature, no product was observed and mostly starting material was retained. At room temperature, the conditions were too harsh for the sulfate group. An enzymatic method was used as an alternative approach for ester hydrolysis. Pig liver esterase was used in various buffer systems. However, no product was observed even after prolonged reaction time. t-Butyl ammonium hydroxide was also used to facilitate the hydrolysis of ester group. It also failed to

give desired the product at room temperature. Under microwave radiations for 20 minutes at 80 °C, degradation of starting material was observed. High temperature conditions were not suitable for the stability of the product. Other bases such as cesium carbonate and NaOH were used. The solvent systems such as methanol, ethanol and water: methanol (1:1) failed to give desired product.

There were several reports on the use of LiOH for hydrolysis of ethyl ester. Initially, it failed to give the desired product in the acetonitrile:DMF (4:1) and THF:water (4:1) solvent systems. The saturated solution of LiOH in methanol led to degradation of starting material. Finally, 3 equivalents of LiOH in methanol at room temperature in 5 hours gave the desired product in good yield.

Table 4. The reaction condition tried for hydrolysis of ethyl ester group of **12a**

Base	Solvent	Condition	Result
K-t-butoxide	DMSO	Water (cat.)	Sulfate removal
K-t-butoxide	DMF	Water (cat.)	Sulfate removal
Pig Liver Esterase	Phosphate buffer	RT	No product
Bu ₄ NOH	THF	RT and MW (80°C)	No product
Cesium Carbonate	Water/methanol	RT	No product
NaOH	Ethanol	RT	Sulfate removed
LiOH	ACN: DMF	RT	No Product
LiOH	THF: water	RT	Degradation
Sat. LiOH	Methanol	RT	Degradation

Reason: The major concern in this step was the stability of the sulfate group. It is known that sulfate groups are not stable under strong basic conditions as well as under moderate acidic conditions, limiting the use to stronger bases and higher temperatures. Secondly, both ester groups were sterically hindered, which limits the access of bulkier bases. The steric issue was further exacerbated by Π -stacking of aromatic rings. The planar nature of these molecules increases the probability of Π -stacking and aggregation.

3.2.4 Reduction Benzofuran Dimer to Diversify the Number and Position of Sulfate Group

In order to observe the effect of sulfate group at the 3- position, we tried to convert ethyl ester to hydroxyl and methyl hydroxyl group at this position. For the introduction of 3-hydroxy and 3-methylhydroxy groups, the Baeyer-Villiger reaction and reduction of ester were tried.

Procedure for Baeyer-Villiger Reaction: To a solution of **3a** (1 mmol) in dry methylene chloride was added meta-chloroperoxy benzoic acid (mCPBA, 2 mmol) and a catalytic amount of *p*-toluene sulfonic acid. The reaction mixture was stirred for 12 hours at room temperature. The product formation was monitored using thin layer chromatography and ^1H -NMR on the crude as well as after initial work up using brine and methylene chloride. The reaction failed to give the desired product. To optimize the reaction conditions, the reaction was performed at 50 °C to overcome the energy barrier, but still no product was observed. The reaction conditions were further modified using different equivalents of mCPBA and by varying the amount of *p*-toluene sulfonic acid. All the above reaction conditions failed to give the desired product.

Procedure for Reduction Using Lithium Aluminum Hydride: To a solution of **2a**, **3a** and **11a-reduced** (1 mmol) in dry THF was added lithium aluminum hydride (2 mmol). The reaction mixture was stirred at room temperature for 3 hours and then quenched by adding a small

amount of water. The reaction product was extracted between brine and methylene chloride layers. The organic layer was concentrated and purified by flash chromatography using a silica gel column. The product formation was monitored using thin layer chromatography and ^1H -NMR of crude as well as the purified product. No product was observed. In order to check the efficiency of the reducing agent, lithium borohydride was used, but still no product was observed. It was concluded that the reducing agent was either not of sufficient activity or had been deactivated by moisture. Further, an excess of LAH was used and thus was transferred under nitrogen atmosphere to prevent the deactivation by air moisture. When a large excess of LAH (5-8 equiv) was used, product was observed in 70% yield. Reaction was purified using silica gel flash chromatography using ethyl acetate in hexanes (10-50%) as solvent.

The product obtained was sulfated using a microwave-based protocol. The triethyl amine salts of sulfated **6**, **7** and **16** were purified by flash chromatography using a silica gel column. Ethyl acetate in hexanes (30%-80%) was used as solvent. It was observed that the product started degrading after purification. Initially, it was believed that the acidic nature of silica might be responsible for degradation as it is known that the sulfate group is unstable in acidic condition. To overcome this, a neutral alumina column was used for purification, but still degradation was a major issue. To check the stability of the product, a small ^1H -NMR study was performed to check the stability of the product in various solvents. The ^1H -NMR for **7** was recorded in various solvents over times of 10 minutes to few days. It was observed that the product was stable in CH_3CN even after 10 days. In methanol, extra peaks corresponding to degradation product started appearing in the proton spectra over the period of 2 hours and complete degradation of product was observed in 2 days. In methanol-water (1:1), prominent peaks of degraded product were observed after both 10 minutes and 2 hours. In the case of water as solvent, degradation of

product started immediately and significant excess peaks started appearing in proton spectra in just 10 minutes. Furthermore, no peaks corresponding to **6** were observed after separation on a cation-exchange column, which is consistent with instability of the product in water. Based on these studies, it can be concluded that **6** is stable in polar aprotic solvents, but starts degrading in protic solvents. The nature of protic solvents to stabilize ions and promote protonation, might be the factor responsible for degradation. The position of the sulfate group and resonance effects may lead to the removal of the 3- position sulfate group.

Reason: The reason for the instability of these molecules in aqueous solvents is not fully understood. But based on ^1H -NMR data, it can be postulated that the electronic effects of the sulfate group as well as of the aromatic ring play a major role. The sulfate group is highly electron withdrawing in nature causing electron “pull” from the aromatic unit, which is further supported by the electron donating nature of the oxygen atom. This movement of electrons can lead to removal of the sulfate group as well as the resonance of aromatic unit to hydroquinone.

3.3 Results and Discussion

3.3.1 Design of the Sulfated Benzofuran Scaffold

Sulfated LMWLs, which recognize exosite II of thrombin, are based on an aromatic scaffold, a scaffold dramatically different from the highly anionic polysaccharide scaffold of heparin.²¹⁶ Nevertheless, sulfated LMWLs retain one characteristic of heparin – structural complexity arising from the presence of multiple inter-monomeric linkages, such as β -5, β - β , β -O4, and 5-5 (Figure 16). A simple calculation suggests that LMWL molecules as small as a tetramer can exhibit nearly 1400 distinct structures even if sulfation and inter-residue linkage are

the only variables considered. To uncover distinct structures that may be the seat of anticoagulant activity, we visualized lignin structure as concatenated, aromatic units, instead of repetitions of 4-hydroxy-cinnamic acid monomers joined together through different inter-residue linkages. In this alternative analysis, oligomeric lignin can be considered as a combinatorial library of dihydro-benzofuran, phenoxy-propanoic acid, biphenyl and fused furan monomers (Figure 16). We reasoned that one or more of these aromatic units with appropriate sulfate groups could be the seat of thrombin recognition and inhibition.

To begin assessing the contribution of these individual aromatic units, we focused on the benzofuran unit, which is a common scaffold used in many synthetic studies. In a preliminary investigation, we had prepared a library of sulfated and carboxylated benzofuran monomers, of which a small group of molecules were found to inhibit thrombin, *albeit* with IC_{50} in the millimolar range. Interestingly, mechanistic studies had suggested allosteric inhibition by these molecules.²¹⁸ This promise led us to explore a more diverse set of sulfated benzofuran monomers and dimers as potential inhibitors of thrombin (Figure 17).

3.3.2 Overall Description of the Sulfated Benzofuran Library

The benzofuran unit of sulfated LMWLs contains substitutions at the 2, 3, 5- positions (Fig. 17). Of these, the 2- and 5- positions are utilized for inter-monomeric linkage and the 3- position may bear a carboxylate or an alkylsulfate group. Considering these variations, charged, polar and hydrophobic substitutions were engineered on this scaffold to obtain a structurally diverse library. Figure 17 describes the multi-modal approach developed to synthesize 15 sulfated monomers and 13 sulfated dimers. This library reflects significant variations in: 1) the number of negatively charged groups (1 to 3 anions); 2) the position of anionic and polar

substitutions from the terminal to the center of the scaffold; 3) the size and nature of hydrophobic groups; and 4) inter-residue linkage geometry. A characteristic feature is that each member of the library is nearly fully water soluble because of the presence of one or more sulfate groups, despite the primarily hydrophobic benzofuran backbone. This combination of water solubility and hydrophobicity has been known to introduce novel physicochemical characteristics in the sulfated lignin-based scaffold, e.g., higher than expected partition coefficient,²¹⁹ and greater proportion of non-ionic forces in binding to proteins.²²⁰

3.3.3 Synthesis of Sulfated Benzofuran Monomers

The first step in the synthesis of the library was the generation of base structures, 5,6-dihydroxy-benzofuran-3-carboxylic acid esters **1a** – **1e** (Figure 17), from catechol in one step using oxidative Michael addition conditions following the report of Pei et al.²¹⁷ The reaction was strongly susceptible to substituent effects, which required extensive optimization of reaction conditions, especially the organic base, reaction time and solvent. Eventually, products **1a** – **1e** were obtained in reasonably good yields (50–65%). Monoalkylation or acylation of dihydroxybenzofurans proceeded smoothly to selective 6-substituted derivatives **2a** – **2j**. That the substitution occurred at the 6-position of the benzofuran ring was confirmed through two dimensional nuclear Overhauser spectroscopy experiments (ROESY), which showed a correlation between the protons of the 3-alkyl ester and 6-alkoxy groups (not shown). The monomeric benzofurans **2a** – **2j** so synthesized in two steps formed one major group of precursors for library construction. Another set of monomer precursors **3a** – **3g** and **4a** – **4g** were synthesized from **2a** – **2j** through silyl protection and bromination, respectively (Figure 17).

Mono-sulfated benzofurans **5a** – **5j** were prepared by direct sulfation of precursors **2a** – **2j**. Phenolic molecules are typically more challenging to sulfate than alcoholic molecules.²²¹ We had previously developed a microwave-based sulfation protocol for introducing multiple sulfate groups in a crowded environment using the triethylamine-sulfur trioxide complex at 100 °C.^{218, 222} This method gave good yields of mono-sulfated benzofurans **5a** – **5j** in their ammonium salt forms, which were exchanged for sodium using a Sephadex C-25 exchange column. To test whether the number and location of sulfate groups on the benzofuran scaffold play a significant role in recognizing thrombin, we also introduced a sulfate group at the 3- position. Thus, benzofurans **2a** and **3a** were reduced with LAH and sulfated to yield **6** and **7**, respectively. However, both **6** and **7** were found to degrade within a couple of hours after dissolution in water at room temperature. The reason for the reduced aqueous stability of these 3-methylene sulfated benzofurans is not clear, although the dual combination of electron pull by sulfate groups and electron push by ring oxygen may be cause of more rapid desulfation.

To assess the importance of the nature of the carbonyl group at the 3-position, silyl-protected benzofuran ester **3** was directly converted to morpholinyl and 4-methylpiperidinyl amides **8a** and **8b**, respectively. Desilylation and sulfation gave mono-sulfated benzofuran amides **9a** and **9b** in excellent yields. Finally, 2-morpholino monomer **10** was prepared from **4a** to study the effect of varying the 2-substituent.

3.3.4 Synthesis of Sulfated Benzofuran Dimers

The construction of the library of dimers relied on the nucleophilic displacement of the allylic bromide at the 2- position by free phenolic group at the 5-position. The apparent simplicity of this reaction and the availability of ten nucleophilic monomers **2a – 2j** and seven allylic bromides **4a – 4g** enticed us to construct a combinatorial library (Figure 17). However, the coupling was challenging on both synthesis and purification fronts. Steric crowding around both the nucleophile and the electrophile resulted in less than optimal yields (<50%) of **11a – 11f**. In addition, the synthesized dimers typically co-eluted with monomers in a wide range of multi-solvent systems, thus creating significant purification issues. We suspected that co-elution may be occurring because of Π -stacking at high concentrations. Thus, a higher yielding dimerization reaction was desirable, which was made possible through implementation of microwave coupling. Using this strategy silylated dimers **11a – 11f** were synthesized in excellent yields (>90%). These were then de-protected and sulfated to yield mono-sulfated benzofuran dimers **12a – 12f**. Likewise, mono-sulfated benzofuran dimers **13** and **14**, which contain a morpholine ring at 2- and 3- positions, respectively, were synthesized starting from monomers **4a** and **8a**, respectively, through a series of silyl protection, allylic bromination, deprotection, nucleophilic coupling and sulfation steps (Figure 17).

To evaluate the role of multiple anionic groups on the small hydrophobic scaffold, **12a** was hydrolyzed in alcoholic LiOH^{223} to yield **15**, a mono-sulfated, dicarboxylated dimer. Likewise, **11a** was reduced with LAH and sulfated to yield **16**, which is a di-sulfated dimer, but as with monomers **6**, **7** and **16** was found to degrade rapidly in water. Finally, coupling of **4a** with **1a** followed by desilylation and sulfation gave **17**, which is also a di-sulfated dimer, but with a structure completely different from **16**. Likewise, another variant of di-sulfated dimer, i.e.,

18, was synthesized by coupling **1a** and **2a** in five steps (Figure. 17). In combination, dimers **15** – **18** display anionic groups around three key positions (3, 5, and 6) of the benzofuran scaffold. These contain either two or three negative charges, which approximate the number of charges typically found on a heparin disaccharide.

3.4 Experimental Section

3.4.1 Chemicals, Reagents and Analytical Chemistry

Microwave-based sulfation reactions were performed using a CEM-Discover synthesizer (Matthews, NC) in sealed reaction vessels (7 mL) at 50 W. The temperature of the reaction was maintained at the desired setting using cooled nitrogen (45 psi) flow. Reagents and chemicals used in reactions were purchased from either Sigma-Aldrich (Milwaukee, WI) or Fisher (Pittsburgh, PA) and used as supplied. Analytical thin layer chromatography (TLC) was performed using UNIPLATETM silica gel GHLF 250 μ m pre-coated plates (ANALTECH, Newark, DE) that were analyzed by fluorescence (254 nm).

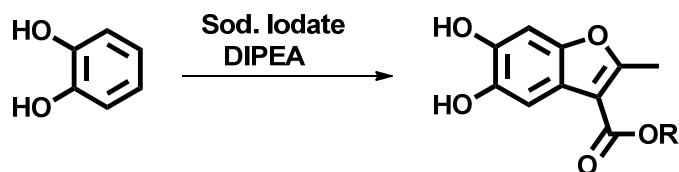
Column chromatography was performed using a Teledyne ISCO (Lincoln, NE) Combi flash RF system and disposable normal silica cartridges of 30 – 50 μ m particle size, 230 – 400 mesh size and 60 Å pore size. Sodium exchange chromatography was performed using SP Sephadex C-25 sodium cation exchange columns from GE Healthcare Life Sciences (Piscataway, NJ). An approximately 100 mg sulfated sample was loaded onto 10 g of the cation exchanger in a 10 \times 460 mm column and eluted with either water or 20% EtOH/H₂O at 0.5 mL/min. Anhydrous reactions were carried out under nitrogen atmosphere in glassware dried at high temperature. Reagent solutions and solvents were handled under nitrogen atmosphere using syringe techniques. The HPLC purification of sulfated benzofurans was carried out on a Jasco chromatography system (Easton, MD) using a 250 \times 10 mm Varian Dynamax Microsorb C4

column. An acetonitrile – water gradient (5 to 100% acetonitrile in 20 min) at 3 mL/min was used to purify the compounds on milligram scale. The eluents were detected at 300 nm.

^1H and ^{13}C NMR spectra were recorded at either 300 or 400 MHz (Varian Mercury or Bruker UltrashieldTM Plus) in appropriate deuterated solvents including CDCl_3 , $\text{DMSO}-d_6$, CD_3OD , acetone- d_6 , or D_2O . All signals are reported in ppm with the internal chloroform, DMSO, acetone, and D_2O signals at 7.26, 2.50, 3.31, 2.05, and 4.79, respectively, as standards. The data is reported as: chemical shifts (ppm), multiplicity (s = singlet, d = doublet, t = triplet, m = multiplet), coupling constant(s) (Hz), and integration. Mass spectrometry was performed on all synthesized molecules using a Micromass ZMD 4000 single quadrupole mass spectrometer with ESI ionization probe operating in negative ion mode (Waters Corp., Milford, MA). The samples, dissolved in acetonitrile containing formic acid (5% v/v), were infused at 10 $\mu\text{L}/\text{min}$. The source block temperature and the probe temperature were typically held at 100 and 120 $^\circ\text{C}$, respectively, while corona and cone voltages were selected through manual optimization. The desolvation nitrogen flow was 500 L/hour. Mass spectra were acquired in the mass range from 110 to 1000 Daltons at 400 amu/sec.

3.4.2 Detailed Description of Syntheses

Syntheses of (1a–e)



To a solution of catechol (20 mmol) in 75 mL of ethanol were added the ester of acetoacetate (20 mmol) and N, N-Diisopropylethylamine (40 mmol). The reaction mixture was stirred for 5 min. To this mixture was added sodium iodate (20 mmol) and stirred vigorously for 5 min and then 25

mL of water was added. The reaction mixture was stirred for 10 hours at room temperature and quenched with 400 mL of ethyl acetate and extracted with 150 mL of brine and 30 mL of 0.5 N HCl. The organic layer was dried over magnesium sulfate and concentrated. The product was purified by passing through plug of silica (1 inch in height) using 2% methanol in methylene chloride. The product was concentrated and dried under vacuum to provide yield of 40% (see Appendix, Page 239-241 for NMR spectra).

1a: ^1H NMR (Acetone- d_6 , 300 MHz) δ 1.36 (t, $J=3$ Hz, 3H), 2.63 (s, 3H), 4.31 (q, $J=6$ Hz, 2H), 6.95 (s, 1H), 7.37 (s, 1H). ^{13}C NMR (CDCl_3) δ 14.79, 14.96, 60.54, 98.53, 106.62, 108.83, 117.56, 144.09, 144.92, 147.79, 161.79, 164.48.

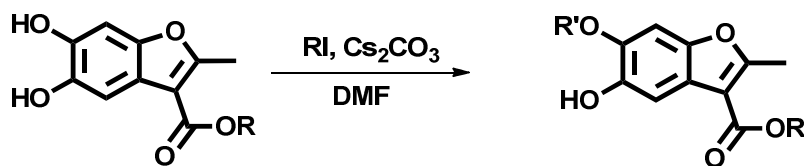
1b: ^1H NMR (CDCl_3 , 300 MHz) δ 2.65 (s, 3H), 3.97 (s, 3H), 6.99 (s, 1H), 7.43 (s, 1H).

1c: ^1H NMR (CDCl_3 , 300 MHz) δ 1.60 (s, 9H), 2.63 (s, 3H), 6.96 (s, 1H), 7.39 (s, 1H).

1d: ^1H NMR (CDCl_3 , 300 MHz) 2.63 (s, 3H), 3.41 (s, 3H), 3.72 (t, $J=12$ Hz, 2H), 4.46 (t, $J=12$ Hz, 2H), 6.96 (s, 1H), 7.39 (s, 1H).

1e: ^1H NMR (CDCl_3 , 300 MHz) 2.71 (s, 3H), 4.85 (d, 2H), 5.22 (d, 1H), 5.36 (d, 2H), 6.00 (m, 1H), 6.91 (s, 1H), 7.46 (s, 1H).

Synthesis of (2a–2j)



To a solution of **1a–1e** (1.44 mmol) in DMF (12 mL) were added cesium carbonate (0.72 mmol) and acyl or alkyl halide (1.44 mmol) and stirred for 15 hours under an N_2 atmosphere. The reaction was quenched by adding 0.5 N HCl and extracted with ethyl acetate. The organic extract

was dried over magnesium sulfate, concentrated and purified on silica gel (0-25% ethyl acetate in hexanes) to give product in 53% yield (see Appendix, Page 242-247 for NMR spectra).

2a: ^1H NMR (CDCl_3 , 300 MHz) δ 1.46 (t, $J=6$ Hz, 3H), 2.75 (s, 3H), 3.96 (s, 3H), 4.39 (q, $J=6$ Hz, 2H), 5.58 (s, 1H), 6.95 (s, 1H), 7.37 (s, 1H). ^{13}C NMR (CDCl_3 , 300 MHz) δ 14.60, 14.66, 56.54, 60.43, 94.33, 106.04, 109.23, 119.19, 143.37, 145.18, 147.86, 162.87, 164.88.

2b: ^1H NMR (CDCl_3 , 300 MHz) δ 2.71 (s, 3H), 3.91 (s, 3H), 3.92 (s, 3H), 6.95 (s, 1H), 7.44 (s, 1H).

2c: ^1H NMR (CDCl_3 , 300 MHz) δ 1.60 (s, 9H), 2.63 (s, 3H), 3.92 (s, 3H), 6.92 (s, 1H), 7.39 (s, 1H).

2d: ^1H NMR (CDCl_3 , 300 MHz) δ 2.63 (s, 3H), 3.41 (s, 3H), 3.72 (t, $J=12$ Hz, 2H), 3.82 (s, 3H), 4.46 (t, $J=12$ Hz, 2H), 6.96 (s, 1H), 7.39 (s, 1H).

2e: ^1H NMR (CDCl_3 , 400 MHz) δ 1.45 (s, 6H), 2.70 (s, 3H), 4.13 (d, 2H), 4.36 (d, 2H), 6.93 (s, 1H), 7.43 (s, 1H). ^{13}C NMR (CDCl_3) δ 14.34, 14.43, 14.76, 31.42, 36.45, 60.15, 65.02, 76.69, 77.00, 77.32, 94.97, 105.73, 109.04, 118.95, 143.34, 144.13, 147.63, 162.50, 162.58, 164.63.

2f: ^1H NMR (CDCl_3 , 300 MHz) δ 1.40 (d, $J=1.5$ Hz, 6H), 1.43 (t, $J=1.8$ Hz, 3H), 2.71 (s, 3H), 4.38 (t, $J=1.8$ Hz, 2H), 4.58 (m, 1H), 6.96 (s, 1H), 7.44 (s, 1H).

2g: ^1H NMR (CDCl_3 , 400 MHz) δ 1.45 (t, $J=18$ Hz, 3H), 2.71 (s, 3H), 3.76 (s, 3H), 4.36 (q, $J=18$ Hz, 2H), 5.53 (s, 2H), 7.05 (s, 1H), 7.54 (s, 1H).

2h: ^1H NMR (CDCl_3 , 400 MHz) δ 1.40 (t, $J=18$ Hz, 3H), 2.71 (s, 3H), 3.74 (m, 8H), 4.38 (q, $J=18$ Hz, 2H), 6.95 (s, 1H), 7.58 (s, 1H).

2i: ^1H NMR (CDCl_3 , 400 MHz) δ 2.71 (s, 3H), 3.83 (s, 3H), 4.85 (d, 2H), 5.22 (d, 1H), 5.36 (d, 2H), 6.00 (m, 1H), 6.91 (s, 1H), 7.46 (s, 1H).

2j: ^1H NMR (CDCl_3 , 400 MHz) δ 1.38 (t, $J=18$ Hz, 3H), 2.67 (s, 3H), 3.78 (s, 3H), 4.33 (q, $J=18$ Hz, 2H), 5.02 (s, 2H), 6.89 (d, $J=21$ Hz, 2H), 6.98 (s, 1H), 7.32 (d, $J=21$ Hz, 2H), 7.41 (s, 1H).

Synthesis of (3a–3f)



To a solution of **2a–2f** (3.63 mmol) in DMF (30 mL) was added imidazole (18.15 mmol) and TBDMSCl (21.83 mmol) and the mixture was stirred. After 16 hours the reaction mixture was quenched with water and extracted with diethyl ether. The organic layer was dried over magnesium sulfate, concentrated and purified by flash chromatography on silica gel (0–15% EtOAc in hexanes) to obtain product in 85–90 % (see Appendix, Page 250–254 for NMR spectra).

3a: ^1H NMR (CDCl_3 , 300 MHz) δ 0.17 (s, 6H), 1.01 (s, 9H), 1.46 (t, $J=6$ Hz, 3H), 2.69 (s, 3H), 3.87 (s, 3H), 4.39 (q, $J=6$ Hz, 2H), 7.05 (s, 1H) 7.41 (s, 1H). ^{13}C NMR (CDCl_3 , 300 MHz) δ 4.5, 14.47, 18.73, 22.25, 25.96, 55.99, 61.00, 95.23, 111.31, 112.77, 118.07, 143.56, 149.97, 151.43, 157.60, 163.69.

3b: ^1H NMR (CDCl_3 , 300 MHz) δ 1.16 (s, 6H), 1.02 (s, 9H), 2.70 (s, 3H), 3.83 (s, 3H), 3.91 (s, 3H), 6.93 (s, 1H), 7.37 (s, 1H).

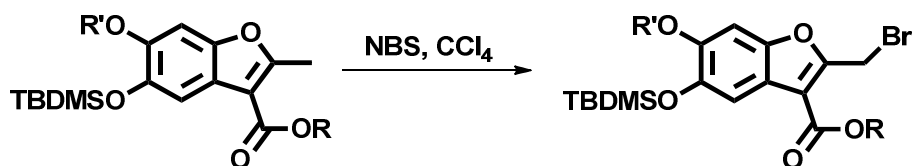
3c: ^1H NMR (CDCl_3 , 300 MHz) δ 0.16 (s, 6H), 1.03 (s, 9H), 1.62 (s, 9H), 2.69 (s, 3H), 3.83 (s, 3H), 6.92 (s, 1H), 7.36 (s, 1H).

3d: ^1H NMR (CDCl_3 , 300 MHz) 0.13 (s, 6H), 1.01 (s, 9H), 2.63 (s, 3H), 3.41 (s, 3H), 3.72 (t, $J=12$ Hz, 2H), 3.82 (s, 3H), 4.46 (t, $J=12$ Hz, 2H), 6.96 (s, 1H), 7.39 (s, 1H).

3e: ^1H NMR (CDCl_3 , 400 MHz) δ 0.11 (s, 6H), 1.04 (s, 9H), 1.46 (s, 6H), 2.71 (s, 3H), 4.03 (d, 2H), 4.35 (d, 2H), 6.93 (s, 1H), 7.40 (s, 1H).

3f: ^1H NMR (CDCl_3 , 400 MHz) δ 0.19 (s, 6H), 1.04 (s, 9H), 1.37 (d, 6H), 1.42 (t, 3H), 2.71 (s, 3H), 4.40 (d, 2H), 6.94 (s, 1H), 7.40 (s, 1H).

Synthesis of (4a–4f)



To the solution of **3a–3f** (1 mmol) in THF (20 mL) was added NBS (1 mmol) and refluxed at 65 °C under a halogen lamp for 1 hour. The reaction mixture was cooled and quenched with water and extracted with hexanes. The organic layer was concentrated and product was obtained in 90–95 % yield (see Appendix, Page 258–260 for NMR spectra).

4a: ^1H NMR (CDCl_3 , 300 MHz) δ 0.17 (s, 6H), 1.01 (s, 9H), 1.46 (t, $J=6$ Hz, 3H), 3.87 (s, 3H), 4.39 (q, $J=6$ Hz, 2H), 4.93 (s, 2H), 7.05 (s, 1H), 7.41 (s, 1H).

4b: ^1H NMR (CDCl_3 , 300 MHz) δ 1.17 (s, 6H), 1.02 (s, 9H), 3.83 (s, 3H), 3.91 (s, 3H), 4.91 (s, 2H), 6.93 (s, 1H), 7.37 (s, 1H).

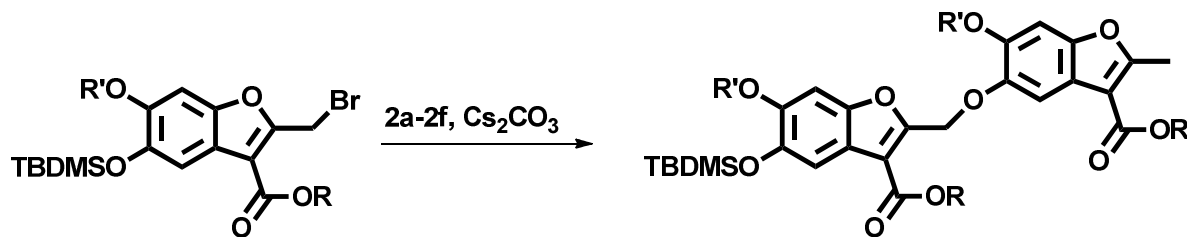
4c: ^1H NMR (CDCl_3 , 300 MHz) δ 0.16 (s, 6H), 1.01 (s, 9H), 1.65 (s, 9H), 3.85 (s, 3H), 4.93 (s, 2H), 6.96 (s, 1H), 7.40 (s, 1H).

4d: ^1H NMR (CDCl_3 , 300 MHz) δ 0.17 (s, 6H), 1.02 (s, 9H), 3.45 (s, 3H), 3.76 (t, $J=12$ Hz, 2H), 3.86 (s, 3H), 4.50 (t, $J=12$ Hz, 2H), 4.96 (s, 2H), 6.98 (s, 1H), 7.45 (s, 1H).

4e: ^1H NMR (CDCl_3 , 400 MHz) δ 0.11 (s, 6H), 1.04 (s, 9H), 1.46 (s, 6H), 4.03 (d, 2H), 4.35 (d, 2H), 4.96 (s, 2H), 6.93 (s, 1H), 7.40 (s, 1H).

4f: ^1H NMR (CDCl_3 , 400 MHz) δ 0.17 (s, 6H), 1.02 (s, 9H), 1.38 (d, 6H), 1.43 (t, 3H), 4.48 (d, 2H), 4.57 (s, 2H), 6.97 (s, 1H), 7.41 (s, 1H).

Synthesis of (11a–11f)



To the solution of **2a–2f** (0.3 mmol) and **4a–4f** (0.4 mmol) in ethyl acetate (4 mL) were added cesium carbonate (0.3 mmol) and anhydrous DMF (1 mL). The reaction mixture was stirred under nitrogen for 15 hours at room temperature. The reaction was quenched with methylene chloride and extracted with brine. The organic layer was dried over magnesium sulfate and concentrated. Purification was done by using flash chromatography on silica gel using (0-20) % ethyl acetate in hexanes. The product was obtained in 60-65 % yield (see Appendix, Page 261-265 for NMR spectra).

11a: ^1H NMR (CDCl_3 , 300 MHz) δ 0.17 (s, 6H), 1.01 (s, 9H), 1.46 (m, 6H), 2.71 (s, 3H), 3.87 (s, 3H), 3.91 (s, 3H), 4.39 (m, 4H), 5.60 (s, 2H), 6.95 (s, 1H), 6.99 (s, 1H), 7.42 (s, 1H), 7.55 (s, 1H). ^{13}C NMR (CDCl_3 , 300 MHz) δ 4.55, 14.41, 14.73, 14.68, 18.92, 25.57, 55.77, 56.62, 60.62, 61.93, 64.47, 95.27, 98.31, 103.47, 109.31, 112.55, 112.73, 117.90, 119.98, 143.29, 146.34, 147.95, 148.08, 151.20, 150.69, 157.66, 162.67, 164.17, 164.83.

11b: ^1H NMR (CDCl_3 , 300 MHz) δ 1.16 (s, 6H), 1.02 (s, 9H), 2.71 (s, 3H), 3.84 (s, 3H), 3.87 (s, 3H), 3.91 (s, 3H), 3.92 (s, 3H), 5.60 (s, 2H), 6.98 (s, 1H), 7.01 (s, 1H), 7.44 (s, 1H), 7.59 (s, 1H)

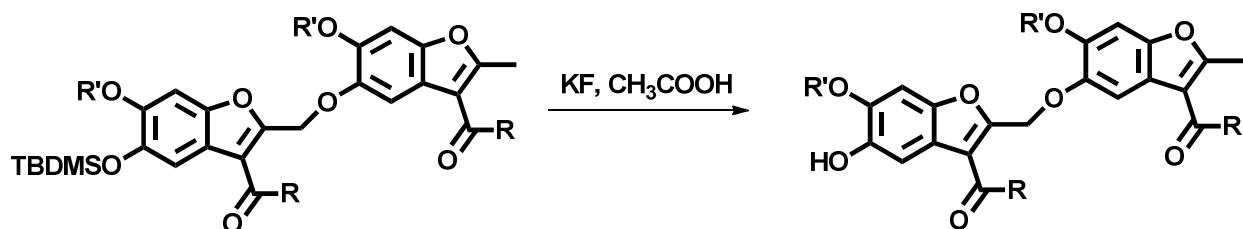
11c: ^1H NMR (CDCl_3 , 300 MHz) δ 0.16 (s, 6H), 1.01 (s, 9H), 1.59 (s, 9H), 1.60 (s, 9H), 2.68 (s, 3H), 3.82 (s, 3H), 3.87 (s, 3H), 5.57 (s, 2H), 6.92 (s, 1H), 6.98 (s, 1H), 7.41 (s, 1H), 7.54 (s, 1H).

11d: ^1H NMR (CDCl_3 , 300 MHz) δ 0.17 (s, 6H), 1.02 (s, 9H), 2.71 (s, 3H), 3.43 (s, 3H), 3.71 (m, 4H), 3.83 (s, 3H), 3.86 (s, 3H), 4.45 (m, 2H), 5.59 (s, 2H), 6.97 (s, 1H), 7.00 (s, 1H), 7.47 (s, 1H), 7.64 (s, 1H).

11e: ^1H NMR (CDCl_3 , 400 MHz) δ 0.17 (s, 6H), 1.03 (s, 9H), 1.37 (s, 12H), 2.70 (s, 3H), 4.08 (d, 4H), 4.33 (d, 4H), 5.57 (s, 2H), 6.98 (d, 2H), 7.44 (s, 1H), 7.58 (s, 1H). ^{13}C NMR (CDCl_3) δ 4.71, 14.19, 14.36, 14.38, 14.68, 14.74, 18.46, 25.75, 60.10, 60.16, 60.46, 64.31, 64.62, 65.01, 76.68, 77.00, 77.20, 77.32, 94.96, 96.01, 96.82, 109.13, 109.26, 111.63, 112.57, 117.85, 118.55, 143.03, 146.17, 148.42, 149.33, 149.90, 149.98, 158.17, 162.49, 163.71, 164.46.

11f: ^1H NMR (CDCl_3 , 400 MHz) δ 0.17 (s, 6H), 1.02 (s, 9H), 1.34 (d, 12H), 1.43 (m, 6H), 2.70 (s, 3H), 4.35 (t, 4H), 4.48 (m, 2H), 5.54 (s, 2H), 6.98 (d, 2H), 7.44 (s, 1H), 7.58 (s, 1H). ^{13}C NMR (CDCl_3 , 400 MHz) δ 4.59, 14.19, 14.38, 18.43, 21.01, 21.92, 21.98, 22.05, 25.78, 60.09, 60.36, 60.43, 64.75, 70.94, 72.65, 76.68, 77.00, 77.32, 98.11, 100.29, 109.13, 109.78, 111.54, 112.74, 118.05, 119.37, 143.96, 147.23, 147.51, 148.54, 149.29, 149.82, 158.39, 162.78, 163.69, 164.43.

Deprotected form of 11a–11f



To a solution of **11a–11f** (0.3 mmol) in DMF (3 mL) were added KF (4 mmol) and glacial acetic acid (10 μL). The reaction mixture was stirred for 5 hours. The reaction was quenched by

methylene chloride and extracted with brine solution. The aqueous layer was again extracted with a fresh batch of methylene chloride. The organic layer was combined and dried over magnesium sulfate and concentrated in vacuum. The solid was precipitated using methanol to obtain product in 90% yield (see Appendix, Page 270-274 for NMR spectra).

11a deprotected form: ^1H NMR (CDCl_3 , 300 MHz) δ 1.46 (m, 6H), 2.71 (s, 3H), 3.80 (s, 3H), 3.85 (s, 3H), 4.39 (m, 4H), 5.35 (s, 2H), 6.95 (s, 1H), 6.99 (s, 1H), 7.42 (s, 1H), 7.55 (s, 1H).

11b deprotected form: ^1H NMR (CDCl_3 , 300 MHz) δ 2.71 (s, 3H), 3.80 (s, 3H), 3.83 (s, 3H), 3.85 (s, 3H), 3.87 (s, 3H), 5.35 (s, 2H), 6.95 (s, 1H), 6.99 (s, 1H), 7.42 (s, 1H), 7.55 (s, 1H).

11c deprotected form: ^1H NMR (CDCl_3 , 300 MHz) δ 1.57 (s, 9H), 1.59 (s, 9H), 2.68 (s, 3H), 3.84 (s, 3H), 3.93 (s, 3H), 5.57 (s, 2H), 6.95 (s, 1H), 7.05 (s, 1H), 7.46 (s, 1H), 7.58 (s, 1H).

11d deprotected form: ^1H NMR (CDCl_3 , 300 MHz) δ 2.71 (s, 3H), 3.43 (s, 3H), 3.71 (m, 4H), 3.83 (s, 3H), 3.86 (s, 3H), 4.45 (m, 2H), 5.59 (s, 2H), 6.97 (s, 1H), 7.01 (s, 1H), 7.50 (s, 1H), 7.63 (s, 1H).

11e deprotected form: ^1H NMR (CDCl_3 , 400 MHz) δ 1.45 (m, 12H), 2.69 (s, 3H), 4.10 (m, 4H), 4.35 (m, 4H), 5.58 (s, 2H), 6.97 (s, 1H), 6.99 (s, 1H), 7.49 (s, 1H), 7.56 (s, 1H).

11f deprotected form: ^1H NMR (CDCl_3 , 400 MHz) δ 1.38 (d, 12H), 1.47 (m, 6H), 2.70 (s, 3H), 4.37 (t, 4H), 4.39 (t, 4H), 5.57 (s, 2H), 7.02 (d, 2H), 7.50 (s, 1H), 7.57 (s, 1H). ^{13}C NMR (CDCl_3 , 400 MHz) δ 14.31, 14.37, 14.38, 21.99, 22.05, 60.11, 60.53, 64.64, 72.40, 72.71, 76.69, 77.01, 77.21, 77.32, 96.70, 100.36, 106.03, 109.12, 109.60, 111.67, 118.50, 119.39, 143.83, 144.45, 147.15, 147.46, 148.66, 149.25, 158.69, 162.79, 163.67, 164.43.

Sulfation of Appropriate Precursors to Yield Sulfated Benzofuran Monomers and Dimers

The synthesis of sulfated benzofurans was developed following our earlier report on the

synthesis of sulfated flavonoids.²²² Briefly, to a solution of unsulfated benzofuran monomer or dimer (typically 50 mg) in acetonitrile: DMF (4:1, 0.45 mL) in a microwave tube were added triethylamine (10 equiv) and trimethylamine-sulfur trioxide complex (15 equiv). The reaction mixture was exposed to microwaves (50 W) for 40 min at 100 °C followed by vacuum concentration to remove all solvent. The solid so obtained was directly loaded on a Sephadex C-25 cation exchange resin and eluted with water. Fractions containing the sulfated product were lyophilized to obtain a solid residue, which was further purified on reverse-phase gradient HPLC to remove residual unsulfated contaminants (see Appendix, Page 282-305 for NMR spectra and Page 307-318 for Mass Spectra).

5a: ¹H NMR (D₂O, 400 MHz) δ 1.45 (t, *J*=6 Hz, 3H), 2.51 (s, 3H), 3.76 (s, 3H), 4.36 (q, *J*=6 Hz, 2H), 5.38 (s, 1H), 7.15 (s, 1H), 7.57 (s, 1H).

5b: ¹H NMR (D₂O, 400 MHz) δ 2.48 (s, 3H), 3.89 (s, 3H), 4.21 (s, 3H), 6.98 (s, 1H), 6.61 (s, 1H). ESI MS (-ve) *m/z* calcd. for C₁₂H₁₁O₈SNa [(M-Na)⁻] 315.02, found 315.01 (M-Na)⁻.

5c: ¹H NMR (D₂O, 400 MHz) δ 1.62 (s, 9H), 2.49 (s, 3H), 3.89 (s, 3H), 6.98 (s, 1H), 6.61 (s, 1H). ¹³C NMR (D₂O, 400 MHz) δ 13.40, 21.22, 61.33, 73.87, 99.93, 107.79, 114.00, 118.54, 139.23, 147.28, 150.45, 164.37, 165.49. ESI MS (-ve) *m/z* calcd for C₁₃H₁₇O₈SNa [(M-Na)⁻] 357.05, found 357.08 (M-Na)⁻.

5d: ¹H NMR (D₂O, 400 MHz) δ 2.48 (s, 3H), 3.21 (s, 3H), 3.62 (t, *J*=12 Hz, 2H), 3.72 (s, 3H), 4.26 (t, *J*=12 Hz, 2H), 6.91 (s, 1H), 7.59 (s, 1H). ESI MS (-ve) *m/z* calcd. for C₁₃H₁₃O₉SNa [(M-Na)⁻] 345.02, found 345.01 (M-Na)⁻.

5e: ¹H NMR (D₂O, 400 MHz) δ 1.70 (m, 6H), 2.99 (s, 3H), 4.41 (q, *J*=17 Hz, 2H), 4.66 (q, *J*= 17 Hz, 2H), 7.55 (s, 1H), 8.21 (s, 1H). ¹³C NMR (D₂O, 400 MHz) δ 16.36, 16.39, 16.76, 63.15,

67.53, 99.69, 110.66, 116.09, 119.96, 141.73, 146.05, 151.33, 152.58, 165.90, 167.00. ESI HRMS (-ve) m/z calcd. for $C_{14}H_{16}O_8SNa [(M-Na)^-]$ 343.0512, found 343.0357 (M-Na)⁻.

5f: 1H NMR (D_2O , 400 MHz) δ 1.37 (m, 9H), 2.36 (s, 3H), 4.23 (q, $J=18$ Hz, 2H), 4.54 (m, 1H), 6.96 (s, 1H), 7.60 (s, 1H). ^{13}C NMR (D_2O) δ 13.40, 13.48, 21.22, 61.33, 73.87, 99.93, 107.79, 114.00, 118.54, 139.23, 147.28, 150.45, 164.37, 165.49. ESI HRMS (-ve) m/z calcd. for $C_{14}H_{15}O_8SNa [(M-Na)^-]$ 357.0532, found 357.0600 (M-Na)⁻.

5g: 1H NMR (D_2O , 400 MHz) δ 1.45 (t, $J=18$ Hz, 3H), 2.50 (s, 3H), 3.64 (s, 3H), 4.31 (q, $J=18$ Hz, 2H), 5.33 (s, 2H), 7.15 (s, 1H), 7.64 (s, 1H). ESI HRMS (-ve) m/z calcd. for $C_{14}H_{15}O_9SNa [(M-Na)^-]$ 359.0420, found 359.0395 (M-Na)⁻.

5h: 1H NMR (D_2O , 400 MHz) δ 1.39 (t, $J=18$ Hz, 3H), 2.57 (s, 3H), 3.87 (m, 8H), 4.29 (q, $J=18$ Hz, 2H), 7.45 (s, 1H), 7.57 (s, 1H). ^{13}C NMR (D_2O , 400 MHz) δ 13.48, 13.72, 44.11, 44.94, 61.53, 61.58, 66.25, 105.77, 106.60, 108.11, 114.53, 123.18, 139.99, 140.26, 149.66, 154.36, 165.33, 166.19. ESI HRMS (-ve) m/z calcd for $C_{17}H_{18}O_{10}SNa [(M-Na)^-]$ 428.0332, found 428.0889 (M-Na)⁻.

5i: 1H NMR (D_2O , 400 MHz) δ 2.51 (s, 3H), 3.63 (s, 3H), 4.65 (d, 2H), 5.02 (d, 1H), 5.16 (d, 2H), 5.91 (m, 1H), 6.81 (s, 1H), 7.56 (s, 1H). ^{13}C NMR (D_2O , 400 MHz) δ 13.40, 55.05, 61.19, 70.68, 97.79, 107.91, 113.75, 114.30, 118.36, 128.61, 128.99, 138.55, 148.09, 150.16, 158.52, 163.59, 165.06. ESI HRMS (+ve) m/z calcd. for $C_{20}H_{19}O_9SNa [(M+Na)^+]$ 481.0632, found 481.1400 (M+Na)⁺.

5j: 1H NMR (D_2O , 400 MHz) δ 1.28 (t, $J=18$ Hz, 3H), 2.09 (s, 3H), 3.54 (s, 3H), 4.12 (q, $J=18$ Hz, 2H), 4.78 (s, 2H), 6.57 (s, 1H), 6.68 (d, $J=21$ Hz, 2H), 7.17 (d, $J=21$ Hz, 2H), 7.67 (s, 1H). ^{13}C NMR (D_2O , 400 MHz) δ 13.40, 55.05, 61.19, 70.68, 97.79, 107.91, 113.75, 114.30, 118.36,

128.61, 128.99, 138.55, 148.09, 150.16, 158.23, 163.59, 165.06. ESI MS (-ve) m/z calcd. for $C_{14}H_{13}O_8SNa [(M-Na)^-]$ 325.03, found 325.04 (M-Na)⁻.

6: 1H NMR (CD_3OD , 300 MHz) δ 2.61 (s, 3H), 3.86 (s, 3H), 6.88 (s, 2H), 7.15 (s, 1H), 7.86 (s, 1H). ^{13}C NMR (CD_3OD , 300 MHz) δ 10.85, 55.78, 59.93, 95.76, 110.69, 112.67, 120.71, 138.55, 150.48, 151.65, 154.22.

7: 1H NMR (CD_3OD , 300 MHz) δ 0.44 (s, 6H), 1.02 (s, 9H), 2.75 (s, 3H), 3.96 (s, 3H), 6.68 (s, 2H), 6.98 (s, 1H), 7.36 (s, 1H). ^{13}C NMR (CD_3OD) δ 4.48, 12.29, 18.70, 26.02, 55.88, 56.04, 95.47, 109.94, 114.31, 120.84, 142.03, 149.32, 149.40, 151.81.

9a: 1H NMR (D_2O , 400 MHz) δ 2.47 (s, 3H), 3.55-3.90 (m, 8H), 3.91 (s, 3H), 7.25 (s, 1H), 7.41 (s, 1H). ^{13}C NMR (D_2O , 400 MHz) δ 12.48, 42.76, 47.82, 56.43, 66.41, 66.79, 96.68, 110.52, 112.70, 118.31, 137.35, 149.74, 151.36, 156.79, 166.23. ESI HRMS (-ve) m/z calcd. for $C_{15}H_{16}NO_8SNa [(M-Na)^-]$ 370.0544, found 370.0652 (M-Na)⁻.

9b: 1H NMR (D_2O , 400 MHz) δ 0.89 (d, $J=17$ Hz, 3H), 1.01 (m, 1H), 1.61-1.81 (m, 4H), 2.39 (s, 3H), 2.92 (m, 1H), 3.08 (m, 1H), 3.56 (m, 1H), 3.92 (s, 3H), 4.45 (m, 1H), 7.27 (s, 1H), 7.64 (s, 1H). ^{13}C NMR (D_2O , 400 MHz) δ 12.47, 12.55, 14.88, 20.89, 30.17, 55.67, 56.59, 96.67, 111.46, 112.63, 118.67, 137.67, 149.82, 151.26, 155.45, 165.32. ESI HRMS (-ve) m/z calcd. for $C_{17}H_{20}NO_7SNa [(M-Na)^-]$ 482.1022, found 382.0847 (M-Na)⁻.

10: 1H NMR (D_2O , 400 MHz) δ 1.47 (t, $J=18$ Hz, 3H), 2.71 (m, 4H), 3.81 (m, 4H), 3.95 (s, 3H), 4.02 (s, 2H), 4.39 (q, $J=18$ Hz, 2H), 7.25 (s, 1H), 7.74 (s, 1H). ^{13}C NMR (D_2O , 400 MHz) δ 13.45, 52.47, 52.64, 56.34, 61.82, 66.07, 96.24, 111.83, 114.82, 117.14, 137.95, 150.45, 151.64, 159.30, 164.77. ESI HRMS (-ve) m/z calcd. for $C_{17}H_{20}NO_9SNa [(M-Na)^-]$ 414.0933, found 414.0847 (M-Na)⁻.

12a: ^1H NMR (CD_3OD , 300 MHz) δ 1.32 (t, $J=6$ Hz, 3H), 2.65 (s, 3H), 3.82 (s, 3H), 3.86 (s, 3H), 4.29 (q, $J=6$ Hz, 2H), 5.52 (s, 2H), 7.12 (s, 1H), 7.22 (s, 1H), 7.43 (s, 1H), 8.04 (s, 1H). ^{13}C NMR (CD_3OD) δ 13.12, 13.53, 13.54, 55.65, 60.20, 60.67, 63.93, 95.54, 95.63, 109.19, 112.32, 115.57, 117.40, 118.31, 139.89, 145.50, 149.74, 152.08, 152.20, 158.70, 162.67, 163.51, 164.48. ESI HRMS (-ve) m/z calcd. for $\text{C}_{26}\text{H}_{25}\text{O}_{13}\text{SNa}[(\text{M}-\text{Na})^-]$ 577.1011, found 577.1146 ($\text{M}-\text{Na})^-$.

12b: ^1H NMR (CD_3OD , 300 MHz) δ 2.67 (s, 3H), 3.83 (s, 3H), 3.84 (s, 3H), 3.85 (s, 3H), 3.86 (s, 3H), 5.55 (s, 2H), 7.13 (s, 1H), 7.24 (s, 1H), 7.47 (s, 1H), 8.03 (s, 1H). ESI HRMS (-ve) m/z calcd. for $\text{C}_{24}\text{H}_{21}\text{O}_{13}\text{SNa}[(\text{M}-\text{Na})^-]$ 549.0723, found 549.0795 ($\text{M}-\text{Na})^-$.

12c: ^1H NMR (CD_3OD , 300 MHz) δ 1.49 (s, 9H), 1.51 (s, 9H), 2.65 (s, 3H), 3.83 (s, 3H), 3.88 (s, 3H), 5.47 (s, 2H), 7.12 (s, 1H), 7.22 (s, 1H), 7.37 (s, 1H), 8.09 (s, 1H). ^{13}C NMR (CD_3OD , 300 MHz) δ 13.09, 27.30, 27.45, 55.59, 55.66, 64.26, 81.00, 81.62, 95.44, 95.56, 109.89, 110.21, 113.55, 115.59, 117.70, 118.42, 139.79, 145.31, 149.83, 151.87, 152.05, 158.16, 162.26, 162.63, 163.80. ESI MS (-ve) m/z calcd. for $\text{C}_{30}\text{H}_{33}\text{O}_{13}\text{SNa}[(\text{M}-\text{Na})^-]$ 633.16, found 633.19 ($\text{M}-\text{Na})^-$.

12d: ^1H NMR (D_2O , 400 MHz) δ 2.30 (s, 3H), 3.26 (s, 3H), 3.32 (s, 3H), 3.57 (m, 2H), 3.63 (m, 5H), 3.77 (s, 3H), 4.18 (m, 2H), 4.27 (m, 2H), 5.17 (s, 2H), 6.49 (s, 1H), 6.89 (s, 1H), 6.93 (s, 1H), 7.67 (s, 1H). ^{13}C NMR (D_2O , 400 MHz) δ 13.49, 55.40, 56.07, 58.13, 58.24, 62.74, 62.96, 63.79, 69.76, 69.89, 93.22, 95.76, 105.85, 107.40, 111.06, 114.98, 116.73, 117.17, 138.28, 144.55, 147.64, 148.10, 150.78, 151.62, 158.55, 162.96, 163.49, 164.40. ESI HRMS (-ve) m/z calcd. for $\text{C}_{28}\text{H}_{29}\text{O}_{115}\text{SNa}[(\text{M}-\text{Na})^-]$ 637.1223, found 637.1161 ($\text{M}-\text{Na})^-$.

12e: ^1H NMR (D_2O , 400 MHz) δ 1.14 (m, 12H), 2.32 (s, 3H), 3.72 (m, 4H), 4.06 (m, 4H), 5.15 (s, 2H), 6.51 (s, 1H), 6.71 (s, 1H), 6.98 (s, 1H), 7.56 (s, 1H). ESI HRMS (-ve) m/z calcd. for $\text{C}_{28}\text{H}_{29}\text{O}_{13}\text{SNa}[(\text{M}-\text{Na})^-]$ 605.1312, found 605.0708 ($\text{M}-\text{Na})^-$.

12f: ^1H NMR (D_2O , 400 MHz) δ 1.07 (m, 18H), 2.27 (s, 3H), 3.99 (m, 4H), 4.20 (m, 2H), 5.05 (s, 2H), 6.64 (s, 1H), 6.67 (s, 1H), 6.99 (s, 1H), 7.81 (s, 1H). ^{13}C NMR (D_2O , 400 MHz) δ 13.29, 13.50, 13.69, 13.78, 20.94, 21.19, 21.40, 60.34, 61.09, 63.81, 71.86, 72.97, 98.90, 108.13, 111.04, 114.71, 117.74, 118.33, 139.92, 146.62, 146.72, 148.33, 148.60, 151.24, 158.69, 162.57, 163.34, 164.08. ESI HRMS (-ve) m/z calcd. for $\text{C}_{30}\text{H}_{33}\text{O}_{13}\text{SNa}$ [(M-Na) $^-$] 633.1236, found 633.1494 (M-Na) $^-$.

13: ^1H NMR (CD_3OD , 400 MHz) δ 1.38 (m, 6H), 2.60 (m, 3H), 3.71 (m, 4H), 3.91 (s, 3H), 3.93 (s, 3H), 4.37 (m, 6H), 5.62 (s, 2H), 7.02 (s, 1H), 7.05 (s, 1H), 7.49 (s, 1H), 8.01 (s, 1H). ESI MS (-ve) m/z calcd. for $\text{C}_{30}\text{H}_{32}\text{NO}_{14}\text{SNa}$ [(M-Na) $^-$] 659.14, found 659.15 (M-Na) $^-$.

14: ^1H NMR (D_2O , 400 MHz) δ 2.40 (s, 3H), 3.24 (m, 8H), 3.67 (m, 8H), 3.81 (s, 3H), 3.92 (s, 3H), 5.30 (s, 2H), 6.85 (s, 1H), 7.14 (s, 1H), 7.33 (s, 1H), 7.43 (s, 1H). ^{13}C NMR (D_2O , 400 MHz) δ 12.36, 42.55, 56.00, 56.40, 63.52, 66.17, 66.36, 96.23, 96.73, 107.16, 110.44, 113.33, 115.29, 116.94, 117.92, 138.10, 143.04, 148.81, 149.45, 151.21, 151.81, 152.46, 156.38, 164.20, 165.93. ESI HRMS (-ve) m/z calcd. for $\text{C}_{30}\text{H}_{31}\text{N}_2\text{O}_{13}\text{SNa}$ [(M-Na) $^-$] 659.1422, found 659.1531 (M-Na) $^-$.

17: ^1H NMR (D_2O , 400 MHz) δ 1.23 (m, 6H), 2.36 (s, 3H), 3.70 (s, 3H), 4.18 (m, 4H), 5.23 (s, 2H), 6.96 (s, 1H), 7.03 (s, 1H), 7.53 (s, 1H), 7.62 (s, 1H). ^{13}C NMR (D_2O , 400 MHz) δ 13.4, 13.51, 13.59, 56.30, 61.53, 62.08, 63.51, 96.28, 99.06, 108.05, 111.73, 114.48, 115.06, 117.13, 119.54, 138.31, 138.82, 147.96, 150.23, 150.94, 152.02, 158.07, 164.50, 164.87, 165.60. ESI HRMS (-ve) m/z calcd. for $\text{C}_{25}\text{H}_{22}\text{O}_{14}\text{S}_2\text{Na}$ [(M-Na) $^-$] 665.0121, found 665.0366 (M-Na) $^-$.

18: ^1H NMR (D_2O , 400 MHz) δ 1.55 (t, $J=18$ Hz, 3H), 1.59 (t, $J=18$ Hz, 3H), 2.41 (s, 3H), 3.81 (s, 3H), 4.18 (q, $J=18$ Hz, 2H), 4.23 (q, $J=18$ Hz, 2H), 5.18 (s, 2H), 6.71 (s, 1H), 6.89 (s, 1H), 7.65 (s, 1H), 7.91 (s, 1H). ^{13}C NMR (D_2O , 400 MHz) δ 13.47, 13.61, 13.63, 56.32, 61.53, 62.18,

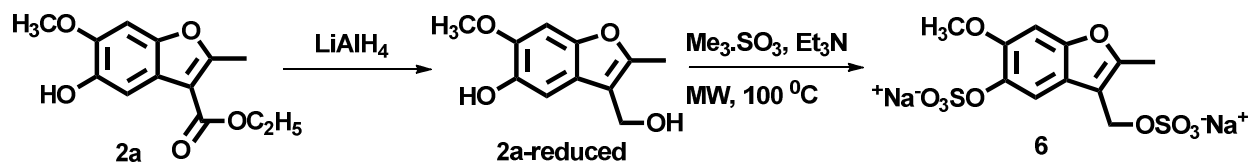
63.61, 96.28, 99.16, 108.01, 111.53, 114.48, 115.06, 117.13, 119.54, 138.31, 138.82, 147.96, 150.23, 150.84, 152.12, 158.17, 164.53, 164.77, 165.60. ESI HRMS (-ve) m/z calcd. for $C_{25}H_{22}O_{14}S_2Na [(M-Na)^-]$ 665.0121, found 665.0277 (M-Na)⁻.

19: ¹H NMR (CDCl₃, 300 MHz) δ 1.39 (m, 6H), 2.67 (s, 3H), 3.85 (s, 3H), 3.88 (s, 3H), 4.36 (m, 4H), 5.55 (s, 2H), 7.22 (s, 1H), 7.23 (s, 1H), 7.43 (s, 1H), 8.07 (s, 1H). ¹³C NMR (CD₃OD, 400 MHz) δ 13.25, 13.38, 13.52, 55.66, 55.77, 60.25, 60.79, 63.16, 95.63, 99.17, 103.95, 108.76, 112.48, 115.58, 117.27, 120.11, 139.90, 146.40, 148.00, 148.45, 152.15, 152.23, 158.27, 163.04, 163.59, 164.61. ESI HRMS (-ve) m/z calcd. for $C_{26}H_{25}O_{13}SNa [(M-Na)^-]$ 577.1011, found 577.1100 (M-Na)⁻.

Synthesis of 15

To a solution of **12a** (100 mg, 0.16 mmol) in 2 mL of methanol was added LiOH (20 mg, 0.8 mmol) and stirred for 5 h at RT. After completion, the reaction mixture was concentrated and purified using HPLC (see Appendix, Page 301 for NMR spectra). ¹H NMR (D₂O, 400 MHz) δ 2.66 (s, 3H), 3.84 (s, 3H), 3.89 (s, 3H), 5.52 (s, 2H), 7.11 (s, 1H), 7.27 (s, 1H), 7.41 (s, 1H), 8.01 (s, 1H). ¹³C NMR (CD₃OD, 400 MHz) δ 13.43, 61.67, 63.73, 95.54, 95.63, 109.19, 112.32, 115.57, 117.40, 118.31, 139.89, 145.50, 149.74, 152.08, 152.20, 158.54, 162.57, 164.51, 165.48. ESI HRMS (-ve) m/z calcd. for $C_{17}H_{20}NO_9SNa [(M-Na)^-]$ 521.0322, found 521.1496 (M-Na)⁻.

Synthesis of 6 from 2a

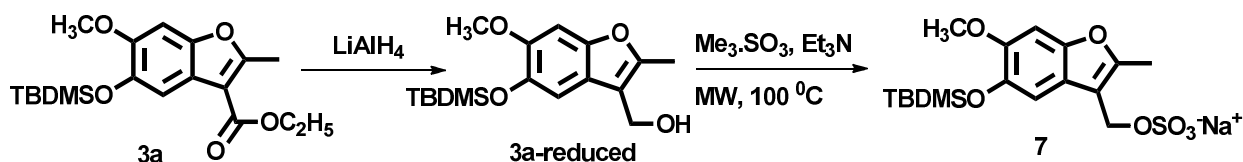


To a solution of **2a** (0.5 mmol) in toluene was added lithium aluminum hydride (2.5 mmol) and stirred for 4 hours at RT. The reaction was quenched by adding water. The reaction mixture was extracted with ethyl ether twice. The organic layer was concentrated under vacuum and purified by flash chromatography using ethyl acetate in hexanes (0-40%). The reduced form of **2a** was sulfated by method described previously in this chapter (see Appendix, Page 250 for NMR spectra).

2a-reduced: ^1H NMR (CDCl_3 , 300 MHz) δ 2.75 (s, 3H), 3.96 (s, 3H), 5.58 (s, 2H), 6.98 (s, 1H), 7.36 (s, 1H).

6: ^1H NMR (CD_3OD , 300 MHz) δ 2.61 (s, 3H), 3.86 (s, 3H), 6.88 (s, 2H), 7.15 (s, 1H), 7.86 (s, 1H). ^{13}C NMR (CD_3OD , 300 MHz) δ 10.85, 55.78, 59.93, 95.76, 110.69, 112.67, 120.71, 138.55, 150.48, 151.65, 154.22.

Synthesis of **7** from **3a**

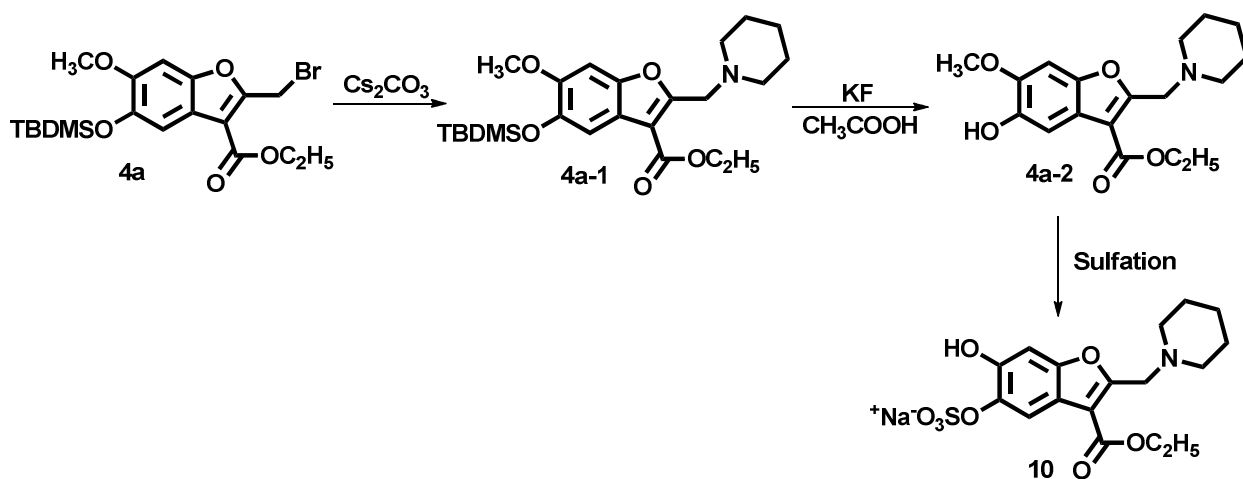


To a solution of **3a** (0.5 mmol) in toluene was added lithium aluminum hydride (4 mmol) and stirred for 4 hours at RT. The reaction was quenched by adding water. The reaction mixture was extracted with ethyl ether twice. The organic layer was concentrated under vacuum and purified by flash chromatography using ethyl acetate in hexanes (0-40%). The reduced form of **3a** is sulfated by method described previously in this chapter (see Appendix, Page 250 for NMR spectra).

3a-reduced: ^1H NMR (CDCl_3 , 300 MHz) δ 0.44 (s, 6H), 1.02 (s, 9H), 2.75 (s, 3H), 3.96 (s, 3H), 5.58 (s, 2H), 6.98 (s, 1H), 7.36 (s, 1H). ^{13}C NMR (CDCl_3 , 300 MHz) δ 4.48, 12.29, 18.70, 26.02, 55.88, 56.04, 95.47, 109.94, 114.31, 120.84, 142.03, 149.32, 149.40, 151.81.

7: ^1H NMR (CD_3OD , 300 MHz) δ 0.44 (s, 6H), 1.02 (s, 9H), 2.75 (s, 3H), 3.96 (s, 3H), 6.68 (s, 2H), 6.98 (s, 1H), 7.36 (s, 1H). ^{13}C NMR (CD_3OD , 300 MHz) δ 4.48, 12.29, 18.70, 26.02, 55.88, 56.04, 95.47, 109.94, 114.31, 120.84, 142.03, 149.32, 149.40, 151.81.

Synthesis of 10 from 4a



To the solution of **4a** (0.3 mmol) in DMF was added Morpholine (0.4 mmol) and cesium carbonate (0.4 mmol) and stirred for 8 hrs at RT. The reaction was quenched by adding methylene chloride and extracted with brine. The organic layer was concentrated and purified by flash chromatography using ethyl acetate in hexanes (0-40%). To the solution of intermediate **4a-1** (0.3 mmol) in DMF (3 mL) were added KF (4 mmol) and acetic acid (10 μL). The reaction mixture was stirred for 5 hours. The reaction was quenched by methylene chloride and extracted with brine solution. The organic layer was combined and dried over magnesium sulfate and concentrated. The solid was precipitated using methanol to obtain intermediate **4a-2** in 90%

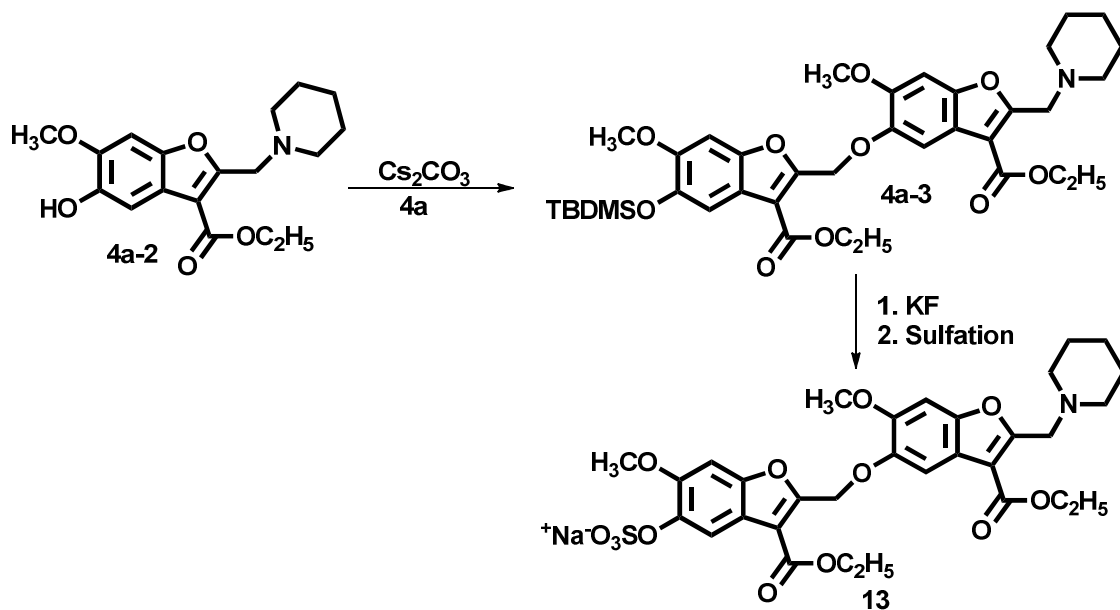
yield. Compound **10** was obtained by the sulfation reaction previously described (see Appendix, Page 252 and 255 for NMR spectra)

4a-1: ^1H NMR (CDCl_3 , 400 MHz) δ 1.44 (t, $J=18$ Hz, 4H), 2.63 (s, 4H), 3.74 (s, 4H), 4.11 (s, 2H), 4.39 (q, $J=18$ Hz, 3H), 7.02 (s, 1H), 7.48 (s, 1H).

4a-2: ^1H NMR (CDCl_3 , 400 MHz) δ 1.45 (t, $J=18$ Hz, 3H), 2.67 (m, 4H), 3.76 (m, 4H), 3.94 (s, 3H), 4.15 (s, 2H), 4.40 (q, $J=18$ Hz, 3H), 7.03 (s, 1H), 7.48 (s, 1H).

10: ^1H NMR (D_2O , 400 MHz) δ 1.47 (t, $J=18$ Hz, 3H), 2.71 (m, 4H), 3.81 (m, 4H), 3.95 (s, 3H), 4.02 (s, 2H), 4.39 (q, $J=18$ Hz, 2H), 7.25 (s, 1H), 7.74 (s, 1H). ^{13}C NMR (D_2O , 400 MHz) δ 13.45, 52.47, 52.64, 56.34, 61.82, 66.07, 96.24, 111.83, 114.82, 117.14, 137.95, 150.45, 151.64, 159.30, 164.77. ESI HRMS (-ve) m/z calcd. for $\text{C}_{17}\text{H}_{20}\text{NO}_9\text{SNa}$ [(M-Na) $^-$] 414.0933, found 414.0847 (M-Na) $^-$.

Synthesis of 13 from 4a



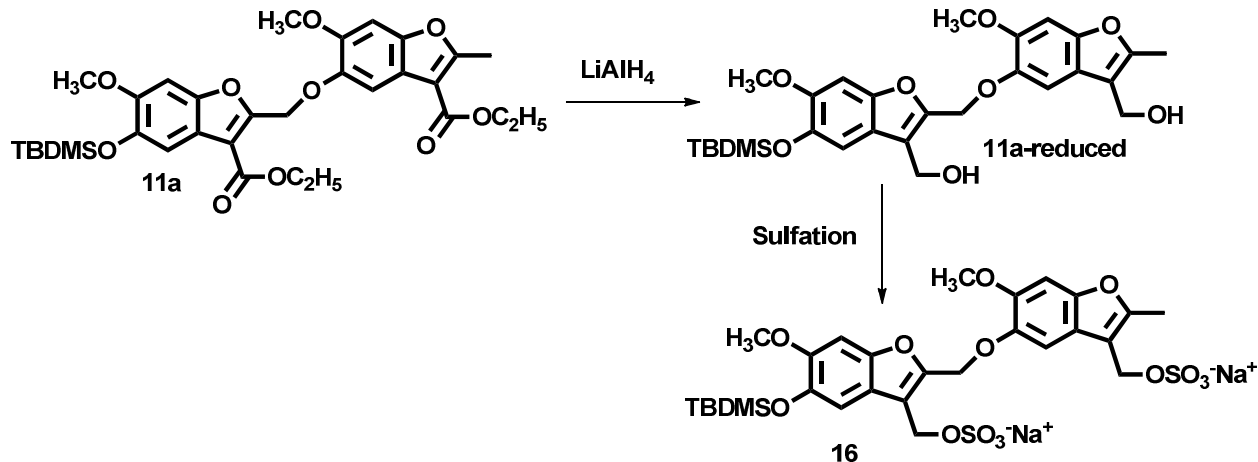
To a solution of **4a-2** (0.3 mmol) and **4a** (0.4 mmol) in ethyl acetate (4 mL) were added cesium carbonate (0.3 mmol) and anhydrous DMF (1 mL). The reaction mixture was stirred under nitrogen for 15 hours at room temperature. The reaction was quenched with methylene chloride and extracted with brine. The organic layer was dried over magnesium sulphate and concentrated. Purification was done by using flash chromatography on silica gel using 0-70% ethyl acetate in hexanes. The product **4a-3** was obtained in 60% yield. The deprotection step followed by sulfation (performed as explained previously) yielded the product **13** (see Appendix, Page 252 and 266 for NMR spectra).

4a-3: ^1H NMR (CDCl_3 , 400 MHz) δ 0.17 (s, 6H), 1.03 (s, 9H), 1.39 (m, 6H), 2.62 (m, 4H), 3.65 (m, 4H), 3.73 (s, 3H), 3.82 (s, 3H), 4.36 (m, 6H), 5.61 (s, 2H), 7.00 (s, 1H), 7.06 (s, 1H), 7.45 (s, 1H), 7.62 (s, 1H).

4a-3 (deprotected form): ^1H NMR (CDCl_3 , 400 MHz) δ 1.38 (m, 6H), 2.60 (m, 3H), 3.71 (m, 4H), 3.91 (s, 3H), 3.93 (s, 3H), 4.37 (m, 6H), 5.62 (s, 2H), 7.02 (s, 1H), 7.05 (s, 1H), 7.49 (s, 1H), 7.59 (s, 1H).

13: ^1H NMR (CD_3OD , 400 MHz) δ 1.38 (m, 6H), 2.60 (m, 3H), 3.71 (m, 4H), 3.91 (s, 3H), 3.93 (s, 3H), 4.37 (m, 6H), 5.62 (s, 2H), 7.02 (s, 1H), 7.05 (s, 1H), 7.49 (s, 1H), 8.01 (s, 1H). ESI MS (-ve) m/z calcd. for $\text{C}_{30}\text{H}_{32}\text{NO}_{14}\text{SNa}$ [(M-Na) $^-$] 659.14, found 659.15 (M-Na) $^-$.

Synthesis of 16 from 11a



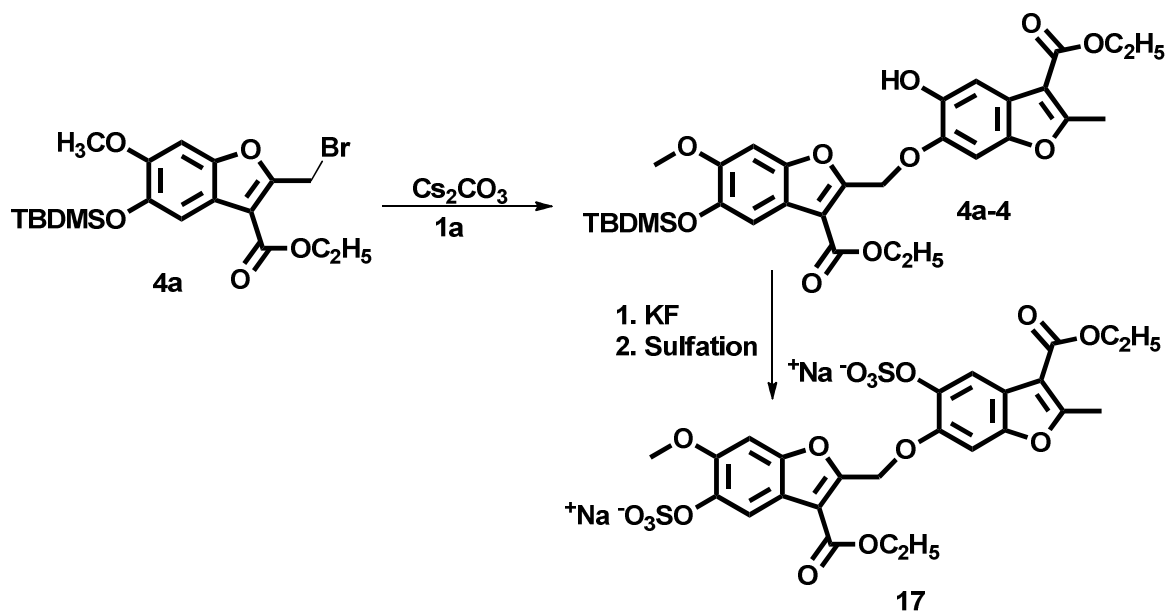
To a solution of **11a** (200 mg, 0.32 mmol) in 10 mL of dry THF was added LiAlH_4 (65 mg, 1.6 mmol) and stirred for 6 hours under nitrogen. After completion, the reaction was quenched by adding 30 mL of water and extracted with 100 mL of ethyl ether twice. The organic layer was concentrated down and purified with flash chromatography using ethyl acetate in hexanes (0–50%). The reduced form of **11a** was sulfated using the general sulfation procedure explained previously (see Appendix, Page 270 for NMR spectra).

11a-reduced: ^1H NMR (CDCl_3 , 300 MHz) δ 0.17 (s, 6H), 1.01 (s, 9H), 2.71 (s, 3H), 3.87 (s, 3H), 3.91 (s, 3H), 5.51 (s, 2H), 5.55 (s, 2H), 5.60 (s, 2H), 6.95 (s, 1H), 6.99 (s, 1H), 7.42 (s, 1H), 7.55 (s, 1H).

16. ^1H NMR (CD_3OD , 300 MHz) δ 0.17 (s, 6H), 1.01 (s, 9H), 2.71 (s, 3H), 3.87 (s, 3H), 3.91 (s, 3H), 5.51 (s, 2H), 6.65 (s, 2H), 6.69 (s, 2H), 7.01 (s, 1H), 7.04 (s, 1H), 7.37 (s, 1H), 7.45 (s, 1H).

^{13}C NMR (CDCl_3 , 300 MHz) δ 4.47, 12.31, 18.70, 26.00, 55.45, 55.81, 55.94, 56.58, 94.60, 95.48, 103.35, 114.35, 118.34, 120.39, 121.24, 142.32, 142.65, 144.82, 148.21, 149.73, 152.05.

Synthesis of 17 from 4a and 1a



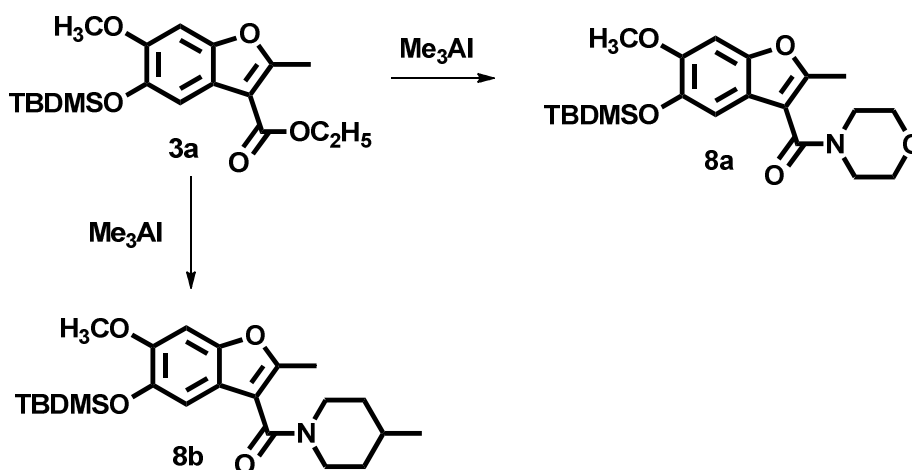
To a solution of **1a** (0.3 mmol) and **4a** (0.4 mmol) in ethyl acetate (4 mL) were added cesium carbonate (0.3 mmol) and anhydrous DMF (1 mL). The reaction mixture was stirred under nitrogen for 15 hours at room temperature. The reaction was quenched with methylene chloride and extracted with brine. The organic layer was dried over magnesium sulfate and concentrated *in vacuo*. Purification was done by using flash chromatography on silica gel using (0-70) % ethyl acetate in hexanes. The product **4a-4** was obtained in 60% yield. The deprotection step followed by the sulfation step (performed as explained previously) yielded the product **17** (see Appendix, Page 264 and 275 for NMR spectra).

4a-4: ^1H NMR (CDCl_3 , 400 MHz) δ 0.03 (s, 6H), 0.04 (s, 6H), 0.96 (s, 9H), 0.97 (s, 9H), 1.36 (m, 6H), 2.72 (s, 3H), 3.81 (s, 3H), 4.15 (m, 4H), 5.34 (s, 2H), 6.78 (s, 1H), 6.80 (s, 1H), 7.22 (s, 1H), 7.37 (s, 1H).

Deprotected 4a-4: ^1H NMR (CDCl_3 , 400 MHz) δ 1.36 (m, 6H), 2.70 (s, 3H), 3.86 (s, 3H), 4.35 (m, 4H), 5.54 (s, 2H), 6.98 (s, 1H), 7.00 (s, 1H), 7.42 (s, 1H), 7.57 (s, 1H).

17: ^1H NMR (D_2O , 400 MHz) δ 1.23 (m, 6H), 2.36 (s, 3H), 3.70 (s, 3H), 4.18 (m, 4H), 5.23 (s, 2H), 6.96 (s, 1H), 7.03 (s, 1H), 7.53 (s, 1H), 7.62 (s, 1H). ^{13}C NMR (D_2O , 400 MHz) δ 13.4, 13.51, 13.59, 56.30, 61.53, 62.08, 63.51, 96.28, 99.06, 108.05, 111.73, 114.48, 115.06, 117.13, 119.54, 138.31, 138.82, 147.96, 150.23, 150.94, 152.02, 158.07, 164.50, 164.87, 165.60. ESI HRMS (-ve) m/z calcd. for $\text{C}_{25}\text{H}_{22}\text{O}_{14}\text{S}_2\text{Na}$ [(M-Na) $^-$] 665.0121, found 665.0366 (M-Na) $^-$.

Synthesis of 8a & 8b from 3a

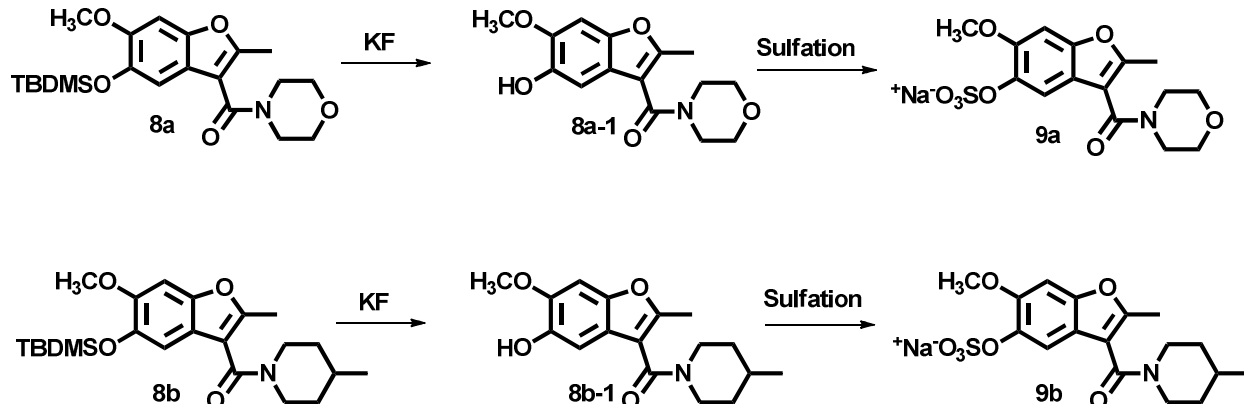


To a solution of trimethyl aluminum (1.5 mmol) in THF was added Morpholine or 4-methyl Piperidine (1.5 mmol). The solution was stirred for 1 hour at RT. The solution of **3a** (1 mmol) in THF was added to drop wise to the above solution over the time of 30 mins. The reaction mixture was stirred at 70 $^\circ\text{C}$ for 24 hours. The reaction was quenched by adding ethyl acetate and extracted with brine. The organic layer was concentrated and purified by flash chromatography using ethyl acetate and hexanes (0-70 %) (See Appendix, Page 256 for NMR spectra).

8a: ^1H NMR (CDCl_3 , 400 MHz) δ 0.13 (s, 6H), 1.00 (s, 9H), 2.48 (s, 3H), 3.64 (m, 8H), 3.78 (s, 3H), 6.84 (s, 1H), 6.93 (s, 1H).

8b: ^1H NMR (CDCl_3 , 400 MHz) δ 0.11 (s, 6H), 0.97 (d, $J=18$ Hz, 3H), 0.98 (s, 9H), 1.65 (m, 4H), 2.44 (s, 3H), 2.88 (m, 2H), 2.98 (m, 2H), 3.80 (s, 3H), 6.86 (s, 1H), 6.93 (s, 1H).

Synthesis of 9a and 9b



The deprotection step followed by the sulfation step (performed as explained previously) yielded the product **9a** and **9b** (see Appendix, Page 248 for NMR spectra).

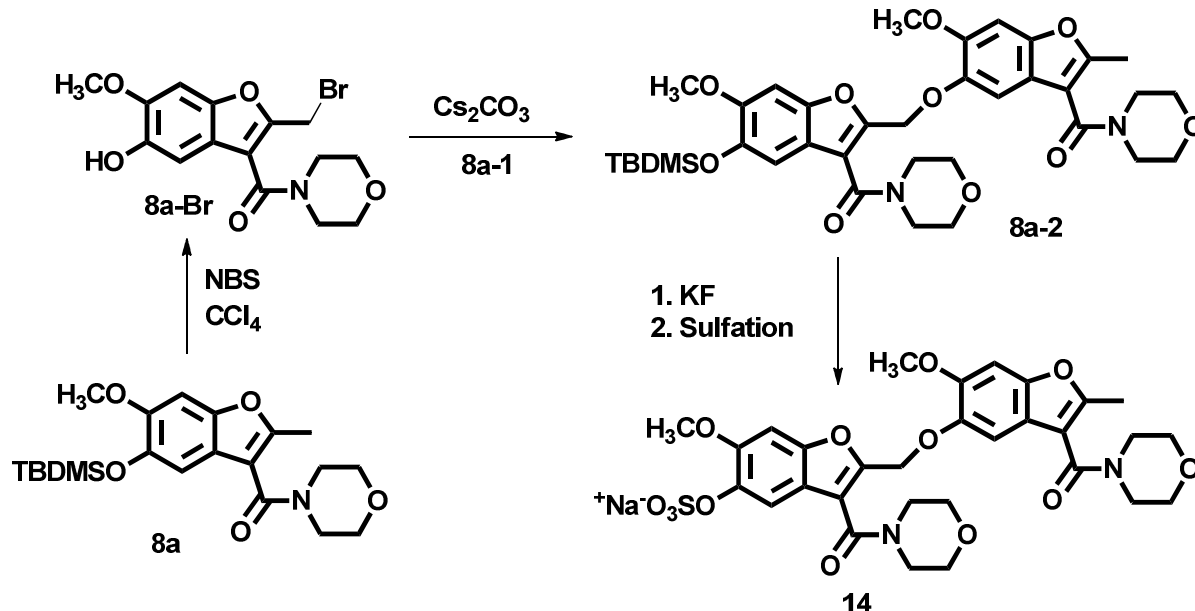
8a-1: ^1H NMR (CDCl_3 , 400 MHz) δ 2.48 (s, 3H), 3.69 (m, 8H), 3.91 (s, 3H), 6.91 (s, 1H), 6.94 (s, 1H).

8b-1: ^1H NMR (CDCl_3 , 400 MHz) δ 0.97 (d, $J=18$ Hz, 3H), 1.67 (m, 4H), 2.46 (s, 3H), 2.88 (m, 2H), 2.98 (m, 2H), 3.80 (s, 3H), 6.86 (s, 1H), 6.93 (s, 1H).

9a: ^1H NMR (D_2O , 400 MHz) δ 2.47 (s, 3H), 3.55-3.90 (m, 8H), 3.91 (s, 3H), 7.25 (s, 1H), 7.41 (s, 1H). ^{13}C NMR (D_2O , 400 MHz) δ 12.48, 42.76, 47.82, 56.43, 66.41, 66.79, 96.68, 110.52, 112.70, 118.31, 137.35, 149.74, 151.36, 156.79, 166.23. ESI HRMS (-ve) m/z calcd. for $\text{C}_{15}\text{H}_{16}\text{NO}_8\text{SNa}$ [(M-Na) $^-$] 370.0544, found 370.0652 (M-Na) $^-$.

9b: ^1H NMR (D_2O , 400 MHz) δ 0.89 (d, $J=17$ Hz, 3H), 1.01 (m, 1H), 1.61-1.81 (m, 4H), 2.39 (s, 3H), 2.92 (m, 1H), 3.08 (m, 1H), 3.56 (m, 1H), 3.92 (s, 3H), 4.45 (m, 1H), 7.27 (s, 1H), 7.64 (s, 1H). ^{13}C NMR (D_2O , 400 MHz) δ 12.47, 12.55, 14.88, 20.89, 30.17, 55.67, 56.59, 96.67, 111.46, 112.63, 118.67, 137.67, 149.82, 151.26, 155.45, 165.32. ESI HRMS (-ve) m/z calcd. for $\text{C}_{17}\text{H}_{20}\text{NO}_7\text{SNa}$ [(M-Na) $^-$] 482.1022, found 382.0847 (M-Na) $^-$.

Synthesis of 14 from 8a



To a solution of **8a** (1 mmol) in THF (20 mL) was added NBS (1 mmol) and the mixture was refluxed at 65 °C under a halogen lamp for 1 hour. The reaction mixture was cooled and extracted using hexanes and water. The organic layer was concentrated and product **8a-Br** was obtained in 90% yield.

To a solution of **8a-1** (0.3 mmol) and **8a-Br** (0.4 mmol) in ethyl acetate (4 mL) were added cesium carbonate (0.3 mmol) and anhydrous DMF (1 mL). The reaction mixture was stirred under nitrogen for 15 hours at room temperature. The reaction was quenched with methylene chloride and extracted with brine. The organic layer was dried over magnesium sulphate and concentrated *in vacuo*. Purification was done by using flash chromatography on silica gel using (0-70) % ethyl acetate in hexanes. The product **4a-4** was obtained in 60% yield. The deprotection step followed by the sulfation step (performed as explained previously) yielded the product **14** (see Appendix, Page 268 and 276 for NMR spectra).

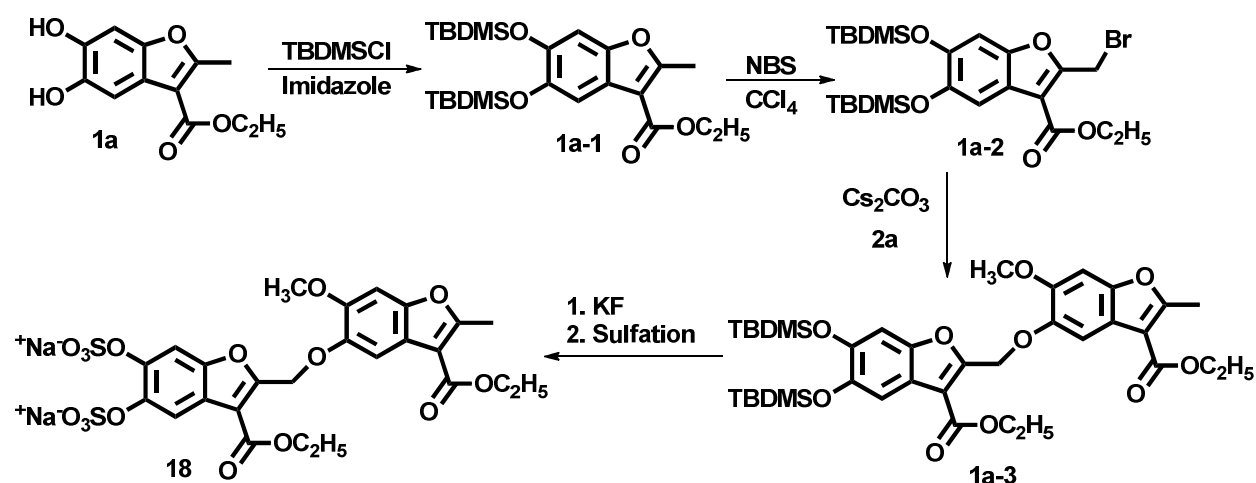
8a-Br: ^1H NMR (CDCl_3 , 400 MHz) δ 0.14 (s, 6H), 1.01 (s, 9H), 3.72 (m, 8H), 3.85 (s, 3H), 4.69 (s, 2H), 6.85 (s, 1H), 6.99 (s, 1H).

8a-2: ^1H NMR (CDCl_3 , 400 MHz) δ 0.14 (s, 6H), 1.01 (s, 9H), 2.49 (s, 3H), 3.74 (m, 16H), 3.85 (s, 3H), 3.87 (s, 3H), 5.24 (s, 2H), 6.90 (s, 1H), 7.00 (s, 1H), 7.02 (s, 1H), 7.11 (s, 1H).

8a-2 (deprotected form): ^1H NMR (CDCl_3 , 400 MHz) δ 2.48 (s, 3H), 3.74 (m, 16H), 3.87 (s, 3H), 3.96 (s, 3H), 5.25 (s, 2H), 6.99 (s, 1H), 7.04 (s, 1H), 7.09 (s, 1H), 7.12 (s, 1H).

14: ^1H NMR (D_2O , 400 MHz) δ 2.40 (s, 3H), 3.24 (m, 8H), 3.67 (m, 8H), 3.81 (s, 3H), 3.92 (s, 3H), 5.30 (s, 2H), 6.85 (s, 1H), 7.14 (s, 1H), 7.33 (s, 1H), 7.43 (s, 1H). ^{13}C NMR (D_2O) δ 12.36, 42.55, 56.00, 56.40, 63.52, 66.17, 66.36, 96.23, 96.73, 107.16, 110.44, 113.33, 115.29, 116.94, 117.92, 138.10, 143.04, 148.81, 149.45, 151.21, 151.81, 152.46, 156.38, 164.20, 165.93. ESI HRMS (-ve) m/z calcd. for $\text{C}_{30}\text{H}_{31}\text{N}_2\text{O}_{13}\text{SNa}$ [(M-Na) $^-$] 659.1422, found 659.1531 (M-Na) $^-$.

Synthesis of 18 from 1a



The protection of the free phenolic groups of **1a** with TBDMSO (as per procedure for synthesis of **3a–3f**) followed by the introduction of the bromo group (as per procedure for synthesis of **4a–4f**) leads to synthesis of intermediate **1a-2**. Coupling intermediate **1a-2** with **2a** using the

procedure described above (synthesis of **5a–5f**) leads to formation of intermediate **1a-3**. The deprotection step followed by the sulfation step (performed as explained previously) yielded the product **18** (see Appendix, Page 256, 260, 266 and 280 for NMR spectra).

1a-1: ^1H NMR (CDCl_3 , 400 MHz) δ 0.12 (s, 12H), 1.05 (s, 18H), 1.37 (t, $J=18$ Hz, 3H), 2.71 (s, 3H), 4.40 (q, $J=18$ Hz, 2H), 6.95 (s, 1H), 7.30 (s, 1H).

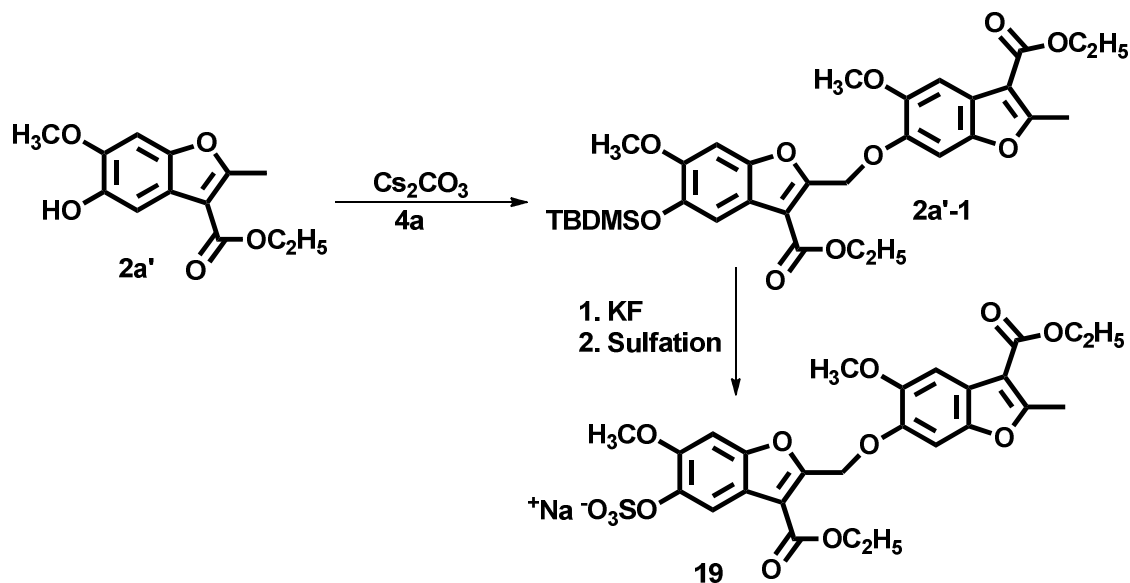
1a-2: ^1H NMR (CDCl_3 , 400 MHz) δ 0.10 (s, 12H), 1.05 (s, 18H), 1.34 (t, $J=18$ Hz, 3H), 4.21 (q, $J=18$ Hz, 2H), 6.99 (s, 1H), 7.23 (s, 1H).

1a-3: ^1H NMR (CDCl_3 , 400 MHz) δ 0.04 (s, 6H), 0.09 (s, 6H), 1.01 (s, 9H), 1.05 (s, 9H), 1.43 (m, 6H), 2.62 (s, 3H), 3.81 (s, 3H), 4.15 (m, 4H), 5.34 (s, 2H), 6.88 (s, 1H), 6.96 (s, 1H), 7.22 (s, 1H), 7.37 (s, 1H).

1a-3 (deprotected form): ^1H NMR (CDCl_3 , 400 MHz) δ 1.35 (m, 6H), 2.71 (s, 3H), 3.84 (s, 3H), 4.37 (m, 4H), 5.52 (s, 2H), 6.98 (s, 1H), 7.12 (s, 1H), 7.35 (s, 1H), 7.47 (s, 1H).

18: ^1H NMR (D_2O , 400 MHz) δ 1.55 (t, $J=18$ Hz, 3H), 1.59 (t, $J=18$ Hz, 3H), 2.41 (s, 3H), 3.81 (s, 3H), 4.18 (q, $J=18$ Hz, 2H), 4.23 (q, $J=18$ Hz, 2H), 5.18 (s, 2H), 6.71 (s, 1H), 6.89 (s, 1H), 7.65 (s, 1H), 7.91 (s, 1H). ^{13}C NMR (D_2O , 400 MHz) δ 13.47, 13.61, 13.63, 56.32, 61.53, 62.18, 63.61, 96.28, 99.16, 108.01, 111.53, 114.48, 115.06, 117.13, 119.54, 138.31, 138.82, 147.96, 150.23, 150.84, 152.12, 158.17, 164.53, 164.77, 165.60. ESI HRMS (-ve) m/z calcd. for $\text{C}_{25}\text{H}_{22}\text{O}_{14}\text{S}_2\text{Na}[(\text{M}-\text{Na})^-]$ 665.0121, found 665.0277 ($\text{M}-\text{Na})^-$.

Synthesis of 19



To a solution of **2a'** (0.3 mmol) and **4a** (0.4 mmol) in ethyl acetate (4 mL) were added cesium carbonate (0.3 mmol) and anhydrous DMF (1 mL). The reaction mixture was stirred under nitrogen for 15 hours at room temperature. The reaction was quenched with methylene chloride and extracted with brine. The organic layer was dried over magnesium sulphate and concentrated *in vacuo*. Purification was done by using flash chromatography on silica gel using 0-70% ethyl acetate in hexanes. The product **2a'-1** was obtained in 60% yield. The deprotection step followed by the sulfation step (performed as explained previously) yielded the product **19** (see Appendix, Page 270 and 277 for NMR spectra).

2a': ^1H NMR (CDCl_3 , 300 MHz) δ 1.48 (t, $J=6$ Hz, 3H), 2.75 (s, 3H), 3.94 (s, 3H), 4.40 (q, $J=6$ Hz, 2H, CH_2), 7.03 (s, 1H), 7.43 (s, 1H).

2a'-1: ^1H NMR (CDCl_3 , 300 MHz) δ 0.16 (s, 6H), 1.01 (s, 9H), 1.41 (m, 6H), 2.70 (s, 3H), 3.83 (s, 3H), 3.92 (s, 3H), 4.39 (m, 4H), 5.60 (s, 2H), 6.99 (s, 1H), 7.21 (s, 1H), 7.43 (s, 1H), 7.44 (s, 1H). ^{13}C NMR (CDCl_3) δ 4.50, 14.46, 14.63, 14.78, 18.72, 25.97, 55.97, 56.62, 60.42, 60.93,

63.47, 95.47, 98.39, 103.77, 109.21, 112.25, 112.73, 117.90, 119.98, 143.29, 146.34, 147.95, 148.08, 150.20, 150.99, 157.66, 162.77, 164.07, 164.79.

2a'-1 (deprotected form): ^1H NMR (CDCl_3 , 300 MHz) δ 1.43 (t, $J=6$ Hz, 6H), 2.72 (s, 3H), 3.92 (s, 6H), 4.39 (m, 4H), 5.60 (s, 2H), 7.00 (s, 1H), 7.19 (s, 1H), 7.41 (s, 1H), 7.44 (s, 1H). ^{13}C NMR (CDCl_3) δ 14.57, 14.63, 14.77, 56.52, 56.65, 60.42, 61.01, 63.57, 94.71, 98.55, 103.83, 106.24, 109.21, 112.35, 118.39, 120.08, 143.81, 146.34, 147.95, 148.12, 149.07, 157.99, 162.82, 164.06, 164.80.

19: ^1H NMR (CDCl_3 , 300 MHz) δ 1.39 (m, 6H), 2.67 (s, 3H), 3.85 (s, 3H), 3.88 (s, 3H), 4.36 (m, 4H), 5.55 (s, 2H), 7.22 (s, 1H), 7.23 (s, 1H), 7.43 (s, 1H), 8.07 (s, 1H). ^{13}C NMR (CD_3OD , 300 MHz) δ 13.25, 13.38, 13.52, 55.66, 55.77, 60.25, 60.79, 63.16, 95.63, 99.17, 103.95, 108.76, 112.48, 115.58, 117.27, 120.11, 139.90, 146.40, 148.00, 148.45, 152.15, 152.23, 158.27, 163.04, 163.59, 164.61. ESI HRMS (-ve) m/z calcd. for $\text{C}_{26}\text{H}_{25}\text{O}_{13}\text{SNa}$ [(M-Na) $^-$] 577.1011, found 577.1100 (M-Na) $^-$.

3.4.3 Determination of Purity by HPLC Method:

HPLC purification was carried out on a Jasco chromatography system using a Varian Dynamax microsorb C4 column of size 250*10 mm. The mobile phase consisted of acetonitrile – water mixture run at a constant flow rate of 3 mL/min. Absorbance was recorded by a Jasco MD-2010 plus UV-VIS detector at 300 nm. The following HPLC method was used:

Table 5. Method used for purity determination

Time	Solvent A (water)	Solvent B (Acetonitrile)
0	95%	5%
5	95%	5%
15	50%	50%
20	0%	100%
25	0%	100%
30	95%	5%

Table 6. Purity of compounds synthesized

Compound	Retention time (mins)	% purity
5a	16.21	98.12
5b	15.38	98.09
5c	16.64	98.56
5d	14.69	96.56
5e	15.85	98.34
5f	16.32	97.87
5g	12.23	78.11
5h	11.60	76.85
5i	16.31	95.15
5j	16.04	98.08
9a	11.22	98.27
9b	11.72	97.59
10^e	13.34	98.52
12a	12.72	99.01
12b	12.01	96.64
12c	13.37	96.22
12d	11.20	95.37
12e	12.97	99.05
12f	13.50	97.52
13	10.34	98.43
14	11.1	98.15
15	8.01	99.13
17	8.34	97.59
18	8.61	98.36
19	12.65	98.27

Chapter 4 Identification of a Novel Binding Site for Allosteric Regulation of Thrombin

4.1 Introduction

In this work, we present the enzyme inhibition and Michaelis-Menten kinetic studies for the library of sulfated benzofuran monomers and dimers, synthesized as described in an earlier chapter, that display a range of inhibition potentials and an allosteric mechanism of inhibition. In this study, we also propose a binding site for sulfated benzofuran dimers (SBDs) based on detailed biochemical studies on the interaction of one of the potent SBDs with thrombin combined with molecular modeling techniques. This will encourage for further rational structure-based drug design. Our work reveals that the SBD interacts with exosite II of thrombin, but in a manner dramatically different from all previously known exosite II ligands, including full-length heparin, heparin octasaccharide, sucrose octasulfate, γ' -fibrinogen peptide, and sulfated LMWLs. The identification of a new site of binding on thrombin together with the molecular size, the novelty of inhibitor structures, the nature of their inhibition and allosteric modulation of thrombin, may lead to a powerful alternative to the competitive inhibitors approved to date. This work puts forward a distinct direction in the terms of the site of binding and thrombin inhibitor structures that will re-direct the search for allosteric modulators of coagulation enzymes, especially thrombin.

4.2 Results

4.2.1 Thrombin Inhibition Potential of Designed Sulfated Benzofuran Monomers and Dimer

Inhibition of thrombin by the designed benzofurans (in Chapter 3) was measured through Spectrozyme TH hydrolysis assay, as described earlier.^{213, 214} This assay relies on the decrease in the initial rate of substrate hydrolysis in the presence of the sulfated benzofuran derivative as a quantitative measure of the inhibition. The fractional decrease in the initial rate of hydrolysis typically shows a sigmoidal profile on a semi-log plot, which is then fitted by a dose – response equation 1 (see experimental section 4.4.2) to derive IC_{50} , HS , Y_0 and Y_M parameters for each potential inhibitor.

Figure 18 shows the semi-log inhibition curves observed for selected benzofuran monomers and dimers from the library shown in Figure 17 (See Chapter 3). Of the 28 potential inhibitors studied in this work, only 11 molecules exhibited reasonable inhibition of human α -thrombin at pH 7.4 and 25 °C. These included the sulfated monomer **5i** and dimers **12a** – **12f**, **13**, and **17** – **19** (Tables 7 and 8). Within this group, inhibitors **12b**, **12c**, and **12f** were the only molecules exhibiting IC_{50} less than 50 μ M. The *t*-butyl derivative **12c** was found to be the most potent thrombin inhibitor with an IC_{50} of 7.3 μ M under physiologically relevant conditions.

The range of inhibition efficacy was found to vary considerably with the structure of the inhibitor. For example, the sulfated dimer **12e** displayed essentially complete inhibition of thrombin (95%, Table 8), while dimer **15** with two carboxylic acid groups inhibited to the extent of only 14% (Table 8). Nearly 85% of the inhibitors displayed 60% or more thrombin inhibition suggesting good overall efficacy for sulfated benzofurans.

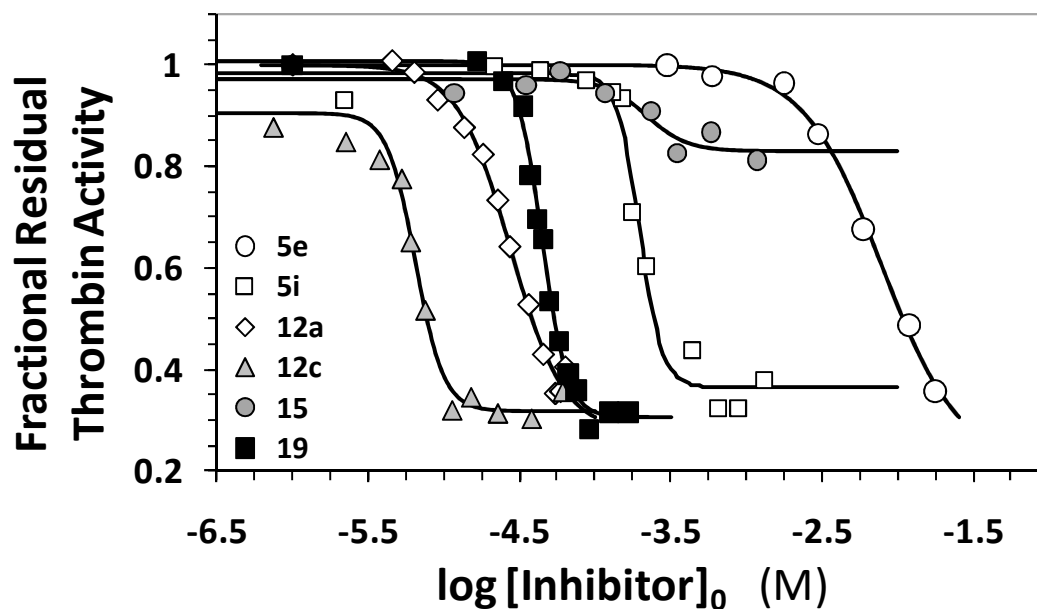


Figure 18. Direct inhibition of thrombin by designed sulfated benzofuran monomers and dimers. The inhibition of human thrombin was determined spectrophotometrically through a Spectrozyme TH hydrolysis assay at pH 7.4 and 25 °C. Solid lines represent sigmoidal fits to the data to obtain IC_{50} , Y_M , and Y_O (equation 1), as described in the experimental section (4.4.2).

Comparison of the two series of benzofuran molecules shows that dimers tend to inhibit thrombin several-fold better than monomers. Of the 15 sulfated monomers studied in this work and 17 sulfated and unsulfated monomers studied earlier,²¹⁸ only **5i** inhibited thrombin with measurable potency (~500 μ M, Table 7). By contrast, most sulfated dimers displayed thrombin inhibition (Table 8). This suggested that larger scaffolds may exhibit higher potency. This also rationalizes the nanomolar potency observed for sulfated LMWL inhibition of thrombin.²¹³

Table 7. Inhibition of Human α -Thrombin by Sulfated Benzofuran Monomers

	R	R'	log IC₅₀ (M)	IC₅₀ (μM)	ΔY
5a	—OCH ₂ CH ₃	—CH ₃	nd ^b	>2500 ^c	-
5b	—OCH ₃	—CH ₃	nd	>3000 ^c	-
5c	—OC(CH ₃) ₃	—CH ₃	nd	>3000 ^c	-
5d	—OCH ₂ CH ₂ OCH ₃	—CH ₃	nd	>2000 ^c	-
5e	—OCH ₂ CH ₃	—CH ₂ CH ₃	-1.7 \pm 0.2 ^d	20560 \pm 8500	0.60
5f	—OCH ₂ CH ₃	—CH(CH ₃) ₂	-1.9 \pm 0.3	13650 \pm 10400	0.75
5g	—OCH ₂ CH ₃	—CH ₂ OCH ₃	nd	>16000 ^c	-
5h	—OCH ₂ CH ₃	Morpholine-4-carbonyl	nd	>25,000 ^c	-
5i	—OCH ₂ CH ₃	Benzoyl- <i>p</i> -methoxy	-3.3 \pm 0.2	520 \pm 280	0.54
5j	—OCH ₂ CH=CH ₂	—CH ₃	nd	>3000	-
9a	<i>N</i> -morpholino	—CH ₃	nd	>2000 ^c	-
9b	<i>N</i> -piperidino	—CH ₃	nd	>2000 ^c	-
10^e	—CH ₂ CH ₃	—CH ₃	nd	>7000 ^c	-

^aThrombin inhibition was measured in spectrophotometric assay through initial rate of Spectrozyme TH hydrolysis as described in Experimental section. ^bNot determined due to incomplete and/or poor inhibition. ^cEstimates on the basis of the highest concentration used in experiment. ^dstandard error shown is ± 1 S.E. ^e**10** contains a morpholine group at the allylic position (instead of a —CH₃ group).

Table 8. Inhibition of Human α -Thrombin by Sulfated Benzofuran Dimers

	R	R'	log IC_{50} (M)	IC_{50} (μM)	ΔY
12a	—OCH ₂ CH ₃	—CH ₃	-4.22 \pm 0.16 ^b	60 \pm 22	0.75
12b	—OCH ₃	—CH ₃	-4.43 \pm 0.12	37 \pm 11	0.68
12c	—OC(CH ₃) ₃	—CH ₃	-5.14 \pm 0.18	7.3 \pm 3.1	0.84
12d	—OCH ₂ CH ₂ OCH ₃	—CH ₃	-3.42 \pm 0.13	375 \pm 109	0.80
12e	—OCH ₂ CH ₃	—CH ₂ CH ₃	-3.92 \pm 0.05	121 \pm 14	0.95
12f	—OCH ₂ CH ₃	—CH(CH ₃) ₂	-4.52 \pm 0.19	30 \pm 13	0.72
13	na ^c	Na	-3.89 \pm 0.20	129 \pm 60	0.62
14	<i>N</i> -morpholino	—CH ₃	Incomplete ^d	>7100	na ^c
15	—OH	—CH ₃	-3.43 \pm 0.37	~374 ^e	0.14
17	na ^c	Na	-3.12 \pm 0.35	~764 ^e	0.95
18	na ^c	Na	-3.44 \pm 0.06	365 \pm 57	0.79
19	na ^c	Na	-4.05 \pm 0.26	89 \pm 54	0.70

^aThrombin inhibition was measured in spectrophotometric assay through initial rate of Spectrozyme TH hydrolysis as described in Experimental section. ^bstandard error shown is ± 1 S.E. ^cNot applicable. See complete structures of **13**, **14**, **15**, **17**, **18** and **19** in Figure 17. ^dFull inhibition profile was not measured. ^eThe error in IC_{50} could not be accurately defined because of insufficient number of data points.

The distinct groups at the 2, 3, 5 and 6- positions on the benzofuran ring result in interesting structure–activity relationships. The sulfate group at the 5- position was found to be the key basis for thrombin inhibition, since all unsulfated precursors studied in this work, monomers as well as dimers, did not inhibit thrombin. Such a high level of dependence on one sulfate group is striking. It also appears to be unusual because thrombin is known to be considerably forgiving in recognizing ligands. For example, ligands as different as heparin and RNA are known to bind in exosite II.^{224, 225} Similarly, hirudin, which contains a sulfated tyrosine, as well as de-sulfated hirudin, i.e., desirudin, binds in exosite I with excellent affinities.^{79, 209, 226}

The stringent requirement for 5-sulfate led to the expectation that multiple sulfate groups on the benzofuran scaffold may induce higher potency. Yet, dimers **17** and **18**, which bear two sulfate groups (5 and 5', and 5 and 6- positions, respectively) inhibited thrombin approximately 6–17-fold weaker (Table 8). Furthermore, the IC_{50} of **15**, which contains the 5-sulfate as well as a carboxylate at each of the 3- positions of the benzofuran rings, also decreases 6.2-fold from its parent **12a**. This implies that any additional anionic group on the benzofuran scaffold is counter-productive, which is contrary to what one would predict on the basis of the thrombin – heparin system.^{212, 224, 226}

Comparison of the IC_{50} s of **12a**, **12b** and **12c** shows that as lipophilicity of the 3-ester increases, the inhibition potency improves 8.2-fold (Table 8). Likewise, change in substitution from ethyl to isopropyl at the 6- position, as in **12e** and **12f**, also increases the potency nearly 4-fold. This implies that hydrophobicity of the scaffold plays an important role in thrombin recognition. In support of this, increase in hydrophilicity of groups markedly decreases potency. For example, the 3-methoxyethyl ester containing **12d** is a 6.2-fold weaker inhibitor of thrombin than the 3-ethyl containing **12a** (Table 8). More importantly, introduction of an *N*-morpholinyl ring (dimer **14**) increased IC_{50} to >2000 μ M, which represents a more than 270-fold loss of affinity from a comparable *t*-butyl ester containing dimer **2c**.

While the above discussion suggests fairly stringent structural requirements on the benzofuran scaffold, two interesting results highlight the possible variances. Dimer **13** containing a morpholine ring at the 2-allylic position displays IC_{50} of 129 μ M, which is only 2.2-fold higher than that of **12a**. This suggests that introduction of a hydrophilic and sterically bulkier group at the terminus opposite the 5-sulfate is not detrimental. Likewise, dimer **19** displays no change in IC_{50} from its comparable parent **12a** (Table 8). Dimer **19** contains a 2-CH₂O-6 inter-monomeric

linkage as compared to a 2-CH₂O-5 linkage present in dimer **12a**. An essentially identical inhibition potency of **19** as compared to **12a** indicates that a change as drastic as a ring flip, or regioisomerism, is well tolerated.

4.2.2 Mechanism of Thrombin Inhibition By Sulfated Benzofuran Dimer **12a**

To elucidate the nature of thrombin inhibition by the designed sulfated benzofurans, the kinetics of Spectrozyme TH hydrolysis by thrombin at pH 7.4 in the presence and absence of **12a** was studied. Spectrozyme TH has been routinely used as a chromogenic substrate of thrombin.²¹³ The initial rate of amidolysis as a function of the substrate concentration displayed a hyperbolic profile, as expected (Figure 19), from which the Michaelis constant (K_M) and maximal velocity of the reaction (V_{MAX}) were derived. The K_M and V_{MAX} for Spectrozyme TH in the absence of **12a** was found to be 18.9 μM and 100 $\text{mAUmin}^{-1}\mu\text{M}^{-1}$, respectively. In the presence of 1.5, 3.0, 10.5 and 30 μM **12a**, the K_M of substrate was found to be 12.6 ± 4.7 , 15.5 ± 5.5 , 15.9 ± 7.4 , and 15.5 ± 3.7 μM . In contrast, the V_{MAX} was measured to be 97 ± 13 , 107 ± 14 , 73 ± 13 and 66 ± 6 $\text{mAUmin}^{-1}\mu\text{M}^{-1}$ in these experiments. This corresponds to ~34% decrease in maximal velocity of reaction upon approximately 50% saturation of the enzyme. This suggests that the presence of **12a** does not significantly affect the binding of the chromogenic substrate to the active site of the enzyme, while significantly reducing its catalytic efficiency.

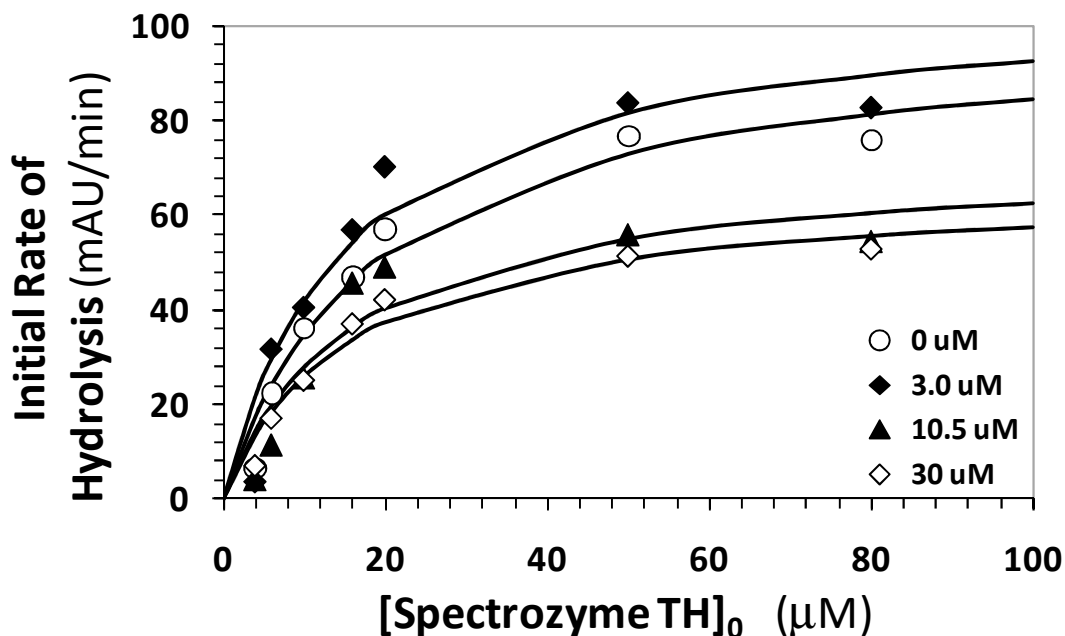


Figure 19. Michaelis-Menten kinetics of Spectrozyme TH hydrolysis by human thrombin in the presence of dimer **12a**. The initial rate of hydrolysis at various substrate concentrations was measured spectrophotometrically in pH 7.4 buffer as described in ‘Experimental Procedures’. The concentrations of **12a** chosen for study include 0 (○), 3.0 (◆), 10.5 (▲), and 30 μM (◇). Solid lines represent non-linear regressional fits to the data by the standard Michaelis-Menten equation to yield K_M and V_{MAX} .

The above Michaelis–Menten kinetics result indicates a non-competitive, allosteric mechanism of thrombin inhibition by **12a** and, by analogy, other sulfated benzofuran molecules. The reduction in catalytic efficiency by these novel inhibitors is primarily brought about by the slow conversion of the thrombin–Spectrozyme TH Michaelis complex, which may arise from the intrinsic change in the rate of chemical reaction or by a change in the structure of the catalytic triad induced by the allosteric inhibitors.

4.2.3 Prolongation of Plasma Clotting Time by Sulfated Benzofurans

Two plasma clotting assays are typically used to assess the anticoagulant potential of new coagulation inhibitors. These are the prothrombin and activated partial thromboplastin time assays (PT and APTT, respectively), which attempt to measure the effect of an inhibitor on the extrinsic and intrinsic flux of coagulation. The concentrations of the inhibitors required to double the PT and APTT were measured, as described earlier for sulfated LMWLs.^{215, 216} The prolongation of plasma clotting time as a function of the concentration of the sulfated benzofurans followed a pattern typical of other well-studied anticoagulants (Figure 20), except for the range of active concentrations. A 2-fold increase in PT required 850 – 2100 μ M concentration of **5i**, **12a** or **12b** (Table 9). In a similar manner, the doubling of APTT required 355 – 1250 μ M of **5i**, **12a**, **12c**, or **12e** (Table 9). Most other monomers or dimers were found to be not effective. These results suggest that the designed small, sulfated benzofurans are about 100 – 250-fold less potent in human plasma than the oligomeric sulfated LMWLs from which they were designed.²¹⁶ This is not too unexpected considering that thrombin inhibition by the smaller synthetic molecules is nearly 400-fold weaker than that of the parent oligomers. Yet, interesting similarities and differences are discernible. For example, dimers are better anticoagulants in plasma than monomers. Within the group of dimers **12a**, **12c** and **12e**, which inhibit thrombin well, are also the best in terms of prolonging APTT. Interestingly, **12b**, which is comparable to **12a** in thrombin inhibition, does not affect APTT at all (Table 9) and the reason for this behavior is not clear. Overall, the plasma studies suggest the feasibility of designing sulfated benzofurans that will function as anticoagulants *in vivo*.

Table 9. Effect of Designed Sulfated Benzofurans on Human Plasma Clotting Time

	<i>APPT</i>	<i>PT</i>
	(μ M)	(μ M)
5i	1,250	1,200
5g	>1,200	ne ^b
5c	>2,000	ne
12a	740	2,100
12b	>1,000	850
12c	355	ne
12d	>1,000	ne
12e	530	ne
14	>1,000	nd ^c
15	>1,000	ne

^a PT and APTT values were deduced in *in vitro* human plasma experiments where the clot initiator is either thromboplastin or ellagic acid, respectively. See Methods for details. ^b no effect.

^c not determined.

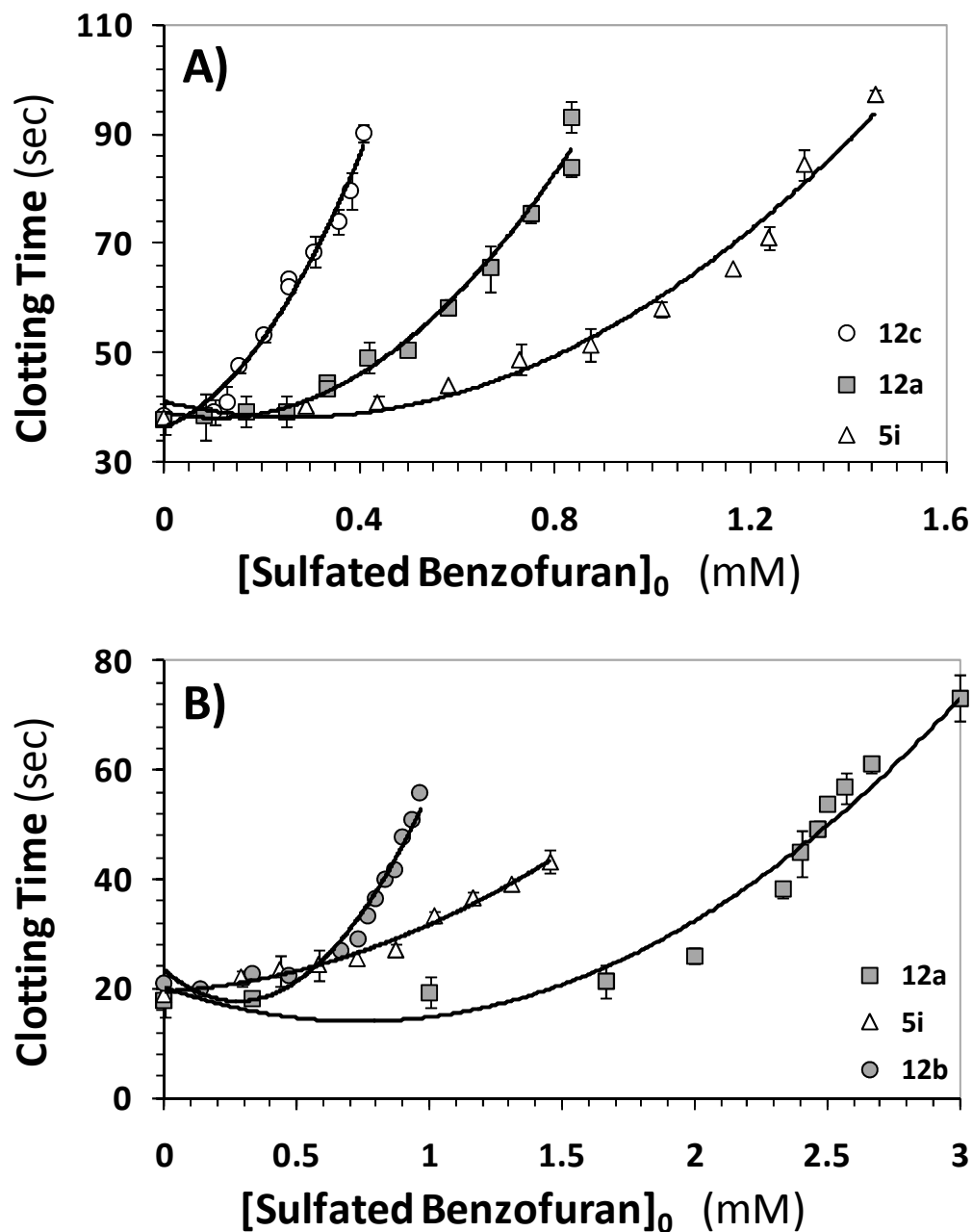


Figure 20. Prolongation of clotting time as a function of concentration of sulfated benzofuran monomers and dimers in either activated partial thromboplastin time assay (A) or prothrombin time assay (B). Solid lines are trend lines, and not non-linear regressional fits. Error bars in the range of symbol size have been omitted. APTT and PT assays were performed as described in the experimental section.

4.2.4 Complementary Biochemical Studies (Studies performed by Dr. Aiye Liang and Ms. May H. Abdel Aziz)

- 1) To test whether dimers bind in exosite I, competition studies with the hirugen analog, [5F]-Hir[54-65](SO₃⁻), were performed. The presence of [5F]-Hir[54-65](SO₃⁻) did not significantly affect the thrombin inhibition profiles indicating that the dimer does not appear to bind in the anion-binding exosite I of thrombin.
- 2) To test whether dimers bind in exosite II, competition studies with three different exosite II binding ligands; porcine unfractionated, heparin, H8, and γ' fibrinogen peptide were performed. A distinct shift in the profiles is observed as the concentration of the γ' fibrinogen peptide increases, suggesting full competition between the two ligands for thrombin binding. This indicates that the dimer and γ' fibrinogen peptide compete for exosite II of thrombin. However, no change in inhibition profile was observed with increasing concentration of heparin octasaccharide H8 and a slight change in inhibition profile was observed with heparin. This indicates that the dimer and H8 do not compete with each other, whereas partial competition is observed with UFH.
- 3) To identify the basic residues that might play an important role in dimer recognition, we studied the inhibition of five thrombin mutants containing single and triple replacements of Arg/Lys to Ala. The dose – response profiles for three of the four single point mutants (Arg175Ala, Lys169Ala, and Lys235Ala) and one triple mutant (Arg93, 97,101Ala) studied in this work were essentially identical to the recombinant wild type enzyme. In striking contrast, the Arg173Ala mutant displayed a 22-fold increase in IC_{50} compared to the wild type enzyme, suggesting its importance for thrombin binding and inhibition by **12a** and related sulfated benzofuran derivatives.

4.2.5 Molecular Docking Identifies a Single Plausible Binding Geometry for **12a** on Thrombin

To identify a plausible binding geometry of sulfated benzofuran dimers on thrombin for structure-based design, we employed a molecular docking and scoring approach. We have previously utilized a similar approach using the automated docking routine GOLD to understand how highly sulfated oligosaccharides recognize proteins.^{227, 228} This approach was also exploited to study the recognition of antithrombin by sulfated LMWLs,²²⁹ which are the parent molecules for the sulfated benzofuran dimers being studied here. Hence, we chose to employ a GOLD-based identification of plausible binding sites and geometries of **12a** on human thrombin.

The GOLD-based docking and scoring approach utilizes a genetic algorithm (GA) to iteratively derive the best binding geometry for each ligand in a pre-defined binding site. Our recent work on the recognition of sulfated LMWLs binding to thrombin mutants revealed that hydrophobic patches in the vicinity of Arg93 may be involved.²³⁰ Considering this, we hypothesized that hydrophobic region(s) near Arg173, which has been implicated by the Arg173Ala thrombin mutant studies presented here, would be important for recognition of **12a** and its related sulfated benzofurans. Several GA docking runs were thus performed to assess how well **12a** could be recognized by the binding site regions surrounding Arg173. Each docking run was performed using a constraint that encouraged the guanidine group of Arg173 to hydrogen bond with the sulfate group of SBD. Only one particular binding site was consistently found to provide a surface complementary to **12a** in which the ligand is bound in an extended, flat conformation. This binding domain was located between Arg173 and the active site of human thrombin, exhibits a high degree of shape complementarity with the ligand and consists of hydrophobic areas suitable for recognizing the benzofuran rings and their substituents. To

more rigorously test whether low occupancy, alternate binding site(s) are possible, a ‘diverse-docking’ experiment was performed in which GOLD was forced to identify solutions with alternative binding sites of **12a** that differ by at least 1.5 Å from the binding mode described above. With this directive, GOLD identified binding sites vastly different from that shown in Figure 21 but with no complementarity to **12a**. This was also reflected in very poor GOLD scores for these alternative geometries. Additionally, the reproducibility of these geometries was poor, suggesting that the algorithm was not able to converge on a plausible binding pose.

On the basis of these initial docking results as well as the FibP and Arg173Ala thrombin studies described above, we concluded that the class of sulfated benzofuran dimers being studied here do recognize this highly complementary domain. To test this prediction further, the library of sulfated benzofuran dimers studied earlier was docked onto human thrombin.²³¹ Three crystal structures of human thrombin (PDB ID = 3EQ0, 1H8D and 2UUF)^{232, 233} with resolution between 1.5 and 2.5 Å were used to test the consistency of binding of the entire library. Each thrombin crystal structure was bound by both an active site inhibitor and a hirudin peptide in exosite II. All of the residues within reach of an Arg173-associated SBD were completely resolved in these three thrombin structures. Overall, the three structures were similar in terms of the resolution of residues in exosite II (backbone RMSD = 0.2 Å; Figure 22).

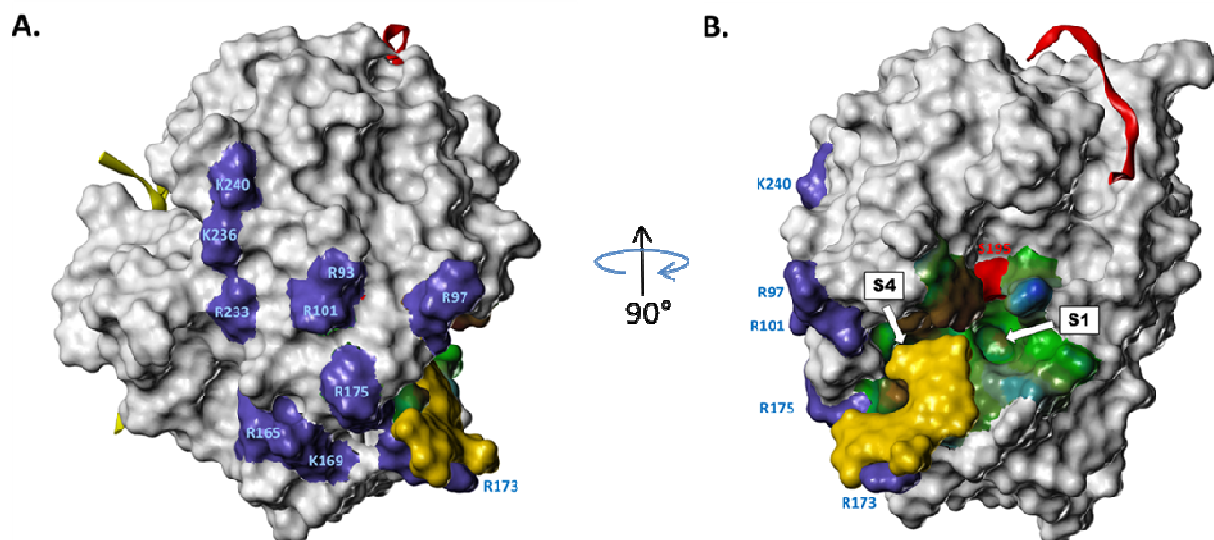


Figure 21. Connolly surface of thrombin (PDB ID = 3EQ0), showing the location of several electropositive basic residues, including those contributing to exosite II and the γ' -fibrinogen peptide binding site (purple patches). The putative binding site and mode of the lead sulfated benzofuran dimer **12a** is rendered as a yellow surface and shows the high degree of shape complementarity with its putative binding site. The thrombin light chain (yellow ribbon) and hirudin peptide denoting the location of exosite-I (red ribbon) are also shown. **B)** The same 3D image rotated by 90°, further highlighting the high degree of shape complementarity between the ligand dimer and its proposed binding site. The active site is displayed with a hydrophobic potential map (blue = hydrophilic, green = amphipathic, brown = hydrophobic) with the nucleophilic serine S195 shown as a red patch. The S1 and S4 substrate specificity pockets are indicated; the hydrophobic S4 pocket is occluded because it is occupied by the ethyl group of the 3'-ethyl ester of **12a**.

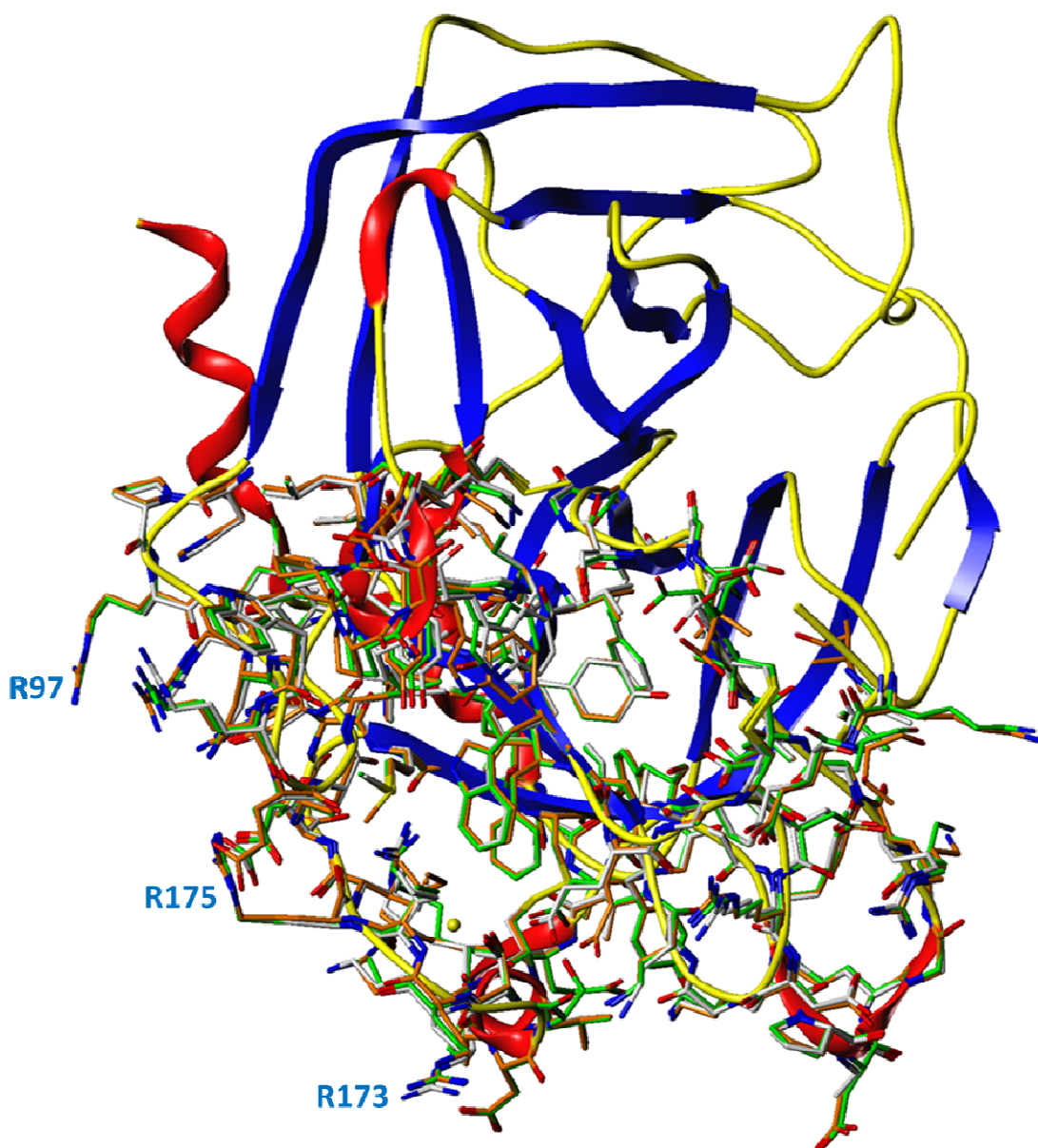


Figure 22. GOLD binding site definitions for 3EQ0, 1H8D and 2UUF (22 Å radius about R173) highlighting the conformational similarity among the three proteins. The thrombin heavy chain is shown as a colored ribbon (red = helix, blue = sheet/strand, yellow = coil) and the residues are rendered as capped sticks (white carbon atoms, 3EQ0; orange carbon atoms, 1H8D; green carbon atoms, 2UUF). The inter-heavy chain backbone RMSD among the three proteins is 0.2 Å.

For the inhibitors studied as a part of the docking library, the binding site between Arg173 and the active site was found to satisfy known thrombin inhibition characteristics. In

addition, the GOLDScores of the compounds in the library showed a modest correlation with their inhibitory activity; compounds with significant, minimal and no inhibitory activity were effectively distinguished (Tables 10 and Figure 23). The docking pose of **12a** onto 3EQ0 thrombin could be used explain interactions at an atomic level. For example, in this pose the 4-sulfate group of **12a** forms a bidentate hydrogen-bond with Arg173, which supports the observation that all molecules devoid of 4-sulfate group are completely devoid of thrombin inhibition activity.²³¹ This consistency was expected due to the inclusion of the Arg173 hydrogen-bond docking constraint. In the proposed binding mode, the Arg173 side chain is in fact surrounded by atoms of the first monomer: the sulfate group forms a double hydrogen-bond salt bridge with the guanidinium group, the 3-ethyl ester group is in a sterically unhindered region adjacent to the guanidinium group and may engage in pi-stacking interactions with it, and the benzofuran core is closely associated with the alkyl portion of the Arg173 side chain.

Table 10. Comparison of GOLD scores obtained from docking studies and IC₅₀ obtained from experimental data.

Inhibitor	GoldScore	IC ₅₀ (μM)
12a	64.37	60±22
12b	62.92	37±11
12c	64.01	7.3±3.1
12d	59.94	375±109
12e	64.60	121±14
12f	64.37	30±13
13	63.16	129±60
14	56.70	>7100
15	59.43	~374

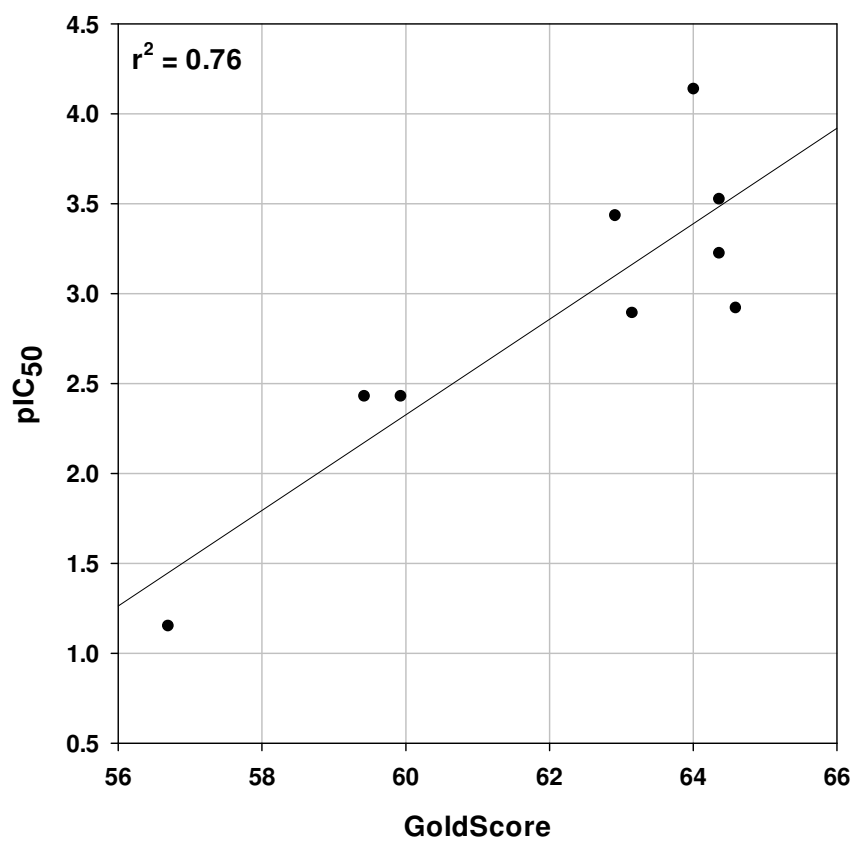


Figure 23. Scatter Plot of GOLDScore vs. pIC₅₀ Values for Docked SBDs.

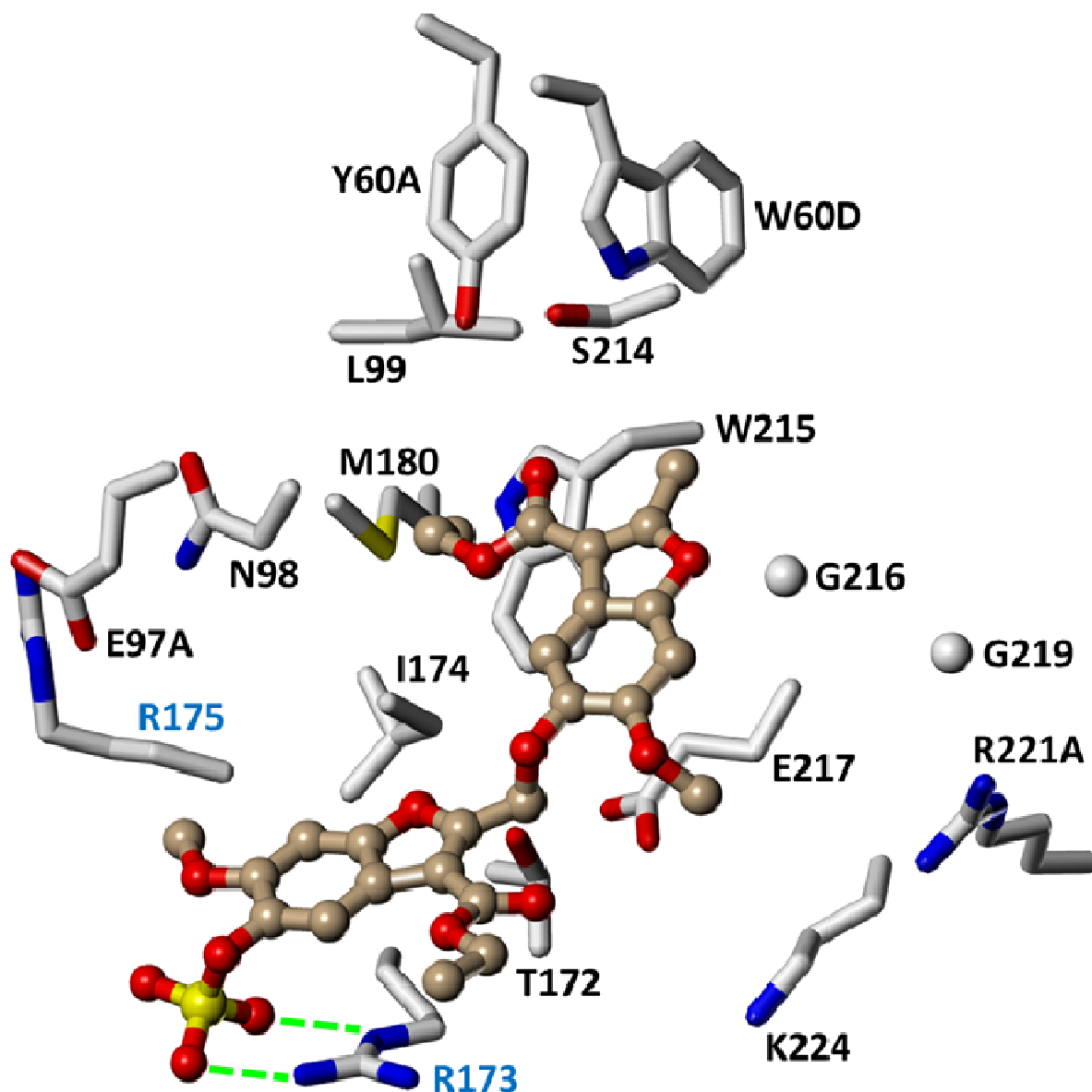
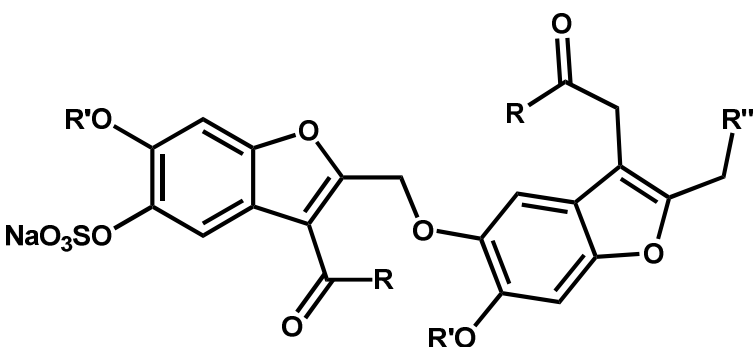


Figure 24. Expanded view of the interaction of **12a** with its putative binding site. The ligand is rendered as a ball-and-stick figure and binding site residues rendered as capped sticks. All binding site side chains within 5 Å of **12a** are displayed. Hydrogen bonds between Arg173 and the ligand sulfate group are shown as green dotted lines.

Additionally, the 3'-ethyl ester group on the second monomeric unit binds in a shallow hydrophobic pocket lined by Asn98, Ile174, Ile176 and Trp215 (i.e., the S4 substrate specificity pocket). Interaction of the 3'-ester group here is consistent with the higher potency of inhibitors

12a, **12b**, and **12c** (see Table 11 for structures). As the hydrophobic character of groups at the 3'-position increases, the potency possibly also increases because of more favorable interactions in the hydrophobic S4 pocket. In contrast, inhibitors **12d**, **14** and **15**, which contains larger and/or polar groups at this position have poorer thrombin inhibition potential.²³¹

Table 11. Structure of sulfated benzofuran dimers **12a–f** and **13–15** found to potently inhibit human thrombin.



	R'	R	R''
12a	-CH ₃	-OC ₂ H ₅	-H
12b	-CH ₃	-OCH ₃	-H
12c	-CH ₃	-OC(CH ₃) ₃	-H
12d	-CH ₃	-OC ₂ H ₄ OCH ₃	-H
12e	-C ₂ H ₅	-OC ₂ H ₅	-H
12f	-CH(CH ₃) ₂	-OC ₂ H ₅	-H
13	-CH ₃	-OC ₂ H ₅	<i>N</i> -morpholino
14	-CH ₃	<i>N</i> -morpholino	-H
15	-CH ₃	-OH	-H

The 6-methoxy group of **12a** is suggested to bind in a region lined by the amide backbones of Arg175, Glu97A, and Ile174, whereas the 6'-methoxy group binds in region formed largely by Asp217 and Lys224 side chains. Both these pockets appear to possess a

combination of hydrophobic and polar properties and are significantly sterically unhindered, which implies they can accommodate larger groups. In fact, the inhibition potency increases as we move from **12a** to **12b** to **12c**, which display increasing homologation at these positions.

The 2'-allylic position is located in an amphiphilic region near Trp215 between the S1 and S4 substrate binding pockets and is oriented toward S1. The model indicates that this region is moderately sterically constrained, which helps us understand why inhibitor **13** containing a 2'-morpholino ring substituent is essentially inactive. The larger and much more polar morpholine ring at 2'-region is likely to prevent the SBD from binding in this pocket resulting in loss of activity.

A key aspect of this binding geometry is that the benzofuran scaffold appears to be an effective core structure because it places its substituents into stereoelectronically favorable pockets on thrombin. It remains to be seen whether or not other planar hydrophobic scaffolds can improve inhibitor potency. Thus, at present it is difficult to discount the value of benzofuran rings to inhibition potency.

4.2.6 Screening Against Other Serine Proteases

The library of sulfated benzofuran monomers and dimers was screened against the panel of coagulation proteases. It includes factors VIIa, IXa, Xa, XIa and XIIa, which are involved in either the intrinsic or extrinsic pathways. The assay is based on hydrolysis of a chromogenic substrate by the protease, the rate of which is decreased in the presence of inhibitor. Screening was performed at single concentration of inhibitors using substrate hydrolysis assay in 96 well-plates. This assay is based on the decrease in the initial rate of substrate hydrolysis in the presence of inhibitor. The decrease in initial rate of hydrolysis typically provides the fractional

residual activity of enzyme. The details of experimental conditions are provided in the Experimental Section (4.4.6).

Tables 12 and 13 show the percentage residual activity of all proteases at a final concentration of 365 μM of each inhibitor. Seven representative monomers were selected to cover a range of substitutions from hydrophobic to polar characteristics as well as the number of sulfate groups. None of these monomers inhibited the factors VIIa, IXa, Xa and XII more than 20% at the concentration of 365 μM . This was expected as monomers showed very poor potency for thrombin except **5i** ($\text{IC}_{50} \sim 500 \mu\text{M}$). The inhibitor **5i** was not able to inhibit any protease except factor XIa greater than 20% at the given concentration. **5i** completely inhibited factor XIa at given concentration, showing its higher potency (Figure 25).

Similarly, seven representative molecules were selected from the library of dimers. None of the dimers inhibited factors VIIa, IXa and XIIa greater than 30% at given concentration showing selectivity of the designed benzofuran dimer derivatives against these proteases (Figure 26). The molecules **12a**, **12e** and **20** inhibited factor Xa activity more than 40%. It is hypothesized that these molecules have the potential to inhibit factor Xa that moderates potency. It has been observed from data on thrombin inhibition that a library of dimers was only able to inhibit thrombin 60% or less. Beside factor Xa, **12e** and **21** were also able to completely inhibit factor XIa at the given concentration. The results are again consistent with the library of monomers and dimers, which showed inhibition potential for both thrombin and factor XIa. Thus, it can be concluded that sulfated benzofuran derivatives bind at a site that have high homology in thrombin and factor XIa.

Table 12. Residual activity of various proteases obtained by screening the library of monomers

	Factor IXa	Factor Xa	Factor VIIa	Factor XIa	Factor XIIa
5c	92±2.7	73±3.9	102±4.2	92±3	100±2
5f	90±1.3	94±1.6	105±5.6	85±4	102±6
5g	104±7	101±5	96±4	96±3.5	104±4
5i	104±5.5	113±16	56±3.2	7±4.1	102±3.3
9a	127±9.9	104±7.8	97±3.2	100±3	105±6
9b	117±22	112±10	100±2.5	106±6	100±4
5j	121±9	106±8	75±3.5	65±3	90±2.5

Table -13. Residual activity of various proteases obtained by screening the library of monomers

	Factor IXa	Factor Xa	Factor VIIa	Factor XIa	Factor XIIa
12a	81±3	61±2	100±3.5	88±2	100±3
12e	89±3	59±4	101±6	6±2	103±6
14	82±3.5	100±4	90±2	89±2	91±1
12d	96±6	114±17	83±3	77±1.6	94±5
15	91±4	101±3	91±2	85±4	94±5
20	82±3	57±3.5	87±1	103±6	96±5
21	83±2	108±10	85±2	51±3	104±5

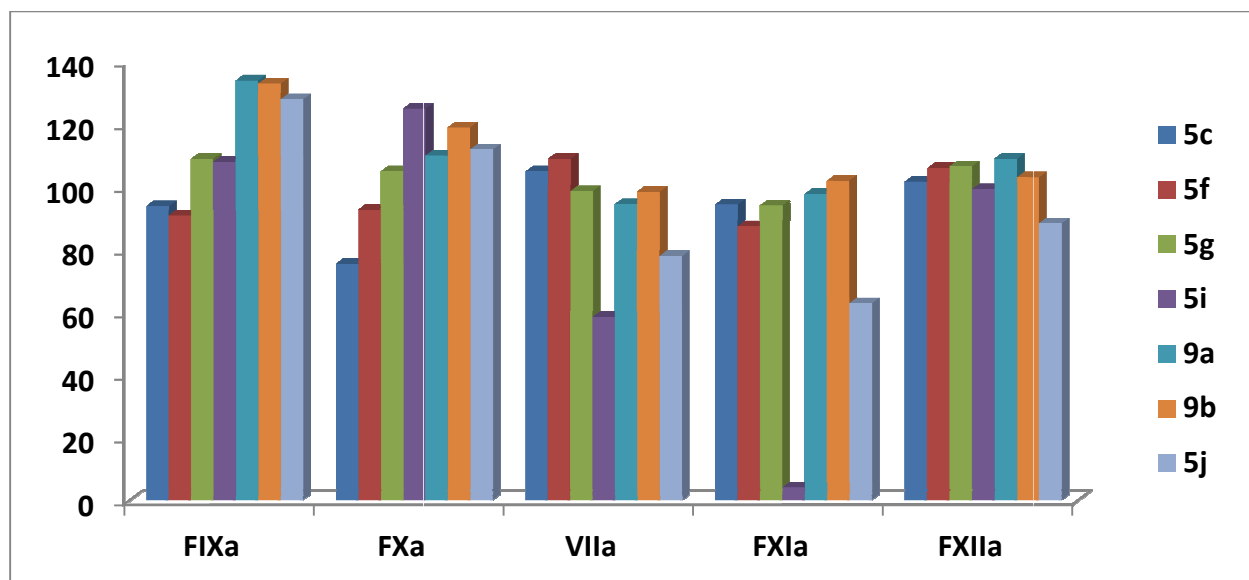


Figure 25. Bar graph showing the % residual activity of given proteases at single concentration of each inhibitor

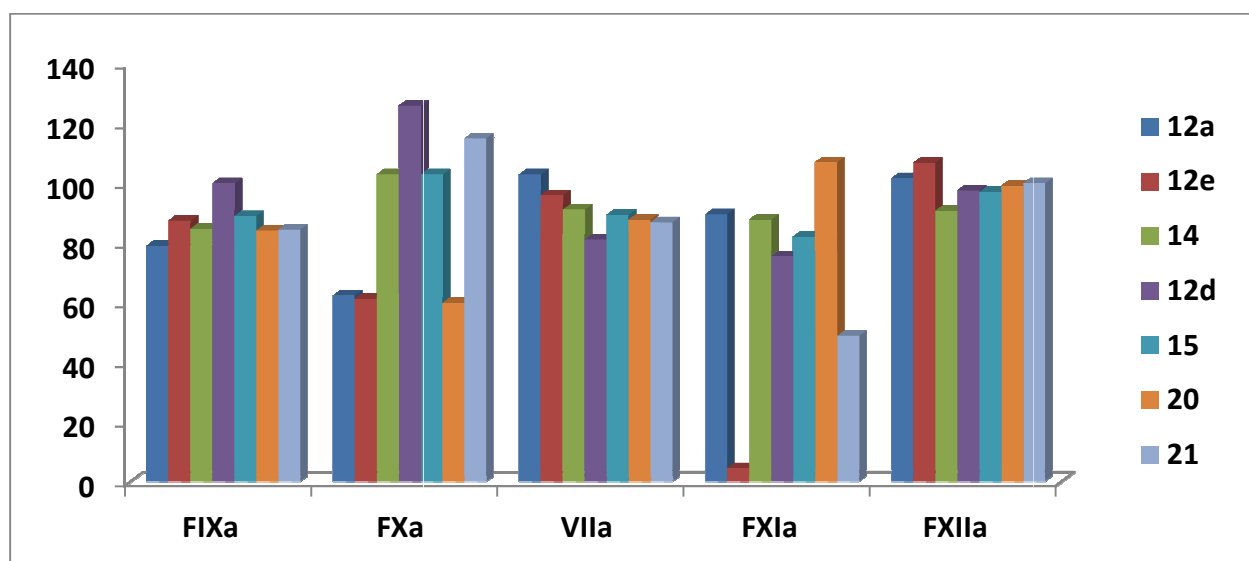


Figure 26. Bar graph showing the % residual activity of given proteases at single concentration of each inhibitor

4.3 Discussion

The range of thrombin inhibition potency and efficacy discovered for sulfated benzofurans suggests that the designed sulfated benzofuran scaffold may be an excellent lead in developing anticoagulants radically different from those studied to-date. The β -5 inter-monomer linkage is only one of the many units present in sulfated LMWLs,^{213, 216} which implies that computational structure-based design may be necessary to identify the most appropriate ‘small’ structure from the large number of potential molecules. One such strategy, e.g., combinatorial virtual library screening, has been put forward for highly sulfated molecules²²⁸ and also been found useful for sulfated lignins binding to antithrombin.²³⁴

This work presents small synthetic sulfated aromatic structures as novel allosteric modulators of thrombin function. Allosteric exosite II-based modulators of thrombin are of special interest because they afford the possibility of controlled inhibition of this key protease that takes part in a number of physiological processes.⁷⁹ Excess inhibition could, in principle, be reversed by highly sulfated small molecules, e.g., sucrose octasulfate, that are also expected to bind in this region without inducing significant reduction in thrombin’s catalytic activity. Allosteric exosite II-mediated inhibitors with nanomolar potency, other than sulfated LMWLs,²¹³ have not been designed as yet and thus, sulfated benzofurans represent first molecules in a new class of thrombin modulators.

Although the potency of our first allosteric inhibitors is not high, it is not a major concern because rational design of these molecules from the parent polymers invoked a rather drastic reduction in molecular weight. Whereas sulfated LMWLs are oligomeric chains with an average molecular weight of 5000, sulfated benzofurans range from 500 to 1000.²¹⁵ Thus, a relatively

easy approach to higher potency would be to prepare appropriate tri- and tetramers of sulfated benzofurans.

This work suggests that SBDs utilize a hydrophobic cavity, which overlaps with the S4 binding pocket (see Figure 21). Although designed as mimetics of heparin, SBDs do not engage the traditional exosite II ligand residues including Arg101, Arg126, Lys235, Lys236 and Lys240. SBDs recognize Arg173, a heparin-binding residue. Yet, the predicted binding mode and orientation of **12a** (see Figure 21 and 24) is likely to be dramatically different from that of polymeric heparin with its chain oriented along the highly electropositive surface.²²⁴ In fact, **12a** binds in a region different from that predicted for sulfated LMWLs, which appear to bind in a linear hydrophobic segment present in exosite II on either sides of residues Arg93 and Arg101.²³⁵ The competition of **12a** with FibP coupled with the known structure of FibP – thrombin complex bodes well for designing peptidomimetics based on the FibP sequence that recognizes the new binding site.²³⁶ These peptidomimetics are likely to possess structures different from our SBDs.

Molecule **12a** does not compete with the chromogenic substrate and yet reduces the rate of substrate hydrolysis²³¹ suggesting that the new binding site is energetically coupled to the active site. The affinity of **12a** for thrombin at pH 7.4 and 25 °C is approximately 6 μ M, which implies a reasonably high affinity interaction. In fact, other than the antithrombin-binding heparin pentasaccharide, which binds with an affinity of ~50 nM,²³⁷ no small, sulfated molecule is known to bind with such high affinity. A recent study of a group of synthetic heparin octasaccharides that target herpes virus glycoproteins with ~20 μ M affinity further support this observation. The reason for the very high affinity of antithrombin-binding heparin pentasaccharide is marvelous engineering by nature over millions of years. Thus, the ~6 μ M

affinity of **12a**, which is ~1000-fold higher than that of its monomer precursor,²³⁸ is a good lead. In fact, the putative binding site presents excellent opportunities advancing the design. For example, Lys224 and Arg221A are within 5 to 8 Å of the carboxylic acid ester. Likewise, several hydrophobic residues are also available for targeting.

Molecule **12a** reduces thrombin's catalytic activity approximately 50% in comparison to known inhibitors that target the active site and exosite I.^{20, 197} This implies that **12a** does not completely inhibit the procoagulant signal. Whereas this could be traditionally considered as a defect of design, considering the problems of over-anticoagulation induced by thrombin inhibitors, the less than perfect reduction in catalytic activity of thrombin may serve to foster the fine balance between procoagulant and anticoagulant signals. More importantly, detailed inhibition profiles reveal that some SBDs exhibit efficacies of greater than 50%, while only between 10 and 20% for others.²³¹ This implies that the SBD binding site may be a 'tunable' binding site and appropriate molecules may be designed with variable efficacies to treat varying levels of procoagulant tendencies.

Finally, this work also highlights the opportunity of exploring allosteric modulators of other coagulation enzymes, e.g., factors Xa, IXa and XIa, through sulfated lignin scaffolds. Considering the wealth of structural diversity accessible with the lignin scaffold, it may be possible to design allosteric inhibitors that target these enzymes in a highly specific manner.

4.4 Experimental Section

4.4.1 Enzyme and Chemicals for Biological Experiments

Human α -thrombin, factors Xa, XIa, IXa, VIIa and recombinant tissue factor were purchased from Haematologic Technologies (Essex Junction, VT). Factor XIIa was purchased

from Enzyme Research Laboratories (South Bend, IN). Stock solutions of thrombin were prepared in 20 mM sodium phosphate buffer, pH 7.4, containing 100 mM NaCl. The chromogenic substrates Spectrozyme TH, Spectrozyme FXa, Spectrozyme FXIIa, Spectrozyme FIXa (299), Spectrozyme VIIa, and Spectrozyme CTY were obtained from American Diagnostica (Greenwich, CT). Citrated human plasma for coagulation time assays was purchased from Valley Biomedical (Winchester, VA). Thromboplastin and ellagic acid were obtained from Fisher Diagnostics (Middletown, VA).

4.4.2 Inhibition of Thrombin

Direct inhibition of thrombin by sulfated benzofuran derivatives was measured through a chromogenic substrate hydrolysis assay.^{213, 214} The buffer used in these experiments was 20 mM Tris-HCl buffer, pH 7.4, containing 100 mM NaCl, 2.5 mM CaCl₂, and 0.1% polyethylene glycol (PEG) 8000. Benzofuran derivatives (2 to 30 μ L) at concentrations ranging from 4 μ g/mL to 5 mg/mL were diluted with the appropriate volume of assay buffer in PEG 20,000-coated acrylic cuvettes at 25 °C. To this solution was added 5 μ L of thrombin solution to give approximately 5 nM initial thrombin concentration. After 10 min of incubation, 20 μ L of 1 mM Spectrozyme TH was rapidly added and the residual thrombin activity was measured from the initial rate of increase in absorbance at 405 nm. Relative residual thrombin activity at each concentration of the inhibitor was calculated from the ratio of thrombin activity in the presence and absence of inhibitor. Logistic equation 1 was used to fit the dose-dependence of residual proteinase activity to obtain the IC_{50} and the efficacy ΔY ($= Y_M - Y_0$) of inhibition.

$$Y = Y_0 + \frac{Y_M - Y_0}{1 + 10^{(\log[I]_0 - \log IC_{50}) \times HS}} \quad \text{Equation 1}$$

In this equation, Y is the ratio of residual thrombin activity in the presence of inhibitor to that in its absence (fractional residual activity), Y_M and Y_O are the maximum and minimum possible values of the fractional residual proteinase activity, IC_{50} is the concentration of the inhibitor that results in 50% inhibition of enzyme activity, and HS is the Hill Slope, which was set constant at 1. A current version of SigmaPlot (SPSS, Inc. Chicago, IL) was used to perform non-linear curve fitting in which Y_M , Y_O and IC_{50} were allowed to float.

4.4.3 Michaelis-Menten Kinetics of Spectrozyme TH Hydrolysis

The initial rate of Spectrozyme TH hydrolysis by 5 – 10 nM thrombin was monitored from the linear increase in absorbance at 405 nm corresponding to less than 10% consumption of the substrate, as described earlier.^{213, 214} The initial rate was measured as a function of various concentrations of the substrate (10 to 600 μ M) in the presence of fixed concentration of dimer **12a** (0–30 μ M) in 20 mM Tris-HCl buffer, pH 7.4, at 37 °C. The data were fitted by Michaelis-Menten equation 2 to determine K_M and V_{MAX} .

$$V_i = \frac{V_{MAX} \times [S]}{K_M + [S]} \quad \text{Equation 2}$$

4.4.4 Prothrombin Time and Activated Partial Thromboplastin Time

Clotting time was measured in a standard 1-stage recalcification assay with a BBL Fibrosystem fibrometer (Becton-Dickinson, Sparks, MD), as described previously.^{215, 216} For PT assays, thromboplastin was reconstituted according to manufacturer's directions and warmed to 37 °C. A 10 μ L sample of the sulfated benzofuran, to give the desired concentration, was brought up to 100 μ L with citrated human plasma, incubated for 30 s at 37 °C followed by addition of 200

μL pre-warmed thromboplastin. Clotting time in the absence of an anticoagulant was determined using 10 μL deionized water. For the APTT assay, 10 μL inhibitor was mixed with 90 μL citrated human plasma and 100 μL of pre-warmed APTT reagent (0.2% ellagic acid). After incubation for 4 minutes, clotting was initiated by adding 100 μL of 25 mM CaCl₂ (37 °C) and time to clot was noted. Each clotting assay was performed in duplicate. The data were fit to a quadratic trendline, which was used to determine the concentration of the inhibitor necessary to double the clotting time, 2×APTT or 2×PT.

4.4.5 Molecular Modeling Studies

Molecular docking studies to identify potential binding poses require an accurate 3D crystal structure of thrombin with high resolution and well-defined side chains. The crystal structure of thrombin bound to its allosteric exosite I ligand hirugen at 1.53 Å resolution was obtained from the Protein Data Bank (PDB ID = 3EQ0), as well as two additional thrombin structures (PDB IDs = 1H8D and 2UUF).^{29,30} All the residues in region of Arg173 were manually inspected to insure that the side chains were completely resolved. Each of the acidic and basic residues was modeled in its most predominant ionization state at physiological pH (i.e., anionic Asp and Glu; cationic Arg and Lys). The inorganic salts and water molecules were deleted from the crystal structure, and hydrogen atoms were added using SYBYL 8.1 (Tripos International, St. Louis, MO). To prepare the structure for docking and scoring protocol, the newly-added hydrogen atoms were energy-minimized using the Tripos Force Field (Gasteiger–Hückel charges; termination criterion of 0.05 kcal/(mol×Å) or 1×10^5 iterations; distance-dependent dielectric constant $\epsilon = 4.0$).

Substituted benzofuran-based dimers **12a–f** and **13–15**, each studied previously,²⁴ were prepared in SYBYL for virtual library screening. Using in-house SYBYL Programming Language (SPL) scripts, compounds contained in the resulting virtual library were post-processed to (1) assign appropriate atom types to the sulfate groups (sulfur atom = S.o2; terminal oxygen atoms = O.co2); (2) assign an initial set of 3D coordinates using the CONCORD module within SYBYL; (3) add missing hydrogen atoms and (4) energy-minimize the resulting structures using the Tripos Force Field as described for the protein (*vide supra*).

Docking of the synthesized inhibitors onto the defined binding site of the thrombin was performed using GOLD 4.1 (Cambridge Crystallographic Data Centre, Cambridge, UK). The binding site was defined to include all atoms within 22 Å around the Arg173 C^α atom. Default parameters were employed during the GOLD docking runs with the following exceptions: a protein hydrogen bonding constraint was added such that the score was reduced by 10.0 GoldScore units if the ligand did not form an H-bond with the guanidinium group of Arg173. Amide bonds were allowed to flip. The number of GA runs was increased to 30 in order to more accurately screen all possible binding geometries, and early termination was disabled. The docking was driven by the GOLDScore fitness function and the docked solutions were ranked based on the unmodified GOLDScore obtained. To assess the reproducibility of the docked poses, the docking runs were performed in triplicate.

4.4.6 Screening for other proteases

Screening of library for Factor VIIa inhibition - Direct inhibition of factor VIIa by the library of sulfated benzofuran derivatives was measured through a one-point chromogenic substrate hydrolysis assay. The buffer used in these experiments was 20 mM Tris-HCl buffer, pH 7.4,

containing 100 mM NaCl, 2.5 mM CaCl₂, 0.1% polyethylene glycol (PEG) 8000 and 0.02% Tween 80. Benzofuran derivatives (5 µL) at concentrations 20 mM were diluted with 75 µL volume of assay buffer in flat bottom 96 well-plates (BD Falcon) at 37 °C. To this solution was added 10 µL of factor VIIa solution to give approximately 80 nM initial factor VIIa concentration and 5 µL of tissue factor solution to give 800 nM. After 10 min of incubation, 5 µL of 20 mM Spectrozyme factor VIIa was rapidly added and the residual factor VIIa activity was measured from the initial rate of increase in absorbance at 405 nm. The plate was read using a microplate reader (FlexStation III, Molecular Devices). Relative residual factor VIIa activity was calculated from the ratio of thrombin activity in the presence and absence of inhibitor. The percent residual activity was calculated using the equation 3:

$$\% \text{ Residual Activity} = [(slope \text{ of blank} - slope \text{ of well with inhibitor})/slope \text{ of blank}] \times 100$$

A cut off of **40%** was selected, and those compounds which showed a % residual activity lower than 40% were selected for full inhibition profile.

Screening of library for Factor IXa inhibition - Direct inhibition of factor IXa by the library of sulfated benzofuran derivatives was measured through a one-point chromogenic substrate hydrolysis assay. The buffer used in these experiments was 20 mM Tris-HCl buffer, pH 7.4, containing 100 mM NaCl, 2.5 mM CaCl₂, 0.1% polyethylene glycol (PEG) 8000, 0.02% Tween 80 and 33% v/v ethylene glycol. Benzofuran derivatives (5 µL) at concentrations 20 mM were diluted with 80 µL volume of assay buffer in flat bottom 96 well-plates (BD Falcon) at 25 °C. To this solution was added 5 µL of factor IXa solution to give approximately 1780 nM initial factor IXa concentration. After 10 min of incubation, 10 µL of 8.5 mM Spectrozyme factor IXa was

rapidly added and the residual factor IXa activity was measured from the initial rate of increase in absorbance at 405 nm. The plate was read using a microplate reader (FlexStation III, Molecular Devices). Relative residual factor IXa activity was calculated from the ratio of thrombin activity in the presence and absence of inhibitor. The percent residual activity was calculated using the equation 3.

Screening of library for Factor Xa inhibition - Direct inhibition of Factor Xa by the library of sulfated benzofuran derivatives was measured through a one-point chromogenic substrate hydrolysis assay. The buffer used in these experiments was 20 mM Tris-HCl buffer, pH 7.4, containing 100 mM NaCl, 2.5 mM CaCl₂, 0.1% polyethylene glycol (PEG) 8000 and 0.02% Tween 80. Benzofuran derivatives (5 μ L) at concentrations 20 mM were diluted with 185 μ L volume of assay buffer in flat bottom 96 well-plates (BD Falcon) at 37 °C. To this solution was added 5 μ L of factor Xa solution to give approximately 43.5 nM initial factor Xa concentration. After 10 min of incubation, 5 μ L of 5 mM Spectrozyme factor Xa was rapidly added and the residual factor Xa activity was measured from the initial rate of increase in absorbance at 405 nm. The plate was read using a microplate reader (FlexStation III, Molecular Devices). Relative residual factor Xa activity was calculated from the ratio of thrombin activity in the presence and absence of inhibitor. The percent residual activity was calculated using the equation 3.

Screening of library for Factor XIa inhibition - Direct inhibition of factor XIa by the library of sulfated benzofuran derivatives was measured through a one-point chromogenic substrate hydrolysis assay. The buffer used in these experiments was 20 mM Tris-HCl buffer, pH 7.4, containing 100 mM NaCl, 0.1% polyethylene glycol (PEG) 8000 and 0.02% Tween 80. Benzofuran derivatives (5 μ L) at concentrations 20 mM were diluted with 85 μ L volume of assay buffer in flat bottom 96 well-plates (BD Falcon) at 25 °C. To this solution was added 5 μ L of

factor XIa solution to give approximately 15.3 nM initial factor XIa concentration. After 10 min of incubation, 5 μ L of 6.6 mM Spectrozyme factor XIa was rapidly added and the residual factor XIa activity was measured from the initial rate of increase in absorbance at 405 nm. The plate was read using a microplate reader (FlexStation III, Molecular Devices). Relative residual factor XIa activity was calculated from the ratio of thrombin activity in the presence and absence of inhibitor. The percent residual activity was calculated using the equation 3.

Screening of library for Factor XIIa inhibition - Direct inhibition of factor XIIa by the library of sulfated benzofuran derivatives was measured through a one-point chromogenic substrate hydrolysis assay. The buffer used in these experiments was 20 mM Tris-HCl buffer, pH 7.4, containing 100 mM NaCl, 0.1% polyethylene glycol (PEG) 8000 and 0.02% Tween 80. Benzofuran derivatives (5 μ L) at concentrations 20 mM were diluted with 185 μ L volume of assay buffer in flat bottom 96 well-plates (BD Falcon) at 25 °C. To this solution was added 5 μ L of factor XIIa solution to give approximately 200 nM initial factor XIIa concentration. After 10 min of incubation, 5 μ L of 5 mM Spectrozyme factor XIIa was rapidly added and the residual factor XIIa activity was measured from the initial rate of increase in absorbance at 405 nm. The plate was read using a microplate reader (FlexStation III, Molecular Devices). Relative residual factor XIIa activity was calculated from the ratio of thrombin activity in the presence and absence of inhibitor. The percent residual activity was calculated using the equation 3.

Chapter 5 Synthesis and Biochemical Evaluation of 2nd Generation Sulfated Benzofurans

5.1 Introduction

The previous chapters describe the successful design and synthesis of small molecules that display an antithrombotic effect through an allosteric mechanism.^{23, 12, 18} Those were the first reported small molecules that reduced the catalytic efficiency of thrombin by binding to an allosteric site. In order to improve the potency of benzofuran dimeric units, we designed a library of 2nd generation compounds. From the SAR studies of the sulfated benzofuran monomers and dimers, we found that substitution at the 2'-allylic position of the sulfated benzofuran dimer does not have a detrimental effect on potency.²³¹ This led us to design a second generation library containing three linked benzofuran units as the backbone scaffold and various substitutions at the first benzofuran unit to improve the potency and solubility of the compounds. In this work, we report the synthesis, biological activity, mechanistic and blood plasma studies of a library of eleven sulfated benzofuran trimers and tetramer. Based on substrate hydrolysis assay and through Michaelis-Menten kinetic studies, we can state that these molecules are potent small synthetic allosteric inhibitors of thrombin. The strong competition with heparin suggests that

these molecules bind at exosite II. Finally, plasma studies showed that these molecules are potent anticoagulants in whole human plasma.

5.2 Results and Discussion

5.2.1 Design and Synthesis of the 2nd Generation Sulfated Benzofuran Scaffold

Previously, we reported that the sulfated low molecular weight lignins (LMWLs) are potent allosteric inhibitors of thrombin and are structurally very different from heparin with less anionic charge and a more hydrophobic scaffold.²³⁹ Similar to heparin, LMWLs are constituted of a mixture of different structures arising from varying inter-residue linkages and degrees of sulfations. It is well known that the β -5 linkage is the most abundant linkage present in natural lignins.^{200, 202} Based on this assumption and its synthetic feasibility, the benzofuran scaffold was designed. In preliminary work, we synthesized a diverse library of sulfated benzofuran monomers and dimers to study the effects of various substitutions on their potency of thrombin inhibition.²³¹ Among the members of this library, a few structures were found to inhibit thrombin with moderate potency in the range of 5-50 μ M. A mechanistic study divulged that these molecules inhibit the catalytic efficiency of thrombin in an allosteric fashion, similar to the parent LMWLs. SAR studies revealed very interesting findings and guided the design 2nd generation compounds. It had been known that one sulfate group at the 5- position is optimal for potency. In addition, any increase in the number of anionic charges, either from sulfate or carboxylate, is detrimental. The presence of hydrophobic groups at the 3-ester and 6-hydroxy positions is favorable. The most striking feature in the SAR that leads to the design of 2nd generation compounds was tolerance of steric group at the 2'-allylic position of sulfated benzofuran dimer.²³¹ Along with this, a 1000-fold improvement in potency on moving from

monomers to dimers led us to add an additional substituted benzofuran unit to the existing dimeric scaffold.

Incorporating the above, a pilot 2nd generation library of ten sulfated benzofuran trimers was designed and synthesized. In this library, the terminal two benzofuran units were kept the same and variations were made at 3, 4 and 5- positions of the first benzofuran units. The variation at the 3-carboxylate ester position included both hydrophilic and bulky hydrophobic groups, while the position and number of anionic group and hydrophobic groups at 6- position were also varied.

5.2.2 Chemistry

Syntheses of β -5-like trimeric units were described in Figure 27-30. Figure 27 described the synthesis of various reactive handles **T4a–T4h** starting from the readily available catechol. The first step leads to formation of 5, 6-dihydroxy-benzofuran-3-carboxylic acid esters using conditions published previously.²³¹ The highly functionalized benzofuran unit **T1a–T1e** was synthesized in one step using an oxidative-Michael addition reaction. The selective mono-alkylation of the 6-hydroxy group of compounds **T1a–T1e** was achieved under basic condition to afford **T2a–T2g** in 60% yield. This reaction also resulted in formation of another regio-isomer **T2h** in minor amounts (< 10 %), causing an unfortunate difficulty in purification. The separation can be achieved by careful purification using flash chromatography. Subsequently, protection of the 5-hydroxy group was achieved by *t*-butyltrimethylsilyl chloride in the presence of imadazole, this led to formation of **T3a–T3h** in very high yield. The bromination of the allylic position in the presence of *N*-bromosuccinimide leads to the synthesis of reactive handles **T4a–T4h**.

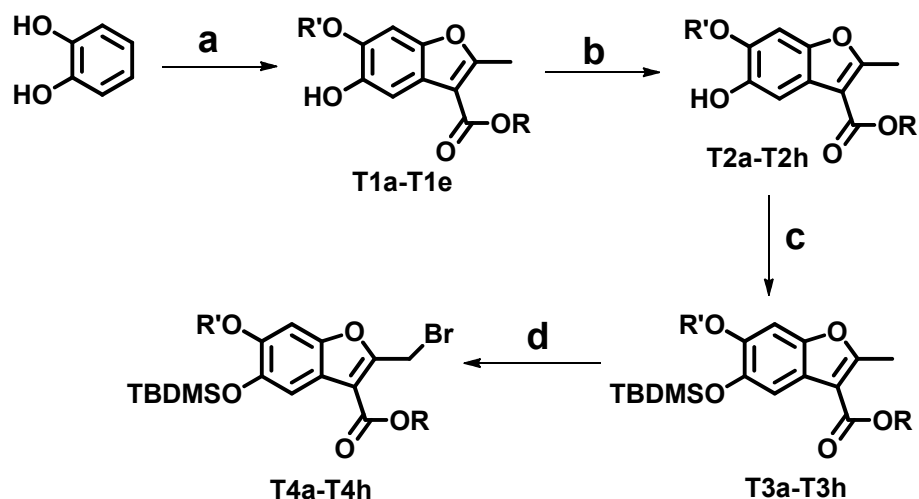


Figure 27. Description of synthesis of a library reactive handles **T4a–T4h** for synthesis of library of sulfated benzofuran trimers. Reactions: a) Alkyl aceto-acetate, NaIO₄, DIPEA, ethanol: water (3:1); b) Cs₂CO₃, alkyl or acyl halide, anh. DMF; c) TBDMSCl, Imidazole, DMF; d) NBS, CCl₄.

As shown in Figure 28, synthesis of compound **T5a–T5b** was afforded by nucleophilic displacement of the allylic bromide of **T4a** by a free phenolic group at the 5- position of **T2a** and **T2e** under basic condition. The coupling reaction was low yielding <50% due to steric interference around both nucleophilic (allylic bromide) and electrophilic (phenolic group) positions. The required handle **T6a–T6b** was achieved by removal of the protecting silyl group from 5- position using potassium fluoride and a catalytic amount of glacial acetic acid.

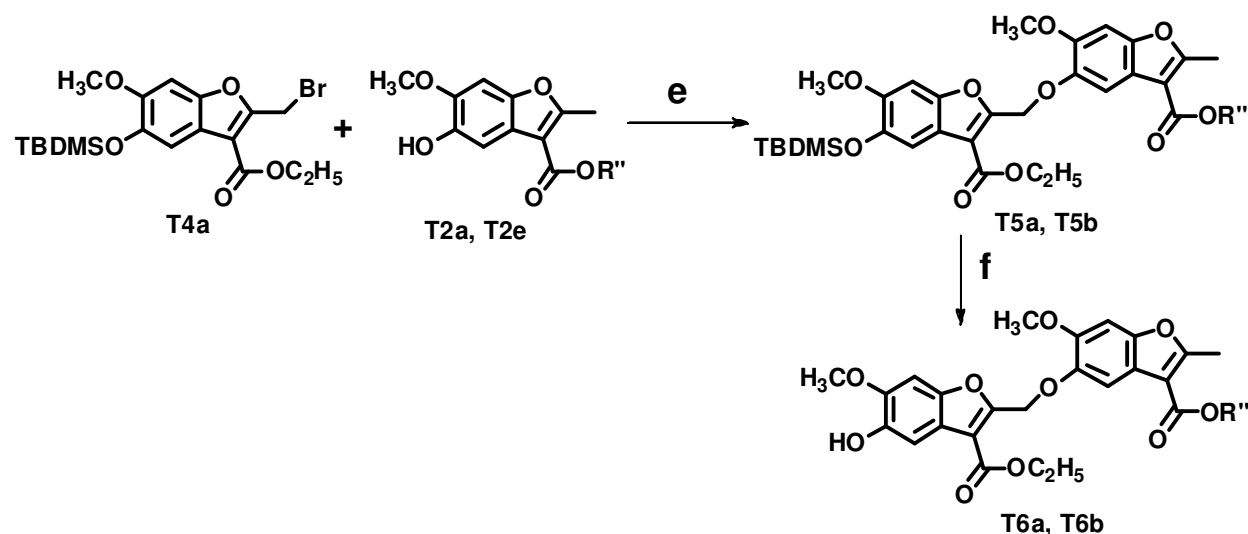


Figure 28. Description of synthesis of reactive handles **T6a–T6b** for synthesis of library of sulfated benzofuran trimers. Reactions: e) Cs_2CO_3 , **T2a** & **T2e**; DMF; f) KF , CH_3COOH , DMF.

Figure 29 describes the synthesis of the nine desired sulfated trimeric units **T9a–T9h** and **T14**. The coupling of the two reactive handles **T4a–T4h** and **T6a–T6b** were achieved using microwave radiation to afford trimeric units **T7a–T7h**. Unlike the coupling reactions for dimeric unit **T5a–T5b**, coupling for trimers failed at room temperature due to solubility and steric issues. Microwave-based coupling reaction afforded the desired compounds in a reaction time of 80 minutes with 50% yield. The compounds **T8a–T8h** were obtained by removal of the protecting silyl group similar to condition used above (synthesis of **T6a–T6b**, Figure 27). The selective hydrolysis of the allyl ester of **T8e** is achieved by a catalytic amount of $\text{Pd}(\text{PPh}_3)_3$ in the presence of base to give **T13** in good yield. The targeted compounds **T9a–T9h** and **T14** were accessed by addition of a sulfate group using the microwave-based conditions previously developed in our laboratory.²²² The cation exchange from triethylamine to sodium was performed using weak cation exchange resin and purified using flash chromatography. In Figure 30, intermediate **T8a** and **T4a** were coupled together under basic conditions using the microwave method described

above in synthesis of **T7a–T7h**. This followed by removal of the protecting group and sulfation afforded the desired compound **T12**.

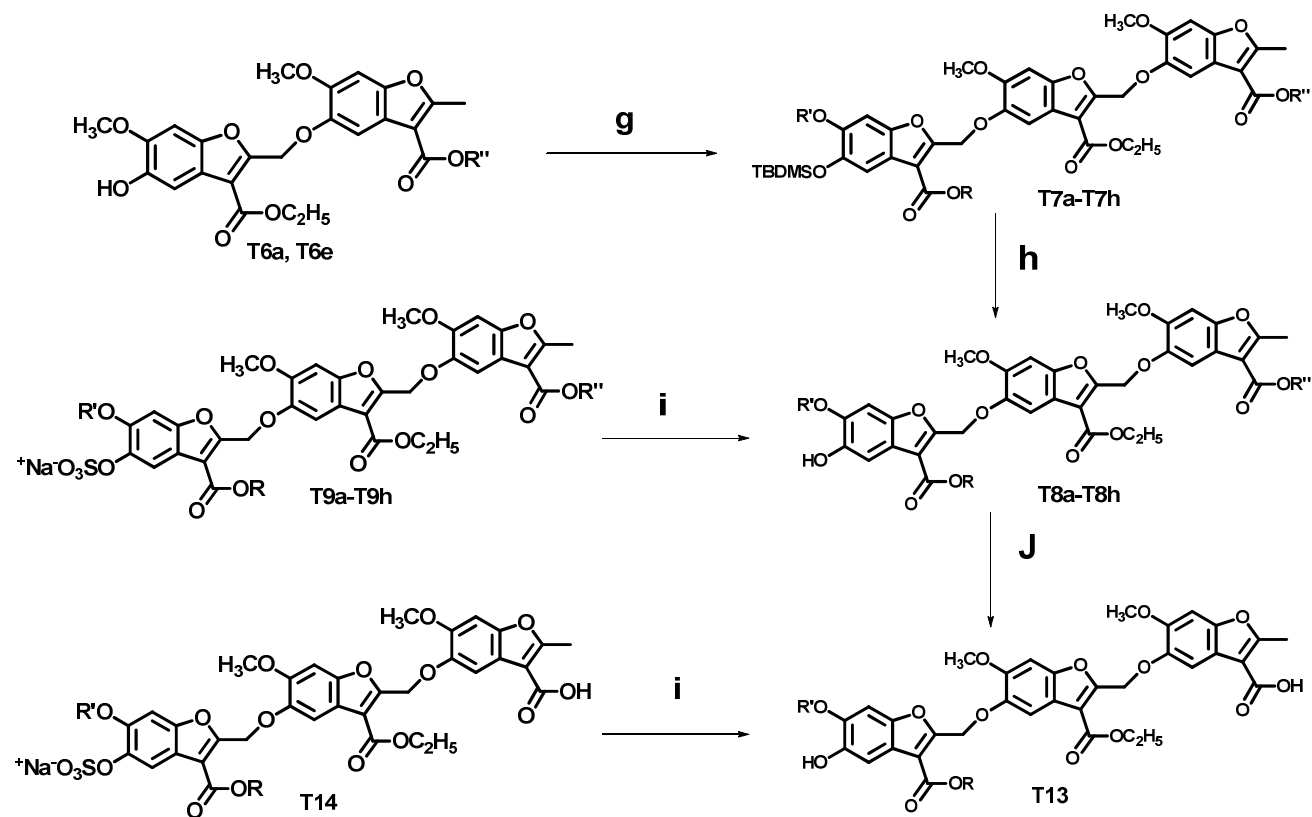


Figure 29. Description of synthesis of library of sulfated benzofuran trimers **T9a–T9h** and **T14**. Reactions: g) Cs_2CO_3 , **2**; DMF; h) KF, CH_3COOH , DMF; i) $\text{Et}_3\text{N}:\text{SO}_3$, $\text{CH}_3\text{CN}:\text{DMF}$ (4:1), MW; j) $\text{Pd}(\text{PPh}_3)_3$, PPh_3 , pyrrolidine.

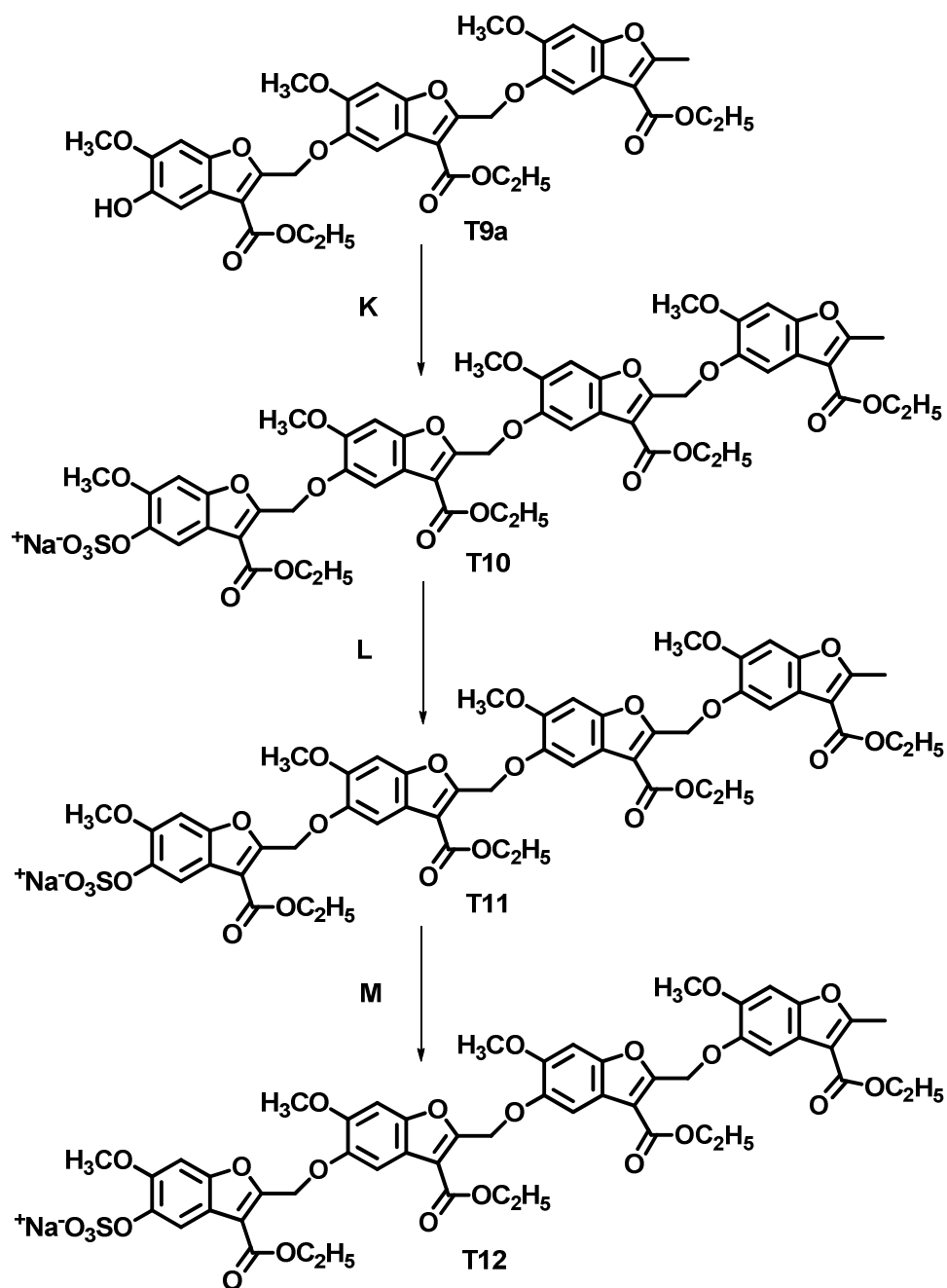


Figure 30. Description of synthesis of sulfated benzofuran tetramer **T12**. Reactions: k) Cs_2CO_3 , **T2a**; DMF; L) KF , CH_3COOH , DMF; M) $\text{Et}_3\text{N}:\text{SO}_3$, $\text{CH}_3\text{CN}:\text{DMF}$ (4:1).

5.2.3 Substrate Hydrolysis Assay

The inhibition potencies of sulfated benzofuran trimers and tetramer for thrombin were measured using the Spectrozyme TH hydrolysis-based assay.²⁰² This assay measures the decrease in the initial rate of substrate hydrolysis in the presence of the inhibitors as a quantitative measure of the inhibition. The fractional decrease in the initial rate of hydrolysis typically gives a sigmoidal curve on a semi-log plot, which is then fitted by a dose - response equation 4 (see Experimental Section 5.4.3) to calculate IC_{50} , HS and ΔY parameters for each potential inhibitor.

The semi-log inhibition profile observed for sulfated benzofuran trimers are shown in Figure 31. From the library of 11 inhibitors, ten molecules demonstrated potent inhibition of human α -thrombin at pH 7.4 and 25 °C. These include sulfated trimers **T9a–T9h**, **T14** and the sulfated tetramer **T12** (Tables 14). The inhibitor **T9a** showed the most potent inhibition with an IC_{50} of 670 nM under physiologically relevant conditions. The range of inhibition efficacy (45 to 95 %, Table 14) was found to vary considerably with the structure of the inhibitor. Nearly all of the inhibitors studied inhibited thrombin to more than 50% suggesting reasonably good overall efficacy in this series of sulfated benzofurans.

Table 14. Inhibition of human thrombin by sulfated benzofuran trimers

	R'	R	log IC_{50} (M)	IC_{50} (μM)	ΔY
T9a	—OCH ₂ CH ₃	—CH ₃	-3.17 \pm 0.02	0.67 \pm 0.04	44.1
T9b	—OCH ₃	—CH ₃	-2.59 \pm 0.12	2.5 \pm 0.2	54.9
T9c	—OC(CH ₃) ₃	—CH ₃	-0.77 \pm 0.03	149.24 \pm 0.04	92.8
T9d	—OCH ₂ CH ₂ OCH ₃	—CH ₃	-1.05 \pm 0.01	88.49 \pm 0.01	67.8
T9f	—OCH ₂ CH ₃	—CH ₂ CH ₃	-2.29 \pm 0.01	5.1 \pm 0.1	41.4
T9g	—OCH ₂ CH ₃	—CH(CH ₃) ₂	-0.48 \pm 0.01	324 \pm 0.1	83.8
T9e	—OCH ₂ CHCH ₂	—CH ₃	-1.12 \pm 0.04	75.64 \pm 0.02	64.3
T9h	na	na	-0.79 \pm 0.3	162 \pm 1	88.6
T12	na	na	-0.97 \pm 0.25	107 \pm 1	50.88
T13	na	na		>500	
T14	—OH	—CH ₃	-0.84 \pm 0.03	143 \pm 0.04	47.72

Spectrozyme TH was used as the substrates and the residual enzyme activity in the presence of the trimer was assessed by measuring the initial rate of substrate hydrolysis at 405 nm. Equation 3 was used to fit the dose dependence of the residual enzyme activity to obtain log IC_{50} , Y_0 , and Y_M values.

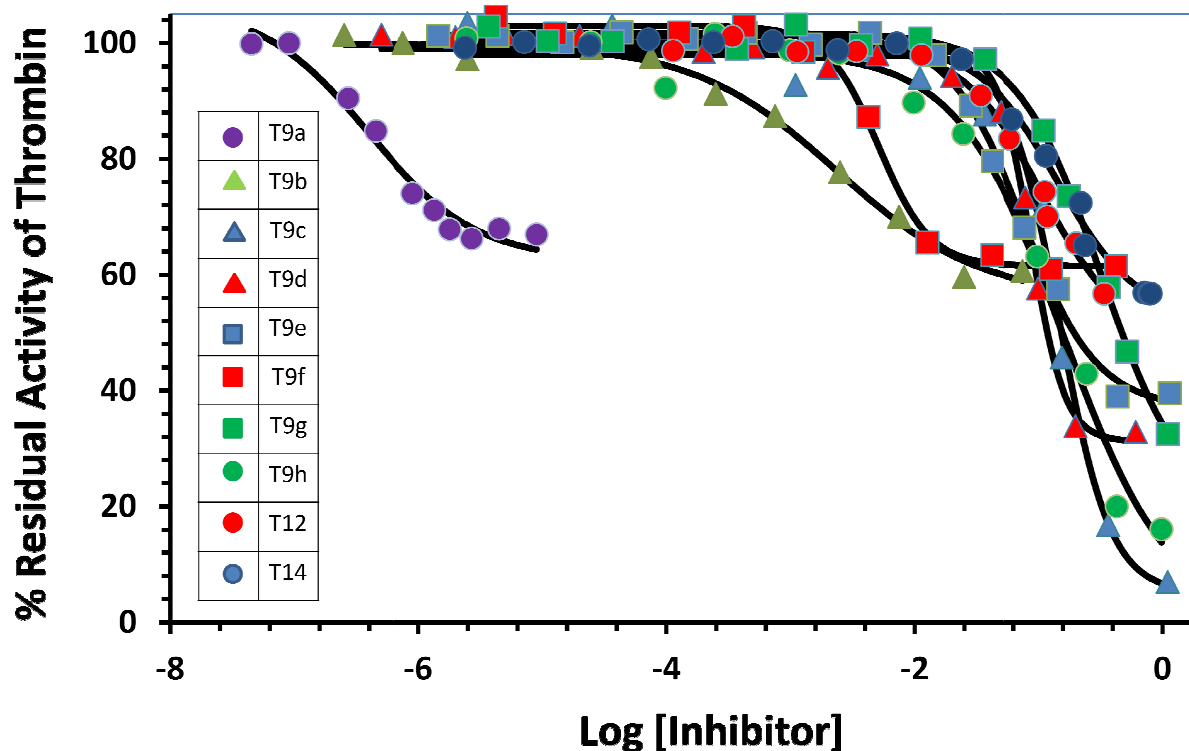


Figure 31. Direct inhibition of thrombin by designed sulfated benzofuran trimers and tetramer. The inhibition of human thrombin was determined spectrophotometrically through a Spectrozyme TH hydrolysis assay at pH 7.4 and 25 °C.

Comparison of the IC_{50} of **T9b**, **T9c**, **T9d** and **T9e** shows that as the size of the 3-ester increases, the inhibition potency decreases by 30 to 60-fold (Table 14). For example, **T9c** containing the highly hydrophobic and bulky t-butyl is 60-fold less potent than **T9b** containing the small methyl group. Whereas, in the cases of **T9d** and **T9e**, having methoxy methyl and allyl group, respectively, IC_{50} dropped only 30-fold. Although the potency of inhibition is decreased on steric crowding, polar groups are tolerated well than hydrophobic groups of the same size. The exceptionally high potency displayed by **T9a** having an ethyl ester at the 3- position is not well understood. This may be due to a stringent requirement of an ethyl ester at 3- position suggesting a highly conserved binding region here.

Similarly for **T9f** and **T9g** potency decreased 65-fold by changing the substitution from ethyl to isopropyl at the 6- position. These imply that Hydrophobicity, as well as the size of the substitution at the 6- position, plays an important role. Increasing the anionic charge, as seen in **T14**, decreases the potency by 220-fold. This suggests that the terminal benzofuran unit binds in a hydrophobic pocket that cannot tolerate the highly charged carboxylate group. This is a significant finding about the nature of this binding pocket. The trimer unit was found to be optimal for activity. Increasing the oligomeric chain to the tetramer as in **T12** decreased activity by 150-fold.

Comparing the effect of the sulfate group with the carboxylate group, it was found that the carboxylate group is not polar enough to solubilize the aromatic trimer scaffold. The molecule **T13** was found to precipitate at a higher concentration, thus causing problems in determination of the full inhibition profile. Thus, we can conclude that carboxylate group cannot successfully replace the sulfate group in this series for direct thrombin inhibition.

5.2.4 Biochemical Studies

- 1) Michaelis-Menten studies show no change in K_M , while there are significant changes in V_{Max} with increasing concentration of inhibitor. This suggests that the presence of the trimer does not affect the binding of the chromogenic substrate to the active site of the enzyme, but significantly reduces its catalytic efficiency. This indicates an uncompetitive, allosteric mechanism of thrombin inhibition by the trimer.
- 2) To test whether trimers binds in exosite I, competition studies with the hirugen analog, [5F]-Hir[54-65](SO₃⁻), were performed. The presence of [5F]-Hir[54-65](SO₃⁻) did not

significantly affect the thrombin inhibition profiles indicating that the trimer does not appear to bind in the anion-binding exosite I of thrombin.

- 3) To test whether trimers binds in exosite II, competition studies with three different exosite II binding ligands; porcine unfractionated heparin, H8, and γ' Fibrinogen peptide were performed. A distinct shift in these profiles is observed as the concentration of the UFH increases, suggesting competition between the two ligands for thrombin binding. This indicates that the trimer and full-length heparin compete for exosite II of thrombin. However, there was no change in inhibition profile observed with increasing concentration of heparin octasaccharide H8 and γ' Fibrinogen peptide. This indicates that the trimer and H8 do not compete with each other, although both are exosite II ligands.

5.2.5 Prolongation of Plasma Clotting Time by T9a

Typically, two plasma clotting assays are performed to evaluate the anticoagulant potency in plasma for new coagulation inhibitors. Prothrombin time (PT) and activated partial thromboplastin time (APTT) assays are used to measure the effect of an inhibitor on the extrinsic and intrinsic flux of coagulation, respectively. The concentrations of the inhibitors required to double the PT and APTT were measured and reported as described earlier (Chapter 4) for our first generation compounds (see Table 15).

A 2-fold increase in PT required 568 μ M concentration of **T9a**. In a similar manner, the doubling of APTT required 139 μ M of **T9a**. The higher potency for the APTT assay as compared to the PT assay suggests a more profound effect on intrinsic pathway. These results also suggest that the 2nd generation library of sulfated trimeric benzofurans is 10-fold more potent in human plasma than 1st generation compounds. These results were expected and prove

the validity of our design. The 2nd generation compounds are only 10 times less potent than our LMWLs, from which the benzofuran scaffold was designed. To further evaluate the mechanism of anticoagulation of these inhibitors in plasma, we performed plasma studies on various factor-deficient human plasmas. When the APTT test was performed on factors IX and XI-deficient human plasma, we measured that concentrations required to double the APTT time were 135 μ M and 120 μ M respectively (see Table 15). There was no significant change in 2^xAPPT time compared to normal human plasma suggesting a less significant role factors IX and XI with respect to the anticoagulation effect of these inhibitors. Similarly, 2^xPT value for factor VII deficient plasma was 518 μ M, which is not significantly different from normal human plasma. Thus, we can conclude that our designed inhibitors are not inhibiting factors IX, XI and VII in human whole plasma. Overall, the plasma studies suggest the feasibility of designing sulfated benzofurans that will function as anticoagulants *in vivo*.

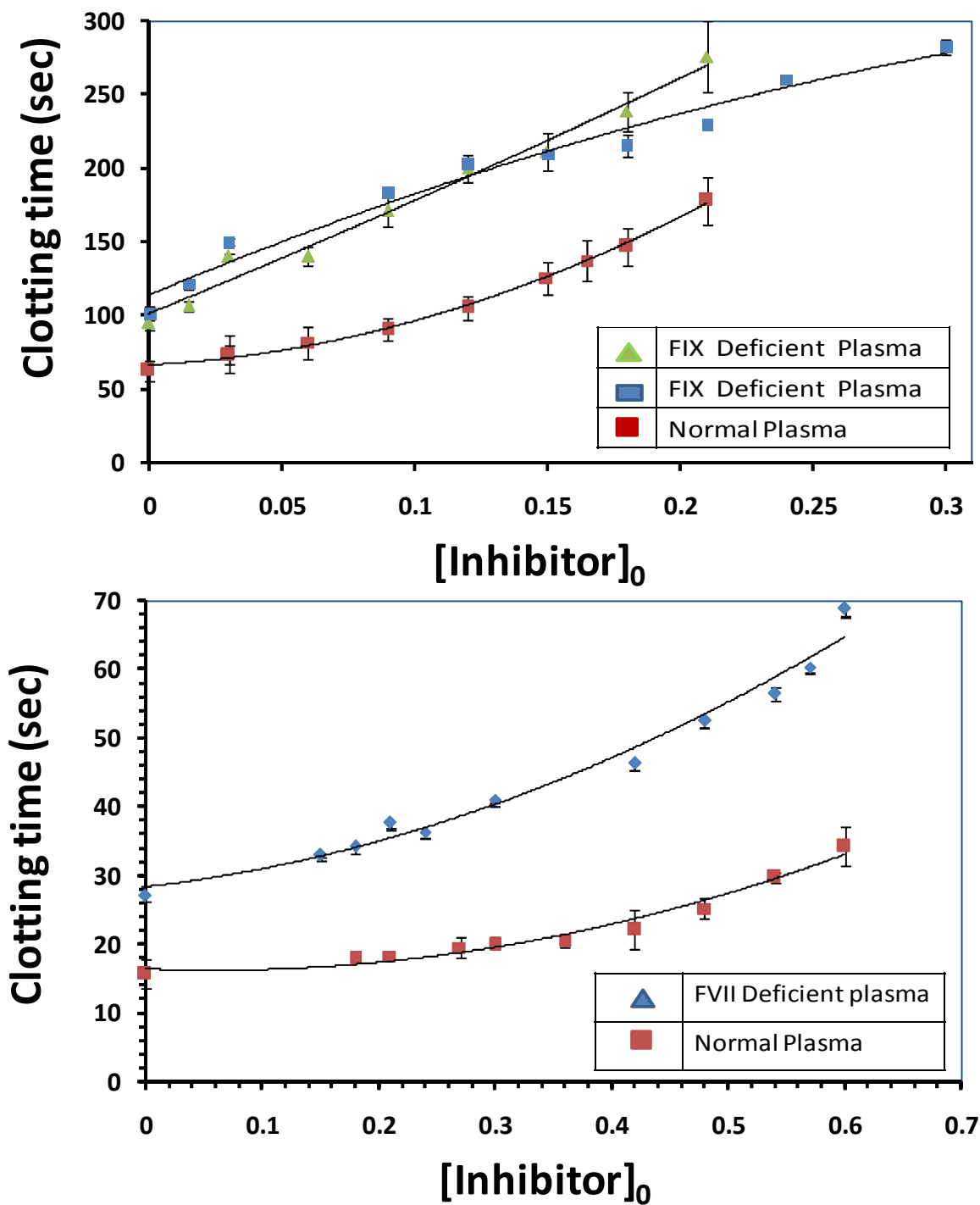


Figure 32 Prolongation of clotting time as a function of concentration of sulfated benzofuran trimer and tetramer in either activated partial thromboplastin time assay (top) or prothrombin time assay (bottom). Solid lines are trend lines, and not non-linear regressional fits.

Table 15. The PT and APTT assay results for **T9a** in normal as well as factor deficient plasma

APTT Assay	2 ^x PT (μM)	2 ^x APTT
Normal Plasma	568	139
Factor XI Deficient Plasma	NA	135
Factor IX Deficient Plasma	NA	120
Factor VII deficient Plasma	518	NA

PT and APTT values were deduced in *in vitro* human plasma experiments where the clot initiator is either thromboplastin or ellagic acid, respectively.

5.2.6 Screening against Other Serine Proteases

The library of sulfated benzofuran trimers was screened against the panel of coagulation proteases including factors VIIa, IXa, Xa, XIa and XIIa, all of which are either involved in intrinsic or extrinsic pathways of the coagulation cascade. These assays are based on the rate of hydrolysis of a chromogenic substrate by the protease, which decreases in the presence of an inhibitor. Screening was performed at a single concentration of inhibitors using a substrate hydrolysis assay in 96-well plates. The decrease in initial rate of hydrolysis provided the fractional residual activity of enzyme. The details of experimental conditions are provided in the Experimental Section (5.4.6).

Table 16 shows the residual activity of all proteases at a final concentration of 365 μM of each inhibitor. The library of trimers contains molecules with varying substitutions ranging from hydrophobic to polar as well multiple anionic groups. None of these trimers inhibited factor XIIa more than 20% at this concentration. In the screening against factor VIIa, molecules **T9b** and

T9e inhibited factor VIIa activity more than 70%, this showing potential for potent inhibition. These two molecules were selected for further inhibition study. Similarly, several trimers showed higher potential for inhibition of factor IXa. Molecules **T9a**, **T9b**, **T9e**, **T9f**, **T12** and **T15** inhibited factor IXa activity greater than 80% at the given concentration. These inhibitors were selected for detailed inhibition profile and thus have potential for the design into better inhibitors of factor IXa.

Table 16. Residual activity of proteases (in %) at single concentration (365 μ M) of each inhibitor

	Factor VIIa	Factor IXa	Factor Xa	Factor XIa	Factor XIIa
T9a	72 \pm 3	1 \pm 1.5	84 \pm 2	2 \pm 3	103 \pm 5
T9b	26 \pm 3.5	3 \pm 3	38 \pm 3	3 \pm 5	86 \pm 3
T9c	92 \pm 3.5	103 \pm 6	31 \pm 2	11 \pm 1	92 \pm 3
T9e	37 \pm 3	16 \pm 2	69 \pm 2	1 \pm 1.5	93 \pm 3
T9f	98 \pm 4	31 \pm 2	73 \pm 3	5 \pm 7	98 \pm 6
T9g	101 \pm 3	82 \pm 3	85 \pm 3	39 \pm 2.5	98 \pm 3
T9h	104 \pm 7	96 \pm 6	76 \pm 2	6 \pm 2	96 \pm 4
T12	100 \pm 6	11 \pm 6	66 \pm 3	3 \pm 2.5	86 \pm 2
T14	74. \pm 1	103 \pm 8	102 \pm 4	11 \pm 5	47 \pm 1.5
T15	100 \pm 4	17 \pm 1	70 \pm 3	4 \pm 3	99 \pm 3.5

In screening against factor Xa, with the exception of inhibitors **T9b** and **T9c**, the majority of trimers showed minimal activity against factor Xa. Although the inhibitory abilities of **T9b** and **T9c** are just 40%, which were much less as compared to inhibition by other proteases, these molecules were selected for detailed inhibition profiles. As expected from the results of inhibition by monomers and dimers, the library of trimers showed potent inhibition against factor

XIa. The trimers inhibited the factor XIa activity greater than 80% at the given concentration. The entire library of trimers was selected for detailed inhibition profile.

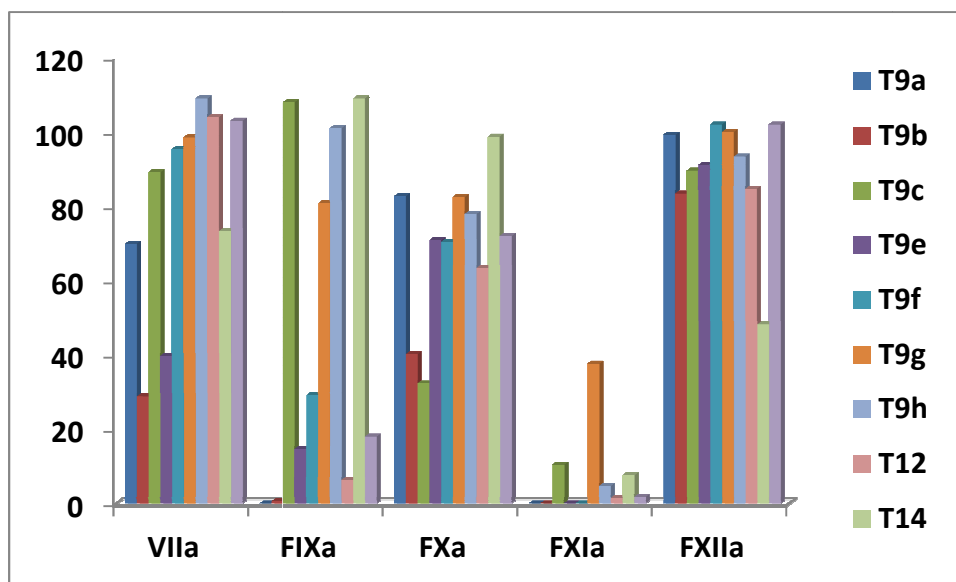


Figure 33. Bar graph showing the % residual activity of given proteases at single concentration of each inhibitor

5.2.7 Factor VIIa Inhibition Potential of Designed Sulfated Benzofuran Trimers

The full Inhibition profile of factor VIIa by sulfated benzofuran trimers was measured with the Spectrozyme TH hydrolysis assay, as described in Experimental Section (5.4.3). This assay analyzes the decrease in the initial rate of substrate hydrolysis in the presence of the sulfated benzofuran with respect to the initial rate of substrate hydrolysis in absence of the inhibitor, to provide a measure of % inhibition of the enzyme. The fractional decrease in initial rate of hydrolysis typically shows a sigmoidal profile on a semi-log plot, which is then fitted by a dose – response to derive IC_{50} , HS , Y_0 and Y_M parameters for each potential inhibitor.

Figure 34 shows the semi-log inhibition curves obtained from selected sulfated trimer compounds. The selected trimer molecules exhibited reasonable inhibition of human factor VIIa at pH 7.4 and 37 °C. Out of the library of 10 trimers, only **T9b** and **T9e** exhibited moderate

inhibition potency for factor VIIa. **T9e** is the most potent with an IC_{50} of $82.5 \pm 0.1 \mu M$, while **T9b** exhibited an IC_{50} of $239 \pm 1 \mu M$ under physiologically relevant conditions. Although **T9b** displayed lower potency compared to **T9e**, it showed a better inhibition efficacy (85%, Table 17) than **T9e** (45%, Table 17). Although this study is too small to predict SAR, these molecules can still serve as potential leads to design inhibitors for factor VIIa.

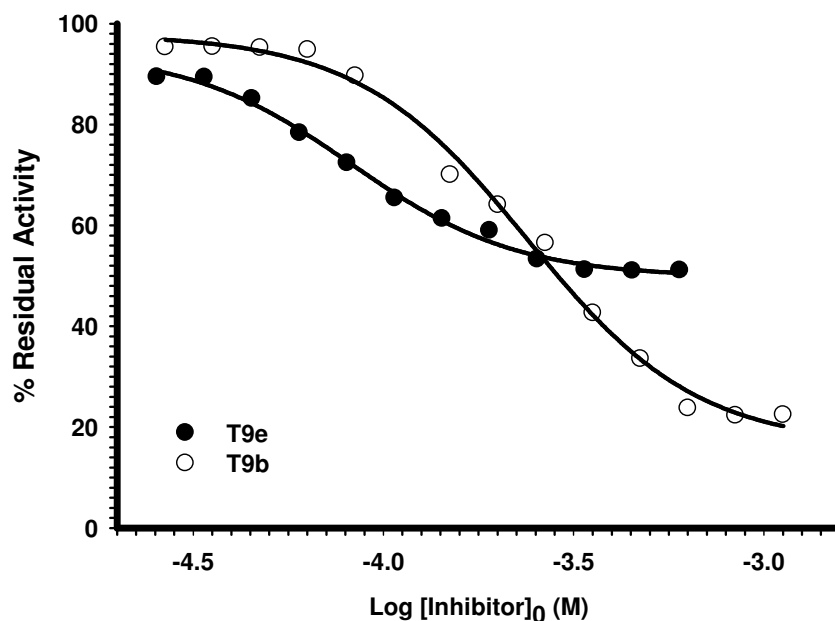


Figure 34. Direct inhibition of factor VII by inhibitors **T9e** and **T9b**. The inhibition of human factor VIIa was determined spectrophotometrically through a Spectrozyme factor VIIa hydrolysis assay at pH 7.4 and 37 °C. Solid lines represent sigmoidal fits to the data to obtain IC_{50} , Y_M , and Y_O , as described in the experimental section.

Table 17. Inhibition of sulfated benzofuran trimers

	Log IC₅₀	IC₅₀ (μM)	ΔY
T9b	-3.62 ± 0.01	239 ± 0.02	83.6
T9e	-4.08 ± 0.01	82.4 ± 0.02	45.3

5.2.8 Factor IXa Inhibition Potential of Designed Sulfated Benzofuran Trimers

Figure 35 shows the semi-log inhibition curves observed obtained from the selected sulfated trimers. The selected trimer molecules exhibited reasonable inhibition of human factor VIIa at pH 7.4 and 37 °C. Out of the library of 10 trimers, five trimers exhibited moderate inhibition potency for factor VIIa. **T9f** is most potent with an IC₅₀ of 9.2 μM and displayed complete inhibition efficacy (95%, Table 18). The other trimers **T9c**, **T9d**, **T12** and **T15** displayed potencies of 25.7 μM, 22.3 μM, 65.5 μM and 23.8 μM, respectively. These trimers displayed inhibition efficacy of 80-90% (Table 18). However, a clear trend of SAR is not observed from this small library of molecules. However, more hydrophobic scaffolds displayed higher potency and efficacy for inhibition of factor IXa. The most potent inhibitor **T9f** has a hydrophobic isopropyl group at the 6- position. Similarly, **T9c**, **T9d** and **T15** with hydrophobic substitutions at the 6- and 3- positions displayed similar potency. The presence of a terminal carboxylate group in **T15** is well tolerated. Increasing the chain length with additional benzofuran units (**T12**) reduces the inhibition potency by 2-fold. Thus, it can be concluded that the trimer is optimal with hydrophobic substitutions at the first unit.

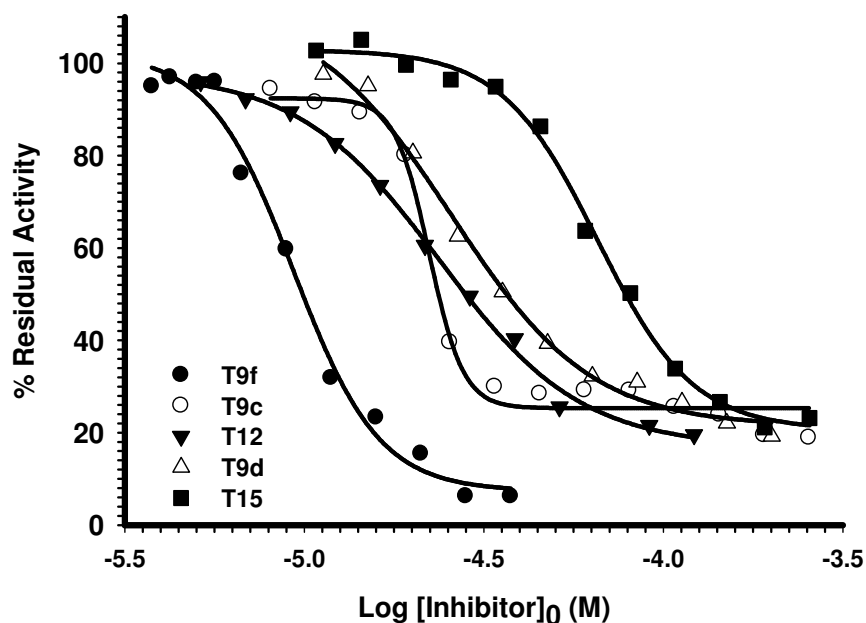


Figure 35. Direct inhibition of factor IXa by inhibitors **T9c**, **T9d**, **T9f**, **T12** and **T15**. The inhibition of human factor IXa was determined spectrophotometrically through a Spectrozyme factor IXa hydrolysis assay at pH 7.4 and 37 °C. Solid lines represent sigmoidal fits to the data to obtain IC_{50} , Y_M , and Y_O , as described in the Experimental Section (5.4.8).

Table 18. Inhibition of human factor IXa by sulfated benzofuran trimer

	Log IC_{50}	IC_{50} (μM)	ΔY
T9c	-4.59 ± 0.02	25.7 ± 0.04	81.3
T9d	-4.65 ± 0.01	22.2 ± 0.01	67
T9f	-5.03 ± 0.01	9.2 ± 0.02	95.8
T12	-4.18 ± 0.01	65.5 ± 0.01	82.2
T15	-4.62 ± 0.01	23.7 ± 0.02	81.3

5.2.9 Factor Xa Inhibition Potential of Designed Sulfated Benzofuran Trimers

Figure 36 shows the semi-log inhibition curves obtained from selected sulfated trimers. The selected trimer molecules exhibited reasonable inhibition of human factor Xa at pH 7.4 and 37

°C. Out of a library of 10 trimers, only **T9b** and **T9d** exhibited moderate inhibition potency. **T9b** is the most potent with an IC_{50} of 61 μ M and **T9d** displayed a potency of 103 μ M (Table 19). These molecules displayed inhibition efficacy of 80-100%. Although this study is too small to predict any SAR, these molecules can serve as potential lead to design inhibitors for factor Xa.

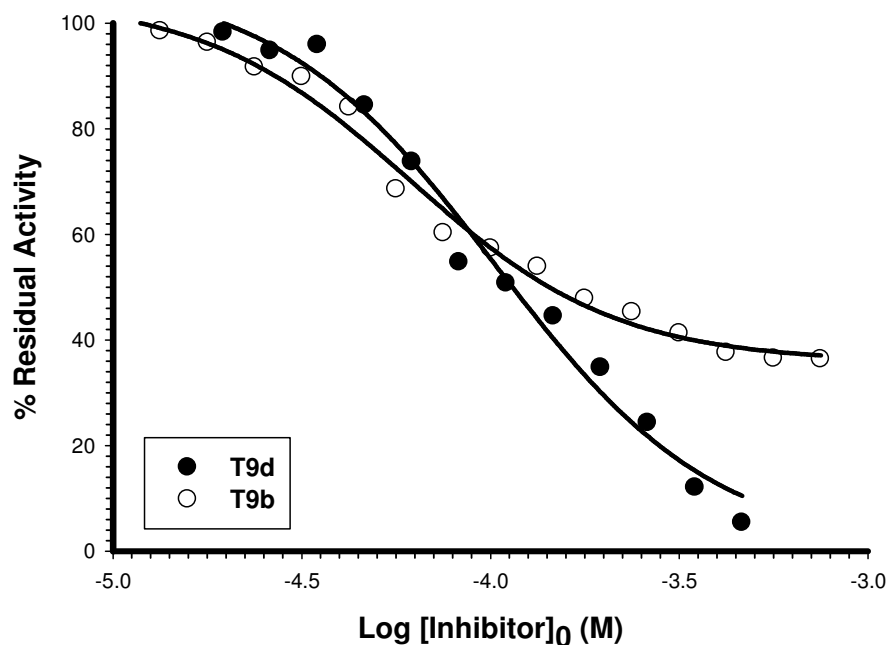


Figure 36. Direct inhibition of factor Xa by inhibitors **T9b**, and **T9d**. The inhibition of human factor Xa was determined spectrophotometrically through a Spectrozyme factor Xa hydrolysis assay at pH 7.4 and 37 °C. Solid lines represent sigmoidal fits to the data to obtain IC_{50} , Y_M , and Y_O , as described in the Experimental Section (5.4.7).

Table 19 Inhibiton of human factor Xa by sulfated benzofuran trimers

	Log IC₅₀	IC₅₀ (μM)	ΔY
T9b	-4.21 ± 0.02	61.1 ± 0.03	68.9
T9d	-3.98 ± 0.04	103.0 ± 0.05	99

5.3 Significance

This work presents a library of small homogenous sulfated aromatic scaffolds as novel inhibitors of thrombin with an allosteric mode of action. These are the first known small aromatic molecules as allosteric inhibitors of thrombin with nanomolar potency. The allosteric inhibition of thrombin offers advantages of controlled inhibition and ease of design of antidote.

Finally, the successful design of allosteric inhibitors of thrombin opens a path for designing allosteric inhibitors for other upstream proteases of the coagulation cascade. The recognition of the heparin binding site by these aromatic inhibitors may extend the inhibition activity for other proteases that are known to bind heparin. By exploring the other structural features of lignins, it may be possible find scaffolds inhibiting other proteases in highly specific manners.

5.4 Experimental Procedures

5.4.1 Chemicals, Reagents and Analytical Chemistry

Reagents, chemicals and solvents were purchased either from Sigma-Aldrich (Milwaukee, WI) or Fisher (Pittsburgh, PA) and were used as received. Reagent solutions and chemicals were handled under inert nitrogen atmosphere using syringe techniques for liquid and dried spatula for solids. All glassware was dried in the oven overnight before use. All organic layers obtained during work-up were dried using anhydrous sodium sulfate. Reaction progress was monitored using analytical thin layer chromatography (TLC) using UNIPLATETM silica gel GHLF 250 μm pre-coated plates (ANALTECH, Newark, DE) and detected by UV (254 nm). Column chromatography was performed using Teledyne ISCO (Lincoln, NE) Combiflash RF system and disposable normal silica cartridges of 30 – 50 μm particle size, 230 – 400 mesh size and 60 Å pore size. Sodium exchange chromatography was performed using SP Sephadex C-25 sodium cation exchange resin from GE Healthcare Life Sciences (Piscataway, NJ). Approximately 100 mg of each sulfated sample was loaded onto 10 g of the cation exchanger in a 10 \times 460 mm column and eluted with water at 0.5 mL/min. Microwave-based sulfation and coupling reactions were performed using a CEM-Discover synthesizer (Matthews, NC) in sealed reaction vessels (7 mL) at 50 W. Temperature of the reaction was maintained at the desired setting using cooled nitrogen (45 psi) flow.

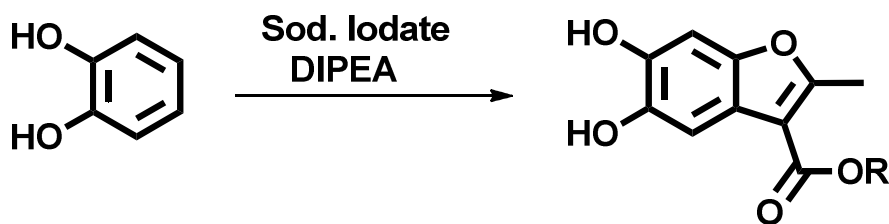
¹H and ¹³C NMR spectra were recorded at either 300 or 400 MHz (Varian Mercury or Bruker UltrashieldTMPlus) in appropriate deuterated solvents including CDCl₃, DMSO-*d*₆, or D₂O. All signals are reported in ppm with the internal chloroform, DMSO, and D₂O signals at 7.26, 2.50, 2.05, and 4.79, respectively, as standards. The data is reported as chemical shifts (ppm) and splitting pattern is described as (s = singlet, d = doublet, t = triplet, m = multiplet) with coupling constant(s) (Hz), and integration. Mass spectrometry was performed on all

synthesized molecules using a Micromass ZMD4000 single quadrupole mass spectrometer with ESI ionization probe operating in negative ion mode (Waters Corp., Milford, MA). The samples, dissolved in acetonitrile containing formic acid (5% v/v), were infused at 10 μ L/min. The source block temperature and the probe temperature were typically held at 100 and 120 $^{\circ}$ C, respectively, while corona and cone voltages were selected through manual optimization. The desolvation nitrogen flow was 500 L/hour. Mass spectra were acquired in the mass range from 110 to 1000 Daltons at 400 amu/sec.

Chromogenic substrate Spectrozyme TH (H-*D*-hexahydrotyrosol-Ala-Arg-*p*-nitroanilide) was purchased from American Diagnostica (Greenwich, CT). Unfractionated porcine heparin was purchased from Sigma (St. Louis, MO). Heparin octasaccharide H8 was purchased from V-Labs (Covington, LA). All other chemicals were analytical reagent grade from either Sigma Chemicals (St. Louis, MO) or Fisher (Pittsburgh, PA) and used as such.

5.4.2 Synthesis Protocols

Synthesis of 5, 6-dihydroxy-2-methylbenzofuran-3-carboxylate esters (T1a–T1e).



To a solution of catechol (20 mmol) in 75 mL of ethanol were added ester of acetoacetate (20 mmol) and N, N-Diisopropylethylamine (40 mmol). The reaction mixture was stirred for 5 min. To this mixture was added sodium iodate (20 mmol) and the solution stirred vigorously for 5 min and then 25 mL of water was added. The reaction mixture was stirred for 10 hours at room

temperature and quenched with 400 mL of ethyl acetate and extracted with 150 mL of brine and 30 mL of 0.5 N HCl. The organic layer was dried over magnesium sulfate and concentrated. The product was purified by passing through a plug of silica (1 inch in height) using 2% methanol in methylene chloride. The product was concentrated and dried under vacuum to provide a yield of 40%.

T1a: ^1H NMR (Acetone- d_6 , 300 MHz) δ 1.36 (t, J = 3 Hz, 3H), 2.63 (s, 3H), 4.31 (q, J = 6 Hz, 2H), 6.95 (s, 1H), 7.37 (s, 1H). ^{13}C NMR (CDCl_3) δ 14.79, 14.96, 60.54, 98.53, 106.62, 108.83, 117.56, 144.09, 144.92, 147.79, 161.79, 164.48.

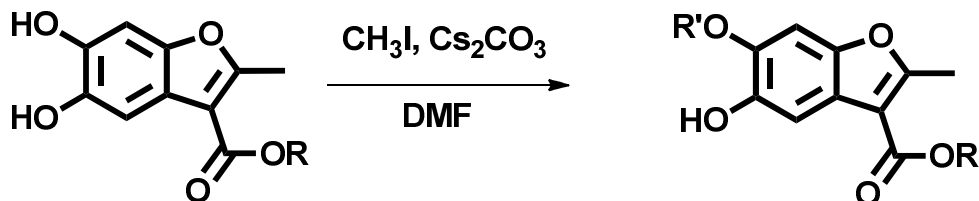
T1b: ^1H NMR (CDCl_3 , 300 MHz) δ 2.65 (s, 3H), 3.97 (s, 3H), 6.99 (s, 1H), 7.43 (s, 1H).

T1c: ^1H NMR (CDCl_3 , 300 MHz) δ 1.60 (s, 9H), 2.63 (s, 3H), 6.96 (s, 1H), 7.39 (s, 1H).

T1d: ^1H NMR (CDCl_3 , 300 MHz) 2.63 (s, 3H), 3.41 (s, 3H), 3.72 (t, J = 12 Hz, 2H), 4.46 (t, J = 12 Hz, 2H), 6.96 (s, 1H), 7.39 (s, 1H).

T1e: ^1H NMR (CDCl_3 , 300 MHz) 2.71 (s, 3H), 4.85 (d, 2H), 5.22 (d, 1H), 5.36 (d, 2H), 6.00 (m, 1H), 6.91 (s, 1H), 7.46 (s, 1H).

Synthesis of 5-hydroxy-6-alkoxy-2-methylbenzofuran-3-carboxylate esters (T2a-T2h)



To a solution of **T1a–T1e** (1.44 mmol) in DMF (12 mL) were added cesium carbonate (0.72 mmol) and acyl or alkyl halide (1.44 mmol) and stirred for 15 hours under an N_2 atmosphere. The reaction was quenched by adding 0.5 N HCl and extracted with ethyl acetate. The organic

extract was dried over magnesium sulfate, concentrated and purified on silica gel (0-25% ethyl acetate in hexanes) to give product in 53% yield.

T2a: ^1H NMR (CDCl_3 , 300 MHz) δ 1.46 (t, $J=6$ Hz, 3H), 2.75 (s, 3H), 3.96 (s, 3H), 4.39 (q, $J=6$ Hz, 2H), 5.58 (s, 1H), 6.95 (s, 1H), 7.37 (s, 1H). ^{13}C NMR (CDCl_3) δ 14.60, 14.66, 56.54, 60.43, 94.33, 106.04, 109.23, 119.19, 143.37, 145.18, 147.86, 162.87, 164.88.

T2b: ^1H NMR (CDCl_3 , 300 MHz) δ 2.71 (s, 3H), 3.91 (s, 3H), 3.92 (s, 3H), 6.95 (s, 1H), 7.44 (s, 1H).

T2c: ^1H NMR (CDCl_3 , 300 MHz) δ 1.60 (s, 9H), 2.63 (s, 3H), 3.92 (s, 3H), 6.92 (s, 1H), 7.39 (s, 1H).

T2d: ^1H NMR (CDCl_3 , 300 MHz) δ 2.63 (s, 3H), 3.41 (s, 3H), 3.72 (t, $J=12$ Hz, 2H), 3.82 (s, 3H), 4.46 (t, $J=12$ Hz, 2H), 6.96 (s, 1H), 7.39 (s, 1H).

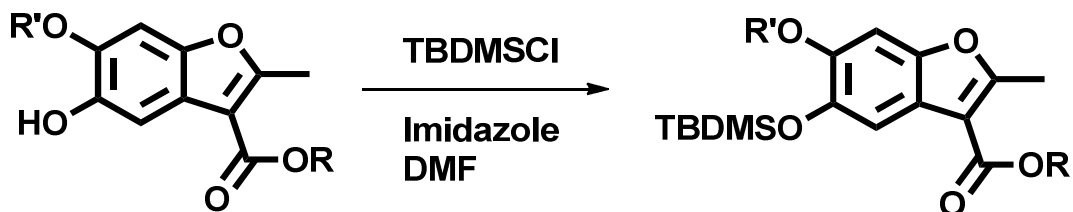
T2e: ^1H NMR (CDCl_3 , 300 MHz) δ 2.71 (s, 3H), 3.83 (s, 3H), 4.85 (d, 2H), 5.22 (d, 1H), 5.36 (d, 2H), 6.00 (m, 1H), 6.91 (s, 1H), 7.46 (s, 1H).

T2f: ^1H NMR (CDCl_3 , 400 MHz) δ 1.45 (s, 6H), 2.70 (s, 3H), 4.13 (d, 2H), 4.36 (d, 2H), 6.93 (s, 1H), 7.43 (s, 1H). ^{13}C NMR (CDCl_3) δ 14.34, 14.43, 14.76, 31.42, 36.45, 60.15, 65.02, 76.69, 77.00, 77.32, 94.97, 105.73, 109.04, 118.95, 143.34, 144.13, 147.63, 162.50, 162.58, 164.63.

T2g: ^1H NMR (CDCl_3 , 300 MHz) δ 1.40 (d, $J=1.5$ Hz, 6H), 1.43 (t, $J=1.8$ Hz, 3H), 2.71 (s, 3H), 4.38 (t, $J=1.8$ Hz, 2H), 4.58 (m, 1H), 6.96 (s, 1H), 7.44 (s, 1H).

T2h: ^1H NMR (CDCl_3 , 300 MHz) δ 1.46 (t, $J=6$ Hz, 3H), 2.75 (s, 3H), 3.96 (s, 3H), 4.39 (q, $J=6$ Hz, 2H), 5.58 (s, 1H), 7.01 (s, 1H), 7.31 (s, 1H).

Synthesis of 5-((t-butyldimethylsilyl)oxy)-6-alkoxy-2-methylbenzofuran-3-carboxylate ester (T3a–T3h).



To a solution of **T2a–T2f** (3.63 mmol) in DMF (30 mL) were added imidazole (18.15 mmol) and TBDMSCl (21.83 mmol) and the mixture was stirred. After 16 hours the reaction mixture was quenched with water and extracted with diethyl ether. The organic layer was dried over magnesium sulfate, concentrated and purified by flash chromatography on silica gel (0-15% EtOAc in hexanes) to obtain product in yield of 85-90 %.

T3a: ^1H NMR (CDCl_3 , 300 MHz) δ 0.17 (s, 6H), 1.01 (s, 9H), 1.46 (t, $J=6$ Hz, 3H), 2.69 (s, 3H), 3.87 (s, 3H), 4.39 (q, $J=6$ Hz, 2H), 7.05 (s, 1H) and 7.41 (s, 1H). ^{13}C NMR (CDCl_3) δ 4.5, 14.47, 18.73, 22.25, 25.96, 55.99, 61.00, 95.23, 111.31, 112.77, 118.07, 143.56, 149.97, 151.43, 157.60, 163.69.

T3b: ^1H NMR (CDCl_3 , 300 MHz) δ 1.16 (s, 6H), 1.02 (s, 9H), 2.70 (s, 3H), 3.83 (s, 3H), 3.91 (s, 3H), 6.93 (s, 1H), 7.37 (s, 1H).

T3c: ^1H NMR (CDCl_3 , 300 MHz) δ 0.16 (s, 6H), 1.03 (s, 9H), 1.62 (s, 9H), 2.69 (s, 3H), 3.83 (s, 3H), 6.92 (s, 1H), 7.36 (s, 1H).

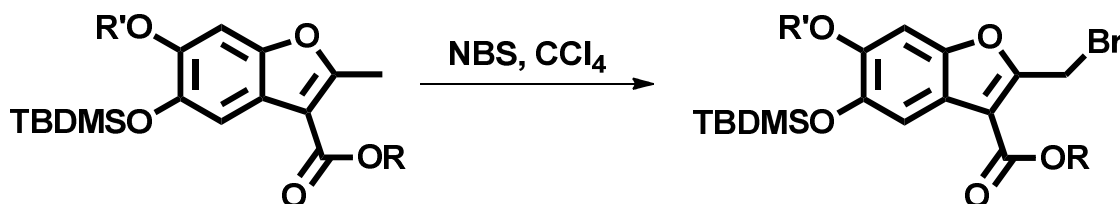
T3d: ^1H NMR (CDCl_3 , 300 MHz) δ 0.13 (s, 6H), 1.01 (s, 9H), 2.63 (s, 3H), 3.41 (s, 3H), 3.72 (t, $J=12$ Hz, 2H), 3.82 (s, 3H), 4.46 (t, $J=12$ Hz, 2H), 6.96 (s, 1H), 7.39 (s, 1H).

T3f: ^1H NMR (CDCl_3 , 400 MHz) δ 0.11 (s, 6H), 1.04 (s, 9H), 1.46 (s, 6H), 2.71 (s, 3H), 4.03 (d, 2H), 4.35 (d, 2H), 6.93 (s, 1H), 7.40 (s, 1H).

T3g: ^1H NMR (CDCl_3 , 400 MHz) δ 0.19 (s, 6H), 1.04 (s, 9H), 1.37 (d, 6H), 1.42 (t, 3H), 2.71 (s, 3H), 4.40 (d, 2H), 6.94 (s, 1H), 7.40 (s, 1H).

T3h: ^1H NMR (CDCl_3 , 300 MHz) δ 0.17 (s, 6H), 1.01 (s, 9H), 1.46 (t, $J=6$ Hz, 3H), 2.69 (s, 3H), 3.87 (s, 3H), 4.39 (q, $J=6$ Hz, 2H), 7.08 (s, 1H), 7.35 (s, 1H).

Synthesis of 2-(bromomethyl)-5-((tert-butyldimethylsilyl)oxy)-6-alkoxybenzofuran-3-carboxylate ester (T4a–T4h).



To a solution of **T3a–T3f** (1 mmol) in THF (20 mL) was added NBS (1 mmol) and the solution was refluxed at 65 °C under a halogen lamp for 1 hour. The reaction mixture was cooled and quenched with water and extracted with hexanes. The organic layer was concentrated and product was obtained in 90-95 % yield.

T4a: ^1H NMR (CDCl_3 , 300 MHz) δ 0.17 (s, 6H), 1.01 (s, 9H), 1.46 (t, $J=6$ Hz, 3H), 3.87 (s, 3H), 4.39 (q, $J=6$ Hz, 2H), 4.93 (s, 2H), 7.05 (s, 1H), 7.41 (s, 1H).

T4b: ^1H NMR (CDCl_3 , 300 MHz) δ 1.17 (s, 6H), 1.02 (s, 9H), 3.83 (s, 3H), 3.91 (s, 3H), 4.91 (s, 2H), 6.93 (s, 1H), 7.37 (s, 1H).

T4c: ^1H NMR (CDCl_3 , 300 MHz) δ 0.16 (s, 6H), 1.01 (s, 9H), 1.65 (s, 9H), 3.85 (s, 3H), 4.93 (s, 2H), 6.96 (s, 1H), 7.40 (s, 1H).

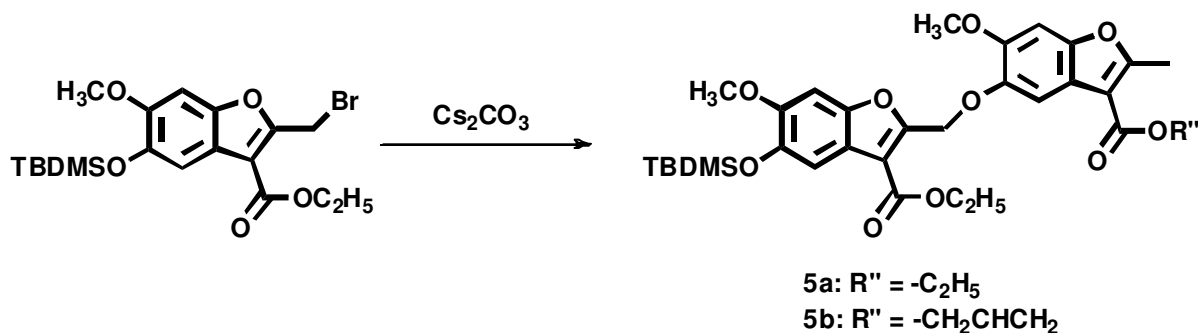
T4d: ^1H NMR (CDCl_3 , 300 MHz) δ 0.17 (s, 6H), 1.02 (s, 9H), 3.45 (s, 3H), 3.76 (t, $J=12$ Hz, 2H), 3.86 (s, 3H), 4.50 (t, $J=12$ Hz, 2H), 4.96 (s, 2H), 6.98 (s, 1H), 7.45 (s, 1H).

T4f: ^1H NMR (CDCl_3 , 400 MHz) δ 0.11(s, 6H), 1.04 (s, 9H), 1.46 (s, 6H), 4.03 (d, 2H), 4.35 (d, 2H), 4.96 (s, 2H), 6.93(s, 1H), 7.40(s, 1H).

T4g: ^1H NMR (CDCl_3 , 400 MHz) δ 0.17 (s, 6H), 1.02 (s, 9H), 1.38 (d, 6H), 1.43 (t, 3H), 4.48 (d, 2H), 4.57 (s, 2H), 6.97 (s, 1H), 7.41 (s, 1H).

T4h: ^1H NMR (CDCl_3 , 300 MHz) δ 0.17 (s, 6H), 1.01 (s, 9H), 1.46 (t, $J=6$ Hz, 3H), 3.87 (s, 3H), 4.39 (q, $J=6$ Hz, 2H), 4.93 (s, 2H), 7.08 (s, 1H) 7.35 (s, 1H).

Synthesis of ethyl 5-((tert-butyldimethylsilyl)oxy)-2-(((3-(ethoxycarbonyl)-6-methoxy-2-methylbenzofuran-5-yl)oxy)methyl)-6-methoxybenzofuran-3-carboxylate (T5a–T5b).



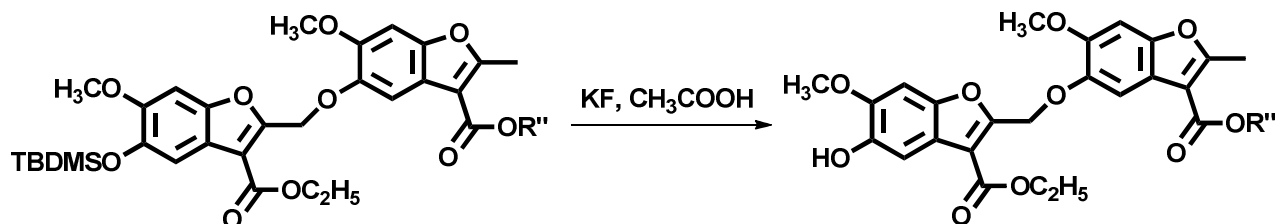
To a solution of **T2a** or **T2e** (0.3 mmol) and **T4a** (0.4 mmol) in ethyl acetate (4 mL) were added cesium carbonate (0.3 mmol) and anhydrous DMF (1 mL). The reaction mixture was stirred under nitrogen for 15 hours at room temperature. The reaction was quenched with methylene chloride and extracted with brine. The organic layer was dried over magnesium sulfate and concentrated. Purification was done by using flash chromatography on silica gel using (0-20) % ethyl acetate in hexanes. The product was obtained in 60-65 % yield.

T5a: ^1H NMR (CDCl_3 , 300 MHz) δ 0.17 (s, 6H), 1.01 (s, 9H), 1.46 (m, 6H), 2.71 (s, 3H), 3.87 (s, 3H), 3.91 (s, 3H), 4.39 (m, 4H), 5.60 (s, 2H), 6.95 (s, 1H), 6.99 (s, 1H), 7.42 (s, 1H), 7.55 (s, 1H). ^{13}C NMR (CDCl_3) δ 4.55, 14.41, 14.73, 14.68, 18.92, 25.57, 55.77, 56.62, 60.62, 61.93,

64.47, 95.27, 98.31, 103.47, 109.31, 112.55, 112.73, 117.90, 119.98, 143.29, 146.34, 147.95, 148.08, 151.20, 150.69, 157.66, 162.67, 164.17, 164.83.

T5b: ^1H NMR (CDCl_3 , 400 MHz) δ 0.15 (s, 6H), 1.00 (s, 9H), 1.37 (t, $J=10.2$ Hz, 3H), 2.70 (s, 3H), 3.82 (s, 3H), 3.85 (s, 3H), 4.35 (q, $J=10.2$ Hz, 2H), 4.80 (d, $J=5.6$ Hz, 2H), 5.20 (m, 1H), 5.38 (m, 1H), 5.57 (s, 2H), 5.99 (m, 1H), 6.97 (s, 1H), 6.98 (s, 1H), 7.24 (s, 1H), 7.44 (s, 1H), 7.59 (s, 1H). ^{13}C NMR (CDCl_3) δ 4.72, 14.20, 14.46, 18.49, 25.75, 55.77, 56.31, 60.52, 63.93, 64.78, 95.32, 107.68, 108.93, 11.88, 118.33, 132.39, 143.07, 145.83, 148.91, 149.09, 149.94, 150.70, 157.79, 162.62, 163.67.

Synthesis of ethyl 5-(hydroxy)-2-(((3-(ethoxycarbonyl)-6-methoxy-2-methylbenzofuran-5-yl)oxy)methyl)-6-methoxybenzofuran-3-carboxylate (T6a-T6b).

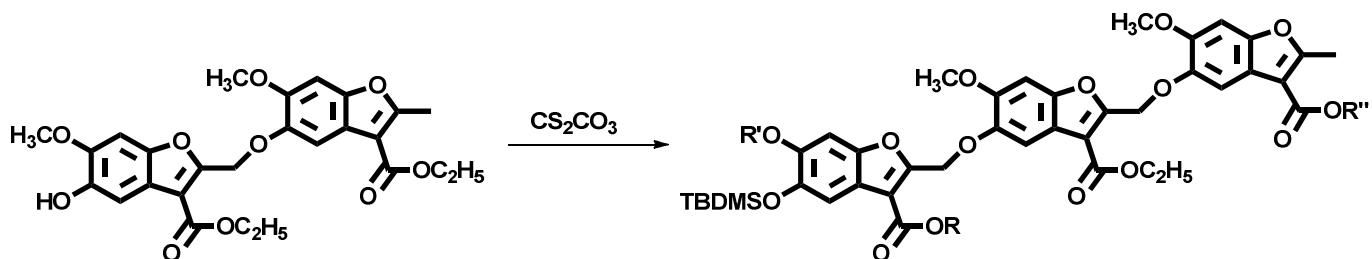


To a solution of **T5a – T5b** (0.3 mmol) in DMF (3 mL) were added KF (4 mmol) and acetic acid (10 μL). The reaction mixture was stirred for 5 hours. The reaction was quenched by methylene chloride and extracted with brine solution. The aqueous layer was again extracted with fresh methylene chloride. The organic layer was combined and dried over magnesium sulfate and concentrated in vacuum. The solid was precipitated using methanol to obtain product in 90% yield.

T6a: ^1H NMR (CDCl_3 , 300 MHz) δ 1.46 (m, 6H), 2.71 (s, 3H), 3.80 (s, 3H), 3.85 (s, 3H), 4.39 (m, 4H), 5.35 (s, 2H), 6.95 (s, 1H), 6.99 (s, 1H), 7.42 (s, 1H), 7.55 (s, 1H). ^{13}C NMR (CDCl_3) δ 14.41, 14.73, 14.68, 25.57, 55.77, 56.62, 60.62, 61.93, 64.47, 95.27, 98.31, 103.47, 109.31, 112.55, 112.73, 117.90, 119.98, 143.29, 146.34, 147.95, 148.08, 151.20, 150.69, 157.66, 162.67, 164.17, 164.83.

T6b: ^1H NMR (CDCl_3 , 400 MHz) δ 1.39 (t, $J=10.2$ Hz, 3H), 2.71 (s, 3H), 3.87 (s, 3H), 3.3 (s, 3H), 4.36 (q, $J=10.2$ Hz, 2H), 4.80 (d, $J=5.6$ Hz, 2H), 5.23 (m, 1H), 5.38 (m, 1H), 5.60 (s, 2H), 5.99 (m, 1H), 6.98 (s, 1H), 7.02 (s, 1H), 7.50 (s, 1H), 7.59 (s, 1H). ^{13}C NMR (CDCl_3) δ 14.15, 14.37, 56.26, 60.64, 64.02, 84.81, 64.91, 94.63, 95.37, 105.85, 106.05, 107.84, 118.09, 118.28, 132.25, 143.70, 145.69, 146.51, 147.68, 148.80, 148.88, 149.11, 157.92, 162.72, 162.81, 163.82.

Synthesis of T7a–T7h



	R	R'	R''
T7a	-C ₂ H ₅	- CH ₃	-H
T7b	- CH ₃	- CH ₃	-H
T7c	-C(CH ₃) ₃	- CH ₃	-H
T7d	-C ₂ H ₄ OCH ₃	- CH ₃	-H
T7e	-C ₂ H ₅	-CH ₃	-CH ₂ CHCH ₂
T7f	-C ₂ H ₅	- C ₂ H ₅	-H
T7g	-C ₂ H ₅	- CH(CH ₃) ₂	-H
T7h	-C ₂ H ₅	-CH ₃	-H

To a solution of **T6a-T6b** (0.3 mmol) and **T4a-T4h** (0.4 mmol) in ethyl acetate (3 mL) were added cesium carbonate (0.3 mmol) and anhydrous DMF (0.5 mL) in a microwave tube (10 mL). The reaction mixture was stirred under microwave radiation at 90 °C for 80 minutes. The reaction was quenched with methylene chloride and extracted with brine. The organic layer was dried over magnesium sulfate and concentrated. Purification was by using flash chromatography on silica gel using 20-60) % ethyl acetate in hexanes. The product was obtained in 50 % yield (see Appendix, Page 318-325 for NMR spectra).

T7a: ¹H NMR (CDCl₃, 400 MHz) δ 0.16 (s, 6H), 1.02 (s, 9H), 1.37 (m, 9H), 2.71 (s, 3H), 3.83 (s, 3H), 3.86 (s, 3H), 3.87 (s, 3H), 4.35 (m, 6H), 5.59 (s, 2H), 5.60 (s, 2H), 6.98 (s, 1H), 7.00 (s, 1H), 7.05 (s, 1H), 7.45 (s, 1H), 7.57 (s, 1H), 7.63 (s, 1H). ¹³C NMR (CDCl₃) δ 4.73, 14.20,

14.23, 14.28, 14.36, 14.39, 25.74, 55.76, 56.25, 56.29, 60.11, 60.56, 60.70, 63.77, 64.02, 95.28, 95.53, 106.05, 107.59, 107.82, 109.10, 111.93, 112.04, 112.52, 117.72, 117.86, 118.39, 143.08, 145.66, 146.07, 148.86, 149.10, 149.84, 149.94, 150.14, 150.72, 157.68, 157.89, 162.37, 163.49, 163.68, 164.40.

T7b: ^1H NMR (CDCl_3 , 400 MHz) δ 0.16 (s, 6H), 1.02 (s, 9H), 1.35 (m, 6H), 2.70 (s, 3H), 3.83 (s, 3H), 3.86 (s, 3H), 3.87 (s, 3H), 3.91 (s, 3H), 4.34 (s, 4H), 5.58 (s, 2H), 5.59 (s, 2H), 6.98 (s, 1H), 7.00 (s, 1H), 7.05 (s, 1H), 7.43 (s, 1H), 7.57 (s, 1H), 7.63 (s, 1H). ^{13}C NMR (CDCl_3 , 400 MHz) δ 4.72, 14.23, 14.37, 14.39, 18.49, 25.76, 51.63, 55.71, 56.26, 56.31, 60.11, 60.57, 63.86, 64.06, 95.23, 95.32, 95.56, 107.74, 107.89, 109.12, 111.78, 112.03, 112.44, 117.77, 117.86, 118.42, 143.15, 145.68, 146.05, 148.89, 149.12, 149.88, 149.95, 150.75, 157.67, 157.91, 162.38, 163.49, 163.78, 164.40.

T7c: ^1H NMR (CDCl_3 , 400 MHz) δ 0.16 (s, 6H), 1.02 (s, 9H), 1.35 (m, 6H), 1.58 (s, 9H), 2.70 (s, 3H), 3.83 (s, 3H), 3.86 (s, 3H), 3.87 (s, 3H), 4.33 (m, 4H), 5.57 (s, 2H), 5.59 (s, 2H), 6.97 (s, 1H), 6.99 (s, 1H), 7.05 (s, 1H), 7.42 (s, 1H), 7.57 (s, 1H), 7.63 (s, 1H). ^{13}C NMR (CDCl_3 , 400 MHz) δ 4.74, 14.25, 14.37, 14.39, 18.47, 25.75, 28.33, 55.74, 56.24, 56.31, 60.12, 60.56, 63.91, 64.05, 81.41, 95.23, 95.32, 95.53, 107.64, 107.90, 109.12, 112.05, 112.66, 113.14, 117.75, 118.08, 118.42, 142.91, 145.68, 146.23, 148.89, 149.12, 149.87, 150.14, 150.59, 157.34, 157.88, 162.38, 162.51, 162.86, 163.50, 164.40.

T7d: ^1H NMR (CDCl_3 , 400 MHz) δ 0.16 (s, 6H), 1.02 (s, 9H), 1.33 (m, 6H), 2.70 (s, 3H), 3.37 (s, 3H), 3.71 (m, 2H), 3.83 (s, 3H), 3.85 (s, 3H), 3.87 (s, 3H), 4.34 (m, 4H), 4.45 (m, 2H), 5.58 (s, 2H), 5.61 (s, 2H), 6.97 (s, 1H), 6.99 (s, 1H), 7.05 (s, 1H), 7.46 (s, 1H), 7.57 (s, 1H), 7.63 (s, 1H). ^{13}C NMR (CDCl_3 , 400 MHz) δ 4.7, 14.25, 14.28, 14.38, 18.49, 25.76, 55.70, 56.27, 56.32, 58.94,

60.12, 60.57, 63.51, 63.75, 64.07, 70.40, 95.28, 95.33, 95.56, 107.47, 107.90, 109.12, 111.77, 112.50, 112.60, 117.75, 117.83, 118.43, 143.16, 145.69, 146.13, 148.90, 149.12, 149.82, 149.97, 150.32, 157.89, 157.97, 162.38, 163.49, 163.60, 164.40.

T7e: ^1H NMR (CDCl_3 , 400 MHz) δ 0.02 (s, 6H), 1.02 (s, 9H), 1.37 (m, 6H), 2.72 (s, 3H), 3.84 (s, 3H), 3.86 (m, 2H), 3.88 (s, 3H), 4.26 (m, 4H), 4.62 (m, 2H), 5.22 (s, 1H), 5.25 (s, 1H), 5.58 (s, 2H), 5.62 (s, 2H), 6.01 (m, 1H), 6.98 (s, 1H), 7.00 (s, 1H), 7.05 (s, 1H), 7.45 (s, 1H), 7.60 (s, 1H), 7.64 (s, 1H). ^{13}C NMR (CDCl_3 , 400 MHz) δ 4.72, 14.20, 14.24, 14.47, 18.49, 25.75, 55.76, 56.26, 56.31, 60.56, 63.79, 64.00, 64.78, 95.30, 95.33, 95.56, 107.64, 107.76, 108.92, 111.94, 112.08, 112.53, 117.75, 117.89, 118.11, 118.33, 132.37, 143.09, 145.76, 146.09, 148.91, 149.11, 149.86, 149.95, 150.16, 150.73, 157.70, 157.82, 162.63, 163.47.

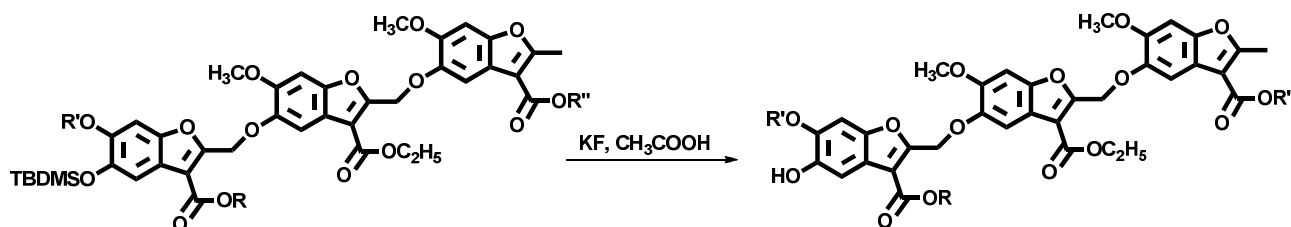
T7f: ^1H NMR (CDCl_3 , 400 MHz) δ -0.17 (s, 6H), 1.03 (s, 9H), 1.34 (m, 12H), 2.71 (s, 3H), 3.86 (s, 3H), 3.87 (s, 3H), 4.18 (m, 2H), 4.35 (m, 6H), 5.58 (s, 3H), 5.60 (s, 3H), 6.98 (s, 1H), 6.99 (s, 1H), 7.05 (s, 1H), 7.45 (s, 1H), 7.58 (s, 1H), 7.64 (s, 1H). ^{13}C NMR (CDCl_3) δ 4.71, 14.21, 14.23, 14.27, 14.29, 14.36, 14.38, 25.71, 55.77, 56.27, 56.30, 60.14, 60.56, 60.72, 63.77, 64.12, 95.30, 95.52, 95.99, 106.05, 107.61, 107.82, 109.13, 111.83, 112.10, 112.52, 117.62, 117.84, 118.44, 143.08, 145.61, 146.17, 148.76, 149.11, 149.83, 149.94, 150.14, 150.72, 157.68, 157.89, 162.33, 163.43, 163.65, 164.42.

T7g: ^1H NMR (CDCl_3 , 400 MHz) δ 0.17 (s, 6H), 1.02 (s, 9H), 1.35 (m, 15H), 2.70 (s, 3H), 3.85 (s, 3H), 3.87 (s, 3H), 4.35 (m, 6H), 4.58 (m, 1H), 5.58 (s, 3H), 5.60 (s, 3H), 6.97 (s, 1H), 6.99 (s, 1H), 7.05 (s, 1H), 7.43 (s, 1H), 7.57 (s, 1H), 7.63 (s, 1H). ^{13}C NMR (CDCl_3 , 400 MHz) δ 4.74, 14.24, 14.27, 14.28, 14.30, 14.36, 14.35, 25.71, 55.75, 56.27, 56.31, 60.14, 60.58, 60.72, 63.74, 64.12, 95.31, 95.55, 95.91, 106.05, 107.61, 107.85, 109.13, 111.83, 112.13, 112.52, 117.64,

117.84, 118.44, 143.12, 145.61, 146.11, 148.76, 149.19, 149.73, 149.94, 150.24, 150.72, 157.58, 157.89, 162.33, 163.43, 163.67, 164.48.

T7h: ^1H NMR (CDCl_3 , 400 MHz) δ 0.16 (s, 6H), 1.00 (s, 9H), 1.35 (m, 9H), 2.70 (s, 3H), 3.86 (s, 3H), 3.87 (s, 9H), 4.35 (m, 6H), 5.58 (s, 4H), 6.97 (s, 1H), 7.03 (s, 1H), 7.05 (s, 1H), 7.44 (s, 1H), 7.57 (s, 1H), 7.64 (s, 1H). ^{13}C NMR (CDCl_3 , 400 MHz) δ 4.72, 14.26, 14.37 (2C), 18.49, 25.70, 28.26, 55.88, 56.26, 56.31, 60.11, 60.57, 60.59, 60.66, 64.07, 95.33, 95.57, 103.47, 103.61, 103.85, 103.95, 107.91, 107.95, 109.12, 111.99, 112.03, 117.78, 118.43, 119.08, 144.71, 145.69, 146.10, 148.90, 149.13, 149.58, 149.95, 150.23, 157.70, 157.93, 162.38, 163.70, 164.40.

Synthesis of T8a–T8g



To a solution of **T7a–T7g** (0.3 mmol) in DMF (3 mL) were added KF (4 mmol) and acetic acid (10 μL). The reaction mixture was stirred for 5 hours. The reaction was quenched by methylene chloride and extracted with brine solution. The aqueous layer was again extracted with methylene chloride. The organic layer was combined and dried over magnesium sulfate and concentrated in vacuum. The solid was precipitated using methanol to obtain product in 90% yield (see Appendix, Page 326-332 for NMR spectra).

T8a: ^1H NMR (CDCl_3 , 400 MHz) δ 1.35 (m, 9H), 2.72 (s, 3H), 3.86 (s, 3H), 3.88 (s, 3H), 3.93 (s, 3H), 4.35 (m, 6H), 5.58 (s, 2H), 5.62 (s, 2H), 6.97 (s, 1H), 7.02 (s, 1H), 7.15 (s, 1H), 7.39 (s, 1H), 7.51 (s, 1H), 7.59 (s, 1H). ^{13}C NMR (CDCl_3 , 400 MHz) δ 14.22, 14.31, 14.36, 14.39, 56.24, 56.31, 60.11, 60.56, 60.64, 63.83, 64.06, 94.49, 95.33, 95.58, 106.07, 107.71, 107.90, 109.12, 112.02, 117.76, 118.35, 118.42, 143.59, 145.68, 146.04, 146.09, 148.72, 148.88, 149.12, 149.75, 150.46, 157.93, 158.12, 162.39, 163.37, 163.68, 164.43.

T8b: ^1H NMR (CDCl_3 , 400 MHz) δ 1.34 (m, 6H), 2.70 (s, 3H), 3.85 (s, 3H), 3.88 (s, 3H), 3.92 (s, 3H), 3.93 (s, 3H), 4.34 (m, 4H), 5.58 (s, 2H), 5.61 (s, 2H), 6.97 (s, 1H), 7.01 (s, 1H), 7.05 (s, 1H), 7.49 (s, 1H), 7.56 (s, 1H), 7.62 (s, 1H). ^{13}C NMR (CDCl_3 , 400 MHz) δ 14.21, 14.36, 14.39, 51.63, 56.28, 56.31, 60.11, 60.57, 63.80, 64.06, 94.49, 95.33, 95.58, 106.05, 107.76, 107.90, 109.11, 111.85, 112.02, 117.77, 118.27, 118.43, 143.66, 145.68, 145.98, 146.16, 148.82, 148.89, 149.12, 149.86, 150.17, 157.93, 158.05, 162.39, 162.69, 163.47, 164.08, 164.40.

T8c: ^1H NMR (CDCl_3 , 400 MHz) δ 1.34 (m, 6H), 1.57 (s, 9H), 2.70 (s, 3H), 3.85 (s, 3H), 3.86 (s, 3H), 3.92 (s, 3H), 4.34 (m, 4H), 5.58 (s, 2H), 5.59 (s, 2H), 6.97 (s, 1H), 7.00 (s, 1H), 7.05 (s, 1H), 7.46 (s, 1H), 7.58 (s, 1H), 7.61 (s, 1H). ^{13}C NMR (CDCl_3 , 400 MHz) δ 14.23, 14.36, 14.38, 28.33, 56.25, 56.28, 56.32, 60.12, 60.56, 64.00, 64.05, 81.58, 94.43, 95.34, 95.56, 106.08, 107.79, 107.91, 109.12, 112.04, 113.19, 117.77, 118.43, 118.61, 143.49, 145.68, 146.00, 146.16, 148.71, 148.90, 149.12, 149.89, 150.16, 157.48, 157.90, 162.38, 162.66, 162.85, 163.47.

T8d: ^1H NMR (CDCl_3 , 400 MHz) δ 1.33 (m, 6H), 2.70 (s, 3H), 3.37 (s, 3H), 3.70 (m, 3H), 3.85 (s, 3H), 3.87 (s, 3H), 3.92 (s, 3H), 4.34 (m, 4H), 4.47 (m, 2H), 5.58 (s, 2H), 5.61 (s, 2H), 6.97 (s, 1H), 7.01 (s, 1H), 7.05 (s, 1H), 7.50 (s, 1H), 7.56 (s, 1H), 7.62 (s, 1H). ^{13}C NMR (CDCl_3 , 400 MHz) δ 14.22, 14.37, 28.25, 35.48, 56.29, 58.93, 60.12, 60.58, 63.47, 63.81, 64.08, 70.38, 70.46,

94.43, 95.34, 95.56, 106.07, 107.54, 107.93, 109.12, 111.82, 112.04, 117.78, 118.34, 118.44, 143.70, 145.70, 146.09, 146.19, 148.84, 148.91, 149.13, 149.81, 150.13, 157.91, 158.17, 162.38, 162.64, 163.46, 164.40.

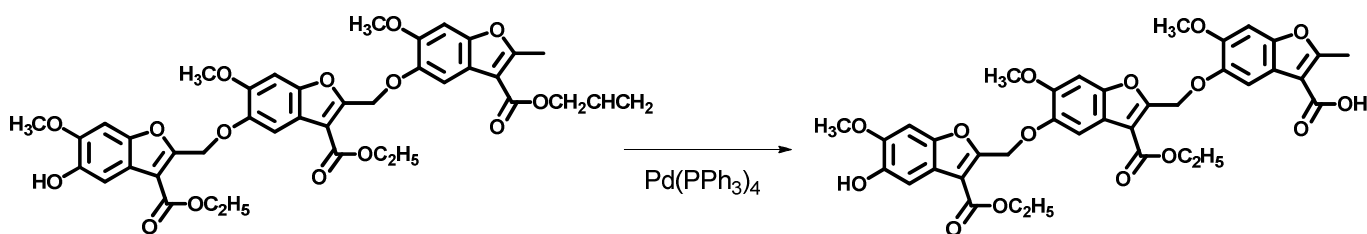
T8e: ^1H NMR (CDCl_3 , 400 MHz) δ 1.31 (t, $J=6.8$ Hz, 3H), 1.39 (t, $J=6.8$ Hz, 3H), 2.71 (s, 3H), 3.87 (s, 3H), 3.88 (s, 3H), 3.92 (s, 3H), 4.37 (m, 4H), 4.79 (d, $J=5.6$ Hz, 2H), 5.22 (m, 2H), 5.33 (m, 2H), 5.57 (s, 2H), 5.62 (s, 2H), 6.00 (m, 1H), 6.97 (s, 1H), 7.01 (s, 1H), 7.04 (s, 1H), 7.49 (s, 1H), 7.59 (s, 1H), 7.62 (s, 1H). ^{13}C NMR (CDCl_3) δ 14.20, 14.24, 14.47, 25.75, 55.76, 56.26, 56.31, 60.56, 63.79, 64.00, 64.78, 95.30, 95.33, 95.56, 107.64, 107.76, 108.92, 11.94, 112.08, 112.53, 116.05, 117.79, 119.11, 119.93, 131.35, 143.09, 145.76, 146.09, 148.59, 149.01, 149.53, 148.75, 151.06, 151.71, 157.38, 167.92, 163.61, 164.07.

T8f: ^1H NMR (CDCl_3 , 400 MHz) δ 1.35 (m, 12H), 2.71 (s, 3H), 3.86 (s, 3H), 3.88 (s, 3H), 4.17 (m, 2H), 4.35 (m, 6H), 5.58 (s, 3H), 5.62 (s, 3H), 6.98 (s, 1H), 7.00 (s, 1H), 7.05 (s, 1H), 7.50 (s, 1H), 7.57 (s, 1H), 7.62 (s, 1H). ^{13}C NMR (CDCl_3) δ 14.20, 14.24, 14.29, 14.31, 14.36, 14.38, 55.78, 56.29, 56.32, 60.15, 60.57, 60.74, 63.77, 64.19, 95.34, 95.52, 95.89, 106.15, 107.61, 107.85, 109.13, 111.73, 112.10, 112.42, 117.65, 117.84, 118.44, 143.08, 145.65, 146.17, 148.76, 149.21, 149.83, 149.94, 150.14, 150.72, 157.68, 157.85, 162.33, 163.47, 163.65, 164.42.

T8g: ^1H NMR (CDCl_3 , 400 MHz) δ 1.37 (m, 15H), 2.70 (s, 3H), 3.86 (s, 3H), 3.88 (s, 3H), 4.36 (m, 6H), 4.58 (m, 1H), 5.58 (s, 3H), 5.62 (s, 3H), 6.97 (s, 1H), 7.02 (s, 1H), 7.05 (s, 1H), 7.49 (s, 1H), 7.57 (s, 1H), 7.63 (s, 1H). ^{13}C NMR (CDCl_3 , 400 MHz) δ 14.21, 14.25, 14.27, 14.34, 14.36, 14.38, 55.79, 56.25, 56.40, 60.12, 60.56, 60.62, 63.77, 64.12, 95.40, 95.52, 95.79, 106.15, 107.51, 107.72, 109.43, 111.63, 112.10, 112.52, 117.52, 117.83, 118.44, 143.08, 145.51, 146.17, 148.66, 149.11, 149.53, 149.64, 150.24, 150.72, 157.88, 157.92, 162.33, 163.33, 163.65, 164.32.

T8h: ^1H NMR (CDCl_3 , 400 MHz) δ 1.35 (m, 9H), 2.72 (s, 3H), 3.86 (s, 3H), 3.88 (s, 3H), 3.93 (s, 3H), 4.35 (m, 6H), 5.58 (s, 2H), 5.62 (s, 2H), 6.97 (s, 1H), 7.02 (s, 1H), 7.15 (s, 1H), 7.39 (s, 1H), 7.51 (s, 1H), 7.59 (s, 1H). ^{13}C NMR (CDCl_3 , 400 MHz) δ 14.22, 14.31, 14.36, 14.39, 56.24, 56.31, 60.11, 60.56, 60.64, 63.83, 64.06, 94.49, 95.33, 95.58, 106.07, 107.71, 107.90, 109.12, 112.02, 117.76, 118.35, 118.42, 143.59, 145.68, 146.04, 146.09, 148.72, 148.88, 149.12, 149.75, 150.46, 157.93, 158.12, 162.39, 163.37, 163.68, 164.43.

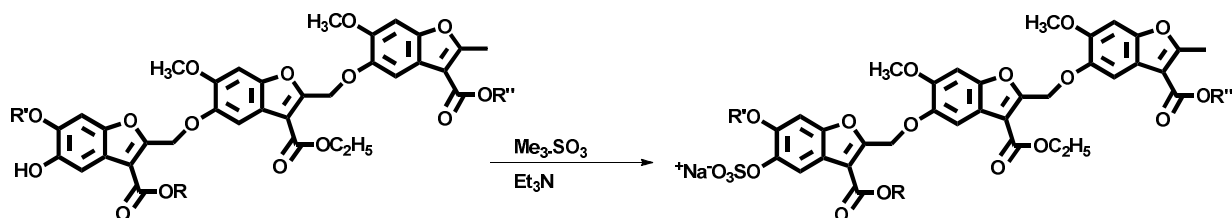
Synthesis of T13



To a solution of **T8e** (0.19 mmol) in methylene chloride (1.5 mL) were added $\text{Pd}(\text{PPh}_3)_4$ (0.009 mmol) and PPh_3 (0.018 mmol). The reaction mixture was stirred for 10 minutes in ice bath to bring temperature down. To this mixture was added pyrrolidine (0.21 mmol) and it was stirred for 30 minutes. The reaction was quenched by methylene chloride and extracted with brine solution. The aqueous layer was again extracted with methylene chloride. The organic layer was combined and dried over magnesium sulfate and concentrated in vacuum. The solid obtained was washed with hexane several times to remove excess of PPh_3 and purified by flash chromatography using ethyl acetate and hexanes (40% to 80%) as the solvent system (see Appendix, Page 331 for NMR spectra).

T13: ^1H NMR (DMSO- d_6 , 400 MHz) δ 1.25 (t, $J=7.2$ Hz, 3H), 1.30 (t, $J=7.2$ Hz, 3H), 2.66 (s, 3H), 3.78 (s, 3H), 3.82 (s, 6H), 4.29 (m, 4H), 5.50 (s, 2H), 5.52 (s, 2H), 7.26 (s, 1H), 7.30 (s, 1H), 7.32 (s, 1H), 7.41 (s, 1H), 7.48 (s, 2H). ^{13}C NMR (DMSO- d_6 , 400 MHz) δ 13.85, 13.96, 54.85, 55.95, 55.99, 56.04, 60.38, 60.50, 62.62, 62.74, 95.67, 95.95, 96.17, 105.93, 106.24, 108.95, 111.22, 111.43, 116.59, 116.99, 117.95, 144.82, 145.06, 145.63, 147.89, 147.97, 148.30, 148.36, 149.32, 149.61, 157.17, 157.59, 161.68, 162.58, 162.90, 165.02. MS (-ve) m/z calcd. for $\text{C}_{39}\text{H}_{37}\text{O}_{15}$ [(M-H) $^-$] 717.37, found 717.26 (M-H) $^-$.

Synthesis of T9a–T9g and T14



To a solution of **T8a–T8g** (0.07 mmol) in acetonitrile: DMF (4:1, 0.45 mL) in a microwave tube were added triethylamine (10 equiv) and trimethylamine-sulfur trioxide complex (15 equiv). The reaction mixture was exposed to microwaves (50 W) for 40 min at 100 °C followed by vacuum concentration to remove all solvent. The solid so obtained was directly loaded on a Sephadex C-25 cation exchange resin and eluted with water. Fractions containing the sulfated product were lyophilized to obtain a solid residue, which was further purified on flash chromatography using 0-20% methanol in methylene chloride (see Appendix, Page 334-342 for NMR spectra and page 344-348 for Mass Spectra).

T9a: ^1H NMR (DMSO- d_6 , 400 MHz) δ 1.24 (m, 12H), 2.65 (s, 3H), 3.77 (s, 6H), 3.80 (s, 3H), 4.26 (m, 6H), 5.49 (s, 2H), 5.53 (s, 2H), 7.30 (s, 1H), 7.32 (s, 1H), 7.36 (s, 1H), 7.41 (s, 1H), 7.46 (s, 1H), 8.03 (s, 1H). ^{13}C NMR (DMSO- d_6 , 400 MHz) δ 13.84, 14.01, 14.16, 14.29, 56.04, 56.11, 60.23, 60.59, 60.74, 63.73, 64.16, 94.56, 95.44, 95.58, 106.17, 107.71, 107.94, 109.12, 112.12, 117.44, 118.35, 118.22, 143.59, 145.68, 146.04, 146.09, 148.72, 148.88, 149.12, 149.75, 150.46, 156.93, 157.12, 161.39, 162.37, 162.68, 163.43. MS (-ve) m/z calcd. for $\text{C}_{39}\text{H}_{37}\text{O}_{18}\text{S} [(\text{M}-\text{Na})^-]$ 825.17, found 825.23 (M-Na) $^-$.

T9b: ^1H NMR (DMSO- d_6 , 400 MHz) δ 1.25 (m, 6H), 2.68 (s, 3H), 3.80 (s, 6H), 3.84 (s, 3H), 3.86 (s, 3H), 4.27 (m, 4H), 5.52 (s, 2H), 5.56 (s, 2H), 7.32 (s, 1H), 7.34 (s, 1H), 7.40 (s, 1H), 7.43 (s, 1H), 7.49 (s, 1H), 8.00 (s, 1H). ^{13}C NMR (DMSO- d_6 , 400 MHz) δ 13.85, 14.00, 48.56, 51.76, 56.04, 56.09, 59.92, 60.47, 62.80, 62.97, 95.97, 96.06, 96.23, 106.53, 106.73, 108.26, 111.35, 111.39, 113.15, 116.28, 116.60, 117.31, 140.86, 145.10, 145.54, 148.51, 148.62, 149.39, 149.65, 150.21, 150.85, 157.63, 157.82, 162.07, 162.62, 163.18, 163.34. MS (-ve) m/z calcd. for $\text{C}_{38}\text{H}_{35}\text{O}_{18}\text{S} [(\text{M}-\text{Na})^-]$ 811.15, found 811.43 (M-Na) $^-$.

T9c: ^1H NMR (DMSO- d_6 , 400 MHz) δ 1.25 (m, 6H), 1.50 (s, 9H), 2.68 (s, 3H), 3.80(s, 3H), 3.81 (s, 3H), 3.82 (s, 3H), 4.27 (m, 4H), 5.51 (s, 2H), 5.53 (s, 2H), 7.31 (s, 1H), 7.32 (s, 1H), 7.40 (s, 1H), 7.43 (s, 1H), 7.48 (s, 1H), 8.11 (s, 1H). ^{13}C NMR (DMSO- d_6 , 400 MHz) δ 13.87, 14.01, 14.04, 27.76, 56.01, 56.04, 56.07, 59.70, 59.92, 60.46, 62.93, 63.07, 95.60, 96.06, 96.23, 106.75, 106.84, 108.29, 111.38, 112.69, 113.08, 116.64, 116.74, 117.33, 140.86, 145.10, 145.70, 148.51, 148.64, 149.45, 149.74, 149.96, 150.52, 156.98, 157.83, 161.92, 162.05, 162.61, 163.34. HRMS (-ve) m/z calcd. for $\text{C}_{41}\text{H}_{41}\text{O}_{18}\text{S} [(\text{M}-\text{Na})^-]$ 853.20, found 853.46 (M-Na) $^-$.

T9d: ^1H NMR (DMSO- d_6 , 400 MHz) δ 1.24 (m, 6H), 2.65 (s, 3H), 3.21 (s, 3H), 3.76 (m, 3H), 3.83 (s, 3H), 3.86 (s, 3H), 3.96 (s, 2H), 4.24 (m, 4H), 4.57 (m, 2H), 5.51 (s, 2H), 5.59 (s, 2H), 7.31 (s, 1H), 7.34 (s, 1H), 7.38 (s, 1H), 7.40 (s, 1H), 7.44 (s, 1H), 8.05 (s, 1H). ^{13}C NMR (DMSO- d_6 , 400 MHz) δ 13.57, 14.17, 28.15, 35.41, 57.29, 58.83, 60.22, 60.51, 63.27, 63.61, 64.18, 70.48, 70.56, 94.73, 95.44, 95.66, 106.17, 107.54, 107.93, 109.12, 111.82, 112.04, 117.78, 118.34, 118.44, 143.70, 145.70, 146.09, 146.19, 148.84, 148.91, 149.13, 149.81, 151.13, 157.61, 158.11, 162.28, 162.44, 163.36, 164.10. MS (-ve) m/z calcd. for $\text{C}_{39}\text{H}_{37}\text{O}_{19}\text{S}$ [(M-Na) $^-$] 841.16 found 841.42 (M-Na) $^-$.

T9e: ^1H NMR (DMSO- d_6 , 400 MHz) δ 1.29 (m, 6H), 2.68 (s, 3H), 3.76 (s, 3H), 3.79 (s, 3H), 3.84 (s, 3H), 4.30 (m, 4H), 5.46 (s, 2H), 5.55 (s, 2H), 7.30 (s, 1H), 7.34 (s, 1H), 7.48 (s, 1H), 7.50 (s, 1H), 7.57 (s, 1H), 8.05 (s, 1H). ^{13}C NMR (DMSO- d_6 , 400 MHz) δ 13.52, 13.89, 13.92, 14.05, 48.56, 52.81, 56.03, 56.05, 60.48, 60.53, 62.85, 63.22, 95.77, 96.06, 96.26, 96.36, 106.42, 107.37, 108.75, 111.42, 111.55, 113.19, 116.44, 116.63, 117.64, 140.85, 145.24, 145.63, 148.37, 148.62, 148.77, 149.40, 149.66, 150.17, 150.77, 157.45, 157.56, 157.67, 159.52, 162.24, 162.60, 162.68. MS (-ve) m/z calcd. for $\text{C}_{40}\text{H}_{37}\text{O}_{18}\text{S}$ [(M-Na) $^-$] 837.16, found 837.42 (M-Na) $^-$.

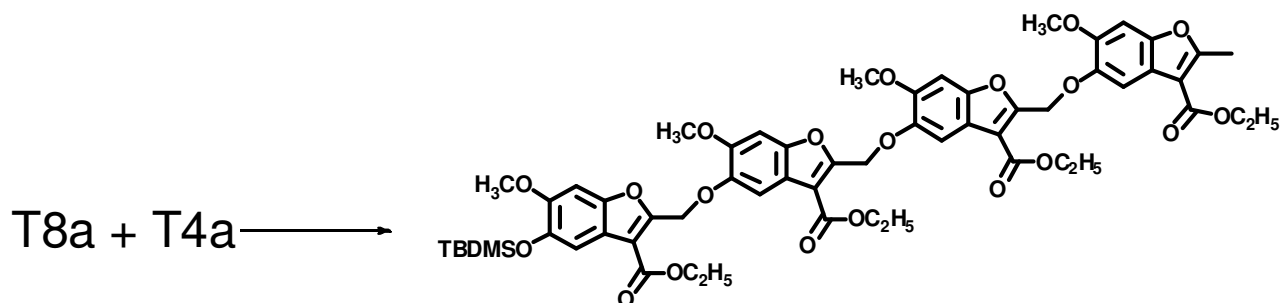
T9f: ^1H NMR (DMSO- d_6 , 400 MHz) δ 1.25 (m, 12H), 2.66 (s, 3H), 3.81 (s, 3H), 3.89 (s, 3H), 4.12 (m, 2H), 4.25 (m, 6H), 5.51 (s, 3H), 5.58 (s, 3H), 7.30 (s, 1H), 7.32 (s, 1H), 7.35 (s, 1H), 7.39 (s, 1H), 7.42 (s, 1H), 8.02 (s, 1H). ^{13}C NMR (DMSO- d_6 , 400 MHz) δ 13.86, 14.04, 14.19, 14.23, 14.31, 14.34, 56.78, 56.99, 57.32, 60.35, 60.59, 60.84, 63.47, 64.59, 95.84, 95.92, 96.19, 106.55, 107.41, 107.84, 109.43, 111.763, 112.13, 113.42, 117.65, 117.84, 118.44, 143.08, 145.65, 146.17, 148.56, 149.01, 149.73, 149.84, 150.74, 151.72, 156.68, 156.85, 161.33, 163.27, 163.45, 164.22. MS (-ve) m/z calcd. for $\text{C}_{40}\text{H}_{39}\text{O}_{18}\text{S}$ [(M-Na) $^-$] 839.18, found 839.41 (M-Na) $^-$.

T9g: ^1H NMR (DMSO- d_6 , 400 MHz) δ 1.27 (m, 15H), 2.64 (s, 3H), 3.81 (s, 3H), 3.87 (s, 3H), 4.26 (m, 6H), 4.42 (m, 1H), 5.52 (s, 3H), 5.59 (s, 3H), 7.30 (s, 1H), 7.32 (s, 1H), 7.37 (s, 1H), 7.39 (s, 1H), 7.43 (s, 1H), 8.00 (s, 1H). ^{13}C NMR (DMSO- d_6 , 400 MHz) δ 13.88, 14.15, 14.26, 14.31, 14.33, 14.37, 56.79, 57.25, 57.40, 60.62, 60.76, 60.68, 63.57, 64.33, 95.63, 95.72, 95.89, 107.15, 107.58, 107.92, 109.83, 112.63, 112.90, 113.52, 117.52, 117.83, 118.44, 143.08, 145.51, 146.17, 148.66, 149.11, 149.53, 149.64, 150.24, 151.72, 158.88, 158.92, 162.63, 163.13, 163.45, 164.12. MS (-ve) m/z calcd. for $\text{C}_{41}\text{H}_{41}\text{O}_{18}\text{S} [(\text{M}-\text{Na})^-]$ 853.20, found 853.47 (M-Na) $^-$.

T9h: ^1H NMR (DMSO- d_6 , 400 MHz) δ 1.25 (m, 9H), 2.64 (s, 3H), 3.82 (s, 3H), 3.87 (s, 3H), 3.91 (s, 3H), 4.25 (m, 6H), 5.51 (s, 2H), 5.58 (s, 2H), 7.31 (s, 1H), 7.34 (s, 1H), 7.35 (s, 1H), 7.41 (s, 1H), 7.46 (s, 1H), 8.02 (s, 1H). ^{13}C NMR (DMSO- d_6 , 400 MHz) δ 13.82, 14.11, 14.26, 14.31, 56.84, 56.91, 60.41, 60.76, 60.94, 63.63, 64.16, 94.79, 95.93, 96.18, 106.27, 107.74, 107.98, 109.52, 112.02, 117.76, 118.35, 118.42, 141.59, 144.68, 144.84, 145.09, 148.12, 148.48, 149.02, 149.75, 150.36, 157.63, 157.92, 162.49, 163.07, 163.48, 164.13. MS (-ve) m/z calcd. for $\text{C}_{39}\text{H}_{37}\text{O}_{18}\text{S} [(\text{M}-\text{Na})^-]$ 825.17, found 825.29 (M-Na) $^-$.

T14: ^1H NMR (DMSO- d_6 , 400 MHz) δ 1.29 (m, 6H), 2.68 (s, 3H), 3.76 (s, 3H), 3.79 (s, 3H), 3.84 (s, 3H), 4.30 (m, 4H), 5.46 (s, 2H), 5.55 (s, 2H), 7.30 (s, 1H), 7.34 (s, 1H), 7.48 (s, 1H), 7.50 (s, 1H), 7.57 (s, 1H), 8.05 (s, 1H). ^{13}C NMR (DMSO- d_6 , 400 MHz) δ 13.52, 13.89, 13.92, 14.05, 48.56, 52.81, 56.03, 56.05, 60.48, 60.53, 62.85, 63.22, 95.77, 96.06, 96.26, 96.36, 106.42, 107.37, 108.75, 111.42, 111.55, 113.19, 116.44, 116.63, 117.64, 140.85, 145.24, 145.63, 148.37, 148.62, 148.77, 149.40, 149.66, 150.17, 150.77, 157.45, 157.56, 157.67, 159.52, 162.24, 162.60, 162.68. MS (-ve) m/z calcd. for $\text{C}_{37}\text{H}_{33}\text{O}_{18}\text{S} [(\text{M}-\text{Na})^-]$ 793.13, found 793.27 (M-Na) $^-$.

Synthesis of T10

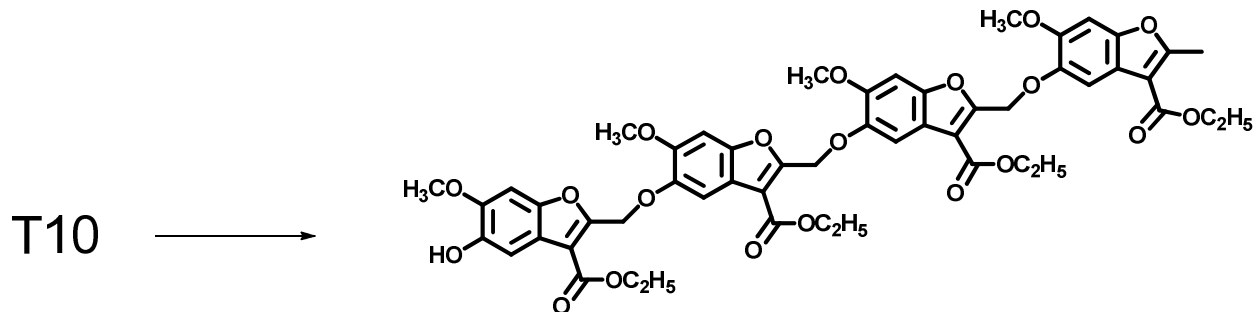


To a solution of **T8a** (0.3 mmol) and **T4a** (0.4 mmol) in ethyl acetate (3 mL) were added cesium carbonate (0.3 mmol) and anhydrous DMF (0.5 mL) in a microwave tube (10 mL). The reaction mixture was stirred under microwave radiation at 90 °C for 80 minutes. The reaction was quenched with methylene chloride and extracted with brine. The organic layer was dried over magnesium sulfate and concentrated. Purification was done by using flash chromatography on silica gel using 30-70% ethyl acetate in hexanes. The product was obtained in 50 % yield (see Appendix, Page 341 for NMR spectra).

^1H NMR (CDCl_3 , 400 MHz) δ 0.17 (s, 6H), 1.02 (s, 9H), 1.35 (m, 12H), 2.71 (s, 3H), 3.83 (s, 3H), 3.86 (s, 3H), 3.87 (s, 3H), 3.88 (s, 3H), 4.35 (m, 8H), 5.58 (s, 2H), 5.60 (s, 2H), 5.61 (s, 2H), 6.98 (s, 1H), 7.00 (s, 1H), 7.05 (s, 2H), 7.45 (s, 1H), 7.58 (s, 1H), 7.63 (s, 1H), 7.64 (s, 1H).

^{13}C NMR (CDCl_3 , 400 MHz) δ 4.71, 14.08 (2C), 14.20, 14.24, 14.37, 18.48, 25.75, 55.77, 56.27 (2C), 56.23, 60.10, 60.55 (2C), 60.58, 63.86, 63.91, 64.09, 95.32 (2C), 95.36, 95.59, 107.77, 107.97, 109.13, 111.93, 112.03, 112.13, 112.53, 117.72, 117.80, 117.91, 118.45, 143.12, 145.72, 146.10, 146.15, 148.93, 149.14, 149.90, 149.95 (2C), 150.19 (2C), 150.74, 157.71 (2C), 157.75, 157.95, 162.37, 163.47, 163.67, 164.38.

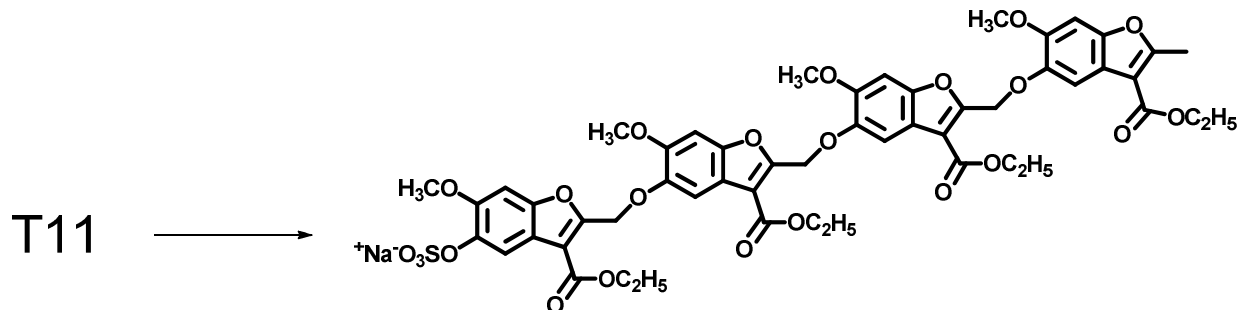
Synthesis of T11



To a solution of **T10** (0.3 mmol) in DMF (3 mL) were added KF (4 mmol) and acetic acid (10 μ L). The reaction mixture was stirred for 5 hours. The reaction was quenched by methylene chloride and extracted with brine solution. The aqueous layer was again extracted with methylene chloride. The organic layer was combined and dried over magnesium sulfate and concentrated in vacuum. The solid was precipitated using methanol to obtain product in 90% yield (see Appendix, Page 342 for NMR spectra).

¹H NMR (CDCl₃, 400 MHz) δ 1.35 (m, 12H), 2.70 (s, 3H), 3.86 (s, 3H), 3.87 (s, 3H), 3.88 (s, 3H), 3.93 (s, 3H), 4.35 (m, 8H), 5.58 (s, 2H), 5.59 (s, 2H), 5.62 (s, 2H), 6.98 (s, 1H), 7.02 (s, 1H), 7.05 (s, 2H), 7.49 (s, 1H), 7.57 (s, 1H), 7.62 (s, 2H). ¹³C NMR (CDCl₃, 400 MHz) δ 14.22, 14.29 (2C), 14.36, 14.39, 56.28 (4C), 60.12, 60.57, 60.60 (2C), 60.64, 63.81 (2C), 64.03, 94.48 (2C), 95.32, 95.56, 106.07 (2C), 107.66, 107.71, 107.84, 109.10, 112.00, 112.12, 117.68, 117.75, 118.30, 118.41, 143.63 (2C), 145.67, 146.05, 146.16, 148.81 (2C), 148.87, 149.11, 149.87, 150.16 (2C), 157.72, 157.91, 157.97 (2C), 162.38, 162.73, 163.46, 163.67.

Synthesis of T12



To a solution of **T11** (0.05 mmol) in acetonitrile: DMF (4:1, 0.45 mL) in a microwave tube were added triethylamine (10 equiv) and trimethylamine-sulfur trioxide complex (15 equiv). The reaction mixture was exposed to microwaves (50 W) for 40 min at 100 °C followed by vacuum concentration to remove all solvent. The solid so obtained was directly loaded on a Sephadex C-25 cation exchange resin and eluted with water. Fractions containing the sulfated product were lyophilized to obtain a solid residue, which was further purified on flash chromatography using 0-20% methanol in methylene chloride (see Appendix, Page 343 for NMR spectra).

^1H NMR (DMSO- d_6 , 400 MHz) δ 1.30 (m, 12H), 2.66 (s, 3H), 3.79 (s, 6H), 3.81 (s, 3H), 3.82 (s, 3H), 4.28 (m, 8H), 5.51 (s, 2H), 5.53 (s, 2H), 5.55 (s, 2H), 7.31 (s, 1H), 7.33 (s, 1H), 7.37 (s, 2H), 7.42 (s, 2H), 7.49 (s, 1H), 8.05 (s, 1H). ^{13}C NMR (DMSO- d_6 , 400 MHz) δ 13.79, 13.87, 14.00, 14.01, 56.02 (4C), 56.08, 59.90, 60.60 (2C), 60.45, 62.89 (2C), 95.72 (2C), 96.07, 96.25, 106.57 (2C), 106.67, 107.71, 107.84, 109.10, 112.00, 112.12, 117.68, 117.75, 118.30, 118.41, 143.63 (2C), 145.67, 146.05, 146.16, 148.81 (2C), 148.87, 149.11, 149.87, 150.16 (2C), 157.42

162.08, 162.62, 162.68, 163.34. MS (-ve) m/z calcd. for $C_{52}H_{49}O_{23}S [(M-Na)^-]$ 1073.44, found 1073.67 $(M-Na)^-$.

5.4.3 Substrate Hydrolysis Assay

Thrombin activity in the presence of inhibitors was studied using a chromogenic substrate hydrolysis assay in 20 mM Tris-HCl buffer, pH 7.4, containing 100 mM NaCl, 2.5 mM $CaCl_2$ and 0.1 % polyethylene glycol (PEG) 8000 in PEG 20,000-coated acrylic cuvettes. Spectrozyme TH was used as substrate and the residual thrombin activity was quantified by measuring the initial rate of hydrolysis from the linear increase in absorbance at 405 nm as a function of time. Briefly, a solution of 10 μ L of the inhibitors to form final concentrations ranging from 4.5 – 900 μ M, was diluted with 970 μ L of buffer and 5 μ L of 1 μ M thrombin (5 nM) and incubated. This was followed by addition of 15 μ L of 2 mM Spectrozyme TH (30 μ M) and the initial rate was quickly measured. Logistic equation 4 was used to fit the dose dependence of residual thrombin activity to obtain IC_{50} .

$$Y = Y_0 + \frac{Y_M - Y_0}{1 + 10^{(\log[I]_0 - \log IC_{50}) \times HS}} \quad \text{Equation 4}$$

In this equation, Y is the ratio of residual thrombin activity in the presence of the inhibitor to that in its absence; Y_M and Y_0 are the maximum and minimum possible values of the fractional residual thrombin activity, respectively; and IC_{50} is the concentration of inhibitors that results in 50% inhibition of enzyme activity. Sigmaplot 8.0 (SPSS, Inc. Chicago, IL) was used to perform non-linear curve fitting in which Y_M , Y_0 , and IC_{50} were allowed optimized.

5.4.4 Michaelis-Menten Kinetics of Substrate Hydrolysis by Thrombin in Presence of T9a

The initial rate of Spectrozyme TH hydrolysis by 5 nM thrombin was monitored from the linear increase in absorbance at 405 nm corresponding to less than 10% consumption of the substrate. The initial rate was measured as a function of various concentrations of the substrate (2 – 80 μ M) in the presence of fixed concentrations of **9a** (0–3.6 μ M), from one or three different stock solutions, incubated with thrombin either overnight at 25°C or for two hours at 37°C in 20 mM Tris-HCl buffer, pH 7.4, to ensure the prevention of aggregation at both conditions. The data was fitted by the standard Michaelis-Menten equation to determine K_M and V_{MAX} .

5.4.5 Plasma Studies (Prothrombin Time and Activated Partial Thromboplastin Time)

For both PT and APTT assays, standard 1-stage recalcification assay with a BBL Fibrosystem fibrometer (Becton-Dickinson, Sparks, MD) was used to measure the clotting time. For the APTT assay, 90 μ L citrated human plasma, 10 μ L inhibitor (or vehicle for blank test), and 100 μ L of pre-warmed APTT reagent (0.2% ellagic acid) were mixed and incubated for 4 minutes. The clotting was initiated by adding 100 μ L of 25 mM $CaCl_2$ (37 °C) and the time to clot was recorded. For Prothrombin (PT) assays, a 10 μ L sample of the inhibitor (or vehicle for blank test), and 90 μ L of citrated human plasma were mixed and incubated for 30 seconds at 37 °C followed by addition of 200 μ L pre-warmed thromboplastin (Reconstituted as per directions provided by manufacturer). Each clotting assay was performed in duplicate. The data were fit to a quadratic trend line, which was used to determine the concentration of the inhibitor necessary to double the clotting time, 2×APTT or 2×PT.

5.4.6 Screening Protocols

Screening of library for Factor VIIa inhibition—Direct inhibition of factor VIIa by the library of sulfated benzofuran derivatives was measured through a one-point chromogenic substrate hydrolysis assay. The buffer used in these experiments was 20 mM Tris-HCl buffer, pH 7.4, containing 100 mM NaCl, 2.5 mM CaCl₂, 0.1% polyethylene glycol (PEG) 8000 and 0.02% Tween 80. Benzofuran derivatives (5 µL) at concentrations 20 mM were diluted with 75 µL volume of assay buffer in flat bottom 96 well-plates (BD Falcon) at 37 °C. To this solution was added 10 µL of FVIIa solution to give approximately 80 nM initial FVIIa concentration and 5 µL of tissue factor solution to give 800 nM. After 10 min of incubation, 5 µL of 20 mM Spectrozyme factor VIIa was rapidly added and the residual factor VIIa activity was measured from the initial rate of increase in absorbance at 405 nm. The plate was read using a microplate reader (FlexStation III, Molecular Devices). Relative residual factor VIIa activity was calculated from the ratio of thrombin activity in the presence and absence of inhibitor. The percent residual activity was calculated using the equation 5.

$$\% \text{ Residual Activity} = [(slope \text{ of blank} - slope \text{ of well with inhibitor})/slope \text{ of blank}] \times 100$$

A cut off of **40%** was selected, and those compounds which showed a % residual activity lower than 40% were selected for full inhibition profile.

Screening of library for Factor IXa inhibition—Direct inhibition of factor IXa by the library of sulfated benzofuran derivatives was measured through a one-point chromogenic substrate hydrolysis assay. The buffer used in these experiments was 20 mM Tris-HCl buffer, pH 7.4, containing 100 mM NaCl, 2.5 mM CaCl₂, 0.1% polyethylene glycol (PEG) 8000, 0.02% Tween

80 and 33% v/v ethylene glycol. Benzofuran derivatives (5 μ L) at concentrations 20 mM were diluted with 80 μ L volume of assay buffer in flat bottom 96 well-plates (BD Falcon) at 25 °C. To this solution was added 5 μ L of factor IXa solution to give approximately 1780 nM initial factor IXa concentration. After 10 min of incubation, 10 μ L of 8.5 mM Spectrozyme factor IXa was rapidly added and the residual factor IXa activity was measured from the initial rate of increase in absorbance at 405 nm. The plate was read using a microplate reader (FlexStation III, Molecular Devices). Relative residual factor IXa activity was calculated from the ratio of thrombin activity in the presence and absence of inhibitor. The percent residual activity was calculated using the equation 5.

Screening of library for Factor Xa inhibition—Direct inhibition of Factor Xa by the library of sulfated benzofuran derivatives was measured through a one-point chromogenic substrate hydrolysis assay. The buffer used in these experiments was 20 mM Tris-HCl buffer, pH 7.4, containing 100 mM NaCl, 2.5 mM CaCl₂, 0.1% polyethylene glycol (PEG) 8000 and 0.02% Tween 80. Benzofuran derivatives (5 μ L) at concentrations 20 mM were diluted with 185 μ L volume of assay buffer in flat bottom 96 well-plates (BD Falcon) at 37 °C. To this solution was added 5 μ L of factor Xa solution to give approximately 43.5 nM initial factor Xa concentration. After 10 min of incubation, 5 μ L of 5 mM Spectrozyme factor Xa was rapidly added and the residual factor Xa activity was measured from the initial rate of increase in absorbance at 405 nm. The plate was read using a microplate reader (FlexStation III, Molecular Devices). Relative residual factor Xa activity was calculated from the ratio of thrombin activity in the presence and absence of inhibitor. The percent residual activity was calculated using the equation 5.

Screening of library for Factor XIa inhibition—Direct inhibition of factor XIa by the library of sulfated benzofuran derivatives was measured through a one-point chromogenic substrate

hydrolysis assay. The buffer used in these experiments was 20 mM Tris-HCl buffer, pH 7.4, containing 100 mM NaCl, 0.1% polyethylene glycol (PEG) 8000 and 0.02% Tween 80. Benzofuran derivatives (5 μ L) at concentrations 20 mM were diluted with 85 μ L volume of assay buffer in flat bottom 96 well-plates (BD Falcon) at 25 °C. To this solution was added 5 μ L of factor XIa solution to give approximately 15.3 nM initial factor XIa concentration. After 10 min of incubation, 5 μ L of 6.6 mM Spectrozyme factor XIa was rapidly added and the residual factor XIa activity was measured from the initial rate of increase in absorbance at 405 nm. The plate was read using a microplate reader (FlexStation III, Molecular Devices). Relative residual factor XIa activity was calculated from the ratio of thrombin activity in the presence and absence of inhibitor. The percent residual activity was calculated using the equation 5.

Screening of library for Factor XIIa inhibition—Direct inhibition of factor XIIa by the library of sulfated benzofuran derivatives was measured through a one-point chromogenic substrate hydrolysis assay. The buffer used in these experiments was 20 mM Tris-HCl buffer, pH 7.4, containing 100 mM NaCl, 0.1% polyethylene glycol (PEG) 8000 and 0.02% Tween 80. Benzofuran derivatives (5 μ L) at concentrations 20 mM were diluted with 185 μ L volume of assay buffer in flat bottom 96 well-plates (BD Falcon) at 25 °C. To this solution was added 5 μ L of factor XIIa solution to give approximately 200 nM initial factor XIIa concentration. After 10 min of incubation, 5 μ L of 5 mM Spectrozyme factor XIIa was rapidly added and the residual factor XIIa activity was measured from the initial rate of increase in absorbance at 405 nm. The plate was read using a microplate reader (FlexStation III, Molecular Devices). Relative residual factor XIIa activity was calculated from the ratio of thrombin activity in the presence and absence of inhibitor. The percent residual activity was calculated using the equation 5.

5.4.7 Inhibition of Factor VIIa

Direct inhibition of factor VIIa by the sulfated benzofuran trimer was measured through a chromogenic substrate hydrolysis assay. The buffer used in these experiments was 20 mM Tris-HCl buffer, pH 7.4, containing 100 mM NaCl, 2.5 mM CaCl₂, 0.1% polyethylene glycol (PEG) 8000 and 0.02% Tween 80. Benzofuran derivatives (5 µL) at various concentrations were diluted with 75 µL volume of assay buffer in flat bottom 96 well-plates (BD Falcon) at 37 °C. To this solution was added 10 µL of factor VIIa solution to give approximately 80 nM initial factor VIIa concentration and 5 µL of tissue factor solution to give 800 nM. After 10 min of incubation, 5 µL of 20 mM Spectrozyme factor VIIa was rapidly added and the residual factor VIIa activity was measured from the initial rate of increase in absorbance at 405 nm. The plate was read using a microplate reader (FlexStation III, Molecular Devices). Relative residual VIIa activity was calculated from the ratio of thrombin activity in the presence and absence of inhibitor. Equation 6 was used to fit the dose-dependence of residual proteinase activity to obtain the *IC*₅₀ and the efficacy $\Delta Y (= Y_M - Y_0)$ of inhibition.

$$Y = Y_0 + \frac{Y_M - Y_0}{1 + 10^{(\log[I]_0 - \log IC_{50}) \times HS}} \quad \text{Equation 6}$$

In this equation, Y is the ratio of residual thrombin activity in the presence of inhibitor to that in its absence (fractional residual activity), *Y*_M and *Y*_O are the maximum and minimum possible values of the fractional residual proteinase activity, *IC*₅₀ is the concentration of the inhibitor that results in 50% inhibition of enzyme activity, and HS is the Hill Slope, which was set constant at 1. A current version of SigmaPlot (SPSS, Inc. Chicago, IL) was used to perform non-linear curve fitting in which *Y*_M, *Y*_O and *IC*₅₀ were optimized.

5. 4.8 Inhibition of Factor IXa

Direct inhibition of factor IXa by sulfated benzofuran trimer was measured through a chromogenic substrate hydrolysis assay. The buffer used in these experiments was 20 mM Tris-HCl buffer, pH 7.4, containing 100 mM NaCl, 2.5 mM CaCl₂, 0.1% polyethylene glycol (PEG) 8000, 0.02% Tween 80 and 33% v/v ethylene glycol. Benzofuran derivatives (5 µL) at concentrations 20 mM were diluted with 80 µL volume of assay buffer in flat bottom 96 well-plates (BD Falcon) at 25 °C. To this solution was added 5 µL of factor IXa solution to give approximately 1780 nM initial factor IXa concentration. After 10 min of incubation, 10 µL of 8.5 mM Spectrozyme factor IXa was rapidly added and the residual factor IXa activity was measured from the initial rate of increase in absorbance at 405 nm. The plate was read using a microplate reader (FlexStation III, Molecular Devices). Relative residual factor IXa activity was calculated as described in Experimental Section 5.4.7.

5.4.9 Inhibition of Factor Xa

Direct inhibition of factor Xa by sulfated benzofuran trimer was measured through a chromogenic substrate hydrolysis assay. The buffer used in these experiments was 20 mM Tris-HCl buffer, pH 7.4, containing 100 mM NaCl, 2.5 mM CaCl₂, 0.1% polyethylene glycol (PEG) 8000 and 0.02% Tween 80. Benzofuran derivatives (5 µL) at concentrations 20 mM were diluted with 185 µL volume of assay buffer in flat bottom 96 well-plates (BD Falcon) at 37 °C. To this solution was added 5 µL of factor Xa solution to give approximately 43.5 nM initial factor Xa concentration. After 10 min of incubation, 5 µL of 5 mM Spectrozyme Xa was rapidly added and the residual factor Xa activity was measured from the initial rate of increase in absorbance at 405

nm. The plate was read using a microplate reader (FlexStation III, Molecular Devices). Relative residual factor Xa activity was calculated as described in Experimental Section 5.4.7.

Chapter 6 Identification of Novel Allosteric Inhibitor by Exploring a Larger Chemical Space

6.1 Introduction

High throughput screening (HTS) and virtual screening (VS) are two most widely used techniques to discover new lead molecules.²⁴⁰ In the last few decades, there has been an enormous growth in the availability of databases of molecules, which in turn has led to increased screening costs and a reduction in hit rate making the HTS approach less appealing.²⁴¹ Computational methods such as VS may offer a time saving and cost saving solution for this problem.²⁴² VS has been validated for performance in several studies for identifying hits.²⁴³ The increasing requirement for improvement in the drug discovery process has sparked the path away from traditional HTS to high speed and cost efficient VS methods.²⁴⁴ The main goal of VS is to come up with novel chemical structures with unique pharmacological profiles. Hence, VS can be called as rational alternative to traditional HTS.²⁴⁰

VS can be classified into two categories: structure-based and ligand-based methods. Structure-based docking is used when the structure of the target is known. The success of this method is compromised, however, by the inability of available scoring functions to identify the

most appropriate binding mode.²⁴³ In addition, it is very time consuming and may not consider the flexibility of the binding site.²⁴⁵ In contrast to structure-based methods, ligand-based methods focus on specific key interactions responsible for protein-ligand binding to generate lead candidates. The major disadvantage is its inability to consider the shape of the binding site. Thus, both of these methods face major drawbacks in terms of predictability. In order to overcome drawbacks associated with both methods, a combination approach may be used.²⁴⁶

The aim of this study is to utilize a combination of both ligand-based and docking-based VS approaches to identify new scaffolds in the design of potential allosteric inhibitors of thrombin. Virtual screening was performed based on the pharmacophore query developed from the SAR results of a library of sulfated benzofuran dimers (see Chapter 4). The hits generated from VS were further validated by docking to a crystal structure of thrombin to identify molecules having high predicted affinity and specificity for the binding site. Three molecules selected from these VS and docking studies were purchased and tested for thrombin inhibition.

6.2 Results and Discussion

6.2.1 Pharmacophore Generation

A pharmacophore was generated based on the results obtained from SAR studies of sulfated benzofuran dimers synthesized previously (Chapter 4),²³¹ as shown in Figure 37. Based on this SAR, it was found that the potency of sulfated monomers improved 1000-fold on addition of one benzofuran unit. Thus, it can be concluded that at least two benzofuran (or aromatic) units are necessary for higher potency. The average distances between these two aromatic regions from their aromatic centroids were measured and found out to be 8.13 ± 0.5 Å. Additionally,

there was a requirement that a hydrophobic group be present at the 3- position on each unit. The average distance to these groups was measured to be 7.35 ± 1 Å from the aromatic centroid. The most stringent requirement was the presence of negative charge (sulfate group) at the first aromatic unit. There are few molecules present in commercial libraries that contain negative charge in the form of sulfate group. To make the search successful, the sulfate group was replaced with a hydroxyl group, which can be later added both *in silico* and by synthesis to place negative charge in the specified region. Based on these features, the query for virtual screening was designed using the tools present in the UNITY search program.

6.2.2 Virtual Screening

The virtual search was performed on the ZINC database (Shoichet Laboratory, UCSF, CA) containing around 1 million compounds. It was performed using the UNITY search tool present in SYBYL 8.1. To narrow down the drug like molecules, Lipinski's rule of five was applied. The following constraints for Lipinski's rule were applied; Maximum weight – 500, maximum donor – 5, maximum acceptor – 10, maximum LogP – 4.15. One deviation from the rule was allowed. The minimum gradient for tweak was set to 0.001. In order to get maximum hits, rings were made flexible and no limit was placed on rotatable bonds. Using the 3D pharmacophore query, a flexible 3D search was performed on the entire ZINC database. Based on similarity in topological and electronic features, 4560 hits were obtained. These hits were pre-processed to add sulfate group using a script that identifies the free phenolic group and performs an *in silico* sulfation. The modified database was used for molecular docking studies.

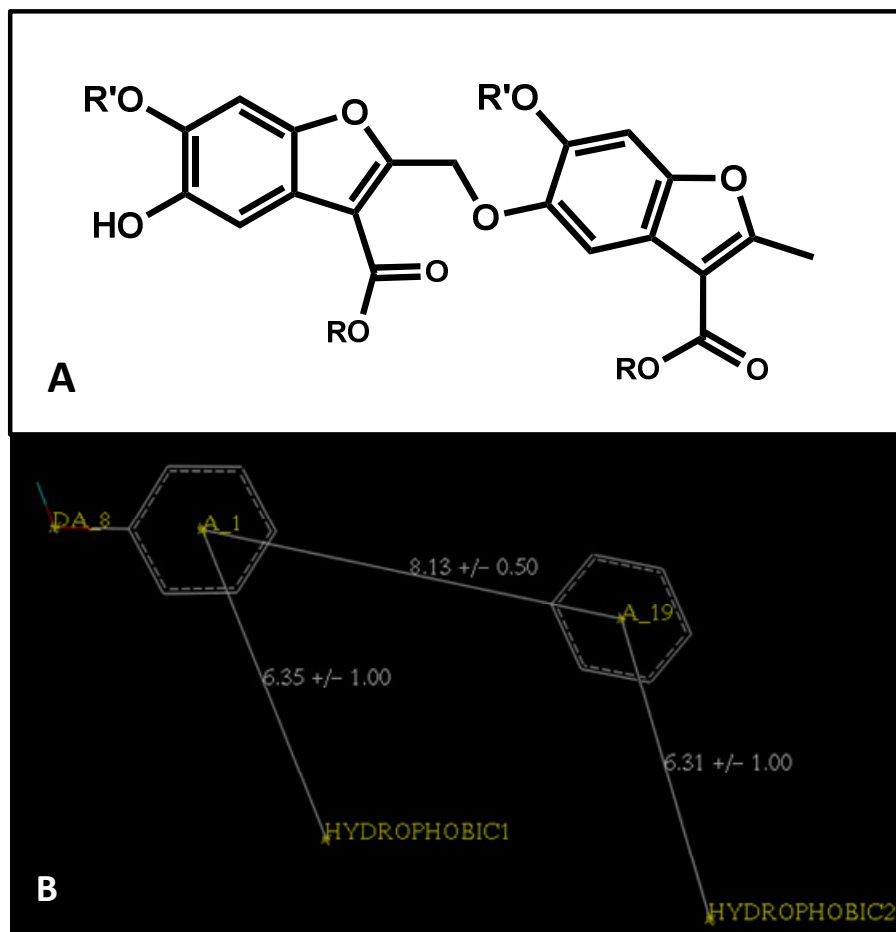


Figure 37. A) Represent atom of the common scaffold for the library of sulfated benzofuran dimers. B) 3D pharmacophore query used for virtual screening of ZINC database to identify the new scaffold with similar electronic and topological features. The query defines the important regions required for defining the activity of inhibitors like aromatic units, hydrophobic centers and the presence of an electron donating center.

6.2.3 Docking Studies

The docking studies were performed using a two-step method with the GOLD docking suite, shown in Figure 38. The aim of the first step is to narrow down the large library of hits obtained from virtual screening by identifying the structures having high affinity for thrombin. In

this step, an initial single docking experiment was performed with the crystal structure of thrombin (PDB: 3EQO). The GA run was set to “10” and early termination was set “ON” to save the CPU time. The molecules were selected based on the GOLDScore. 138 structures were considered as high affinity based on GOLDScore (> 70). In the second step, docking studies were performed in triplicate to identify the structures which bind consistently in the same binding pose over three independent runs. The purpose of three independent runs was to gain confidence in binding geometry and to identify correct binding poses. In three independent runs, GA was set to “30” and early terminal was set “OFF” to identify the best binding pose. The binding poses from three runs were superimposed to calculate the root mean square deviation (RMSD). The structures having $\text{RMSD} < 2$ were selected. Ten molecules were identified which met the requirement of both filters. These molecules have high GOLDScore, which correspond to high affinity for the binding site and consistent binding geometry over three independent runs. Based on this two-step docking study and commercial availability, three molecules were purchased. The molecules **V1**, **V2** and **V3** was purchased from Spec (RI, USA), ChemBridge Corporation (CA, USA) and ChemDiv (CA, USA), respectively.

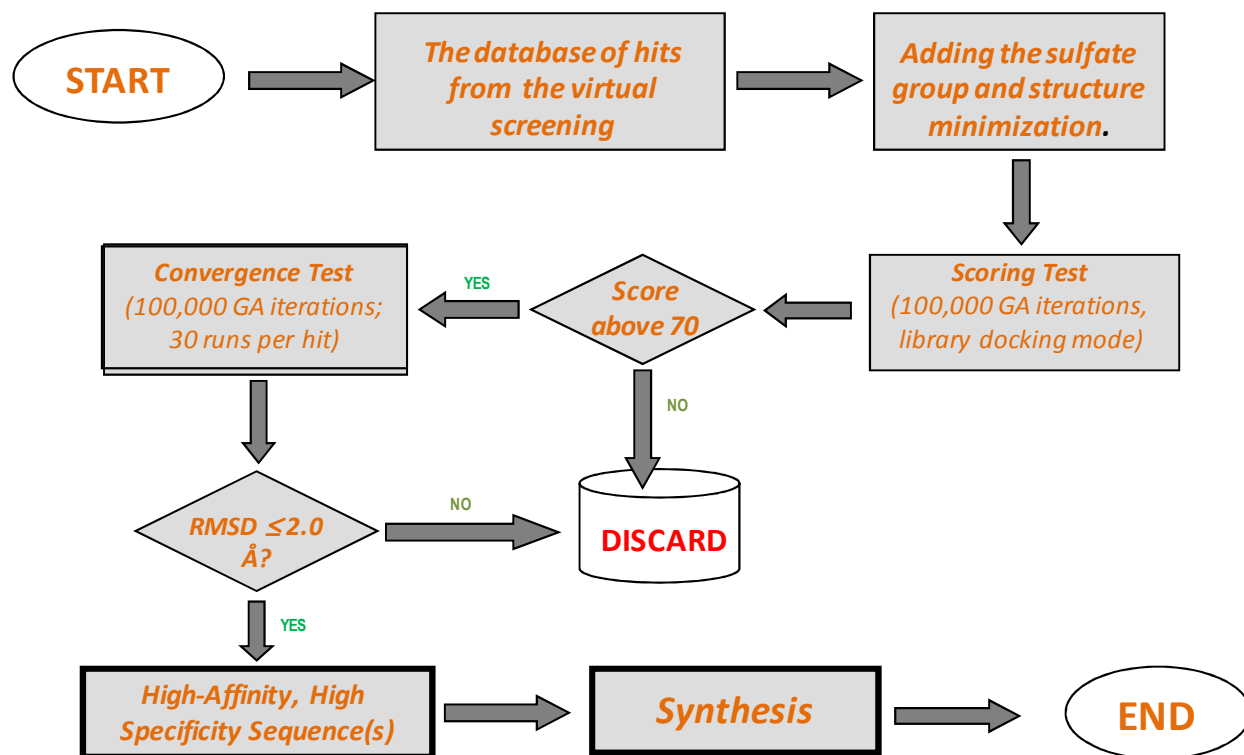


Figure 38. Graphical representation of docking protocol using the two-step approach to identify new hits. Figure explains the two filters and cutoff limit to pass both filters. The figure is adapted from Raghuraman *et al.* (2006) *J. Med. Chem.* 49, 3553-3562.

6.2.4 Chemistry

To meet the requirement of pharmacophore query, sulfate groups need to be added. In the final step, the sulfate group was added on the three purchased compound using the microwave-based sulfation method developed in our laboratory.²²² To the solution of unsulfated compound (typically 50 mg) in acetonitrile: DMF (4:1, 0.45 mL) in a microwave tube were added triethylamine (10 equiv) and trimethylamine-sulfur trioxide complex (15 equiv). The reaction mixture was exposed to microwaves (50 W) for 40 min at 100 °C followed by vacuum concentration to remove all solvent. The solid so obtained was directly loaded on a Sephadex C-25 cation exchange resin and eluted with water. Fractions containing the sulfated product were

lyophilized to obtain a solid residue, which was further purified on reverse-phase gradient HPLC to remove residual unsulfated contaminants. The final molecules are obtained in good yield (see Appendix, Page 352-354 for NMR spectra).

V1: ^1H NMR (CDCl_3 , 400 MHz) δ 4.25 (s, 2H), 4.66 (s, 2H), 6.40 (d, $J=8.4$ Hz, 1H), 6.64 (d, $J=8.4$ Hz, 2H), 6.85 (d, $J=8.4$ Hz, 1H), 6.90 (m, 2H), 6.95 (m, 4H), 7.04 (m, 2H).

V1S: ^1H NMR (D_2O , 400 MHz) δ 4.78 (s, 2H), 5.15 (s, 2H), 7.18 (d, $J=8.8$ Hz, 2H), 7.35 (m, 4H), 7.40 (m, 1H), 7.47 (m, 1H), 7.66 (m, 2H), 7.92 (s, 1H).

V2: ^1H NMR (CDCl_3 , 400 MHz) δ 6.18 (m, 4H), 6.96 (m, 6H), 7.46 (m, 3H), 7.92 (m, 1H), 8.08 (s, 1H), 9.32 (s, 1H), 9.66 (s, 1H).

V2S: ^1H NMR (D_2O , 400 MHz) δ 7.23 (m, 4H), 7.48 (m, 4H), 7.51 (m, 2H), 7.72 (s, 1H), 7.79 (m, 1H), 7.82 (d, $J=8$ Hz, 1H), 8.05 (s, 1H), 8.16 (m, 1H).

V3: ^1H NMR (DMSO-d_6 , 400 MHz) δ 2.27 (s, 3H), 3.77 (d, $J=15$ Hz, 1H), 4.93 (d, $J=15$ Hz, 1H), 5.31 (s, 1H), 6.62 (t, $J=2$ Hz, 1H), 6.69 (m, 1H), 6.74 (m, 1H), 7.05 (m, 2H), 7.13 (m, 3H), 7.55 (m, 1H), 7.88 (m, 2H), 8.03 (m, 1H).

V3S: ^1H NMR (DMSO , 400 MHz) δ 2.18 (s, 3H), 3.84 (d, $J=15$ Hz, 1H), 4.84 (d, $J=15$ Hz, 1H), 5.35 (s, 1H), 6.97 (m, 4H), 7.05 (m, 2H), 7.18 (m, 1H), 7.29 (m, 1H), 7.49 (m, 1H), 7.76 (m, 1H), 7.82 (m, 1H), 7.97 (m, 1H).

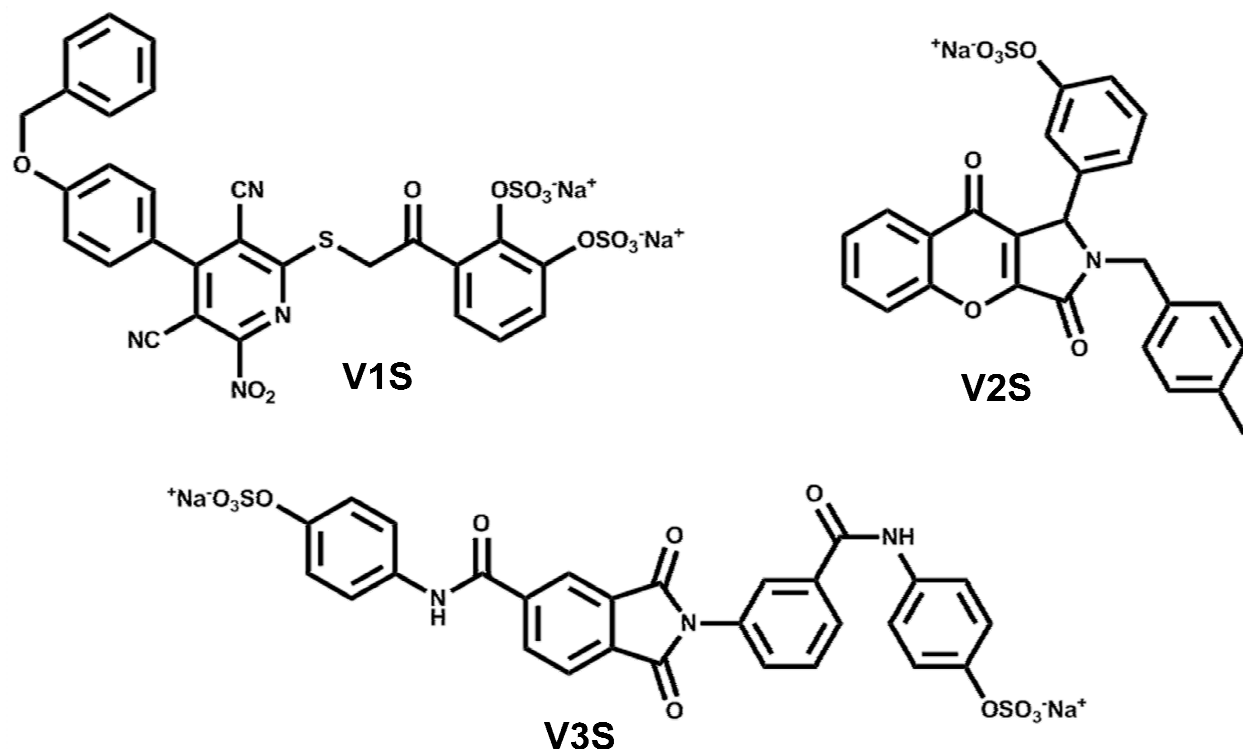


Figure 39. Structures of a library of sulfated compounds as potential allosteric regulators of thrombin. These molecules were purchased from Spec, Chembridge and ChemDiv and then sulfated. Sulfation protocol is described in chemistry section.

6.2.5 Inhibition of Thrombin by Sulfated Molecules

Inhibition of thrombin by the inhibitors was measured through Spectrozyme TH hydrolysis assay. The assay is based on the principle that the initial rate of substrate hydrolysis decreases in the presence of the inhibitor quantitatively. The fractional decrease in initial rate of hydrolysis shows a sigmoidal profile on a semi-log plot, which is fitted by a dose – response equation 5 (Experimental Section 6.4.5) to derive IC_{50} , HS , Y_0 and Y_M parameters for each potential inhibitor. The semi-log inhibition curves observed for inhibitors are shown in Figure 40. Three inhibitors studied in this work showed reasonable inhibition of human α -thrombin at

pH 7.4 and 25 °C. The inhibitors **V1S**, **V2S**, and **V3S** exhibited IC_{50} 65.9 μ M, 192.9 μ M and 285.6 μ M (see Table 20 and Figure 40). The potency for thrombin inhibition for these molecules is comparable to library of sulfated benzofuran dimers. Thus, these molecules can serve as additional lead structures for designing allosteric inhibitors of thrombin.

Table 20. Inhibition of Human α -Thrombin by Sulfated molecules

	log IC_{50} (M)	IC_{50} (μM)	ΔY
V1S	-4.18 \pm 0.16	65.9 \pm 1.1	0.614
V2S	-3.71 \pm 0.12	192 \pm 11	0.425
V3S	-3.54 \pm 0.18	285.6 \pm 1.1	0.890

Thrombin inhibition was measured in spectrophotometric assay through initial rate of Spectrozyme TH hydrolysis as described in Experimental section. Standard error shown is \pm 1 S.E.

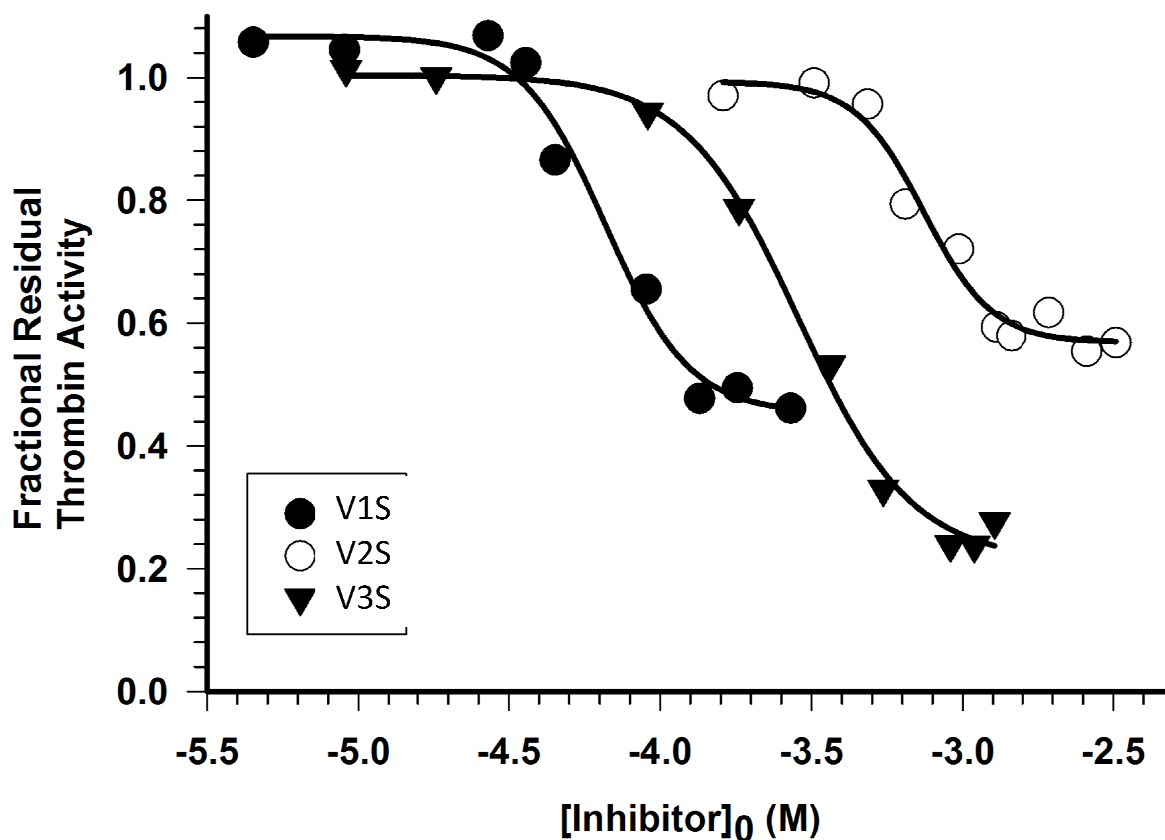


Figure 40. Direct inhibition of thrombin by designed **V1S**, **V2S** and **V3S**. The inhibition of human thrombin was determined spectrophotometrically through a Spectrozyme TH hydrolysis assay at pH 7.4 and 25 °C. Solid lines represent sigmoidal fits to the data to obtain IC_{50} , Y_M , and Y_O .

6.2.6 Prolongation of Plasma Clotting Time by Sulfated Compounds

Two types of plasma clotting assays are performed to evaluate the anticoagulant potency in plasma for new coagulation inhibitors. Prothrombin (PT) and activated partial thromboplastin time (APTT) assays are used to measure the effect of an inhibitor on the extrinsic and intrinsic flux of coagulation, respectively. The concentrations of the inhibitors required to double the PT and APTT were measured and reported, shown in Table 21. A 2-fold increase in PT required 606 μ M concentrations of **1S**. In a similar manner, the doubling of APTT required 550 μ M of **V1S**.

These results suggest that the sulfated compound **V1S** is significantly potent in human plasma and hence proves our design and model for allosteric inhibition of thrombin.

To further evaluate the effect of various factors in anticoagulation mechanism by inhibitor **1S** in plasma, we performed plasma studies on various factor deficient human plasma. The APTT test was performed on factor IX and XI deficient human plasma; it was found that the concentration required to double the APTT time were 380 μM and 368 μM , respectively (see Table 21, Figure 41). These results suggest that there was no significant change in APTT time than normal human plasma; hence factors IX and XI do not play a role in the anticoagulation effect of these inhibitors. Similarly, the PT test was performed on factor VII deficient plasma giving 2*PT of 779.24 μM (see Table 21), which is significantly different from the value obtained in normal human plasma. Thus, we can conclude that our designed inhibitor **V1S** is interacting with factor VII in human plasma to show an anticoagulant effect. Overall, the plasma studies suggest the feasibility of designing small molecules that will function as anticoagulants *in vivo*.

Table 21. Effect of Designed Sulfated Benzofurans on Human Plasma Clotting Time.^a

Plasma	2*PT (μM)	2*APTT (μM)
Human Plasma	606.8	550
FIX Deficient Plasma	nd ^b	368.83
FXI Deficient Plasma	nd ^b	380
FVII Deficient Plasma	779.24	nd ^b

^a PT and APTT values were deduced in *in vitro* human plasma experiments where the clot initiator is either thromboplastin or ellagic acid, respectively. ^b not determined.

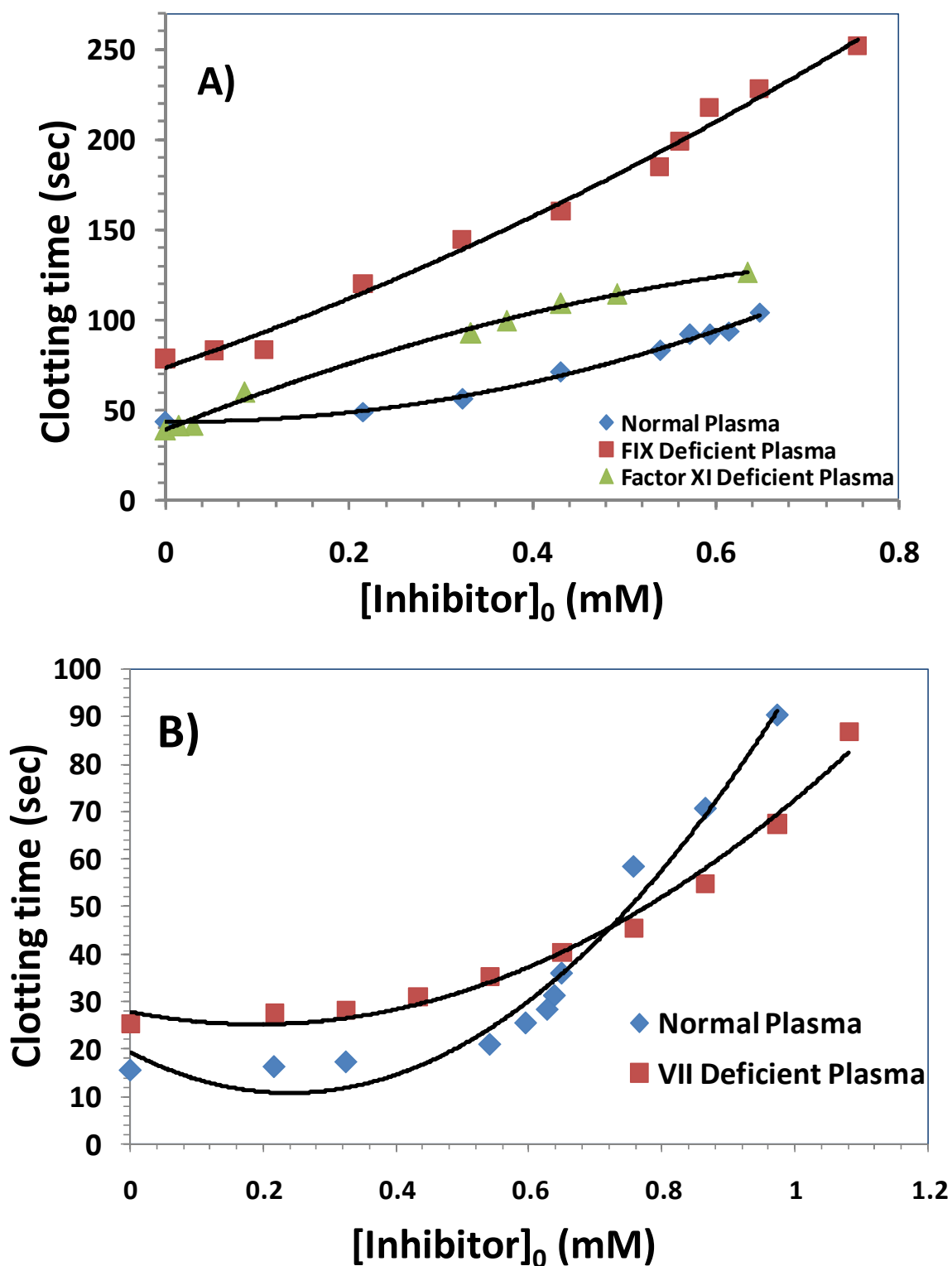


Figure 41. Prolongation of clotting time as a function of concentration of **V1S** in either activated partial thromboplastin time assay (A) or prothrombin time assay (B). Solid lines are trend lines, and not non-linear regressional fits.

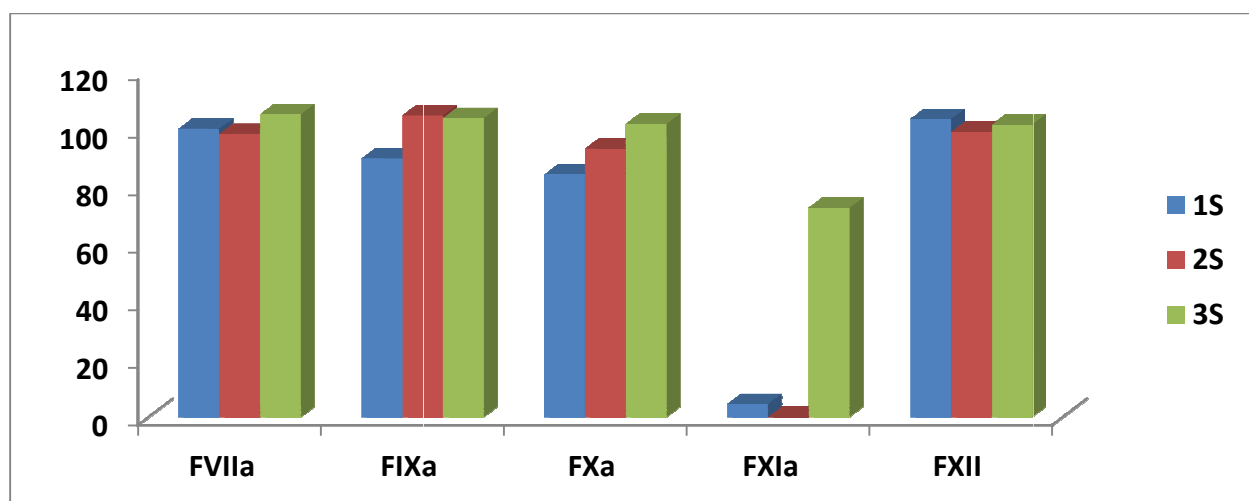
6.2.7 Screening against Other Serine Proteases

The library of sulfated molecules obtained from virtual screening were screened against the panel of coagulation proteases including factors VIIa, IXa, Xa, XIa and XIIa, which are either involved in the intrinsic or extrinsic pathways. The assay is based on hydrolysis of a chromogenic substrate by the protease, the rate of which is decreased in the presence of inhibitor. Screening was performed at a single concentration of inhibitors using a substrate hydrolysis assay in 96 well-plates. This assay is based on the decrease in the initial rate of substrate hydrolysis in the presence of inhibitor. The decrease in initial rate of hydrolysis typically provides the fractional residual activity of enzyme.

Table 22 shows the percentage residual activity of all proteases at the final concentration of 365 μ M of each inhibitor. None of these molecules inhibited the factors VIIa, IXa, Xa and XII by more than 20% at the concentration of 365 μ M (see Figure 42). In screening against factor XIa, molecules **V1S** and **V2S** completely inhibited factor XIa activity. These results were consistent with library of sulfated benzofuran dimers from which they are derived. Similar to dimers, these molecules showed selectivity against factors VIIa, IXa and XIIa and completely inhibited factor XIa. Thus, this selectivity filter further validates the computational model for designing the allosteric inhibitor of thrombin.

Table 22. Residual enzyme activity for various proteases at 365 μ M inhibitor concentration

	Factor VIIa	Factor IXa	Factor Xa	Factor XIa	Factor XII
V1S	98 \pm 3	91 \pm 2	86 \pm 3	7 \pm 4	100 \pm 5
V2S	100 \pm 2.5	101 \pm 5	91 \pm 4	6 \pm 8	96 \pm 3
V3S	102 \pm 4	107 \pm 4	97 \pm 7	76 \pm 4	97 \pm 7

**Figure 42.** Bar graph for residual activity for screening against various proteases

6.3 Discussion

Computational structure-based design provides an excellent tool set to identify the most appropriate ‘small’ molecule structure from a large number of potential molecules. The thrombin inhibition potency and efficacy discovered for three sulfated molecules designed using computational tools suggest that these scaffolds may serve as leads in developing new allosteric inhibitors of thrombin. The moderate potency displayed by these inhibitors validates the computational model design; we employed to identify inhibitors that modulate the thrombin activity by an allosteric mechanism.

This work presents the combination of ligand-based and docking-based approaches to identify and design small synthetic sulfated aromatic structures as novel allosteric modulators of thrombin function. The allosteric inhibitors of thrombin are advantageous in terms of their controlled inhibition of protease and the ability to reverse excess inhibition. The success of our computational model for allosteric inhibition of thrombin give us confidence to extend it toward for developing allosteric inhibitors for other proteases such as factors VIIa, Xa, IXa and XIa.

6.4 Experimental Section

6.4.1 Protein preparation

The docking studies required an accurate 3D structure of thrombin with high resolution. The crystal structure of thrombin bound to its allosteric exosite I ligand hirugen with resolution of 1.53 Å was obtained from the protein data bank (ID: 3EQ0). All the heavy atoms in the region of Arg173 were resolved. The inorganic salts and water molecules were deleted. Hydrogen atoms were added to the protein using the “Add Hydrogen” function of Sybyl 8.1. The protein was minimized to adjust the hydrogen position using the minimizing tool in Sybyl 8.1, by using the Tripos force field to reach the terminating gradient of 0.05 kcal/mol/Å or a maximum of 100000 iterations. The Gasteiger-Huckel type charge was assigned to each atom. The thrombin binding site was defined to include all the amino acid residues in a radius of 22 Å around the Cα carbon of Arg173.

6.4.2 Chemical database for virtual screening

A virtual screening of the commercially available database “ZINC” using our pharmacophore was carried out. The ZINC database contains the structural information of approximately 1

million molecules. These molecules are supplied by various companies such as Key Organics, Maybridge, Chemdiv, Otava, Life Chemicals, Specs, Asinex, etc. The compound collection was obtained as Structure-Data files and stored. The virtual screening was performed using “Unity Search” available in Sybyl 8.1. The flexible 3D search option was used for screening the database against the pharmacophore query (Figure 37). To reduce the number of hits obtained from the search, constraints such as Lipinski rules, were applied.

6.4.3 Docking Protocol

Docking of the potential hits obtained from virtual screening onto the defined binding site of the thrombin was performed with GOLD 4.1 (Cambridge Crystallographic Data Center, UK). The binding site is comprised of Arg173 and all the amino acid residues within a radius of 22 Å around it. GOLD is a “soft docking” method that implicitly handles local protein flexibility by allowing a small degree of interpenetration, or van der Waals overlap, of ligand and protein atoms. GOLD optimizes the orientation of hydrogen-bond donating atoms on the residues such as Ser, Thr, Tyr, Lys and Arg as part of the docking process. Except for the automated number of iterations, the allowed amide bond flip and the prohibited early termination, default parameters were employed during the GOLD docking runs. Docking was driven by the GOLD scoring function and molecules were ranked based on the GOLDScore obtained. The protein hydrogen binding constraints were added for five hydrogen atoms of the guanidine group of Arg173 and penalty of 10 GOLD score units were assigned.

Docking of the synthesized inhibitors onto the defined binding site of the thrombin were also performed with GOLD 4.1. Default parameters were employed with the following exceptions: A protein hydrogen bonding constraint was added such that the score was reduced by

10.0 GoldScore units if the ligand did not form an H-bond with the guanidinium group of Arg173. Again, amide bonds were allowed to flip. The number of GA runs was increased to 30 to more accurately screen all possible binding geometries, and early termination was disabled. The docking was driven by the GOLDScore fitness function and the docked solutions were ranked based on the unmodified GOLDScore obtained. To assess the reproducibility of the docked poses, the docking runs were performed in triplicate.

6.4.4 Chemicals, Reagents and Analytical Chemistry

Reagents, chemicals and solvents were purchased either from Sigma-Aldrich (Milwaukee, WI) or Fisher (Pittsburgh, PA) and were used as received. Reagent solutions and chemicals were handled under inert nitrogen atmosphere using syringe techniques for liquid and dried spatula for solids. All glassware was dried in the oven overnight before use. Sodium exchange chromatography was performed using SP Sephadex C-25 cation exchange resin from GE Healthcare Life Sciences (Piscataway, NJ). Approximately 100 mg sulfated sample was loaded onto 10 g of the cation exchanger in a 10 × 460 mm column and eluted with either water at 0.5 mL/min. Microwave-based sulfation and coupling reactions were performed using a CEM-Discover synthesizer (Matthews, NC) in sealed reaction vessels (7 mL) at 50 W. The temperature of the reaction was maintained at the desired setting using cooled nitrogen (45 psi) flow.

^1H and ^{13}C NMR spectra were recorded at either 300 or 400 MHz (Varian Mercury or Bruker UltrashieldTM Plus) in appropriate deuterated solvents including CDCl_3 , $\text{DMSO}-d_6$, or D_2O . All signals are reported in ppm with the internal chloroform, DMSO, and D_2O signals at 7.26, 2.50, 2.05, and 4.79, respectively, as standards. The data is reported as chemical shifts

(ppm) and splitting pattern is described as (s = singlet, d = doublet, t = triplet, m = multiplet) with coupling constant(s) (Hz), and integration. Mass spectrometry was performed on all synthesized molecules using a Micromass ZMD4000 single quadrupole mass spectrometer with ESI ionization probe operating in negative ion mode (Waters Corp., Milford, MA). The samples, dissolved in acetonitrile containing formic acid (5% v/v), were infused at 10 μ L/min. The source block temperature and the probe temperature were typically held at 100 and 120 °C, respectively, while corona and cone voltages were selected through manual optimization. The desolvation nitrogen flow was 500 L/hour. Mass spectra were acquired in the mass range from 110 to 1000 Daltons at 400 amu/sec. The chromogenic substrate Spectrozyme TH (H-*D*-hexahydrotyrosol-Ala-Arg-*p*-nitroanilide) was purchased from American Diagnostica (Greenwich, CT). Unfractionated porcine heparin was purchased from Sigma (St. Louis, MO). All other chemicals were analytical reagent grade from either Sigma Chemicals (St. Louis, MO) or Fisher (Pittsburgh, PA) and used as such.

6.4.5 Substrate hydrolysis assay

Thrombin activity in the presence of inhibitors was studied using chromogenic substrate hydrolysis assay in 20 mM Tris-HCl buffer, pH 7.4, containing 100 mM NaCl, 2.5 mM CaCl₂ and 0.1% polyethylene glycol (PEG) 8000 in PEG 20,000-coated acrylic cuvettes. Spectrozyme TH was used as substrate and the residual thrombin activity was quantified by measuring the initial rate of hydrolysis from the linear increase in absorbance at 405 nm as a function of time. Briefly, a solution of 10 μ L of the inhibitors to form final concentrations ranging from 4.5 – 900 μ M, was diluted with 970 μ L of buffer and 5 μ L of 1 μ M thrombin (5 nM) and incubated. This was followed by addition of 15 μ L of 2 mM Spectrozyme TH (30 μ M) and the initial rate was

rapidly measured. Equation 6 was used to fit the dose dependence of residual thrombin activity to obtain IC_{50} .

$$Y = Y_0 + \frac{Y_M - Y_0}{1 + 10^{(\log[I]_0 - \log IC_{50}) \times HS}} \quad \text{Equation 6}$$

In this equation Y is the ratio of residual thrombin activity in the presence of the inhibitor to that in its absence; Y_M and Y_0 are the maximum and minimum possible values of the fractional residual thrombin activity, respectively; and IC_{50} is the concentration of inhibitors that results in 50% inhibition of enzyme activity. Sigmaplot 8.0 (SPSS, Inc. Chicago, IL) was used to perform non-linear curve fitting in which Y_M , Y_0 , and IC_{50} were optimized.

6.4.6 Plasma studies (Prothrombin Time and Activated Partial Thromboplastin Time)

For both PT and APTT assays, standard 1-stage recalcification assay with a BBL Fibrosystem fibrometer (Becton-Dickinson, Sparks, MD) was used to measure the clotting time. For the APTT assay, 90 μ L citrated human plasma, 10 μ L inhibitor (or vehicle for blank test), and 100 μ L of pre-warmed APTT reagent (0.2% ellagic acid) were mixed and incubated for 4 minutes. The clotting was initiated by adding 100 μ L of 25 mM $CaCl_2$ (37 °C) and the time to clot was recorded. For prothrombin (PT) assays, 10 μ L sample of the inhibitor (or vehicle for blank test) and 90 μ L of citrated human plasma were mixed and incubated for 30 second at 37 °C followed by addition of 200 μ L pre-warmed thromboplastin (reconstituted as per directions provided by manufacturer). Each clotting assay was performed in duplicate. The data were fit to a quadratic trend line, which was used to determine the concentration of the inhibitor necessary to double the clotting time, 2×APTT or 2×PT.

Chapter 7 Conclusion

Designing allosteric inhibitors offers the opportunity to regulate thrombin for maintaining balance between its procoagulant and anticoagulant activities. Thus, allosteric inhibitors could help in overcoming the side effects such as enhanced risk of excessive bleeding and in eliminating the need for regular laboratory monitoring. To design novel anticoagulants as allosteric inhibitors of thrombin based on the β -5 linkage of LMWLs, benzofuran-based sulfated monomers and oligomers were designed.

A diversified library of monomers and dimers was synthesized and found to exhibit moderately potent inhibition of thrombin. From this library, **12c** was found to be the most potent allosteric inhibitor designed so far. Interesting structure-activity relationships were observed. Sulfated dimers were found to be 1000-fold more potent than sulfated monomers. A strict requirement of a key sulfate group was found, as un-sulfated precursors were found to be inactive. However, increasing the number of anionic groups was found to be deleterious for potency. The presence of hydrophobic groups at 3- and 3'-positions improved potency, but substitution with hydrophilic and bulky groups at these positions led to a decrease in potency. Similarly, the presence of bulky and hydrophobic groups at 6 and 6' positions improved the inhibition potency.

Michaelis-Menten kinetics study suggested a non-competitive, allosteric mode of inhibition by these inhibitors. Screening of sulfated monomers and dimers against the panel of coagulation factors such as factors VIIa, IXa, Xa, XIa and XIIa suggested high selectivity for thrombin. However, a few dimers were able to inhibit factor XIa also. The *in vitro* anticoagulant potency of these inhibitors was translated into higher system, such as human plasma. Based on competitive and mutagenesis studies, it was found that Arg173 residue played a crucial role in recognition of these inhibitors. A plausible binding mode was identified using molecular docking and scoring approaches. The proposed binding mode was able to explain majority of the SAR findings and GOLDScore correlated well with the experimental IC_{50} value. Thus, the proposed binding model offers an excellent opportunity to design new inhibitors with improved inhibition potency.

In a quest to improve the thrombin inhibition potency, a small library of sulfated benzofuran trimers and tetramer was synthesized. It was found that extension of oligomeric chain to trimer improved the potency nearly 10-fold. However, increasing the chain length further to tetramer was detrimental for potency. This observation suggests that trimer is an optimal oligomeric chain length for potency. The allosteric mode of inhibition was also retained in higher oligomers. However, competitive studies suggest that sulfated trimers recognized a site different from sulfated dimers. The range of thrombin inhibition potency and efficacy discovered for sulfated benzofurans monomers and higher oligomers suggest that the designed sulfated benzofuran scaffold may be an excellent lead in developing anticoagulants radically different from those studied to-date.

Finally, a pharmacophore query was designed based on the SAR results obtained from the library of sulfated dimers to virtually screen a larger chemical space. The combination of

both ligand-based and docking-based approach was used to identify new scaffolds as potential leads for allosteric inhibitors of thrombin. Three molecules were selected to purchase and sulfated to match the query. It was found that all three sulfated molecules were moderate inhibitors of thrombin with potency similar to that of the sulfated dimers. The anticoagulant potency of these new inhibitors translated well into human plasma. Thus, we identified three new scaffolds, which can serve as starting point to design the new inhibitors for thrombin. Overall, this work highlights the opportunity of exploring allosteric modulators of thrombin and other coagulation enzymes, e.g., factors Xa, IXa and XIa, through sulfated lignin scaffolds.

References

1. Brenner, B.; Hoffman, R. Emerging options in the treatment of deep vein thrombosis and pulmonary embolism. *Blood Rev.* **2011**, *25*, 215-221.
2. Harenberg, J.; Marx, S.; Wehling, M.; Krejczy, M. New Anticoagulants - Promising and Failed Developments. *Br. J. Pharmacol.* **2011**, *In Press*.
3. Sakhuja, R.; Yeh, R. W.; Bhatt, D. L. Anticoagulant agents in acute coronary syndromes. *Curr. Probl. Cardiol.* **2011**, *36*, 127-168.
4. Hart, R. G.; Halperin, J. L. Atrial fibrillation and thromboembolism: a decade of progress in stroke prevention. *Ann. Intern. Med.* **1999**, *131*, 688-695.
5. Hoppensteadt, D. A.; Jeske, W.; Walenga, J.; Fareed, J. The future of anticoagulation. *Semin. Respir. Crit. Care. Med.* **2008**, *29*, 90-99.
6. Fernandez, P. M.; Patierno, S. R.; Rickles, F. R. Tissue factor and fibrin in tumor angiogenesis. *Semin. Thromb. Hemost.* **2004**, *30*, 31-44.
7. Sans, S.; Kesteloot, H.; Kromhout, D. The burden of cardiovascular diseases mortality in Europe. Task Force of the European Society of Cardiology on Cardiovascular Mortality and Morbidity Statistics in Europe. *Eur. Heart J.* **1997**, *18*, 1231-1248.
8. Fenton, J. W., 2nd; Ofosu, F. A.; Brezniak, D. V.; Hassouna, H. I. Understanding thrombin and hemostasis. *Hematol. Oncol. Clin. North Am.* **1993**, *7*, 1107-1119.

9. Hoffman, M.; Monroe, D. M.,3rd A cell-based model of hemostasis. *Thromb. Haemost.* **2001**, 85, 958-965.
10. Frederick, R.; Pochet, L.; Charlier, C.; Masereel, B. Modulators of the coagulation cascade: focus and recent advances in inhibitors of tissue factor, factor VIIa and their complex. *Curr. Med. Chem.* **2005**, 12, 397-417.
11. Monroe, D. M.; Hoffman, M. What does it take to make the perfect clot? *Arterioscler. Thromb. Vasc. Biol.* **2006**, 26, 41-48.
12. Crawley, J. T.; Lane, D. A. The haemostatic role of tissue factor pathway inhibitor. *Arterioscler. Thromb. Vasc. Biol.* **2008**, 28, 233-242.
13. Hack, C. E. Tissue factor pathway of coagulation in sepsis. *Crit. Care Med.* **2000**, 28, S25-30.
14. Carmeliet, P.; Collen, D. Tissue factor. *Int. J. Biochem. Cell Biol.* **1998**, 30, 661-667.
15. Macfarlane, R. G. An Enzyme Cascade in the Blood Clotting Mechanism, and its Function as a Biochemical Amplifier. *Nature* **1964**, 202, 498-499.
16. Berntorp, E. Prophylaxis and treatment of bleeding complications in von Willebrand disease type 3. *Semin. Thromb. Hemost.* **2006**, 32, 621-625.
17. Monroe, D. M.; Hoffman, M.; Roberts, H. R. Transmission of a procoagulant signal from tissue factor-bearing cell to platelets. *Blood Coagul. Fibrinolysis* **1996**, 7, 459-464.

18. Larkin, D.; Murphy, D.; Reilly, D. F.; Cahill, M.; Sattler, E.; Harriott, P.; Cahill, D. J.; Moran, N. ICln, a novel integrin α IIb β 3-associated protein, functionally regulates platelet activation. *J. Biol. Chem.* **2004**, *279*, 27286-27293.
19. Pidard, D. The platelet fibrinogen receptor: a model for the analysis of cellular adhesion mechanisms and their modification in pathology. *Pathol. Biol. (Paris)* **1989**, *37*, 1107-1113.
20. Saiah, E.; Soares, C. Small molecule coagulation cascade inhibitors in the clinic. *Curr. Top. Med. Chem.* **2005**, *5*, 1677-1695.
21. Davie, E. W.; Ratnoff, O. D. Waterfall Sequence for Intrinsic Blood Clotting. *Science* **1964**, *145*, 1310-1312.
22. Griffin, J. H. Blood coagulation. The thrombin paradox. *Nature* **1995**, *378*, 337-338.
23. Nesheim, M. Thrombin and fibrinolysis. *Chest* **2003**, *124*, 33S-9S.
24. Di Cera, E. Thrombin. *Mol. Aspects Med.* **2008**, *29*, 203-254.
25. Giesen, P. L.; Rauch, U.; Bohrmann, B.; Kling, D.; Roque, M.; Fallon, J. T.; Badimon, J. J.; Himber, J.; Riederer, M. A.; Nemerson, Y. Blood-borne tissue factor: another view of thrombosis. *Proc. Natl. Acad. Sci. U. S. A.* **1999**, *96*, 2311-2315.
26. Eisenberg, P. R.; Siegel, J. E.; Abendschein, D. R.; Miletich, J. P. Importance of factor Xa in determining the procoagulant activity of whole-blood clots. *J. Clin. Invest.* **1993**, *91*, 1877-1883.
27. Suzuki, K.; Dahlback, B.; Stenflo, J. Thrombin-catalyzed activation of human coagulation factor V. *J. Biol. Chem.* **1982**, *257*, 6556-6564.

28. Mosesson, M. W. Fibrinogen and fibrin structure and functions. *J. Thromb. Haemost.* **2005**, 3, 1894-1904.
29. Fulcher, C. A.; Roberts, J. R.; Zimmerman, T. S. Thrombin proteolysis of purified factor viii procoagulant protein: correlation of activation with generation of a specific polypeptide. *Blood* **1983**, 61, 807-811.
30. Mosesson, M. W.; Siebenlist, K. R.; Meh, D. A. The structure and biological features of fibrinogen and fibrin. *Ann. N. Y. Acad. Sci.* **2001**, 936, 11-30.
31. Sadler, J. E. Medicine: K is for koagulation. *Nature* **2004**, 427, 493-494.
32. Anand, K.; Pallares, I.; Valnickova, Z.; Christensen, T.; Vendrell, J.; Wendt, K. U.; Schreuder, H. A.; Enghild, J. J.; Aviles, F. X. The crystal structure of thrombin-activable fibrinolysis inhibitor (TAFI) provides the structural basis for its intrinsic activity and the short half-life of TAFIa. *J. Biol. Chem.* **2008**, 283, 29416-29423.
33. Li, W.; Huntington, J. A. The heparin binding site of protein C inhibitor is protease-dependent. *J. Biol. Chem.* **2008**, 283, 36039-36045.
34. Lundblad, R. L.; Bradshaw, R. A.; Gabriel, D.; Ortel, T. L.; Lawson, J.; Mann, K. G. A review of the therapeutic uses of thrombin. *Thromb. Haemost.* **2004**, 91, 851-860.
35. Li, W.; Johnson, D. J.; Esmon, C. T.; Huntington, J. A. Structure of the antithrombin-thrombin-heparin ternary complex reveals the antithrombotic mechanism of heparin. *Nat. Struct. Mol. Biol.* **2004**, 11, 857-862.

36. Weitz, J. I.; Hudoba, M.; Massel, D.; Maraganore, J.; Hirsh, J. Clot-bound thrombin is protected from inhibition by heparin-antithrombin III but is susceptible to inactivation by antithrombin III-independent inhibitors. *J. Clin. Invest.* **1990**, *86*, 385-391.
37. Walenga, J. M.; Hoppensteadt, D. A. Monitoring the new antithrombotic drugs. *Semin. Thromb. Hemost.* **2004**, *30*, 683-695.
38. Davidson, B. L. Preparing for the new anticoagulants. *J. Thromb. Thrombolysis* **2003**, *16*, 49-54.
39. Fareed, J.; Thethi, I.; Hoppensteadt, D. Old Versus New Oral Anticoagulants: Focus on Pharmacology. *Annu. Rev. Pharmacol. Toxicol.* **2011**, .
40. Palareti, G.; Manotti, C.; D'Angelo, A.; Pengo, V.; Erba, N.; Moia, M.; Ciavarella, N.; Devoto, G.; Berrettini, M.; Leali, N.; Poggi, M.; Legnani, C.; Musolesi, S.; Coccheri, S. Thrombotic events during oral anticoagulant treatment: results of the inception-cohort, prospective, collaborative ISCOAT study: ISCOAT study group (Italian Study on Complications of Oral Anticoagulant Therapy). *Thromb. Haemost.* **1997**, *78*, 1438-1443.
41. Iqbal, C. W.; Cima, R. R.; Pemberton, J. H. Bleeding and Thromboembolic Outcomes for Patients on Oral Anticoagulation Undergoing Elective Colon and Rectal Abdominal Operations. *J. Gastrointest. Surg.* **2011**, .
42. Weitz, J. I. Low-molecular-weight heparins. *N. Engl. J. Med.* **1997**, *337*, 688-698.

43. Langdown, J.; Belzar, K. J.; Savory, W. J.; Baglin, T. P.; Huntington, J. A. The critical role of hinge-region expulsion in the induced-fit heparin binding mechanism of antithrombin. *J. Mol. Biol.* **2009**, *386*, 1278-1289.
44. Gomez-Outes, A.; Suarez-Gea, M. L.; Calvo-Rojas, G.; Lecumberri, R.; Rocha, E.; Pozo-Hernandez, C.; Terleira-Fernandez, A. I.; Vargas-Castrillon, E. Discovery of Anticoagulant Drugs: A Historical Perspective. *Curr. Drug Discov. Technol.* **2011**, .
45. Hirsh, J.; Bauer, K. A.; Donati, M. B.; Gould, M.; Samama, M. M.; Weitz, J. I.; American College of Chest Physicians Parenteral anticoagulants: American College of Chest Physicians Evidence-Based Clinical Practice Guidelines (8th Edition). *Chest* **2008**, *133*, 141S-159S.
46. Warkentin, T. E.; Greinacher, A. Heparin-induced thrombocytopenia: recognition, treatment, and prevention: the Seventh ACCP Conference on Antithrombotic and Thrombolytic Therapy. *Chest* **2004**, *126*, 311S-337S.
47. Bates, S. M.; Weitz, J. I. New anticoagulants: beyond heparin, low-molecular-weight heparin and warfarin. *Br. J. Pharmacol.* **2005**, *144*, 1017-1028.
48. Carrasco, P. Pharmacology of second generation low molecular weight heparins. *Pathophysiol. Haemost. Thromb.* **2002**, *32*, 401-402.
49. Turpie, A. G. Fondaparinux: a Factor Xa inhibitor for antithrombotic therapy. *Expert Opin. Pharmacother.* **2004**, *5*, 1373-1384.
50. Tran, A. H.; Lee, G. Fondaparinux for prevention of venous thromboembolism in major orthopedic surgery. *Ann. Pharmacother.* **2003**, *37*, 1632-1643.

51. Turpie, A. G.; Gallus, A. S.; Hoek, J. A.; Pentasaccharide Investigators A synthetic pentasaccharide for the prevention of deep-vein thrombosis after total hip replacement. *N. Engl. J. Med.* **2001**, *344*, 619-625.
52. Greinacher, A.; Warkentin, T. E. The direct thrombin inhibitor hirudin. *Thromb. Haemost.* **2008**, *99*, 819-829.
53. Stone, S. R.; Hofsteenge, J. Kinetics of the inhibition of thrombin by hirudin. *Biochemistry* **1986**, *25*, 4622-4628.
54. Hogg, P. J.; Jackson, C. M. Fibrin monomer protects thrombin from inactivation by heparin-antithrombin III: implications for heparin efficacy. *Proc. Natl. Acad. Sci. U. S. A.* **1989**, *86*, 3619-3623.
55. Glusa, E.; Markwardt, F. Platelet functions in recombinant hirudin-anticoagulated blood. *Haemostasis* **1990**, *20*, 112-118.
56. Fox, I.; Dawson, A.; Loynds, P.; Eisner, J.; Findlen, K.; Levin, E.; Hanson, D.; Mant, T.; Wagner, J.; Maraganore, J. Anticoagulant activity of Hirulog, a direct thrombin inhibitor, in humans. *Thromb. Haemost.* **1993**, *69*, 157-163.
57. Matsuo, T.; Koide, M.; Kario, K. Development of argatroban, a direct thrombin inhibitor, and its clinical application. *Semin. Thromb. Hemost.* **1997**, *23*, 517-522.
58. Weitz, J. I.; Hudoba, M.; Massel, D.; Maraganore, J.; Hirsh, J. Clot-bound thrombin is protected from inhibition by heparin-antithrombin III but is susceptible to inactivation by antithrombin III-independent inhibitors. *J. Clin. Invest.* **1990**, *86*, 385-391.

59. Wille-Jorgensen, P. The potential role of new therapies in deep-vein thrombosis prophylaxis. *Semin. Hematol.* **2001**, 38, 20-30.
60. Van Aken, H.; Bode, C.; Darius, H.; Diehm, C.; Encke, A.; Gulba, D. C.; Haas, S.; Hacke, W.; Puhl, W.; Quante, M.; Riess, H.; Scharf, R.; Schellong, S.; Schror, T.; Schulte, K. L.; Tebbe, U. Anticoagulation: the present and future. *Clin. Appl. Thromb. Hemost.* **2001**, 7, 195-204.
61. Tasset, D. M.; Kubik, M. F.; Steiner, W. Oligonucleotide inhibitors of human thrombin that bind distinct epitopes. *J. Mol. Biol.* **1997**, 272, 688-698.
62. White, R.; Rusconi, C.; Scardino, E.; Wolberg, A.; Lawson, J.; Hoffman, M.; Sullenger, B. Generation of species cross-reactive aptamers using "toggle" SELEX. *Mol. Ther.* **2001**, 4, 567-573.
63. De Cristofaro, R.; De Candia, E.; Rutella, S.; Weitz, J. I. The Asp(272)-Glu(282) region of platelet glycoprotein Ibalpha interacts with the heparin-binding site of alpha-thrombin and protects the enzyme from the heparin-catalyzed inhibition by antithrombin III. *J. Biol. Chem.* **2000**, 275, 3887-3895.
64. Leung, L. L. Application of combinatorial libraries and protein engineering to the discovery of novel anti-thrombotic drugs. *Thromb. Haemost.* **1995**, 74, 373-376.
65. Petitou, M.; Duchaussoy, P.; Herbert, J. M.; Duc, G.; El Hajji, M.; Branellec, J. F.; Donat, F.; Necciari, J.; Cariou, R.; Bouthier, J.; Garrigou, E. The synthetic pentasaccharide fondaparinux: first in the class of antithrombotic agents that selectively inhibit coagulation factor Xa. *Semin. Thromb. Hemost.* **2002**, 28, 393-402.

66. Buller, H. R.; Davidson, B. L.; Decousus, H.; Gallus, A.; Gent, M.; Piovella, F.; Prins, M. H.; Raskob, G.; Segers, A. E.; Cariou, R.; Leeuwenkamp, O.; Lensing, A. W.; Matisse Investigators. Fondaparinux or enoxaparin for the initial treatment of symptomatic deep venous thrombosis: a randomized trial. *Ann. Intern. Med.* **2004**, *140*, 867-873.
67. Turpie, A. G. Fondaparinux: a Factor Xa inhibitor for antithrombotic therapy. *Expert Opin. Pharmacother.* **2004**, *5*, 1373-1384.
68. Gerotziafas, G. T.; Samama, M. M. Heterogeneity of synthetic factor Xa inhibitors. *Curr. Pharm. Des.* **2005**, *11*, 3855-3876.
69. Weitz, J. I.; Bates, S. M. New anticoagulants. *J. Thromb. Haemost.* **2005**, *3*, 1843-1853.
70. Dahl, O. E. Mechanisms of hypercoagulability. *Thromb. Haemost.* **1999**, *82*, 902-906.
71. Hirsh, J.; O'Donnell, M.; Weitz, J. I. New anticoagulants. *Blood* **2005**, *105*, 453-463.
72. Lee, A.; Agnelli, G.; Buller, H.; Ginsberg, J.; Heit, J.; Rote, W.; Vlasuk, G.; Costantini, L.; Julian, J.; Comp, P.; van Der Meer, J.; Piovella, F.; Raskob, G.; Gent, M. Dose-response study of recombinant factor VIIa/tissue factor inhibitor recombinant nematode anticoagulant protein c2 in prevention of postoperative venous thromboembolism in patients undergoing total knee replacement. *Circulation* **2001**, *104*, 74-78.
73. Mousa, S. A.; Mohamed, S. Inhibition of endothelial cell tube formation by the low molecular weight heparin, tinzaparin, is mediated by tissue factor pathway inhibitor. *Thromb. Haemost.* **2004**, *92*, 627-633.

74. Davidson, B. L. Preparing for the new anticoagulants. *J. Thromb. Thrombolysis* **2003**, *16*, 49-54.
75. Nutescu, E. A.; Wittkowsky, A. K. Direct thrombin inhibitors for anticoagulation. *Ann. Pharmacother.* **2004**, *38*, 99-109.
76. Di Cera, E.; Page, M. J.; Bah, A.; Bush-Pelc, L.; Garvey, L. C. Thrombin allostery. *Phys. Chem. Chem. Phys.* **2007**, *9*, 1291-1306.
77. Wolberg, A. S. Thrombin generation and fibrin clot structure. *Blood Rev.* **2007**, *21*, 131-142.
78. Lane, D. A.; Philippou, H.; Huntington, J. A. Directing thrombin. *Blood* **2005**, *106*, 2605-2612.
79. Huntington, J. A. Molecular recognition mechanisms of thrombin. *J. Thromb. Haemost.* **2005**, *3*, 1861-1872.
80. Steinmetzer, T.; Sturzebecher, J. Progress in the development of synthetic thrombin inhibitors as new orally active anticoagulants. *Curr. Med. Chem.* **2004**, *11*, 2297-2321.
81. Nutescu, E. A.; Wittkowsky, A. K. Direct thrombin inhibitors for anticoagulation. *Ann. Pharmacother.* **2004**, *38*, 99-109.
82. Hofsteenge, J.; Braun, P. J.; Stone, S. R. Enzymatic properties of proteolytic derivatives of human alpha-thrombin. *Biochemistry* **1988**, *27*, 2144-2151.
83. Monroe, D. M.; Hoffman, M.; Roberts, H. R. Platelets and thrombin generation. *Arterioscler. Thromb. Vasc. Biol.* **2002**, *22*, 1381-1389.

84. Steinmetzer, T.; Hauptmann, J.; Sturzebecher, J. Advances in the development of thrombin inhibitors. *Expert Opin. Investig. Drugs* **2001**, *10*, 845-864.
85. Dang, O. D.; Vindigni, A.; Di Cera, E. An allosteric switch controls the procoagulant and anticoagulant activities of thrombin. *Proc. Natl. Acad. Sci. U. S. A.* **1995**, *92*, 5977-5981.
86. Hortin, G. L.; Trimpe, B. L. Allosteric changes in thrombin's activity produced by peptides corresponding to segments of natural inhibitors and substrates. *J. Biol. Chem.* **1991**, *266*, 6866-6871.
87. Bailey, K.; Bettelheim, F. R.; Lorand, L.; Middlebrook, W. R. Action of thrombin in the clotting of fibrinogen. *Nature* **1951**, *167*, 233-234.
88. Fenton, J. W. Thrombin specificity. *Ann. N. Y. Acad. Sci.* **1981**, *370*, 468-495.
89. Vu, T. K.; Wheaton, V. I.; Hung, D. T.; Charo, I.; Coughlin, S. R. Domains specifying thrombin-receptor interaction. *Nature* **1991**, *353*, 674-677.
90. Liu, L. W.; Vu, T. K.; Esmon, C. T.; Coughlin, S. R. The region of the thrombin receptor resembling hirudin binds to thrombin and alters enzyme specificity. *J. Biol. Chem.* **1991**, *266*, 16977-16980.
91. Lawson, J. H.; Kalafatis, M.; Stram, S.; Mann, K. G. A model for the tissue factor pathway to thrombin. I. An empirical study. *J. Biol. Chem.* **1994**, *269*, 23357-23366.

92. Nimjee, S. M.; Oney, S.; Volovyk, Z.; Bompiani, K. M.; Long, S. B.; Hoffman, M.; Sullenger, B. A. Synergistic effect of aptamers that inhibit exosites 1 and 2 on thrombin. *RNA* **2009**, *15*, 2105-2111.
93. Monteiro, R. Q.; Raposo, J. G.; Wisner, A.; Guimaraes, J. A.; Bon, C.; Zingali, R. B. Allosteric changes of thrombin catalytic site induced by interaction of bothrojaracin with anion-binding exosites I and II. *Biochem. Biophys. Res. Commun.* **1999**, *262*, 819-822.
94. Esmon, C. T.; Lollar, P. Involvement of thrombin anion-binding exosites 1 and 2 in the activation of factor V and factor VIII. *J. Biol. Chem.* **1996**, *271*, 13882-13887.
95. Fredenburgh, J. C.; Stafford, A. R.; Leslie, B. A.; Weitz, J. I. Bivalent binding to gammaA/gamma'-fibrin engages both exosites of thrombin and protects it from inhibition by the antithrombin-heparin complex. *J. Biol. Chem.* **2008**, *283*, 2470-2477.
96. Mattsson, C.; Menschik-Lundin, A.; Nylander, S.; Gyzander, E.; Deinum, J. Effect of different types of thrombin inhibitors on thrombin/thrombomodulin modulated activation of protein C in vitro. *Thromb. Res.* **2001**, *104*, 475-486.
97. de Amorim, H. L.; Netz, P. A.; Guimaraes, J. A. Thrombin allosteric modulation revisited: a molecular dynamics study. *J. Mol. Model.* **2010**, *16*, 725-735.
98. Gandhi, P. S.; Chen, Z.; Di Cera, E. Crystal structure of thrombin bound to the uncleaved extracellular fragment of PAR1. *J. Biol. Chem.* **2010**, *285*, 15393-15398.

99. Myles, T.; Le Bonniec, B. F.; Stone, S. R. The dual role of thrombin's anion-binding exosite-I in the recognition and cleavage of the protease-activated receptor 1. *Eur. J. Biochem.* **2001**, *268*, 70-77.
100. Kahn, M. L.; Zheng, Y. W.; Huang, W.; Bigornia, V.; Zeng, D.; Moff, S.; Farese, R. V., Jr; Tam, C.; Coughlin, S. R. A dual thrombin receptor system for platelet activation. *Nature* **1998**, *394*, 690-694.
101. Monteiro, R. Q.; Raposo, J. G.; Wisner, A.; Guimaraes, J. A.; Bon, C.; Zingali, R. B. Allosteric changes of thrombin catalytic site induced by interaction of bothrojaracin with anion-binding exosites I and II. *Biochem. Biophys. Res. Commun.* **1999**, *262*, 819-822.
102. Monteiro, R. Q. Targeting exosites on blood coagulation proteases. *An. Acad. Bras. Cienc.* **2005**, *77*, 275-280.
103. Krishnaswamy, S.; Betz, A. Exosites determine macromolecular substrate recognition by prothrombinase. *Biochemistry* **1997**, *36*, 12080-12086.
104. Dang, O. D.; Vindigni, A.; Di Cera, E. An allosteric switch controls the procoagulant and anticoagulant activities of thrombin. *Proc. Natl. Acad. Sci. U. S. A.* **1995**, *92*, 5977-5981.
105. Gibbs, C. S.; Coutre, S. E.; Tsiang, M.; Li, W. X.; Jain, A. K.; Dunn, K. E.; Law, V. S.; Mao, C. T.; Matsumura, S. Y.; Mejza, S. J. Conversion of thrombin into an anticoagulant by protein engineering. *Nature* **1995**, *378*, 413-416.
106. Di Cera, E.; Guinto, E. R.; Vindigni, A.; Dang, Q. D.; Ayala, Y. M.; Wuyi, M.; Tulinsky, A. The Na⁺ binding site of thrombin. *J. Biol. Chem.* **1995**, *270*, 22089-22092.

107. Dang, Q. D.; Sabetta, M.; Di Cera, E. Selective loss of fibrinogen clotting in a loop-less thrombin. *J. Biol. Chem.* **1997**, 272, 19649-19651.
108. Ayala, Y.; Di Cera, E. Molecular recognition by thrombin. Role of the slow-->fast transition, site-specific ion binding energetics and thermodynamic mapping of structural components. *J. Mol. Biol.* **1994**, 235, 733-746.
109. Bah, A.; Garvey, L. C.; Ge, J.; Di Cera, E. Rapid kinetics of Na⁺ binding to thrombin. *J. Biol. Chem.* **2006**, 281, 40049-40056.
110. Di Cera, E.; Page, M. J.; Bah, A.; Bush-Pelc, L. A.; Garvey, L. C. Thrombin allostery. *Phys. Chem. Chem. Phys.* **2007**, 9, 1291-1306.
111. Di Cera, E.; Dang, Q. D.; Ayala, Y. M. Molecular mechanisms of thrombin function. *Cell Mol. Life Sci.* **1997**, 53, 701-730.
112. Di Cera, E. A structural perspective on enzymes activated by monovalent cations. *J. Biol. Chem.* **2006**, 281, 1305-1308.
113. Dang, Q. D.; Guinto, E. R.; di Cera, E. Rational engineering of activity and specificity in a serine protease. *Nat. Biotechnol.* **1997**, 15, 146-149.
114. Dang, Q. D.; Di Cera, E. Residue 225 determines the Na(+)-induced allosteric regulation of catalytic activity in serine proteases. *Proc. Natl. Acad. Sci. U. S. A.* **1996**, 93, 10653-10656.

115. Degen, S. J.; McDowell, S. A.; Sparks, L. M.; Scharer, I. Prothrombin Frankfurt: a dysfunctional prothrombin characterized by substitution of Glu-466 by Ala. *Thromb. Haemost.* **1995**, *73*, 203-209.
116. Miyata, T.; Aruga, R.; Umeyama, H.; Bezeaud, A.; Guillin, M. C.; Iwanaga, S. Prothrombin Salakta: substitution of glutamic acid-466 by alanine reduces the fibrinogen clotting activity and the esterase activity. *Biochemistry* **1992**, *31*, 7457-7462.
117. Henriksen, R. A.; Dunham, C. K.; Miller, L. D.; Casey, J. T.; Menke, J. B.; Knupp, C. L.; Usala, S. J. Prothrombin Greenville, Arg517-->Gln, identified in an individual heterozygous for dysprothrombinemia. *Blood* **1998**, *91*, 2026-2031.
118. Mann, K. G. Biochemistry and physiology of blood coagulation. *Thromb. Haemost.* **1999**, *82*, 165-174.
119. Sambrano, G. R.; Weiss, E. J.; Zheng, Y. W.; Huang, W.; Coughlin, S. R. Role of thrombin signalling in platelets in haemostasis and thrombosis. *Nature* **2001**, *413*, 74-78.
120. Coughlin, S. R. Thrombin signalling and protease-activated receptors. *Nature* **2000**, *407*, 258-264.
121. Vu, T. K.; Wheaton, V. I.; Hung, D. T.; Charo, I.; Coughlin, S. R. Domains specifying thrombin-receptor interaction. *Nature* **1991**, *353*, 674-677.
122. Davey, M. G.; Luscher, E. F. Actions of thrombin and other coagulant and proteolytic enzymes on blood platelets. *Nature* **1967**, *216*, 857-858.

123. De Marco, L.; Mazzucato, M.; Masotti, A.; Fenton, J. W., 2nd; Ruggeri, Z. M. Function of glycoprotein Ib alpha in platelet activation induced by alpha-thrombin. *J. Biol. Chem.* **1991**, 266, 23776-23783.
124. Ishihara, H.; Connolly, A. J.; Zeng, D.; Kahn, M. L.; Zheng, Y. W.; Timmons, C.; Tram, T.; Coughlin, S. R. Protease-activated receptor 3 is a second thrombin receptor in humans. *Nature* **1997**, 386, 502-506.
125. Vu, T. K.; Hung, D. T.; Wheaton, V. I.; Coughlin, S. R. Molecular cloning of a functional thrombin receptor reveals a novel proteolytic mechanism of receptor activation. *Cell* **1991**, 64, 1057-1068.
126. Vassallo, R. R., Jr; Kieber-Emmons, T.; Cichowski, K.; Brass, L. F. Structure-function relationships in the activation of platelet thrombin receptors by receptor-derived peptides. *J. Biol. Chem.* **1992**, 267, 6081-6085.
127. Seegers, W. H.; Warner, E. D.; Brinkhous, K. M.; Smith, H. P. The use of Purified Thrombin as an Hemostatic Agent. *Science* **1939**, 89, 86.
128. Gomez, M.; Logsetty, S.; Fish, J. S. Reduced blood loss during burn surgery. *J. Burn Care Rehabil.* **2001**, 22, 111-117.
129. Light, R. U. The antigenicity of bovine thrombin; clinical evaluation. *J. Neurosurg.* **1945**, 2, 516-523.
130. Jackson, C. M.; Nemerson, Y. Blood coagulation. *Annu. Rev. Biochem.* **1980**, 49, 765-811.

131. Osterud, B.; Rapaport, S. I. Activation of factor IX by the reaction product of tissue factor and factor VII: additional pathway for initiating blood coagulation. *Proc. Natl. Acad. Sci. U. S. A.* **1977**, *74*, 5260-5264.
132. Butenas, S.; Mann, K. G. Kinetics of human factor VII activation. *Biochemistry* **1996**, *35*, 1904-1910.
133. Bajaj, S. P.; Rapaport, S. I.; Brown, S. F. Isolation and characterization of human factor VII. Activation of factor VII by factor Xa. *J. Biol. Chem.* **1981**, *256*, 253-259.
134. Radcliffe, R.; Bagdasarian, A.; Colman, R.; Nemerson, Y. Activation of bovine factor VII by hageman factor fragments. *Blood* **1977**, *50*, 611-617.
135. Radcliffe, R.; Nemerson, Y. Mechanism of activation of bovine factor VII. Products of cleavage by factor Xa. *J. Biol. Chem.* **1976**, *251*, 4749-4802.
136. Radcliffe, R.; Nemerson, Y. Activation and control of factor VII by activated factor X and thrombin. Isolation and characterization of a single chain form of factor VII. *J. Biol. Chem.* **1975**, *250*, 388-395.
137. Higashi, S.; Matsumoto, N.; Iwanaga, S. Molecular mechanism of tissue factor-mediated acceleration of factor VIIa activity. *J. Biol. Chem.* **1996**, *271*, 26569-26574.
138. Higashi, S.; Nishimura, H.; Aita, K.; Iwanaga, S. Identification of regions of bovine factor VII essential for binding to tissue factor. *J. Biol. Chem.* **1994**, *269*, 18891-18898.

139. Persson, E.; Olsen, O. H.; Ostergaard, A.; Nielsen, L. S. Ca²⁺ binding to the first epidermal growth factor-like domain of factor VIIa increases amidolytic activity and tissue factor affinity. *J. Biol. Chem.* **1997**, *272*, 19919-19924.
140. Kelly, C. R.; Dickinson, C. D.; Ruf, W. Ca²⁺ binding to the first epidermal growth factor module of coagulation factor VIIa is important for cofactor interaction and proteolytic function. *J. Biol. Chem.* **1997**, *272*, 17467-17472.
141. Astermark, J.; Hogg, P. J.; Bjork, I.; Stenflo, J. Effects of gamma-carboxyglutamic acid and epidermal growth factor-like modules of factor IX on factor X activation. Studies using proteolytic fragments of bovine factor IX. *J. Biol. Chem.* **1992**, *267*, 3249-3256.
142. Morita, T.; Isaacs, B. S.; Esmon, C. T.; Johnson, A. E. Derivatives of blood coagulation factor IX contain a high affinity Ca²⁺-binding site that lacks gamma-carboxyglutamic acid. *J. Biol. Chem.* **1984**, *259*, 5698-5704.
143. Foster, D.; Davie, E. W. Characterization of a cDNA coding for human protein C. *Proc. Natl. Acad. Sci. U. S. A.* **1984**, *81*, 4766-4770.
144. Astermark, J.; Bjork, I.; Ohlin, A. K.; Stenflo, J. Structural requirements for Ca²⁺ binding to the gamma-carboxyglutamic acid and epidermal growth factor-like regions of factor IX. Studies using intact domains isolated from controlled proteolytic digests of bovine factor IX. *J. Biol. Chem.* **1991**, *266*, 2430-2437.
145. Mannhalter, C.; Schiffman, S.; Deutsch, E. Phospholipids accelerate factor IX activation by surface bound factor XIa. *Br. J. Haematol.* **1984**, *56*, 261-271.

146. Cheung, W. F.; Stafford, D. W.; Sugo, T. Localization of a calcium-dependent epitope to the amino terminal region of the Gla domain of human factor IX. *Thromb. Res.* **1996**, *81*, 65-73.
147. Gailani, D.; Renne, T. Intrinsic pathway of coagulation and arterial thrombosis. *Arterioscler. Thromb. Vasc. Biol.* **2007**, *27*, 2507-2513.
148. Bouma, B. N.; Griffin, J. H. Human blood coagulation factor XI. Purification, properties, and mechanism of activation by activated factor XII. *J. Biol. Chem.* **1977**, *252*, 6432-6437.
149. Thompson, R. E.; Mandle, R. Jr.; Kaplan, A. P. Association of factor XI and high molecular weight kininogen in human plasma. *J. Clin. Invest.* **1977**, *60*, 1376-1380.
150. Fujikawa, K.; Chung, D. W.; Hendrickson, L. E.; Davie, E. W. Amino acid sequence of human factor XI, a blood coagulation factor with four tandem repeats that are highly homologous with plasma prekallikrein. *Biochemistry* **1986**, *25*, 2417-2424.
151. Naito, K.; Fujikawa, K. Activation of human blood coagulation factor XI independent of factor XII. Factor XI is activated by thrombin and factor XIa in the presence of negatively charged surfaces. *J. Biol. Chem.* **1991**, *266*, 7353-7358.
152. von dem Borne, P. A.; Meijers, J. C.; Bouma, B. N. Feedback activation of factor XI by thrombin in plasma results in additional formation of thrombin that protects fibrin clots from fibrinolysis. *Blood* **1995**, *86*, 3035-3042.
153. Gailani, D.; Broze, G. J., Jr Factor XI activation in a revised model of blood coagulation. *Science* **1991**, *253*, 909-912.

154. Papagrigoriou, E.; McEwan, P. A.; Walsh, P. N.; Emsley, J. Crystal structure of the factor XI zymogen reveals a pathway for transactivation. *Nat. Struct. Mol. Biol.* **2006**, *13*, 557-558.
155. Tordai, H.; Banyai, L.; Patthy, L. The PAN module: the N-terminal domains of plasminogen and hepatocyte growth factor are homologous with the apple domains of the prekallikrein family and with a novel domain found in numerous nematode proteins. *FEBS Lett.* **1999**, *461*, 63-67.
156. Riley, P. W.; Cheng, H.; Samuel, D.; Roder, H.; Walsh, P. N. Dimer dissociation and unfolding mechanism of coagulation factor XI apple 4 domain: spectroscopic and mutational analysis. *J. Mol. Biol.* **2007**, *367*, 558-573.
157. Cool, D. E.; Edgell, C. J.; Louie, G. V.; Zoller, M. J.; Brayer, G. D.; MacGillivray, R. T. Characterization of human blood coagulation factor XII cDNA. Prediction of the primary structure of factor XII and the tertiary structure of beta-factor XIIa. *J. Biol. Chem.* **1985**, *260*, 13666-13676.
158. Stavrou, E.; Schmaier, A. H. Factor XII: what does it contribute to our understanding of the physiology and pathophysiology of hemostasis & thrombosis. *Thromb. Res.* **2010**, *125*, 210-215.
159. Schmaier, A. H.; Larusch, G. Factor XII: new life for an old protein. *Thromb. Haemost.* **2010**, *104*, 915-918.
160. Revak, S. D.; Cochrane, C. G.; Griffin, J. H. The binding and cleavage characteristics of human Hageman factor during contact activation. A comparison of normal plasma with plasmas

deficient in factor XI, prekallikrein, or high molecular weight kininogen. *J. Clin. Invest.* **1977**, *59*, 1167-1175.

161. Pixley, R. A.; Schapira, M.; Colman, R. W. The regulation of human factor XIIa by plasma proteinase inhibitors. *J. Biol. Chem.* **1985**, *260*, 1723-1729.

162. Pixley, R. A.; Schmaier, A.; Colman, R. W. Effect of negatively charged activating compounds on inactivation of factor XIIa by C1 inhibitor. *Arch. Biochem. Biophys.* **1987**, *256*, 490-498.

163. Schmaier, A. H. Why do we want to know how factor XII levels are modulated? *Thromb. Res.* **2010**, *125*, 105-106.

164. Farsetti, A.; Misiti, S.; Citarella, F.; Felici, A.; Andreoli, M.; Fantoni, A.; Sacchi, A.; Pontecorvi, A. Molecular basis of estrogen regulation of Hageman factor XII gene expression. *Endocrinology* **1995**, *136*, 5076-5083.

165. Dittman, W. A.; Majerus, P. W. Structure and function of thrombomodulin: a natural anticoagulant. *Blood* **1990**, *75*, 329-336.

166. Maruyama, I.; Salem, H. H.; Ishii, H.; Majerus, P. W. Human thrombomodulin is not an efficient inhibitor of the procoagulant activity of thrombin. *J. Clin. Invest.* **1985**, *75*, 987-991.

167. Wen, D. Z.; Dittman, W. A.; Ye, R. D.; Deaven, L. L.; Majerus, P. W.; Sadler, J. E. Human thrombomodulin: complete cDNA sequence and chromosome localization of the gene. *Biochemistry* **1987**, *26*, 4350-4357.

168. Fuentes-Prior, P.; Iwanaga, Y.; Huber, R.; Pagila, R.; Rumennik, G.; Seto, M.; Morser, J.; Light, D. R.; Bode, W. Structural basis for the anticoagulant activity of the thrombin-thrombomodulin complex. *Nature* **2000**, *404*, 518-525.
169. Esmon, C. T. The roles of protein C and thrombomodulin in the regulation of blood coagulation. *J. Biol. Chem.* **1989**, *264*, 4743-4746.
170. Esmon, C. T. Protein C anticoagulant pathway and its role in controlling microvascular thrombosis and inflammation. *Crit. Care Med.* **2001**, *29*, S48-51; discussion 51-2.
171. Stenflo, J. Structure-function relationships of epidermal growth factor modules in vitamin K-dependent clotting factors. *Blood* **1991**, *78*, 1637-1651.
172. Walker, F. J.; Fay, P. J. Regulation of blood coagulation by the protein C system. *FASEB J.* **1992**, *6*, 2561-2567.
173. Castellino, F. J. Human protein C and activated protein C Components of the human anticoagulation system. *Trends Cardiovasc. Med.* **1995**, *5*, 55-62.
174. Stearns-Kurosawa, D. J.; Kurosawa, S.; Mollica, J. S.; Ferrell, G. L.; Esmon, C. T. The endothelial cell protein C receptor augments protein C activation by the thrombin-thrombomodulin complex. *Proc. Natl. Acad. Sci. U. S. A.* **1996**, *93*, 10212-10216.
175. Varadi, K.; Philapitsch, A.; Santa, T.; Schwarz, H. P. Activation and inactivation of human protein C by plasmin. *Thromb. Haemost.* **1994**, *71*, 615-621.

176. Mather, T.; Oganessyan, V.; Hof, P.; Huber, R.; Foundling, S.; Esmon, C.; Bode, W. The 2.8 Å crystal structure of Gla-domainless activated protein C. *EMBO J.* **1996**, *15*, 6822-6831.
177. Dahlback, B. Protein S and C4b-binding protein: components involved in the regulation of the protein C anticoagulant system. *Thromb. Haemost.* **1991**, *66*, 49-61.
178. Suzuki, K.; Kusumoto, H.; Deyashiki, Y.; Nishioka, J.; Maruyama, I.; Zushi, M.; Kawahara, S.; Honda, G.; Yamamoto, S.; Horiguchi, S. Structure and expression of human thrombomodulin, a thrombin receptor on endothelium acting as a cofactor for protein C activation. *EMBO J.* **1987**, *6*, 1891-1897.
179. Bajzar, L.; Morser, J.; Nesheim, M. TAFI, or plasma procarboxypeptidase B, couples the coagulation and fibrinolytic cascades through the thrombin-thrombomodulin complex. *J. Biol. Chem.* **1996**, *271*, 16603-16608.
180. Rezaie, A. R.; Cooper, S. T.; Church, F. C.; Esmon, C. T. Protein C inhibitor is a potent inhibitor of the thrombin-thrombomodulin complex. *J. Biol. Chem.* **1995**, *270*, 25336-25339.
181. Stern, D. M.; Nawroth, P. P.; Harris, K.; Esmon, C. T. Cultured bovine aortic endothelial cells promote activated protein C-protein S-mediated inactivation of factor Va. *J. Biol. Chem.* **1986**, *261*, 713-718.
182. Walker, F. J. Regulation of activated protein C by a new protein. A possible function for bovine protein S. *J. Biol. Chem.* **1980**, *255*, 5521-5524.
183. Mann, K. G.; Jenny, R. J.; Krishnaswamy, S. Cofactor proteins in the assembly and expression of blood clotting enzyme complexes. *Annu. Rev. Biochem.* **1988**, *57*, 915-956.

184. Kalafatis, M.; Rand, M. D.; Mann, K. G. The mechanism of inactivation of human factor V and human factor Va by activated protein C. *J. Biol. Chem.* **1994**, *269*, 31869-31880.
185. Nicolaes, G. A.; Dahlback, B. Factor V and thrombotic disease: description of a janus-faced protein. *Arterioscler. Thromb. Vasc. Biol.* **2002**, *22*, 530-538.
186. Fulcher, C. A.; Gardiner, J. E.; Griffin, J. H.; Zimmerman, T. S. Proteolytic inactivation of human factor VIII procoagulant protein by activated human protein C and its analogy with factor V. *Blood* **1984**, *63*, 486-489.
187. Espana, F.; Medina, P.; Navarro, S.; Zorio, E.; Estelles, A.; Aznar, J. The multifunctional protein C system. *Curr. Med. Chem. Cardiovasc. Hematol. Agents* **2005**, *3*, 119-131.
188. Riewald, M.; Petrovan, R. J.; Donner, A.; Mueller, B. M.; Ruf, W. Activation of endothelial cell protease activated receptor 1 by the protein C pathway. *Science* **2002**, *296*, 1880-1882.
189. Mosnier, L. O.; Zlokovic, B. V.; Griffin, J. H. The cytoprotective protein C pathway. *Blood* **2007**, *109*, 3161-3172.
190. Gibbs, C. S.; Coutre, S. E.; Tsiang, M.; Li, W. X.; Jain, A. K.; Dunn, K. E.; Law, V. S.; Mao, C. T.; Matsumura, S. Y.; Mejza, S. J. Conversion of thrombin into an anticoagulant by protein engineering. *Nature* **1995**, *378*, 413-416.
191. Dang, O. D.; Vindigni, A.; Di Cera, E. An allosteric switch controls the procoagulant and anticoagulant activities of thrombin. *Proc. Natl. Acad. Sci. U. S. A.* **1995**, *92*, 5977-5981.

192. Cantwell, A. M.; Di Cera, E. Rational design of a potent anticoagulant thrombin. *J. Biol. Chem.* **2000**, *275*, 39827-39830.
193. Harbrecht, U. Old and new anticoagulants. *Hamostaseologie* **2011**, *31*, 21-27.
194. Klement, P.; Rak, J. Emerging anticoagulants: mechanism of action and future potential. *Vnitr. Lek.* **2006**, *52 Suppl 1*, 119-122.
195. Hocht, T.; Farhan, S.; Wojta, J.; Huber, K. New anticoagulant agents in acute coronary syndromes. *Heart* **2011**, *97*, 244-252.
196. Eriksson, B. I.; Quinlan, D. J.; Eikelboom, J. W. Novel oral factor Xa and thrombin inhibitors in the management of thromboembolism. *Annu. Rev. Med.* **2011**, *62*, 41-57.
197. Straub, A.; Roehrig, S.; Hillisch, A. Oral, direct thrombin and factor Xa inhibitors: the replacement for warfarin, leeches, and pig intestines? *Angew. Chem. Int. Ed Engl.* **2011**, *50*, 4574-4590.
198. Mannucci, P. M.; Franchini, M. Old and new anticoagulant drugs: a minireview. *Ann. Med.* **2011**, *43*, 116-123.
199. Levi, M.; Eerenberg, E. S.; Kampuisen, P. W. Anticoagulants. Old and new. *Hamostaseologie* **2011**, *31*, .
200. Liang, A.; Thakkar, J. N.; Desai, U. R. Study of physico-chemical properties of novel highly sulfated, aromatic, mimetics of heparin and heparan sulfate. *J. Pharm. Sci.* **2010**, *99*, 1207-1216.

201. Henry, B. L.; Monien, B. H.; Bock, P. E.; Desai, U. R. A novel allosteric pathway of thrombin inhibition: Exosite II mediated potent inhibition of thrombin by chemo-enzymatic, sulfated dehydropolymers of 4-hydroxycinnamic acids. *J. Biol. Chem.* **2007**, *282*, 31891-31899.
202. Monien, B. H.; Henry, B. L.; Raghuraman, A.; Hindle, M.; Desai, U. R. Novel chemo-enzymatic oligomers of cinnamic acids as direct and indirect inhibitors of coagulation proteinases. *Bioorg. Med. Chem.* **2006**, *14*, 7988-7998.
203. Raghuraman, A.; Tiwari, V.; Thakkar, J. N.; Gunnarsson, G. T.; Shukla, D.; Hindle, M.; Desai, U. R. Structural characterization of a serendipitously discovered bioactive macromolecule, lignin sulfate. *Biomacromolecules* **2005**, *6*, 2822-2832.
204. Sidhu, P. S.; Liang, A.; Mehta, A. Y.; Abdel Aziz, M. H.; Zhou, Q.; Desai, U. R. Rational design of potent, small, synthetic allosteric inhibitors of thrombin. *J. Med. Chem.* **2011**, *54*, 5522-5531.
205. Verghese, J.; Liang, A.; Sidhu, P. P.; Hindle, M.; Zhou, Q.; Desai, U. R. First steps in the direction of synthetic, allosteric, direct inhibitors of thrombin and factor Xa. *Bioorg. Med. Chem. Lett.* **2009**, *19*, 4126-4129.
206. Prezelj, A.; Anderluh, P. S.; Peternel, L.; Urleb, U. Recent advances in serine protease inhibitors as anticoagulant agents. *Curr. Pharm. Des.* **2007**, *13*, 287-312.
207. Tucker, T. J.; Brady, S. F.; Lumma, W. C.; Lewis, S. D.; Gardell, S. J.; Naylor-Olsen, A. M.; Yan, Y.; Sisko, J. T.; Stauffer, K. J.; Lucas, B. J.; Lynch, J. J.; Cook, J. J.; Stranieri, M. T.; Holahan, M. A.; Lyle, E. A.; Baskin, E. P.; Chen, I. W.; Dancheck, K. B.; Krueger, J. A.;

Cooper, C. M.; Vacca, J. P. Design and synthesis of a series of potent and orally bioavailable noncovalent thrombin inhibitors that utilize nonbasic groups in the P1 position. *J. Med. Chem.* **1998**, *41*, 3210-3219.

208. Burgey, C. S.; Robinson, K. A.; Lyle, T. A.; Nantermet, P. G.; Selnick, H. G.; Isaacs, R. C.; Lewis, S. D.; Lucas, B. J.; Krueger, J. A.; Singh, R.; Miller-Stein, C.; White, R. B.; Wong, B.; Lyle, E. A.; Stranieri, M. T.; Cook, J. J.; McMasters, D. R.; Pellicore, J. M.; Pal, S.; Wallace, A. A.; Clayton, F. C.; Bohn, D.; Welsh, D. C.; Lynch, J. J., Jr; Yan, Y.; Chen, Z.; Kuo, L.; Gardell, S. J.; Shafer, J. A.; Vacca, J. P. Pharmacokinetic optimization of 3-amino-6-chloropyrazinone acetamide thrombin inhibitors. Implementation of P3 pyridine N-oxides to deliver an orally bioavailable series containing P1 N-benzylamides. *Bioorg. Med. Chem. Lett.* **2003**, *13*, 1353-1357.

209. Liu, L. W.; Vu, T. K.; Esmon, C. T.; Coughlin, S. R. The region of the thrombin receptor resembling hirudin binds to thrombin and alters enzyme specificity. *J. Biol. Chem.* **1991**, *266*, 16977-16980.

210. Ye, J.; Liu, L. W.; Esmon, C. T.; Johnson, A. E. The fifth and sixth growth factor-like domains of thrombomodulin bind to the anion-binding exosite of thrombin and alter its specificity. *J. Biol. Chem.* **1992**, *267*, 11023-11028.

211. Li, W.; Johnson, D. J.; Adams, T. E.; Pozzi, N.; De Filippis, V.; Huntington, J. A. Thrombin inhibition by serpins disrupts exosite II. *J. Biol. Chem.* **2010**, *285*, 38621-38629.

212. Olson, S. T.; Halvorson, H. R.; Bjork, I. Quantitative characterization of the thrombin-heparin interaction. Discrimination between specific and nonspecific binding models. *J. Biol. Chem.* **1991**, *266*, 6342-6352.
213. Henry, B. L.; Monien, B. H.; Bock, P. E.; Desai, U. R. A novel allosteric pathway of thrombin inhibition: Exosite II mediated potent inhibition of thrombin by chemo-enzymatic, sulfated dehydropolymers of 4-hydroxycinnamic acids. *J. Biol. Chem.* **2007**, *282*, 31891-31899.
214. Henry, B. L.; Abdel Aziz, M.; Zhou, Q.; Desai, U. R. Sulfated, low-molecular-weight lignins are potent inhibitors of plasmin, in addition to thrombin and factor Xa: Novel opportunity for controlling complex pathologies. *Thromb. Haemost.* **2010**, *103*, 507-515.
215. Henry, B. L.; Thakkar, J. N.; Martin, E. J.; Brophy, D. F.; Desai, U. R. Characterization of the plasma and blood anticoagulant potential of structurally and mechanistically novel oligomers of 4-hydroxycinnamic acids. *Blood Coagul. Fibrinolysis* **2009**, *20*, 27-34.
216. Monien, B. H.; Henry, B. L.; Raghuraman, A.; Hindle, M.; Desai, U. R. Novel chemo-enzymatic oligomers of cinnamic acids as direct and indirect inhibitors of coagulation proteinases. *Bioorg. Med. Chem.* **2006**, *14*, 7988-7998.
217. Pei, L.; Li, Y.; Bu, X.; Gu, L.; Chan, A. S. C. One-pot synthesis of 5,6-dihydroxylated benzo[b]furan derivatives. *Tetrahedron Lett.* **2006**, *47*, 2615-2618.
218. Verghese, J.; Liang, A.; Sidhu, P. P.; Hindle, M.; Zhou, Q.; Desai, U. R. First steps in the direction of synthetic, allosteric, direct inhibitors of thrombin and factor Xa. *Bioorg. Med. Chem. Lett.* **2009**, *19*, 4126-4129.

219. Liang, A.; Thakkar, J. N.; Desai, U. R. Study of physico-chemical properties of novel highly sulfated, aromatic, mimetics of heparin and heparan sulfate. *J. Pharm. Sci.* **2010**, *99*, 1207-1216.
220. Desai, B. J.; Boothello, R. S.; Mehta, A. Y.; Scarsdale, J. N.; Wright, H. T.; Desai, U. R. Interaction of thrombin with sucrose octasulfate. *Biochemistry* **2011**, *50*, 6973-6982.
221. Al-Horani, R. A.; Desai, U. R. Chemical Sulfation of Small Molecules - Advances and Challenges. *Tetrahedron* **2010**, *66*, 2907-2918.
222. Raghuraman, A.; Riaz, M.; Hindle, M.; Desai, U. R. Rapid and efficient microwave-assisted synthesis of highly sulfated organic scaffolds. *Tetrahedron Lett.* **2007**, *48*, 6754-6758.
223. Dayal, B.; Salen, G.; Toome, B.; Tint, G. S.; Shefer, S.; Padia, J. Lithium hydroxide/aqueous methanol: mild reagent for the hydrolysis of bile acid methyl esters. *Steroids* **1990**, *55*, 233-237.
224. Carter, W. J.; Cama, E.; Huntington, J. A. Crystal structure of thrombin bound to heparin. *J. Biol. Chem.* **2005**, *280*, 2745-2749.
225. Jeter, M. L.; Ly, L. V.; Fortenberry, Y. M.; Whinna, H. C.; White, R. R.; Rusconi, C. P.; Sullenger, B. A.; Church, F. C. RNA aptamer to thrombin binds anion-binding exosite-2 and alters protease inhibition by heparin-binding serpins. *FEBS Lett.* **2004**, *568*, 10-14.
226. Liu, C. C.; Brustad, E.; Liu, W.; Schultz, P. G. Crystal structure of a biosynthetic sulfo-hirudin complexed to thrombin. *J. Am. Chem. Soc.* **2007**, *129*, 10648-10649.

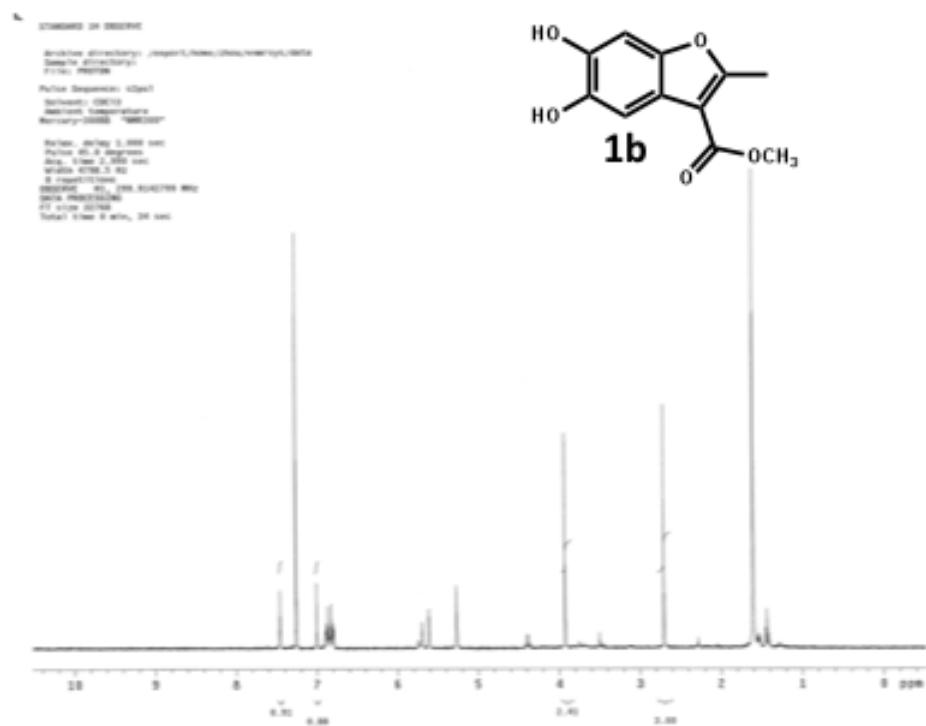
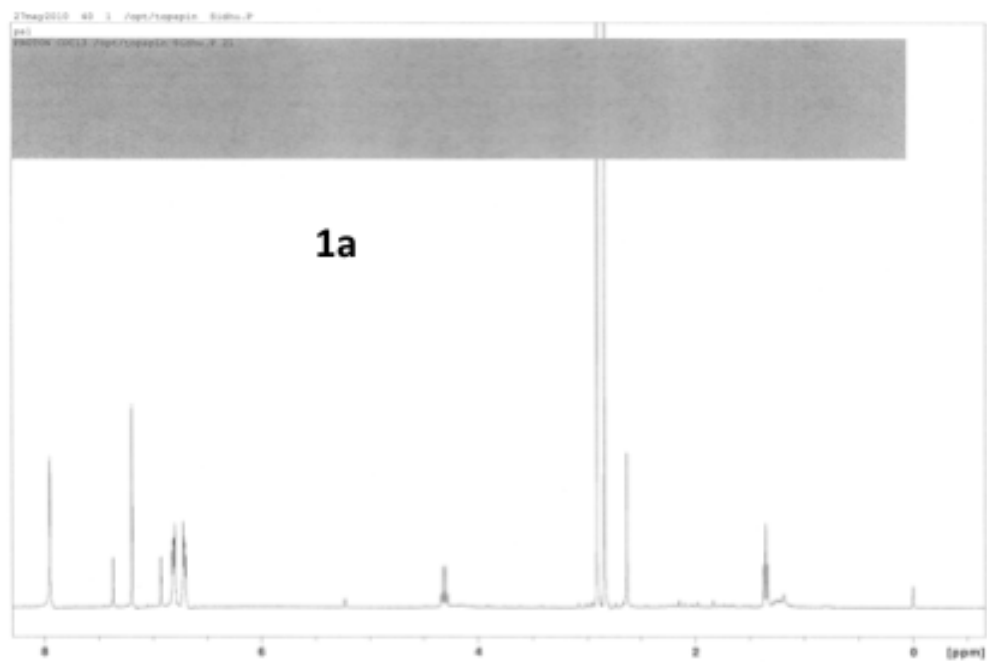
227. Raghuraman, A.; Mosier, P. D.; Desai, U. R. Understanding Dermatan Sulfate-Heparin Cofactor II Interaction through Virtual Library Screening. *ACS Med. Chem. Lett.* **2010**, *1*, 281-285.
228. Raghuraman, A.; Mosier, P. D.; Desai, U. R. Finding a needle in a haystack: development of a combinatorial virtual screening approach for identifying high specificity heparin/heparan sulfate sequence(s). *J. Med. Chem.* **2006**, *49*, 3553-3562.
229. Henry, B. L.; Connell, J.; Liang, A.; Krishnasamy, C.; Desai, U. R. Interaction of antithrombin with sulfated, low molecular weight lignins: opportunities for potent, selective modulation of antithrombin function. *J. Biol. Chem.* **2009**, *284*, 20897-20908.
230. Abdel Aziz, M. H.; Mosier, P. D.; Desai, U. R. Identification of the site of binding of sulfated, low molecular weight lignins on thrombin. *Biochem. Biophys. Res. Commun.* **2011**, *413*, 348-352.
231. Sidhu, P. S.; Liang, A.; Mehta, A. Y.; Abdel Aziz, M. H.; Zhou, Q.; Desai, U. R. Rational design of potent, small, synthetic allosteric inhibitors of thrombin. *J. Med. Chem.* **2011**, *54*, 5522-5531.
232. Skordalakes, E.; Dodson, G. G.; Green, D. S.; Goodwin, C. A.; Scully, M. F.; Hudson, H. R.; Kakkar, V. V.; Deadman, J. J. Inhibition of human alpha-thrombin by a phosphonate tripeptide proceeds via a metastable pentacoordinated phosphorus intermediate. *J. Mol. Biol.* **2001**, *311*, 549-555.

233. Ahmed, H. U.; Blakeley, M. P.; Cianci, M.; Cruickshank, D. W.; Hubbard, J. A.; Helliwell, J. R. The determination of protonation states in proteins. *Acta Crystallogr. D Biol. Crystallogr.* **2007**, *63*, 906-922.
234. Henry, B. L.; Connell, J.; Liang, A.; Krishnasamy, C.; Desai, U. R. Interaction of antithrombin with sulfated, low molecular weight lignins: opportunities for potent, selective modulation of antithrombin function. *J. Biol. Chem.* **2009**, *284*, 20897-20908.
235. Abdel Aziz, M. H.; Mosier, P. D.; Desai, U. R. Identification of the site of binding of sulfated, low molecular weight lignins on thrombin. *Biochem. Biophys. Res. Commun.* **2011**, .
236. Pineda, A. O.; Chen, Z. W.; Marino, F.; Mathews, F. S.; Mosesson, M. W.; Di Cera, E. Crystal structure of thrombin in complex with fibrinogen gamma' peptide. *Biophys. Chem.* **2007**, *125*, 556-559.
237. Desai, U. R. New antithrombin-based anticoagulants. *Med. Res. Rev.* **2004**, *24*, 151-181.
238. Verghese, J.; Liang, A.; Sidhu, P. P. S.; Hindle, M.; Zhou, Q.; Desai, U. R. First steps in the direction of synthetic, allosteric, direct inhibitors of thrombin and factor Xa. *Bioorg. Med. Chem. Lett.* **2009**, *19*, 4126-4129.
239. Henry, B. L.; Abdel Aziz, M.; Zhou, Q.; Desai, U. R. Sulfated, low-molecular-weight lignins are potent inhibitors of plasmin, in addition to thrombin and factor Xa: Novel opportunity for controlling complex pathologies. *Thromb. Haemost.* **2010**, *103*, 507-515.
240. Stahl, M.; Guba, W.; Kansy, M. Integrating molecular design resources within modern drug discovery research: the Roche experience. *Drug Discov. Today* **2006**, *11*, 326-333.

241. Shoichet, B. K. Virtual screening of chemical libraries. *Nature* **2004**, 432, 862-865.
242. Steindl, T. M.; Schuster, D.; Wolber, G.; Laggner, C.; Langer, T. High-throughput structure-based pharmacophore modelling as a basis for successful parallel virtual screening. *J. Comput. Aided Mol. Des.* **2006**, 20, 703-715.
243. Klebe, G. Virtual ligand screening: strategies, perspectives and limitations. *Drug Discov. Today* **2006**, 11, 580-594.
244. Oprea, T. I.; Matter, H. Integrating virtual screening in lead discovery. *Curr. Opin. Chem. Biol.* **2004**, 8, 349-358.
245. Lyne, P. D. Structure-based virtual screening: an overview. *Drug Discov. Today* **2002**, 7, 1047-1055.
246. Kitchen, D. B.; Decornez, H.; Furr, J. R.; Bajorath, J. Docking and scoring in virtual screening for drug discovery: methods and applications. *Nat. Rev. Drug Discov.* **2004**, 3, 935-949.

Appendix

NMR and Mass Spectra



STANDARD IN OBSERVE

Archive directory: /export/home/chem/vwarkey/data
Sample directory:
File: 060306

Pulse Sequence: zgpg30

Solvent: CDCl₃
Nucleic temperature

2000000000

Relax. delay 1.000 sec

Pulse 45.0 degrees

Acq. time 3.750 sec

Waltz 4700.5 Hz

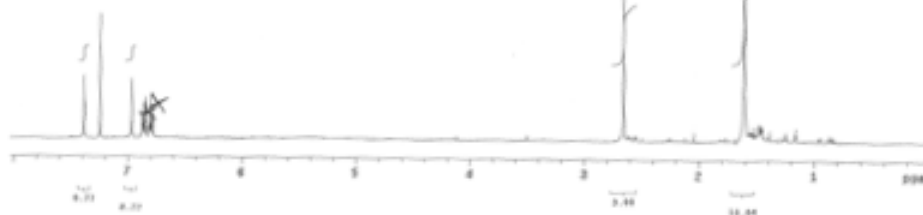
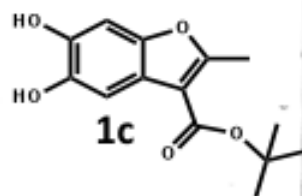
5 repetitions

060306 F1 100.626014 MHz

DATA PROCESSING

FT size 32768

Total time 2 min, 30 sec



STANDARD IN OBSERVE

Archive directory: /export/home/chem/vwarkey/data
Sample directory:
File: 060306

Pulse Sequence: zgpg30

Solvent: CDCl₃
Nucleic temperature

Mercury-2000000000

Relax. delay 1.000 sec

Pulse 45.0 degrees

Acq. time 3.750 sec

Waltz 4700.5 Hz

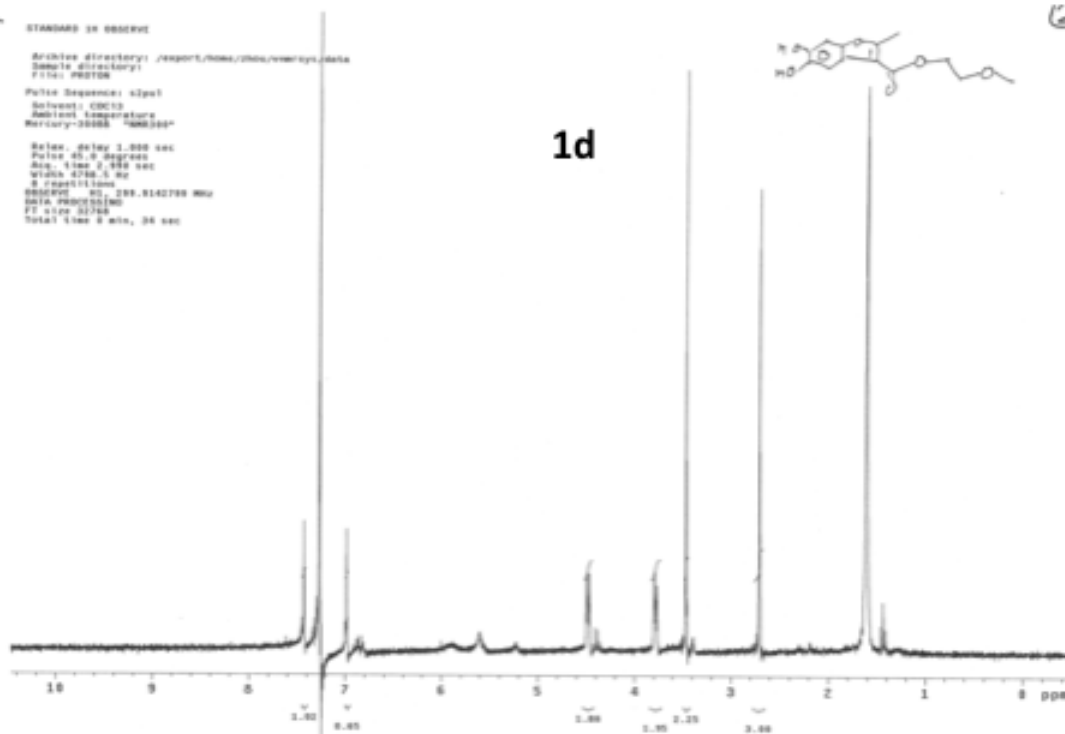
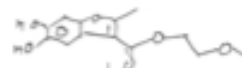
5 repetitions

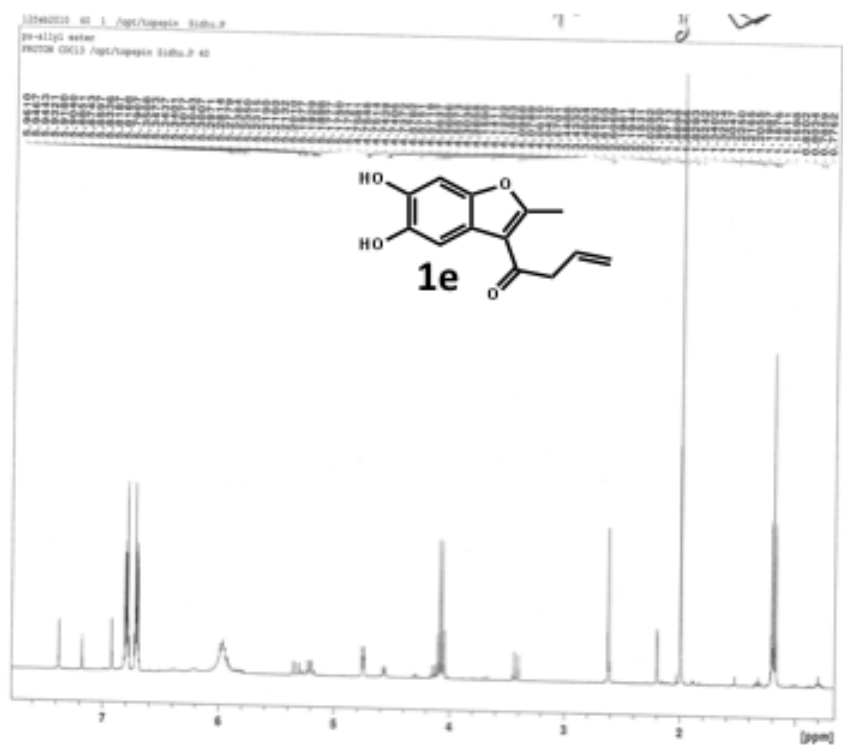
060306 F1 100.626014 MHz

DATA PROCESSING

FT size 32768

Total time 2 min, 30 sec



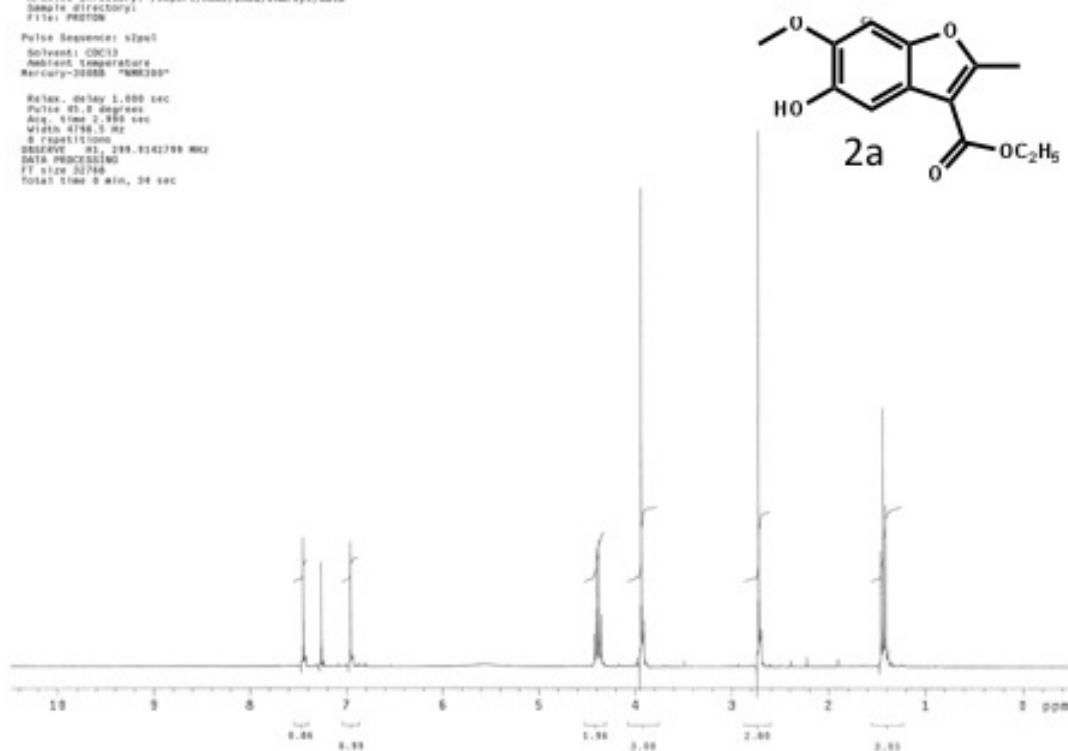


STANDARD IN OBSERVE

Archive directory: /export/home/zhong/nmr/cpi/data
Sample directory:
File: PRETON

Pulse Sequence: zgpg30
Solvent: CDCl3
Ambient Temperature
Mercury-3000S "NMK300"

Relax. delay 1.000 sec
Pulse 45.0 degrees
Acq. time 2.986 sec
Width 4798.5 Hz
0 repetitions
OBSERVED 41, 294.8141789 MHz
DATA PROCESSING
F2 size 32768
Total time 8 min, 34 sec

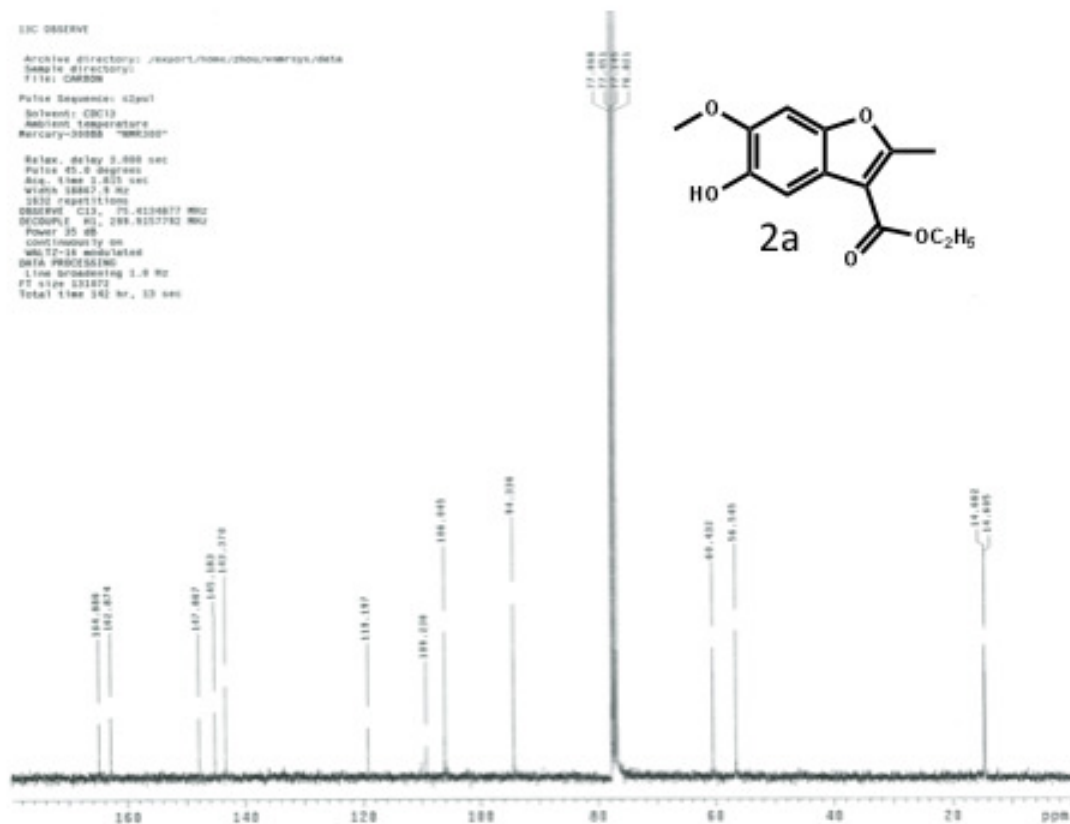


13C OBSERVE

Archive directory: /export/home/zhong/nmr/cpi/data
Sample directory:
File: CARBON

Pulse Sequence: zgpg30
Solvent: CDCl3
Ambient Temperature
Mercury-3000S "NMK300"

Relax. delay 0.000 sec
Pulse 45.0 degrees
Acq. time 2.401 sec
Width 58867.5 Hz
2532 repetitions
OBSERVED C13, 75.4134877 MHz
DECOUPLE 40, 294.8157792 MHz
Power 35 dB
Continuously on
vht-17-18 modulated
DATA PROCESSING
Line broadening 1.0 Hz
F2 size 32768
Total time 141 hr, 53 sec



STANDARD IN OBSERVE

Archive directory: /export/home/chem/vnmrpy/data
 Sample directory:
 Title: PR0706

Pulse Sequence: zgpg30

Solvent: CDCl3

Antenna Temperature

Mercury-30000 "NM0300"

Relax. delay 5.000 sec

Pulse 45.0 degrees

Acq. time 3.486 sec

Width 4788.5 Hz

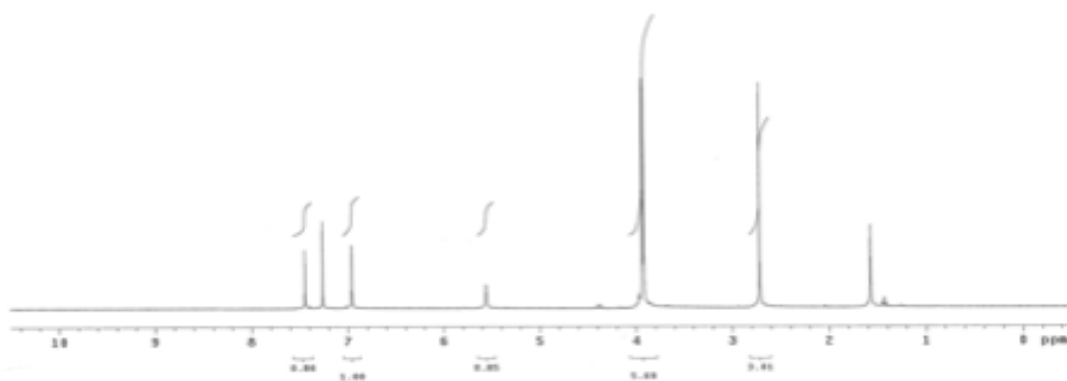
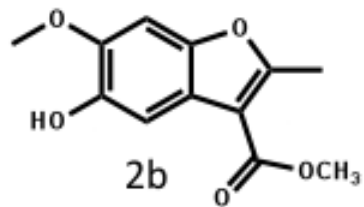
0 repetitions

OBSERVE H1 299.8142755 MHz

DATA PROCESSING

FT size 32768

Total time 8 min, 34 sec



STANDARD IN OBSERVE

Archive directory: /export/home/chem/vnmrpy/data
 Sample directory:
 Title: PR0706

Pulse Sequence: zgpg30

Solvent: CDCl3

Temp. 23.0 C / 235.1 K

INSTR-400 "NM0400"

Relax. delay 5.000 sec

Pulse 45.0 degrees

Acq. time 3.724 sec

Width 4788.5 Hz

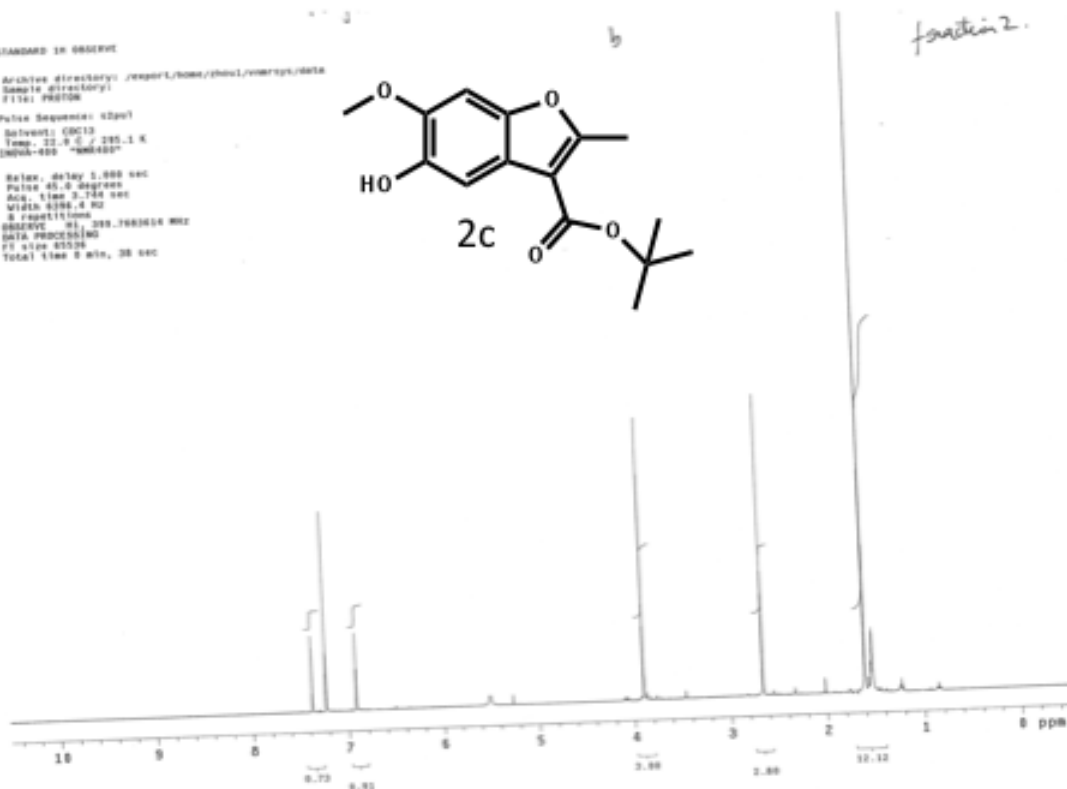
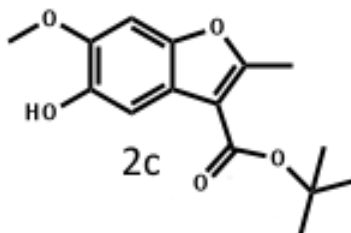
0 repetitions

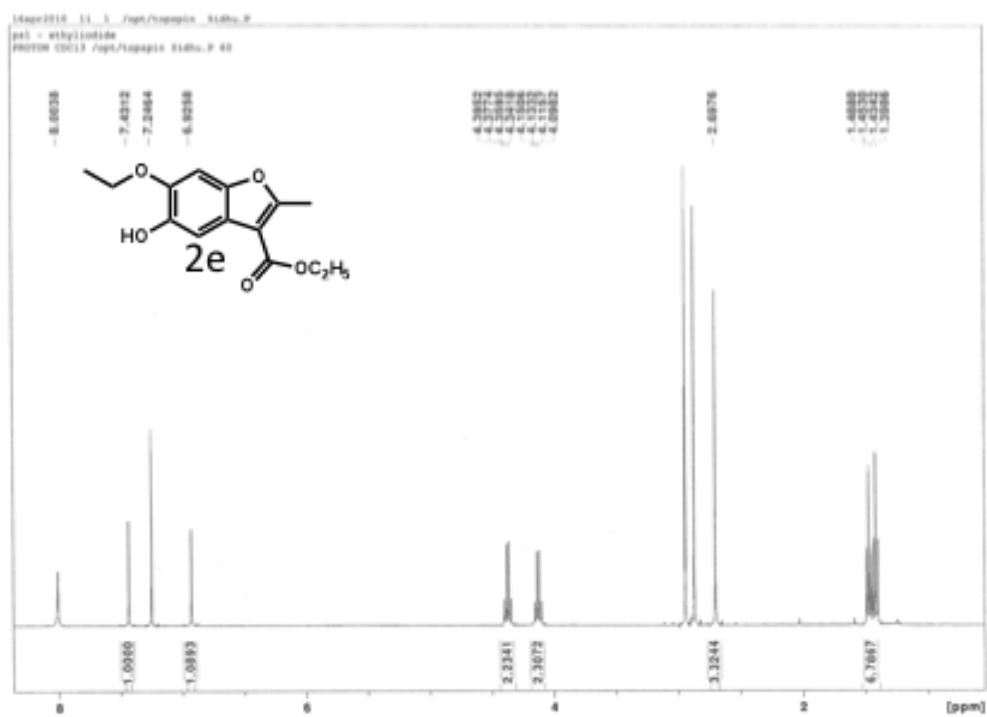
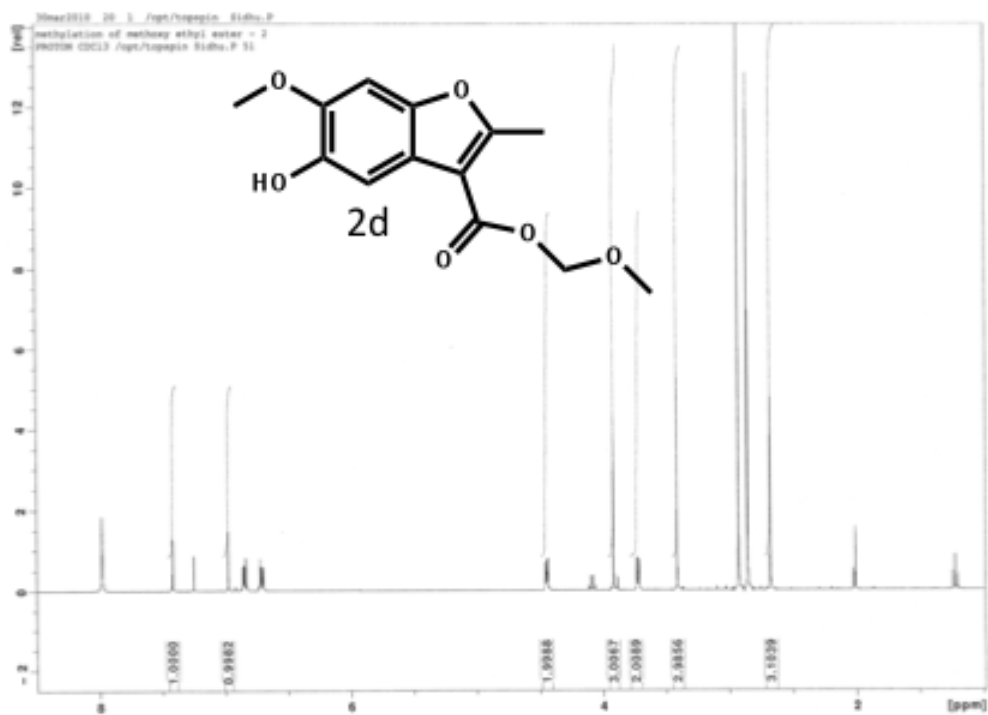
OBSERVE H1 299.7683614 MHz

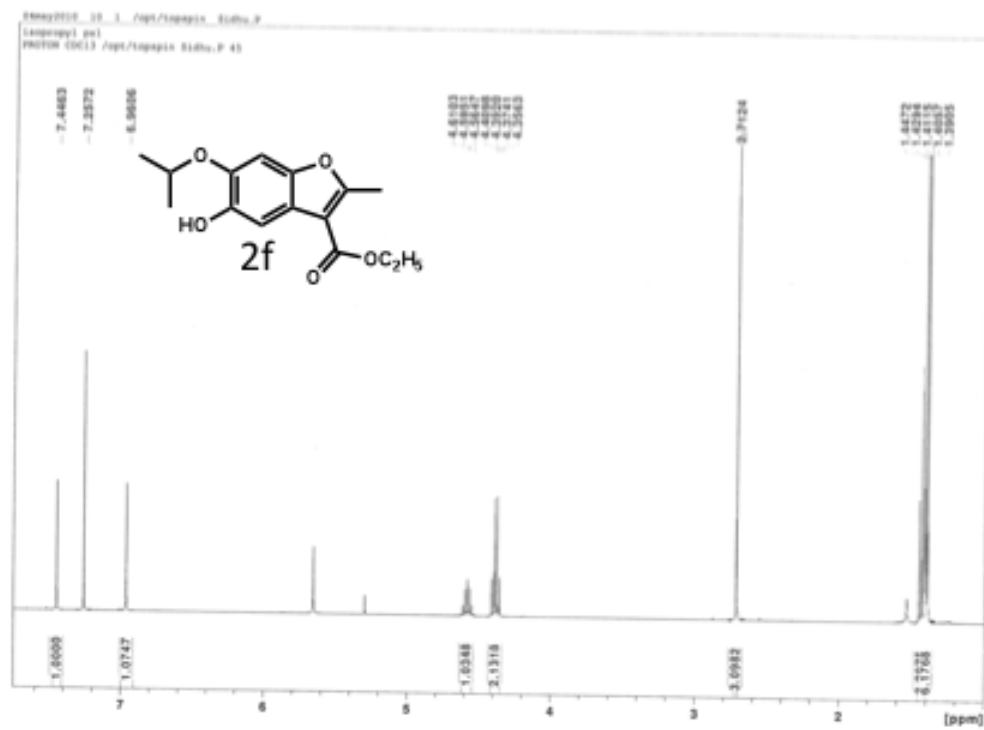
DATA PROCESSING

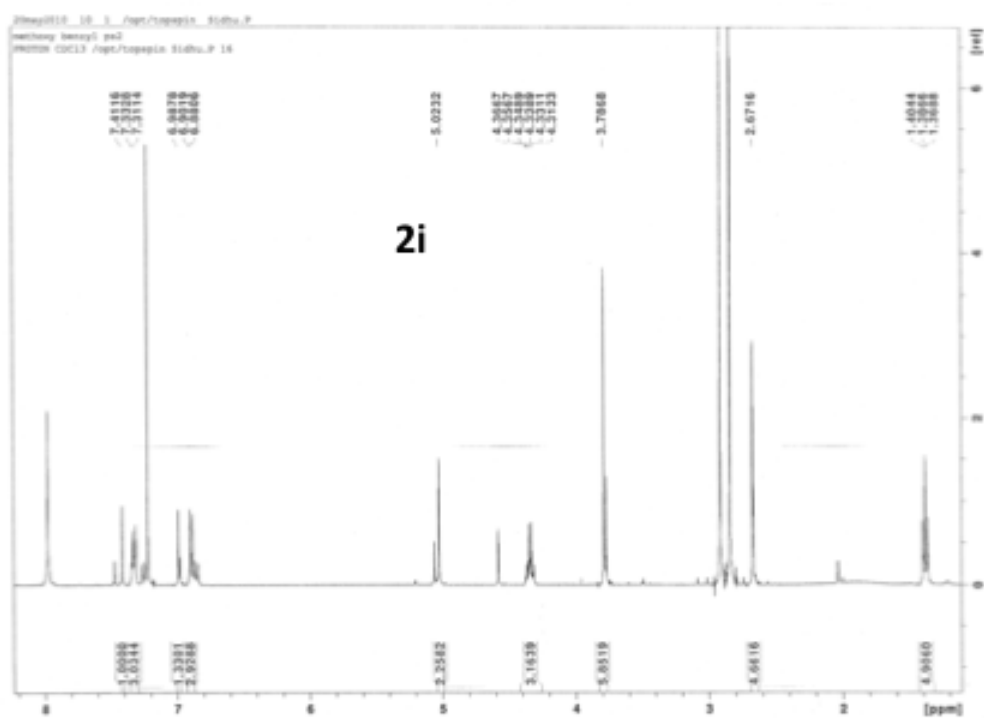
FT size 32768

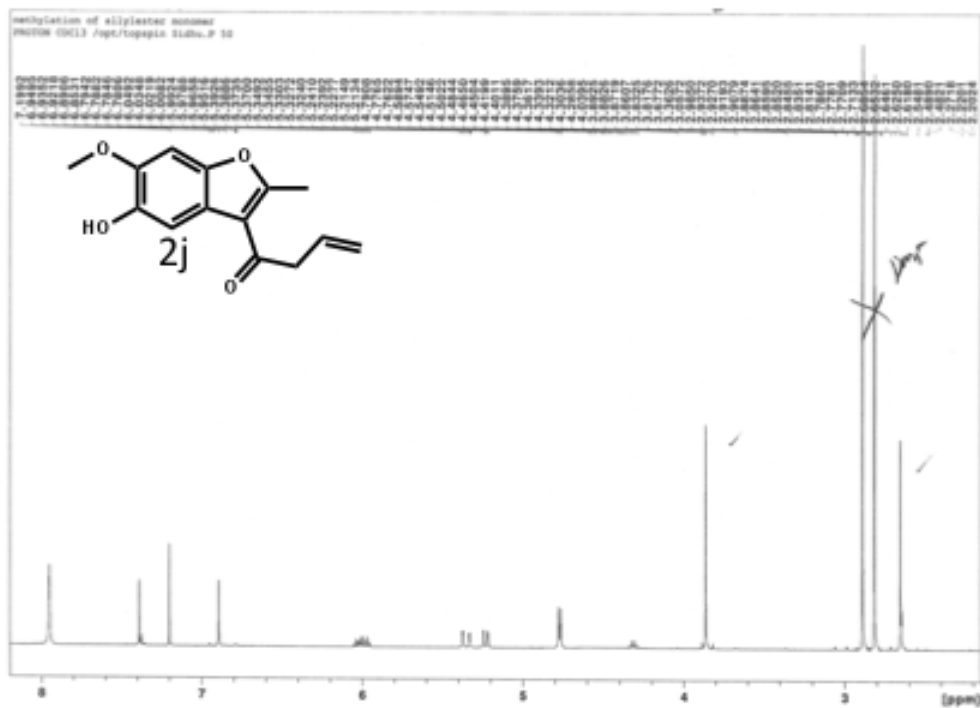
Total time 8 min, 34 sec

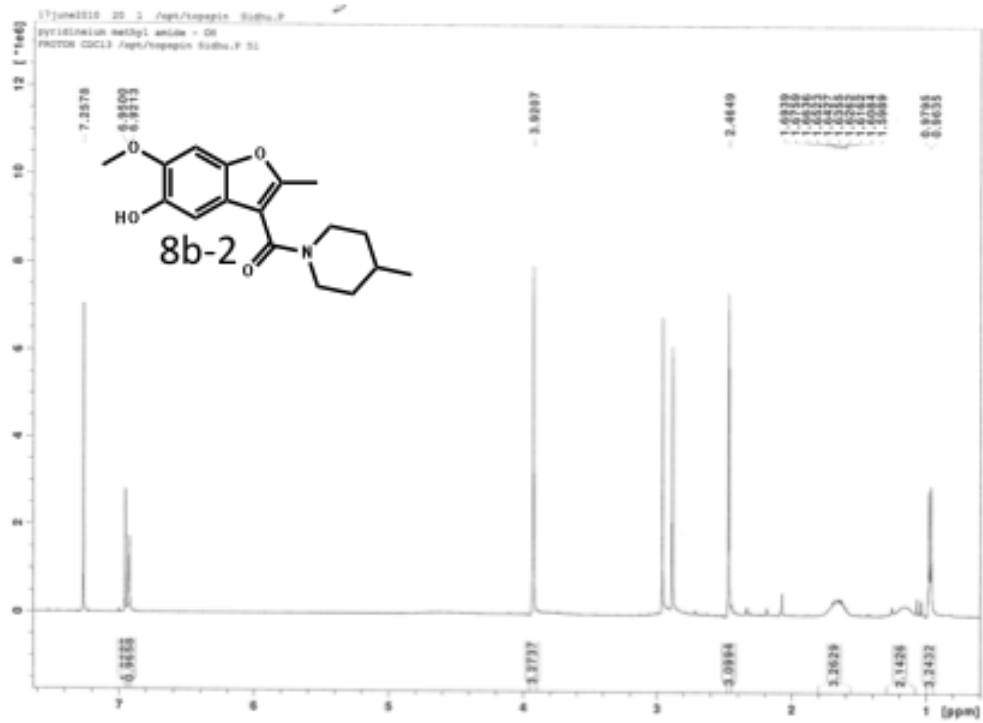
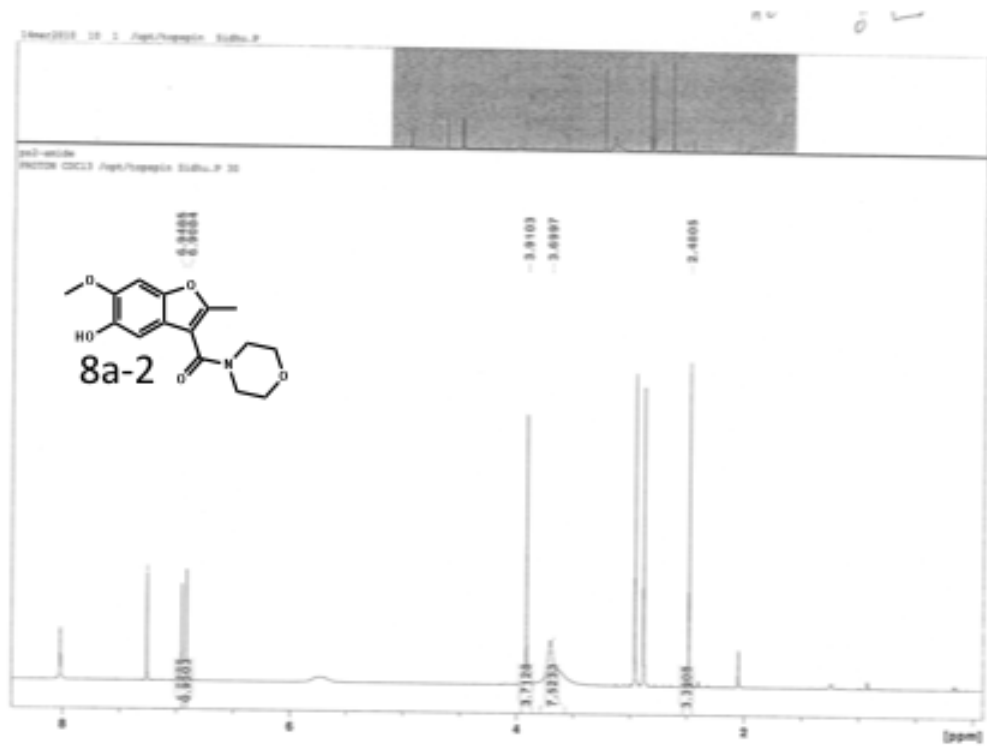


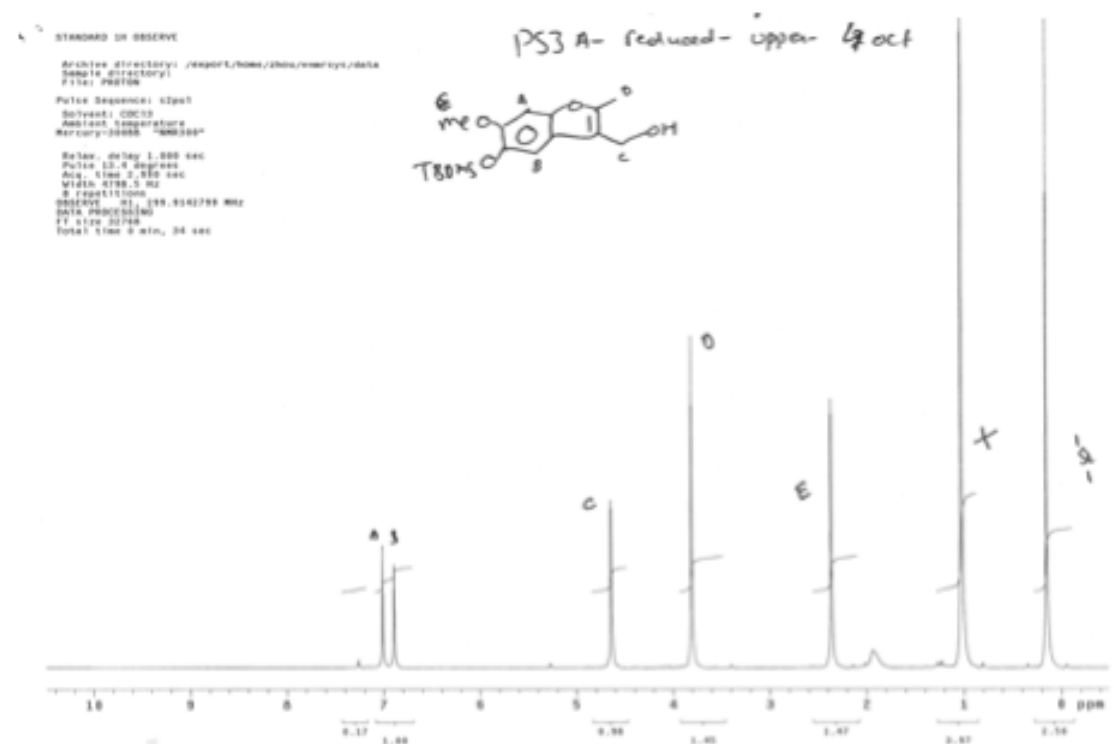
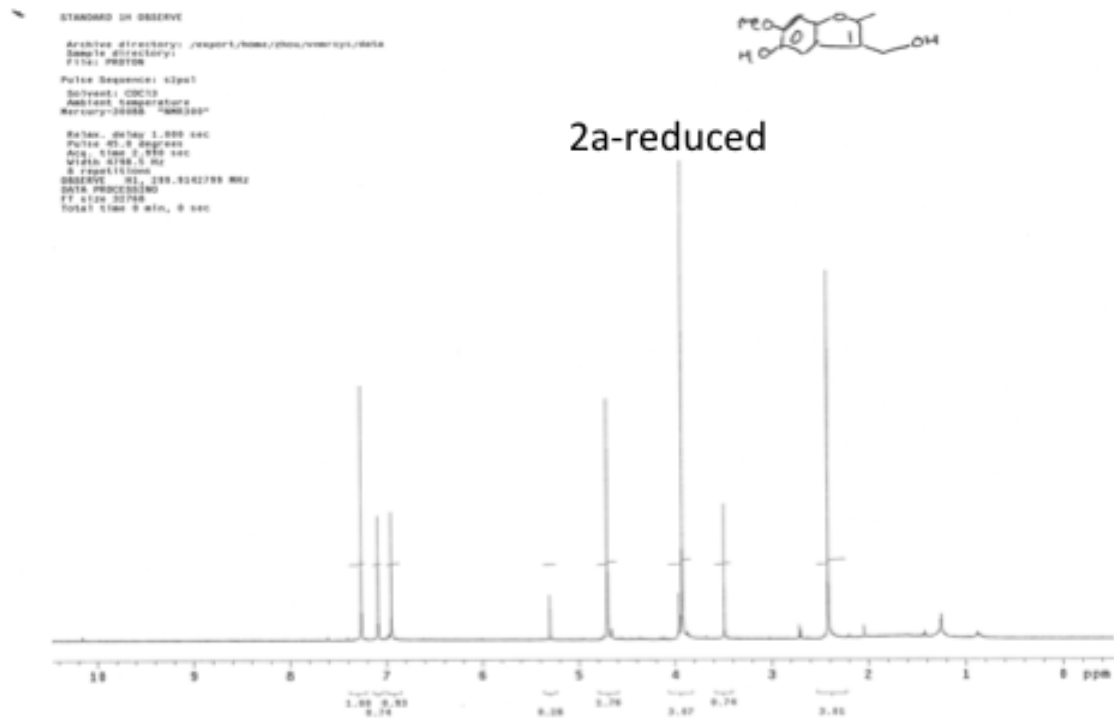








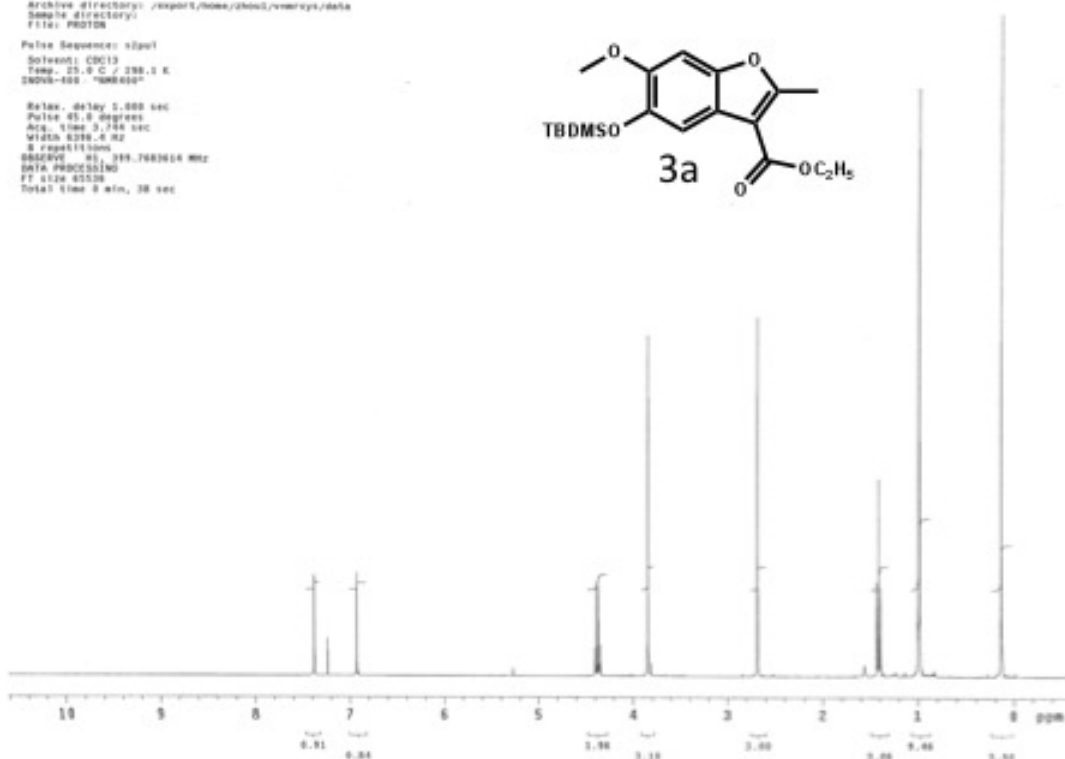
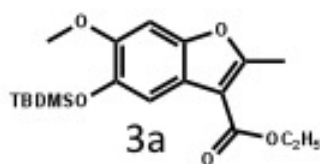




STANDARD IN OBSERVE

Archive directory: /export/home/zhouch/vnmrpy/data
Sample directory:
File: PROTON

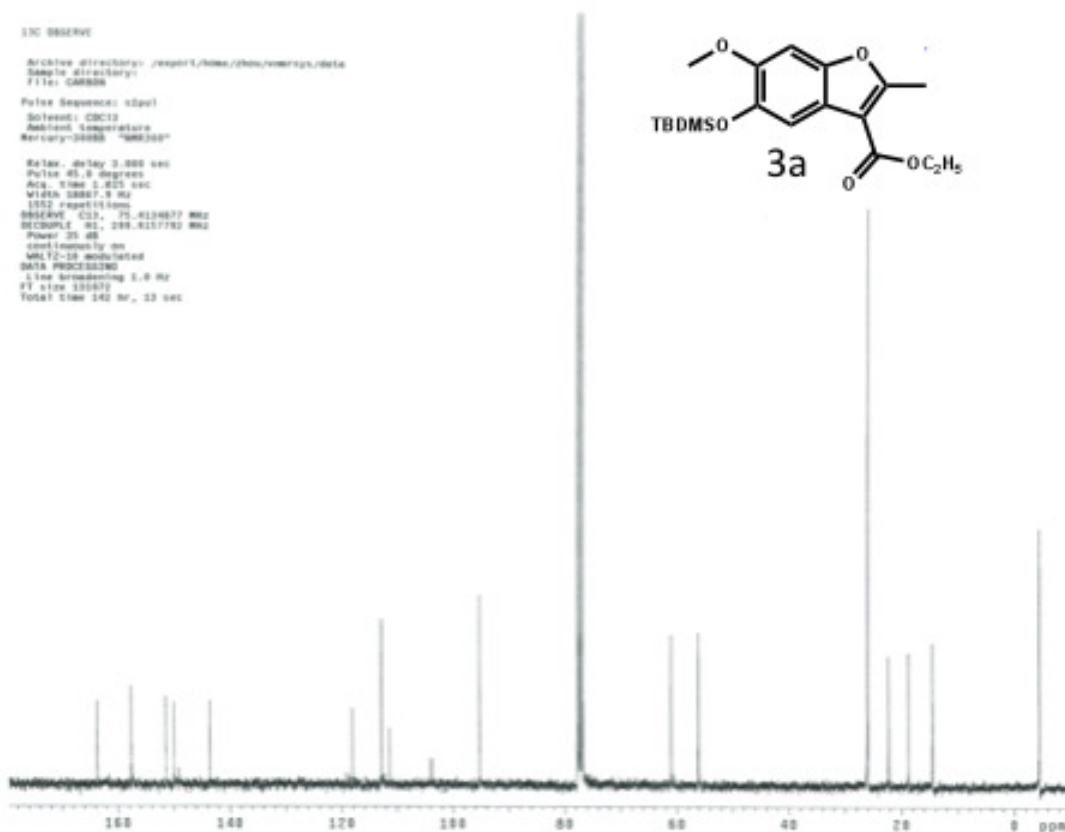
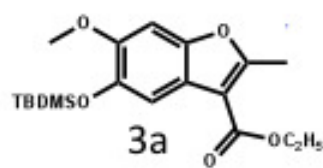
Pulse Sequence: zgpg30
Solvent: CDCl3
Temp.: 25.0 C / 298.1 K
SFOV=600 MHz
Relax. delay 5.000 sec
Pulse 45.0 degrees
Acq. time 0.744 sec
Width 6216.4 Hz
S repetitions
OBSERVE F1: 399.708164 MHz
Data PROCESSING
F1 size 65536
Total time 0 min, 38 sec



13C NMR

Archive directory: /export/home/zhouch/vnmrpy/data
Sample directory:
File: GAMMA

Pulse Sequence: zgpg30
Solvent: CDCl3
Ambient temperature
Mercury=00000 MHz
Relax. delay 3.000 sec
Pulse 45.0 degrees
Acq. time 5.875 sec
Width 38807.9 Hz
1552 repetitions
OBSERVE C13: 101.624677 MHz
DECOUPLE H1: 299.8157782 MHz
Power 20 dB
continuously on
WALTZ-16 modulated
Data PROCESSING
Line broadening 5.0 Hz
F1 size 131072
Total time 140 hr, 12 sec



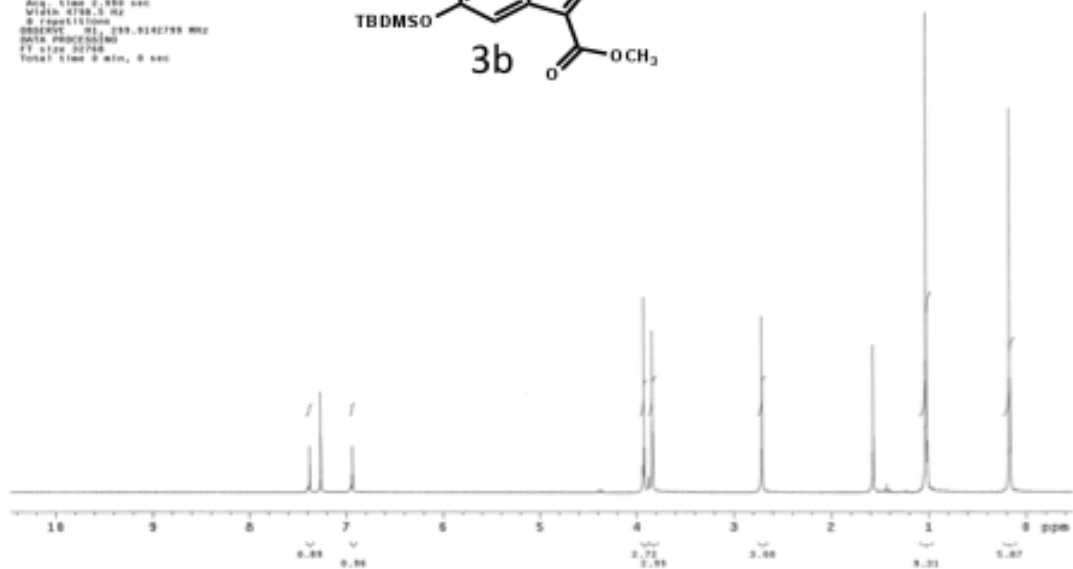
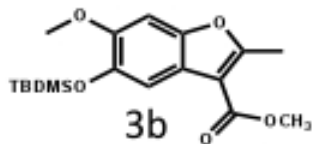
STANDARD OR OBSERVE

Archive directory: /export/home/zhao/vnmrpy/data
 Sample directory:
 File: 000100

Pulse Sequence: zgpg30

Solvent: CDCl3
 Ambient temperature
 Mercury:30000 "400.139"

Pulse delay 1.000 sec
 Pulse on 0 degrees
 Acq. time 2.950 sec
 Width 0.780 Hz
 0 repetitions
 OBSERVE F1 100.6142795 MHz
 DATA PROCESSING
 F1 size 32768
 Total time 0 min, 0 sec



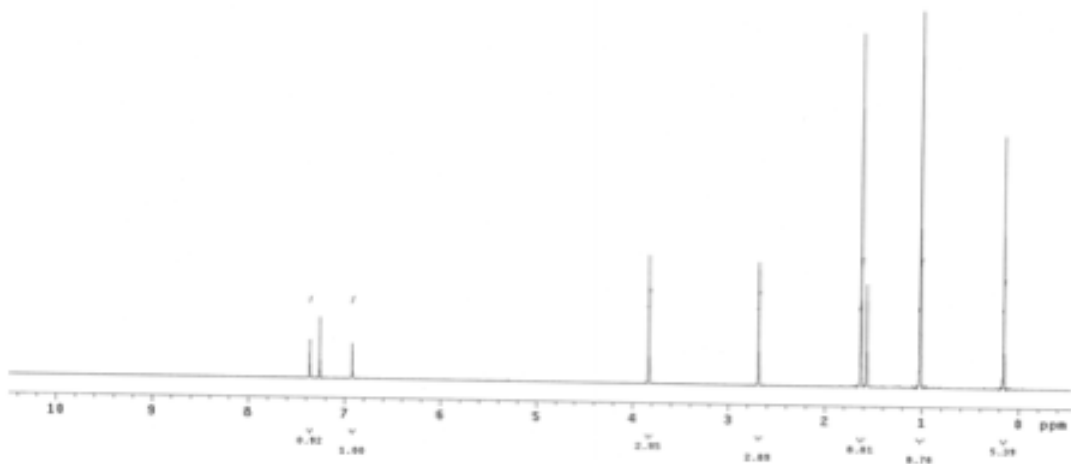
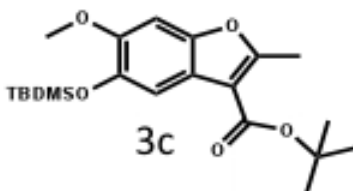
STANDARD OR OBSERVE

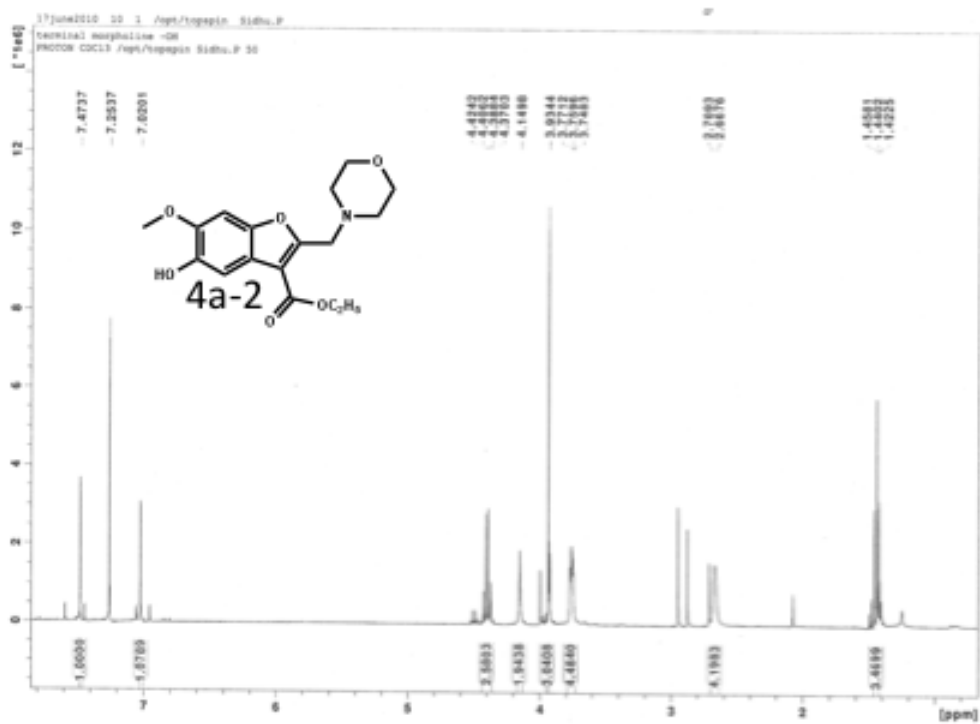
Archive directory: /export/home/zhao/vnmrpy/data
 Sample directory:
 File: 000100

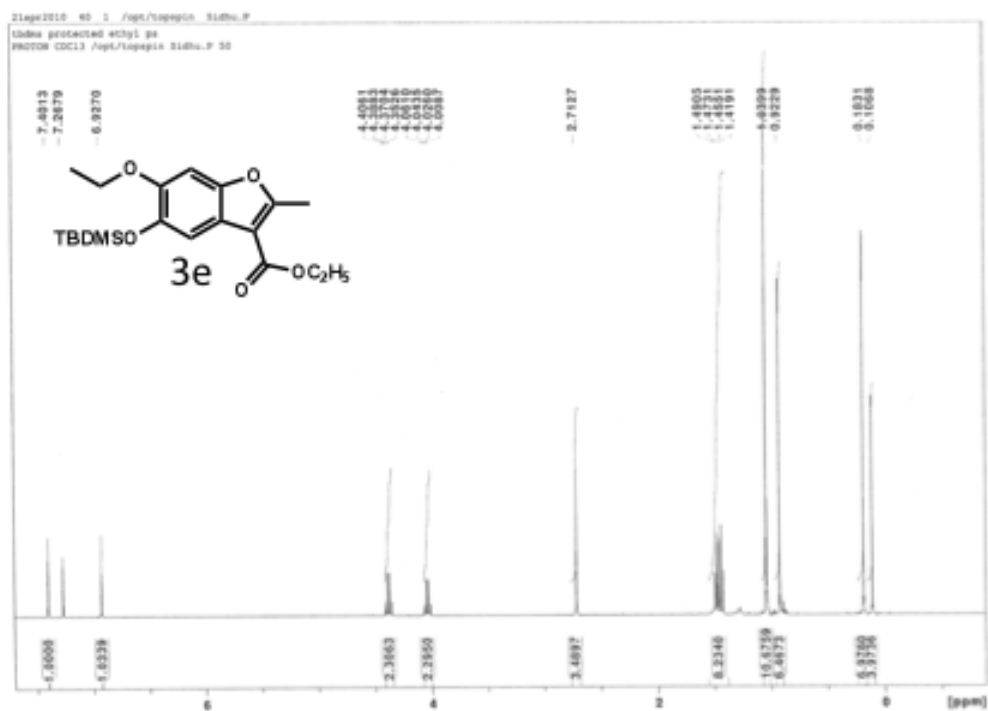
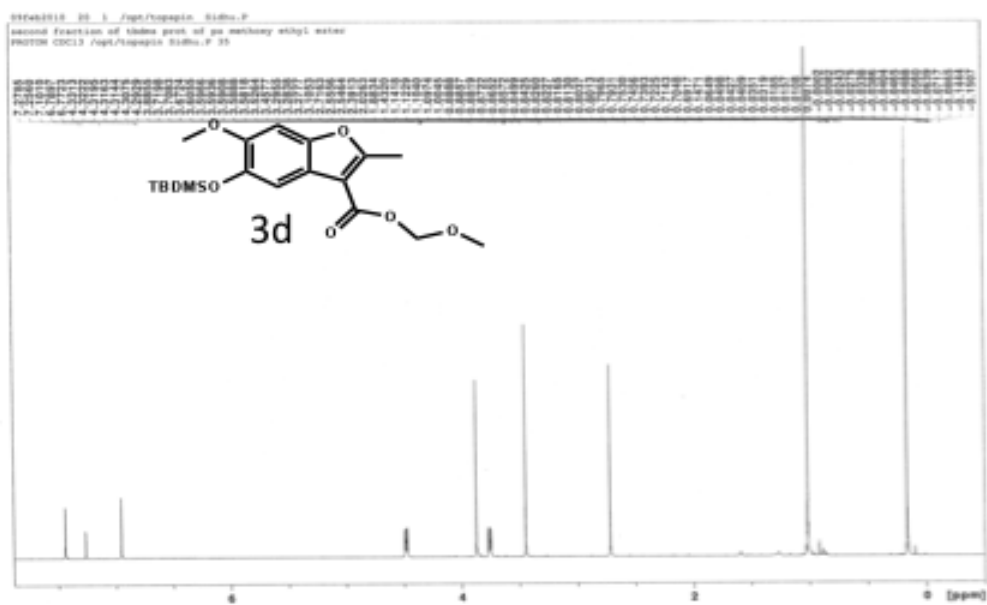
Pulse Sequence: zgpg30

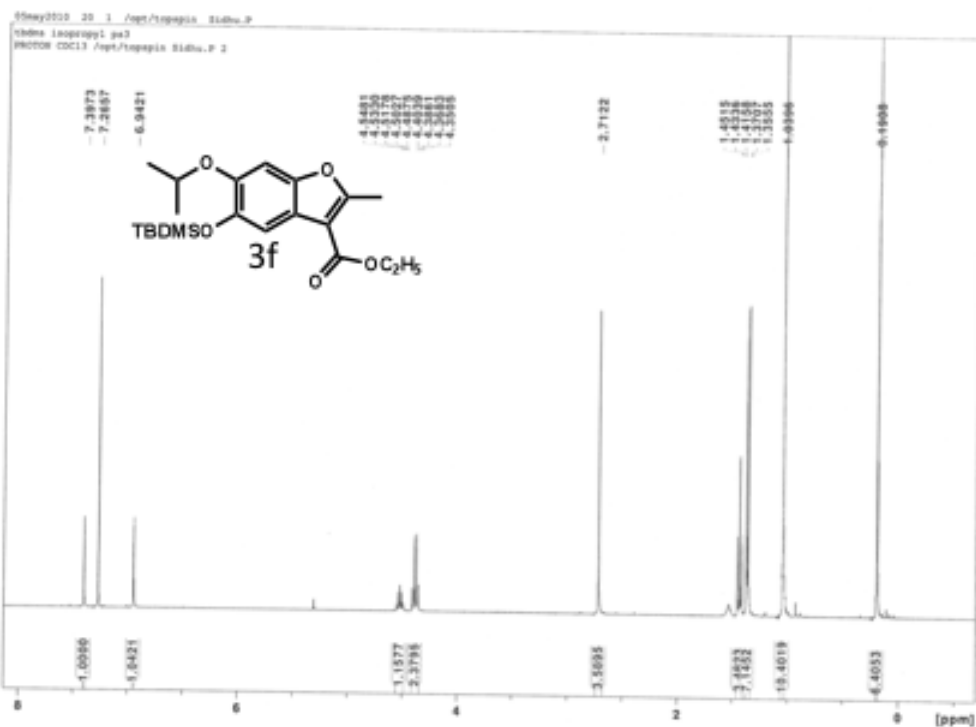
Solvent: CDCl3
 Ambient temperature
 Mercury:30000 "400.139"

Pulse delay 1.000 sec
 Pulse on 0 degrees
 Acq. time 2.950 sec
 Width 0.780 Hz
 0 repetitions
 OBSERVE F1 100.6142795 MHz
 DATA PROCESSING
 F1 size 32768
 Total time 0 min, 0 sec





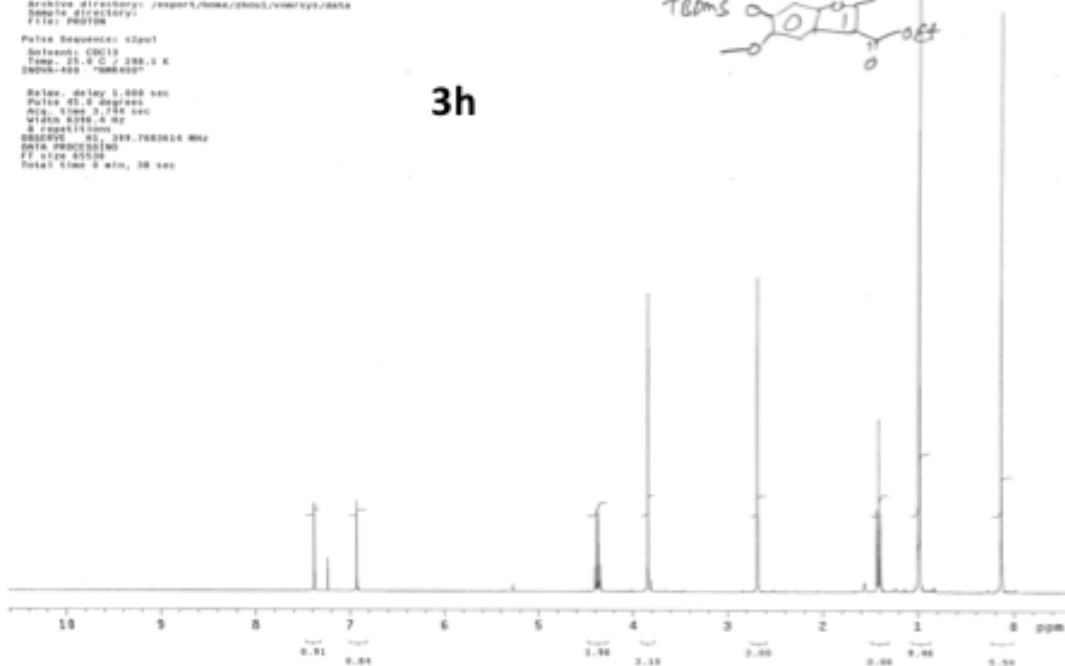
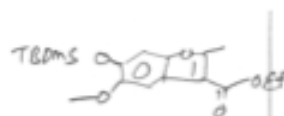


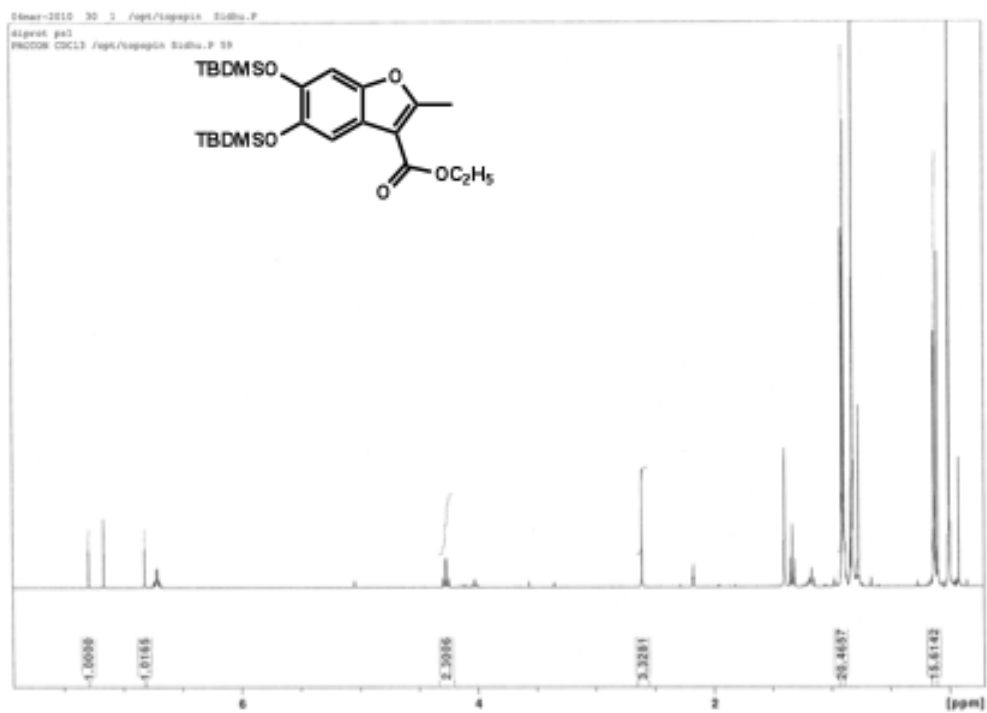
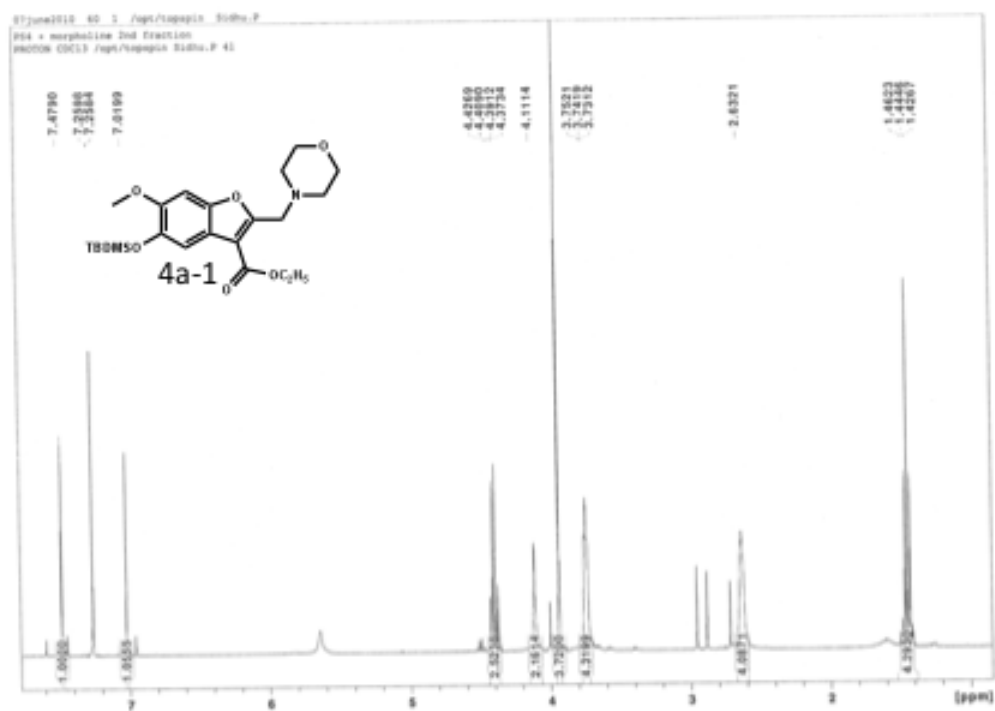


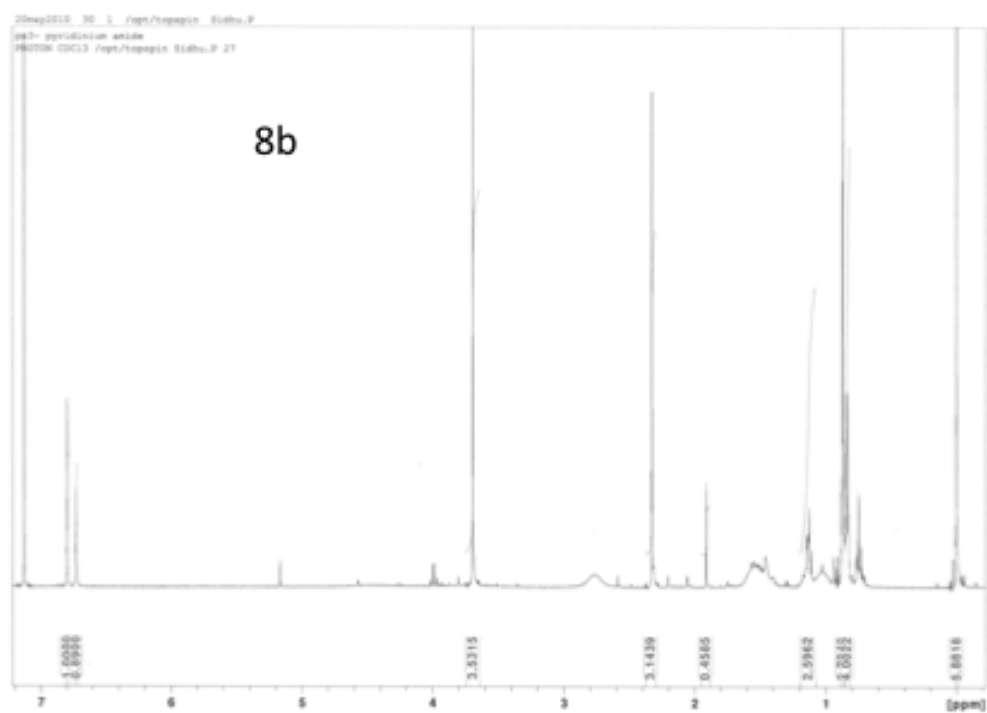
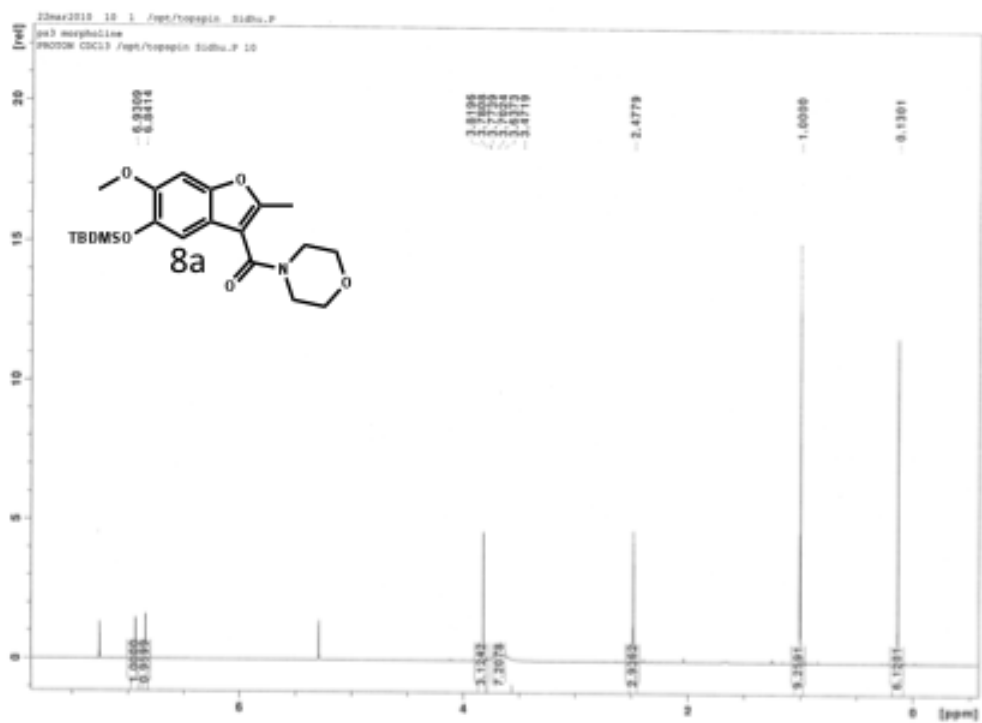
STANDARD IN OBSERVE

Acquire directory: /export/home/ghost/vanderyst/data
 Sample directory:
 File: PROTON
 Pulse Sequence: zgpg30
 Solvent: CDCl3
 Temp: 25.0 C / 298.1 K
 DMSO-d6 - "HMR450"
 Relax. delay: 5.000 sec
 Pulse: 15.0 degrees
 Acq. time: 0.156 sec
 Width: 1016.4 Hz
 6 repetitions
 OBSERVE: H1, 300.1363010 MHz
 DATA PROCESSING
 F1: 300.1363010
 Total time: 0 min, 38 sec

3h



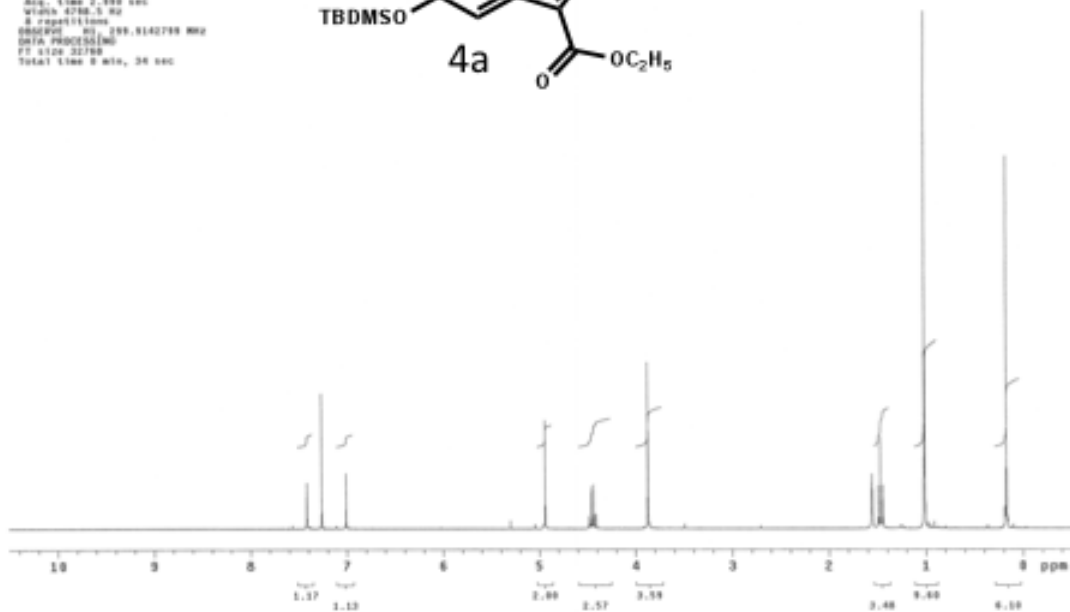
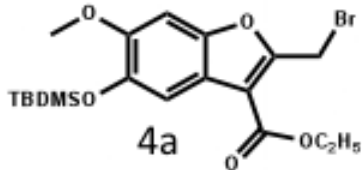




```
Archive directory: /export/home/gibson/vromsys/data
Sample directory:
File: P80206

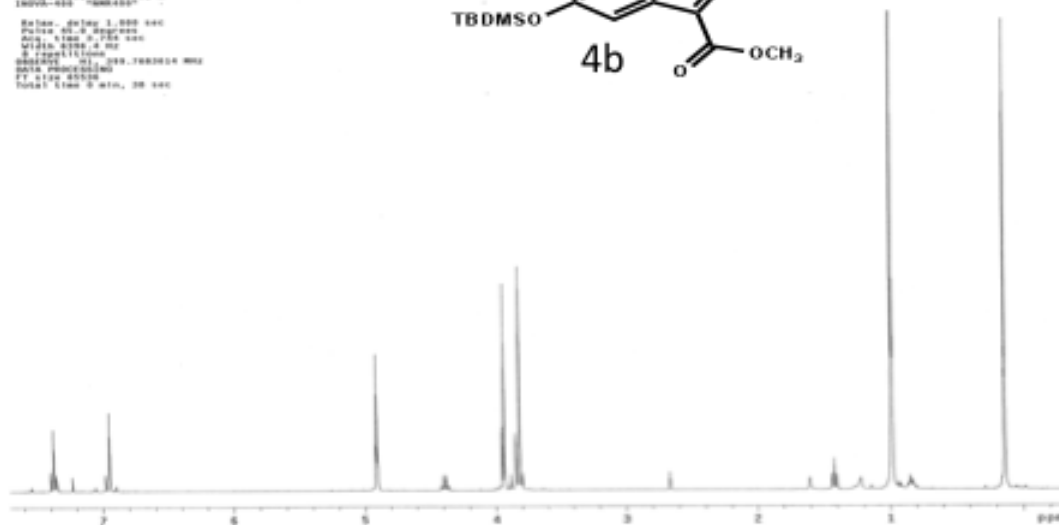
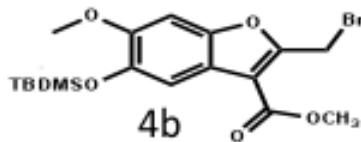
Pulse Sequence: dnpolr
Solvent: CDCl3
Ambient temperature
Recycle: 99999 "999999"

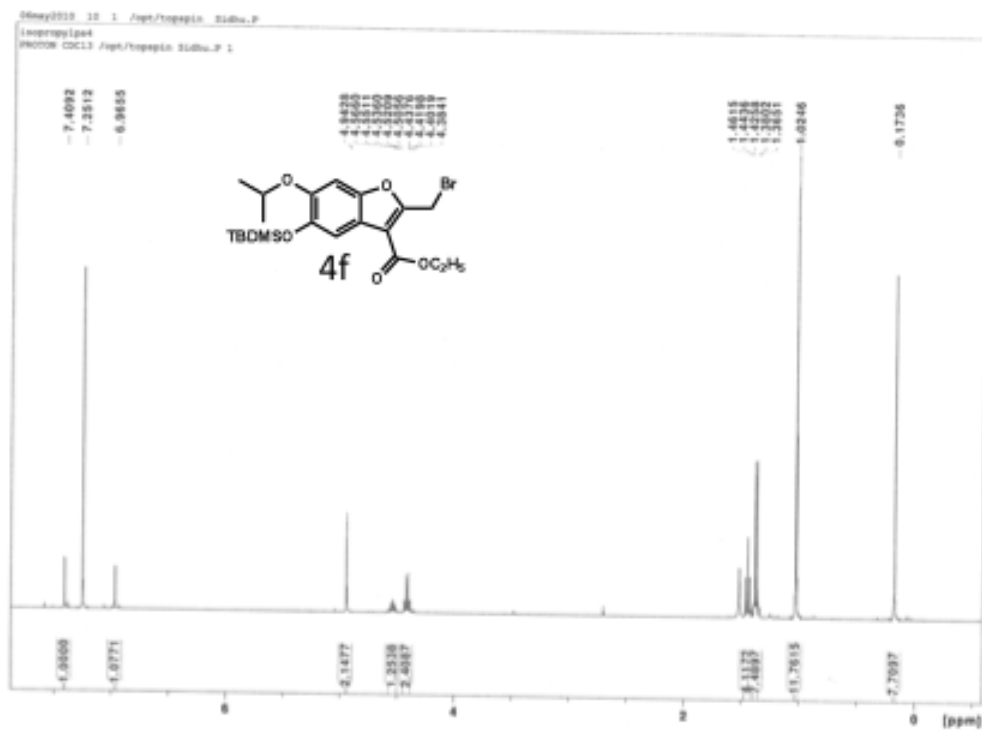
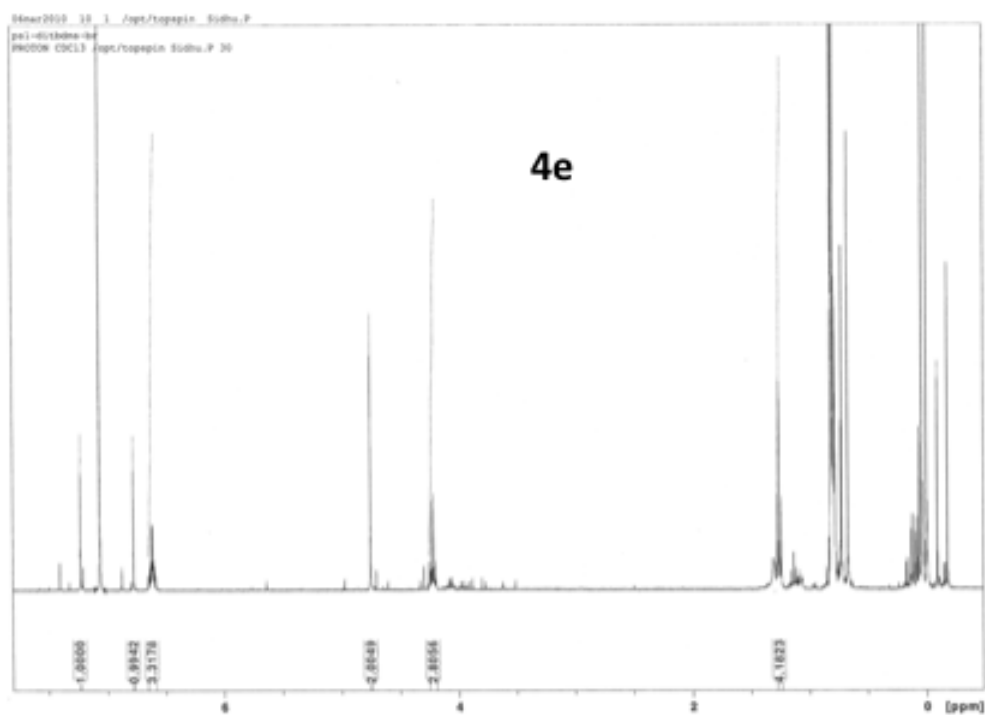
Relax. delay 1.000 sec
Pulse 40.0 degrees
Acq. time 2.000 sec
Width 4700.0 Hz
N = 640000
=====
00000000 Hz [99.9142798 MHz]
Data FWD(155)MHz
PC steps 32768
Total time 8 min, 34 sec
```

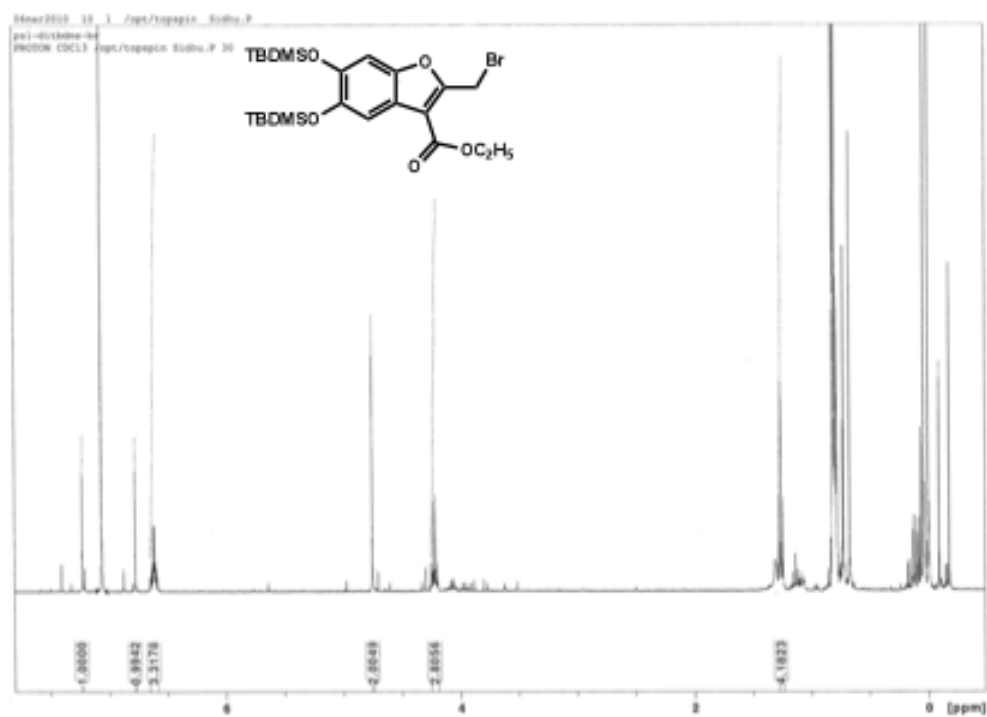


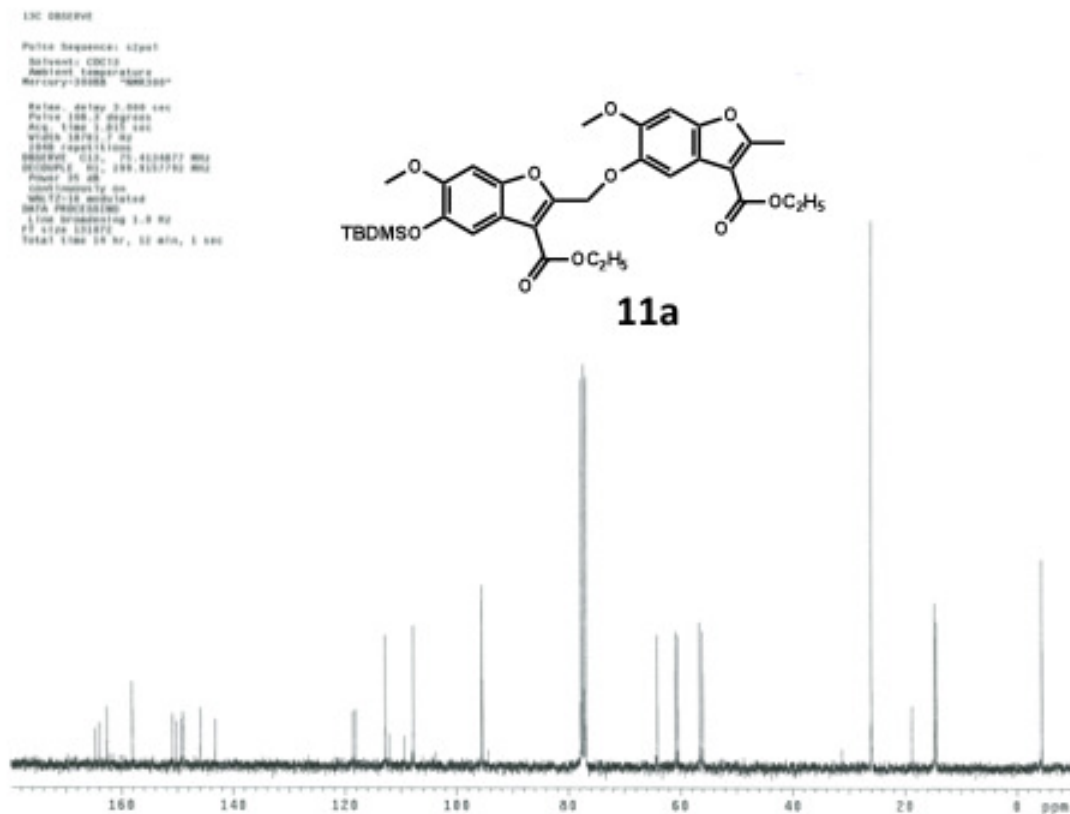
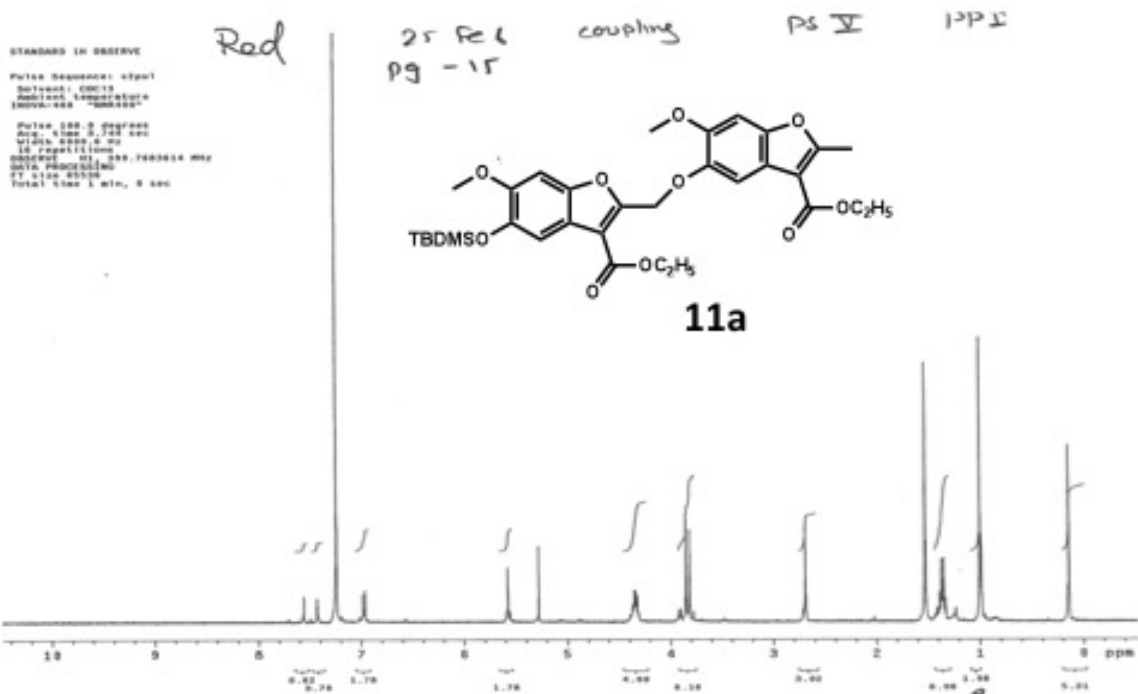
```

$ cat /etc/passwd | grep root | awk '{print $1,$2,$3,$4,$5,$6,$7,$8,$9,$10,$11,$12,$13,$14,$15,$16,$17,$18,$19,$20,$21,$22,$23,$24,$25,$26,$27,$28,$29,$30,$31,$32,$33,$34,$35,$36,$37,$38,$39,$40,$41,$42,$43,$44,$45,$46,$47,$48,$49,$50,$51,$52,$53,$54,$55,$56,$57,$58,$59,$60,$61,$62,$63,$64,$65,$66,$67,$68,$69,$70,$71,$72,$73,$74,$75,$76,$77,$78,$79,$80,$81,$82,$83,$84,$85,$86,$87,$88,$89,$90,$91,$92,$93,$94,$95,$96,$97,$98,$99,$100,$101,$102,$103,$104,$105,$106,$107,$108,$109,$110,$111,$112,$113,$114,$115,$116,$117,$118,$119,$120,$121,$122,$123,$124,$125,$126,$127,$128,$129,$130,$131,$132,$133,$134,$135,$136,$137,$138,$139,$140,$141,$142,$143,$144,$145,$146,$147,$148,$149,$150,$151,$152,$153,$154,$155,$156,$157,$158,$159,$160,$161,$162,$163,$164,$165,$166,$167,$168,$169,$170,$171,$172,$173,$174,$175,$176,$177,$178,$179,$180,$181,$182,$183,$184,$185,$186,$187,$188,$189,$190,$191,$192,$193,$194,$195,$196,$197,$198,$199,$200,$201,$202,$203,$204,$205,$206,$207,$208,$209,$210,$211,$212,$213,$214,$215,$216,$217,$218,$219,$220,$221,$222,$223,$224,$225,$226,$227,$228,$229,$230,$231,$232,$233,$234,$235,$236,$237,$238,$239,$240,$241,$242,$243,$244,$245,$246,$247,$248,$249,$250,$251,$252,$253,$254,$255,$256,$257,$258,$259,$260,$261,$262,$263,$264,$265,$266,$267,$268,$269,$270,$271,$272,$273,$274,$275,$276,$277,$278,$279,$280,$281,$282,$283,$284,$285,$286,$287,$288,$289,$290,$291,$292,$293,$294,$295,$296,$297,$298,$299,$300,$301,$302,$303,$304,$305,$306,$307,$308,$309,$310,$311,$312,$313,$314,$315,$316,$317,$318,$319,$320,$321,$322,$323,$324,$325,$326,$327,$328,$329,$330,$331,$332,$333,$334,$335,$336,$337,$338,$339,$340,$341,$342,$343,$344,$345,$346,$347,$348,$349,$350,$351,$352,$353,$354,$355,$356,$357,$358,$359,$360,$361,$362,$363,$364,$365,$366,$367,$368,$369,$370,$371,$372,$373,$374,$375,$376,$377,$378,$379,$380,$381,$382,$383,$384,$385,$386,$387,$388,$389,$390,$391,$392,$393,$394,$395,$396,$397,$398,$399,$400,$401,$402,$403,$404,$405,$406,$407,$408,$409,$410,$411,$412,$413,$414,$415,$416,$417,$418,$419,$420,$421,$422,$423,$424,$425,$426,$427,$428,$429,$430,$431,$432,$433,$434,$435,$436,$437,$438,$439,$440,$441,$442,$443,$444,$445,$446,$447,$448,$449,$450,$451,$452,$453,$454,$455,$456,$457,$458,$459,$460,$461,$462,$463,$464,$465,$466,$467,$468,$469,$470,$471,$472,$473,$474,$475,$476,$477,$478,$479,$480,$481,$482,$483,$484,$485,$486,$487,$488,$489,$490,$491,$492,$493,$494,$495,$496,$497,$498,$499,$500,$501,$502,$503,$504,$505,$506,$507,$508,$509,$510,$511,$512,$513,$514,$515,$516,$517,$518,$519,$520,$521,$522,$523,$524,$525,$526,$527,$528,$529,$530,$531,$532,$533,$534,$535,$536,$537,$538,$539,$540,$541,$542,$543,$544,$545,$546,$547,$548,$549,$550,$551,$552,$553,$554,$555,$556,$557,$558,$559,$560,$561,$562,$563,$564,$565,$566,$567,$568,$569,$570,$571,$572,$573,$574,$575,$576,$577,$578,$579,$580,$581,$582,$583,$584,$585,$586,$587,$588,$589,$590,$591,$592,$593,$594,$595,$596,$597,$598,$599,$600,$601,$602,$603,$604,$605,$606,$607,$608,$609,$610,$611,$612,$613,$614,$615,$616,$617,$618,$619,$620,$621,$622,$623,$624,$625,$626,$627,$628,$629,$630,$631,$632,$633,$634,$635,$636,$637,$638,$639,$640,$641,$642,$643,$644,$645,$646,$647,$648,$649,$650,$651,$652,$653,$654,$655,$656,$657,$658,$659,$660,$661,$662,$663,$664,$665,$666,$667,$668,$669,$670,$671,$672,$673,$674,$675,$676,$677,$678,$679,$680,$681,$682,$683,$684,$685,$686,$687,$688,$689,$690,$691,$692,$693,$694,$695,$696,$697,$698,$699,$700,$701,$702,$703,$704,$705,$706,$707,$708,$709,$710,$711,$712,$713,$714,$715,$716,$717,$718,$719,$720,$721,$722,$723,$724,$725,$726,$727,$728,$729,$730,$731,$732,$733,$734,$735,$736,$737,$738,$739,$740,$741,$742,$743,$744,$745,$746,$747,$748,$749,$750,$751,$752,$753,$754,$755,$756,$757,$758,$759,$760,$761,$762,$763,$764,$765,$766,$767,$768,$769,$770,$771,$772,$773,$774,$775,$776,$777,$778,$779,$780,$781,$782,$783,$784,$785,$786,$787,$788,$789,$790,$791,$792,$793,$794,$795,$796,$797,$798,$799,$800,$801,$802,$803,$804,$805,$806,$807,$808,$809,$810,$811,$812,$813,$814,$815,$816,$817,$818,$819,$820,$821,$822,$823,$824,$825,$826,$827,$828,$829,$830,$831,$832,$833,$834,$835,$836,$837,$838,$839,$840,$841,$842,$843,$844,$845,$846,$847,$848,$849,$850,$851,$852,$853,$854,$855,$856,$857,$858,$859,$860,$861,$862,$863,$864,$865,$866,$867,$868,$869,$870,$871,$872,$873,$874,$875,$876,$877,$878,$879,$880,$881,$882,$883,$884,$885,$886,$887,$888,$889,$890,$891,$892,$893,$894,$895,$896,$897,$898,$899,$900,$901,$902,$903,$904,$905,$906,$907,$908,$909,$910,$911,$912,$913,$914,$915,$916,$917,$918,$919,$920,$921,$922,$923,$924,$925,$926,$927,$928,$929,$930,$931,$932,$933,$934,$935,$936,$937,$938,$939,$940,$941,$942,$943,$944,$945,$946,$947,$948,$949,$950,$951,$952,$953,$954,$955,$956,$957,$958,$959,$960,$961,$962,$963,$964,$965,$966,$967,$968,$969,$970,$971,$972,$973,$974,$975,$976,$977,$978,$979,$980,$981,$982,$983,$984,$985,$986,$987,$988,$989,$990,$991,$992,$993,$994,$995,$996,$997,$998,$999,$1000,$1001,$1002,$1003,$1004,$1005,$1006,$1007,$1008,$1009,$1010,$1011,$1012,$1013,$1014,$1015,$1016,$1017,$1018,$1019,$1020,$1021,$1022,$1023,$1024,$1025,$1026,$1027,$1028,$1029,$1030,$1031,$1032,$1033,$1034,$1035,$1036,$1037,$1
```



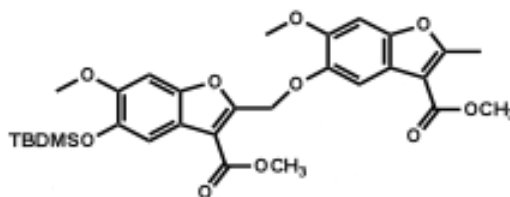




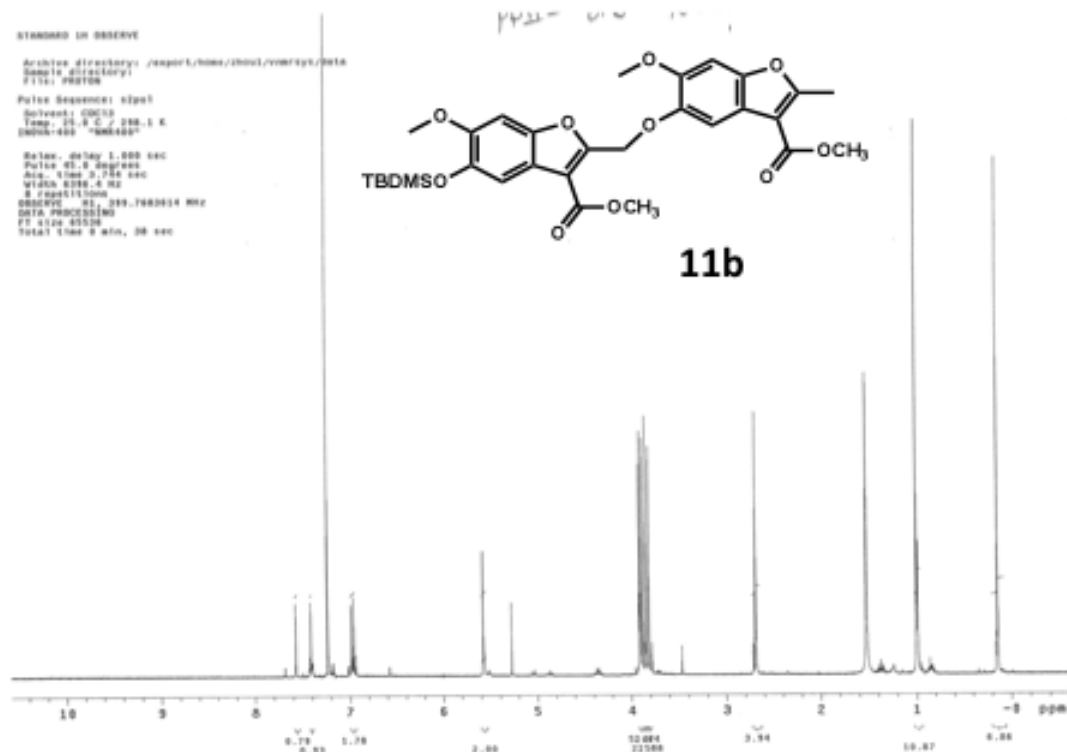


STANDARD IN OBSERVE

Archive directory: /export/home/aboul/emr/typ/1016
Sample directory:
File: 101601
Pulse Sequence: zgpg30
Solvent: CDCl3
Temp: 25.0 C / 298.1 K
DMSO-d6
Relax. delay: 1.000 sec
Pulse: 45.0 degrees
Acq. time: 2.750 sec
Width: 4700.0 Hz
S repetitions: 8
Sweep rate: 313.780000 MHz
DATA PROCESSING
FT size: 4096
Total time: 0 min, 08 sec

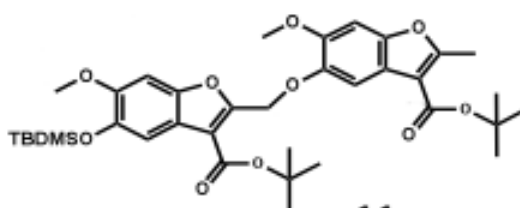


11b

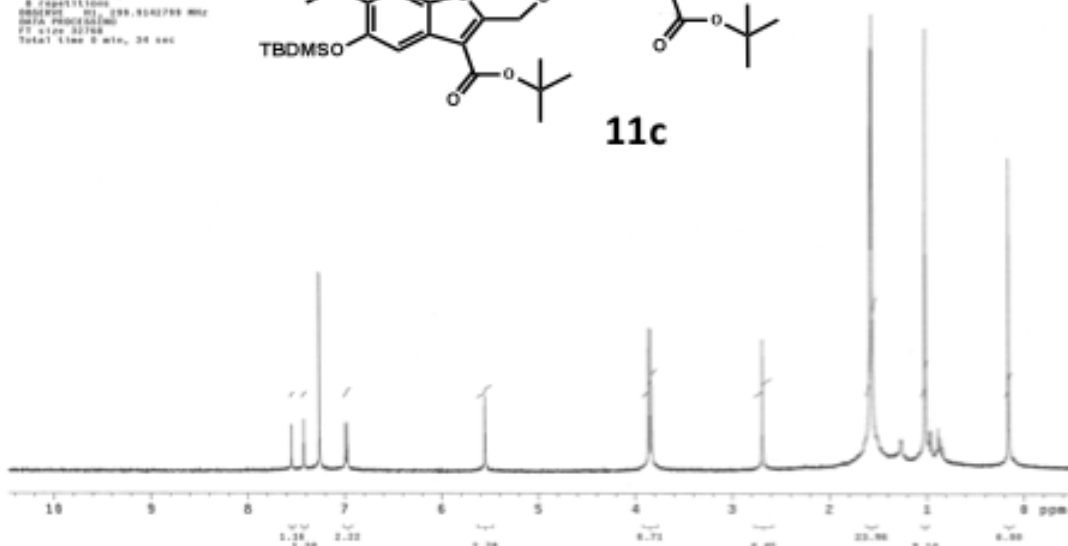


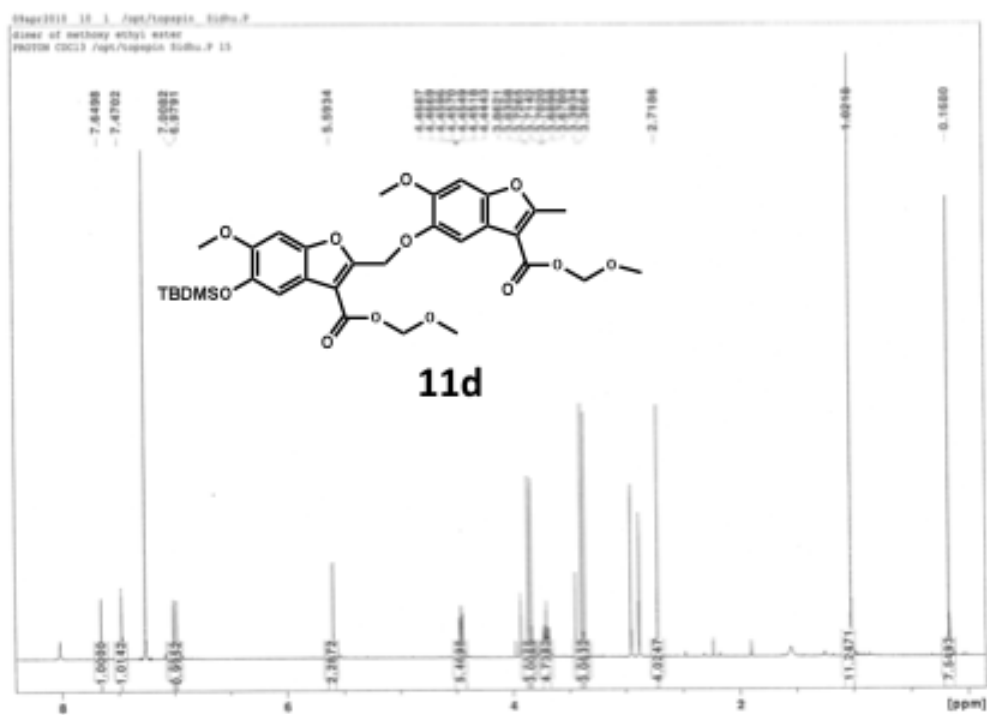
STANDARD IN OBSERVE

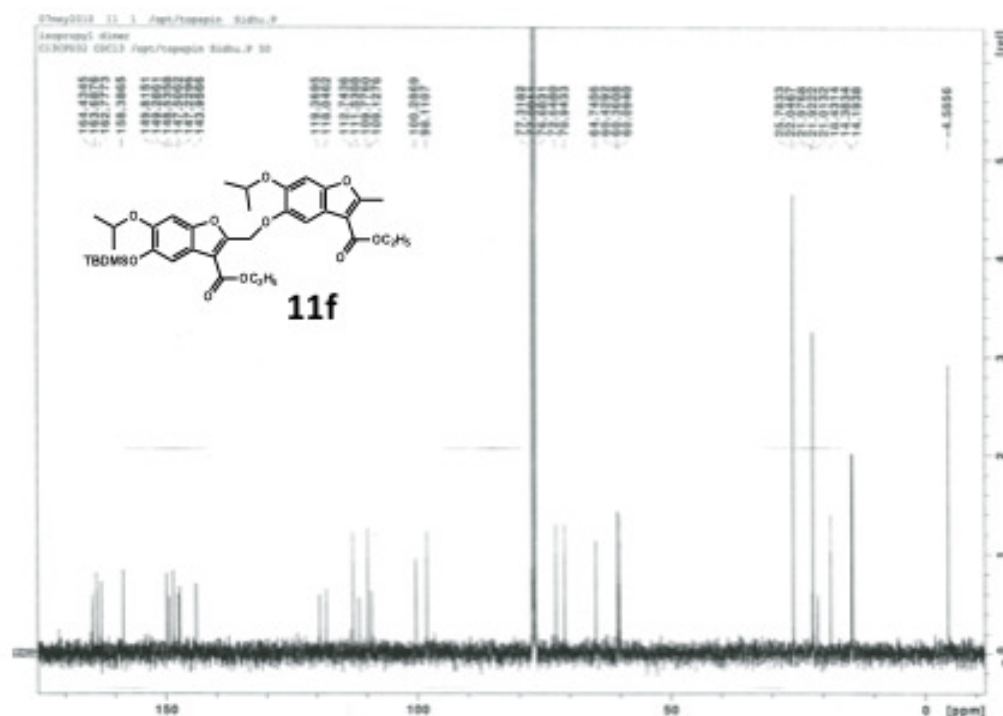
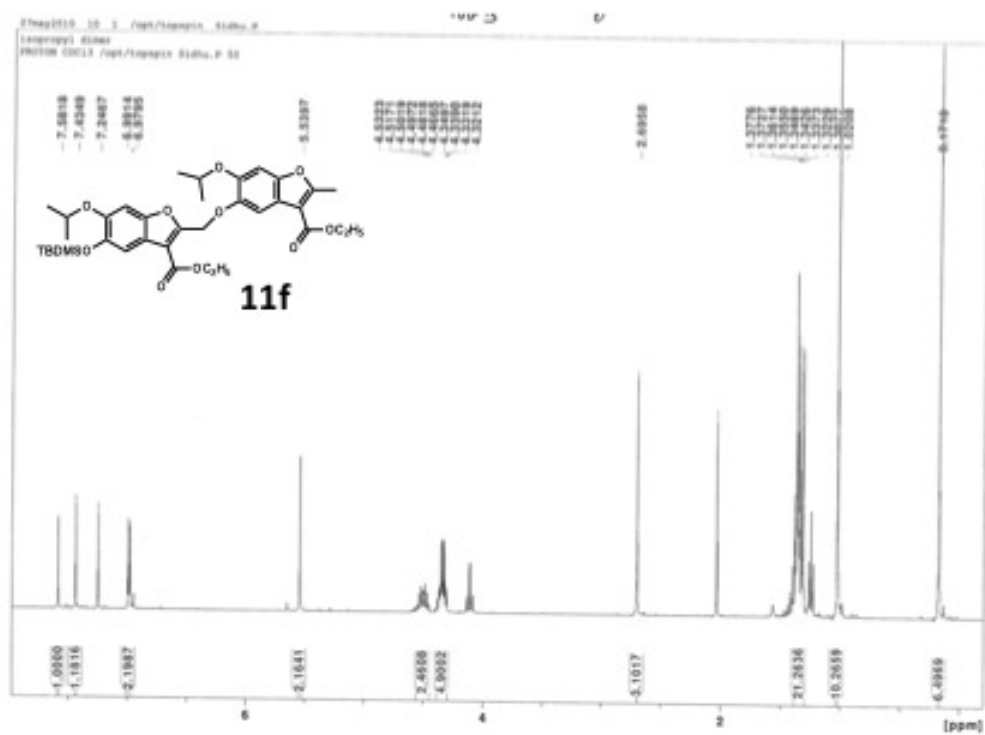
Archive directory: /export/home/aboul/emr/typ/1016
Sample directory:
File: 101601
Pulse Sequence: zgpg30
Solvent: CDCl3
Acquisition Temperature: Mercury-20000
Relax. delay: 1.000 sec
Pulse: 45.0 degrees
Acq. time: 2.750 sec
Width: 4700.0 Hz
S repetitions: 8
Sweep rate: 313.780000 MHz
DATA PROCESSING
FT size: 4096
Total time: 0 min, 08 sec

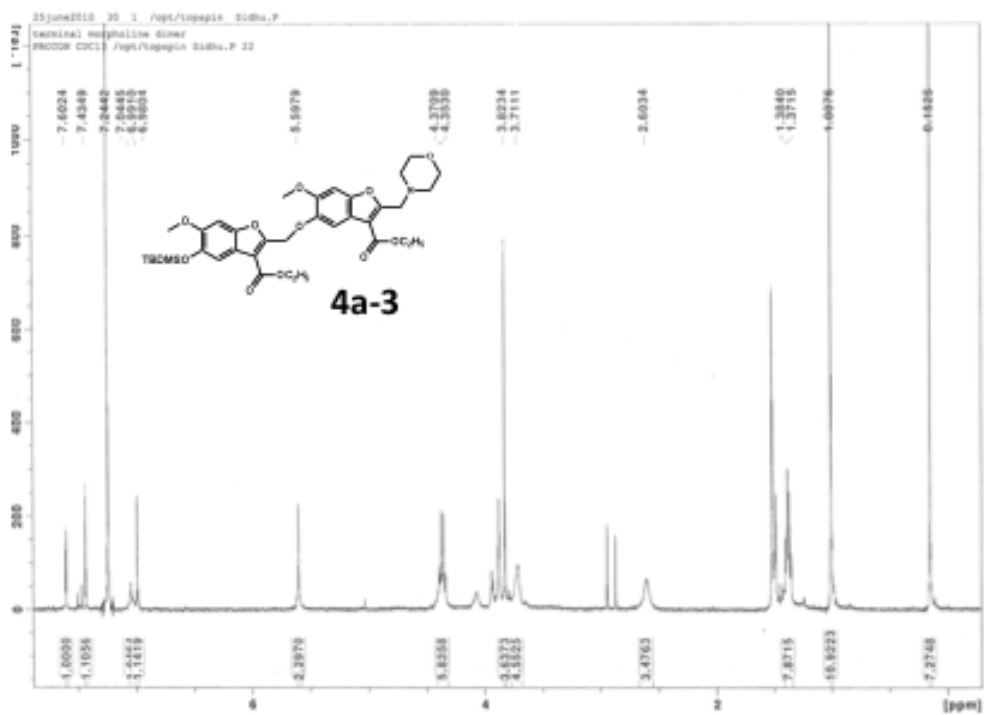
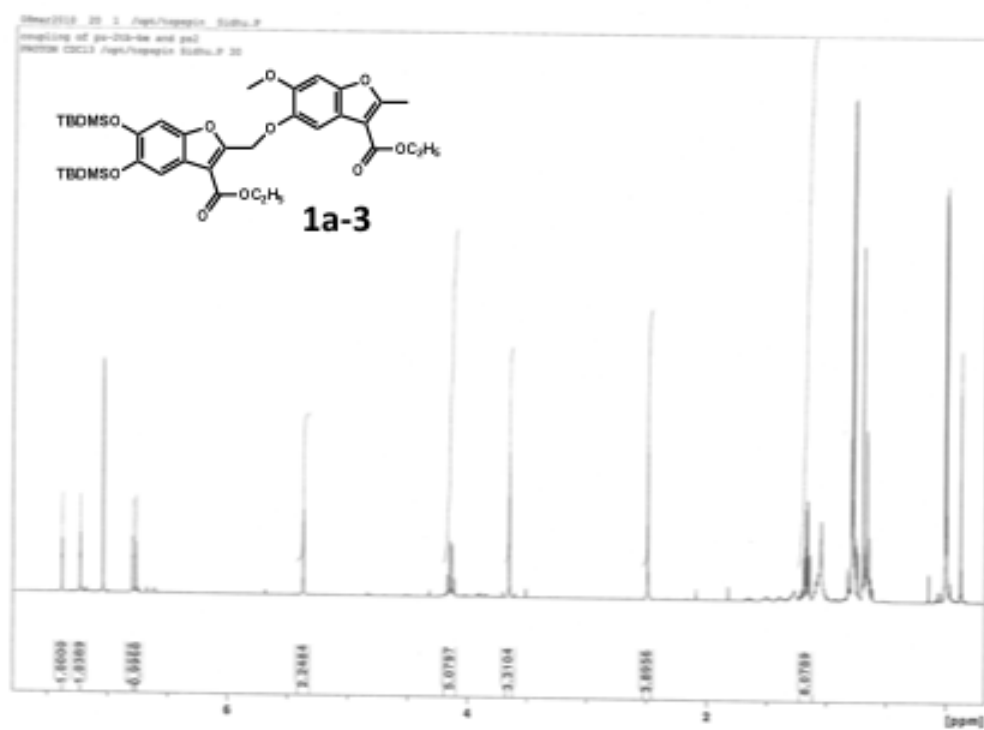


11c









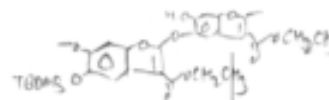
STANDARD IN OBSERVE

Archive directory: /export/home/zhou/mercury/data
Sample directory:
File: PROTON

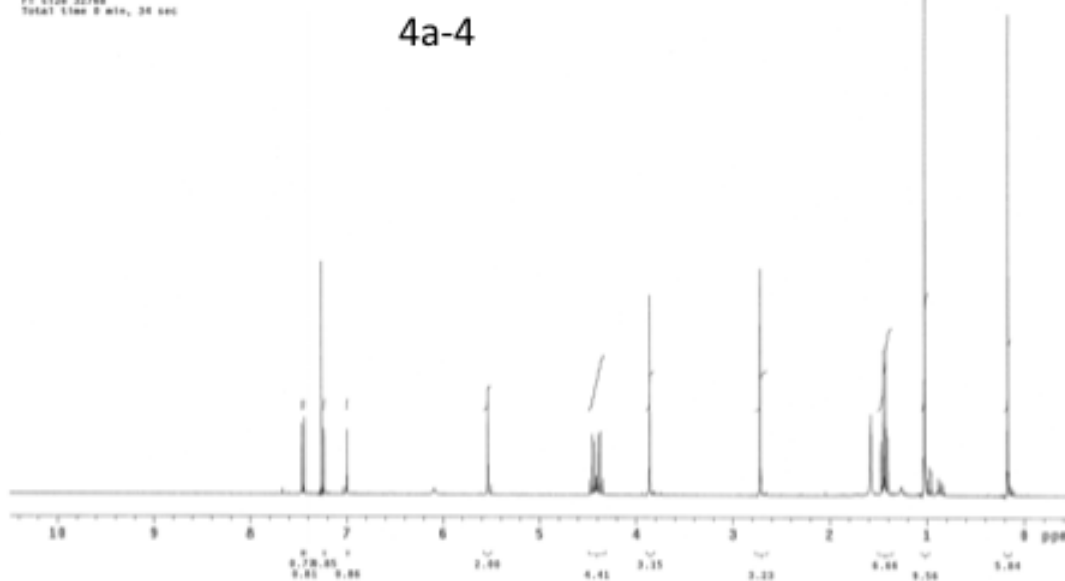
Pulse Sequence: zgpg30

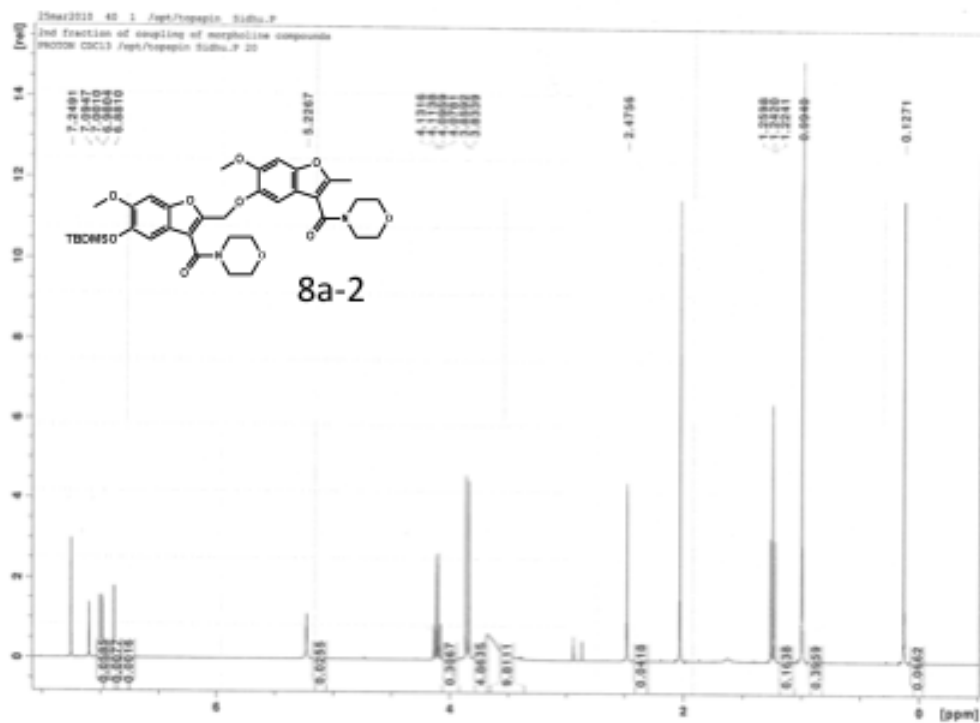
Solvent: CDCl3
Reference temperature
Mercury-3000S 400MHz

Relax. delay 1.000 sec
Pulse 40.0 degrees
Acq. time 0.000 sec
Width 4700.0 Hz
0 repetitions
OBSERVE NO 399.8142758 MHz
DATA PROCESSING
F2 size 32768
Total time 0 min, 36 sec

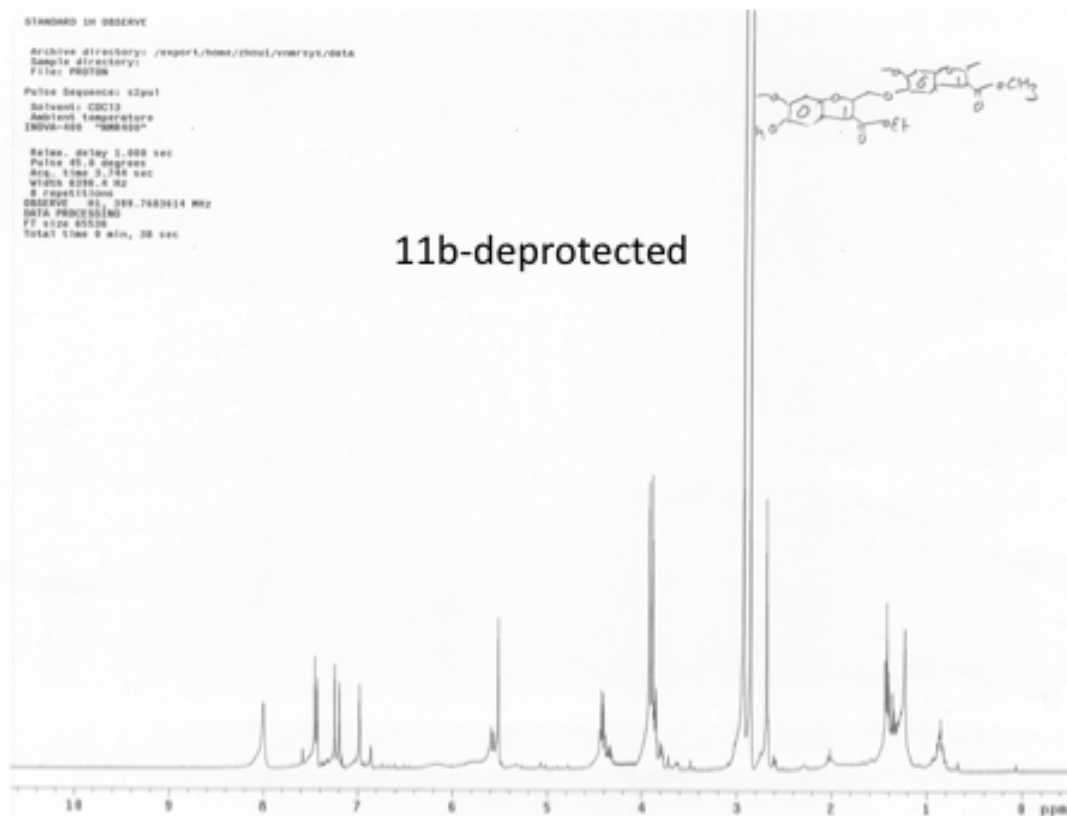
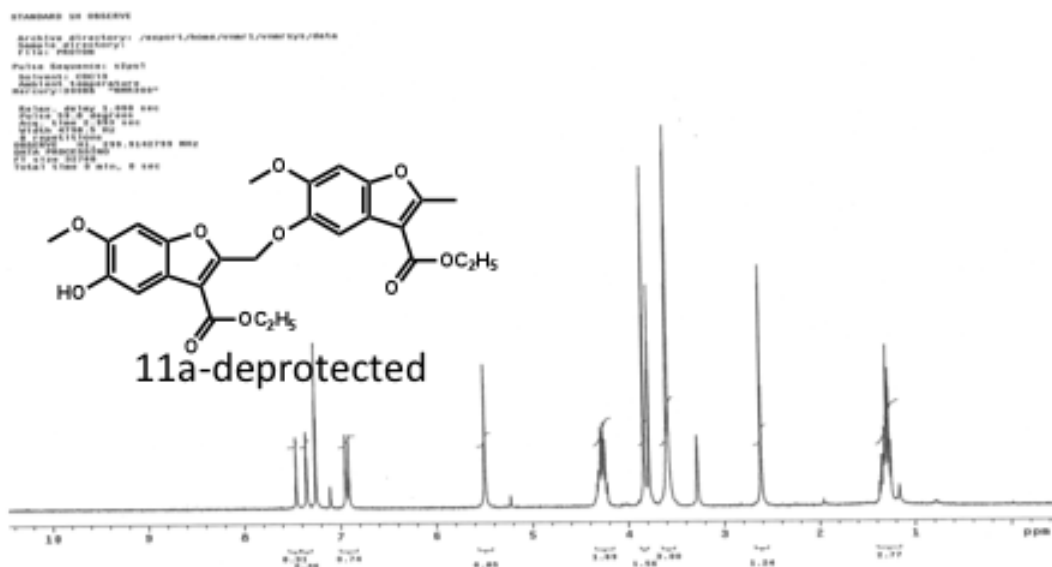


4a-4





270



STANDARD IN OBSERVE

Archive directory: /export/home/zhou/chemistry/data
Sample directory:
File: 111c

Pulse Sequence: zgpg30

Surveyl: CQC13

Acquisition Temperature

Mercury-20000 "WMS300"

Relax. delay 1.000 sec

Pulse 40.0 degrees

Acq. time 2.950 sec

Width 4798.5 Hz

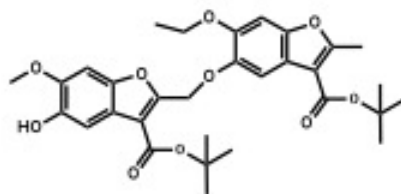
0 Repetitions

Observed: 41, 289, 0140799 Hz

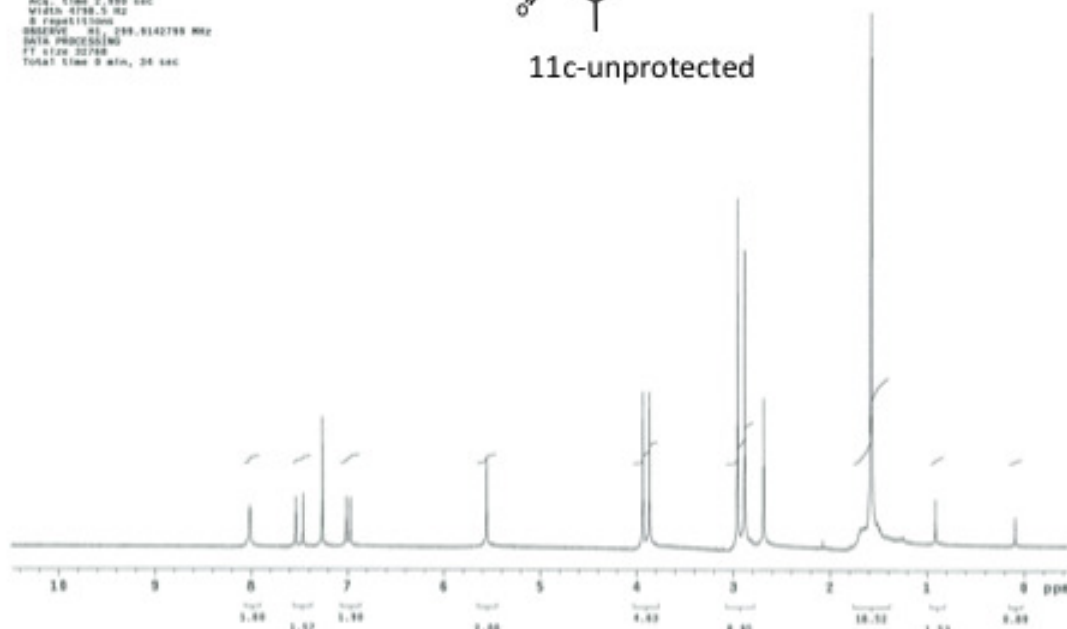
Data Process[ed]

FT size 32768

Total time 5 min, 34 sec



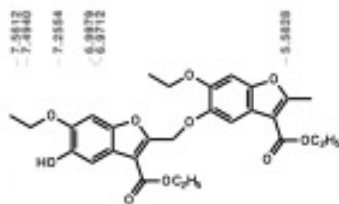
11c-unprotected



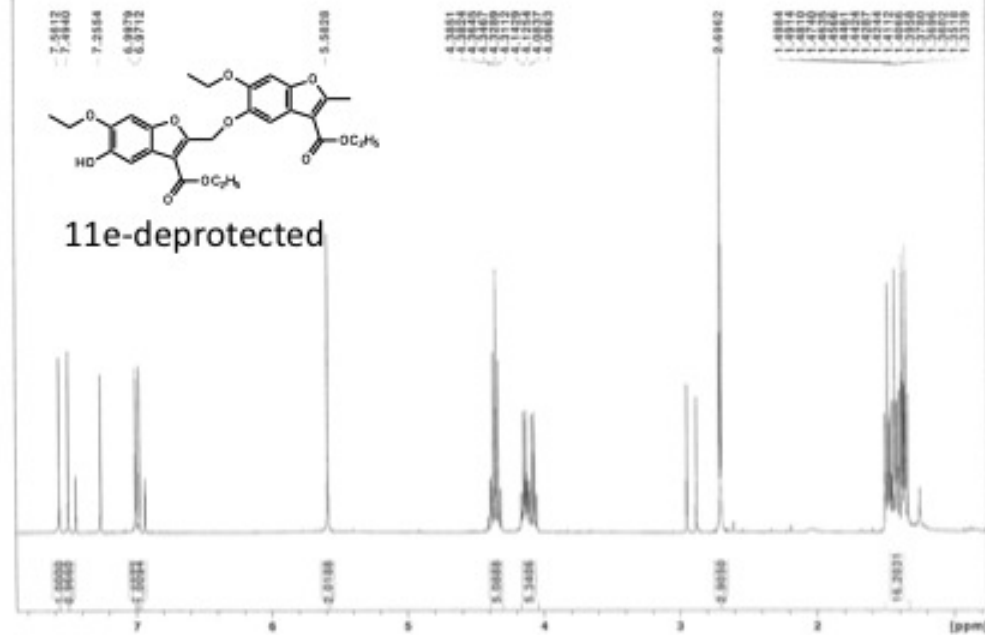
27Apr2010 10 1 /opt/ropepin 514hu.P

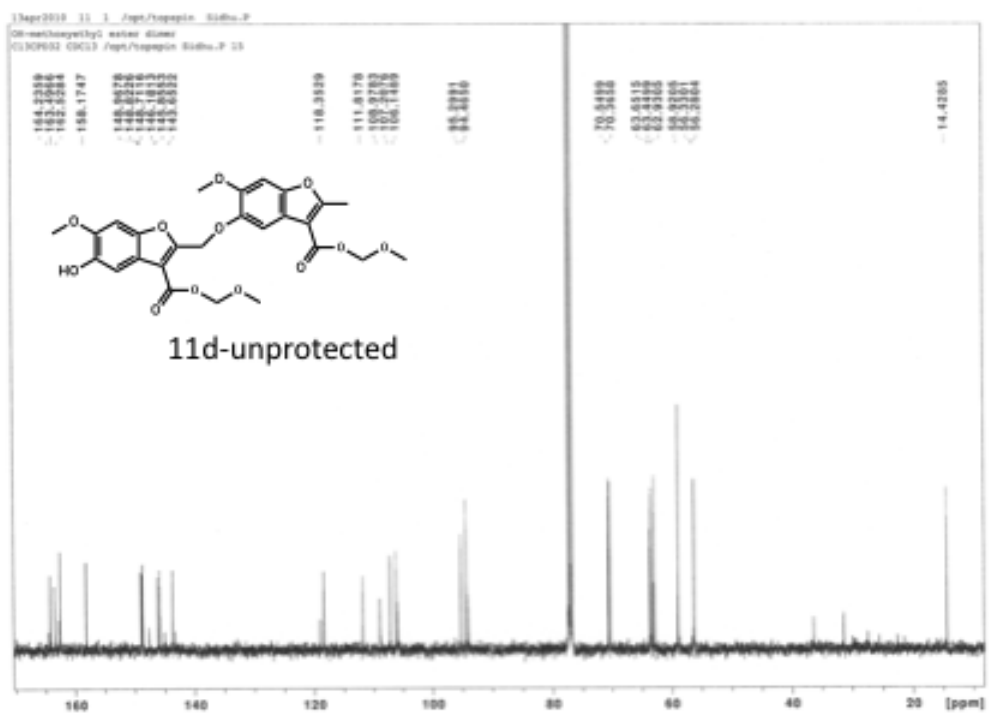
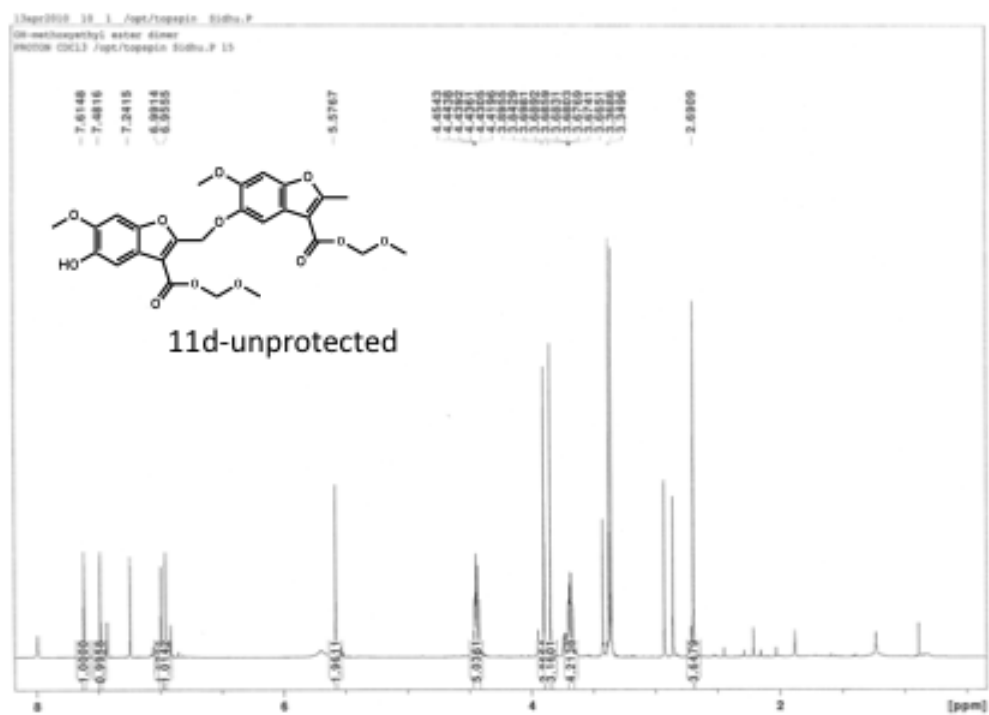
Owner: zh. wily2

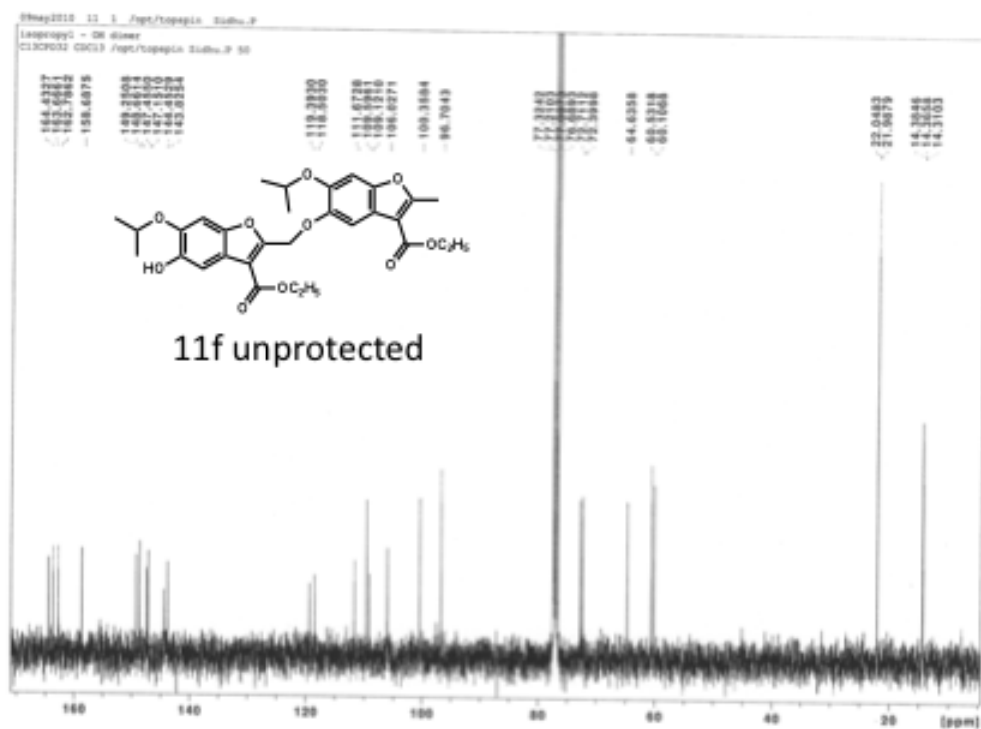
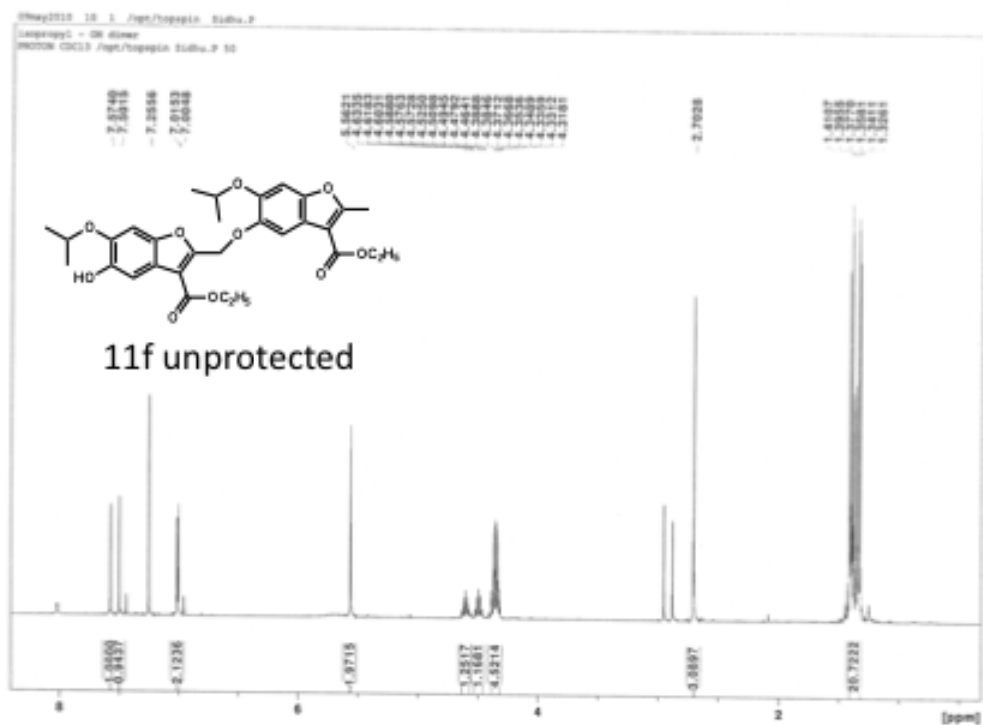
PROTON CQC13 /opt/ropepin 514hu.P 50

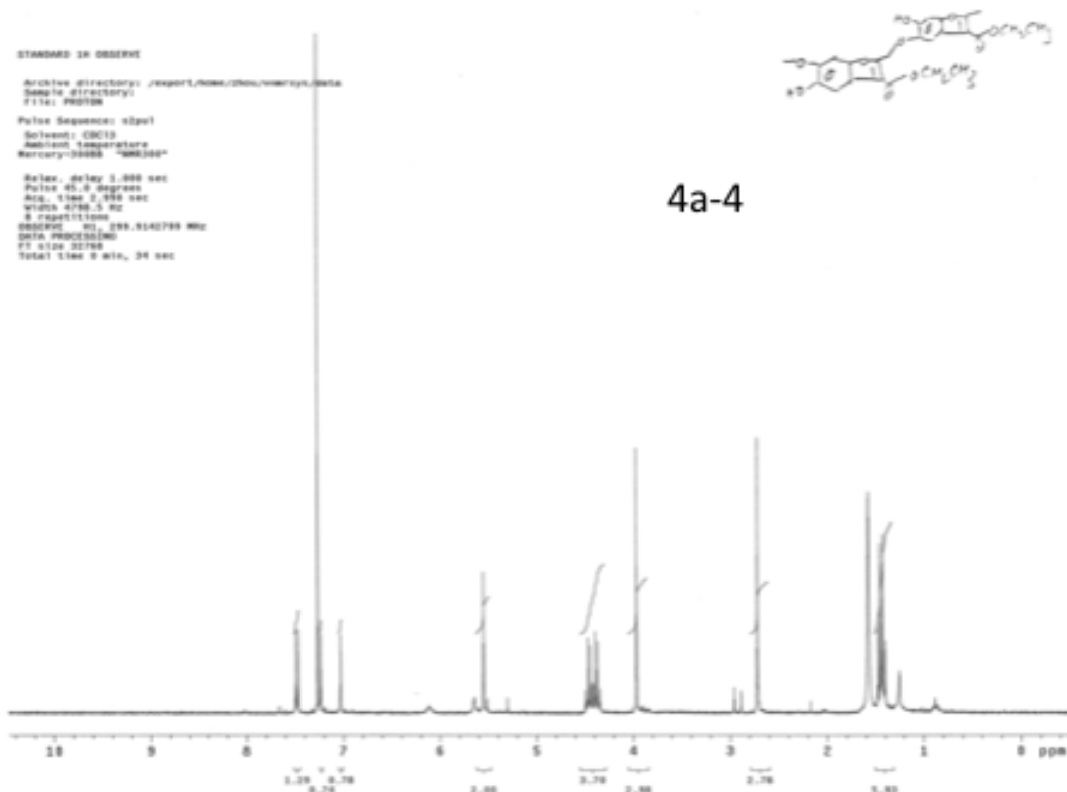
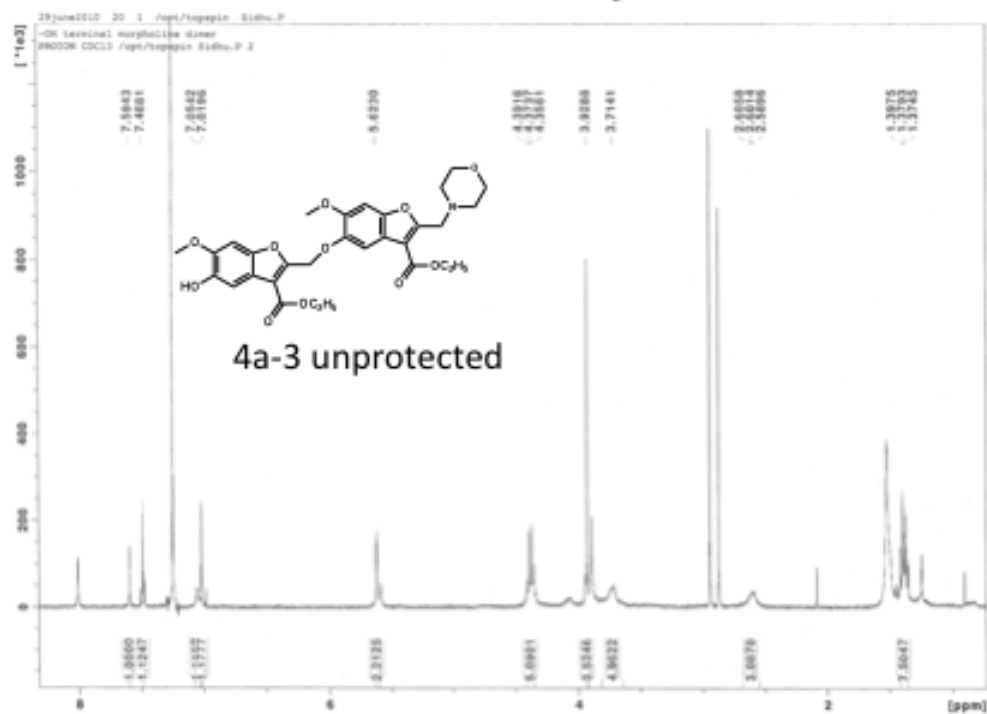


11e-deprotected





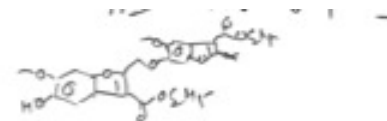




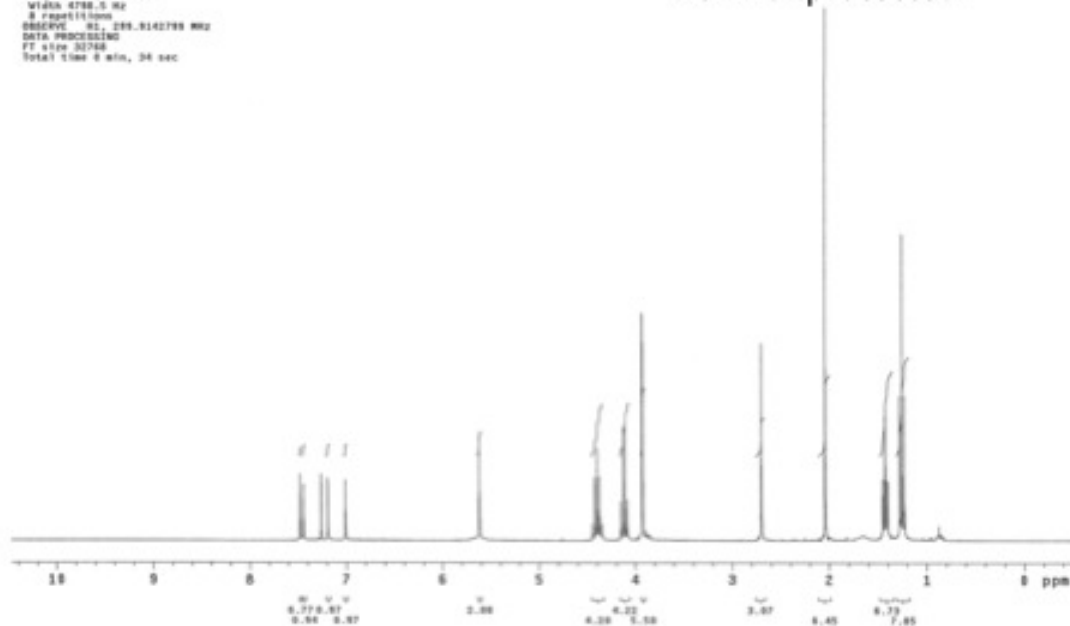
STANDARD 1H OBSERVE

Archive directory: /export/home/zhao/mercury/data
 Sample directory:
 File: P80098
 Pulse Sequence: zgpg30
 Solvent: CDCl3
 Ambient temperature
 Mercury-3000S "900300"

Relax. delay 3.000 sec
 Pulse 45.0 degrees
 Acq. time 2.950 sec
 Width 4788.0 Hz
 8 repetitions
 OBSERVE: 01, 299.9142798 MHz
 DATA PROCESSING
 FT size 32768
 Total time 8 min, 34 sec



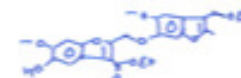
2a'-1 unprotected



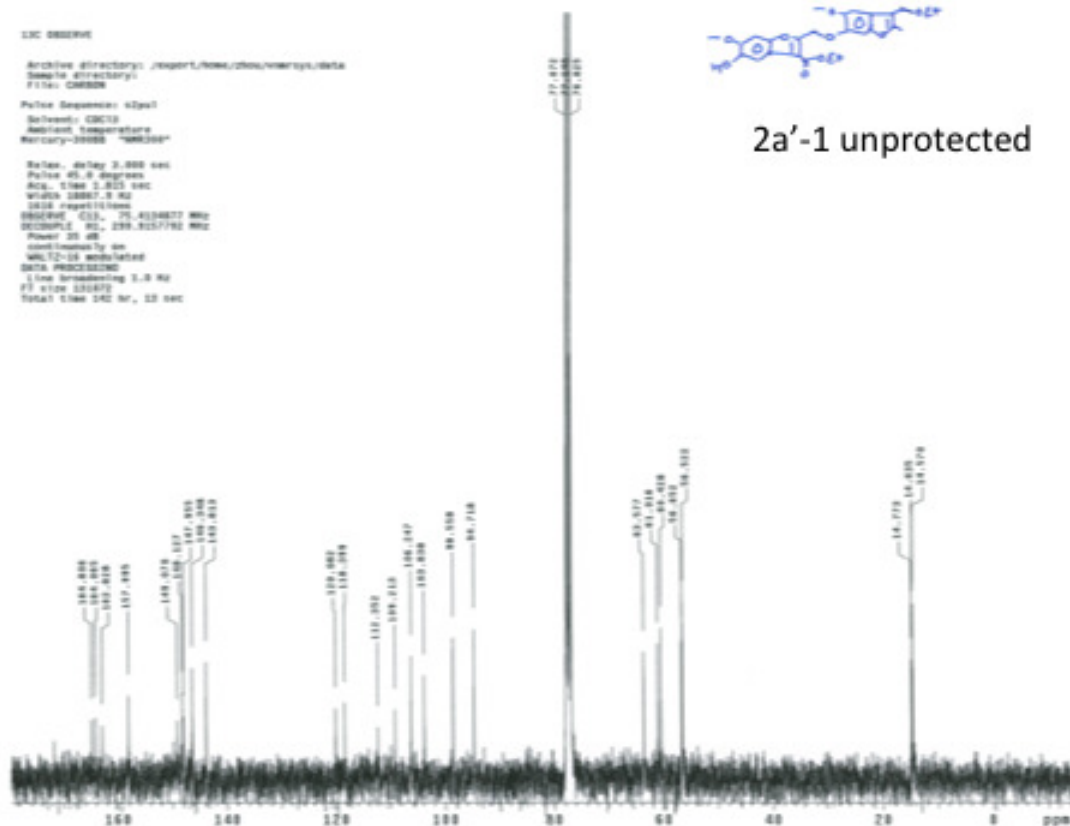
13C OBSERVE

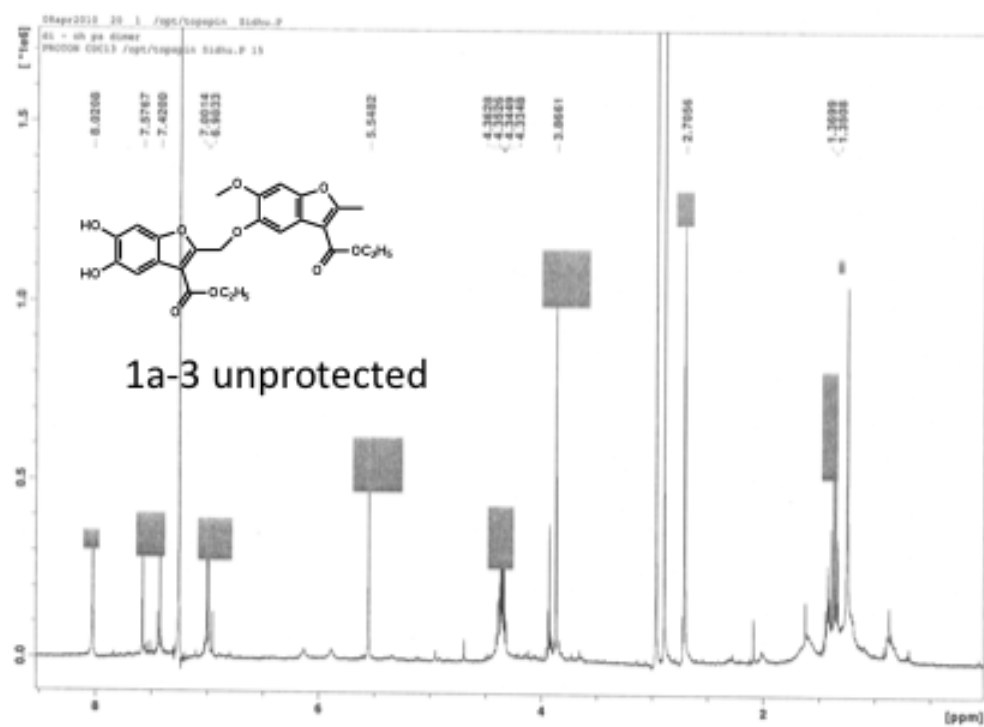
Archive directory: /export/home/zhao/mercury/data
 Sample directory:
 File: C80008
 Pulse Sequence: zgpg30
 Solvent: CDCl3
 Ambient temperature
 Mercury-3000S "900300"

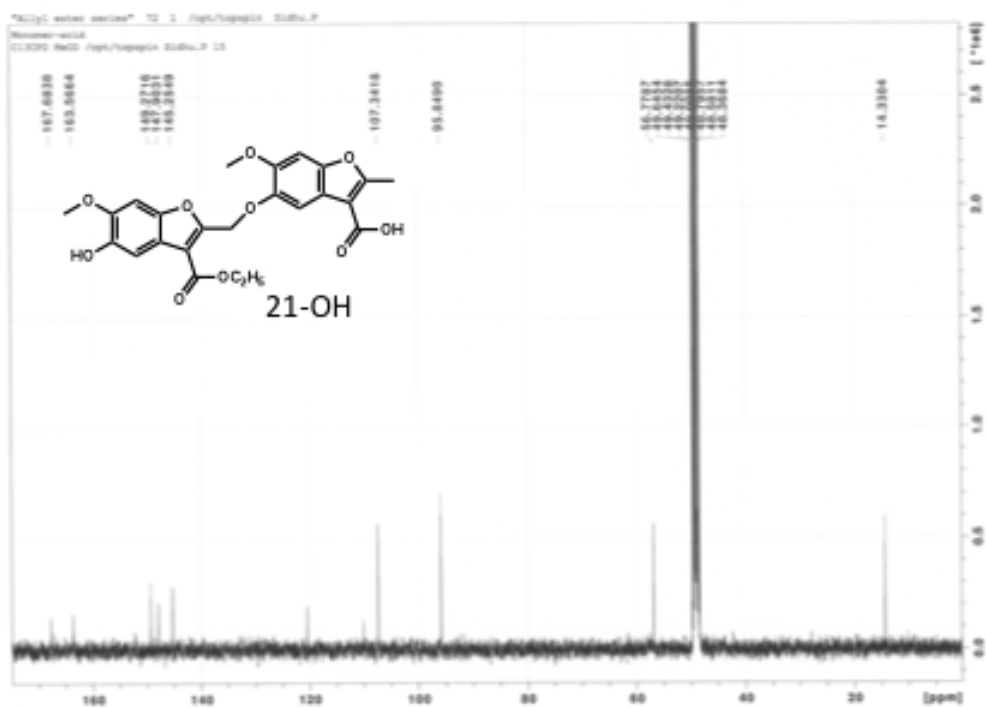
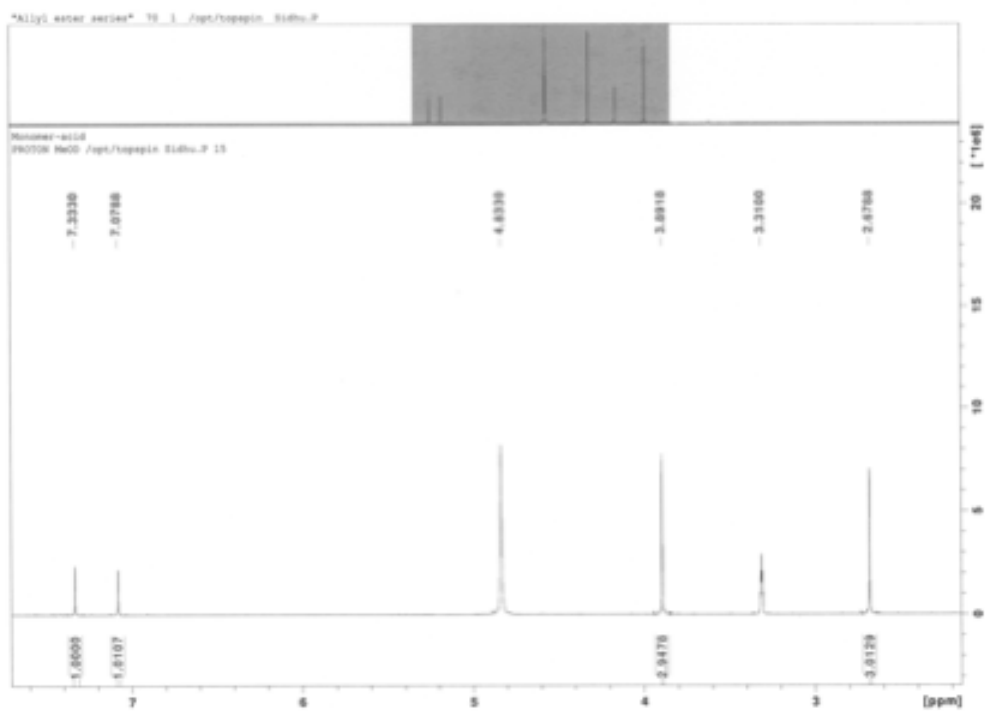
Relax. delay 3.000 sec
 Pulse 45.0 degrees
 Acq. time 3.825 sec
 Width 22887.0 Hz
 1024 repetitions
 OBSERVE: 01, 75.4234877 MHz
 DECOUPLE: 02, 201.8257792 MHz
 Power 25 dB
 cross-polarization on
 WALTZ-16 modulation
 DATA PROCESSING
 Line broadening 3.0 Hz
 FT size 132672
 Total time 242 hr, 12 sec



2a'-1 unprotected







STANDARD IN OBSERVE

Archive directory: /export/home/ghou/vnmr/kyt/data
Sample directory:

Pulse Sequence: zgpg30

Solvent: CDCl3

Ambient temperature

File: zgpg30-d1401-22001

Acquire: 300000 50000000

Relax: delay 5.000 sec

Pulse 45.0 degrees

Acq. time 2.350 sec

Width 4790.5 Hz

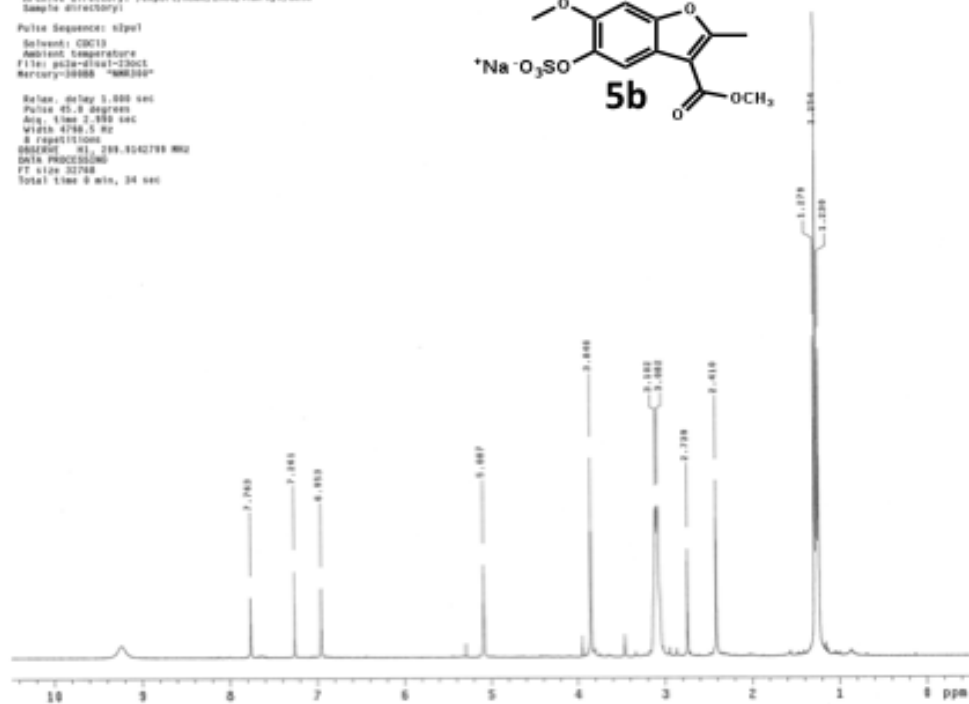
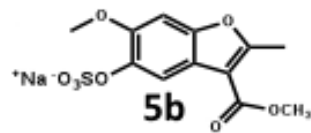
8 repetitions

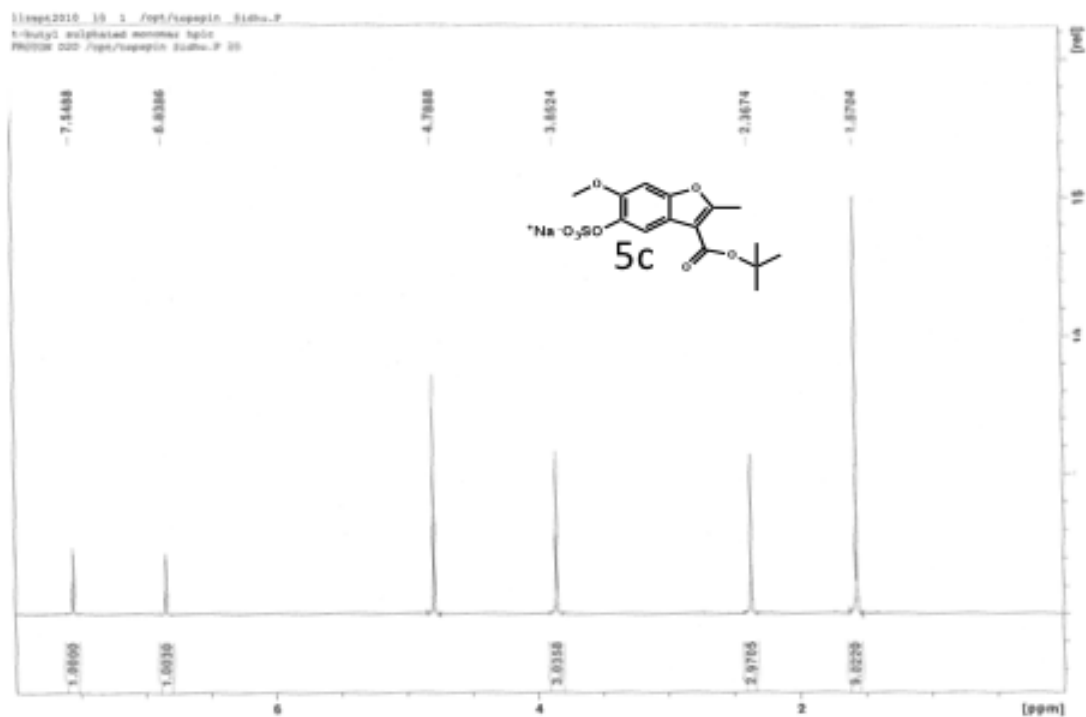
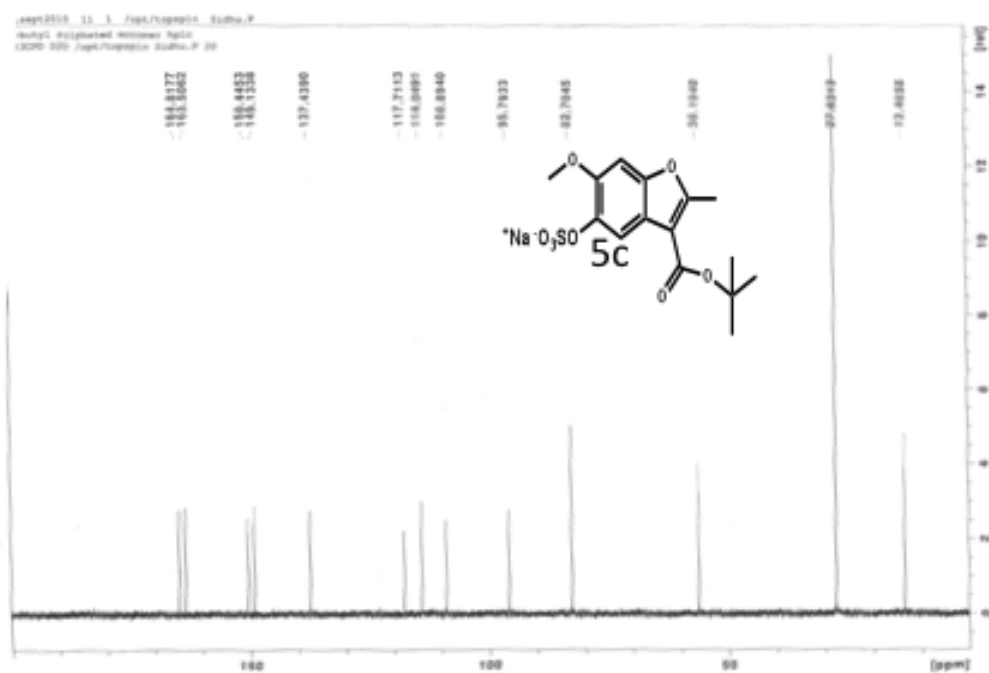
DSF: 401.210.0042790 MHz

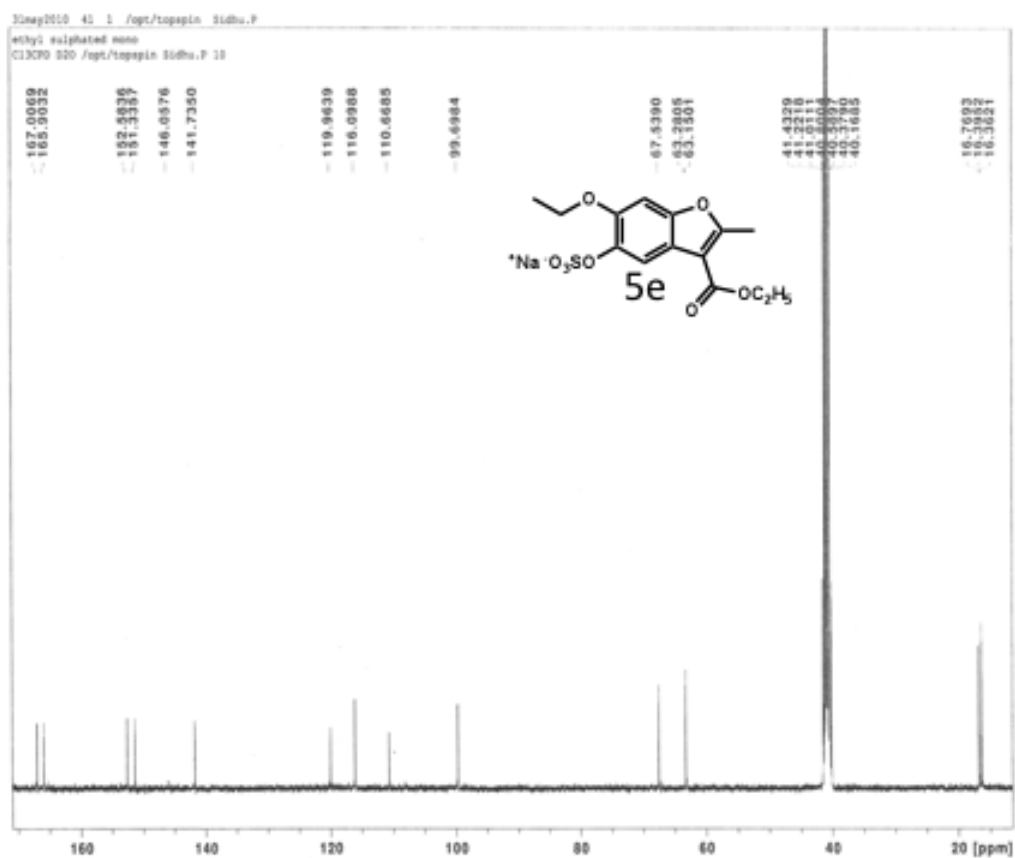
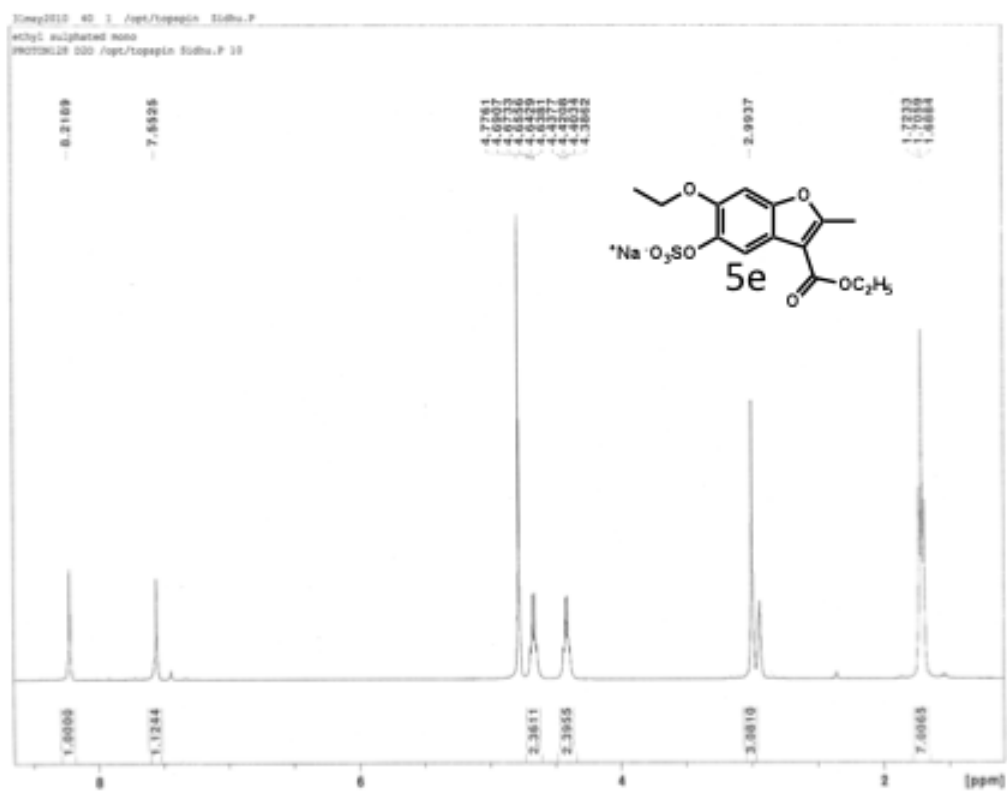
DATA PROCESSING

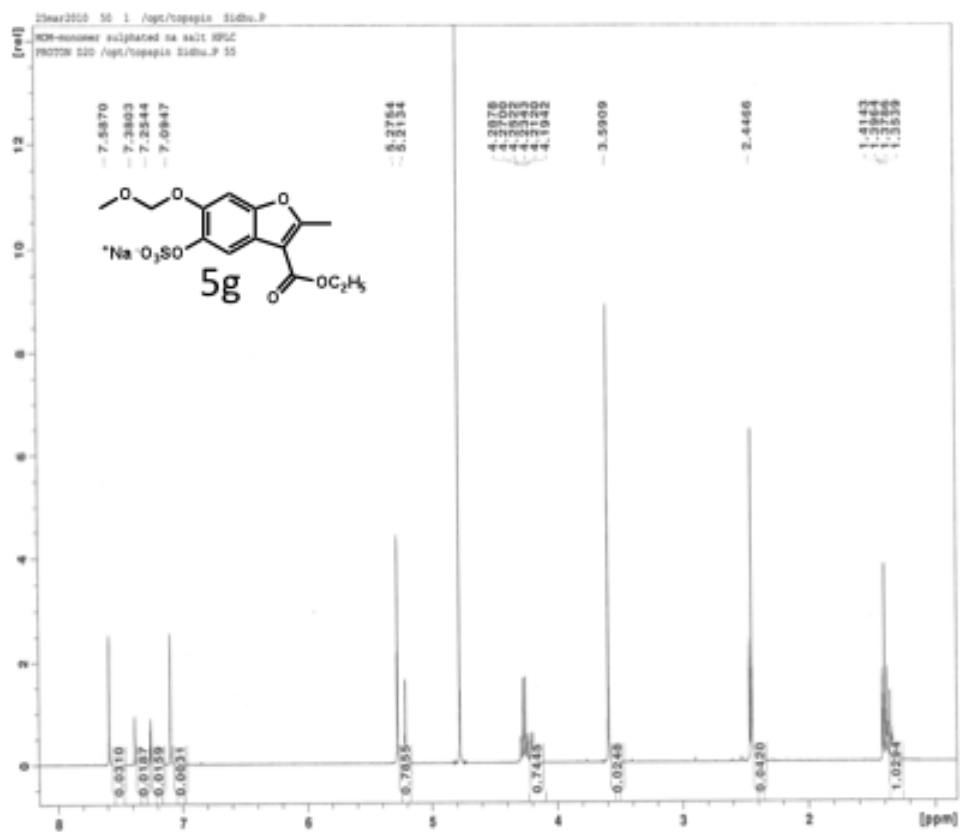
FT size 32768

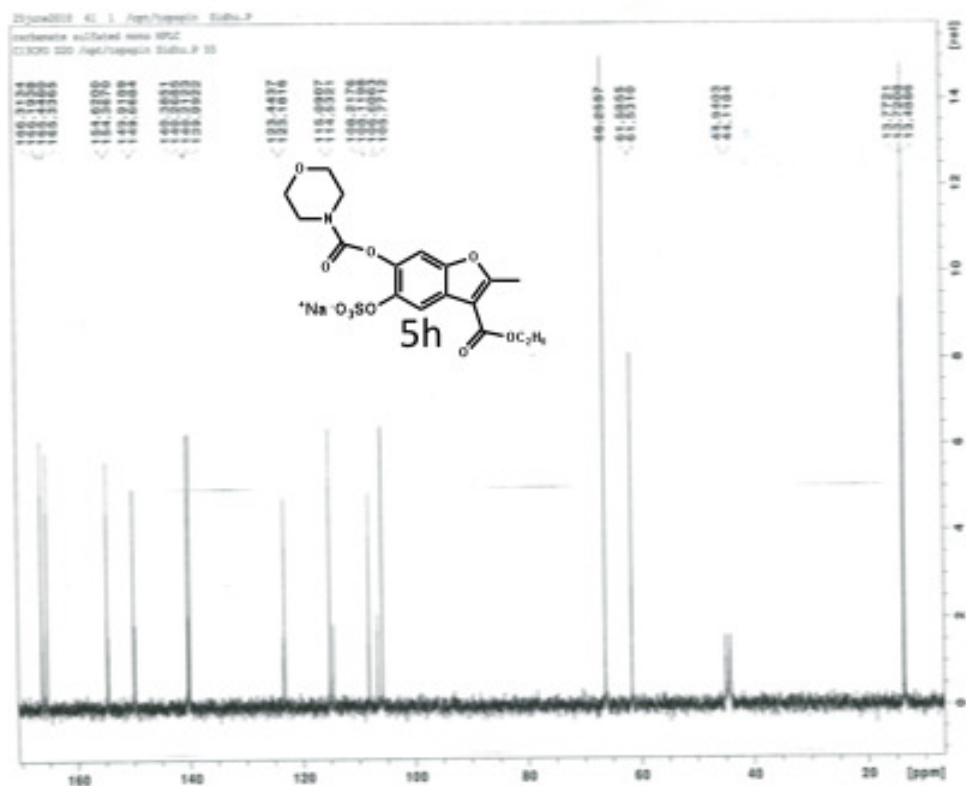
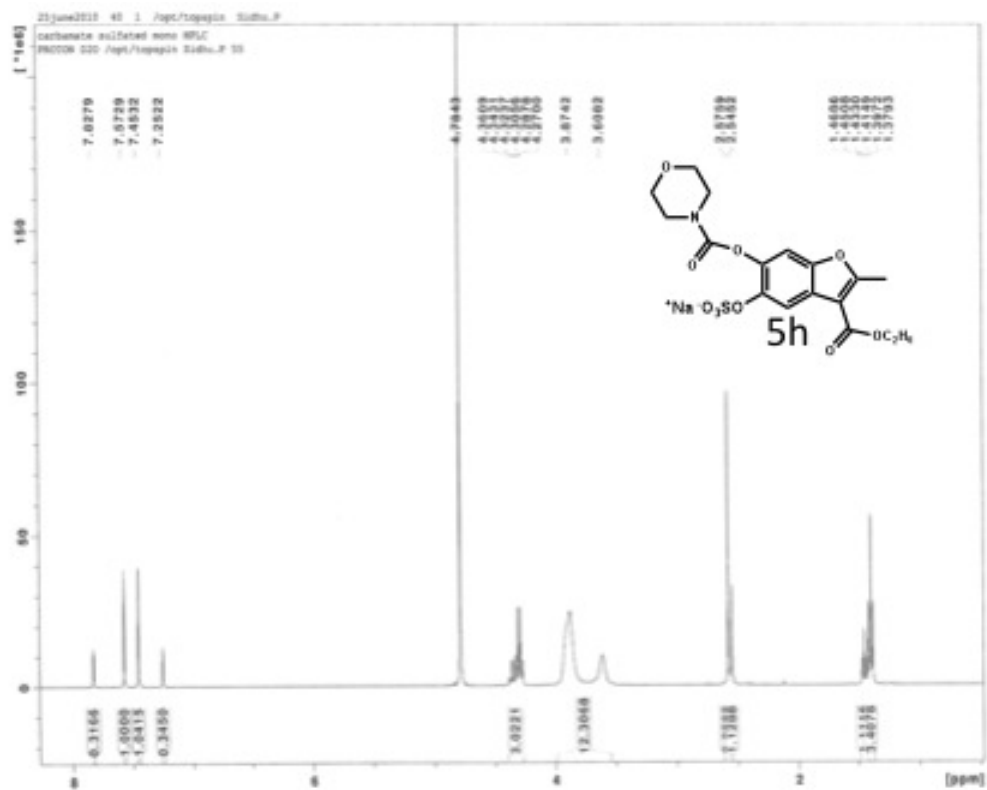
Total time 8 min, 34 sec

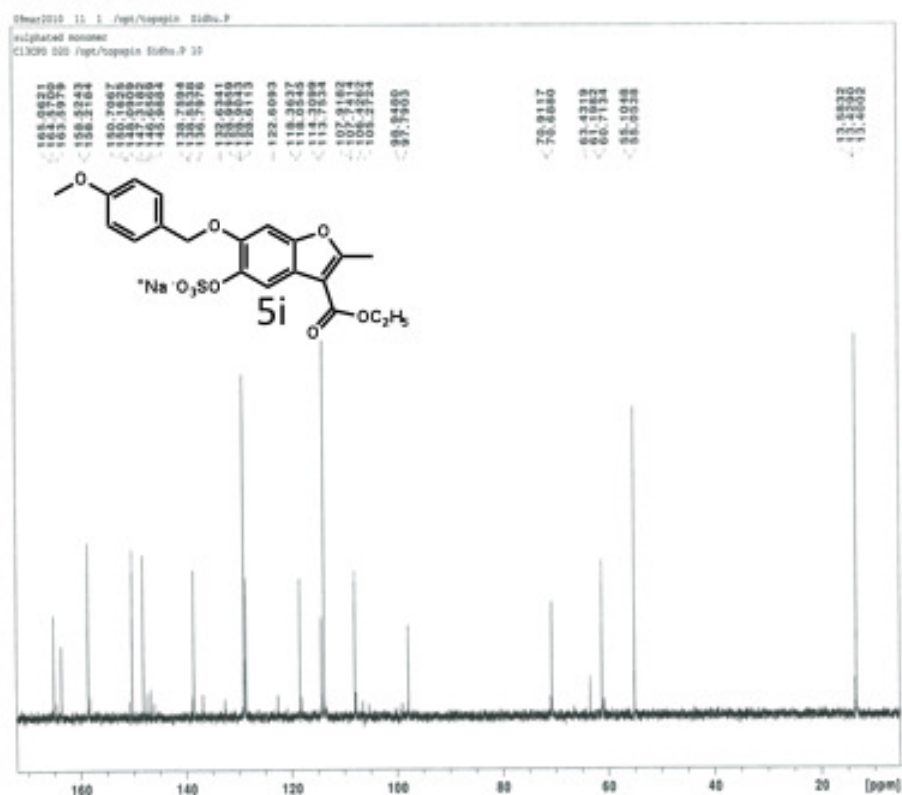
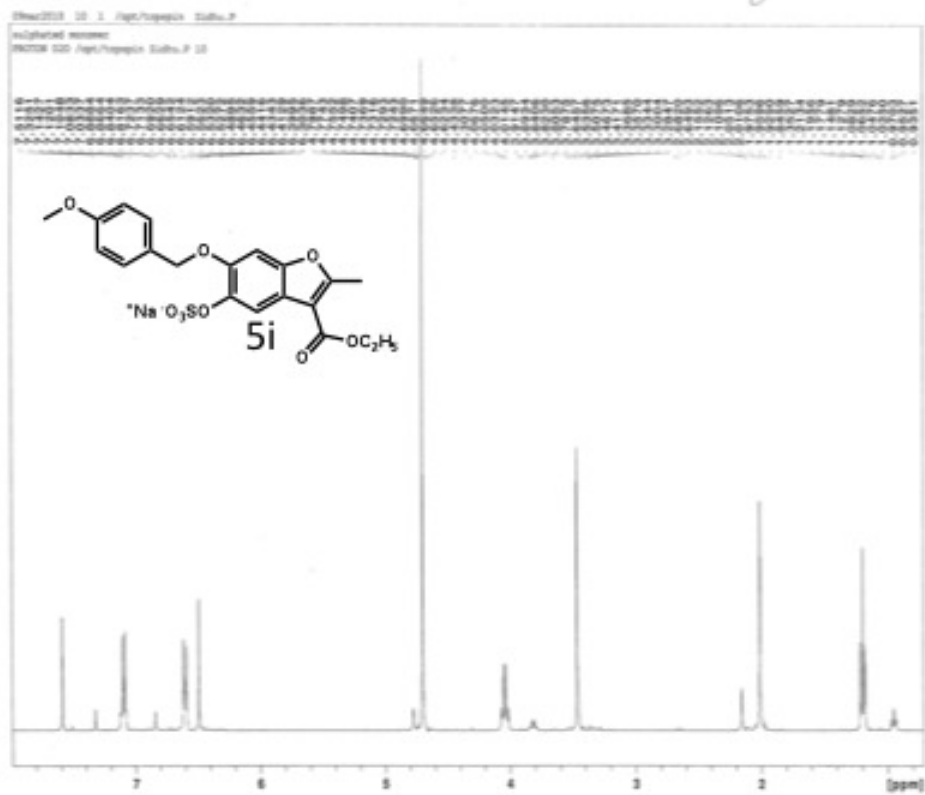












STANDARD 2H OBSERVE

Archive directory: /export/home/chem/vmr/vmr/1/data
Sample directory:
File: P00106

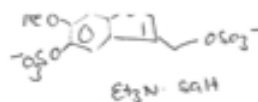
Pulse Sequence: zgpg30

Solvent: CDCl3

Ambient temperature

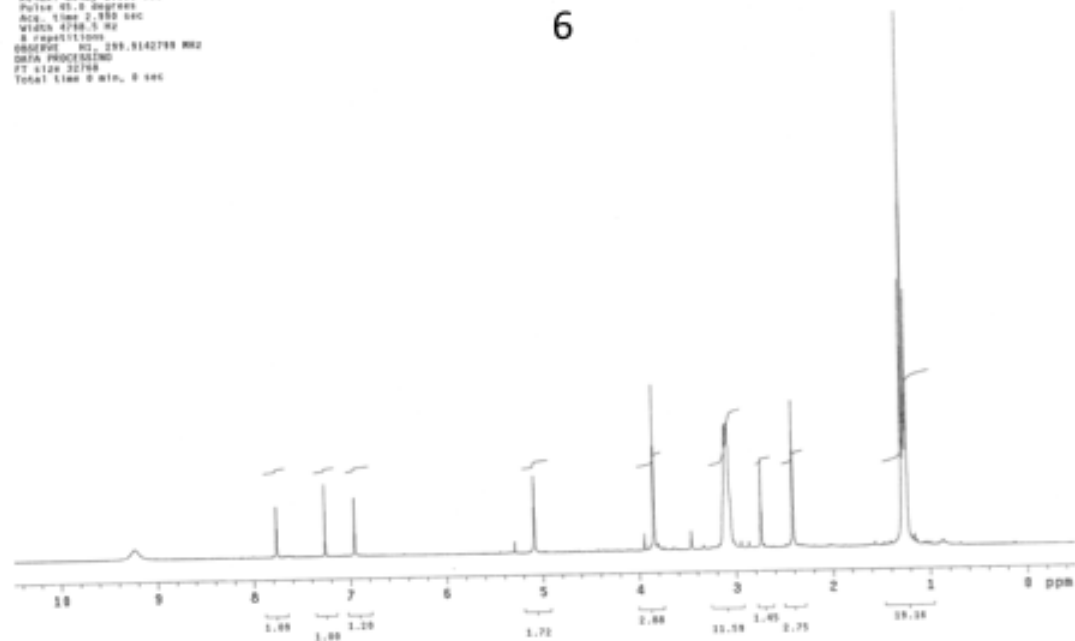
Mercury-300SB "900300"

Relax. delay 1.000 sec
Pulse 45.0 degrees
Acq. time 2.950 sec
Width 4788.5 Hz
repetitions
SFOFREQ Hz 100.6142788 MHz
DATA PROCESSING
F2 size 32768
Total time 9 min. 0 sec

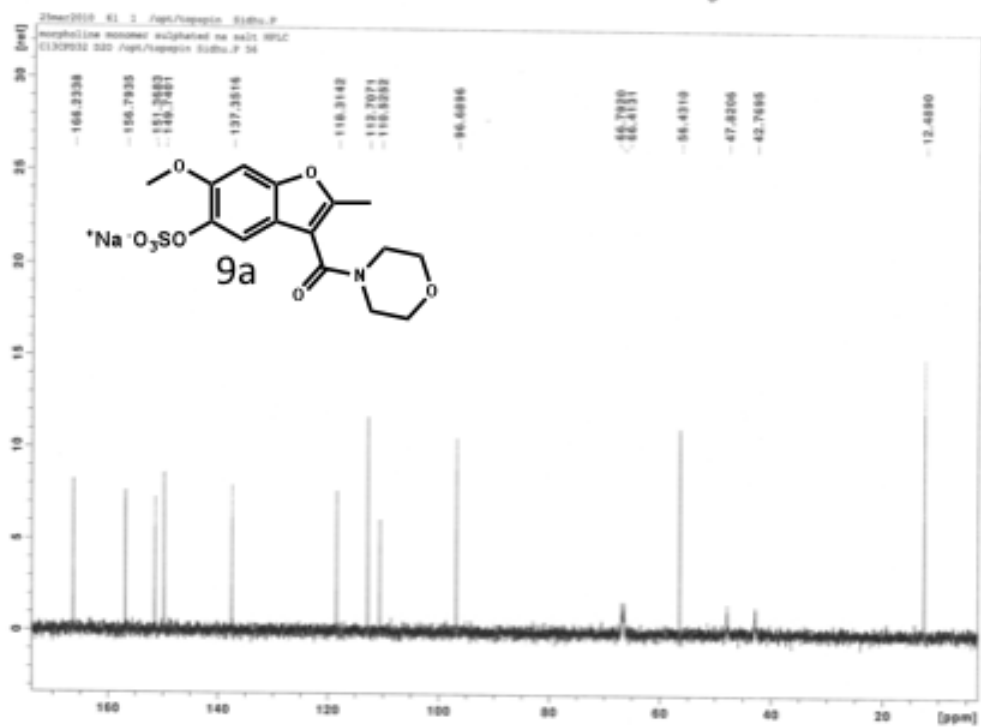
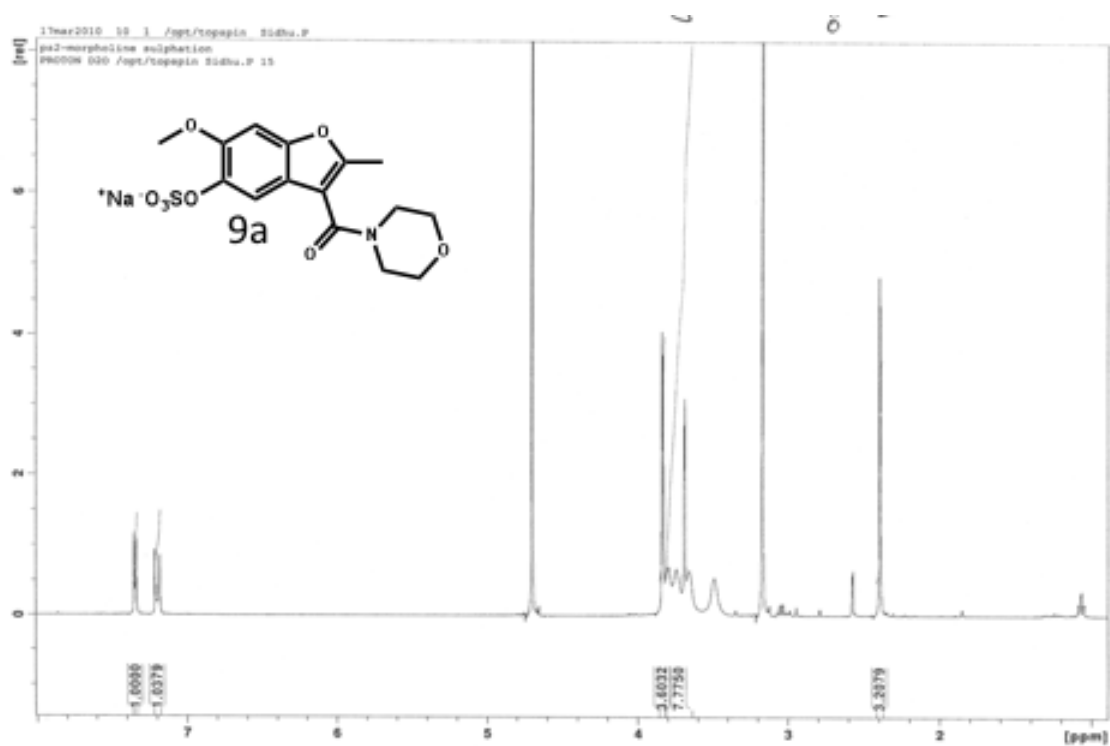


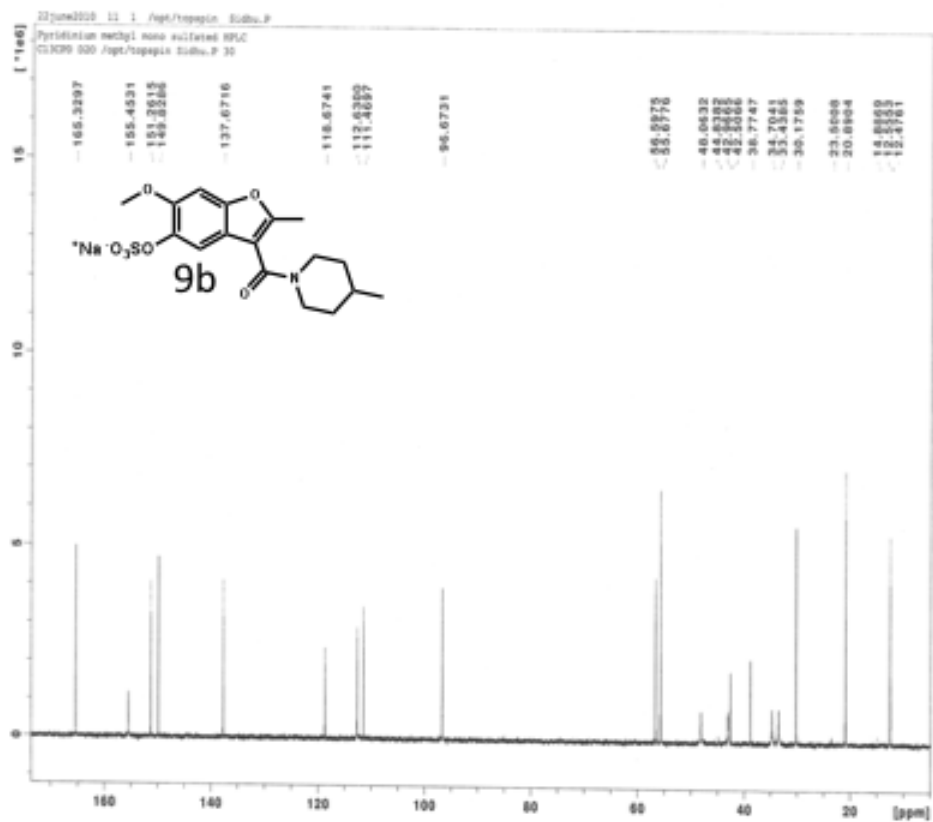
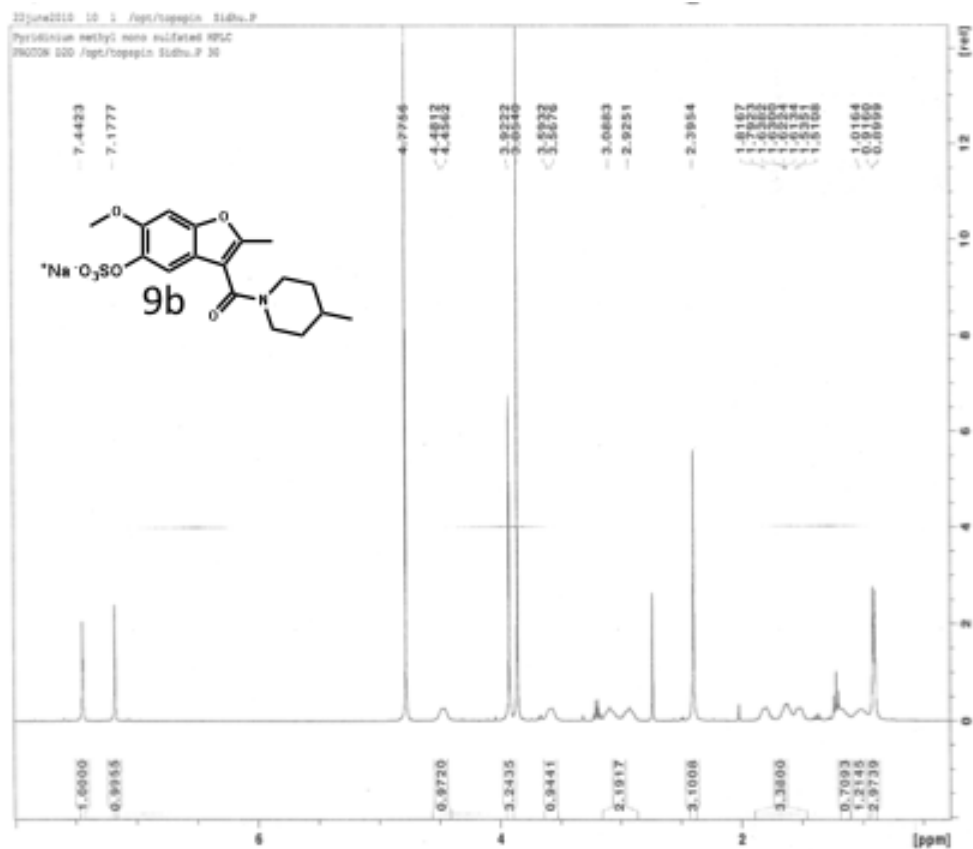
60%

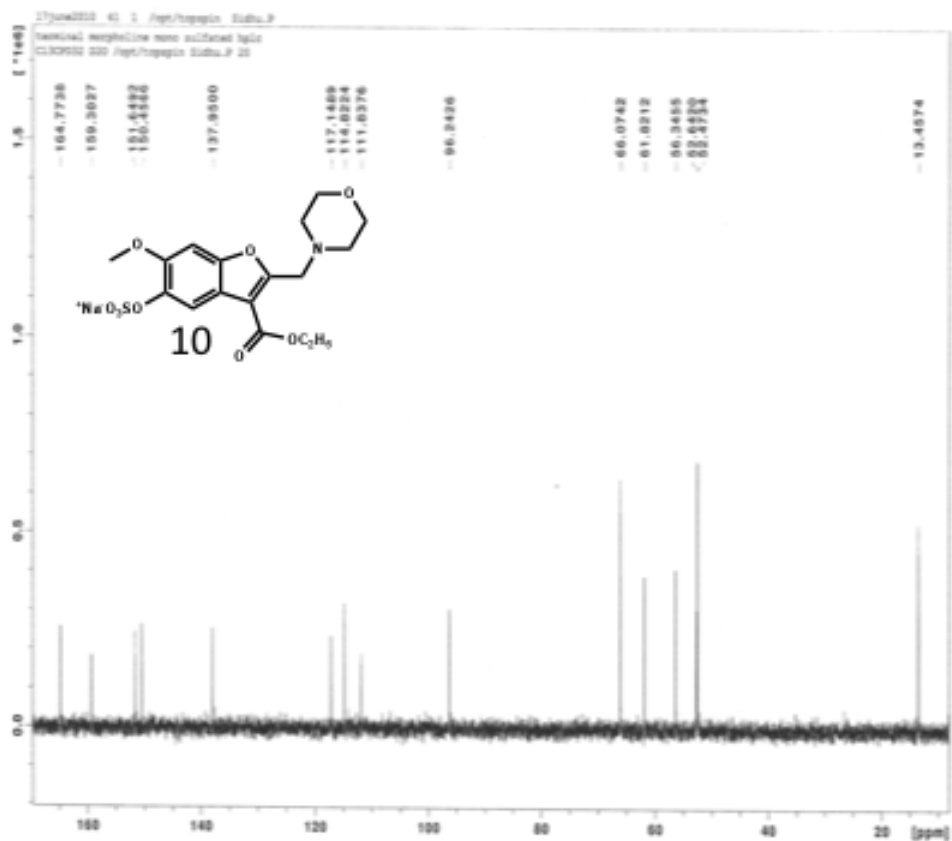
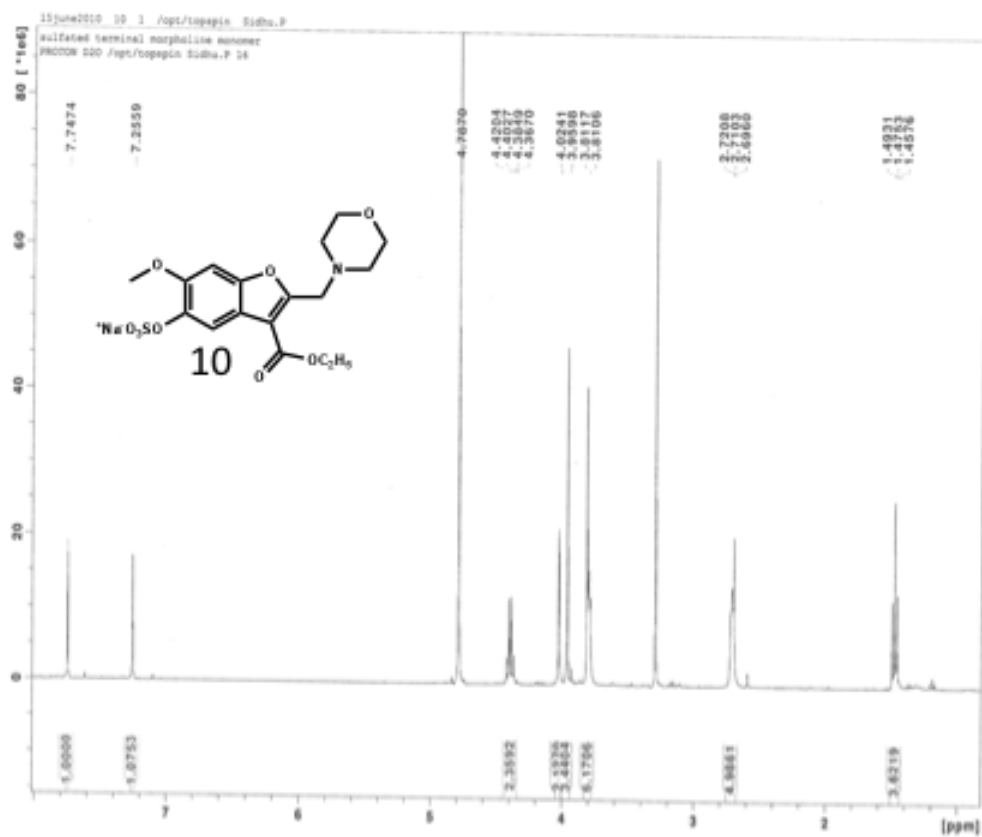
6



7





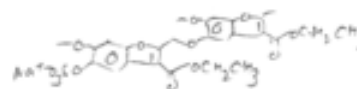


STANDARD 1H OBSERVE

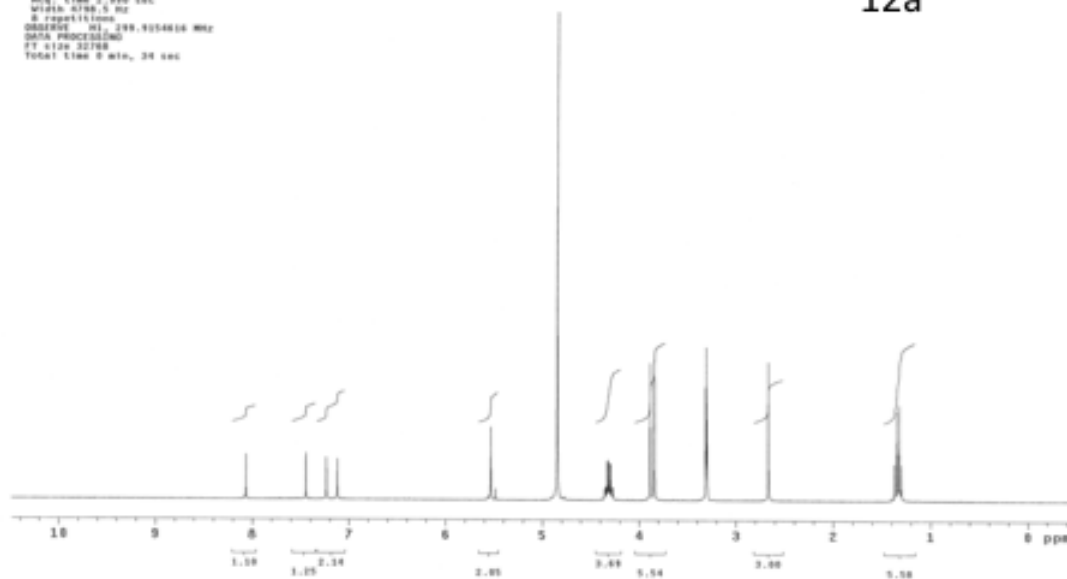
Archive directory: /export/home/ghou/chemsyn/data
Sample directory:
File: 765706

Pulse Sequence: zgpg30
Solvent: CD3OD
Acidic temperature
Mercury-2000B "NMJ300"

Relax. delay 1.000 sec
Pulse 45.0 degrees
Acq. time 2.700 sec
Width 4198.5 Hz
S repetitions
OBSERVE F1, 299.9254616 MHz
DATA PROCESSING
FT size 32768
Total time 0 min, 24 sec



12a

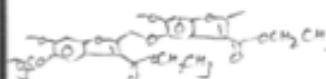


13C OBSERVE

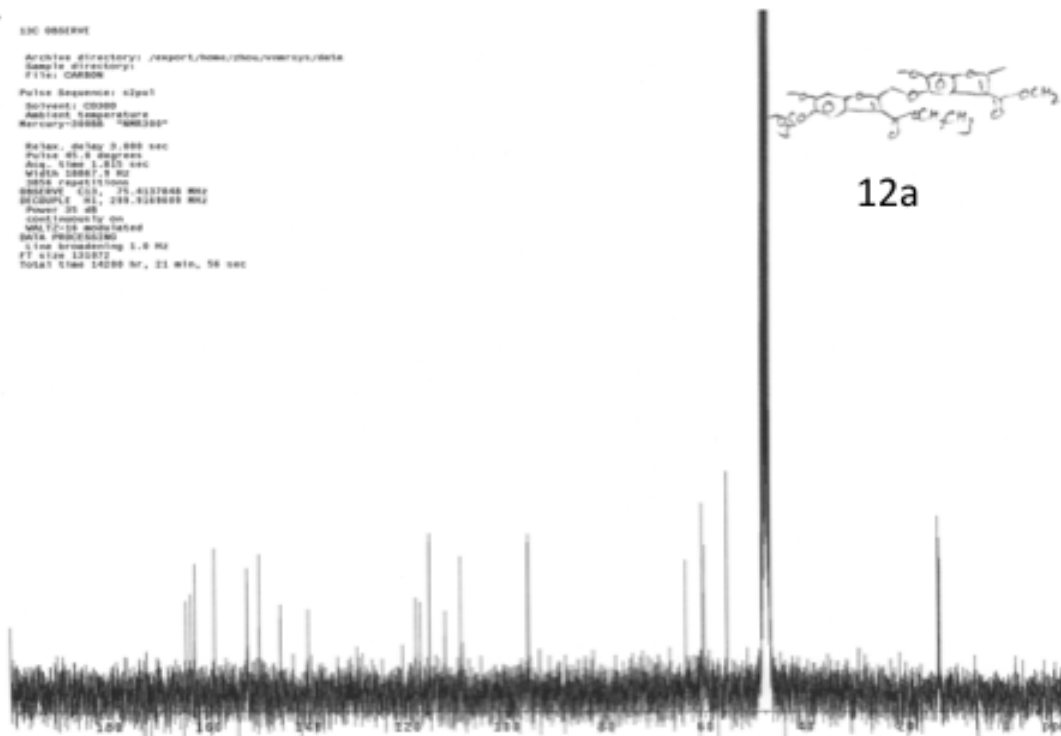
Archive directory: /export/home/ghou/chemsyn/data
Sample directory:
File: 765706

Pulse Sequence: zgpg30
Solvent: CD3OD
Acidic temperature
Mercury-2000B "NMJ300"

Relax. delay 3.000 sec
Pulse 45.0 degrees
Acq. time 1.510 sec
Width 20867.0 Hz
S repetitions
OBSERVE F1, 75.4127648 MHz
PCouple F2, 299.9254616 MHz
Power 35 dB
continuously on
NUC12-16 modulated
DATA PROCESSING
Line broadening 1.0 Hz
FT size 131072
Total time 14209 hr, 21 min, 56 sec



12a

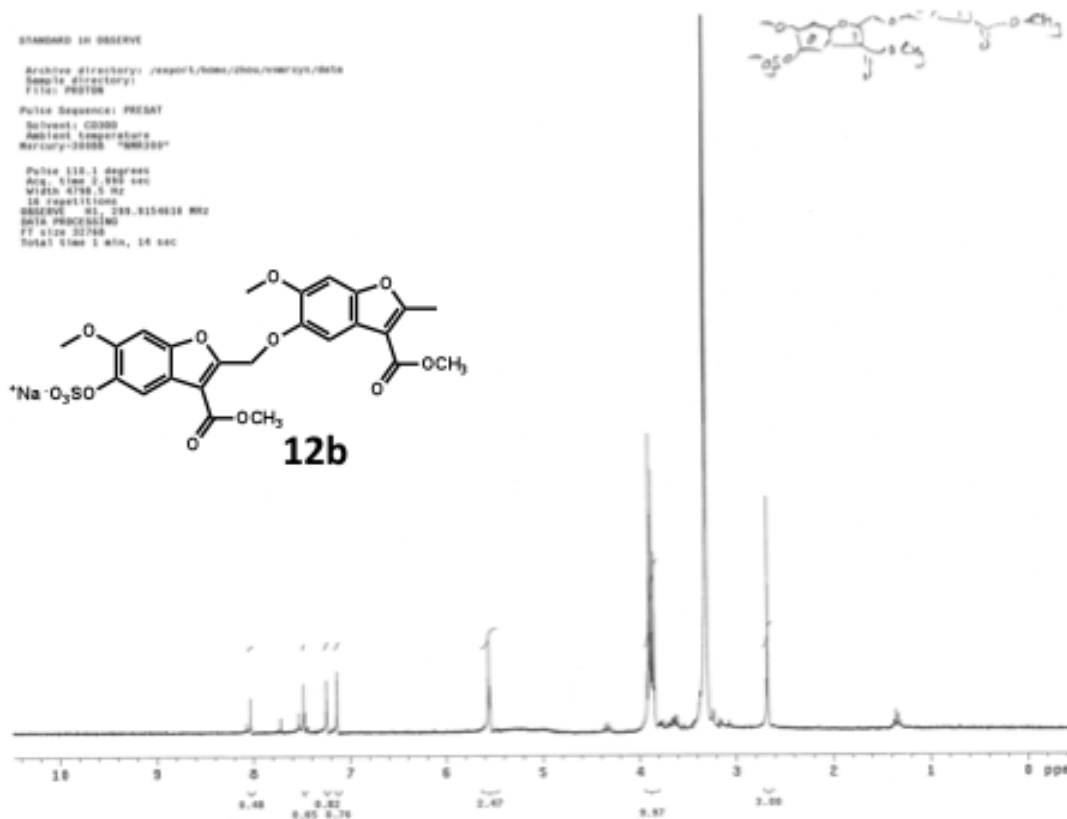
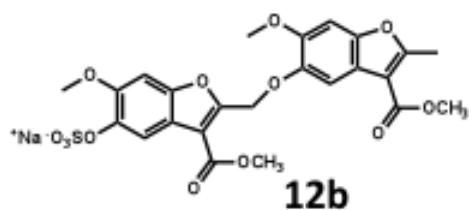


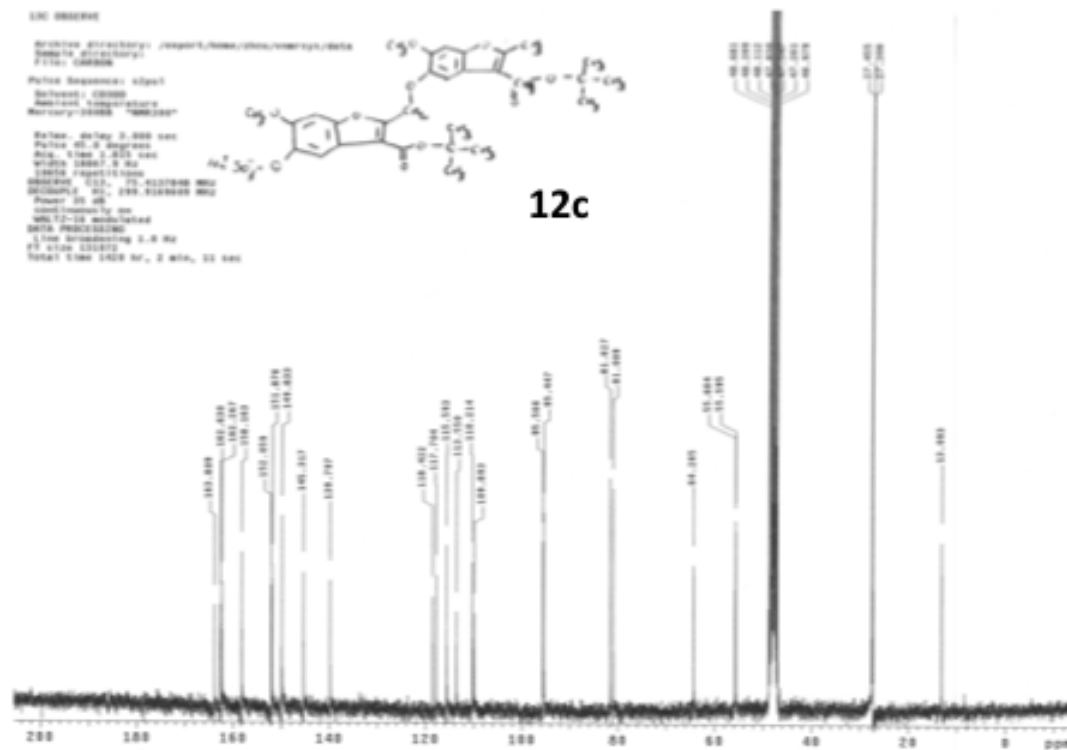
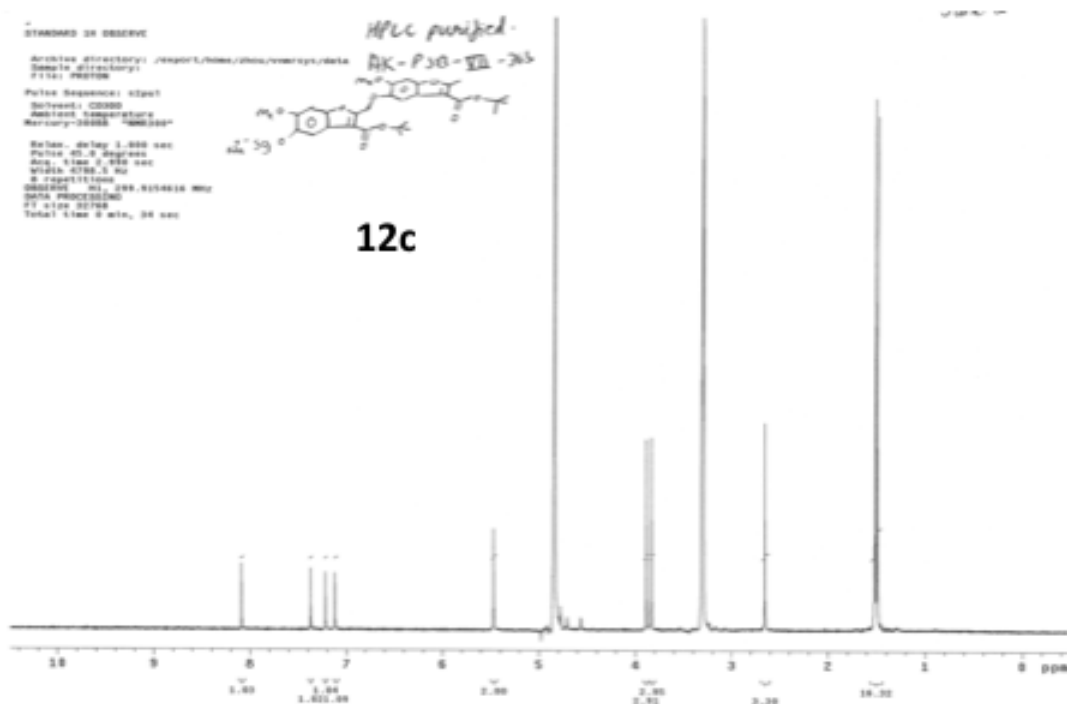
STANDARD IN OBSERVE

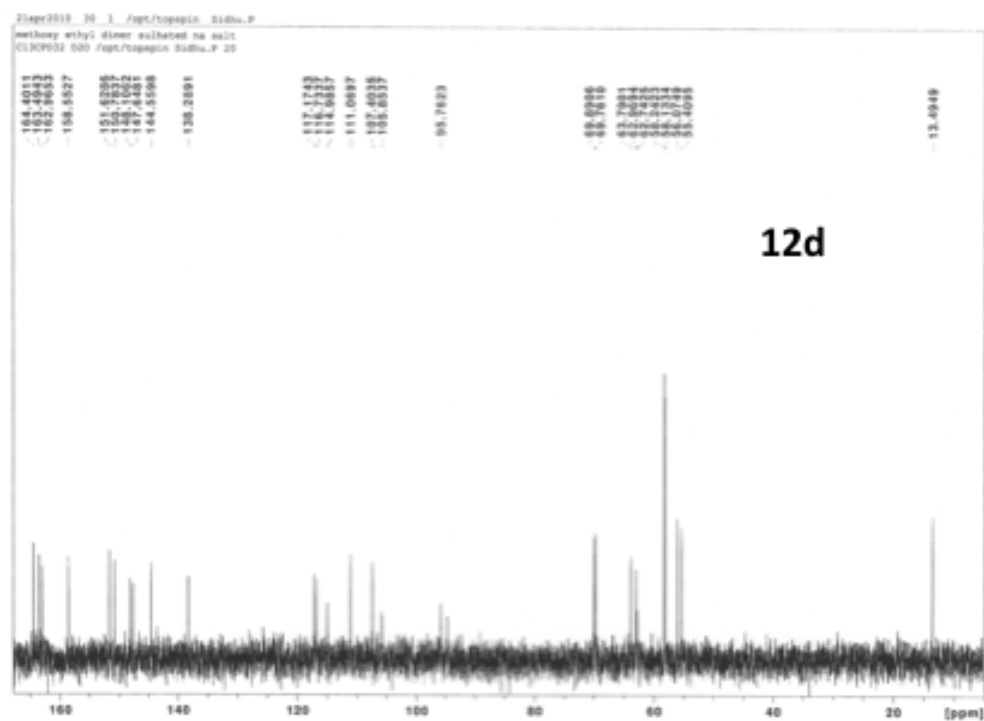
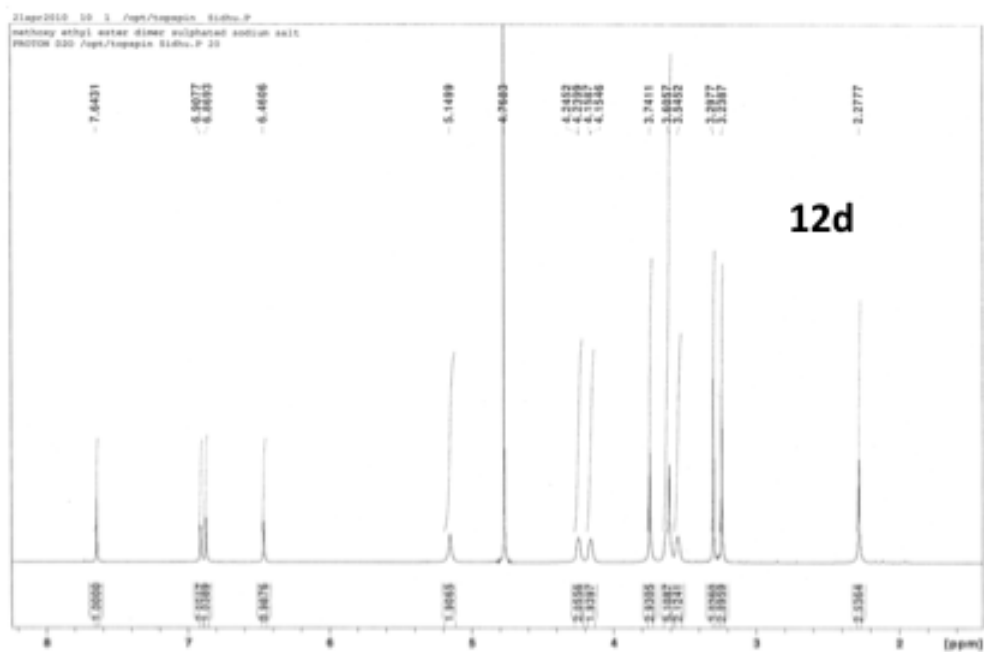
Archive directory: /export/home/chem/mercury/data
Sample directory:
File: PR0106

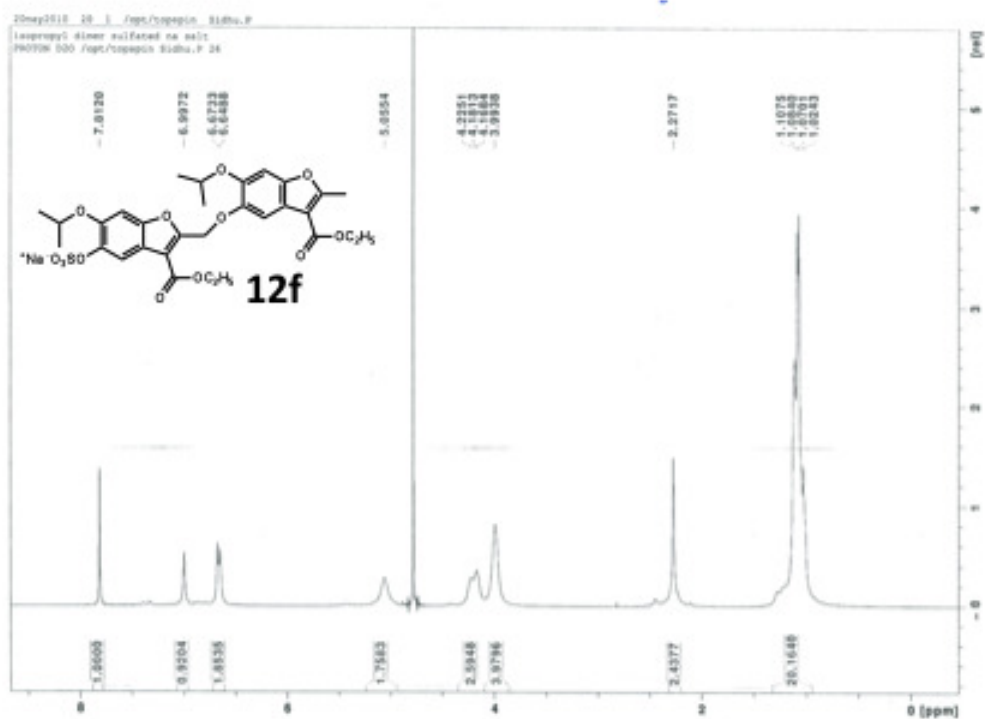
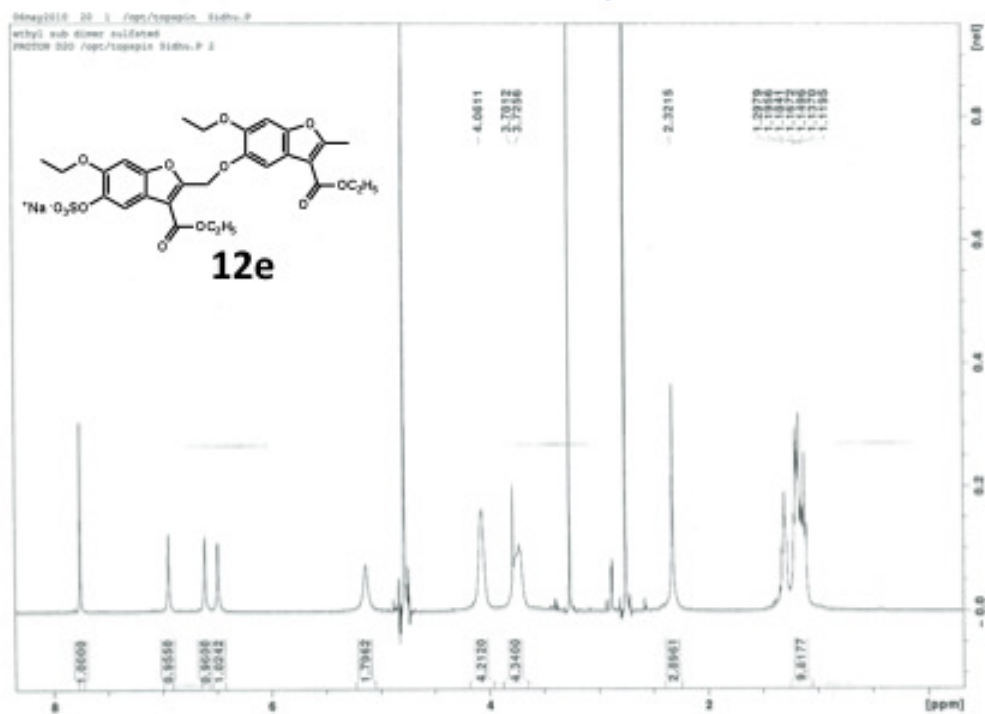
Pulse Sequence: PRESAT
Solvent: CD3OD
Acquisition temperature
Mercury-3000B "NM3000"

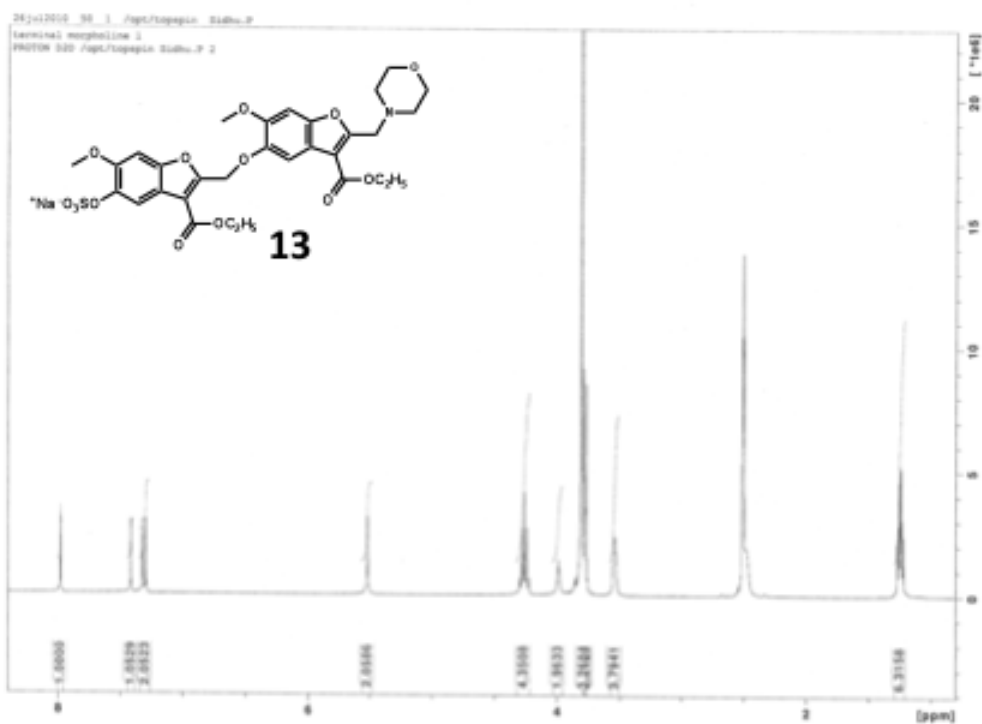
Pulse 110.1 degrees
Acq. time 0.940 sec
Width 4700.0 Hz
10 repetitions
OBSERVE: 31, 200.6150018 MHz
data PROCESSING
FT 0.120 22.740
TOTAL 0.960 1 min, 18 sec

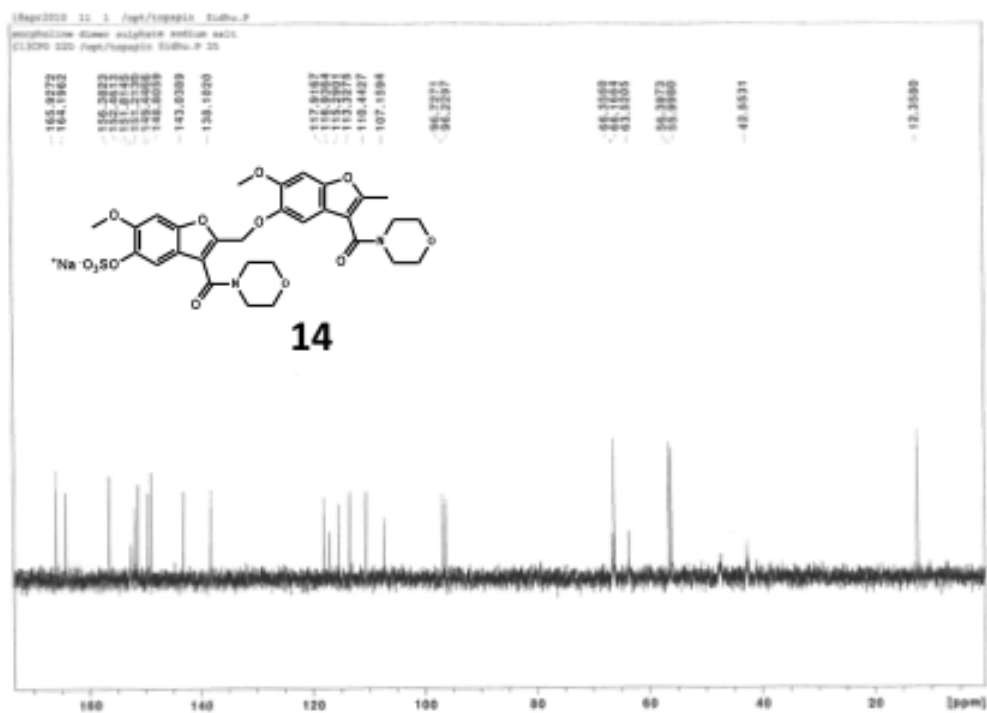
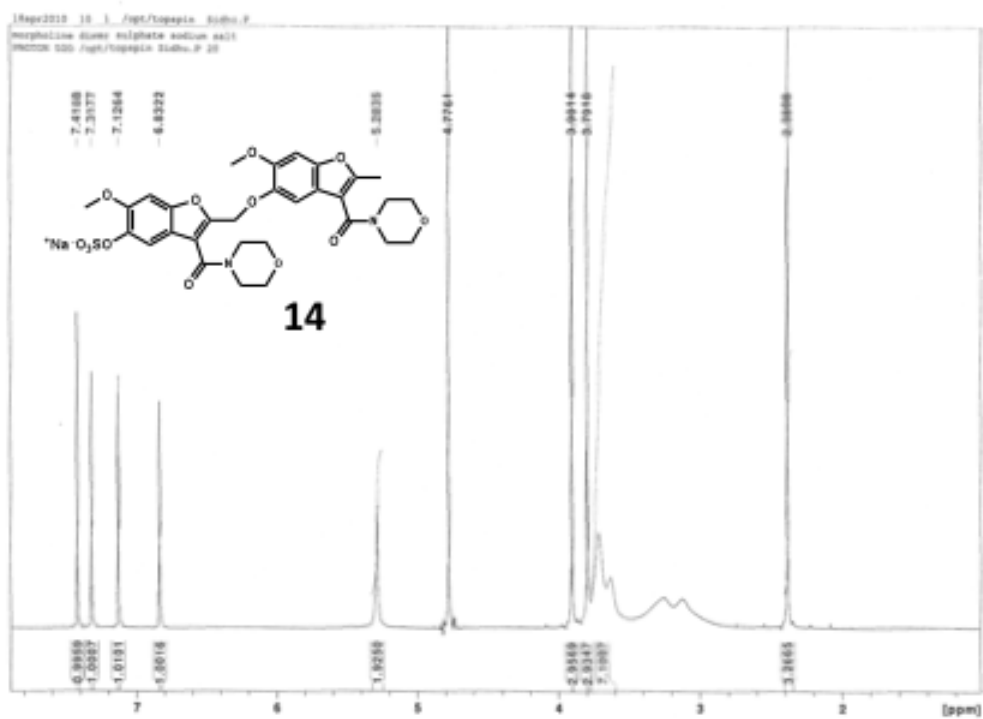












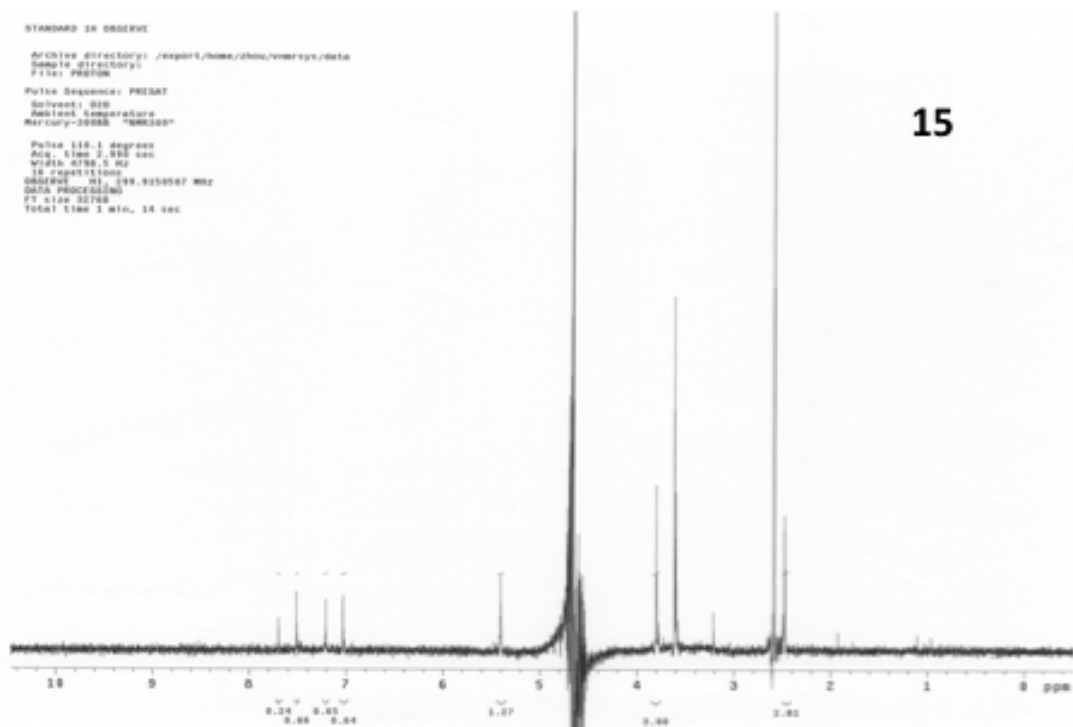
STANDARD 18 OBSERVE

Archive directory: /export/home/zhoul/vmrays/data
 Sample directory:
 File: PR0106

Pulse Sequence: PRISM7

Solvent: D2O
 Ambient temperature
 Mercury-200SD "NM0200"

Pulse 110.1 degrees
 Acq. time 2.955 sec
 Width 6788.3 Hz
 16 repetitions
 OBSERVE F1: 149.9155607 MHz
 DATA PROCESSING
 FT size 32768
 Total time 1 min, 14 sec



15

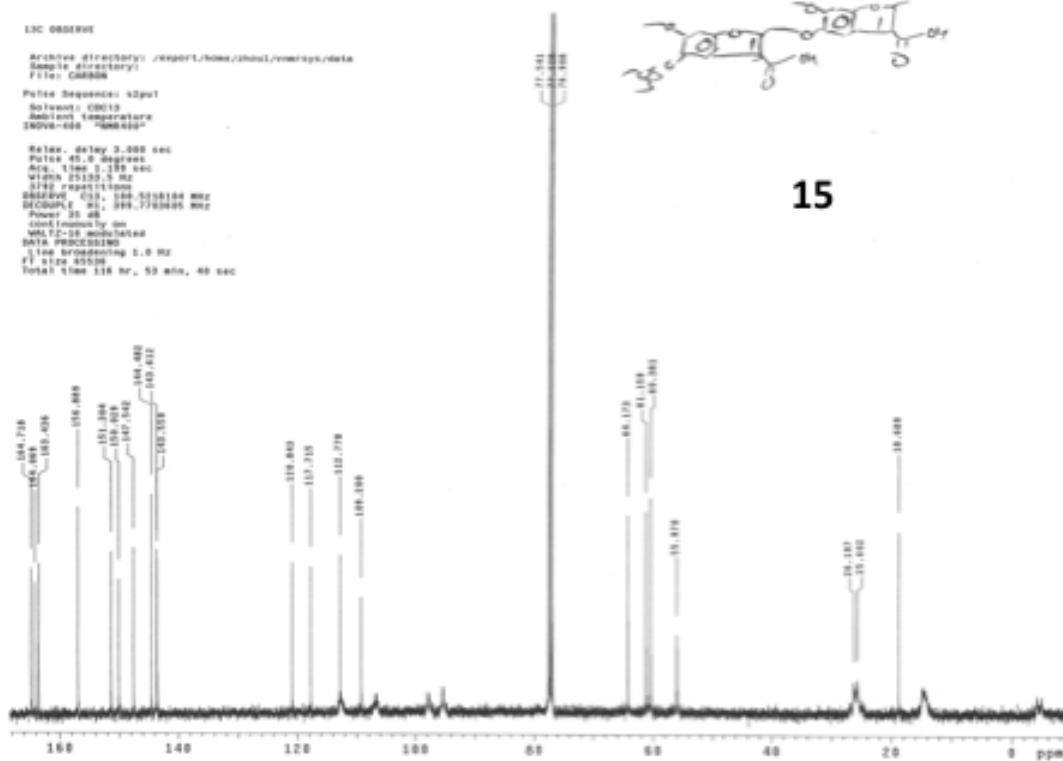
13C OBSERVE

Archive directory: /export/home/zhoul/vmrays/data
 Sample directory:
 File: C00006

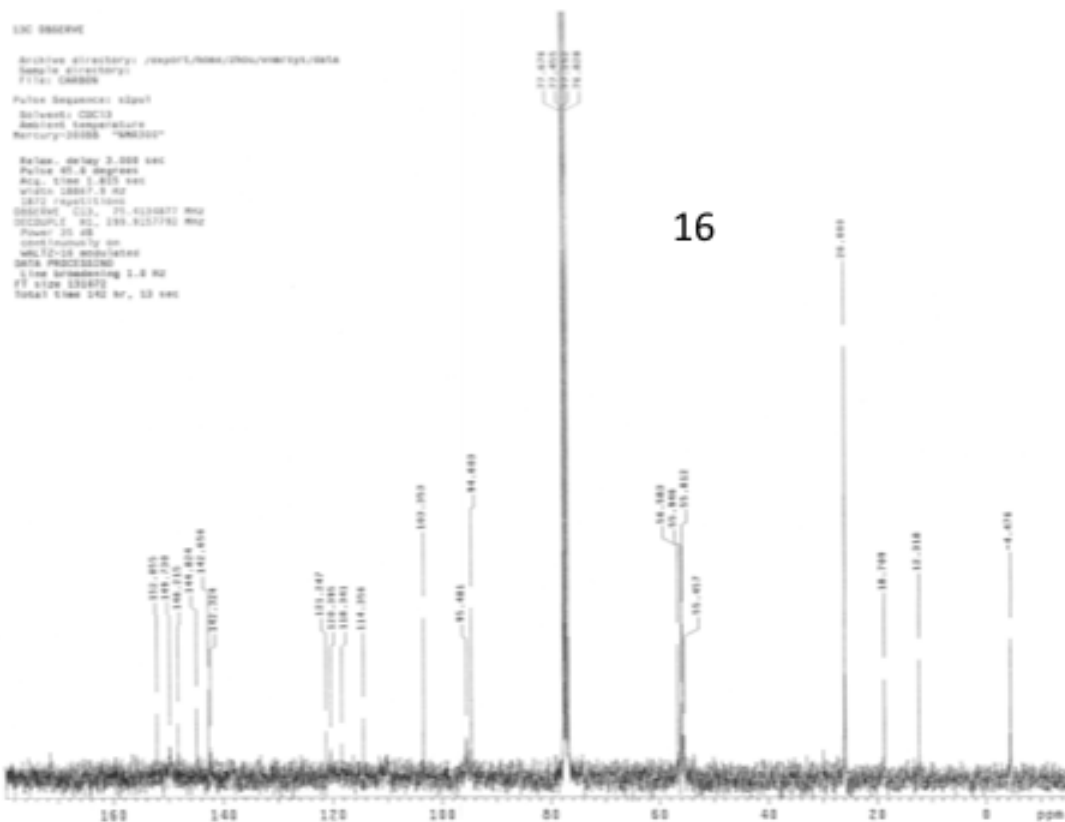
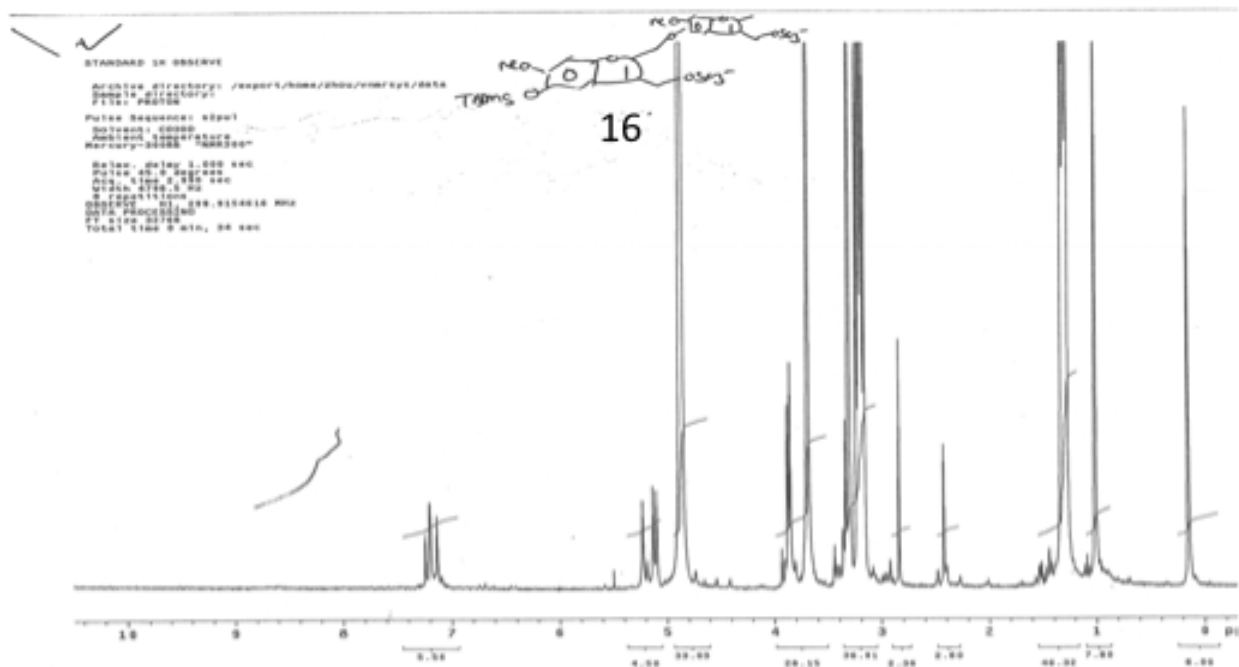
Pulse Sequence: zgpg30

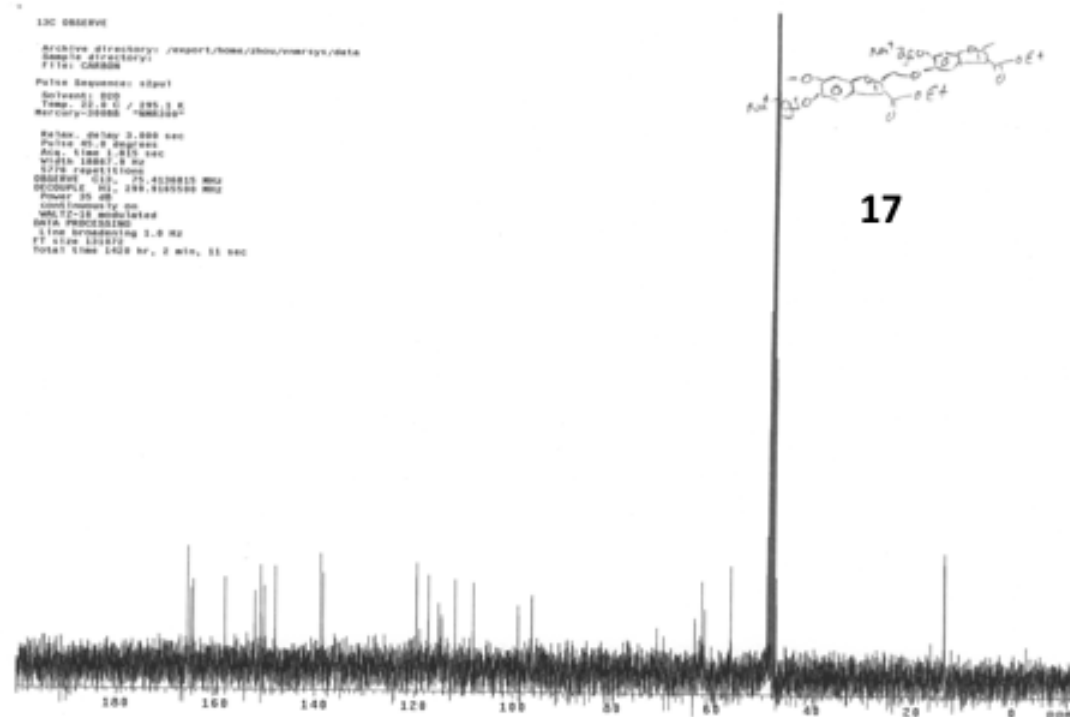
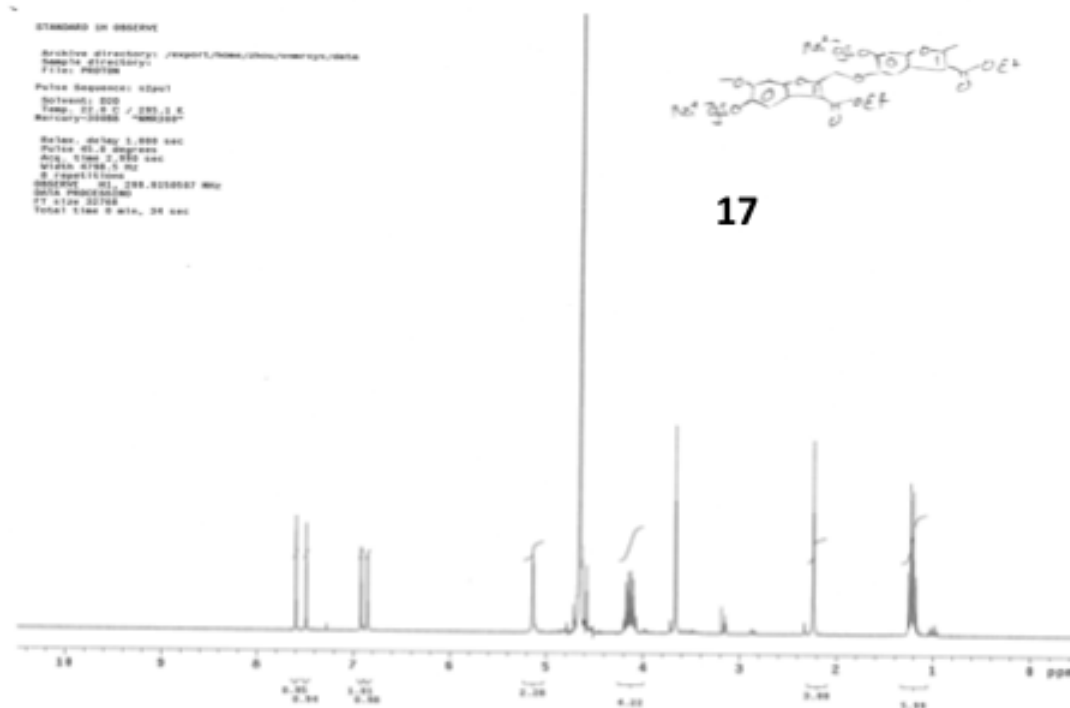
Solvent: CDCl3
 Ambient temperature
 SDDV-600 "NM0600"

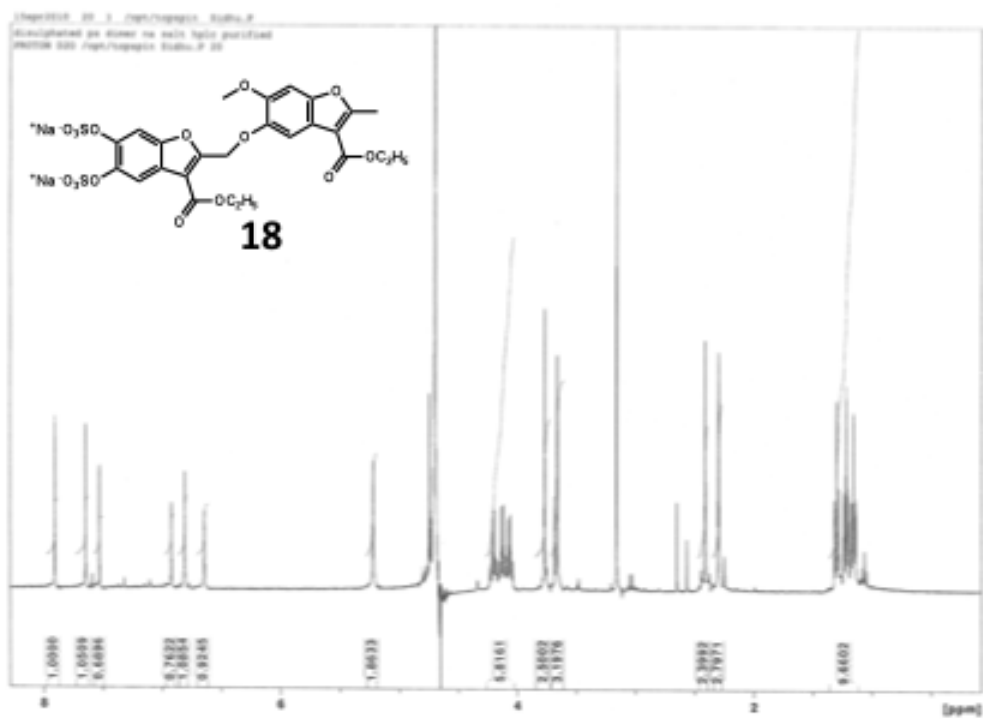
Relax. delay 3.000 sec
 Pulse 40.0 degrees
 Acq. time 1.189 sec
 Width 25133.3 Hz
 16 repetitions
 OBSERVE F1: 100.628164 MHz
 DECOUPLE F2: 149.720365 MHz
 Power 35 dB
 cond. manually on
 WALTZ-16 modulation
 DATA PROCESSING
 Line broadening 0.0 Hz
 FT size 45536
 Total time 118 hr, 53 min, 40 sec

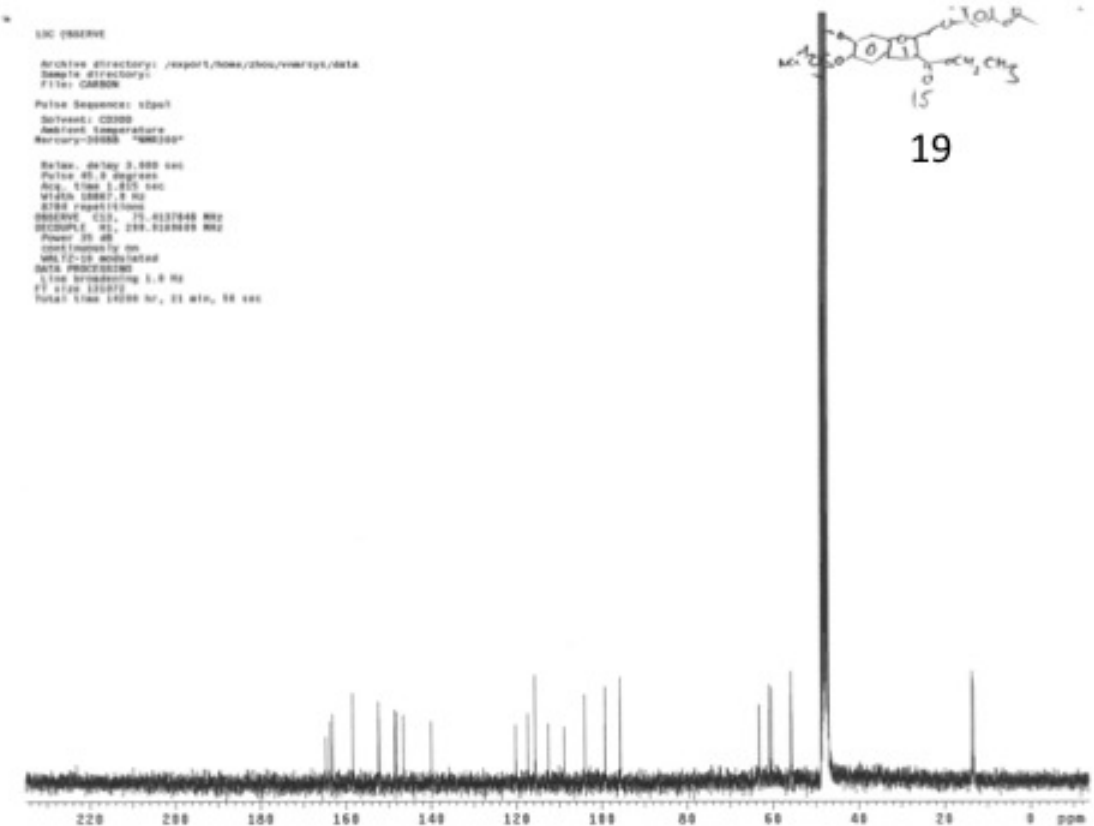
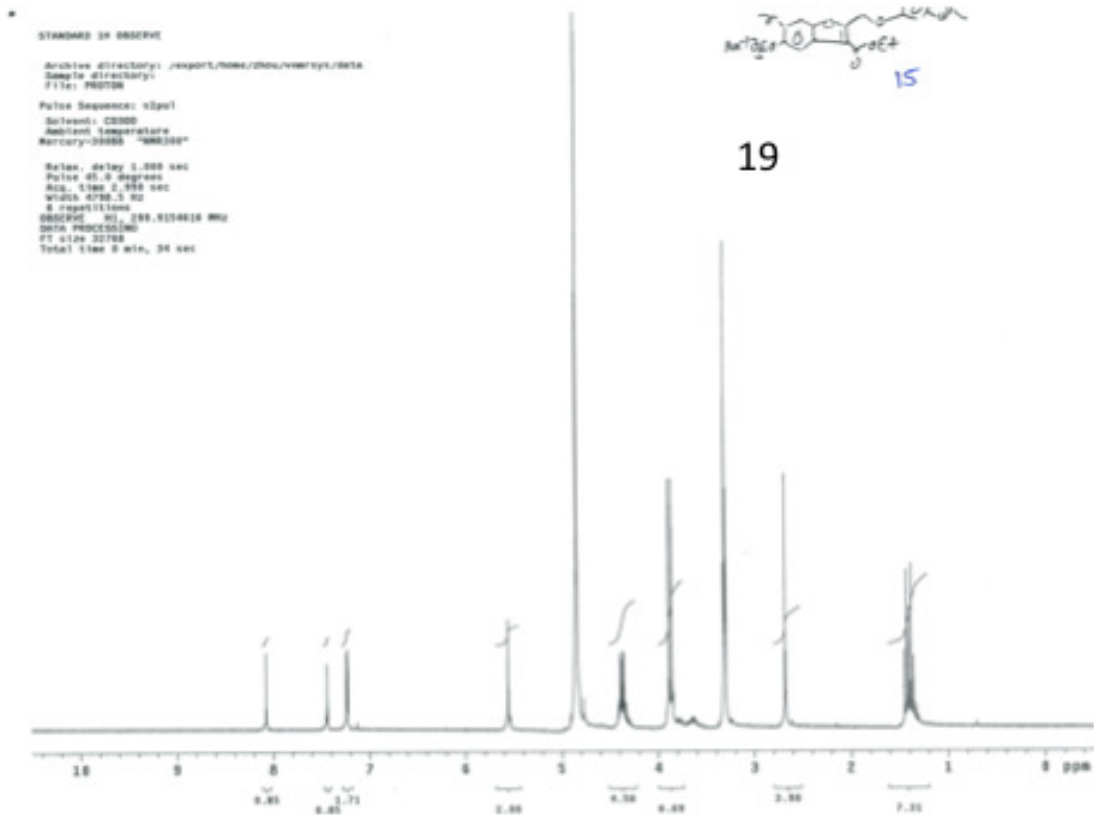


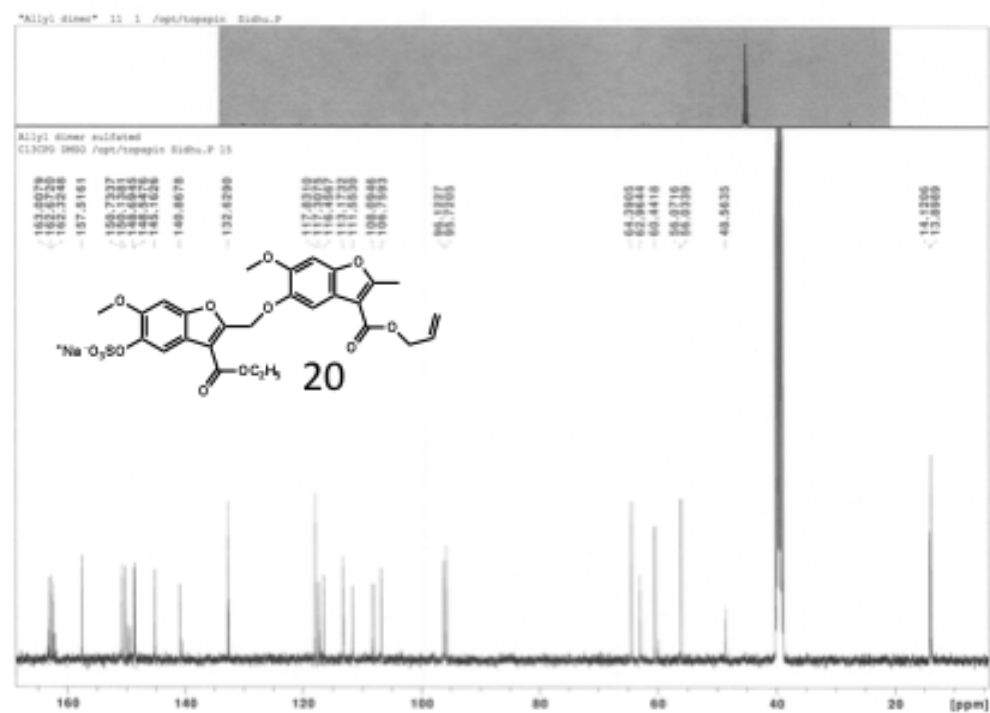
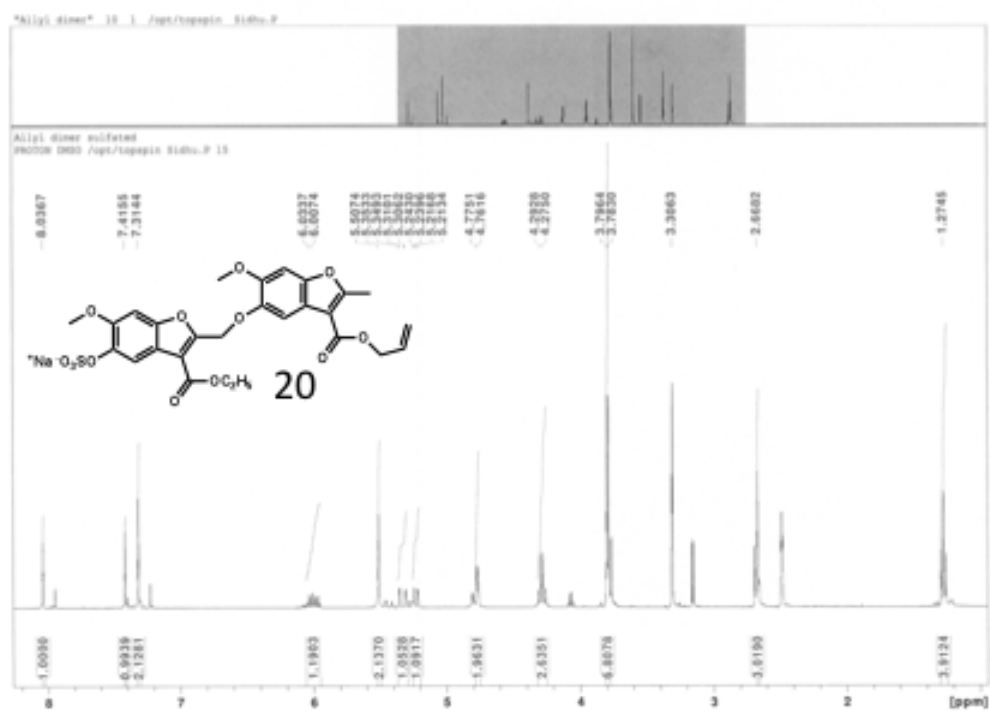
15







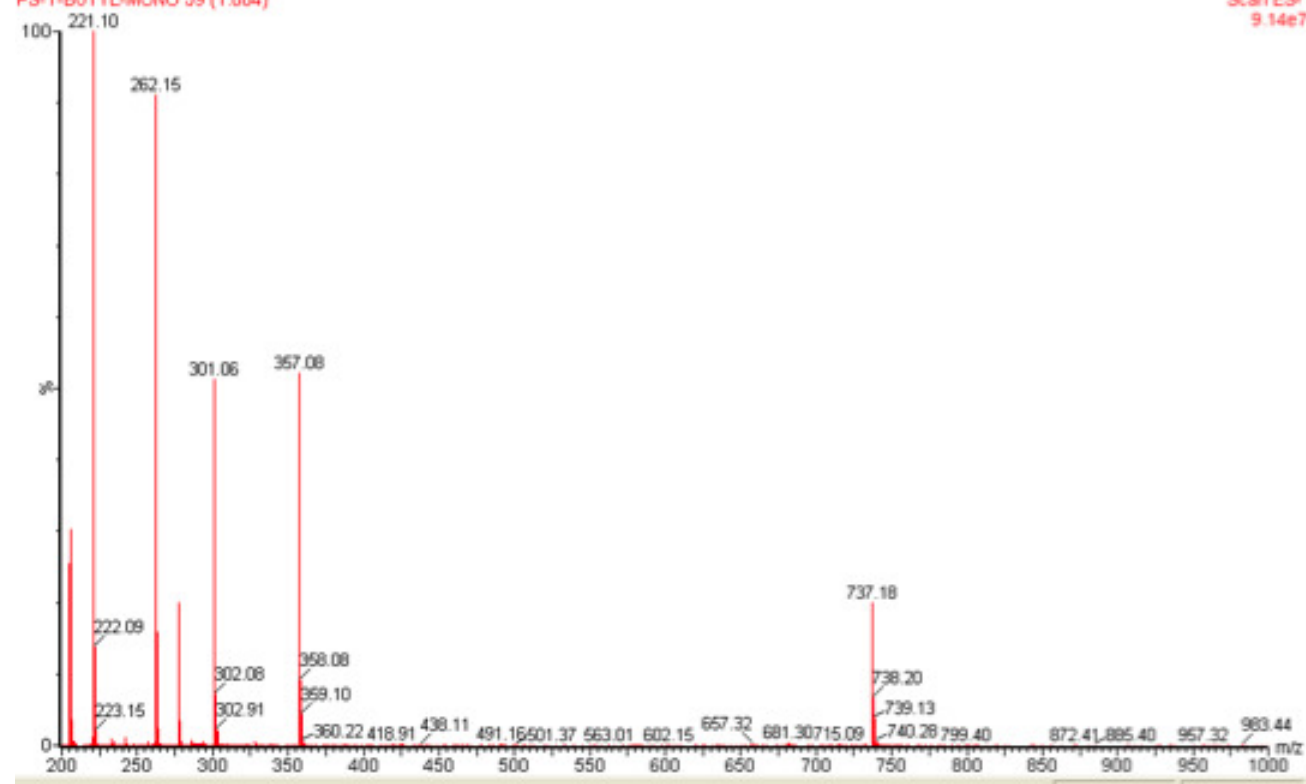




PS-T-BUTYL-MONO

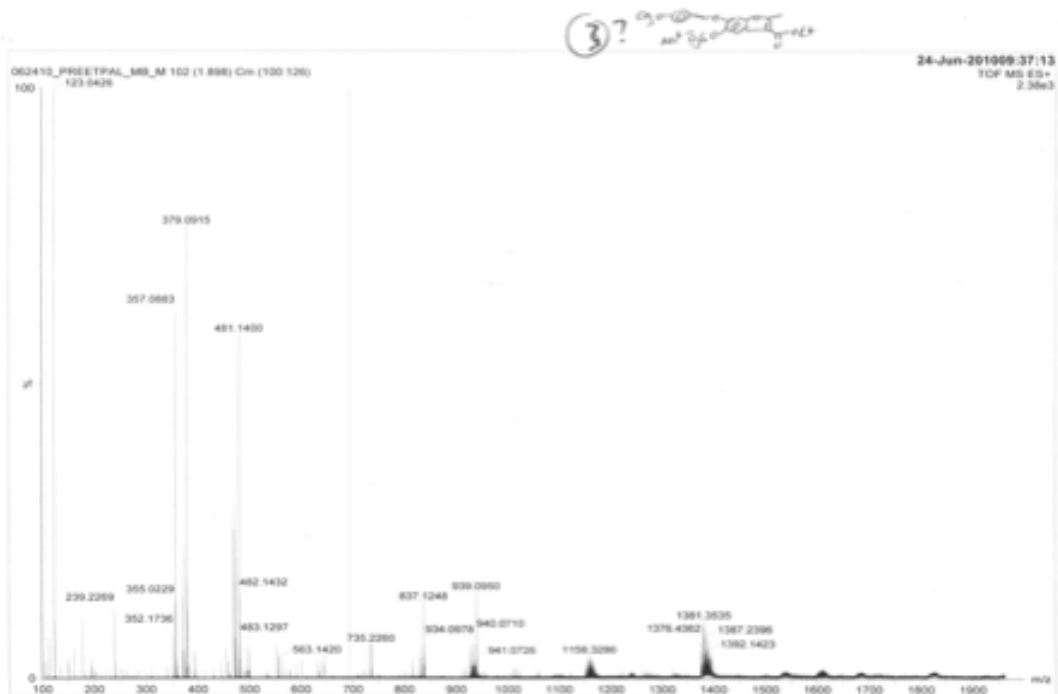
PS-T-BUTYL-MONO 59 (1.004)

Scan ES-
9.14e7



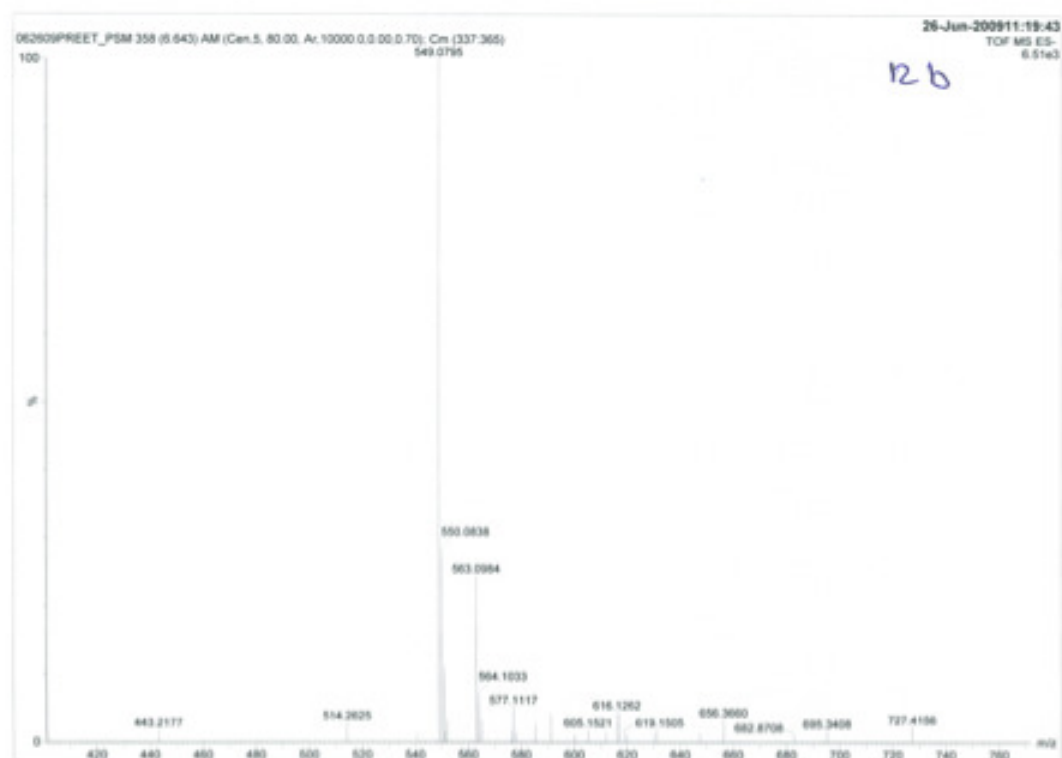
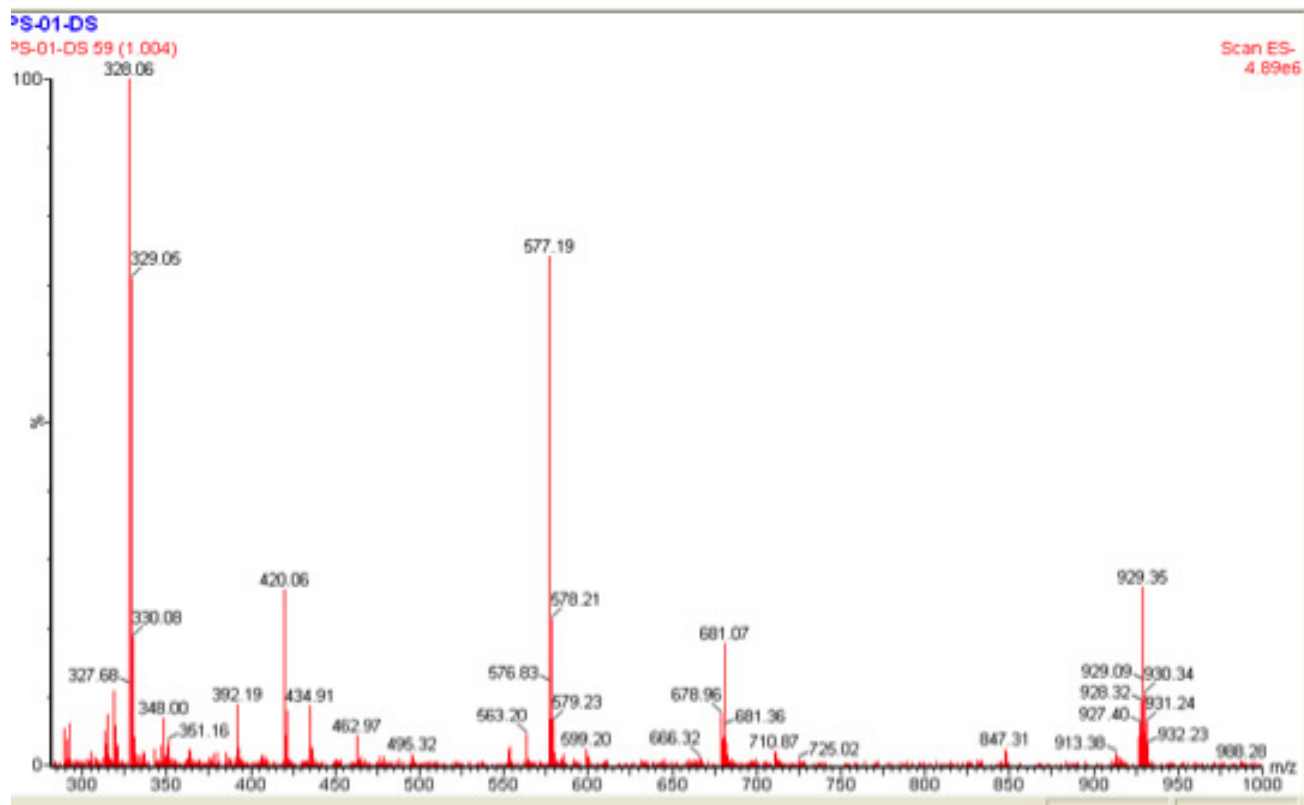


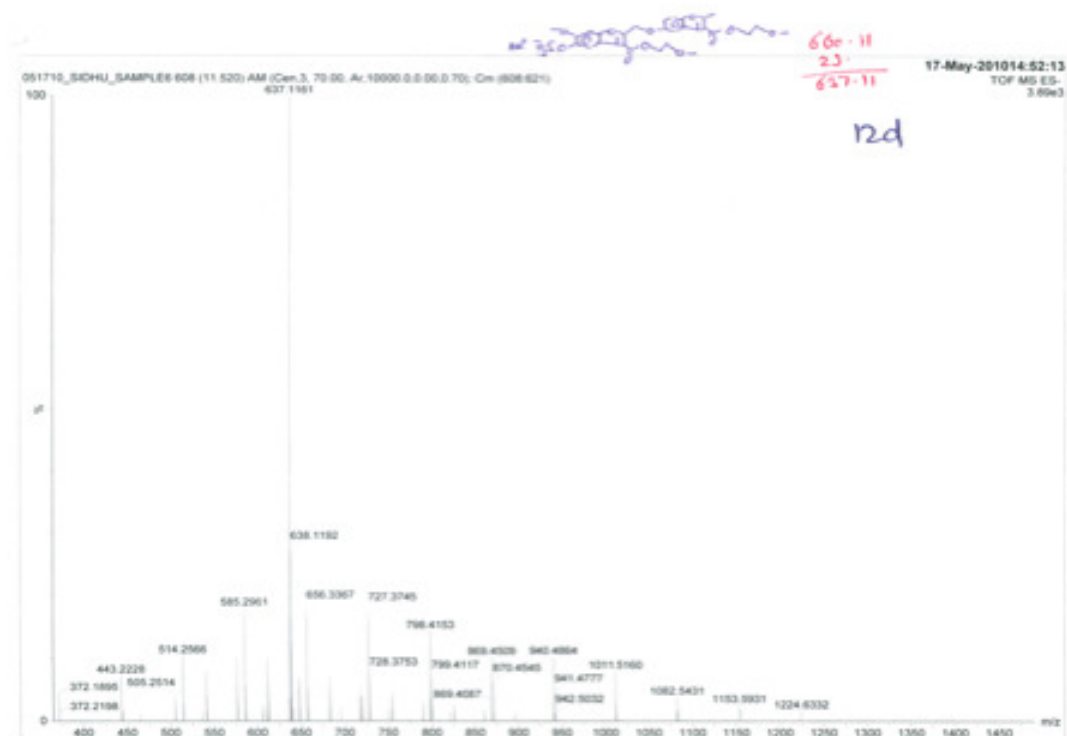
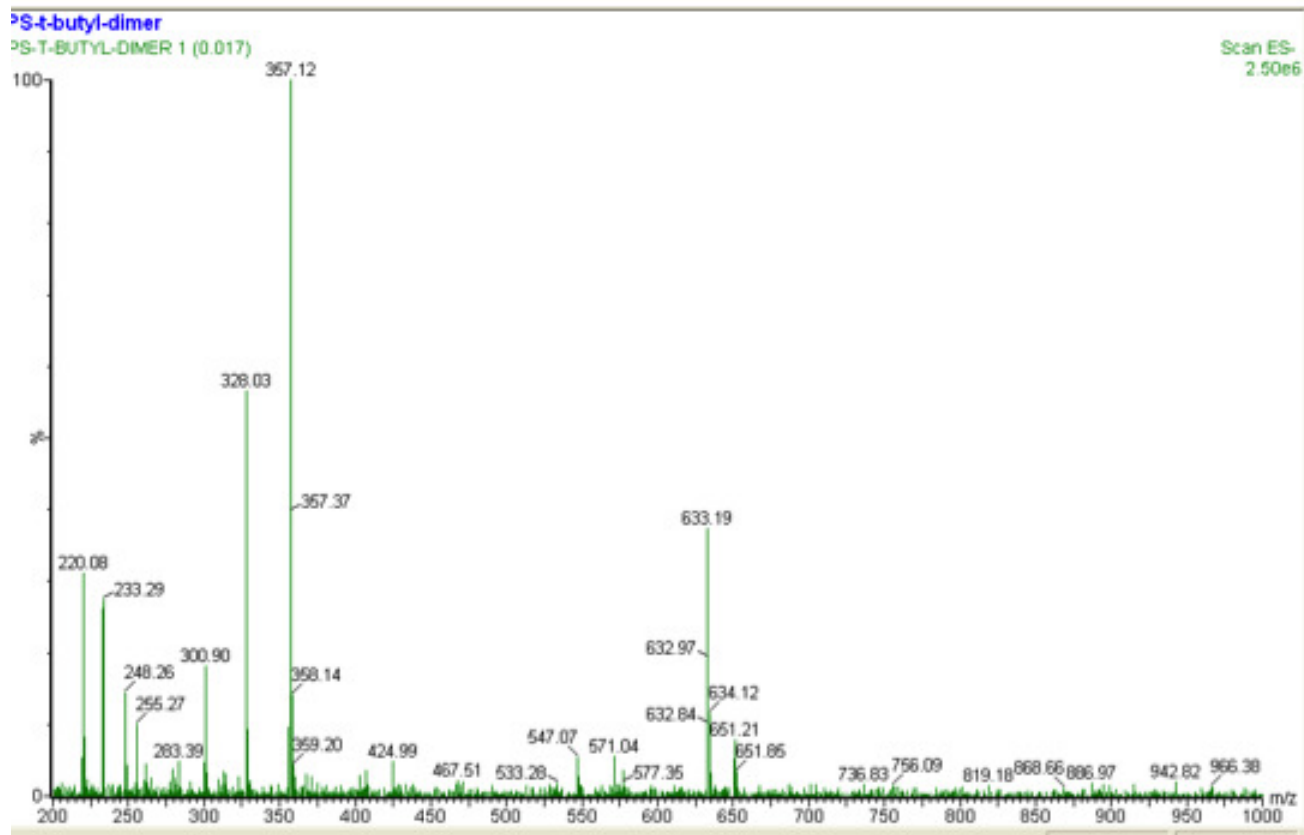


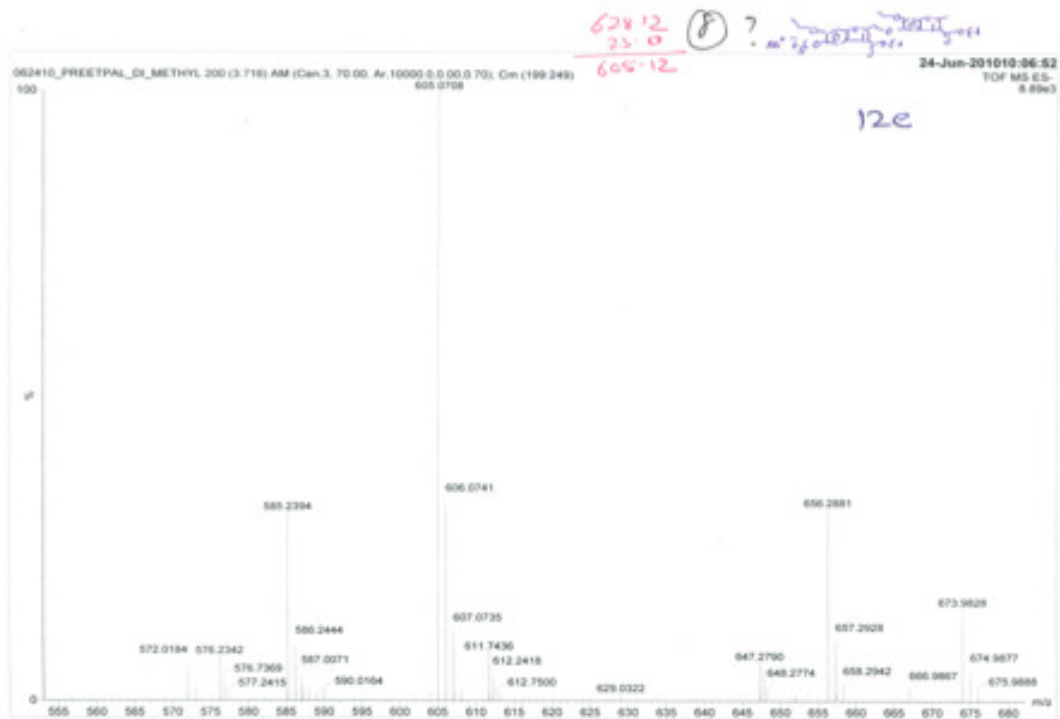


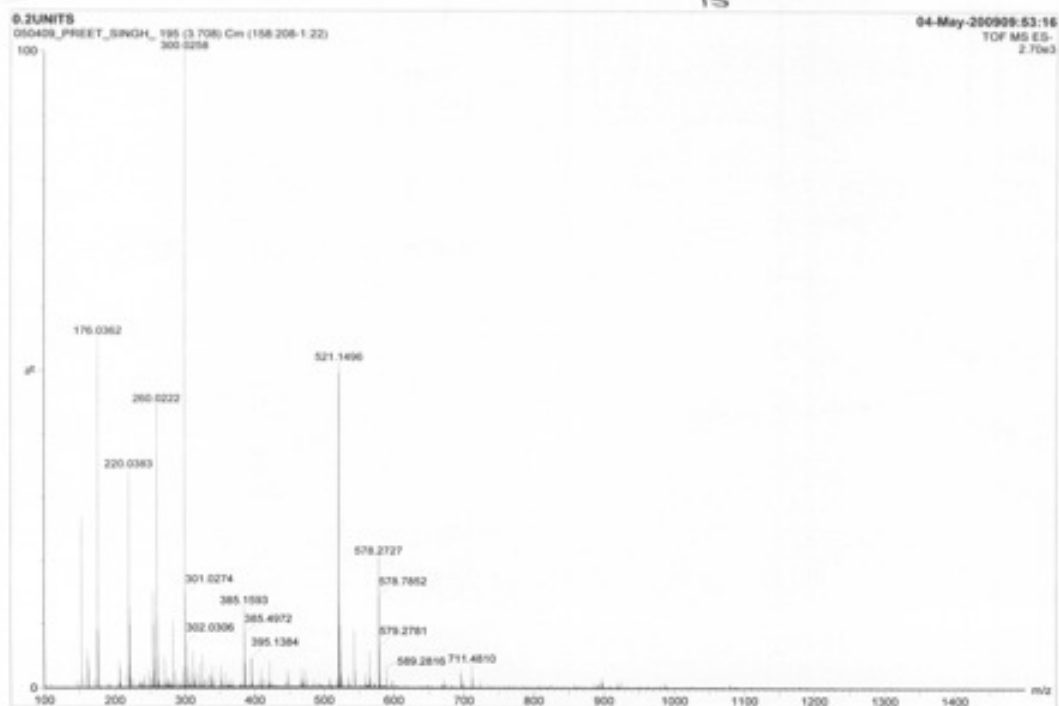


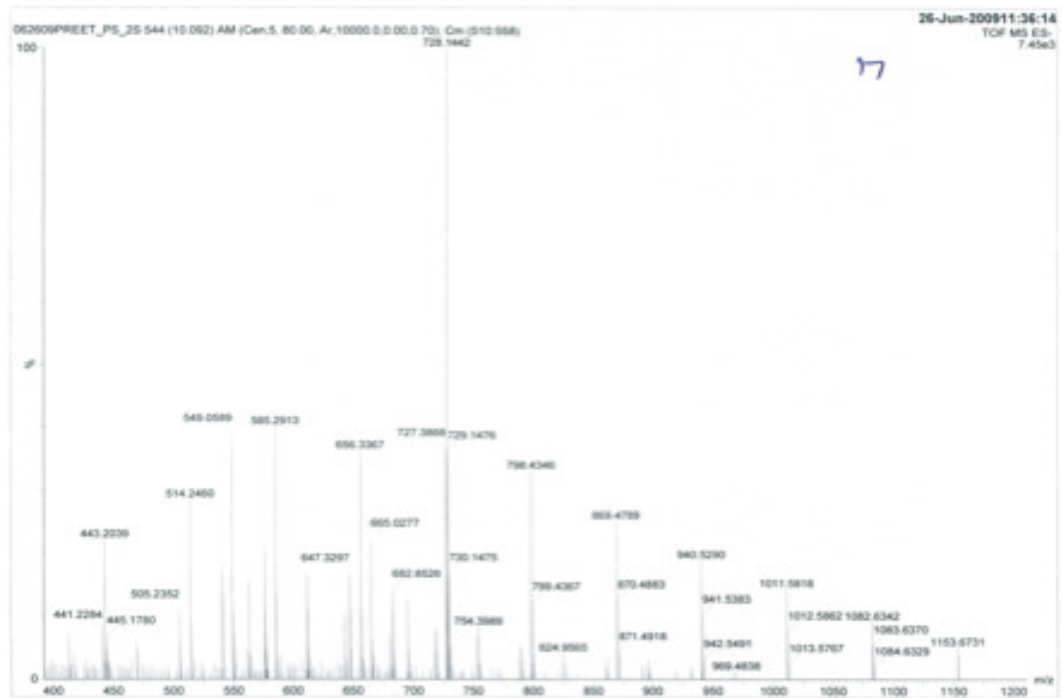


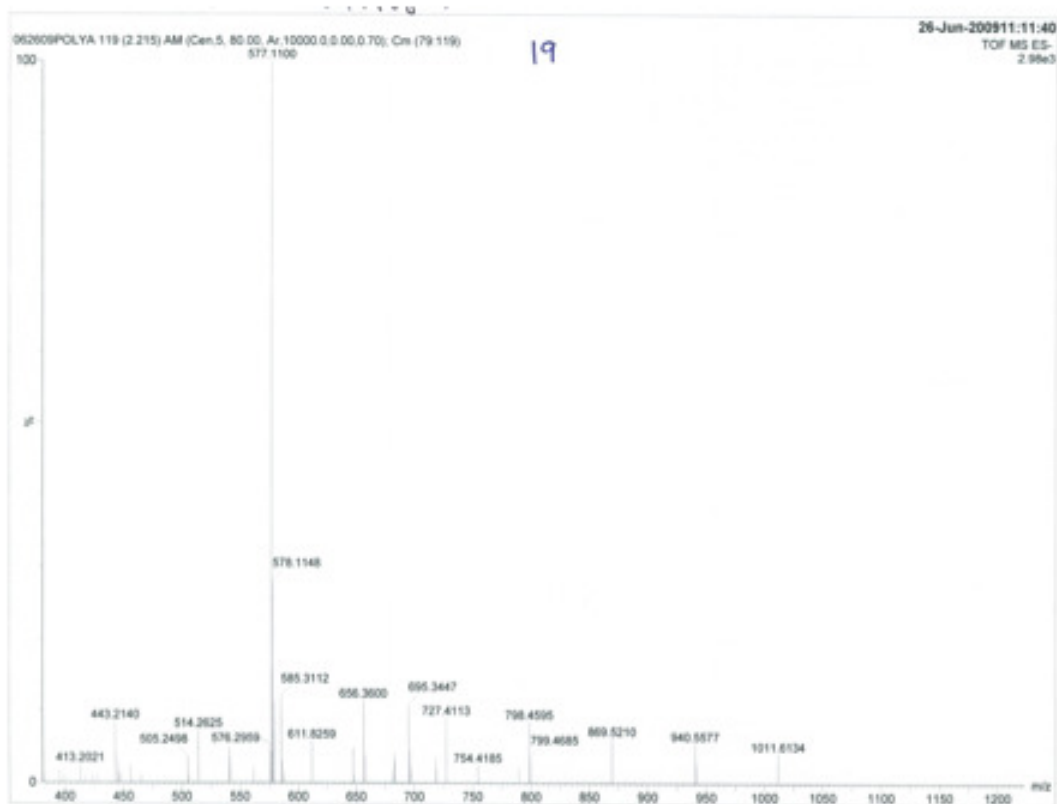


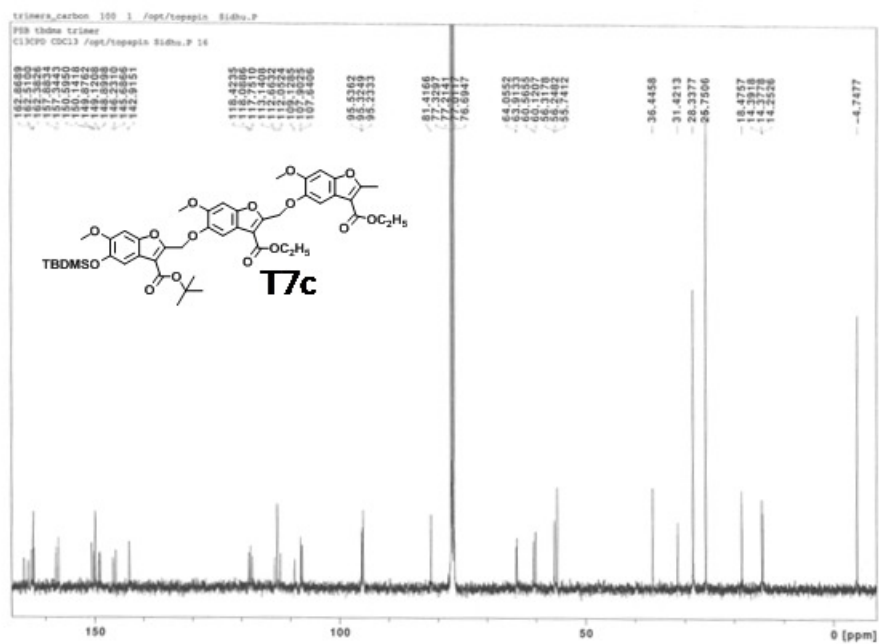
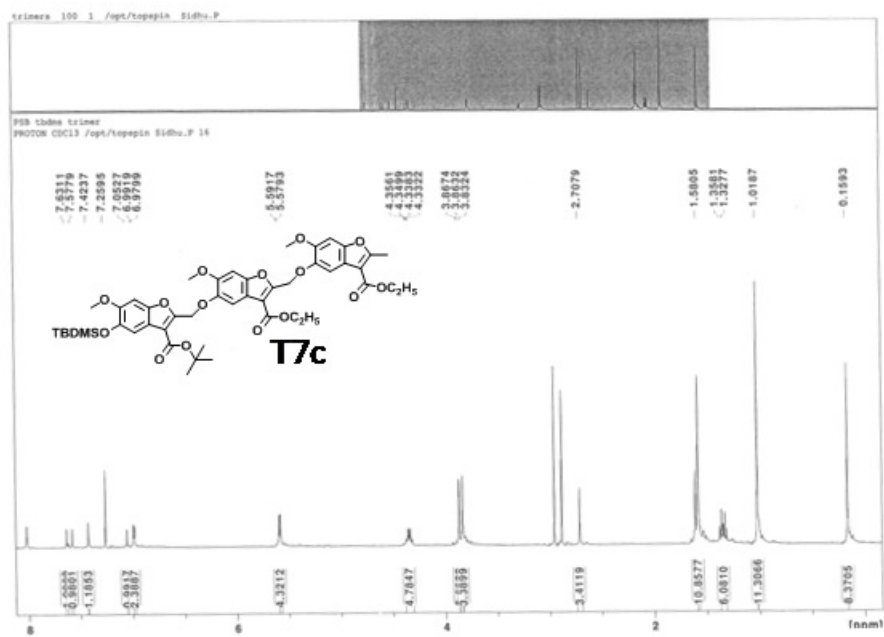


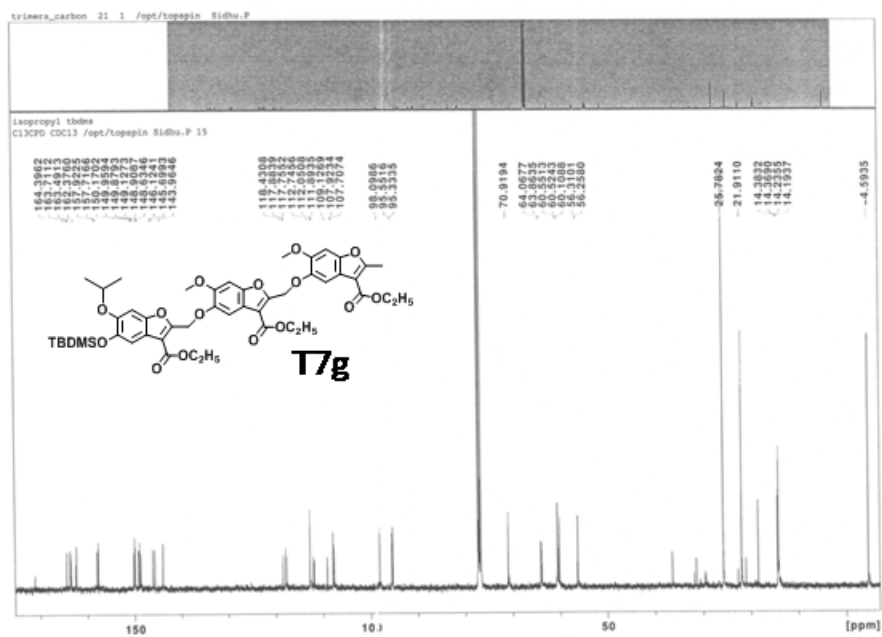
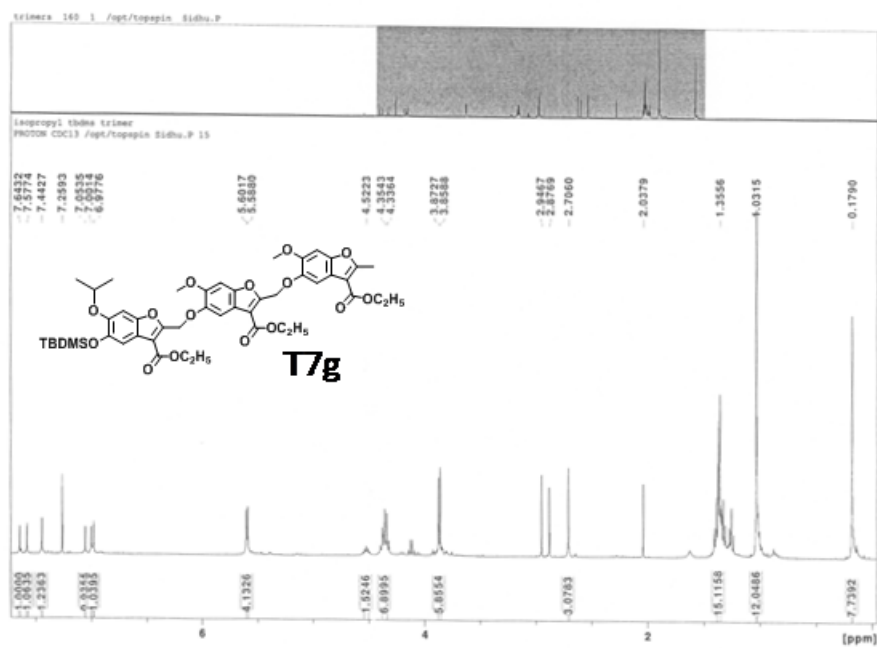


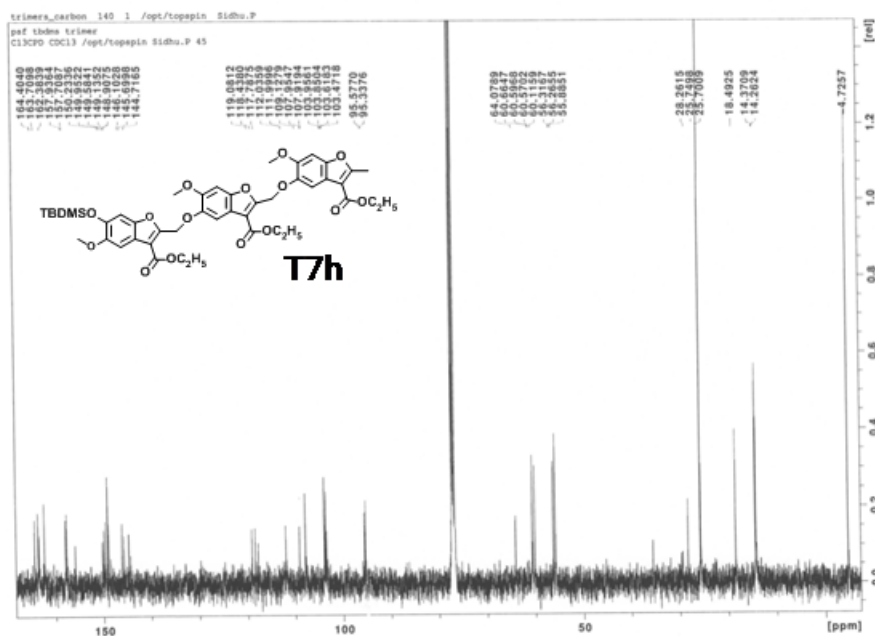
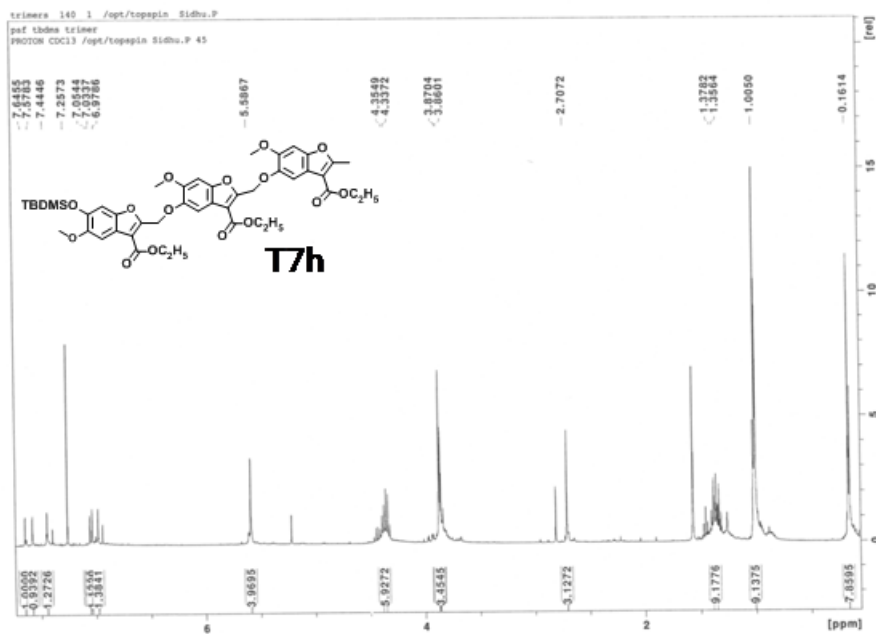


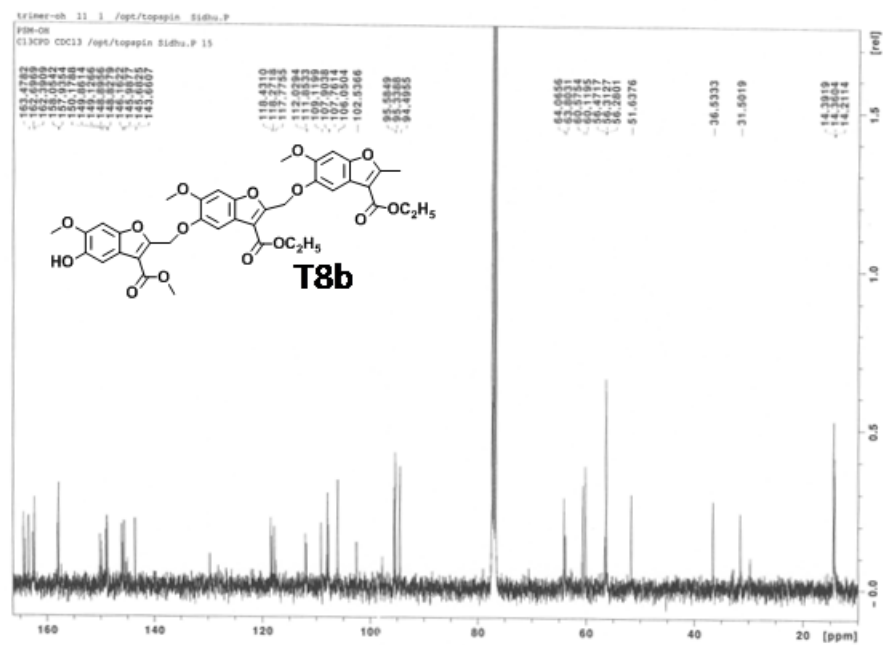
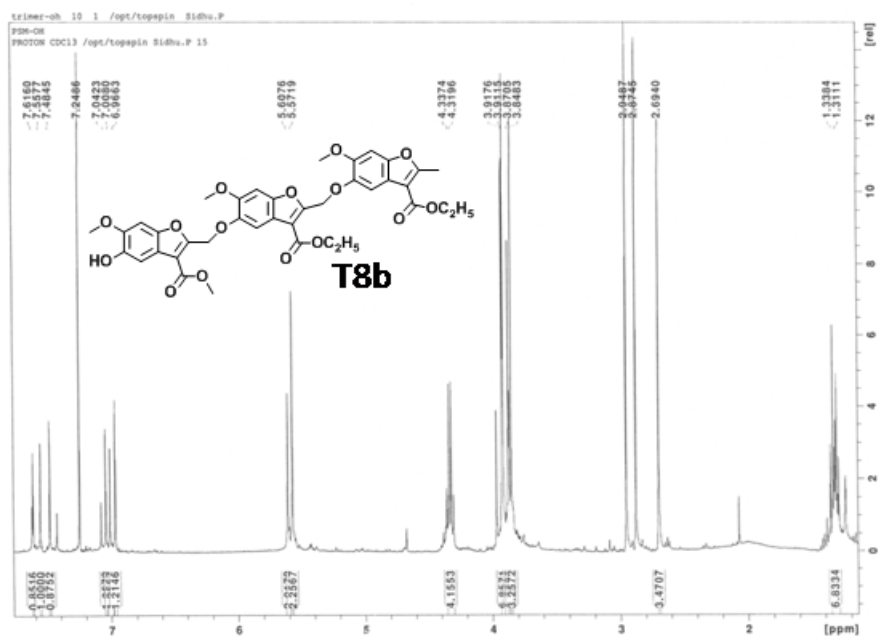


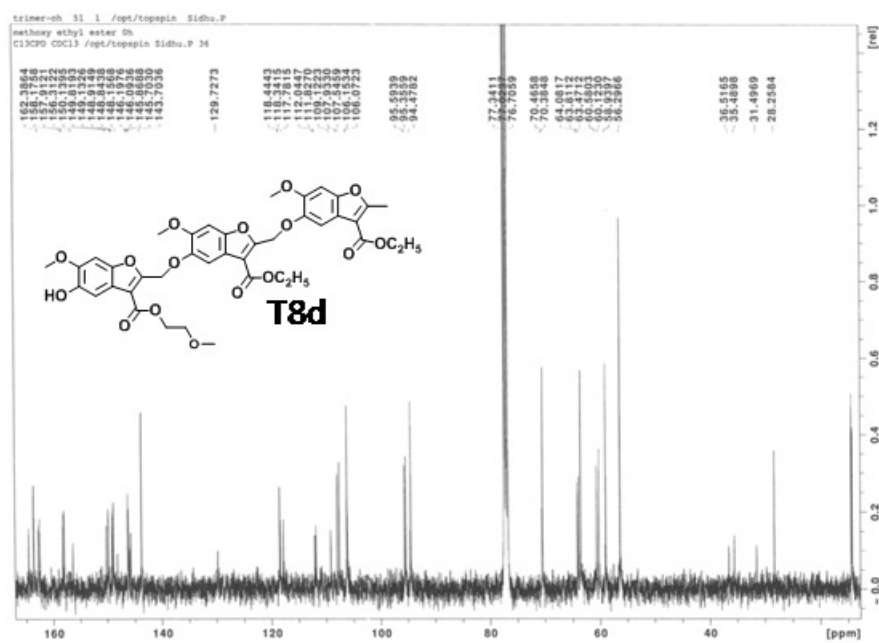
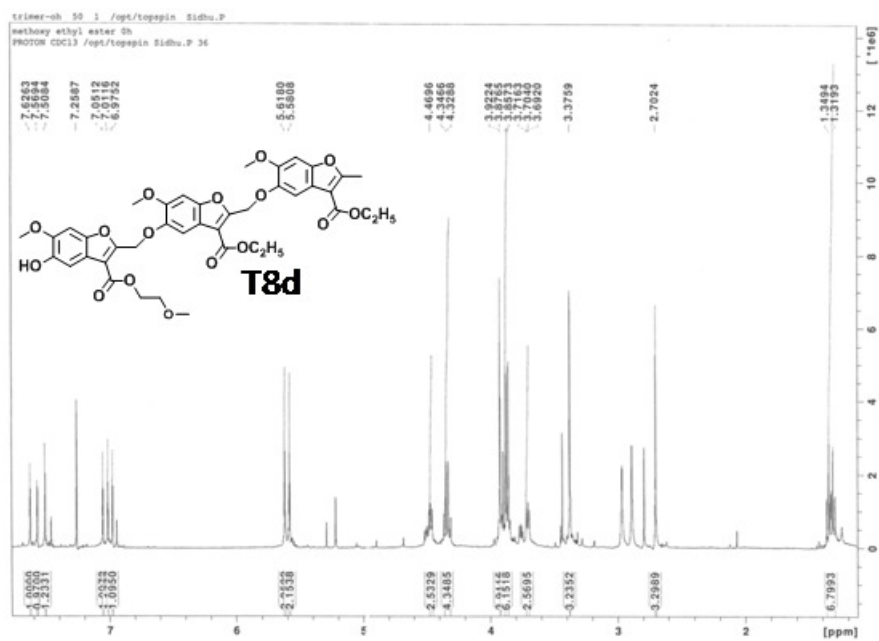


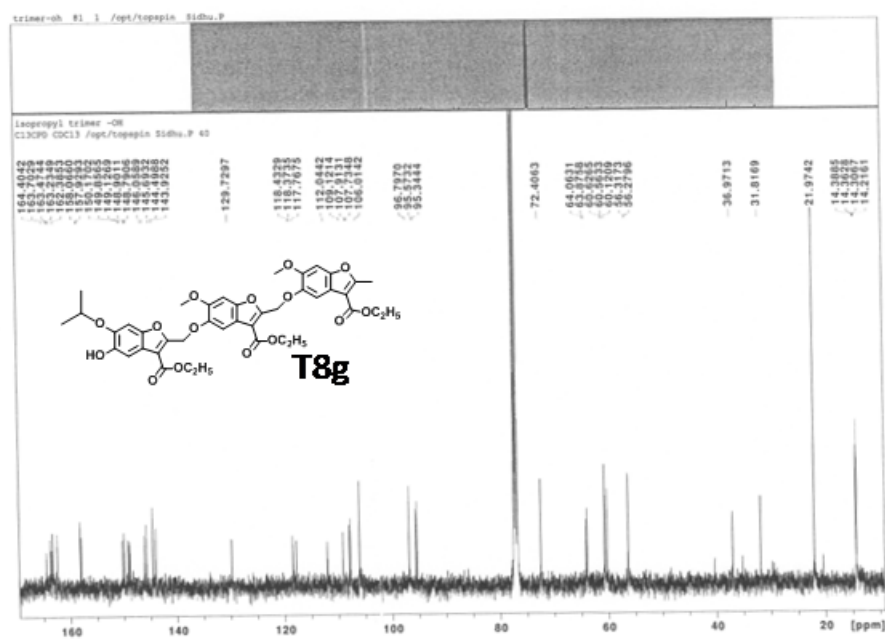
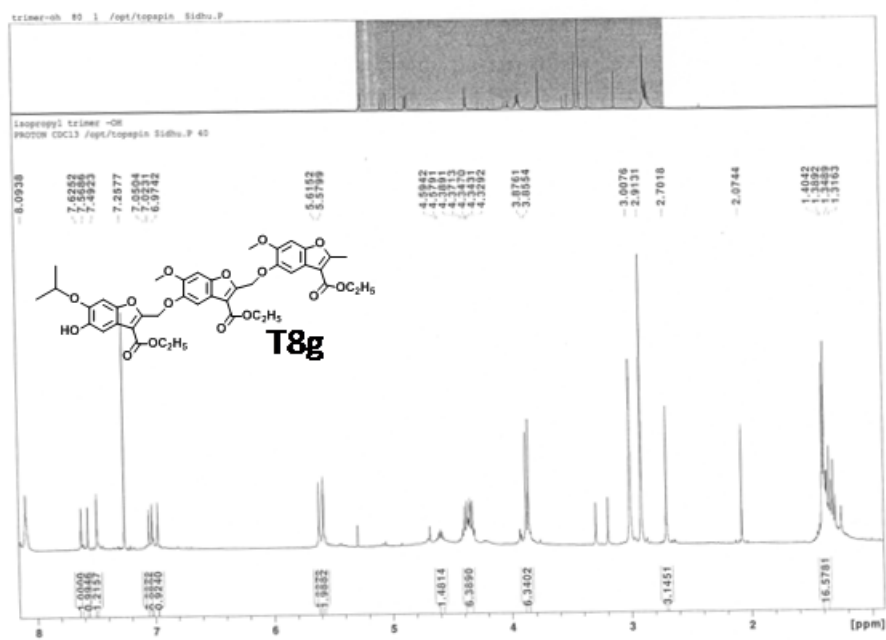


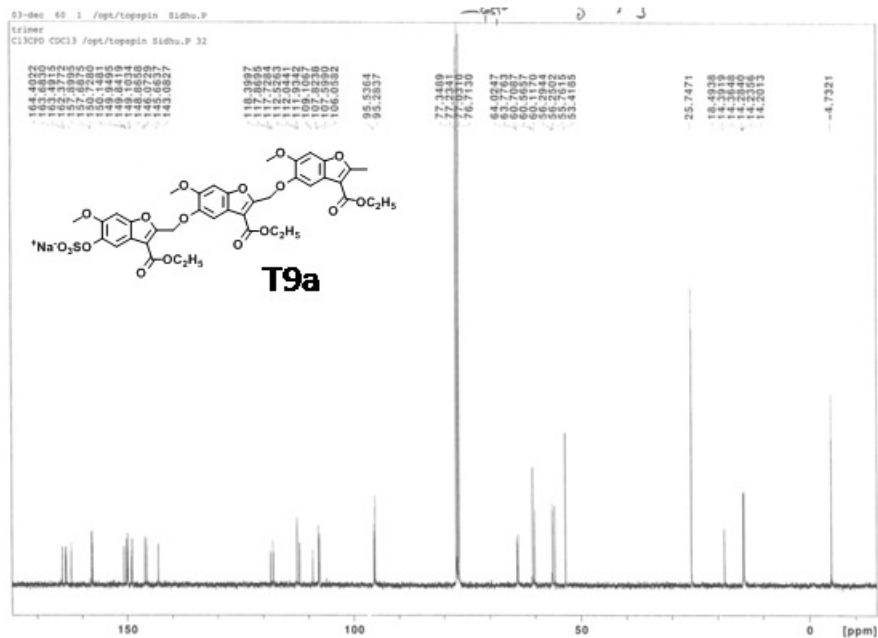
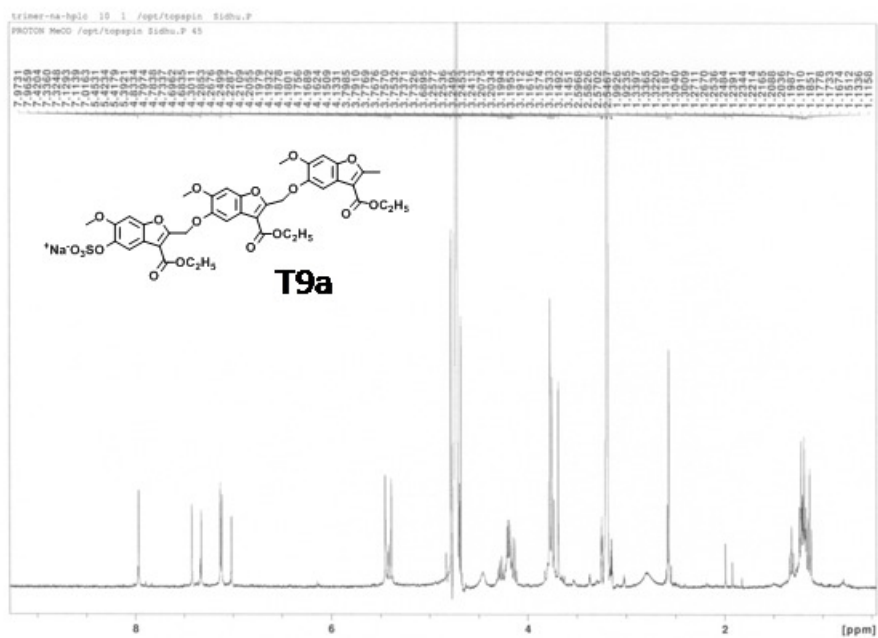


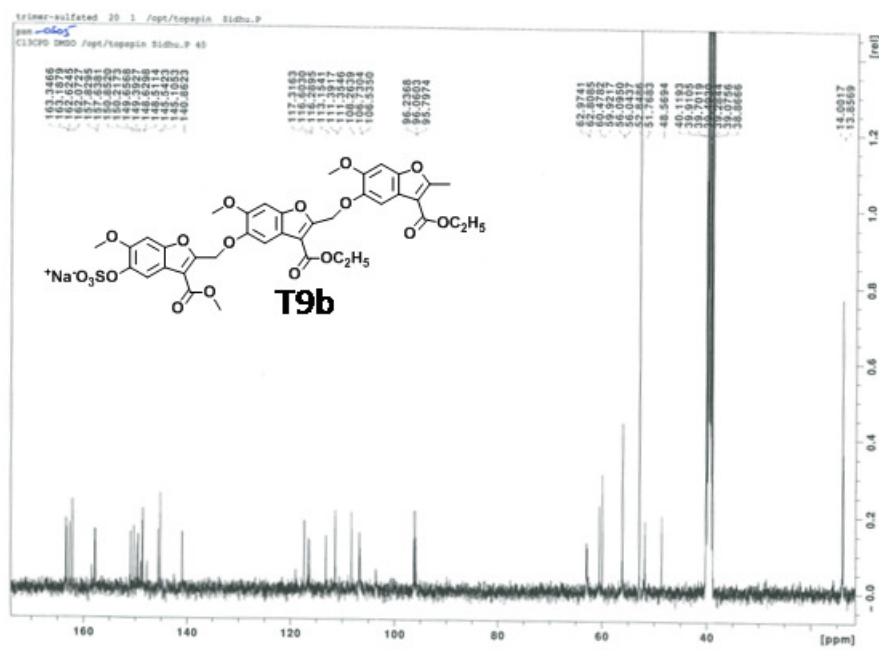
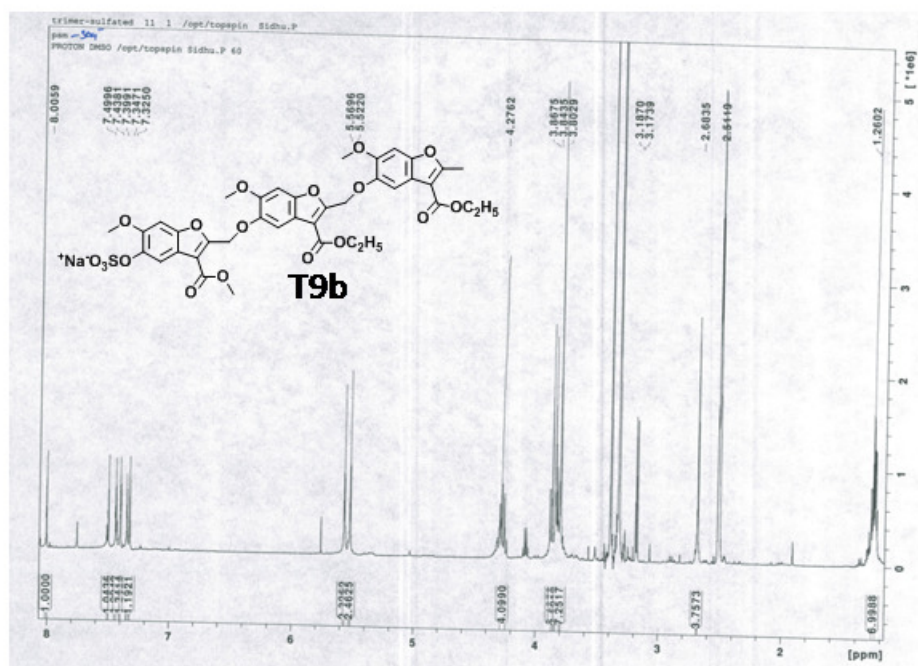


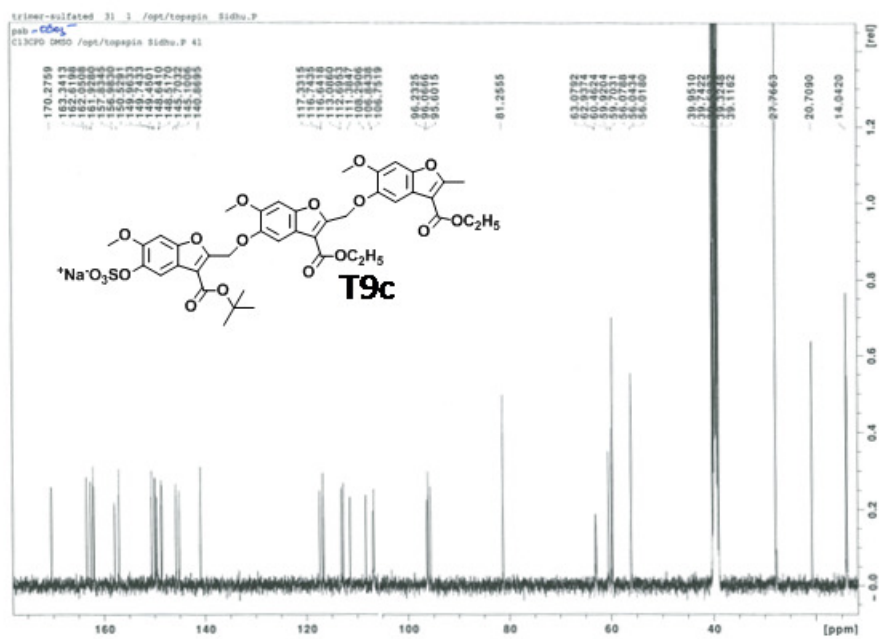
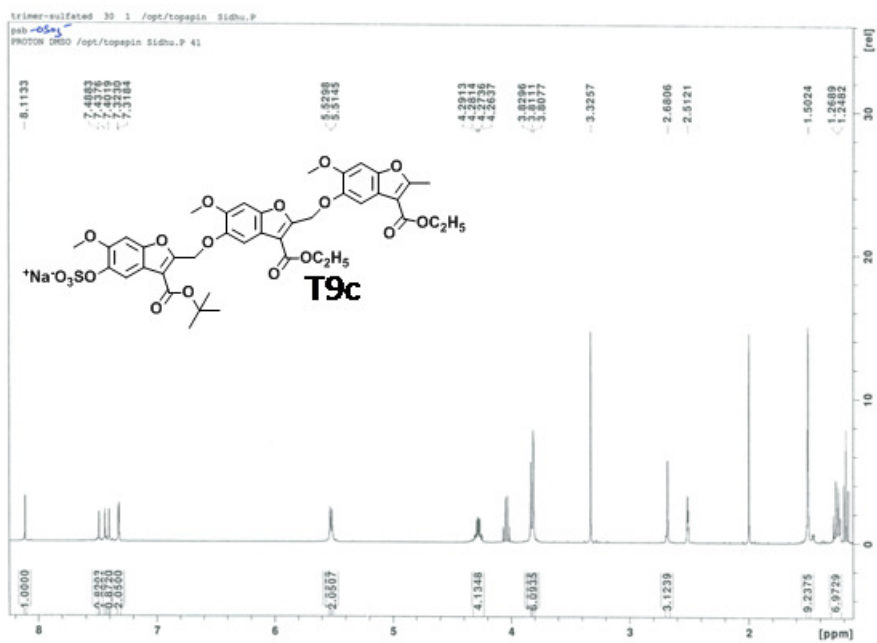


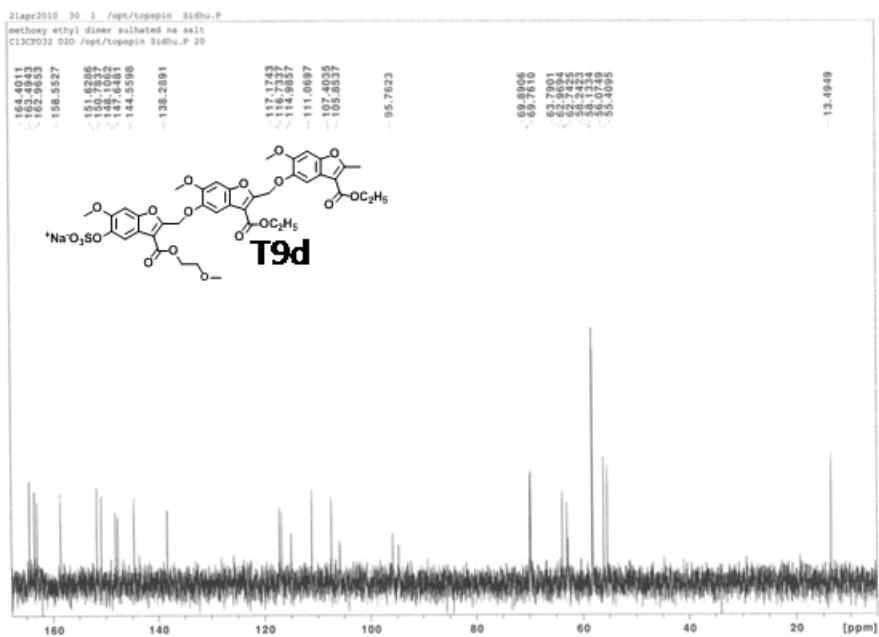
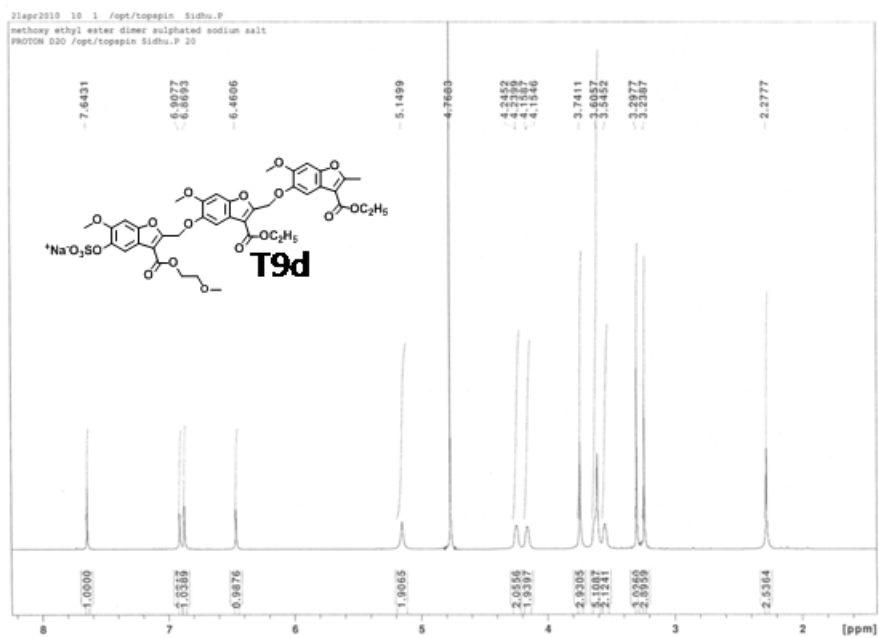


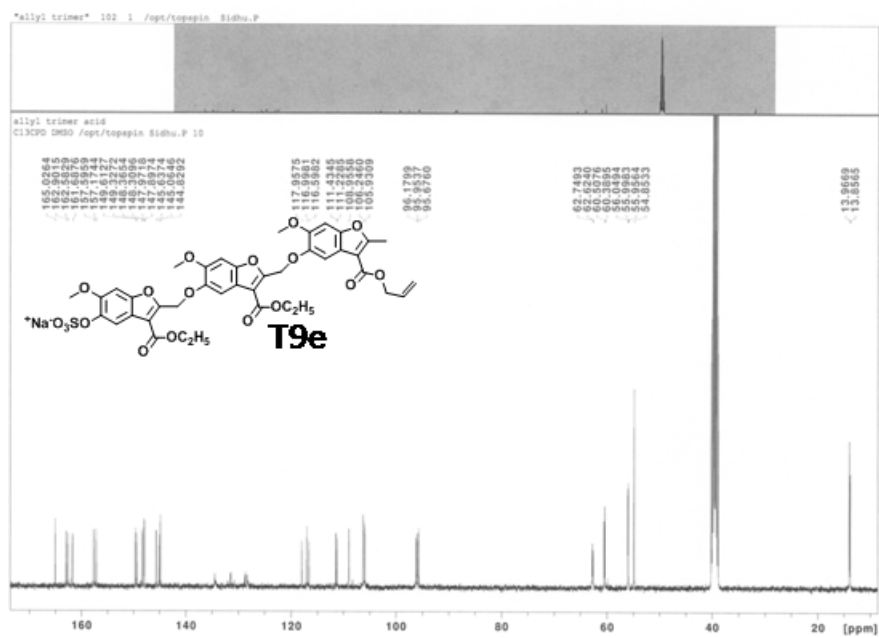
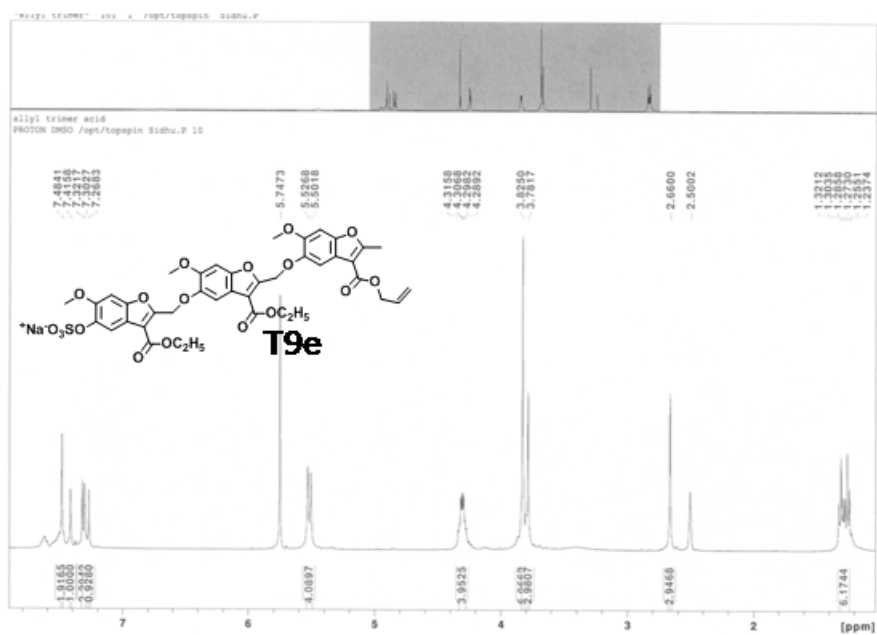


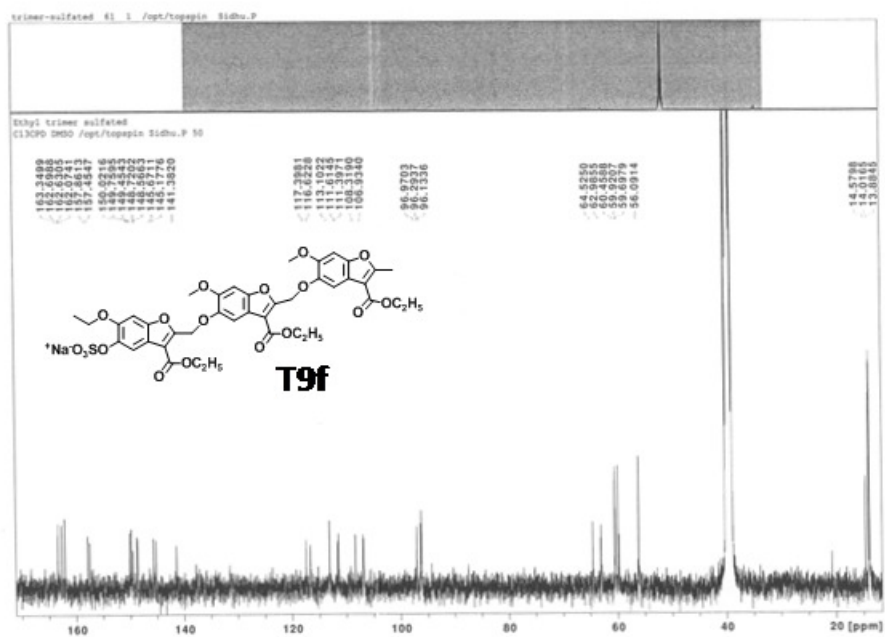
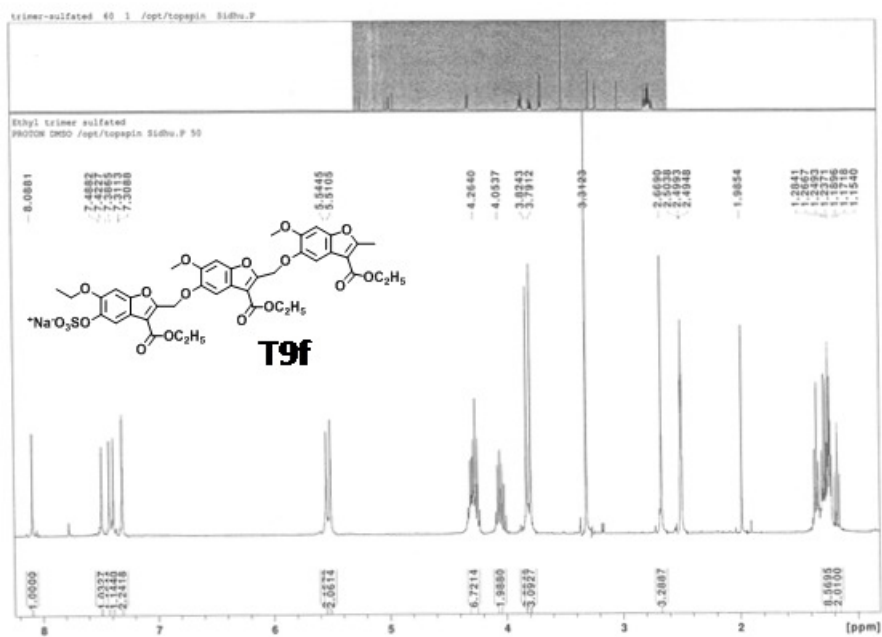


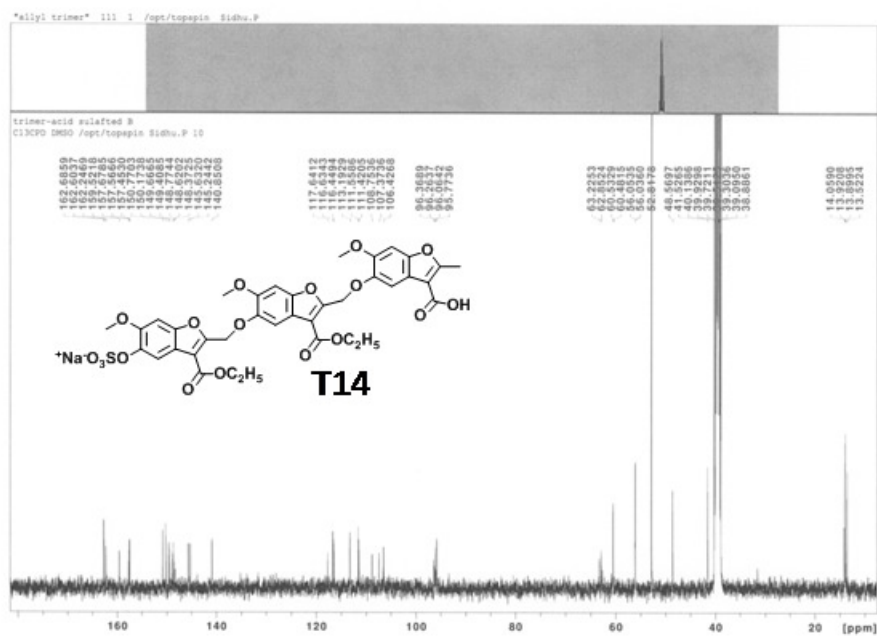
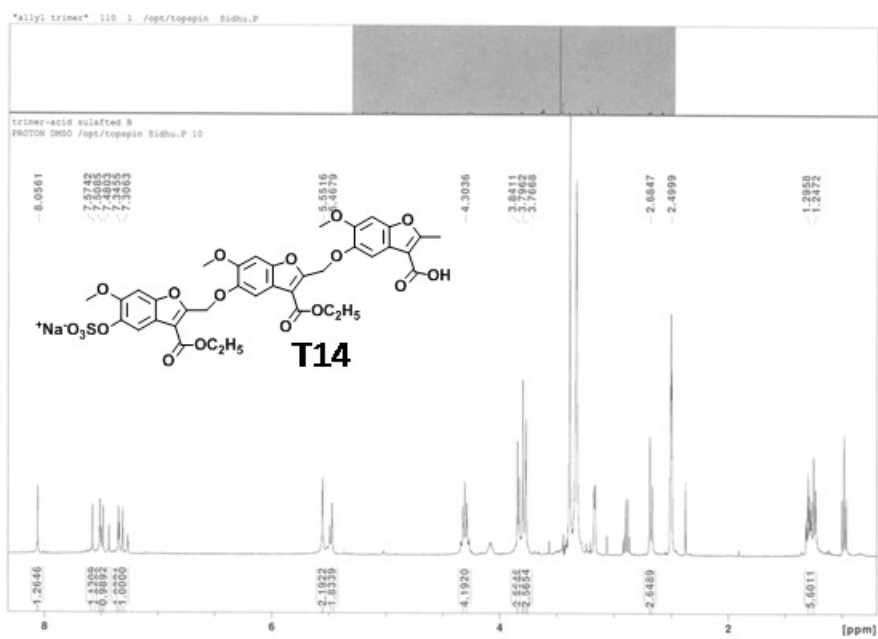


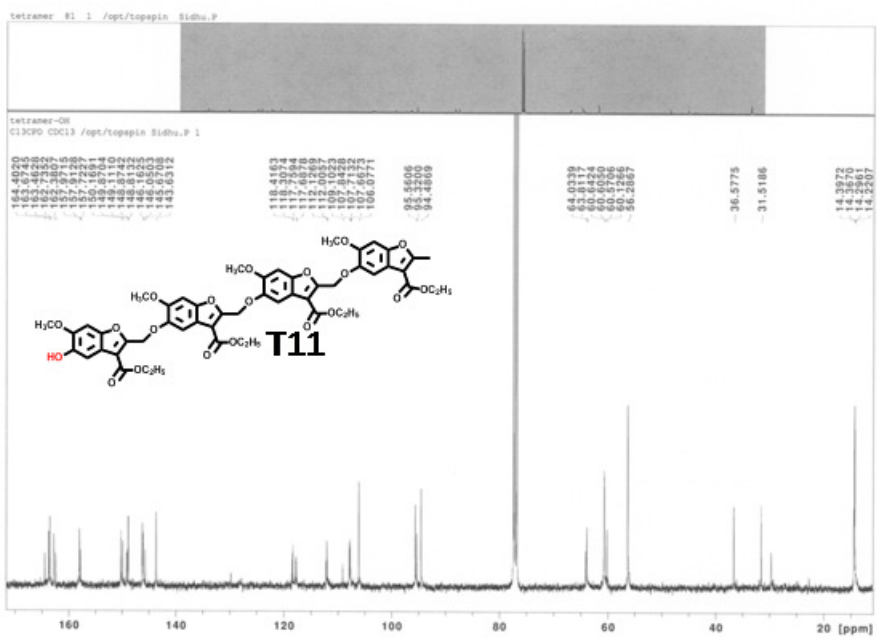
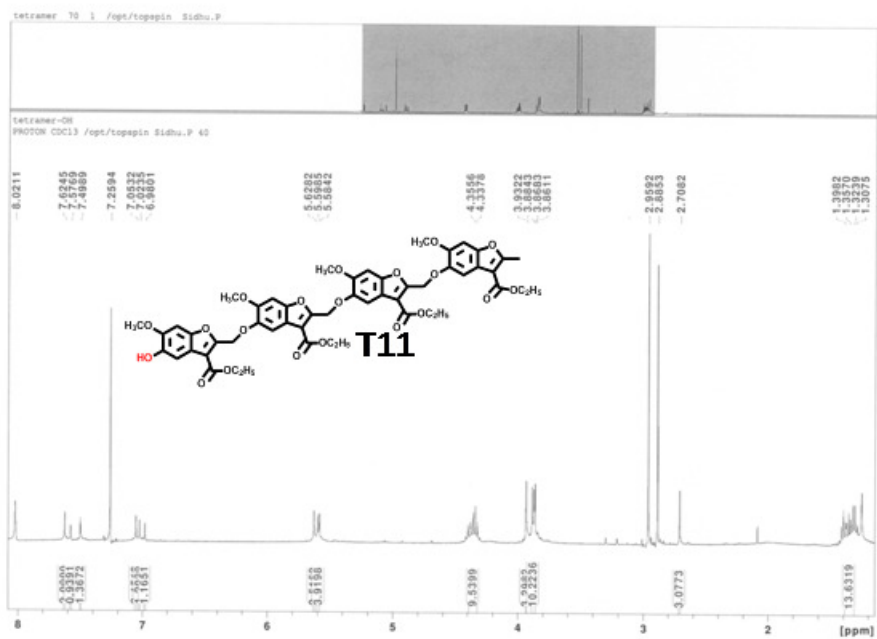


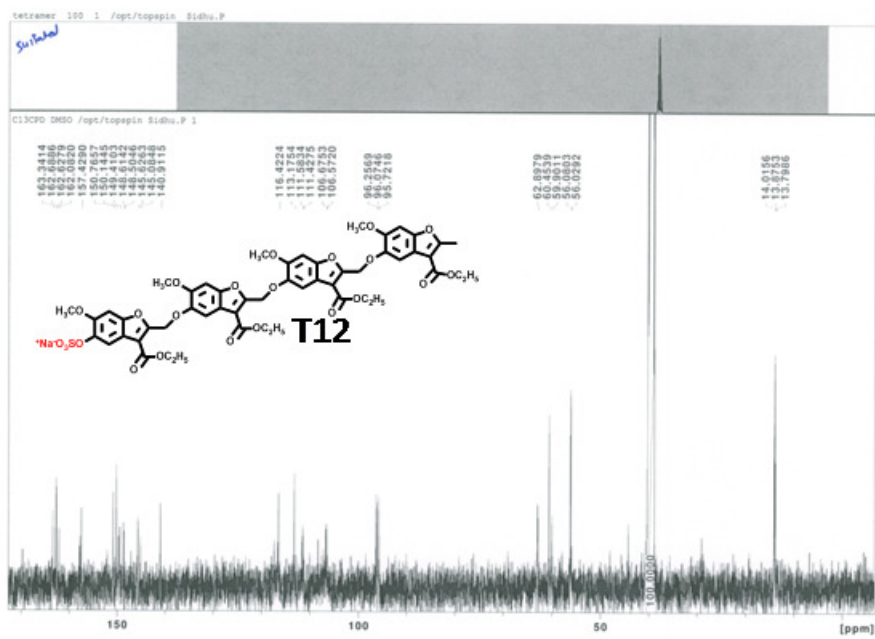
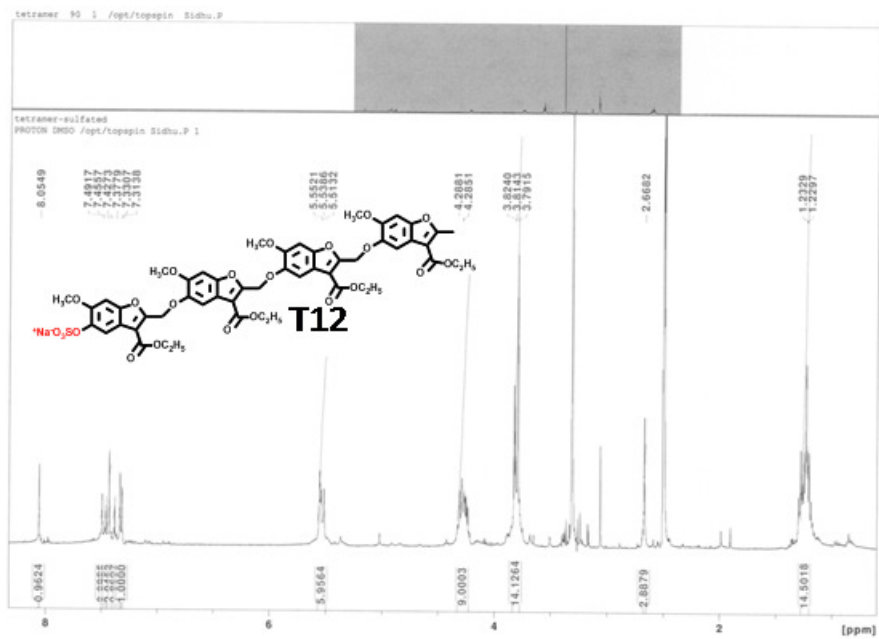






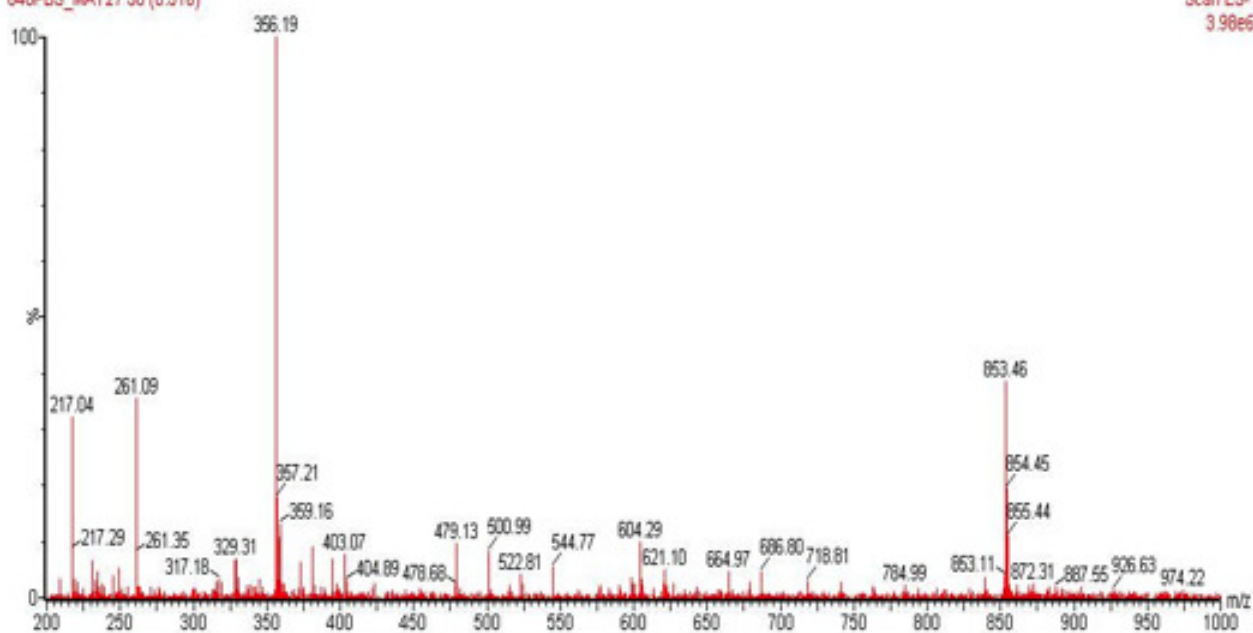






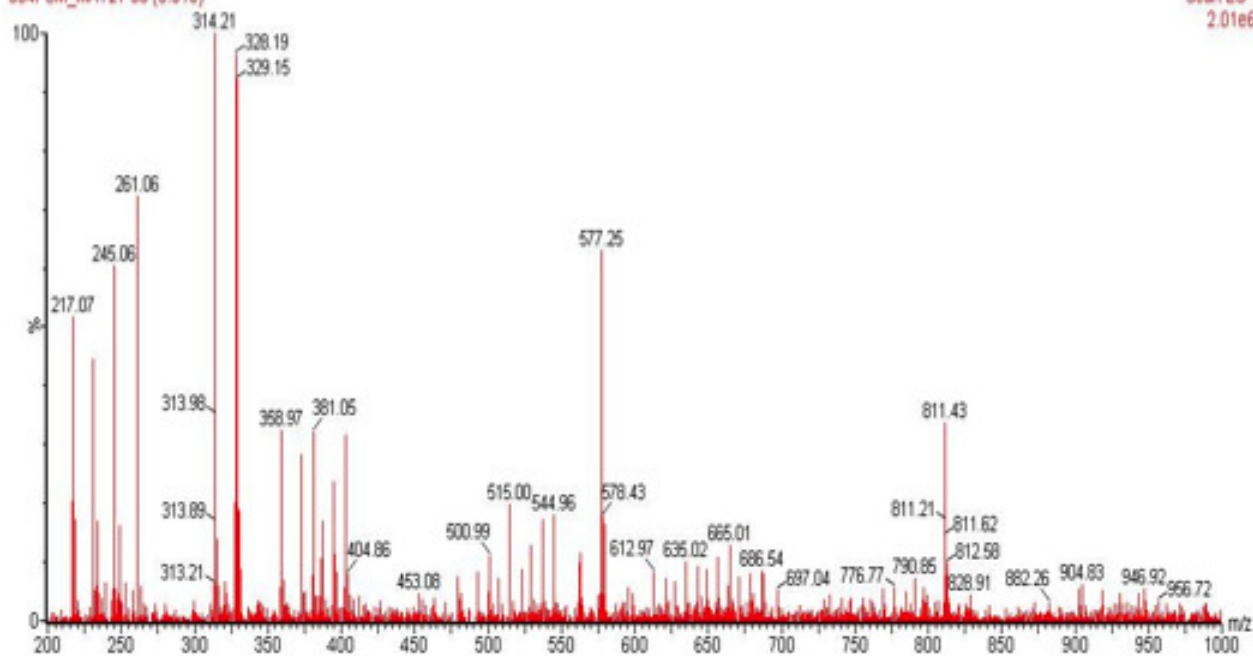
848-monosulfated
848PBS_MAY27 30 (0.516)

Scan ES-
3.98e6



834-monosulfated
834PSM_MAY27 30 (0.515)

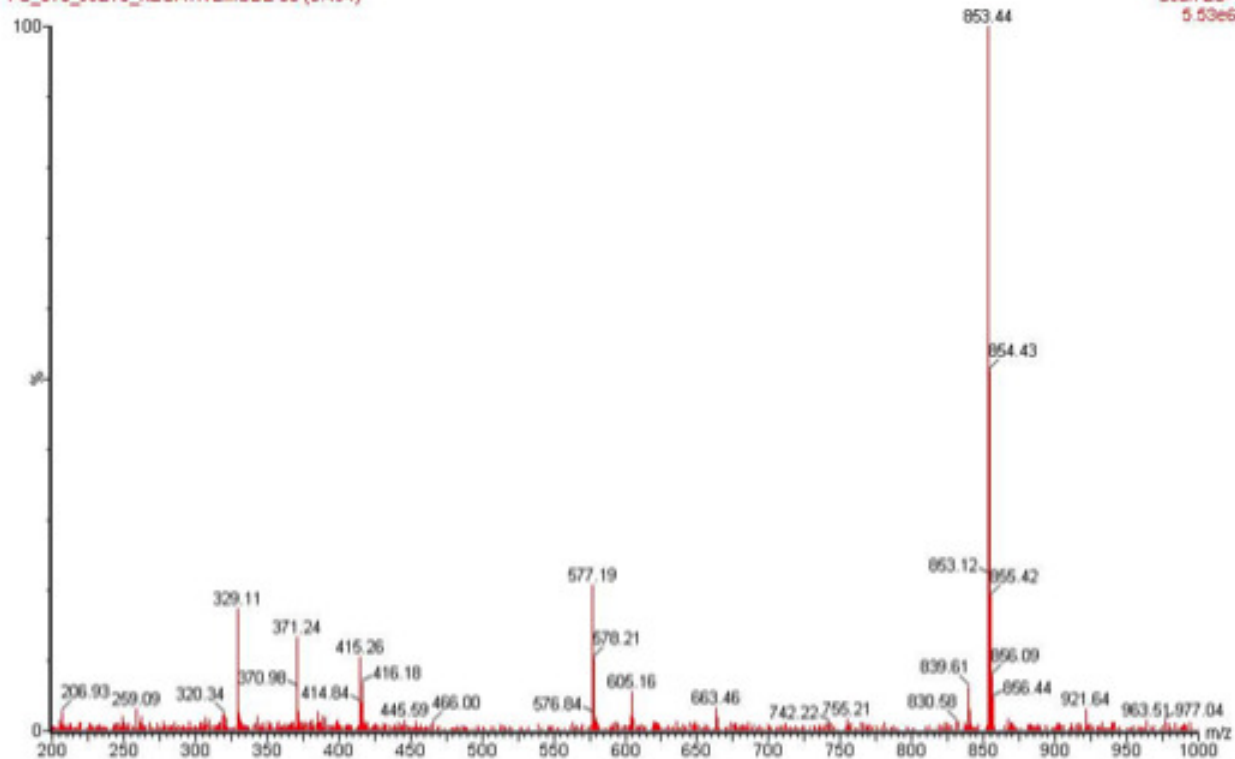
Scan ES-
2.01e6



Isopropyl sulfated trimer

PS_876_JULY5_NEGATIVEMODE 56 (0.494)

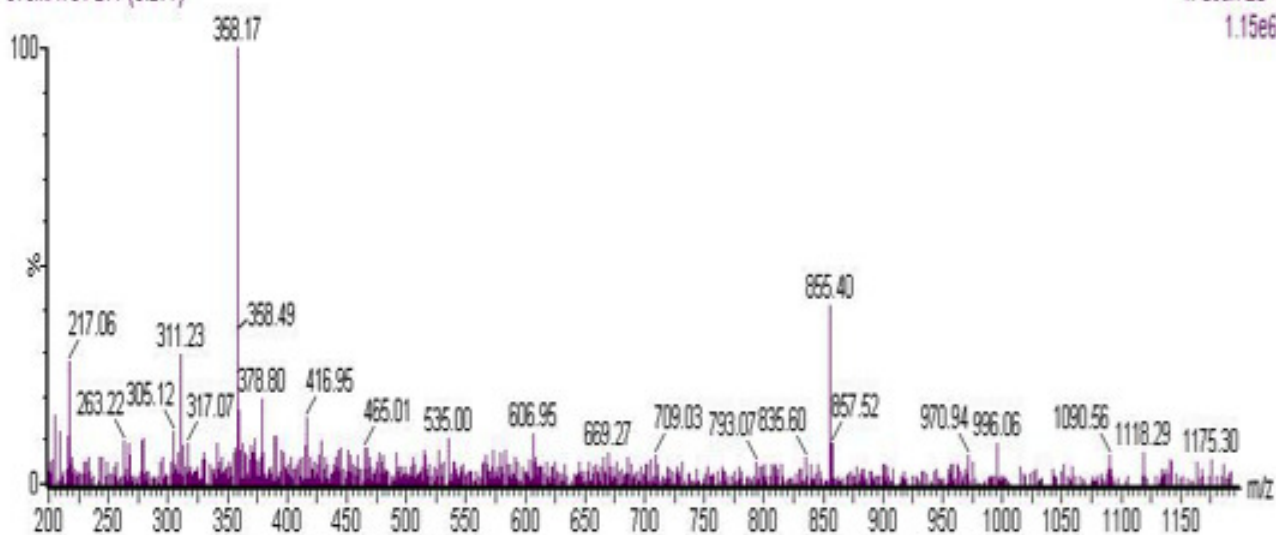
Scan ES-
5.53e6



878

878MAY31 277 (3.277)

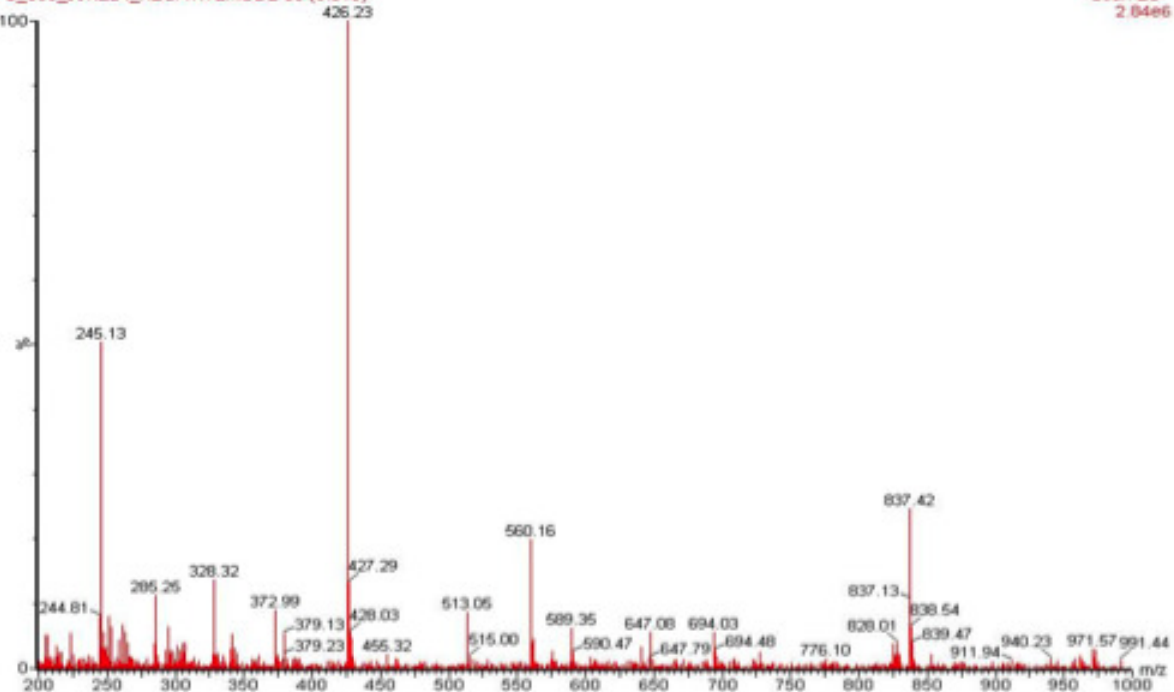
1: Scan ES-
1.15e6



860_monosulfated

PS_860_JUNE24_NEGATIVEMODE 30 (0.515)

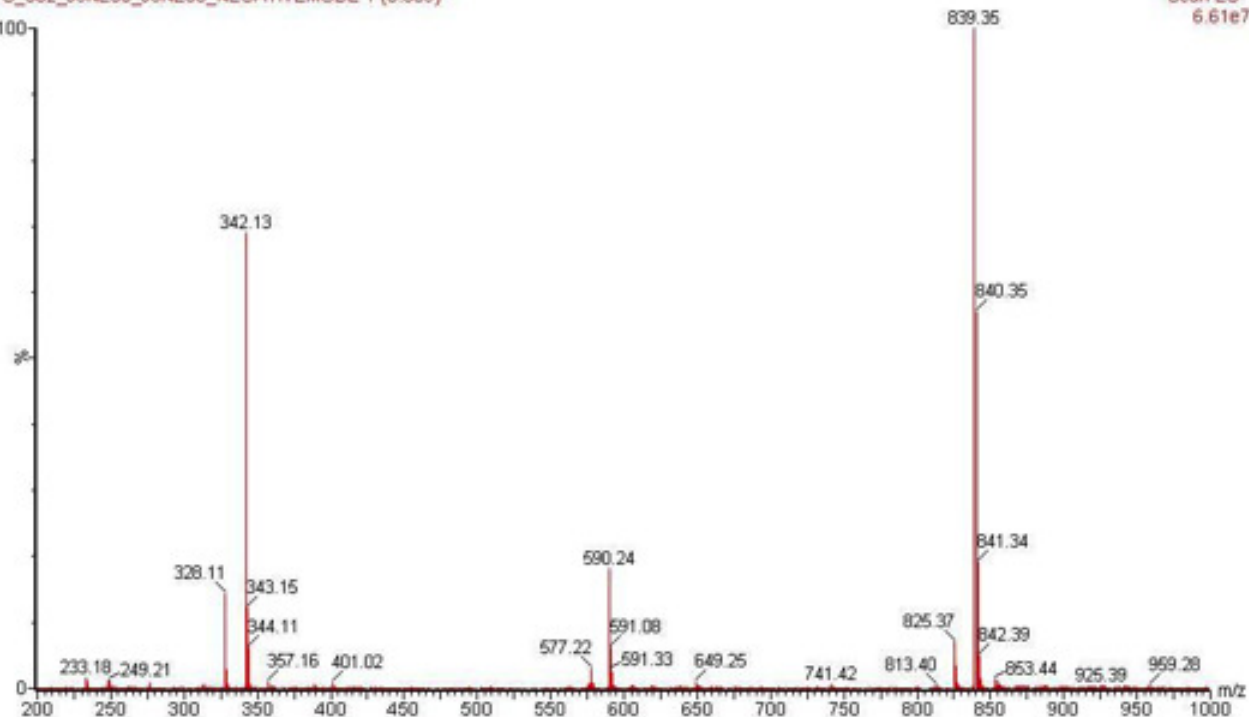
Scan ES-
2.84e6



monosulfated trimer

PS_862_JUNE30_JUNE30_NEGATIVEMODE 1 (0.009)

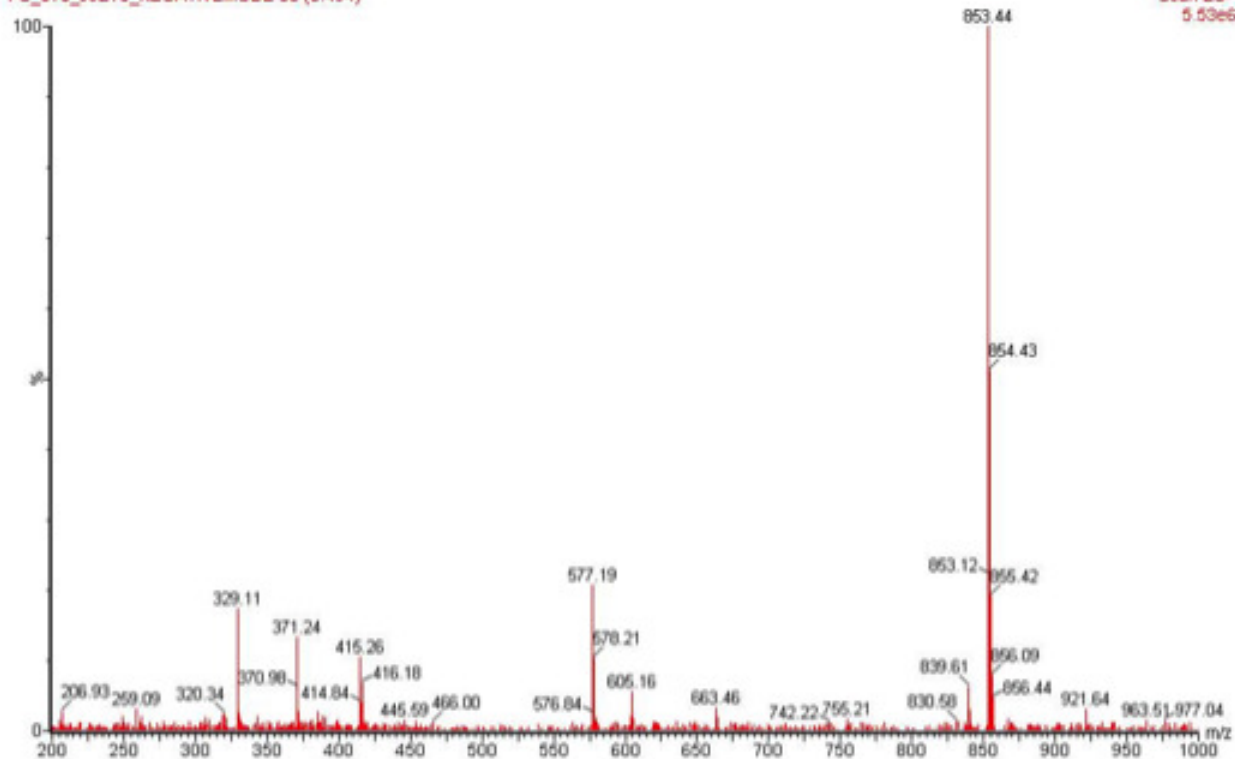
Scan ES-
6.61e7



Isopropyl sulfated trimer

PS_876_JULY5_NEGATIVEMODE 56 (0.494)

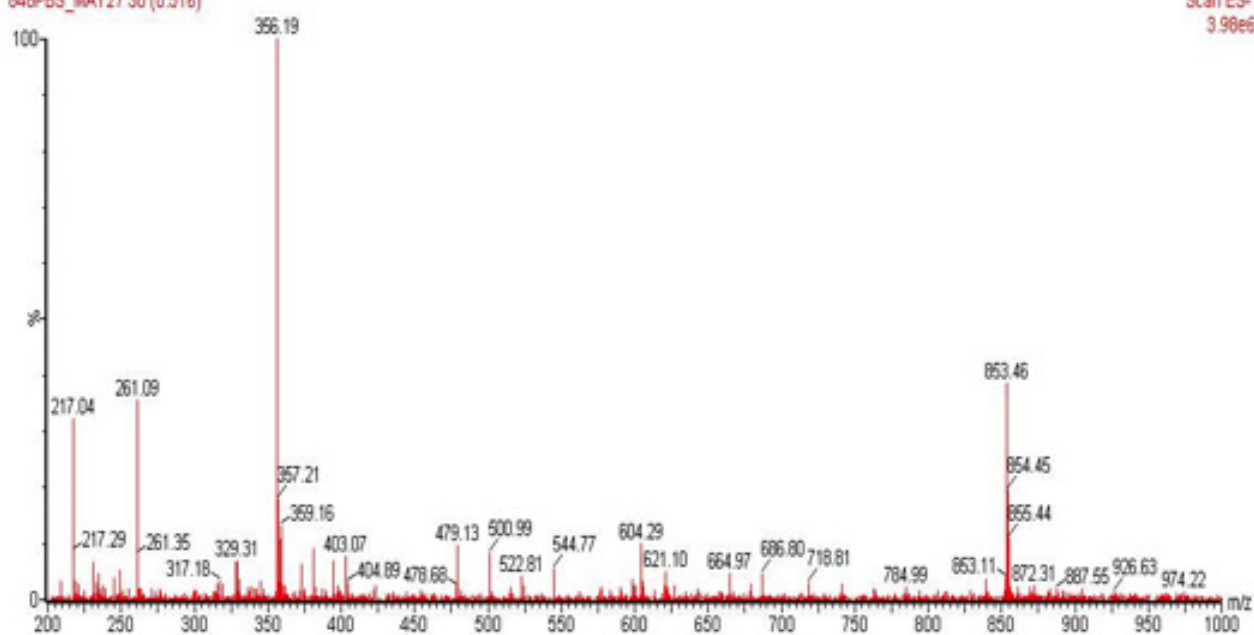
Scan ES-
5.53e6



848-monosulfated

848PBS_MAY27 30 (0.516)

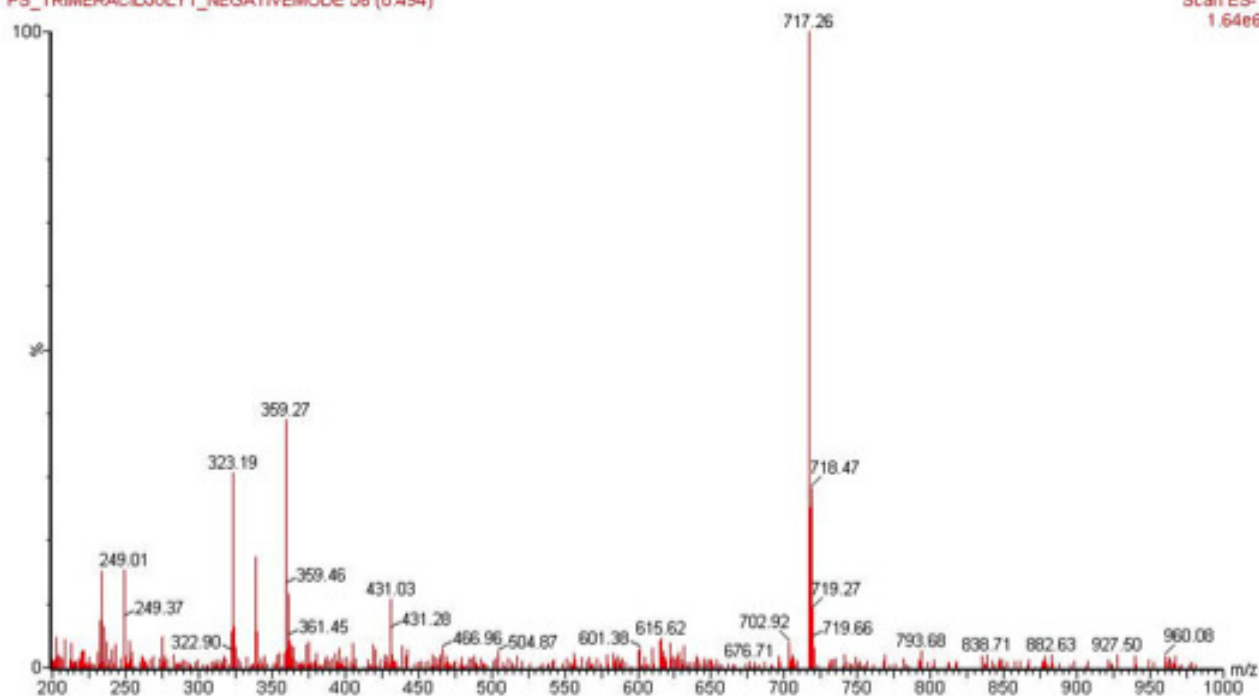
Scan ES-
3.98e6



718

PS_TRIMERACIDJULY1_NEGATIVEMODE 56 (0.494)

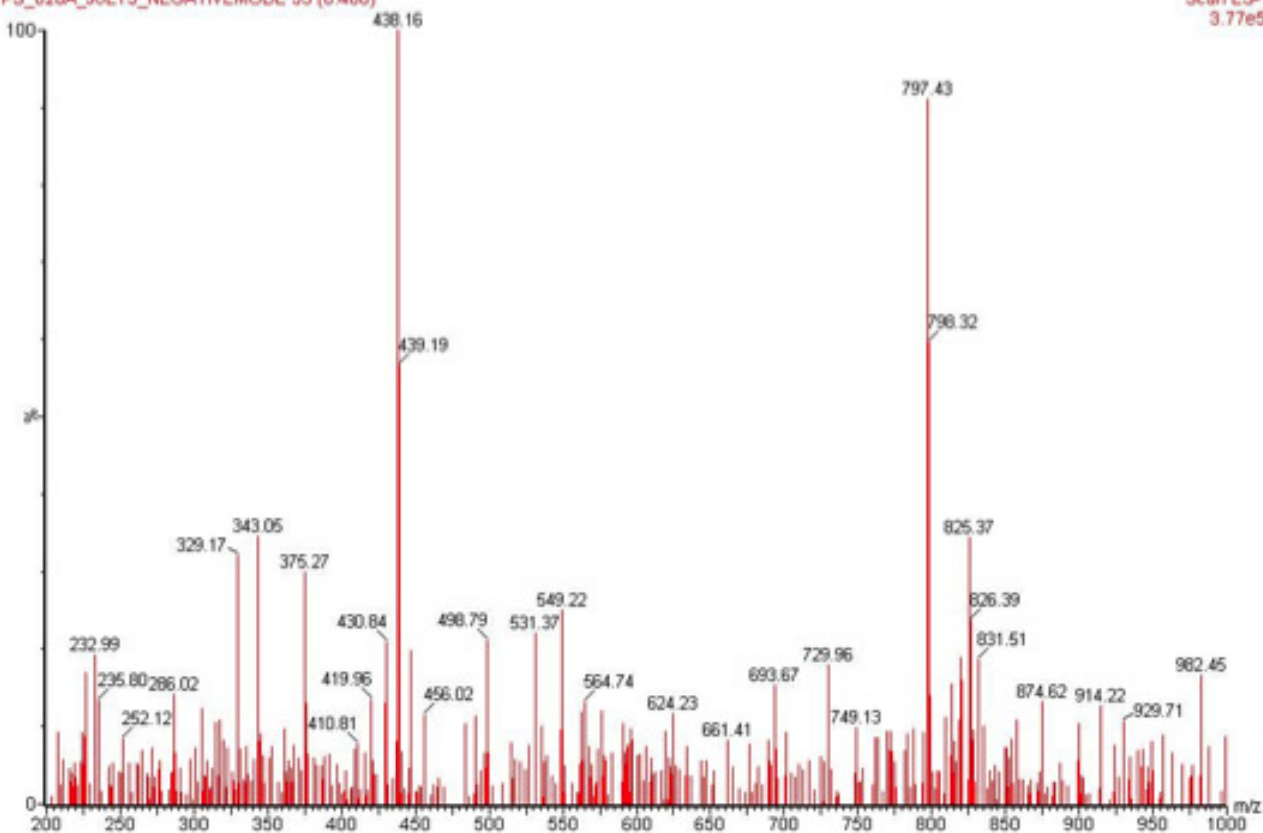
Scan ES-
1.64e6

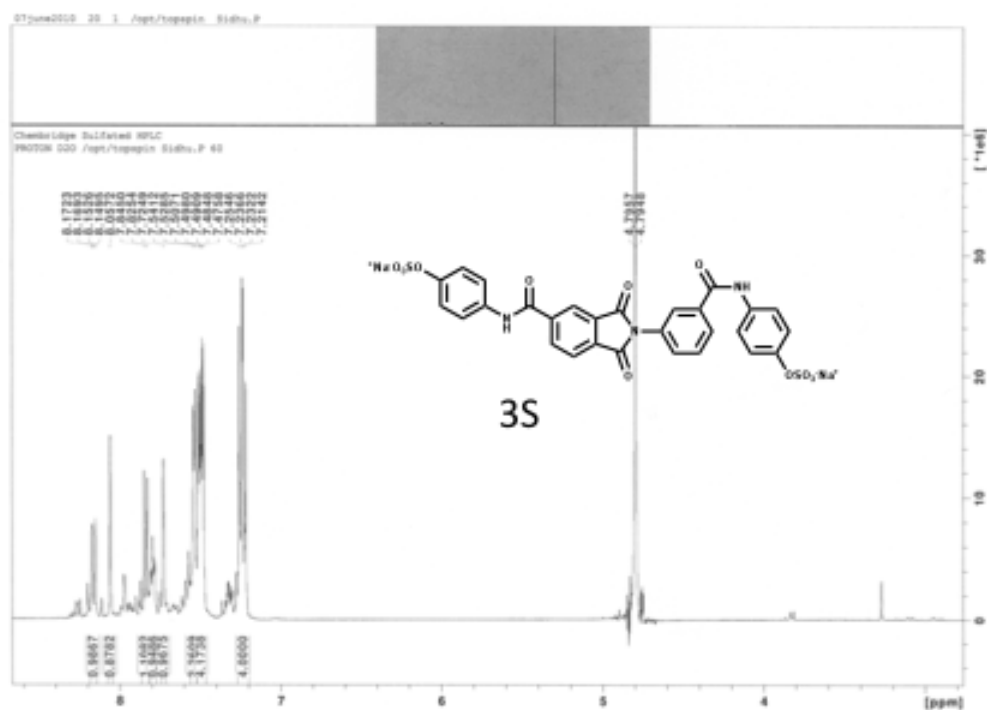
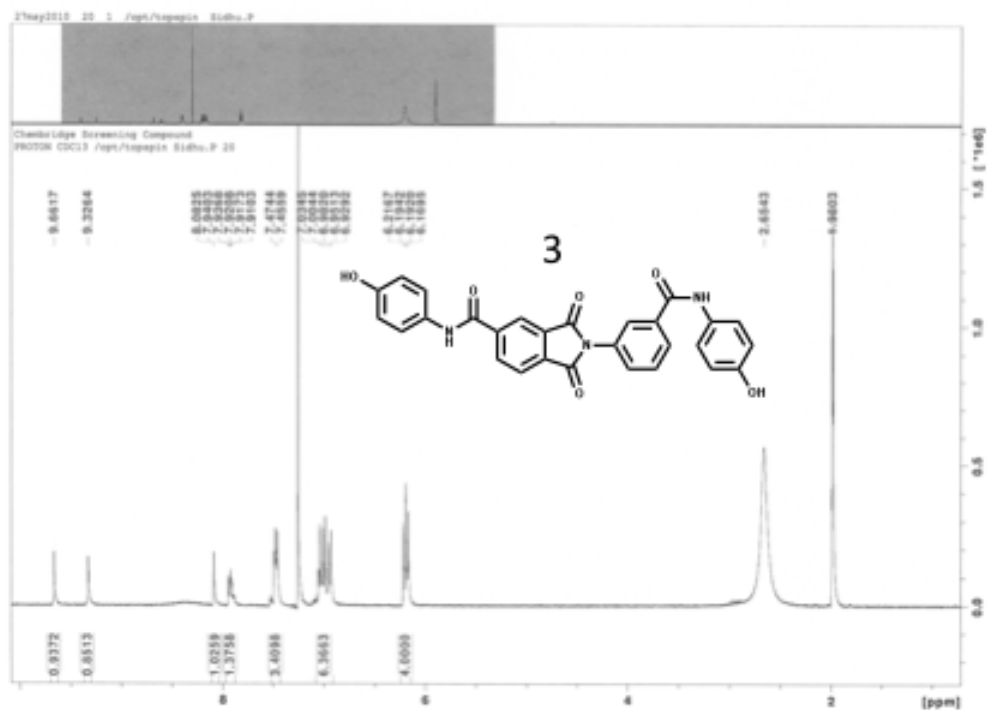


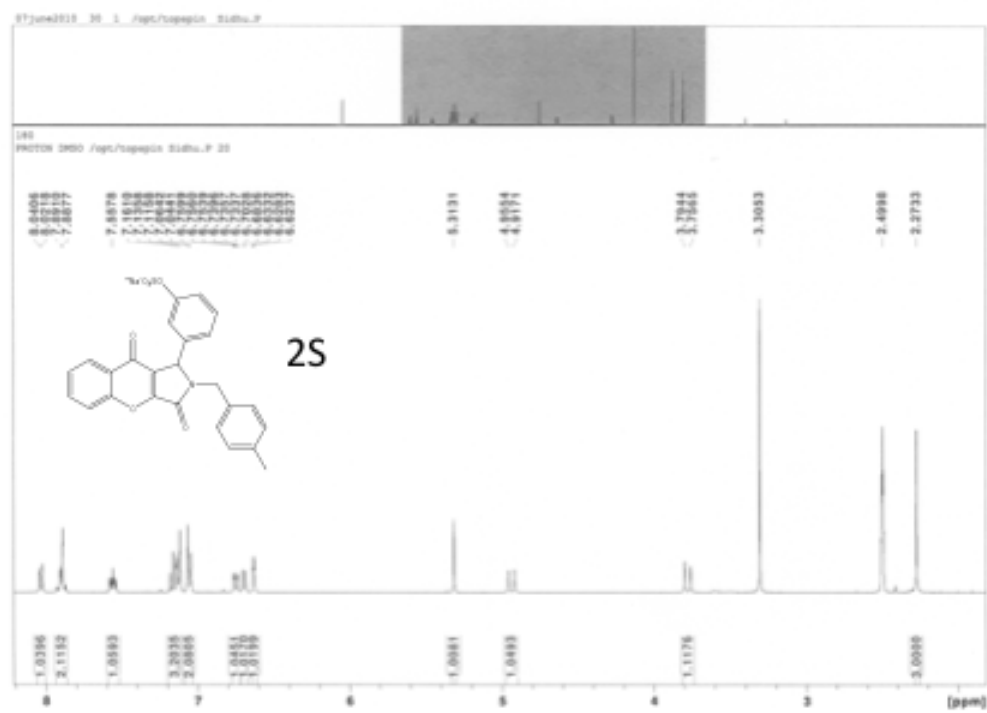
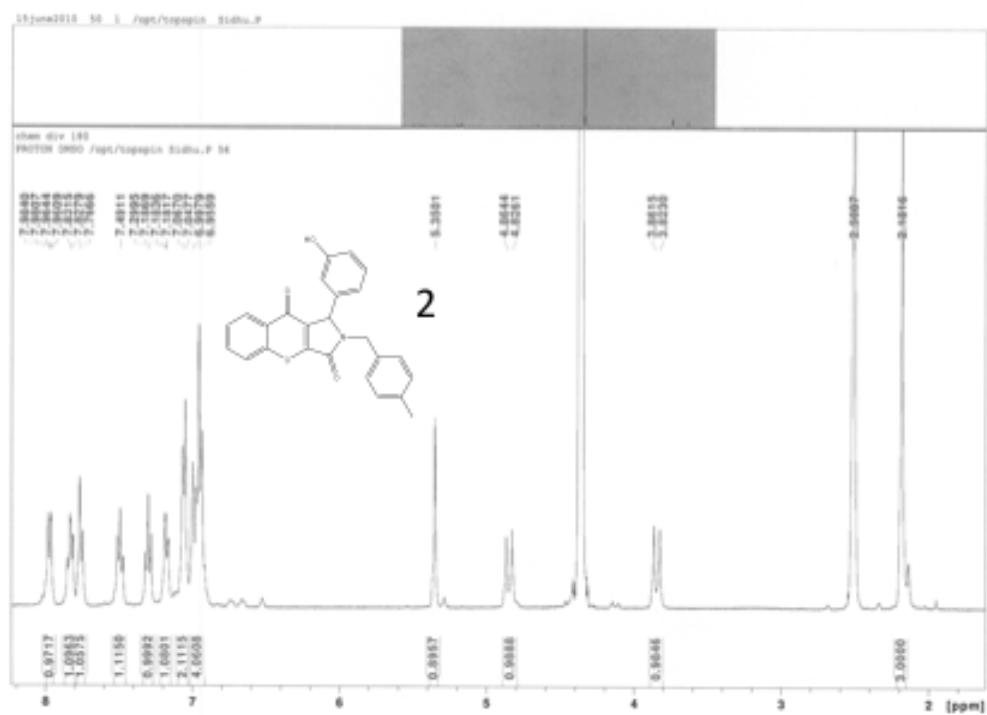
sulfated acid trimer

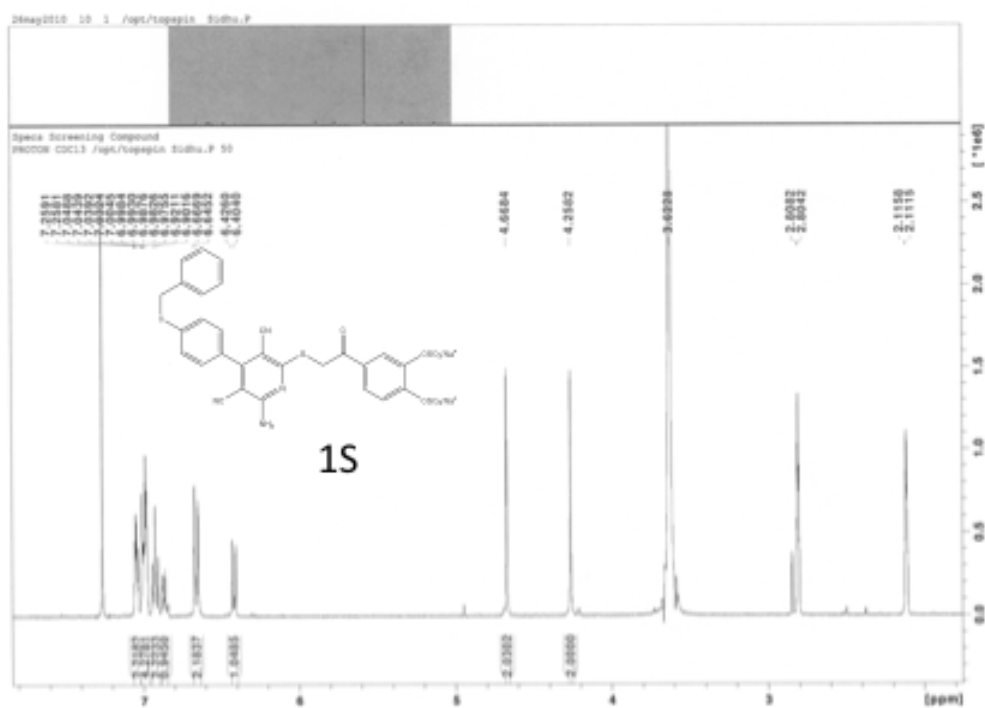
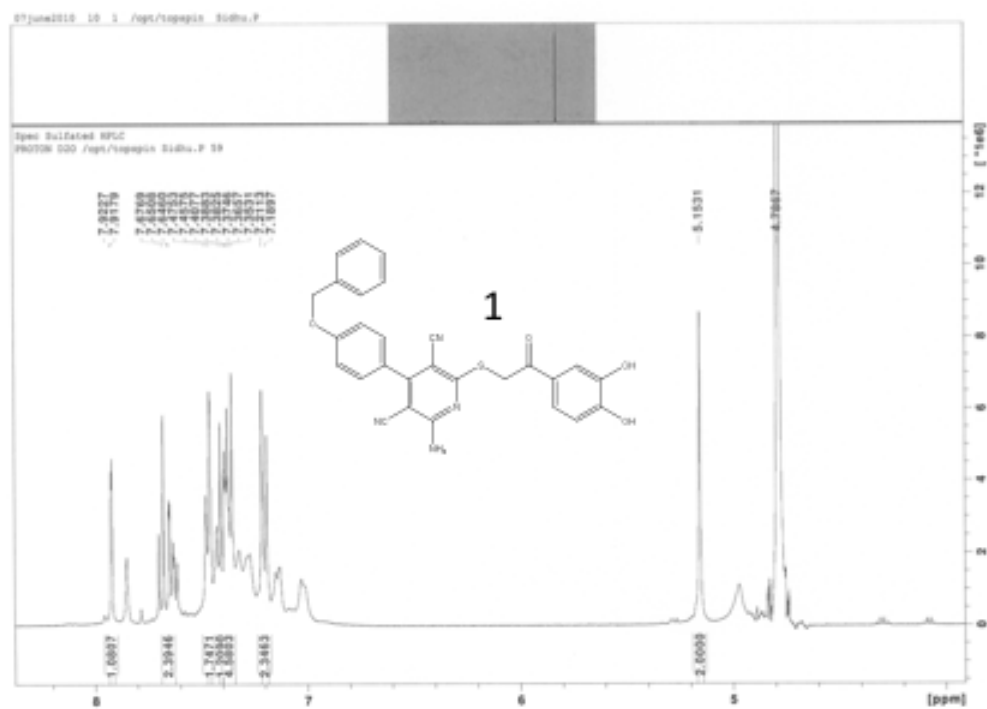
PS_820A_JULY5_NEGATIVEMODE 53 (0.468)

Scan ES-
3.77e5









VITA

Preetpal Singh Sidhu was born on 5th September, 1984 in Dhaban, India and he is currently a citizen of the Republic of India. Preetpal graduated high school from KCVN in 2002. He received his Bachelor of Pharmacy degree from Rajiv Gandhi University of Health Science, Bangalore, India (RGUHS, India) in 2006. In the year 2003 and 2006, he was accorded with “Overall Rank Certificate” from RGUHS. He also received “Industry Diploma in Contract Research and Clinical Trials” and “Certificate in Pharmaceutical Patents” in 2006. He commenced his Ph.D. degree (Fall 2007) in the Department of Medicinal Chemistry under the Pharmaceutical Science program at Virginia Commonwealth University, Richmond, Virginia (USA). In 2009, he also received the AAiPS Research Award.